SSC-347

STRATEGIES FOR NONLINEAR ANALYSIS OF MARINE STRUCTURES
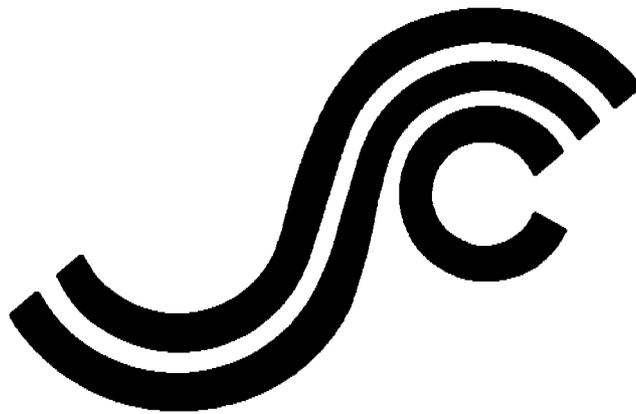
SHIP STRUCTURE COMMITTEE

1991

SHIP STRUCTURE COMMITTEE

The SHIP STRUCTURE COMMITTEE is constituted to prosecute a research program to improve the hull structures of ships and other marine structures by an extension of knowledge pertaining to design, materials, and methods of construction.

RADM J. D. Sipes, USCG, (Chairman)
Chief, Office of Marine Safety, Security
  and Environmental Protection
U. S. Coast Guard

Mr. Alexander Malakhoff
Director, Structural Integrity
  Subgroup (SEA 55Y)
Naval Sea Systems Command

Dr. Donald Liu
Senior Vice President
American Bureau of Shipping

Mr. H. T. Haller
Associate Administrator for Ship-
  building and Ship Operations
Maritime Administration

Mr. Thomas W. Allen
Engineering Officer (N7)
Military Sealift Command

CDR Michael K. Parmelee, USCG,
Secretary, Ship Structure Committee
U. S. Coast Guard

CONTRACTING OFFICER TECHNICAL REPRESENTATIVES

Mr. William J. Siekierka
SEA 55Y3
Naval Sea Systems Command

Mr. Greg D. Woods
SEA 55Y3
Naval Sea Systems Command

SHIP STRUCTURE SUBCOMMITTEE

The SHIP STRUCTURE SUBCOMMITTEE acts for the Ship Structure Committee on technical matters by providing technical coordination for determinating the goals and objectives of the program and by evaluating and interpreting the results in terms of structural design, construction, and operation.

AMERICAN BUREAU OF SHIPPING

Mr. Stephen G. Arntson (Chairman)
Mr. John F. Conlon
Dr. John S. Spencer
Mr. Glenn M. Ashe

MILITARY SEALIFT COMMAND

Mr. Albert J. Attermeyer
Mr. Michael W. Touma
Mr. Jeffery E. Beach

MARITIME ADMINISTRATION

Mr. Frederick Seibold
Mr. Norman O. Hammer
Mr. Chao H. Lin
Dr. Walter M. Maclean

NAVAL SEA SYSTEMS COMMAND

Mr. Robert A. Sielski
Mr. Charles L. Null
Mr. W. Thomas Packard
Mr. Allen H. Engle

U. S. COAST GUARD

CAPT T. E. Thompson
CAPT Donald S. Jensen
CDR Mark E. Noll

SHIP STRUCTURE SUBCOMMITTEE LIAISON MEMBERS

U. S. COAST GUARD ACADEMY

LT Bruce Mustain

U. S. MERCHANT MARINE ACADEMY

Dr. C. B. Kim

U. S. NAVAL ACADEMY

Dr. Ramswar Bhattacharyya

STATE UNIVERSITY OF NEW YORK
  MARITIME COLLEGE

Dr. W. R. Porter

WELDING RESEARCH COUNCIL

Dr. Martin Prager

NATIONAL ACADEMY OF SCIENCES –
  MARINE BOARD

Mr. Alexander B. Stavovy

NATIONAL ACADEMY OF SCIENCES –
  COMMITTEE ON MARINE STRUCTURES

Mr. Stanley G. Stiansen

SOCIETY OF NAVAL ARCHITECTS AND
  MARINE ENGINEERS –
  HYDRODYNAMICS COMMITTEE

Dr. William Sandberg

AMERICAN IRON AND STEEL INSTITUTE

Mr. Alexander D. Wilson

Ship Structure Committee

An Interagency Advisory Committee
Dedicated to the Improvement of Marine Structures

January 31, 1991

SSC-347
SR-1304

STRATEGIES FOR NONLINEAR ANALYSIS
OF MARINE STRUCTURES

Marine structures are designed to withstand the extreme responses caused by environmental factors during its lifetime. This report covers available and emerging techniques to determine extreme responses of nonlinear marine structures and systems. Nonlinear characteristics of wave induced forces and extreme value analyses of nonlinear systems are addressed. The review of procedures for nonlinear analysis and how they may be applied to the probability analysis of extreme events should prove to be useful.

J. D. SIPES
Rear Admiral, U.S. Coast Guard
Chairman, Ship Structure Committee

1. Report No. SSC-347	2. Government Accession No.	3. Recipient's Catalog No.
4. Title and Subtitle Strategies for Nonlinear Analysis of Marine Structures		5. Report Date AUGUST 1988
		6. Performing Organization Code
7. Author's) Subrata K. Chakrabarti		8. Performing Organization Report No. SR-1304
9. Performing Organization Name and Address CBI Research Corporation 1501 North Division Street Plainfield, IL 60544-8929		10. Work Unit No. (TRAIS)
		11. Contract or Grant No. DTCG23-85-C-20069
12. Sponsoring Agency Name and Address Commandant U.S. Coast Guard 2100 Second Street, SW Washington, DC 20593		13. Type of Report and Period Covered Final Report
		14. Sponsoring Agency Code G-M

15. Supplementary Notes

Sponsored by the Ship Structure Committee and its member agencies.

16. Abstract

This report extensively reviews the state-of-the-art of available and emerging techniques for determining extreme responses of nonlinear marine structures and systems. The contents may be categorized into two parts. The first presents the nonlinear characteristics of wave induced forces and corresponding structural responses. The other discusses the extreme value analysis of nonlinear systems relevant to offshore and marine structural design. Generic procedures for the nonlinear analysis of marine structures were reviewed. Discussions of non-Gaussian random processes and the use of extreme value statistics are included. Methods that may be applied to the probability analysis of extreme events were investigated. Different types of nonlinear behavior of interest for various classes of offshore structures were studied. Various statistical analysis methods are summarized and their applicability, assumptions and limitations are discussed.

17. Key Words Marine Structures Nonlinear Analysis Probabilistic Methods Extreme Value Analysis Structural Analysis	18. Distribution Statement Available from: Nat'l Technical Information Service Springfield, VA 22161 or Marine Tech. Information Facility National Maritime Research Center Kings Point, NY 10024-1699		
19. Security Classif. (of this report) Unclassified	20. Security Classif. (of this page) Unclassified	21. No. of Pages 380	22. Price

Form DOT F 1700.7 (8-72)   Reproduction of completed page authorized

METRIC CONVERSION FACTORS

Approximate Conversions to Metric Measures

Symbol	When You Know	Multiply by	To Find	Symbol
		LENGTH		
in	inches	*2.5	centimeters	cm
ft	feet	30	centimeters	cm
yd	yards	0.9	meters	m
mi	miles	1.6	kilometers	km
		AREA		
in^2	square inches	6.5	square centimeters	cm^2
ft^2	square feet	0.09	square meters	m^2
yd^2	square yards	0.8	square meters	m^2
mi^2	square miles	2.6	square kilometers	km^2
	acres	0.4	hectares	ha
		MASS (weight)		
oz	ounces	28	grams	g
lb	pounds	0.45	kilograms	kg
	short tons (2000 lb)	0.9	tonnes	t
		VOLUME		
tsp	teaspoons	5	milliliters	ml
Tbsp	tablespoons	15	milliliters	ml
fl oz	fluid ounces	30	milliliters	ml
c	cups	0.24	liters	l
pt	pints	0.47	liters	l
qt	quarts	0.95	liters	l
gal	gallons	3.8	liters	l
ft^3	cubic feet	0.03	cubic meters	m^3
yd^3	cubic yards	0.76	cubic meters	m^3
		TEMPERATURE (exact)		
°F	Fahrenheit temperature	5/9 (after subtracting 32)	Celsius temperature	°C

*1 in = 2.54 (exactly). For other exact conversions and more detailed tables, see NBS Misc. Publ. 286, Units of Weights and Measures, Price $2.25, SD Catalog No. C13 10 286.

Approximate Conversions from Metric Measures

Symbol	When You Know	Multiply by	To Find	Symbol
		LENGTH		
mm	millimeters	0.04	inches	in
cm	centimeters	0.4	inches	in
m	meters	3.3	feet	ft
m	meters	1.1	yards	yd
km	kilometers	0.6	miles	mi
		AREA		
cm^2	square centimeters	0.16	square inches	in^2
m^2	square meters	1.2	square yards	yd^2
km^2	square kilometers	0.4	square miles	mi^2
ha	hectares (10,000 m^2)	2.5	acres	
		MASS (weight)		
g	grams	0.035	ounces	oz
kg	kilograms	2.2	pounds	lb
t	tonnes (1000 kg)	1.1	short tons	
		VOLUME		
ml	milliliters	0.03	fluid ounces	fl oz
l	liters	2.1	pints	pt
l	liters	1.06	quarts	qt
l	liters	0.26	gallons	gal
m^3	cubic meters	35	cubic feet	ft^3
m^3	cubic meters	1.3	cubic yards	yd^3
		TEMPERATURE (exact)		
°C	Celsius temperature	9/5 (then add 32)	Fahrenheit temperature	°F

```
°F  -40    0    32  40    80  98.6 120   160  200  212 °F
    |-|-|-|-|-|-|-|-|-|-|-|-|-|-|-|-|-|-|-|-|-|
°C  -40   -20    0    20   40   60    80  100 °C
                          37
```
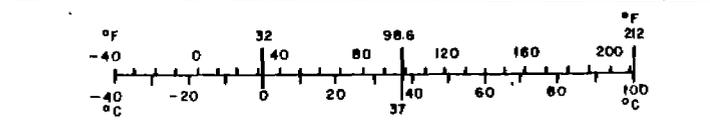
TABLE OF CONTENTS

SUMMARY

LIST OF SYMBOLS

SUMMARY

Marine Structures are employed in the exploration, production and transportation of offshore minerals as well as for transportation of people and products across nations and for the defense of the country. The structures used for the production of oil and gas are generally located at a particular site offshore while others are mobile. These structures are often at the mercy of the harsh environment of the ocean in the form of waves, wind, current and earthquake and must survive the severest storm encountered during its lifetime.

Design of an offshore structure is based on the extreme responses experienced by the components of the structure under the influence of the environment faced by the structure in its lifetime. If the structural components may be treated as a linear system, the derivation of the extreme responses is relatively straightforward. However, most practical offshore systems have nonlinear responses, and these design tools are not applicable.

The purpose of this report is to perform an extensive state-of-the-art review of the available and emerging techniques for the determination of extreme responses of a nonlinear marine structure and system. The contents of this report may be categorized into two parts; one presents the nonlinear characteristics of wave-induced forces and corresponding structural responses, and the other discusses the extreme value analysis of nonlinear systems relevant to offshore and marine structure design. The report reviews the generic procedures for the nonlinear analysis of marine structures and investigates the method in which they may be applied to the probability analysis of extreme events.

Different types of nonlinear behavior of interest for various classes of offshore structures have been studied. Nonlinearities in the analysis of these structures appear at various stages, e.g., waves, material properties, forcing function and motion response. The solutions of the dynamic problem with time dependent loads fall into two main categories: deterministic and nondeterministic (stochastic). Deterministic solutions include both the time domain (time history analysis) and the frequency domain analysis. While the time history analysis can retain most of the nonlinearities in a marine system, frequency domain solutions are necessarily linearized. Review of

these various generic procedures for nonlinear analysis has been made.

In the case of probabilisitc method of obtaining extremes of a response of an offshore structure, distinctions are made regarding short-term versus long-term.

A short term means a period of time which is short enough to describe the sea and the response as a stationary random process. This period of time is on the order of 30 minutes to 3 hours. It is a general practice to assume that the short-term statistical distribution of response amplitudes follows the Rayleigh distribution function. Based on this function, the probabilities of certain extremes over a given short term may be predicted. The waves are assumed Gaussian for this purpose. For responses, the narrow bandedness and linearity are inherent assumptions. However, the response (output) of a nonlinear system is a non-Gaussian random process even though the waves (input) is Gaussian. This fundamental principle has been addressed in the report. The prediction of the statistical properties of marine systems with strong nonlinear characteristics is not possible using a linear analysis. For statistical analysis of nonlinear systems, the probabilistic prediction of non-Gaussian random process is essential. This area has been discussed in the report, and several non-Gaussian random processes have been included.

For extreme value statistics, a long-term (of the order of 20-100 years) distribution of the response parameters is often required. The long-term non-stationary random process is sometimes written as a sum of a large number of short-term stationary process. The extreme values of a given probability level are also obtained by order-statistics. This area is briefly reviewed.

Various available methods in the above areas have been summarized, and their applicability, assumptions and limitations have been discussed. Based on this discusssion, several conclusions and recommendations have been drawn.

iv

LIST OF SYMBOLS

a	amplitude of wave
$\bar{a}$	rms wave amplitude
c	wave celerity
C_D	drag coefficient
$\bar{C}_D$	steady drag coefficient
C_{jk}	restoring force matrix
C_M	inertia (or mass) coefficient
D	cylinder diameter
d	water depth
E	Young's modulus
$\underline{E[\cdot]}$	expected value
F	mean force
f	force per unit length of structure
f_D	drag force per unit length of structure
f_I	inertia force per unit length of structure
f_{max}	maximum force per unit length of structure
g	acceleration due to gravity
H	wave height
H_n	Hermite polynomial of order n
H_{rms}	rms value of wave height
H_S	significant wave height
$\hat{h}$	H / H_{rms}
I	moment of inertia
i	imaginary quantity $(= \sqrt{-1})$
K	ratio of rms drag to rms inertia force
k	wave number $(= \frac{2\pi}{L})$
k_A	$\rho\, C_A\, \frac{\pi}{4}\, D^2$
KC	Keulegan-Carpenter number $(= u_o T / D)$
k_D	$\frac{1}{2} \rho\, C_D\, D$
k_j	cumulants
k_M	$\rho\, C_M\, \frac{\pi}{4}\, D^2$
L	wave length
l	length of mooring line
M_{jk}	added mass matrix
m_{jk}	mass matrix

m_n	nth moment of wave spectral density (n = 0,1,2,...)
N	T_R / T_z ; also, number of wave components
$N(\mu,\sigma^2)$	normal distribution of mean, μ , and standard deviation, σ
N_{jk}^2	linear damping matrix
N_{jk}^1	nonlinear damping matrix
n_x	direction cosine
P(x)	cumulative probability or probability distribution of x
p	dynamic pressure or slope
p(x)	probability density of x
Q	long-term probability of exceedance
q	short-term probability of exceedance or probability density
R	cylinder (structure) radius
Re	Reynolds number $\left(= u_0 D / \upsilon \right)$
R_{xy}	correlation function between functions x(t) and y(t)
r	cosh ky/sinh kd
$S(\omega)$	spectral energy density of wave
$S^*(\omega)$	spectral energy density of wave in current
$S_F(\omega)$	force spectral density
$S_u(\omega)$	spectral energy density of horizontal velocity
T	wave period
T_o	period of cylinder oscillation
T_M	expected time between two successive crests
T_R	record length of time
t	time
U	current velocity
U_W	wind speed
u	horizontal water particle velocity
$\dot{u}$	horizontal water particle acceleration
u_0	amplitude of horizontal velocity
V_R	reduced velocity $\left(= {}^{UT}o /_D \right)$
v	vertical velocity component
v_R	$u - \dot{x}$
v_j	eigenvectors
v_r	relative velocity $\left(= u - \dot{x} \right)$
v(t)	u(t) - U

w	weight per unit length of chain
$\underset{\sim}{w}$	normal velocity vector
X_k	amplitudes of motion
x	coordinate in the horizontal direction
x_k	motion components (k = 1,2,...,6)
y	coordinate in the vertical direction
α	phase angle of force or empirical parameter
α	$\frac{1}{\nu}$ or probability level
β	phase angle of motions or empirical parameter
δ	stretch in mooring line
ϵ	crest front steepness
ϵ	spectral width parameter
$\hat{\epsilon}$	$\epsilon / \epsilon_{rms}$
ζ	incident wave amplitude
η	wave profile or elevation
θ_0	angle of mean wave direction
κ	1 / ln N
λ	vertical asymmetry factor
λ	current strength (U / u_0)
λ_3	skewness
λ_4	kurtosis minus 3
λ_j	eigenvalues
μ	peak rate density
μ	horizontal asymmetry factor
μ_x	mean value of x
ν	kinematic viscosity of water
ρ	correlation coefficient
ρ	mass density of water
σ_x	standard deviation of x
τ	time lag
ν_i	degrees of freedom
ω	wave frequency ($= 2\pi / T$)
ω_0	peak frequency or undamped natural frequency
Φ	velocity potential
$\Phi(u)$	standard normal distribution
$\sim$	vector sign
Γ	gamma function

TABLE 1.1 - TYPES OF OFFSHORE STRUCTURES

```
                    ┌─────────────────────┐
                    │     MARINE AND      │
                    │ OFFSHORE STRUCTURES │
                    └─────────────────────┘
                              │
       ┌──────────────────────┼──────────────────────┐
       │                      │                      │
 ┌───────────┐          ┌───────────┐          ┌───────────┐
 │ FIXED[1,2]│          │FLOATING[2,3]│         │ FLEXIBLE  │
 └───────────┘          └───────────┘          └───────────┘
       │                      │                      │
```

FIXED[1,2]	FLOATING[2,3]	FLEXIBLE
Drilling Jackets Production Platforms Oil Storage Tanks Caissons	Ships Barges Semisubmersibles Buoys TLPs Articulated Buoyant Towers Guyed Towers[4]	Catenary Cables Chains Risers TLP Tendons Marine Hoses
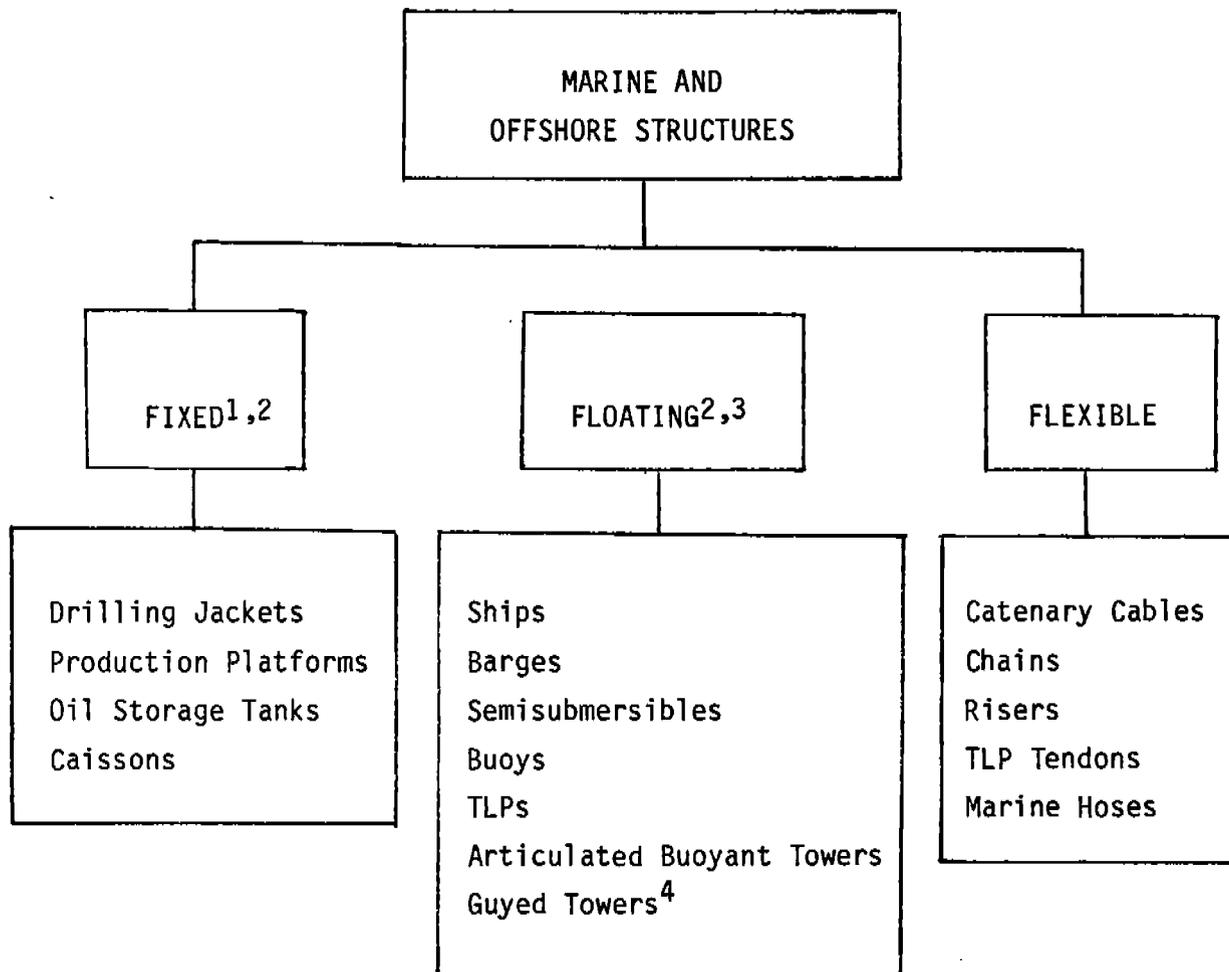
NOTES:

1. Fixed structures may be piled or gravity type.

2. Fixed or floating structures may be rigid or non-rigid. The non-rigid structures will undergo small deflections or displacements under environmental loads.

3. Floating structures are usually moored in place in operational mode.

4. Strictly speaking, guyed towers do not belong to this category; but its analysis is similar to the others in this category.

1.0 INTRODUCTION

The marine and offshore structures and their components may be classified into three broad categories: fixed structures, floating structures and flexible structures. Table 1.1 shows these three classes of structures.

The fixed structures in the open ocean are held in place by their weight or by piling. Generally, jacket type structures consisting of a large number of tubular members in various planes are held in-place by piling. Many such structures may be seen in the Gulf of Mexico. On the other hand, large-volumed production structures made of concrete and steel that exist in the North Sea are gravity-type structures. The weight of these structures provides sufficient bearing pressure to overcome sliding or overturning due to environmental loads, thus fixing their position.

There are two primary types of floating structures. One type is powered to move from one location to another and is used to transport materials across bodies of water. Examples of this type of structures are ships and barges. The other type of floating structures is mechanically connected to the ocean bottom or moored in place for use in offshore operation such as in the production, processing and storing of oil. Such structures may be articulated towers, semisubmersibles, tension leg platforms (TLPs), etc.

Fixed and floating structures may be rigid or non-rigid. Large structural components are considered rigid for the analysis of wave forces and motions. Long members of small cross sections, e.g., in jacket platforms may undergo deflections or displacements which are substantial and should be considered non-rigid. An articulated tower may also experience natural period vibrations in higher vibration modes than the rigid body motion. These members are treated as non-rigid in the response calculation.

The third type of structures, namely, the flexible structures undergo large deformations which must be taken into account when being analyzed. It may be important to update the external forcing function on these structures based on their displaced configuration. Examples of these structures are risers, TLP tendons, catenary lines, hoses, etc.

Because of the nature of these flexible structures, the nonlinearities in the design analyses appear in different phases and are sometimes typical of

1

the structures in question. On the other hand, certain types of nonlinearities are common to most of these structures, depending on the environment experienced by them.

This report discusses the common types of nonlinearities (Chapter 2) encountered in the design of offshore structures. The types of nonlinearities are arranged in the order in which they may enter into the analysis of a structure. Applicability of these nonlinearities to the types of structures included in Table 1.1 is discussed. Examples of the nonlinearities are presented from which the importance of the nonlinear terms may be assessed.

The main thrust of the present report is the extreme value analysis of nonlinear systems relevant to offshore or marine structures. This area is relatively new, but progress in this area in the last several years has been rapid and steady. Because of the complexity of the problem, the extreme value analysis of nonlinear systems makes approximate assumptions in order to make the mathematical problems tractable and fit one of the known extreme value analysis methods. Chapter 3 discusses various probabilistic methods and distribution functions used in predicting short- and long-term extreme response values for an offshore structure. Most of the nonlinear systems which appeared in Chapter 2 are addressed here.

The applicability of the various approximate methods in nonlinear extreme value analysis is discussed in Chapter 4. Some of the assumptions and limitations of these techniques are summarized. Based on this evaluation, consistent methodology applicable to the probabilistic approaches is provided in Chapter 5. As will be clear from the discussions in the earlier chapters, a single methodology may not be appropriate for evaluation of all systems. Therefore, based on certain input parameters depending on the types of nonlinearities, different methodologies and formulations are recommended. Moreover, because of the cost and schedule constraints of this contract, several recommendations are made for possible future work in this area.

2.0 TYPES OF NONLINEARITIES

The nonlinearities enter into an offshore structure analysis at various phases. The first and foremost of these is the environment itself. In describing the environmental conditions that influence the offshore structures, nonlinear theories are often needed. For example, waves are often nonlinear and require a mathematical series expression which depends on various wave parameters (e.g. wave height) in a nonlinear fashion. In describing the effect of the environment on the structure, the external loading may become nonlinear. Examples of such nonlinearities are current load, wind load and wave drag load. The response of the structure resulting from the environmental loads may be nonlinear due to nonlinear damping, for example.

Let us, at this point, explain what is understood about a nonlinear system and how it differs from a linear system.

2.1 DEFINITION OF NONLINEAR SYSTEMS

Consider a nonlinear system. If $y(t)$ is the response at a given time, t, that is single valued and nonlinear due to an excitation $x(t)$ at the same time, t, then

$$y(t) = g[x(t)] \qquad (2.1)$$

where $g(x)$ is a single valued nonlinear function of x. The system $g(x)$ is nonlinear if

$$g(a_1 x_1 + a_2 x_2) \neq a_1 g(x_1) + a_2 g(x_2) \qquad (2.2)$$

where a_1 and a_2 are arbitrary constants. This system is considered a "zero memory" system, meaning that the response of the system does not depend on the past value of the excitation. If the system is a constant parameter nonlinear system and if the excitation $x(t)$ represents a stationary random process, then the response $y(t)$ will also be a stationary random process. In this case, the correlation function of the output, and between input and output are given by

3

$$R_{yy}(\tau) = E[y(t) \; y(t + \tau)] = E[g\{x(t)\} \; g\{x(t + \tau)\}] \qquad (2.3)$$

$$R_{xy}(\tau) = E[x(t) \; y(t + \tau)] = E[g\{x(t)\} \; g\{x(t + \tau)\}] \qquad (2.4)$$

where R refers to the correlation at a time lag, τ, and E refers to the expected value. Examples of zero memory nonlinear systems that are often found in the offshore structure analysis are

- Square-Law System: $y = x^2$
- Cubic System: $y = x^3$
- Square-Law System with Sign: $y = |x|x$

In this section, we shall describe the various types of nonlinearities that are encountered in the marine and offshore structure design. The subjects are introduced in the order mentioned at the beginning of this section. First of all, nonlinearities encountered in describing the environment will be described. Then the external loading from these environments that are nonlinear will be discussed. Finally, the responses from external loadings that are nonlinear will be addressed. It should be noted that the design extreme value analysis should properly account for these nonlinearities.

2.2 NONLINEAR WAVES AND WAVE SIMULATION

In computing the wave loads on the components of an offshore structure, a suitable wave theory must be chosen based on the wave parameters. Numerous water wave theories have been developed which describe the kinematic and dynamic properties of the water particles at or below the free surface of the wave profile. Although the ocean waves are random in nature, the wave theories describe wave profiles that are regular and periodic in nature. There are three basic parameters that are used in describing all wave theories: water depth, wave height and wave period.

The linearity of waves is determined by the wave height or the wave slope. The simplest and most commonly used wave theory is known as Airy theory which is linear with the wave height (hence, also called the linear theory). Because of the linearity of the Airy theory with the wave height,

4

the structural response obtained using this theory is often quite straight-forward, even though not necessarily linear. This is the theory that is almost exclusively used in the extreme value analysis of responses, and forms the basis for the latter chapters.

The free surface boundary conditions are linearized in describing the linear Airy wave theory. Therefore, it is not possible to accurately predict the statistical and spectral properties of particle kinematics in the free surface zone. Anastasiou, et al. (1982) derived the probability density function of particle kinematics in the free surface region, which is correct up to the second order. The wave loads in the free surface zone on a vertical cylinder were computed to demonstrate the nonlinear properties of the particle kinematics.

However, in many physical situations the linear theory is not adequate to accurately describe waves. In this case one has to resort to other theories to match or at least approach the physical data. Besides the linear theory, other commonly used nonlinear theories in the design of offshore structures are (1) Stokes higher order theory [Skelbreia and Hendricksen (1960)], (2) cnoidal theory [Weigel (1960)] and (3) stream function theory [Dean (1965), (1970)].

To offer an example of the differences among theories, Airy linear theory provides an expression for the horizontal water particle velocity as

$$u = \frac{\pi H}{T} \frac{\cosh ky}{\sinh kd} \cos (kx - \omega t) \qquad (2.5)$$

whereas Stokes second order nonlinear theory expresses the same parameter as

$$u = \frac{\pi H}{T} \frac{\cosh ky}{\sinh kd} \cos (kx - \omega t) + \frac{3}{4c} \left(\frac{\pi H}{T} \right)^2 \frac{\cosh 2ky}{\sinh^4 kd} \cos 2(kx - \omega t) \qquad (2.6)$$

where H = wave height, T = wave period, d = water depth, y = vertical coordinate of particle, k = wave number (= $2\pi/L$, L = wave length), x = horizontal coordinate of particle, ω = wave frequency, c = wave celerity, and t = time. The first term on the right hand side of Eq. 2.6 corresponds to the first order theory and is linear with the wave height. However, the second term is proportional to the square of the wave height (or wave slope).

Similarly, the horizontal water particle velocity of an Nth order stream

function theory is given in a series form with terms up to N as follows:

$$u = - \sum_{n=1}^{N} nk \cosh (2n-1)ky [X(2n-1) \cos(2n-1)kx + X(2n) \sin(2n)kx] \qquad (2.7)$$

in which X(n) are the coefficients of the stream function. The statistical distribution properties of nonlinear waves have received some attention in recent years which have been discussed in Chapter 3.

The applicability of the wave theories may be described by two nondimensional parameters, d/gT^2 and H/gT^2 based on the three basic wave parameters, d, H and T. This is described by the regions shown in Fig. 2.1. The limits of validity of the various theories are based on how well the free surface boundary conditions are satisfied, although there has been limited experimental verification. For this reason, in using this chart, one need not strictly adhere to the boundary lines in selecting a theory. In fact, the linear theory has been shown to work quite well in predicting structure responses well beyond its analytic limitations.

These wave theories are used in computing the response function of an offshore structure. High order deterministic wave theories are used extensively in the design of offshore structures despite their inability to model the randomness of a wind generated sea. The extreme values of responses (linear and nonlinear) are predicted invariably in linear random waves. For a linear system this procedure is straight-forward with the use of a wave energy spectrum model as will be described in the next chapter. For a nonlinear response function, the solutions are often obtained in the time domain. This requires the simulation of a time series from the energy spectrum model.

The random waves in the ocean cannot be described by a theoretical model. They are generally described by their energy density spectrum. Often a mathematical formula is used to describe the energy density spectrum of an ocean wave. A commonly used form is the Pierson-Moskowitz spectrum given by

$$S(\omega) = \frac{5}{16} H_s^2 \frac{\omega^{-5}}{\omega_0^{-4}} \exp [-1.25 (\omega/\omega_0)^{-4}] \qquad (2.8)$$

in which $S(\omega)$ is one-sided (i.e. $0 < \omega < \infty$) energy spectral density, H_s = significant wave height and ω_0 = peak frequency corresponding to the energy spectral peak.
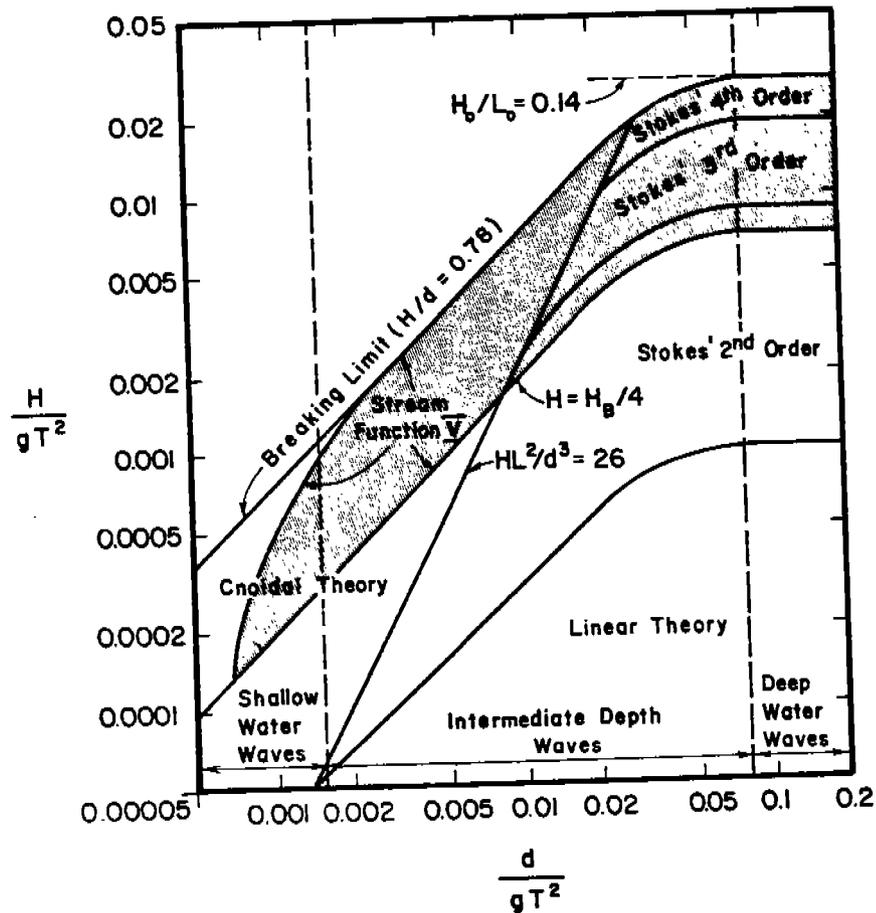
FIGURE 2.1 REGIONS OF VALIDITY FOR VARIOUS WAVE THEORIES [AFTER LEMÉHAUTÉ (1976)]

While the above form of the energy density spectrum may be used as a modified two parameter spectrum having H_s and ω_0 as independent parameters, the P-M spectrum is a one-parameter spectrum of a fully-developed sea in which H_s is related to ω_0 by the relationship

$$\frac{\omega_0^2 H_s}{g} = 0.161 \qquad (2.9)$$

Thus, given a significant wave height, the peak frequency can be determined and vise versa. Recently, Buckley (1986) analyzed ocean wave data obtained from measurements at a platform in the Gulf of Mexico, NOAA data buoys, Navy SOWM data and data from Canadian and Great Lakes waters. Based on the significant wave height and peak period of this set of data, an empirical boundary describing the limiting steepness was obtained as

$$\frac{\omega_0^2 H_s}{g} = 0.306 \qquad (2.10)$$

which is about twice that prescribed by the P-M spectrum.

For a frequency domain analysis, these spectrum formulas (e.g., Eq. 2.8) are used directly. A wave profile is simulated from such a spectrum for a time domain analysis. One of the straight forward methods of simulation of the time series is the linear superposition method of dividing the energy density spectrum into several slices of width, $\Delta\omega$. Then the wave height representing the energy under these slices is given by the formula

$$H_i(\omega_i) = 2 \sqrt{2S(\omega_i)\,\Delta\omega} \qquad (2.11)$$

where ω_i corresponds to the central frequency of the slice. The corresponding period is given by

$$T_i = \frac{2\pi}{\omega_i} \qquad (2.12)$$

This, then, gives the component of the wave representing the frequency interval, i, given by the wave height - period pair, (H_i, T_i). The phase angle is assumed uniformly distributed over $(0, 2\pi)$ and is chosen randomly. Then the profile of the random wave is obtained by adding all the components of the wave thus generated

7

$$\eta(x,t) = \sum_{i=1}^{N} \frac{H_i}{2} \cos(k_i x - \omega_i t + \psi_i) \qquad (2.13)$$

where $k_i = 2\pi/L_i$, L_i = wave length at a frequency ω_i and N = number of slices made in the wave spectrum (typically 50-200).

The random wave profile produced by this method is Gaussian only in the limit as N extends to infinity. In order to avoid this problem [Tucker, et al. (1984)], Eq. 2.13 may be rewritten in terms of two coefficients, a_i, b_i (instead of ψ_i) which are functions of the cosine and sine component of ($k_i x - \omega_i t$). These coefficients are then assumed to be randomly distributed in a Gaussian form to ensure η to be Gaussian. It has been shown [Elgar, et al., (1985)] that the group statistics of the wave profiles by either of the two methods produce similar results.

In a deterministic approach the maximum wave cycle in a random wave field is often used to obtain the design response value. Such cycles are generally highly nonlinear with sharper crests and require higher order wave theory (e.g. stream function theory) to describe the wave cycle.

A method of simulation of nonlinear random seas was provided by Hudspeth (1975). The method involves inverting the Fourier wave amplitude spectral components by a Fast Fourier algorithm. Second order corrections are made to the linear random sea surface. These nonlinear components appear at frequencies that are sums or differences of the linear frequencies and include the product of the linear spectral components. The nonlinear random sea surface is derived from a linear simulation. The kinematic field, i.e. water particle velocity and acceleration are obtained by a digital linear filtering technique.

2.3 WAVES PLUS CURRENT

When current is present along with the waves, the current is often considered steady and its effect is linearly superimposed on the effect of the waves on responses. It is sometimes found that the combined effect of waves and current on the responses may be different from their individual effects linearly superimposed because of wave-current interaction. This is particularly true for a moving structure for which the motion may become quite complex and nonlinear even for linear waves. In addition, however, when

current is in the direction of waves there are additional changes experienced by the waves.

On encountering a current, the characteristics of a wave change. In particular, in the presence of current the wave height and the wave length experience modification. If the current is in the direction of wave propagation, the wave slope decreases and its length increases. On the other hand, if the current opposes the wave, the wave slope increases in magnitude and the wave length shortens. These changes take place due to the interaction between the waves and current.

In deepwater in the presence of a uniform current the wave number, k, is related to the wave frequency, ω, by the generalized dispersion relationship

$$k = \frac{4\omega^2/g}{[1 + (1 + 4U\omega/g)^{1/2}]^2} \qquad (2.14)$$

where U may be positive (in the direction of wave propagation) or negative (opposite to the wave direction). Note that the expression in Eq. 2.12 reduces to the deepwater dispersion relation ($k = \omega^2/g$) in the absence of current ($U = 0$). When U is positive the value of k is smaller so that the wave length is larger. Likewise when U is negative, the value of k increases and the wave length is smaller than the no-current case.

The wave-current interactions in a random wave field show that the wave energy density spectrum likewise undergoes profound changes. Under the action of a steady current in deepwater, the wave energy spectrum takes the form

$$S^*(\omega) = \frac{4\,S(\omega)}{(1 + \frac{4U\omega}{g})^{1/2}\,[1 + (1 + \frac{4U\omega}{g})^{1/2}]^2} \qquad (2.15)$$

When the current speed is negative there is a cut-off frequency in the surface wave spectrum given by the condition $1 + 4U\omega/g = 0$ beyond which no waves exist. Since the phase speed, c ($= \omega/k$), of gravity waves is a monotonically decreasing function of wave number and frequency, the influence of current will be predominant at the higher wave number range. Furthermore, the contribution from the higher wave number range dominates the wave surface slope whereas the current changes the surface slope pattern drastically. This is demonstrated in Fig. 2.2 in which the ratio of $S^*(\omega)/S(\omega)$ is plotted versus ω for different values of steady current with and against the wave

9
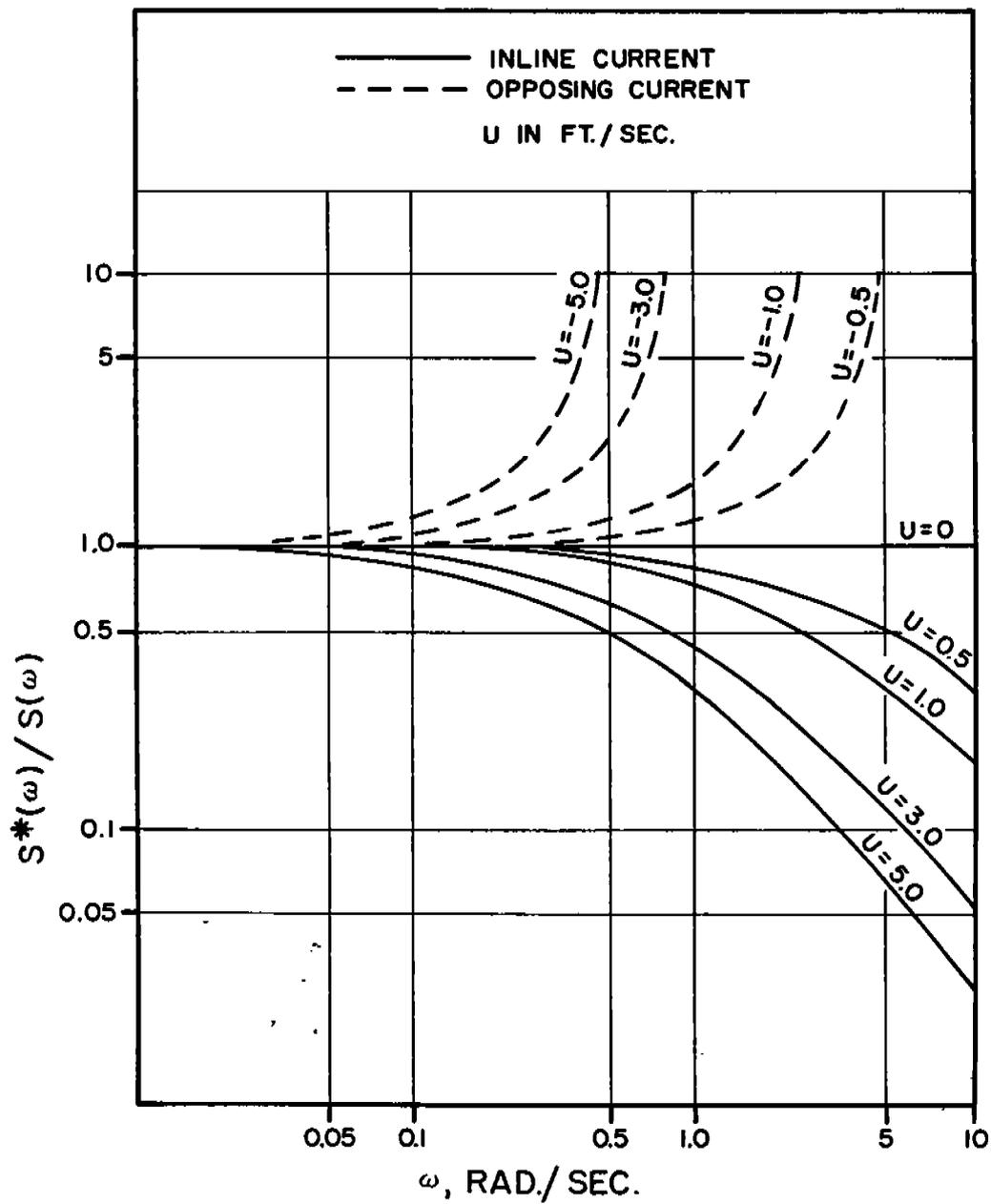
FIGURE 2.2

RATIO OF ENERGY SPECTRA WITH AND WITHOUT CURRENT UNDER
DIFFERENT CURRENT CONDITIONS ; U IN M/SEC [HUANG ET AL. (1972)]
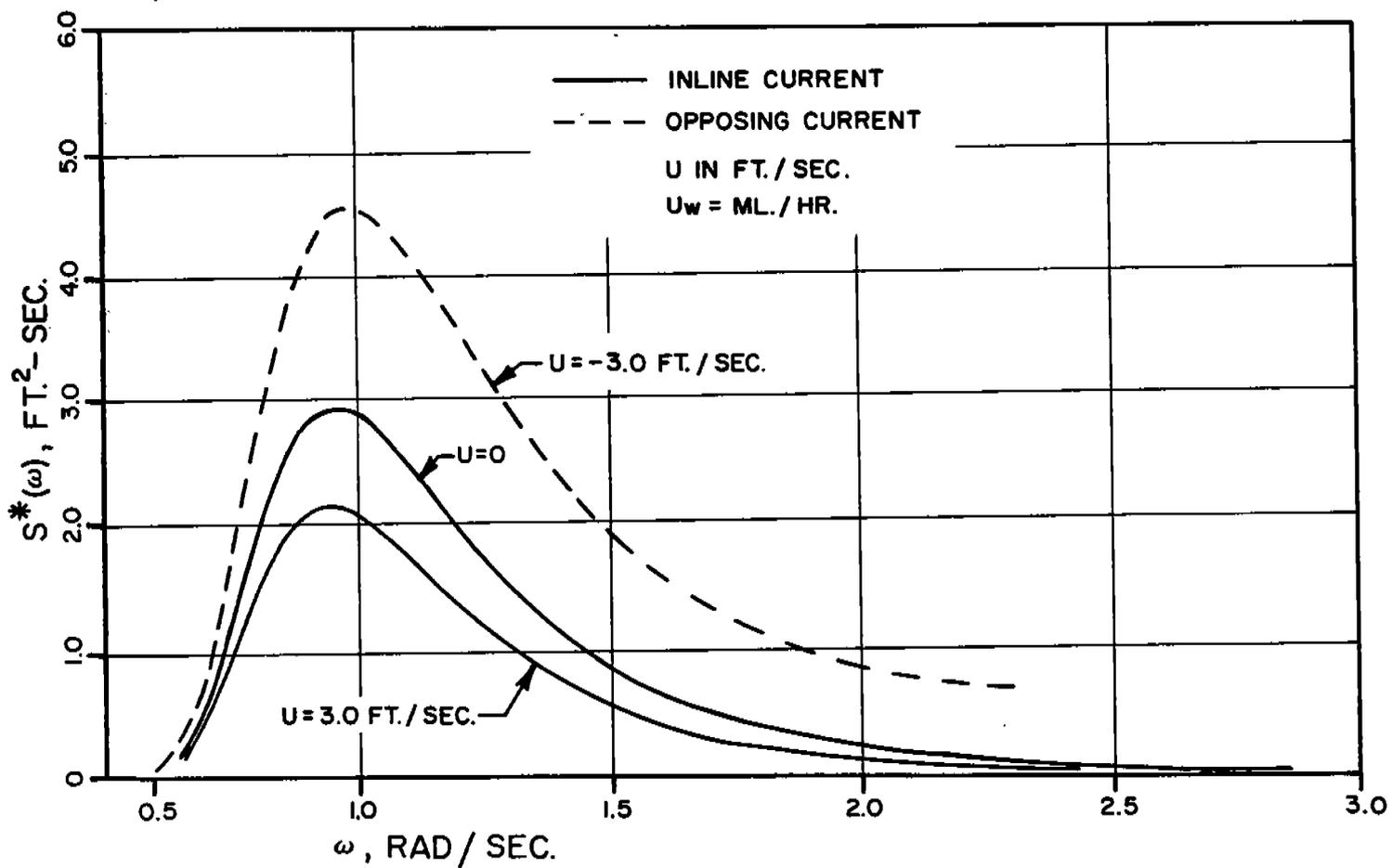
FIGURE 2.3

SURFACE WAVE ENERGY SPECTRA UNDER DIFFERENT CURRENT CONDITIONS

[TUNG AND HUANG (1972)]

direction. It is seen that the effect of current at the low frequency is small. At higher frequencies the effect of current increases energy level when it opposes waves and decreases when it is with the waves. This is further illustrated in Fig. 2.3 where $S^*(\omega)$ is shown versus ω. The wave energy density spectrum, $S(\omega)$ represents a P-M spectrum for a wind speed of U_w = 20 miles/hr. The spectra of fluid particle velocity and acceleration at mean water level are given by

$$S_u^*(\omega) = \omega^2 \, S^*(\omega) \qquad\qquad (2.16)$$

and

$$S_{\dot{u}}^*(\omega) = \omega^4 \, S^*(\omega) \qquad\qquad (2.17)$$

Figure 2.4 shows the effect of wave current interaction on the water particle velocity spectrum, $S^*_u(\omega)$ for different current speeds of $U = \pm 3$ ft/sec. Spectra of water particle acceleration exhibit similar characteristics.

2.4 NONLINEAR FORCE

It is clear from the previous sections that nonlinear waves will produce nonlinear responses even if the transfer mechanism is linear. On the other hand, for a linear wave the responses are nonlinear if the transfer function is nonlinear. Thus the responses of a marine structure will be nonlinear if the exciting forces arising from (linear) waves are nonlinear. One of the most common types of dynamic nonlinearity encountered in the exciting forces is due to the drag force. The nonlinear steady drag force due to wind and current is well-known. Extending this form to the case of waves, adding the inertia component and taking into account of the reversal of force in a wave cycle, an empirical formula was proposed about 25 years ago which is commonly known as the Morison equation.

2.4.1 Morison Equation

The Morison equation was developed by Morison, et. al. (1950) for describing the horizontal forces on a vertical pile. It is written in terms of the water particle velocity and acceleration components as

$$f = k_M \, \dot{u} + k_D |u| u \qquad\qquad (2.18)$$
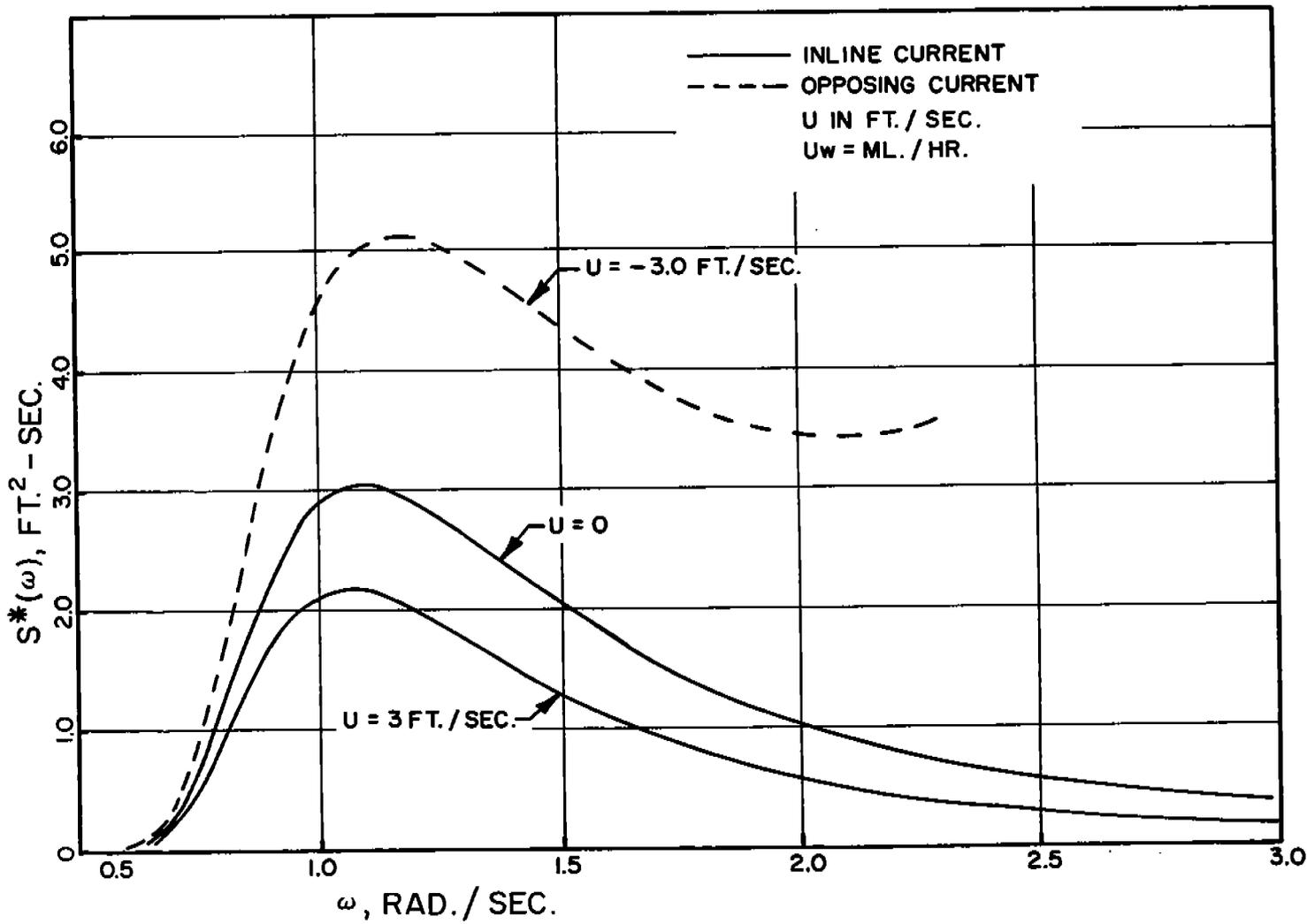
FIGURE 2.4

VELOCITY SPECTRA UNDER DIFFERENT CURRENT CONDITIONS

[TUNG AND HUANG (1972)]
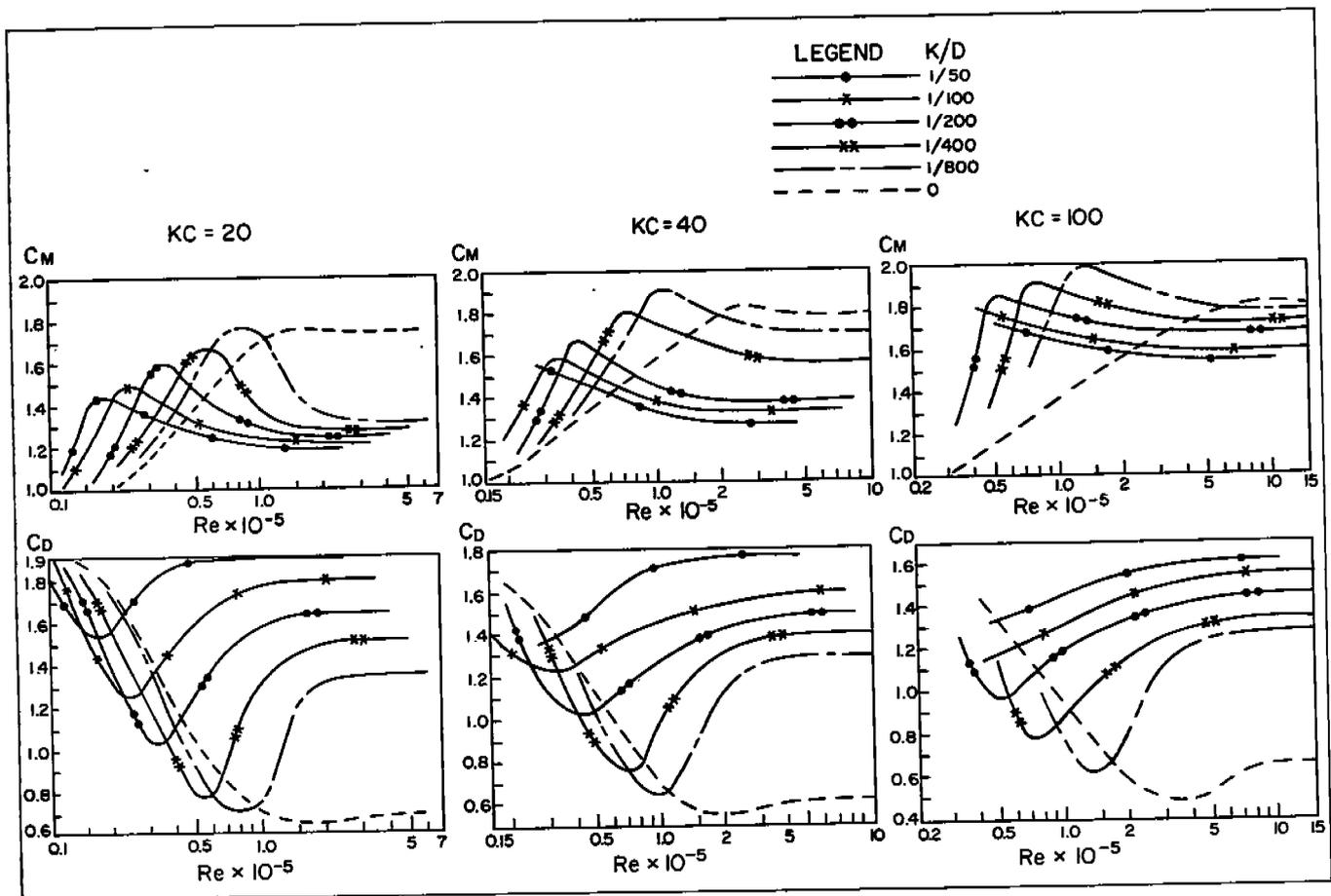
FIGURE 2.5 VALUES OF C_M AND C_D AS FUNCTION OF Re, KC AND ROUGHNESS
COEFFICIENT (K/D) [FROM SARPKAYA ET AL. (1976)]

in which

$$k_M = \rho \, C_M \, \frac{\pi}{4} \, D^2 \qquad\qquad (2.19)$$

and

$$k_D = \frac{1}{2} \, \rho \, C_D \, D \qquad\qquad (2.20)$$

and f = hydrodynamic force per unit length of the vertical cylinder, ρ = mass density of water, D = cylinder diameter, u and $\dot{u}$ = water particle velocity and acceleration, and C_M, C_D = inertia and drag force coefficients respectively.

This empirical force model has been the most widely used method in determining forces on small diameter vertical cylindrical members in an offshore structure. The computation depends on a knowledge of the water particle kinematics and empirically determined coefficients. Extensive research effort has been expended in the past in obtaining the values of the force coefficients, C_M and C_D. In this area, the most noteworthy laboratory results on C_M and C_D were produced by Sarpkaya [see Sarpkaya and Isaacson (1981)] from his U-tube experiments. His data show that these coefficients are functions of the Keulegan-Carpenter number (KC), Reynolds number (Re) and roughness parameter of the cylinder. The Keulegan-Carpenter number is a measure of the water particle orbital amplitude with respect to the cylinder diameter and is defined as KC = $u_0 T/D$ where u_0 is the amplitude of the water particle velocity. Typical results for C_M and C_D from Sarpkaya's experiments for different values of KC are shown in Fig. 2.5. His analysis shows that for smooth cylinders, the value of C_D approaches 0.65 and C_M approaches 1.8 at higher values of Re. In waves, these values from pure 2-D oscillatory flow should probably be considered an upper limit. Limited correlation of these data in waves has been made. One such correlation in a limited range of Re was made by Chakrabarti (1981) in Fig. 2.6. Note that the correlation is quite good except for C_M near KC = 10 and at higher values of KC where Chakrabarti's data are sparse and need further verification.

The Morison equation has been used in the application of both regular waves and random waves. In a design, the coefficients in the random waves are often chosen from the regular wave tests and assumed constant with
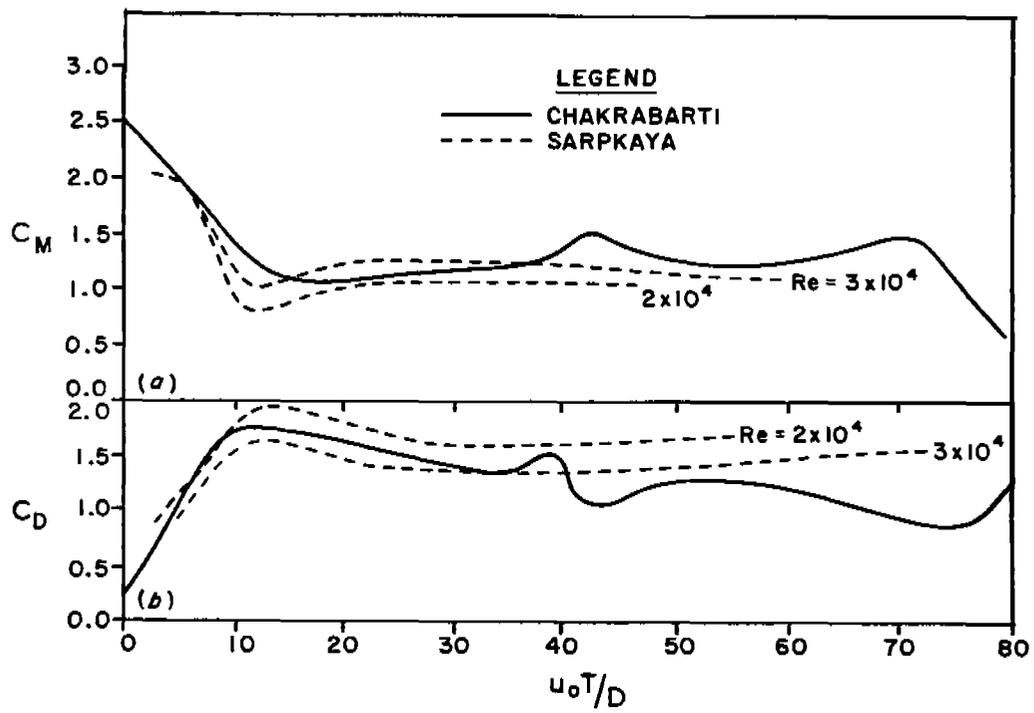
FIGURE 2.6 COMPARISON OF SARPKAYA'S TWO-DIMENSIONAL FLOW TEST RESULTS WITH
WAVE TANK TEST RESULTS
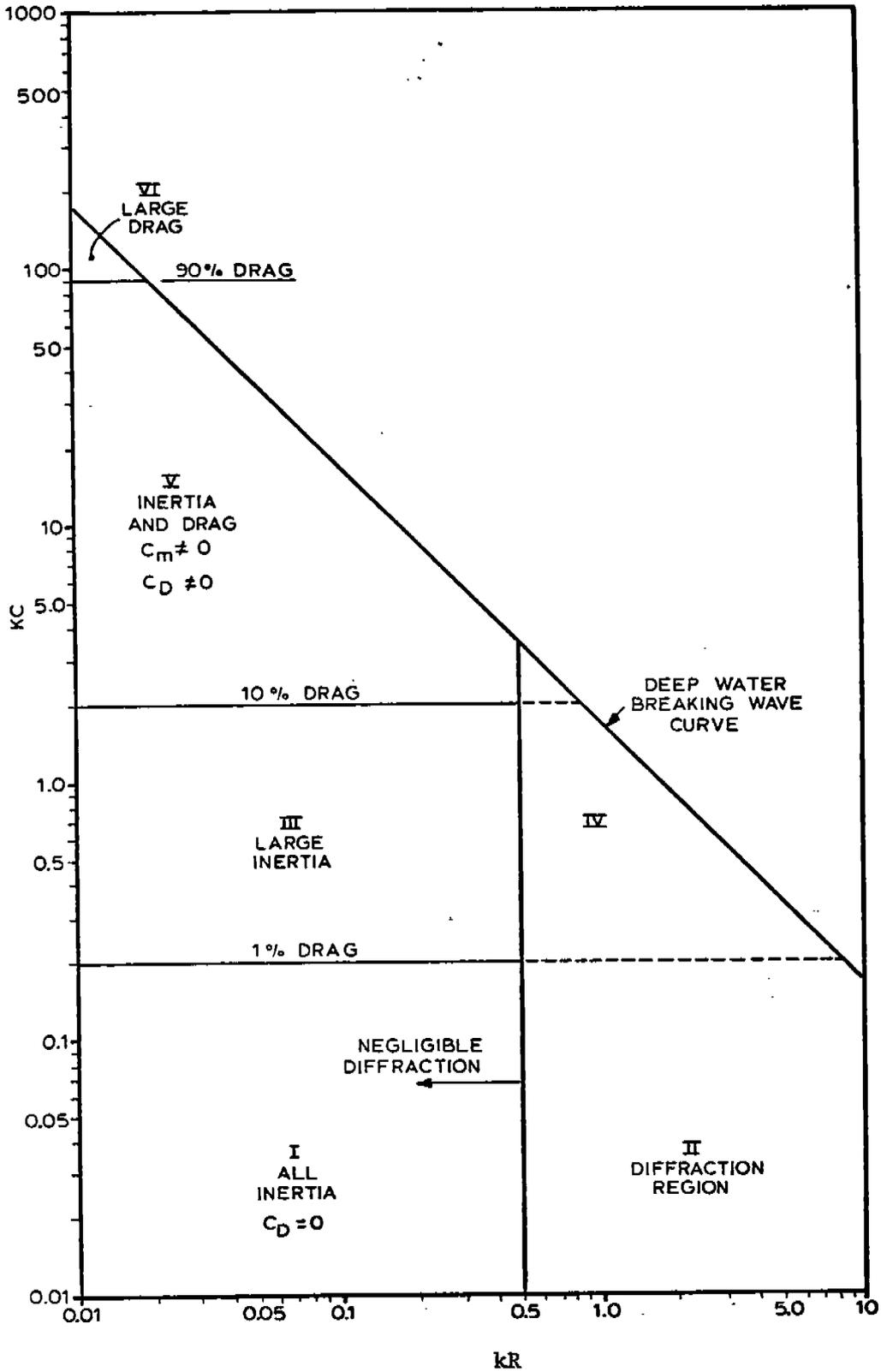
FIGURE 2.7   REGIONS OF APPLICATION OF WAVE FORCE FORMULAS

frequency. The coefficients have generally been derived in the laboratory in oscillating motion or in regular waves. The data from ocean tests have produced large scatter which does not validate the applicability of the Morison equation. In a test with a vertical cylinder in a wave tank, Vugts and Bouquet (1985) measured the forces and corresponding water particle kinematics at a small section of the cylinder in random waves. Then they considered these signals as output and input signals respectively, and applied the measurements to a general transformation model consisting of linear and nonlinear paths. They chose four models, one of which corresponded to the Morison equation. The Morison equation was found to be the best suited, giving a good match between the two signals. The inertia coefficient was found to be reasonably constant for a given frequency spectra while the drag coefficient decreased in value with frequency.

The Morison equation has been extended to inclined cylindrical members of an offshore structure in terms of a normal velocity component, $\underset{\sim}{w}$, and a normal acceleration component, $\underset{\sim}{\dot{w}}$. In this case, the force is written as a vector quantity

$$\underset{\sim}{f} = k_M \underset{\sim}{\dot{w}} + k_D |\underset{\sim}{w}| \underset{\sim}{w} \tag{2.21}$$

The force vector per unit length of cylinder may be decomposed into its three components along 3 axes XYZ by writing

$$\underset{\sim}{w} = u_x \underset{\sim}{i} + u_y \underset{\sim}{j} + u_z \underset{\sim}{k} \tag{2.22}$$

and

$$\underset{\sim}{\dot{w}} = \dot{u}_x \underset{\sim}{i} + \dot{u}_y \underset{\sim}{j} + \dot{u}_z \underset{\sim}{k} \tag{2.23}$$

It has been shown through experiments [Sarpkaya (1984), Garrison (1985)] that the coefficients C_M and C_D for an inclined cylinder may be obtained as those values from the vertical cylinder tests.

The expression for the inclined cylinder, Eq. 2.21, is general enough that the forces on a small cylinder in any plane may be obtained from it. This formula is applicable to derive forces from various types of offshore

structures and structure components. Some of these are jacket structure, risers, tendons, articulated tower, legs of semisubmersible and guyed tower. It should be noted, however, that the applicability of Eq. 2.21 to a randomly oriented cylinder needs further investigation.

The regions of applicability of the Morison equation and, in particular, the areas of drag and inertia force predominance may be discussed in terms of the chart in Fig. 2.7. The chart has been obtained by examining the ratio of the maximum drag force, f_{D_0}, to the maximum inertia force, f_{I_0}, for a cylinder in linear waves. Note that

$$\frac{f_{D_0}}{f_{I_0}} = \frac{C_D}{\pi^2 C_M} (KC) \qquad (2.24)$$

where KC is the Keulegan-Carpenter number. Assuming $C_D = 1$ and $C_M = 2$, the percentage of drag to inertia may be established. The limits are stated in terms of the KC number, and the diffraction parameter, $kR = \pi D/L$, R = cylinder radius. According to this chart the nonlinear force due to the drag effect tends to become important when KC becomes greater than 2. The wave force from the Morison equation becomes mostly drag for KC > 90.

By virtue of the form of the drag term, the drag force component is nonlinear in the time series even if the water particle velocity is sinusoidal. On the other hand, the inertia term is linear if the sinusoidal water particle velocity (e.g. by linear wave theory) is used for the (local) acceleration. If the local horizontal acceleration is replaced by the total horizontal acceleration including convective terms, the inertia term has a nonlinear form.

$$\frac{Du}{Dt} = \frac{\partial u}{\partial t} + u \frac{\partial u}{\partial x} + v \frac{\partial u}{\partial y} + w \frac{\partial u}{\partial z} \qquad (2.25)$$

in which u, v and w are the components of the water particle velocity vector in a rectangular Cartesian coordinate system. Wave force data reduced on the basis of nonlinear (irregular) stream function theory dependent on the measured wave profile and local measured forces have shown satisfactory correlation with measured total forces [Chakrabarti (1980)].

In addition to the extensions of the Morison equation stated above, several modified forms of the formula are used in the offshore structure

13

design. These have to do with combining different environmental effects into the formula. The two most important of these are current and structure motion. Current can be applicable to all three types of structures while the structure motion is important only for a floating or flexible structure.

2.4.2 Fixed Cylinder in Waves and Current

When current is present with waves, the formula for a fixed structure is written in terms of the total velocity including a steady current, U, and an oscillatory component, u as

$$f = k_M \dot{u} + k_D |u \pm U| (u \pm U) \tag{2.26}$$

where -U represents uniform current opposing the direction of wave propagation.

However, it is sometimes argued that a single drag coefficient does not adequately express the total drag force in the presence of waves and current. An alternate form of the Morison equation has been suggested

$$f = k_M \dot{u} + k_D |u|u + \overline{k}_D U^2 \tag{2.27}$$

where $\overline{k}_D$ is defined in terms of a steady drag coefficient, $\overline{C}_D$ as

$$\overline{k}_D = \frac{1}{2} \rho \overline{C}_D D \tag{2.28}$$

The Keulegan-Carpenter number and the Reynolds number in a wave-current field are defined as

$$KC = \frac{(u_0 \pm U)T}{D} \tag{2.29}$$

$$Re = \frac{(u_0 \pm U) D}{\nu} \tag{2.30}$$

where u_0 = amplitude of u and ν = kinematic viscosity of water.

It should be emphasized that the values of the hydrodynamic coefficients in the wave-current field are expected to be different from those in waves alone. Unfortunately, such data are limited. Iwagaki, et al. (1983)

14

presented values of C_M, C_D versus KC from a combined wave-current test. These values shown in Fig. 2.8 are not much different from the wave alone data.

Because of the difficulty of generating waves on a steady current an alternative and often considered equivalent approach is taken. Sarpkaya et al. (1984) had adopted one such method in his U-tube in which the cylinder was moved steadily in an oscillating flow field. They used the relative velocity model (Eq. 2.26) to derive C_M and C_D. Results obtained from such a test on C_M and C_D are shown in Figs. 2.9-2.10. Reference may be made to Sarpkaya's (1984) paper for other similar data.

Moe and Verley (1980) took a slightly different approach. They oscillated a horizontal cylinder sinusoidally in a uniform current field and measured forces on the cylinder. They used the three-term Morison equation, similar to Eq. 2.27, with the exception that u is replaced by $\dot{x}$, $\dot{u}$ by $\ddot{x}$ and k_M by k_A, where x is the amplitude of the oscillating cylinder and $k_A = \rho C_A \pi D^2/4.$. The coefficient, C_A, is defined as the added mass coefficient for the oscillating cylinder and is related to C_M by $C_M = 1 + C_A$ for a buoyant cylinder. They derived the values of $\overline{C_D}$,and Fourier averaged C_A and C_D. The coefficients C_A and C_D showed complex dependencies on the amplitude parameter $\hat{x} = x_0/D$ and the reduced velocity,

$$V_R = UT_0/D \tag{2.31}$$

where T_0 = period of cylinder oscillation. The plot of $\overline{C_D}$ vs. $\hat{x}$ for various values of V_R is shown in Fig. 2.11.

From the above tests it is obvious that the values of the hydrodynamic coefficients are directly related to the form of the force equation used, e.g., independent flow field or relative velocity model. The advantage of the three-term Morison equation is that the steady drag force may be easily separated from the oscillating part, e.g., in the analysis of a structural dynamic problem. However, it seems simpler to use the relative velocity model since it means choosing and working with one less coefficient.

2.4.3 Oscillating Cylinder in Waves

When a rigid structure is free to move in waves, the effect of the structure motion can be combined with the wave effects to form

15
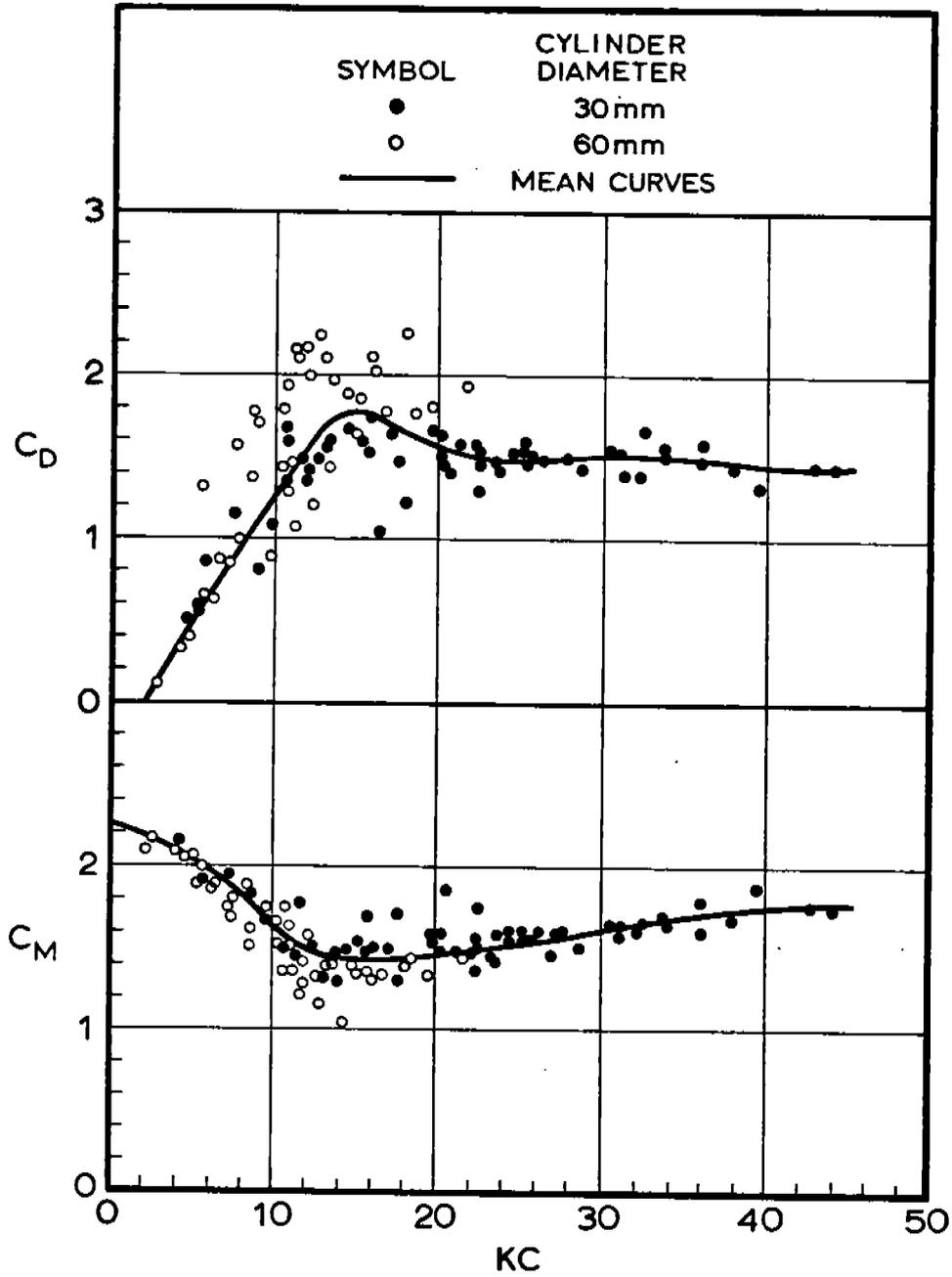
FIGURE 2.8 INERTIA AND DRAG COEFFICIENTS OF FIXED VERTICAL CYLINDER IN A
COMBINED WAVE-CURRENT FIELD [IWAGAKI, ET AL. (1983)]
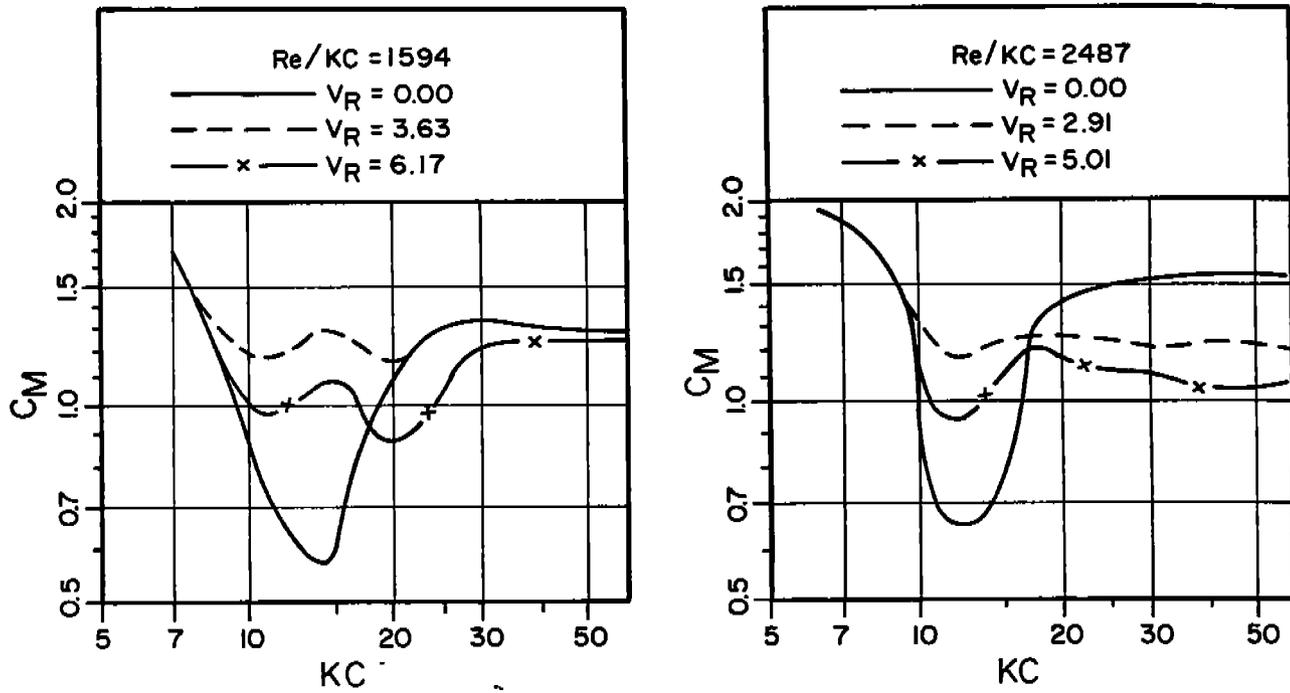
FIGURE 2.9   INERTIA   COEFFICIENT   FOR   A   SMOOTH   OSCILLATING   CYLINDER   IN
UNIFORM COLLINEAR CURRENT (A) Re/KC = 1594 AND (B) Re/KC = 2487
[SARPKAYA ET AL. (1984)]
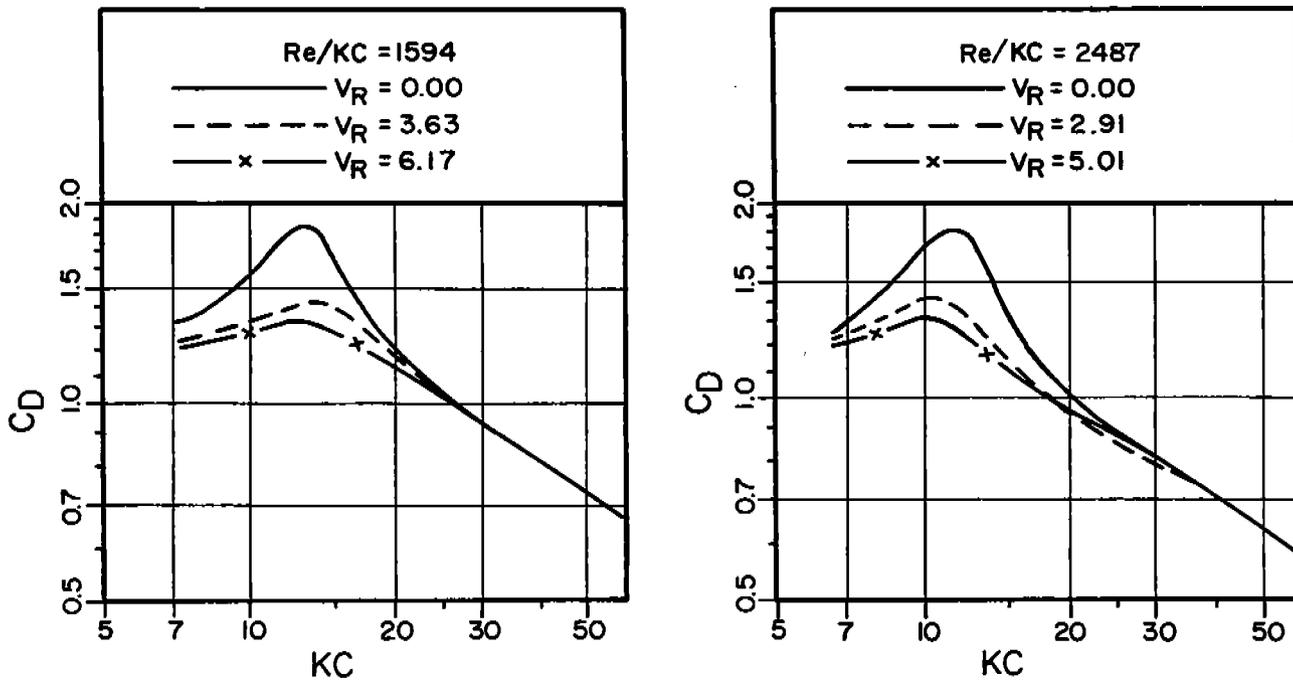
FIGURE 2.10   DRAG COEFFICIENT FOR A SMOOTH OSCILLATING CYLINDER IN UNIFORM
COLLINEAR CURRENT FOR (A) Re/KC = 1594 AND (B) Re/KC = 2487
[SARPKAYA ET AL. (1984)]
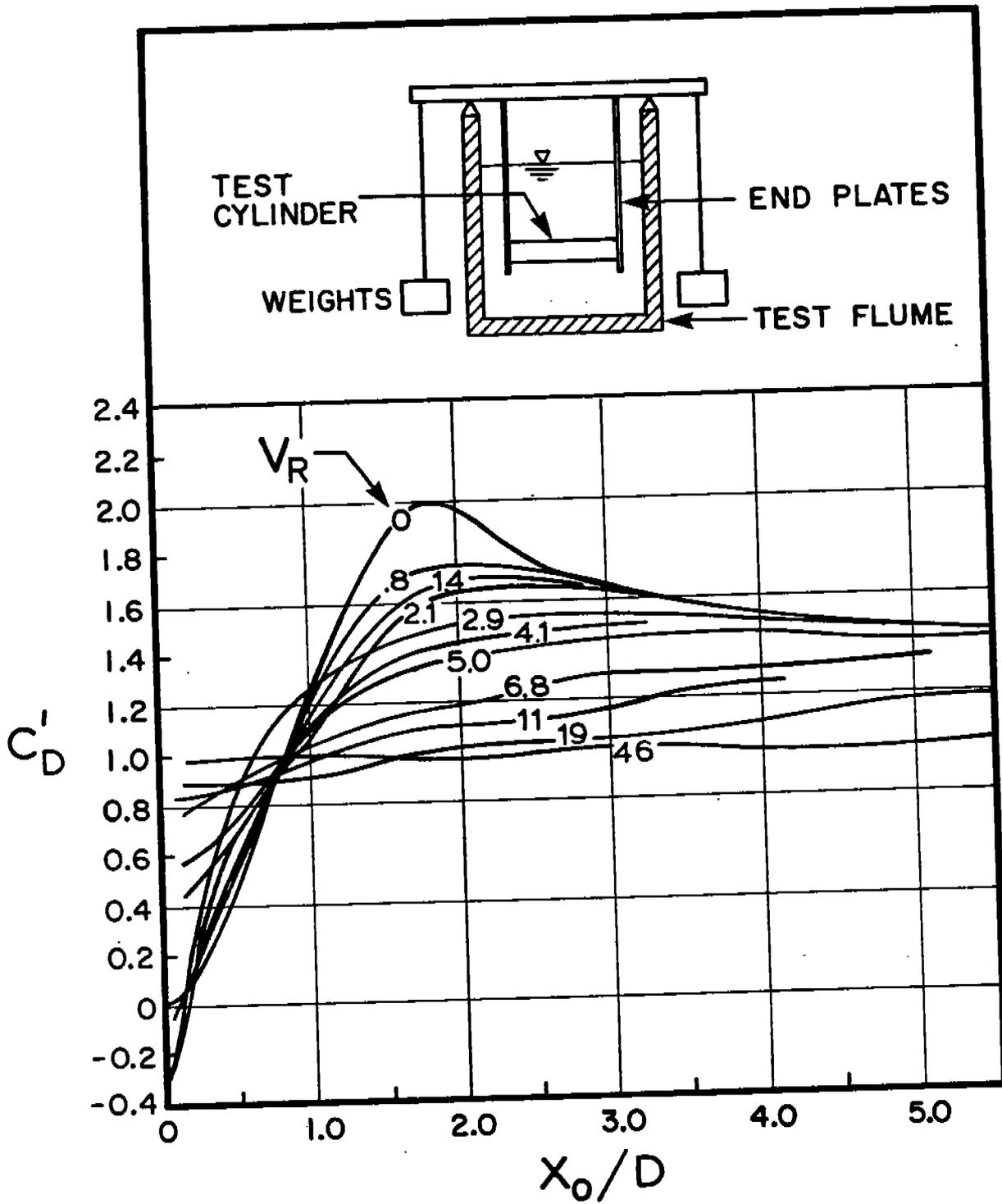
FIGURE 2.11 OSCILLATORY DRAG COEFFICIENT FOR A SINUSOIDALLY OSCILLATING
CYLINDER IN UNIFORM COLLINEAR CURRENT [MOE AND VERLEY (1980)]

$$f = k_M \ddot{u} - k_A \ddot{x} + k_D|u|u - k_D'|\dot{x}|\dot{x} \qquad (2.32)$$

where $k_A = \rho C_A \pi D^2/4$, $k_D' = \frac{1}{2} \rho C_D' D$, C_A = added mass coefficient and C_D' = drag coefficient due to structure motion defined separately from the fluid dynamic drag. This form is known as the independent flow fields; a far field due to the wave motion and relatively unaffected by the structure motion, and a near field resulting from the structure motion. The values of C_M and C_D may be obtained from wave experiments while the coefficients C_A and C_D' are derived from the experiments of an oscillating cylinder in otherwise calm water. The values of the KC and Re numbers are obtained from the respective velocities and periods.

When the forces are written in terms of the relative motion, single coefficients for the inertia and drag are assumed to apply. Thus, the form of the force term including the structure inertia due to its acceleration, ($m\ddot{x}$ term) is

$$f = k_M (\dot{u} - \ddot{x}) + k_D|u - \dot{x}|(u - \dot{x}) \qquad (2.33)$$

This model is known as the relative velocity model. It requires fewer coefficients than Eq. 2.32, and has been used extensively in the past, e.g., to evaluate the stochastic dynamic response of offshore platforms, motions of articulated towers, etc. In this case, the Reynolds number and KC number are defined in terms of the relative velocity, v_r, as

$$KC = \frac{v_{r0} T_r}{D} \qquad\qquad Re = \frac{v_{r0} D}{\nu} \qquad (2.34)$$

where v_{r0} = amplitude of v_r and T_r = combined period of v_r. Note that v_r need not be sinusoidal even if u and $\dot{x}$ are.

It is sometimes convenient to separate the inertia coefficient from the added mass coefficient. As an example, the diffraction-radiation theory provides different values for the force and added mass coefficients. Therefore, a third alternative form of the modified Morison equation is written in terms of the relative velocity, and the acceleration terms are separated.

$$f = k_M \, \ddot{u} - k_A \, \ddot{x} + k_D |u - \dot{x}|(u - \dot{x}) \qquad (2.35)$$

The question arises as to which is the more appropriate form of the modified Morison equation for a structure moving in waves. Since there is a variety of offshore structures, e.g., jacket platforms, articulated columns, risers, tension leg platforms, that fall under this category in which the drag effect is important, it is worthwhile to discuss the appropriate and useful applications of Eqs. 2.32, 2.33 and 2.35. Because the original Morison equation is empirical, it is not possible to justify its extension to other cases and to discuss which one is more "correct". Obviously, coefficients derived from one of these formulations can be justifiably used in the application of that form only. However, experimental data in this area is scarce. An attempt to investigate this area was made by Chakrabarti et al. (1983-1984) through model testing. An articulated column was tested in three modes with the same setup: (1) fixed in waves, (2) harmonically oscillated in still water, and (3) free to move in the plane of the waves. The amplitude of velocity of the structure was comparable to the water particle velocity. The test showed that the relative velocity form of the Morison equation is appropriate, even though the observations were limited. Considerable work is needed to determine the appropriate values of C_M and C_D in the relative velocity model in waves.

An experiment with a submerged articulated tower was performed recently by Dahong, et al. (1982) in which the motions of the tower both in-line and transverse to the direction of waves were measured. From these measurements the values of C_M, C_D from a relative velocity model (Eq. 2.33) and lift coefficient, C_L, were derived. The mean values of these coefficients versus KC are presented in Fig. 2.12.

The region of applicability of the relative velocity and independent flow fields model may be discussed in terms of reduced velocity, V_R (defined by u_0 instead of U in Eq. 2.31) and an amplitude parameter, $\hat{x}$. The limits of applicability are given in Fig. 2.13. The x-axis is the reduced velocity, V_R while the y-axis is the KC number based on the water particle velocity.

For compliant structures, e.g. articulated towers, KC, V_R and $\hat{x}$ are relatively large. For conventional jackets, KC and V_R are large, but $\hat{x}$ is small. In both cases the flow is quasi-steady and the periods of oscillation
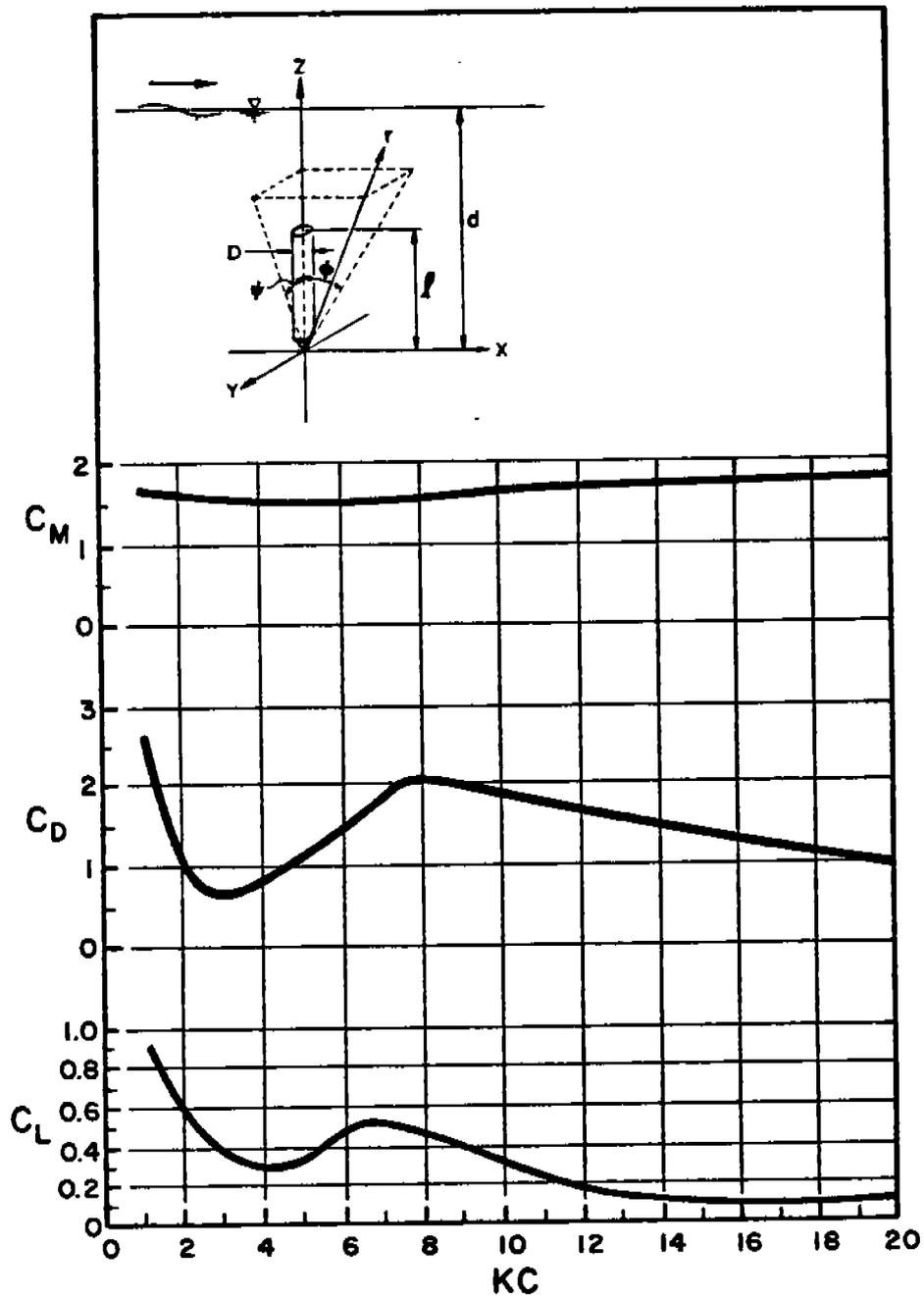
FIGURE 2.12 HYDRODYNAMIC COEFFICIENTS FOR A SUBMERGED ARTICULATED TOWER IN
TWO DEGREES OF MOTION [DAHONG, ET AL. (1982)]
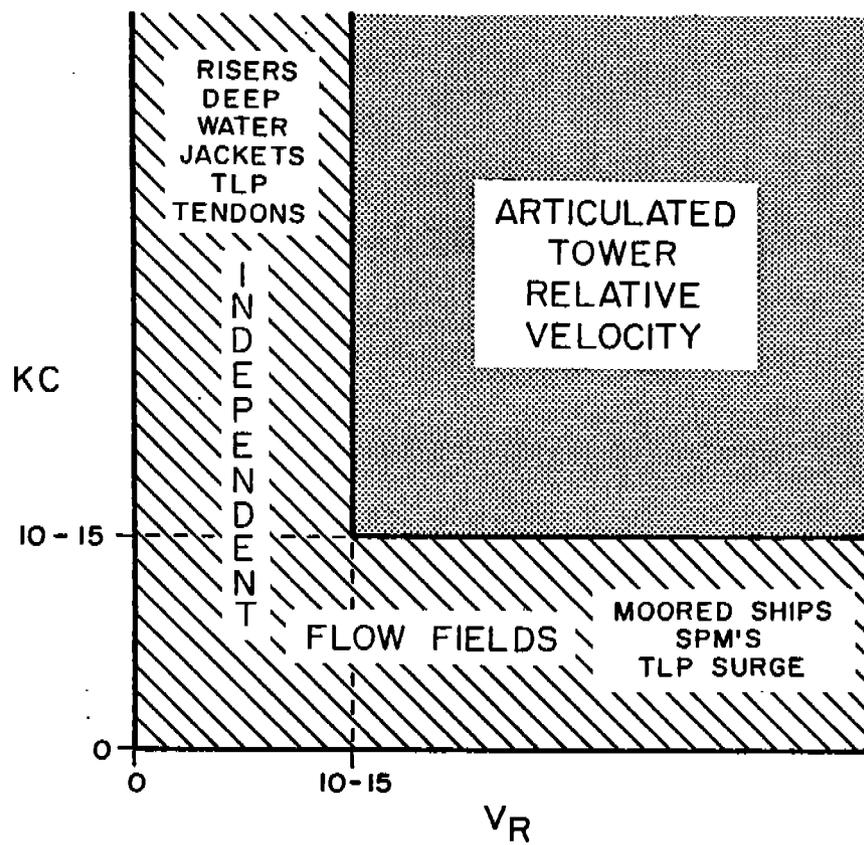
FIGURE 2.13 QUALITATIVE REGION OF APPLICABILITY OF INDEPENDENT FLOW FIELD
AND RELATIVE VELOCITY MODELS

of the structure generally coincide with the periods of the incident waves. The use of the relative velocity term in the computation of the drag force may be appropriate in these cases.

Two other cases may be considered. High KC and small V_R values correspond to a resonating drag dominated structure, i.e. a high-frequency cylinder oscillation in a slowly oscillating external flow. Examples of this case are vibrating structures at high resonant frequency such as riser cables, TLP tendons, etc. Similarly, low KC and high V_R values mean a low frequency cylinder oscillation in a high frequency flow oscillation. This second case includes the slowly-oscillating drift motions of a moored structure, e.g., ships, semisubmersibles, TLP surge, floating caissons, etc. In these two cases, the concept of relative velocity applied in Eqs. 2.33 and 2.35 is highly suspect and the independent flow fields model, Eq. 2.32, is applicable. The main reason for this choice is that the two motions are quite different and relatively independent of each other. Thus, the smaller motions are capable of creating local wakes independent of the larger motions. The relative velocity model accounts for their combined effect, thus ignoring the smaller motions. The two drag coefficients may be chosen from the two types of test data, one from a fixed cylinder in waves and one from an oscillating cylinder in still water (or alternately, oscillating water past a stationary cylinder). The KC and Re numbers are computed from the individual velocities for this purpose.

A simple technique may be employed in determining which of the two models, relative velocity and independent flow field, is applicable in a particular application. When the two flows are comparable, one influences the other and the relative velocity model is applicable. The independent flow fields model may be used when one of the velocities is large compared to the other. The applicable coefficients are chosen based on the test results obtained from the corresponding models.

2.4.4 Oscillating Cylinder in Waves and Current

For a structure free to oscillate in the presence of waves and current, the Morison equation is modified as

$$f = k_M \dot{u} - k_A \ddot{x} + k_D |u \pm U - \dot{x}|(u \pm U - \dot{x}) \qquad (2.36)$$

18

Other forms of Eq. 2.36 may be written as before and have been used in the past. These forms are applicable to moving structures in waves and current whose member sizes are such that the hydrodynamic drag force is significant. Even though the equation is written to define a force term, in a motion analysis, the terms from Eq. 2.36 appear on both sides of the equation of motion. For example, the first term on the right hand side is a forcing function. The second term is an inertia term and belongs to the left hand side of the equation of motion. The third term includes both a force term and a damping term coupled together. If this term is linearized, then the two components may be uncoupled into two terms belonging to the two sides of the equation. In a time domain analysis it is treated as a damping term.

Test results under this condition, however, are almost nonexistent. Considerable work is needed to achieve insight into this most complex problem. The force and the motion are dependent upon the water particle kinematics as well as the velocity and acceleration of the structure itself. Because of the lack of data in this area, the hydrodynamic coefficients for the analysis of such problems are chosen from studies similar to those described in the preceding sections.

2.5 STEADY DRIFT FORCE

The second-order theory for the steady drift force is based on the first-order diffraction-radiation theory and is applicable to regular waves. The regular wave results are then applied to wave groups and irregular waves. In addition, a steady drift force develops from the drag force term at the free surface as well as in current.

In the following section, the steady drift force due to viscous flow is discussed. It is generally applicable to structures that have members in the drag-dominated areas (refer to Fig. 2.7), e.g., in jacket structures, TLP tendons, etc.

2.5.1 Steady Drift Force Due to Viscous Flow

The forces on a small vertical cylinder due to linear waves may be obtained from the Morison formula by substituting $u(t) = u_0 \cos\omega t$ in Eq. 2.18. Then, noting that $\dot{u}(t) = -\omega\, u_0 \sin\omega t$,

$$f = -k_M \omega u_0 \sin \omega t + k_D u_0^2 |\cos \omega t| \cos \omega t \qquad (2.37)$$

This form of the wave force at a submerged location has a zero mean over one wave cycle. If the cylinder is allowed to oscillate harmonically in waves with a displacement amplitude of x_0 at a phase angle of α with respect to the wave so that $x(t) = x_0 \cos(\omega t + \alpha)$, then the relative velocity model (Eq. 2.33) gives

$$f = -k_M \omega V \sin(\omega t + \phi) + k_D V^2 |\cos(\omega t + \phi)| \cos(\omega t + \phi) \qquad (2.38)$$

in which the quantities V and ϕ are defined as

$$V = [u_0^2 + (\omega x_0)^2 - 2 \omega u_0 x_0 \cos \alpha]^{1/2} \qquad (2.39)$$

and

$$\phi = \tan^{-1} \left(\frac{\omega x_0 \sin \alpha}{u_0 - \omega x_0 \cos \alpha} \right) \qquad (2.40)$$

The expression in Eq. 2.38 also has a zero mean. Comparing Eqs. 2.37 and 2.38, it is clear that for a moving structure in waves, u_0 should be replaced by V and ωt by $\omega t + \phi$. Hence, the subsequent derivations are done only for a fixed cylinder.

Note that there are two areas that will produce a non-zero mean viscous drift force. When current is present along with waves, a mean drift force is generated from the drag force at any elevation of the cylinder. Moreover, due to the changing free surface of the waves at the cylinder, the force will produce a mean drift at the still water level (SWL).

In the presence of current, U, the relative velocity drag force may be broken up into two simpler expressions depending on the relative magnitude between U and u_0. For $|U| > u_0$,

$$f_D = \pm k_D \left[U^2 + \frac{1}{2} u_0^2 (1 + \cos 2\omega t) + 2 U u_0 \cos \omega t \right] \qquad (2.41)$$

where the negative sign applies to the case of current opposite to the wave

direction, and for $|U| < u_0$

$$f_D = k_D \left[U^2 + \frac{1}{2} u_0^2 (1 + \cos 2\omega t) + 2 U u_0 \cos \omega t \right] \text{sgn}(u + U) \qquad (2.42)$$

in which sgn is a sign function and takes on values of ± 1 depending on the sign of $u + U$.

When normalized by $k_D u_0^2$, the mean viscous drift force for unit submerged length of a vertical cylinder is given by the following expressions. Defining the quantity, ψ, as

$$\psi = \cos^{-1} \left(-\frac{U}{u_0} \right), \qquad 0 < \psi < \pi \qquad (2.43)$$

we have

$$\frac{\overline{f}_D}{k_D u_0^2} = \pm \left[\frac{1}{2} + \left(\frac{U}{u_0} \right)^2 \right] \qquad \text{for } \frac{|U|}{u_0} > 1 \qquad (2.44)$$

and

$$\frac{\overline{f}_D}{k_D u_0^2} = \frac{1}{\pi} \left\{ \left(\frac{U}{u_0} \right)^2 (2\psi - \pi) + 4 \left(\frac{U}{u_0} \right) \sin \psi + \left(\psi - \frac{\pi}{2} + \frac{1}{2} \sin 2\psi \right) \right\} \text{ for } \frac{|U|}{u_0} < 1$$

$$(2.45)$$

where the bar denotes average value over a cycle. The numerical values of the normalized force are presented in Fig. 2.14 as functions of U/u_0 in the range of -2.0 to 2.0. Note that the curve is asymmetric about U/u_0 and becomes parabolic at higher values of U/u_0. A few experimental data points at low current values are also shown in this figure.

In order to obtain the expressions of the free surface force on a vertical cylinder, use of the Morison equation is made. Current is not included in this derivation since current is generally considered present up to the still water level in the application of the Morison equation. The force per unit length of the cylinder due to wave only is given by Eq. 2.18. According to linear theory, the maximum velocity, u_0 is given as

$$u_0 = \frac{gkH}{2\omega} \frac{\cosh ky}{\cosh kd} \qquad (2.46)$$

21
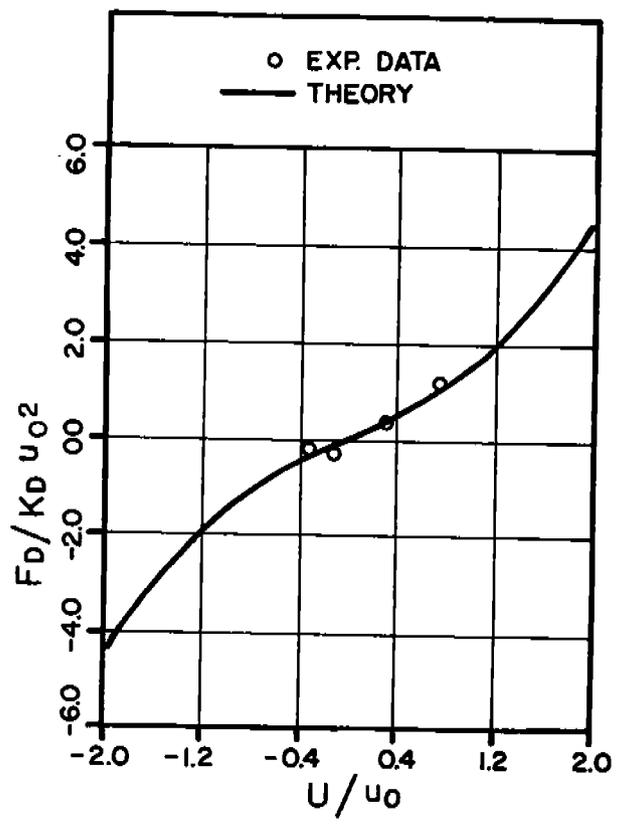
FIGURE 2.14
MEAN VISCOUS DRIFT FORCE ON A FIXED
VERTICAL CYLINDER IN A WAVE-CURRENT FIELD
[CHAKRABARTI (1984)]

TABLE 2.1

VALUES OF C_1 AS FUNCTION OF kH

kH	C_1	kH	C_1
0.05	1.0003	0.10	1.0013
0.15	1.0030	0.20	1.0053
0.25	1.0084	0.30	1.0120
0.35	1.0164	0.40	1.0215
0.45	1.0272	0.50	1.0337
0.55	1.0409	0.60	1.0487
0.65	1.0574	0.70	1.0667
0.75	1.0768	0.80	1.0877
0.85	1.0994	0.90	1.1118
0.95	1.1251	1.00	1.1392

in which g = acceleration due to gravity, k = wave number, H = wave height, d = water depth and y = elevation from bottom. Assuming that the linear theory can be applied up to the free surface, the total force is obtained from the integral

$$F = \int_0^{d+\eta} f \, dy \qquad (2.47)$$

which provides

$$F = -k_M \frac{gH \sinh k(d + \eta)}{2 \cosh kd} \sin \omega t + \frac{1}{2} k_D \left(\frac{gkH}{2\omega \cosh kd} \right)^2$$

$$\left[(d + \eta) + \frac{\sinh 2k (d + \eta)}{2k} \right] |\cos \omega t| \cos \omega t \qquad (2.48)$$

The inertia part of the force has a zero mean. The drag force yields an average value over one wave cycle.

$$\frac{\overline{F}}{2k_D \, g/k^2} = \frac{(kH)^3}{12\pi} \left[\frac{1}{\sinh 2kd} + C_1(kH) \coth 2kd \right] \qquad (2.49)$$

The numerical values of C_1 are shown in Table 2.1 as functions of kH. Note that Eq. 2.49 is due only to the free surface variation even though the integration in Eq. 2.47 is carried out over the entire submerged length. The mean value, however, is a function of the water depth.

Since the linear theory is applicable for infinitesimal wave amplitudes and is valid up to the SWL, use of the expressions for the water particle kinematics up to the free surface of a finite wave is questionable. Therefore, "stretching" formulas have been suggested in finite water depth by which the water particle kinematics at the wave crest and the wave trough assume the same values. If one of these stretching formulas is applied, the water particle velocity is written as

$$u = \frac{gkH}{2\omega} \frac{\cosh ky \left(\frac{d}{d + \eta} \right)}{\cosh kd} \cos \omega t \qquad (2.50)$$

and $\dot{u}$ is expressed in terms of u_0 and ω as done earlier, then the total force up to the free surface is given by

$$F = -k_M \frac{gH}{2d} (d + \eta) \tanh kd \sin \omega t + \frac{1}{2} k_D \left(\frac{gkH}{2\omega \cosh kd} \right)^2$$

$$(d + \eta) \left[1 + \frac{\sinh 2kd}{2kd} \right] |\cos \omega t| \cos \omega t \qquad (2.51)$$

The mean value of F is obtained on integration as before.

$$\frac{\overline{F}}{2k_D \, g/k^2} = \frac{(kH)^3}{12\pi} \left[\frac{1}{\sinh 2kd} + \frac{1}{2kd} \right] \qquad (2.52)$$

Thus, the mean force from the free surface effect of a small vertical cylinder (where viscous effect is important) is a function of the cube of the wave height as opposed to the square of it for the potential drift force, as will be found in the following section.

Note that in deep water, $\omega^2 = gk$ and the expression in Eq. 2.49 approximates as

$$\frac{\overline{F}}{2k_D \, g/k^2} = \frac{C_1}{12\pi} (kH)^3 \qquad (2.53)$$

However, the mean free surface force from Eq. 2.52 approaches zero as the water depth approaches infinity. The mean drift force from Eq. 2.53 have been plotted in Fig. 2.15. Note that the normalized force depends on kH approximately as its cube [Chakrabarti (1984)].

2.5.2 Steady Drift Force Due to Potential Flow

For structures that are large, the force is mainly inertial and potential theory is applicable. The steady drift force is second order and can be shown to arise from the first-order potential. The contribution due to the steady drift force from the potential flow about a floating body has four components which are addressed in the following section.

2.5.2.1 Wave Elevation Drift Force

Consider the extension of pressures above the mean water level to the instantaneous free surface at the body while the body is in motion. Then the integration of this pressure around the object at the water line gives rise to a steady second-order force whose component, $\overline{F}_1$, in the horizontal direction is given by

23
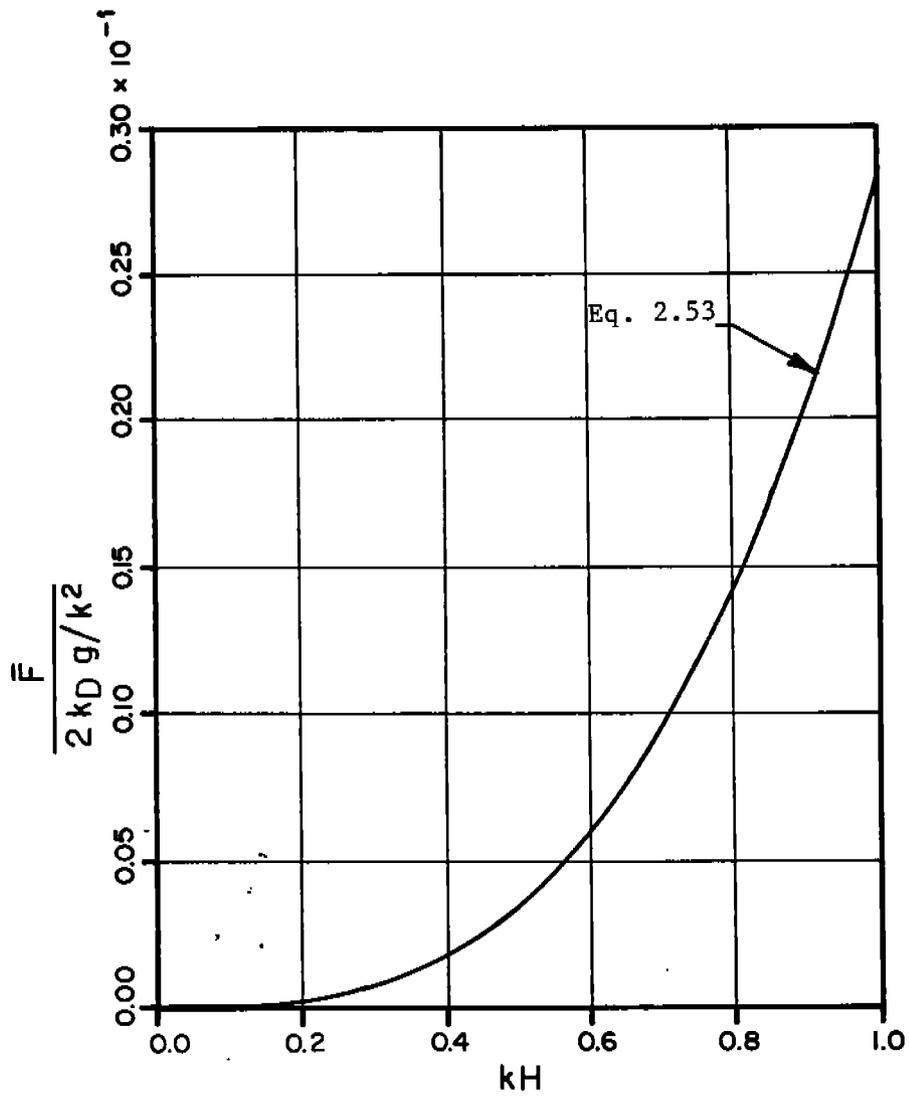
FIGURE 2.15 MEAN VISCOUS DRIFT FORCE FROM FREE SURFACE EFFECT ON A FIXED
VERTICAL CYLINDER IN DEEPWATER (kd < π)
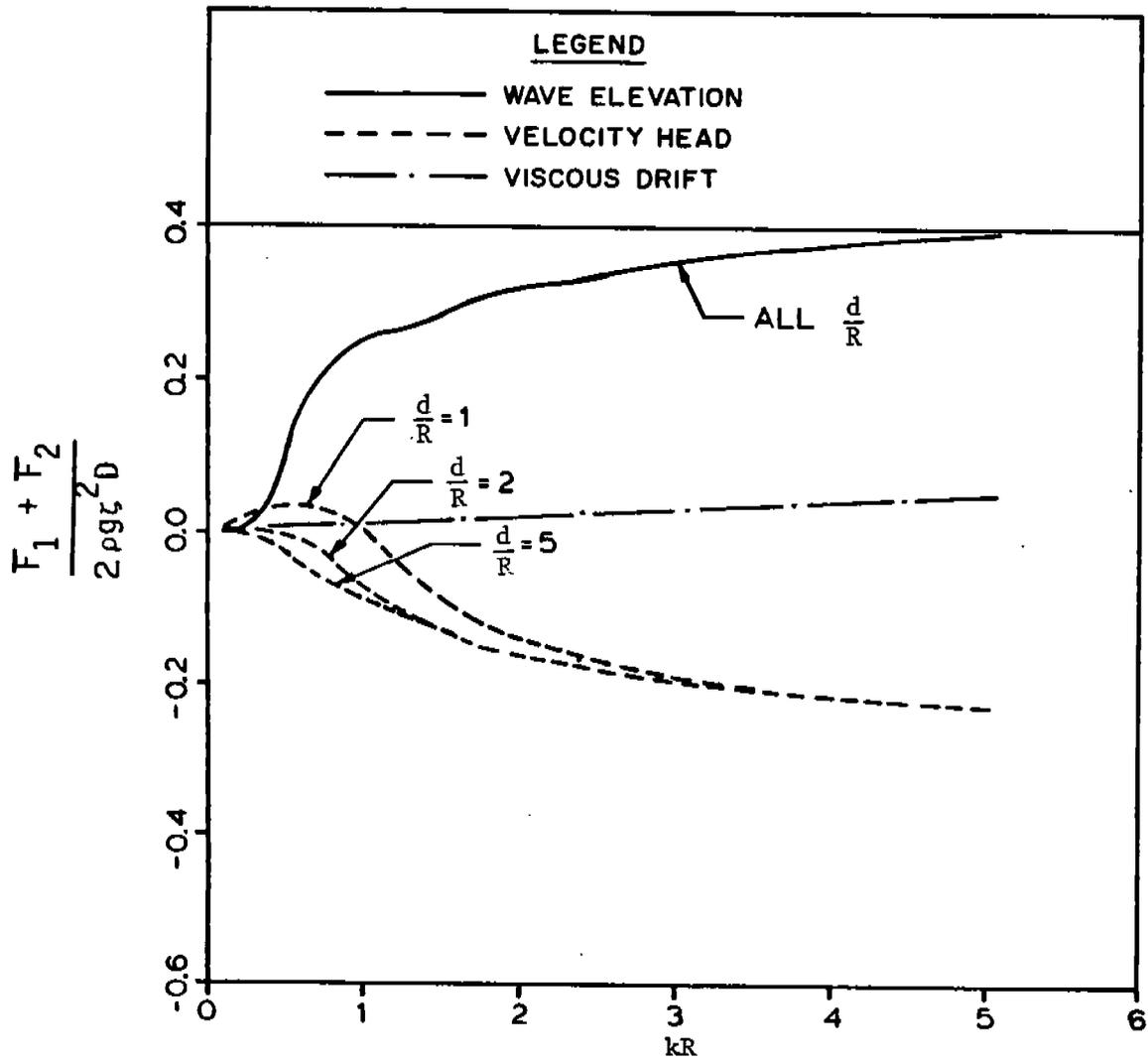
FIGURE 2.16   MEAN POTENTIAL DRIFT FORCE ON A FIXED VERTICAL CYLINDER

$$F_1 = -\frac{1}{2} \rho g \ \overline{\int_{WL} \zeta_1^2 \, n_x \, dl} \qquad (2.54)$$

in which the bar denotes mean value, g = acceleration due to gravity, ζ_1 = first order wave amplitude at a point on the moving body, n_x = direction cosine, and WL = water line at the body surface.

For a fixed vertical cylinder that extends from the free surface to a submerged point where there is no wave action, the body may be treated as two-dimensional and the MacCamy-Fuchs theory is applicable. In this case, the horizontal wave elevation drift force may be obtained in a closed form. The time-independent steady force component may be written as

$$\overline{F}_1 = \frac{4 \rho g \zeta^2 D}{\pi^2 (kR)^3} \sum_{n=0}^{\infty} \left[1 - \frac{n(n+1)}{(kR)^2} \right] \frac{1}{A_n(kR) \, A_{n+1}(kR)} \qquad (2.55)$$

where D = cylinder diameter (= $2R$), ζ = incident wave amplitude (= $H/2$), k = wave number, and $A_n(kR) = J_n'^2(kR) + Y_n'^2(kR)$, J_n, Y_n = Bessel function of order n of the first and second kind respectively, and prime denotes derivative with respect to the arguments.

2.5.2.2 Velocity Head Drift Force

The second term of Bernoulli's equation provides a steady second-order component when the first-order velocity potential including the diffraction-radiation effect is used to compute the pressure. Then the steady horizontal force component may be obtained from the integral

$$\overline{F}_2 = -\frac{1}{2} \rho \ \overline{\int\int_{S} (\nabla \Phi)^2 \, n_x \, ds} \qquad (2.56)$$

in which s = surface of the body and $\nabla \Phi$ = first-order velocity vector.

For the fixed vertical cylinder in deep water, the horizontal velocity head drift force may be calculated using the total velocity potential.

$$\overline{F}_2 = -\frac{2 \rho g \zeta^2 D}{\pi^2 (kR)^3} \sum_{n=0}^{\infty} \left[1 - \left\{ \frac{n(n+1)}{(kR)^2} \right\}^2 \right] \frac{1}{A_n A_{n+1}} \qquad (2.57)$$

Combining Eqs. 2.55 and 2.57 we obtain the total steady force on the fixed vertical cylinder.

24

$$\frac{\overline{F}_1 + \overline{F}_2}{\rho g \zeta^2 D} = \frac{2}{\pi^2 (kR)^3} \sum_{n=0}^{\infty} \left[1 - \frac{n(n+1)}{(kR)^2} \right]^2 \frac{1}{A_n A_{n+1}} \tag{2.58}$$

In intermediate water depths, this force is also a function of the depth.

Numerical values of the wave elevation drift force, $\overline{F}_1$, and the velocity head drift force, $\overline{F}_2$, as well as the total steady force due to the total wave potential in the presence of a fixed vertical cylinder are shown in Fig. 2.16. These quantities are normalized with respect to $\rho g \zeta^2 D$ and plotted versus the diffraction parameter, kR. The numerical values correspond to water depths ranging from $d/R = 1$ to reasonably deep water, $d/R = 5$. Note that the quantity $\overline{F}_1$ is positive while $\overline{F}_2$ is negative over the range of kR considered. Also, the nondimensional steady drift force $(\overline{F}_1 + \overline{F}_2)$ approaches a constant value of 1/3 in deep water at higher values of kR.

For a moving cylinder there are two other components due to the motion of the body contributing to the total steady drift force.

2.5.2.3 Body Motion Drift Force

The first-order wave force on the body is computed at its mean position. However, the body undergoes motion due to waves and assumes a different orientation at the instant this force is calculated. Therefore, if a Taylor series expansion about the mean body position is made, the second-order steady horizontal force term takes the following form:

$$\overline{F}_3 = - \rho \int \int_s \underset{\sim}{x} \cdot \frac{\partial}{\partial t} (\nabla \Phi) \, n_x \, ds \tag{2.59}$$

where $\underset{\sim}{x}$ = motion vector.

2.5.2.4 Rotational Inertia Drift Force

This term arises because the first-order forces due to the pressure are always normal to the surface. As the vessel oscillates the direction of these normals rotate. If the components of these normals in the directions of the fixed coordinate system are considered, a nonlinear drift load develops. Then, mathematically, the second order drift force contribution assumes the form

25
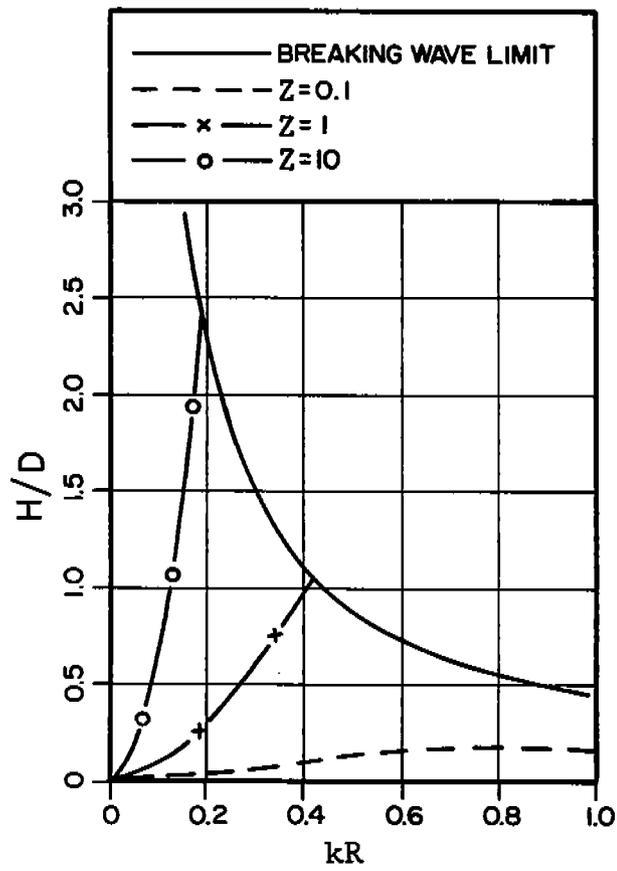
FIGURE 2.17 REGIMES OF POTENTIAL VERSUS VISCOUS DRIFT FORCE ON A FIXED VERTICAL CYLINDER IN DEEPWATER [CHAKRABARTI (1984)]
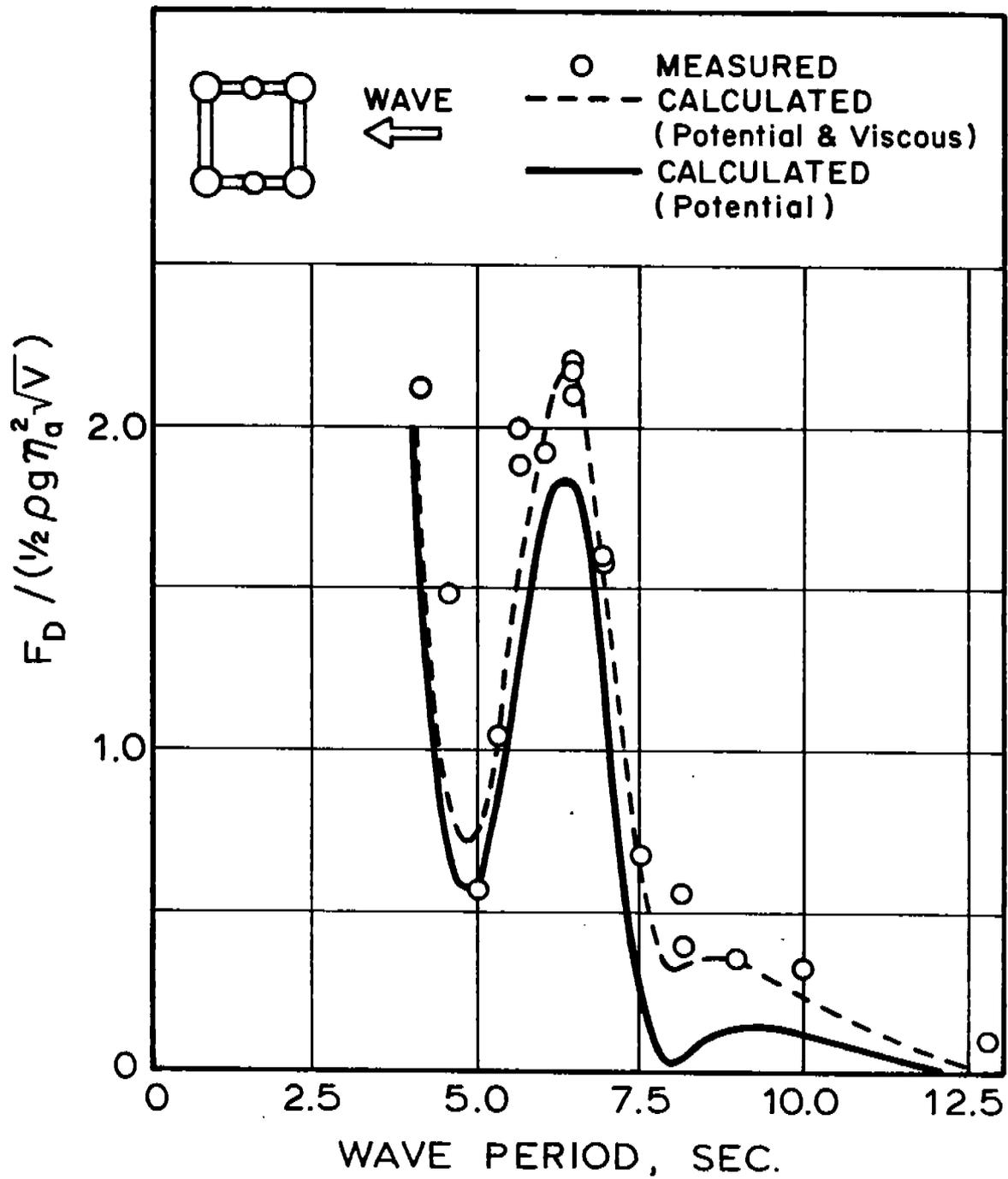
FIGURE 2.18   WAVE DRIFT FORCE ON A TLP IN REGULAR WAVES [KOBSYASHI, ET AL. (1985)]

$$\bar{F}_4 = \overline{\underset{\sim}{\dot{x}} \cdot \underset{\sim}{F}} \tag{2.60}$$

where $\underset{\sim}{F}$ = force vector.

Thus, only the results based on the first-order velocity potential are needed to obtain the steady second order force. The total steady drift force is obtained by adding the four components

$$\bar{F}_p = \bar{F}_1 + \bar{F}_2 + \bar{F}_3 + \bar{F}_4 \tag{2.61}$$

in the direction of surge.

The preceding four contributions arise from the assumption that the fluid flow is irrotational and the potential theory is applicable. In order to determine whether the viscous effect is important, calculations may be made to compute the viscous drag force on the moving body from the drag part of the Morison equation. For a moving cylinder in surge, this calculation takes the form

$$f_D = k_D |u - \dot{x}| (u - \dot{x}) \tag{2.62}$$

in which $\dot{x}$ = surge velocity of the cylinder. When this term is extended up to the free surface above the SWL, a steady component arises which is proportional to the third power of the wave amplitude. A deep water approximation of this expression in the absence of motion gives

$$\bar{F} = \frac{4}{3\pi} k_D (gk) \zeta^3 \tag{2.63}$$

which is comparable to Eq. 2.53 except for the constant C_1 (= 1 here) and which may be written in a form similar to Eq. 2.58 as

$$\frac{\bar{F}}{\rho g \zeta^2 D} = \frac{2C_D}{3\pi} (kR)(\zeta/R) \tag{2.64}$$

The effect of the viscous drift force on the cylinder in relation to the drift force contribution from the potential flow is shown in Fig. 2.16. Consider the radius of the cylinder to be 2 ft. and a wave height of 0.5 ft. for all wave periods so that $\zeta/R = 0.125$. The value of C_D is considered to be

1.0. Then, the values of the viscous drift force are as shown in Fig. 2.16. Note that, in general, the viscous drift force is small compared to the potential force for all values of kR and increases linearly with kR. At kR = 2, the viscous effect is about 15 percent of the potential drift force. For smaller diameter cylinders and higher waves the viscous effect can become more predominant because of its third order dependence on the wave height.

For a general floating body, it is difficult to discuss the ranges of the diffraction parameter, kR and viscosity parameter, H/D (or ζ/R) where the viscous or the potential drift forces are predominant. However, a qualitative assessment of their relative importance may be made by considering a fixed vertical cylinder in deepwater. If Z is considered the ratio of the viscous to the potential drift force, then the region may be constructed as shown in Fig. 2.17 for different values of Z = 0.1, 1 and 10. The middle curve (Z = 1) represents equal contribution from the viscous and potential drift forces. For Z = 10, the potential drift may be neglected just as the viscous drift at Z = 0.1.

An example of the effect of a nonlinear viscous term on the motion of a TLP [Kobsyashi, et al. (1985)] is shown in Fig. 2.18. In this case, steady drift force as a function of the wave period in regular waves is given. The solid line represents the computed values based on potential theory. The dotted line includes the effect of the viscous drift force from the relative velocity model. The correlation of the experimental data is much better with the latter results. Moreover, the contribution of the viscous drift force is much larger than the potential drift force at higher periods (beyond 7.5 secs.) where the ocean waves have much higher energy. Note that for a structure with small members in large waves, such as a compliant tower (where Z is closer to 10), Fig. 2.17 shows the drift force to be primarily viscous.

In order to compute the steady wave drift force due to wave groups and irregular waves, the following procedure is used. The wave energy density spectrum, $S(\omega)$, where ω = wave frequency, for the particular wave group or irregular wave is determined. Then, the steady drift force, $\bar{F}_I$, due to the wave group or the irregular wave is calculated using the regular wave steady drift force $\bar{F}_p(\omega)$ resulting in the transfer function

$$\bar{F}_I = 4 \rho g D \int_{\omega_1}^{\omega_2} S(\omega) \bar{F}_p (\omega) d\omega \qquad (2.65)$$

27

in which ω_1 and ω_2 are the lower and upper frequency limits of the waves.

2.6 NONLINEAR MOTION RESPONSE

A floating structure is connected to the ocean floor in several different ways. An articulated tower is connected to the seafloor via a universal joint which allows certain degrees of freedom of the tower. A ship, barge or a semisubmersible is attached to the seafloor by means of a catenary system through a turntable so that it can weathervane. In this case the structure has all six degrees of freedom. A tension leg platform is held in place by a series of vertical tendons. It is free to surge but has limited heave and pitch motion.

In addition to the forcing function, the equation of motion typically includes an inertia, a linear damping and a restoring force term. The inertia term includes an added mass term. The added mass coefficient is obtained from the linear diffraction/radiation theory for a large structure or from the modified Morison equation for a small member. The limits of applicability in terms of the diffraction parameter ka have been shown in Fig. 2.7. For ka > 0.5 the diffraction becomes important. The linear damping term generally comes from the radiation theory as well. The restoring force term arises from the structure geometry and the type of mooring system. This term is often nonlinear, but may be linearized over the range of application if the motion of the structure is small. The catenary system is described in Section 2.9. The nonlinear viscous damping is often significant and, therefore, needs to be introduced in the equation of motion of the system in the first-order analysis.

2.6.1 First-Order Motions with Nonlinear Drag Damping

The problem of calculating exciting forces using the first-order theory reduces to solving for the total velocity potential, $\Phi(x,y,z,t)$ which can be written as the sum of an incident velocity potential, $\Phi_i(x,y,z,t)$ and a scattered velocity potential, $\Phi_s(x,y,z,t)$. The incident velocity potential, Φ_i is known from the Airy wave theory. The total velocity potential, Φ, satisfies Laplace's equation and the appropriate linearized boundary conditions at the free surface, the ocean bottom and the cylinder surface, as well as the

Sommerfeld radiation condition. The body surface condition states that the normal velocity component on the surface is zero. In the boundary value approach of the problem, on application of this condition, the numerical problem in terms of the unknown scattered potential reduces to a two-dimensional Fredholm integral equation in Green's function. The first-order forces are computed at the mean equilibrium position of the cylinder on the assumption that the motion is small. The first-order pressure on the submerged surface of the cylinder at its equilibrium position is obtained from the first term in Bernoulli's equation,

$$p = \rho \frac{\partial \Phi}{\partial t} + \frac{1}{2} \rho (\nabla \Phi)^2 \qquad (2.66)$$

The added mass and damping coefficients associated with the motions of the body are obtained for the body oscillating harmonically in still water. The formulation of this problem is quite similar to the previous one for fixed structures and uses the same Green's function. The integral equation is modified by the body surface boundary condition which states that the normal velocity component of the fluid at a point on the body is equal to the velocity of the body at that point. In this case, the incident wave potential is absent and the velocity potential for a particular motion of the body e.g., surge, sway, heave, pitch, roll and yaw, Φ_j (j = 1, 2, . . ., 6) replaces the scattered potential in the earlier formulation. Once a particular Φ_j is known, the in-phase and out-of-phase components of the reaction forces constitute the added mass and damping coefficients for that degree of freedom.

Considering that the nonlinear damping is important, the motion of the system may be described by a set of six coupled differential equations of second-order as follows:

$$\sum_{k=1}^{6} [(m_{jk} + M_{jk}) \ddot{x}_k + N_{jk}^1 \dot{x}_k + N_{jk}^2 |\dot{x}_k| \dot{x}_k$$

$$+ C_{jk} x_k] = F_j e^{i(\omega t + \alpha_j)} , \quad j = 1, 2, . . . 6 \qquad (2.67)$$

in which m_{jk} = mass and moment of inertia matrix, M_{jk} = added mass matrix, N_{jk}^1 = linear damping matrix, N_{jk}^2 = nonlinear damping matrix, C_{jk} = restoring force matrix, and F_j, α_j, = exciting force vector and associated phase angles, i = imaginary quantity and ω = wave frequency. The dots

29

represent derivatives of the displacements, x_k, with respect to the time, t. The quantities, F_j and α_j are obtained from the linear diffraction theory while M_{jk} and N^1_{jk} are results of the corresponding radiation problem. The restoring force matrix, C_{jk} is composed of the buoyancy change of the structure and the spring constant in the system. The nonlinear damping term, N^2_{jk} is evaluated from the drag part of the Morison equation and depends on a drag coefficient. This term is particularly important for a motion near the natural period of the structure.

All terms in Eq. 2.67 are linear (on the assumption that the springs in the mooring line are linear) except for the nonlinear damping term. For a simplified solution of the equation of motion, Eq. 2.67, this term is linearized with respect to time in the following way. The motions are assumed harmonic

$$x_k = X_k \, e^{i(\omega t + \beta_k)} \tag{2.68}$$

in which X_k = amplitude of motion not necessarily linear with the wave amplitude and β_k = its phase angle. Then the nonlinear damping term is approximated as

$$|\dot{x}_k| \dot{x}_k \approx \frac{8}{3\pi} (\omega X_k)\dot{x}_k \tag{2.69}$$

The right hand side of Eq. 2.69 is the first term of the Fourier series expansion of the left hand side. On substitution of Eqs. 2.68 and 2.69 in Eq. 2.67 and elimination of time, t, the following matrix equation in unknowns, X_k and β_k are obtained:

$$\sum_{k=1}^{6} \left[-\omega^2(m_{jk} + M_{jk}) + i\omega(N^1_{jk} + \frac{8}{3\pi} N^2_{jk} \, \omega X_k) + C_{jk} \right]$$

$$X_k \, e^{i\beta_k} = F_j \, e^{i\alpha_j}, \quad j = 1, 2, \ldots 6 \tag{2.70}$$

The solution for X_k and β_k are obtained by an iterative scheme in which X_k in the term with N^2_{jk} is assumed zero initially to obtain the first estimate of X_k and β_k through a 6 x 6 matrix inversion. This value of X_k is then substituted for X_k in the term with N^2_{jk} to compute the subsequent solution until a numerical convergence is reached.

Several different variations of the equation of motion are possible and have been used in analyzing the motion of floating structures. When nonlinear (drag) damping effects on the structure are considered small, the equations of motion reduce to

$$\sum_{k=1}^{6} [(m_{jk} + M_{jk}) \ddot{x}_k + N_{jk}^1 \dot{x}_k + C_{jk} x_k] = F_j e^{i(\omega t + \alpha_j)} \qquad (2.71)$$

which is a linear equation whose solution is obtained as Eq. 2.70 for $N_{jk}^2 = 0$.

The correlation of the numerical results with experiments in wave tanks on a variety of floating structures has shown that satisfactory agreement can be obtained by the simplified theory. An example of such an experimental correlation for a conventional barge is shown in Figs. 2.19 and 2.20. The barge was tested in the head sea position in which the surge, heave and pitch motions were significant, (Fig. 2.19) as well as in the beam sea position where sway, heave and roll were important (Fig. 2.20). The cross marks represent the linear theory results. The correlation is quite satisfactory everywhere except near the natural period of the spring-mass system (e.g. in roll). The theory seems to overpredict the motion in this area compared to the experimental data, partly due to the low damping values near the natural period from the linear theory.

In Figs. 2.19 and 2.20, the nonlinear solution obtained from Eq. 2.70 is shown as the solid line. While the scatter in the experimental data may be due to a different amount of nonlinear damping with different wave height (while the theoretical curve is obtained for a given wave height) the correlation is better with this added nonlinear damping term. Thus, the nonlinear damping improves the solution near the natural period of the structure in a particular mode of oscillation.

The coupled nonlinear equations describing the various degrees of motion that include a significant relative-velocity-squared drag term cannot be solved in the frequency domain while retaining their nonlinear characteristics. The use of the independent flow fields model or the relative velocity model in the equations of motion depends on the relative magnitudes of the water particle velocity drag force versus the structure motion damping force. If the two are comparable then the relative velocity model seems appropriate. Otherwise, the independent flow fields model is applicable.

31
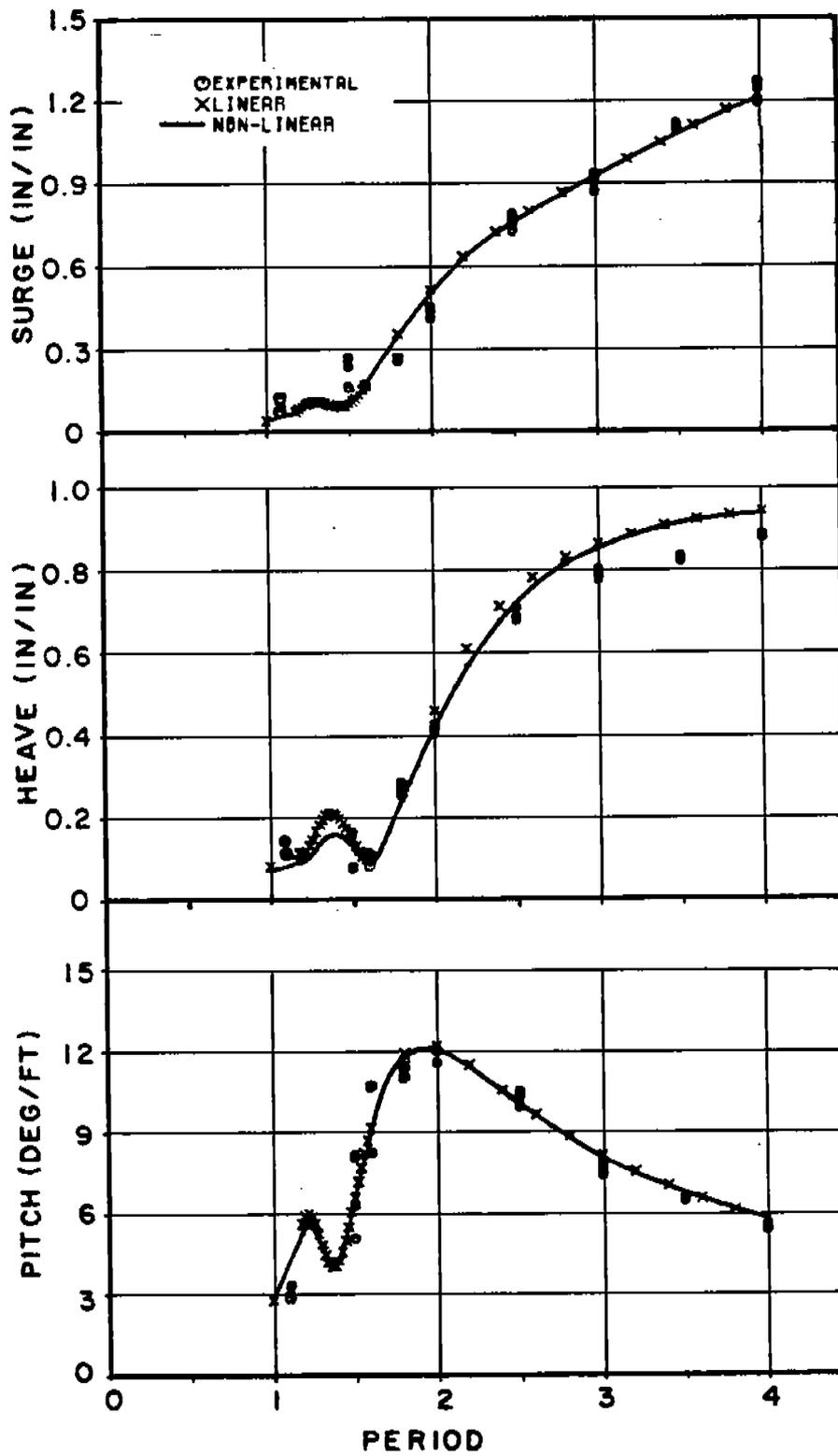
FIGURE 2.19   CORRELATION OF THE MOTIONS OF A MOORED BARGE IN REGULAR WAVES
IN A HEAD SEA [CHAKRABARTI AND COTTER (1983)]
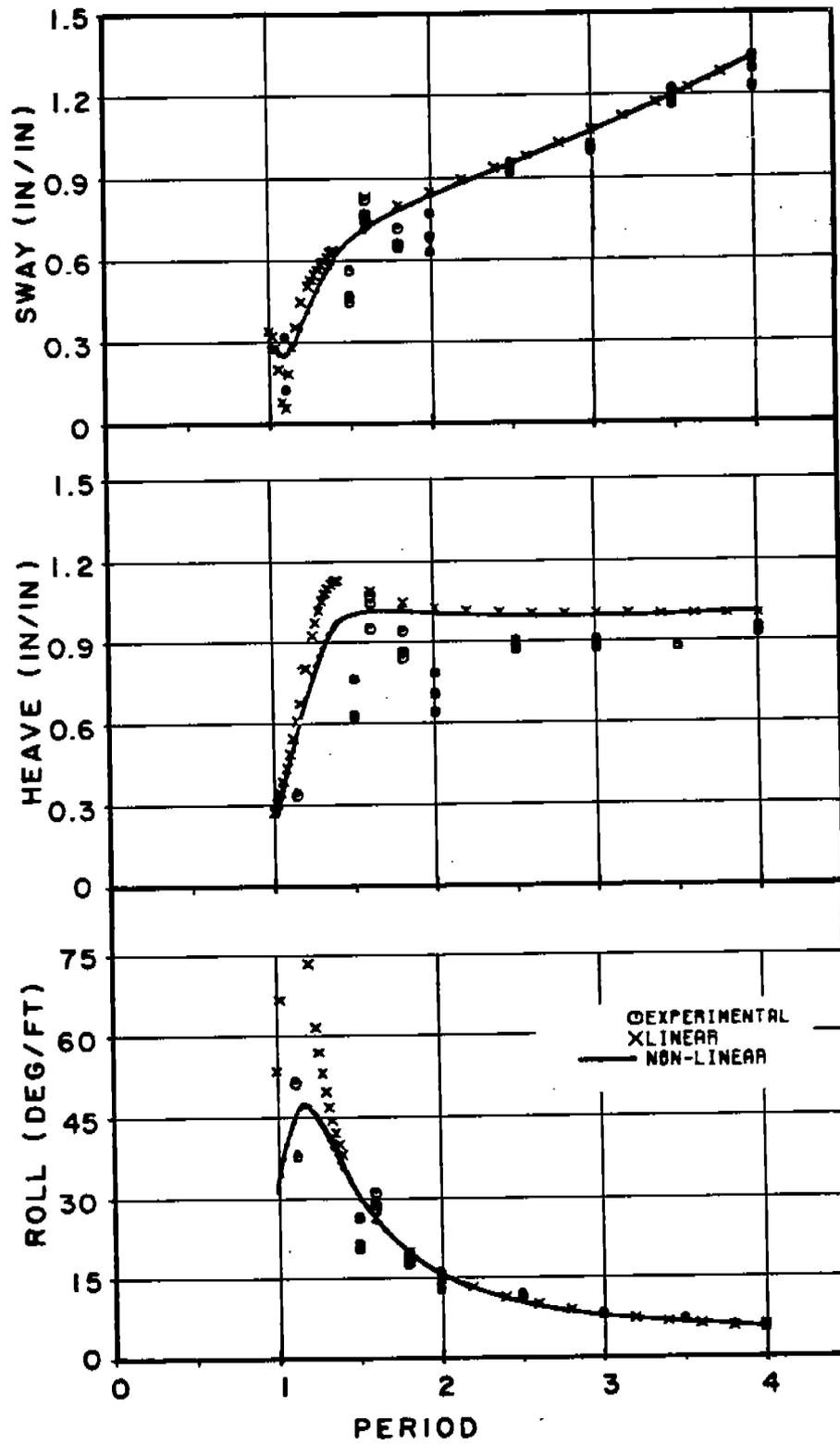
FIGURE 2.20 CORRELATION OF THE MOTIONS OF A MOORED BARGE IN REGULAR WAVES
IN A BEAM SEA [CHAKRABARTI AND COTTER (1983)]

In random waves the equation of motion is written as before except that the added mass and damping coefficients are obtained from the convolution integrals. This is required for a random seastate because these quantities are functions of wave frequencies. Thus, the equation of motion including only the linear damping term becomes

$$\sum_{k=1}^{6} \left[(m_{jk} + M^{*}_{jk}) \, \ddot{x}_k + \int_{-\infty}^{t} N^{*}_{jk} \, (t - \tau) \, \dot{x}_k(\tau) \, d\tau + C_{jk} \, x_k \right] = F_j(t) \qquad (2.72)$$

where

$$N^{*}_{jk}(t) = \frac{2}{\pi} \int_{0}^{\infty} N_{jk} \, (\omega) \cos \omega t \, d\omega \qquad (2.73)$$

and

$$M^{*}_{jk}(\omega) = M_{jk} \, (\omega) + \frac{1}{\omega} \int_{0}^{\infty} N^{*}_{jk} \, (t) \sin \omega t \, dt \qquad (2.74)$$

The quantities M_{jk} and N_{jk} are the frequency dependent added mass and damping coefficients, respectively. It is clear that this set of equation can only be solved in a time domain analysis. The solution method is quite cumbersome and requires considerable computer time.

2.7 LOW FREQUENCY OSCILLATION

The surface profile of a unidirectional random seastate may be represented as its short-term description by a large number, N, of sinusoidal components having frequency, ω_n and random phase, ε_n ($n = 1,2,....N$), as described by Eq. 2.13. The wave profile may be conveniently written in a complex notation

$$\eta(t) = \sum_{n=1}^{N} \sqrt{2S(\omega_n)d\omega} \; \hat{u}_n \; e^{i\omega_n t} \qquad (2.75)$$

where the quantity under the radical sign is the wave amplitude and $\hat{u}_n$ is a complex Gaussian random variable with the following properties:

$$E\left[|\hat{u}_n^2|\right] = 1; \quad E\left[\hat{u}_m \hat{u}_n\right] = 0; \quad E\left[\hat{u}_m \hat{u}_n\right] = 0 \qquad (2.76)$$

where E refers to the expected. value of the argument, m ≠ n and asterisk denotes conjugate.

The steady potential drift force in regular waves has been shown to appear from the second-order terms of the first-order potential. Since an irregular wave has multiple components of frequency, the interaction of two wave components at two frequencies will give rise not only to a steady drift force as before, but also oscillating drift force components at low as well as high frequencies. This is illustrated by a simple example.

There are several contributions to the high and low order components. One of them is the free surface component. Another one is considered in the present example. The pressure at a submerged location of the TLP is given from potential theory by Bernoulli's equation

$$p = \rho \frac{\partial \Phi}{\partial t} + \frac{1}{2} \rho (u^2 + v^2) \tag{2.77}$$

where Φ is the total potential due to the wave field in the presence of TLP, u and v are the corresponding horizontal and vertical velocity components and ρ is the mass density of water. By linear theory, the first term in Eq. 2.77 is a first order pressure while the second term is second-order. Let us consider only the incident wave field and also assume that it is composed of two regular wave components having frequencies ω_1 and ω_2. Then, by linear superposition of Airy theory, the particle velocity components are

$$u = u_1 \cos \omega_1 t + u_2 \cos \omega_2 t \tag{2.78}$$

$$v = v_1 \sin \omega_1 t + v_2 \sin \omega_2 t \tag{2.79}$$

where (u_1, v_1) and (u_2, v_2) are the velocity amplitude components at ω_1 and ω_2 respectively. Then, the second-order pressure term, on expansion, reduced to

$$p_2 = \frac{1}{2} \rho \left[\frac{1}{2} (u_1^2 + u_2^2 + v_1^2 + v_2^2) + \right.$$

$$\frac{1}{2} (u_1^2 - v_1^2) \cos 2\omega_1 t + \frac{1}{2} (u_2^2 - v_2^2) \cos 2\omega_2 t +$$

$$(u_1 u_2 - v_1 v_2) \cos(\omega_1 + \omega_2)t +$$

$$(u_1 u_2 + v_1 v_2) \cos(\omega_1 - \omega_2)t] \qquad\qquad (2.80)$$

The above expression will produce a steady force, a component of force at twice the frequency of the individual components, ω_1 and ω_2, a sum frequency force and a difference frequency force.

Thus, while the energy of wave at the heave and pitch natural frequencies as well as surge frequency is negligible, two individual frequencies within the wave energy may be chosen such that their sum or their difference approaches the high frequency (e.g., heave and pitch of a TLP) periods or the low frequency (surge of a TLP) period. For example, a 6 second period will produce a second harmonic at 3 seconds which may correspond to heave or pitch natural period. Similarly, an 8 second and 4.8 second period would add to a 3 second period. A combination of 8 second and 8.7 second period will produce a difference frequency corresponding to the surge natural period of 99.4 seconds.

The oscillating drift force is computed following the method outlined by Pinkster (1980). In an irregular wave this force appears as a slowly-varying force having the form

$$F_2(t) = \sum_{m=1}^{N} \sum_{n=1}^{N} \zeta_m \zeta_n \{P(\omega_m,\omega_n) \cos[(\omega_m - \omega_n)t - \epsilon_m + \epsilon_n]$$

$$+ Q(\omega_m,\omega_n) \sin[(\omega_m - \omega_n)t - \epsilon_m + \epsilon_n] \} \qquad (2.81)$$

where N = number of wave components of frequencies ω_n (n = 1, 2, . . ., N) in the irregular wave, P (symmetric) is the in-phase component of the wave drift force in a wave group of frequencies ω_m and ω_n, Q (asymmetric) is the corresponding out-of-phase component of the drift force, and ζ_n represents wave amplitudes at frequencies ω_n and phase angles ϵ_n.

The force, F_2, in Eq. 2.73 may be similarly expressed as

$$F_2(t) = \sum_{m=1}^{N} \sum_{n=1}^{N} \overline{H}_{mn} \hat{u}_m \hat{u}_n^* e^{i(\omega_m - \omega_n)t} \qquad\qquad (2.82)$$

where

$$\overline{H}_{mn} = (P_{mn} - iQ_{mn}) \sqrt{2S(\omega_m)d\omega} \sqrt{2S(\omega_n)d\omega} \qquad (2.83)$$

In the above expression for F_2, real parts are assumed.

For a linearly moored lightly damped system, the equation of horizontal motions (to which the second-order force is sensitive) may be written as shown in Eq. 2.71 where the right hand side is replaced by expressions of the form of Eq. 2.82. The solution for this set of equations in the frequency domain may be written as

$$X_j = \sum_{m=1}^{N} \sum_{n=1}^{N} G_{mn}^j \, \hat{u}_m \hat{u}_n^* \, e^{i(\omega_m - \omega_n)t} \qquad (2.84)$$

where

$$G_{mn}^i = \sum_{j=1}^{N} T_{mn}^{ij} \, \bar{H}_{mn}^j \qquad (2.85)$$

and T_{mn}^{ij} is given by

$$T_{mn}^{ij} = [- (\omega_m - \omega_n)^2 (m_{ij} + M_{ij}) + i(\omega_m - \omega_n) N_{ij}^1 + C_{ij}]^{-1} \qquad (2.86)$$

Newman's (1974) approximate solution may be obtained from the above. For a narrow-band spectrum, e.g., for a wave group, it may be assumed that ω_m and ω_n are close to each other so that they may be replaced by their mean values without appreciable error. Then

$$P(\omega_m, \omega_n) = P \left[\frac{\omega_m + \omega_n}{2}, \frac{\omega_m + \omega_n}{2} \right] = P_{mn} \qquad (2.87)$$

$$Q(\omega_m, \omega_n) = Q_{mn} = 0 \qquad (2.88)$$

and

$$F_2(t) = \sum_{m=1}^{N} \sum_{n=1}^{N} \zeta_m \, \zeta_n \, P_{mn} \cos[(\omega_m - \omega_n)t - \epsilon_m + \epsilon_n] \qquad (2.89)$$

where P_{mn} is obtained from the regular wave steady drift force at a frequency corresponding to the mean of the frequencies, ω_m and ω_n.

If it is further assumed that the only frequency that is of any large consequence in determining the slowly-oscillating mooring line load is the natural frequency, ω_N, of the system, then we can assume

$$\omega_m - \omega_n = \omega_N \tag{2.90}$$

and only the diagonal terms in Eq. 2.89 are relatively important which gives

$$F(t) = \bar{F}_p \cos (\omega_N t) \tag{2.91}$$

Since the slowly oscillating mooring line load occurs at or near the natural frequency of the system in surge, a reasonable estimate of its magnitude may be made from the following differential equation:

$$m\ddot{x} + N_1 \dot{x} + N_2 |\dot{x}|\dot{x} + Kx = F(t) \tag{2.92}$$

in which m = total mass of the cylinder including added mass, N_1 = linear damping coefficient, N_2 = nonlinear damping coefficient, K = spring constant of the mooring line and F(t) is given by Eq. 2.91. This equation is similar in form to Eq. 2.67 and an approximate solution is obtained in a similar fashion by assuming x to be sinusoidal

$$x = x_0 \cos (\omega_N t + \varepsilon) \tag{2.93}$$

where x_0 = amplitude of oscillation and ε = its phase angle. The solutions for x_0 and ε are

$$x_0 = \frac{\bar{F}_p}{\{(K - \omega_N^2 m)^2 + \omega_N^2 [N_1 + \frac{8}{3\pi} \omega_N N_2 x_0]^2\}^{1/2}} \tag{2.94}$$

and

$$\tan \varepsilon = - \frac{\omega_N [N_1 + \frac{8}{3\pi} \omega_N N_2 x_0]}{[K - \omega_N^2 m]} \tag{2.95}$$

Once x_0 is known, the mooring line load amplitude is computed as

$$\bar{F}_m = Kx_0 \tag{2.96}$$

2.8 HIGH FREQUENCY SPRINGING FORCE

When a floating structure, e.g., a TLP is restrained in the vertical

36

direction by its tendons, the natural period in heave is small, being of the order of 2-4 seconds. This gives rise to the problem of high frequency oscillation of TLP in heave due to a high frequency second order force. The general design approach for the TLP is not particularly different from any other compliant offshore structures. What makes the dynamics of TLP unique from other floating structures is its response to the high frequency wave exciting forces. Besides the responses at the wave frequency, the platform is subjected to a high frequency tension oscillation of the vertical tethers (often called springing) and a low frequency drift oscillation in surge. The overall damping of the system (including mechanical and hydrodynamic) is extremely small for both the springing and drift oscillation so that they produce a significant load in the tendons and significant motion in surge.

The second-order forces are obtained from the first- and second-order velocity potentials and the complete Bernoulli's equation. The quadratic transfer functions obtained from these expressions are used to derive the difference frequency wave exciting force (drift force) and the sum frequency second order force (springing force). Thus, generalizing Eq. 2.81

$$F^{(2)\pm}(t) = \sum_{i=1}^{N} \sum_{j=1}^{N} \zeta_i \zeta_j \{ P_{ij}^{\pm} \cos [(\omega_i \pm \omega_j)t - (\epsilon_i \pm \epsilon_j)]$$

$$+ Q_{ij}^{\pm} \sin [(\omega_i \pm \omega_j)t - (\epsilon_i \pm \epsilon_j)] \} \qquad (2.97)$$

where $P_{ij}^{\pm}$ and $Q_{ij}^{\pm}$ are the even and odd components of normalized forces due to ω_i and ω_j, ζ_i and ζ_j are the corresponding wave amplitudes, and N is the number of wave components in the random wave simulation. It is clear from the above expressions that in regular waves

$$F^{(2)-}(t) = 0 \qquad (2.98)$$

and

$$F^{(2)+}(t) = \sum_{i=1}^{N} \zeta_i^2 \{ P_{ii}^{+} \cos 2(\omega_i t - \epsilon_i) + Q_{ii}^{+} \sin 2(\omega_i t - \epsilon_i) \} \qquad (2.99)$$

Thus, the low frequency force is absent while the high frequency force appears at twice the regular wave frequency. Moreover, this force is nonlinear, being a function of the square of the wave amplitudes, ζ_i (second-order). The

amplitude and phase of the quadratic transfer function are

$$T_{ii}^+ = [(P_{ii}^+)^2 + (Q_{ii}^+)^2]^{1/2} \qquad (2.100)$$

$$\varepsilon_{ii} = -\tan^{-1} \left(\frac{Q_{ii}^+}{P_{ii}^+} \right) \qquad (2.101)$$

Based on this transfer function then, the tether forces in the high frequency springing may be simply obtained by solving a linearized equation of motion in heave and pitch. A model test was performed on a vertical cylinder in waves in which forces on the fixed cylinder were measured. The waves generated in the tank were regular waves, wave groups and irregular waves. The wave groups consisted of two regular waves whose sum frequencies corresponded to the natural pitch frequency of a hypothetical TLP. An example of the forces measured due to one of the wave groups is shown in Fig. 2.21. The wave profile corresponds to waves of frequencies 0.44 HZ and 0.88 HZ. The force has additional peaks present corresponding to second harmonics of the above frequencies, and their sum frequency component at 1.32 HZ. These higher order loads are small, being on the order of 3 to 5 percent of the first-order loads. The correlation of the second-order fixed cylinder loads in regular waves with the computed load approximated by the first-order potential is shown in Fig. 2.22.

Numerous analyses and model tests have been performed on TLPs which considered different aspects of platform motion and tether dynamics. One of such analyses that included all three areas of response of the TLP was performed by DeBoom, et al. (1984). They analyzed the motion and tether forces for a TLP. The heave and pitch natural periods were almost identical. In random waves, the added mass and damping terms were assumed to be frequency dependent as outlined in Eqs. 2.72. The solution was obtained by a finite difference scheme. DeBoom, et al. (1984) compared results from such an analytical solution with the measured high frequency tether forces in regular waves in a test with a four column TLP model. The correlation is shown in Fig. 2.23. The fore and aft tether forces were found to be almost 180° out of phase. From this, it is concluded that most of the high frequency contribution came from the pitching motion of the TLP. The springing force appeared at the higher (twice for regular waves) frequencies and was nonlinear
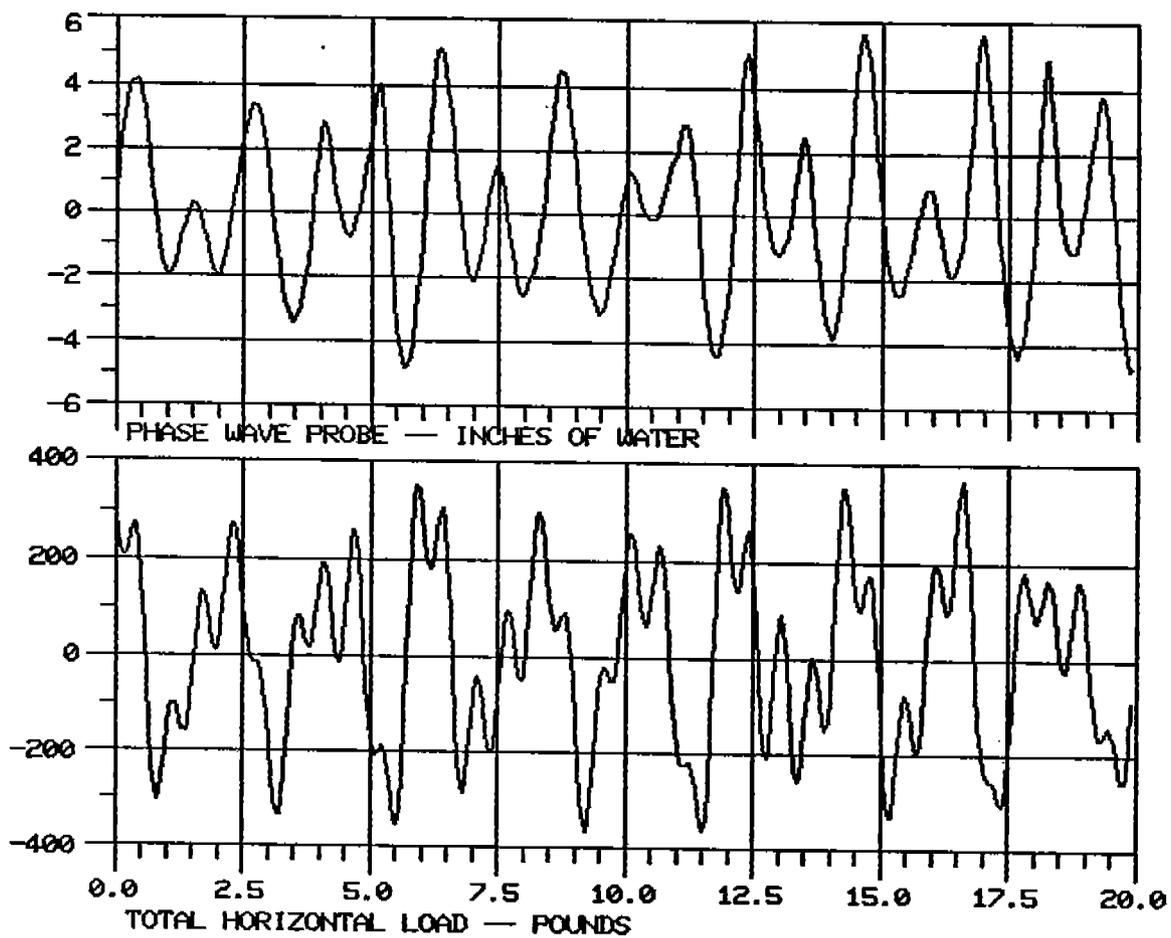
FIGURE 2.21 MEASURED WAVE AND HORIZONTAL FORCE ON A FIXED VERTICAL CYLINDER
IN A PAIRED REGULAR WAVE
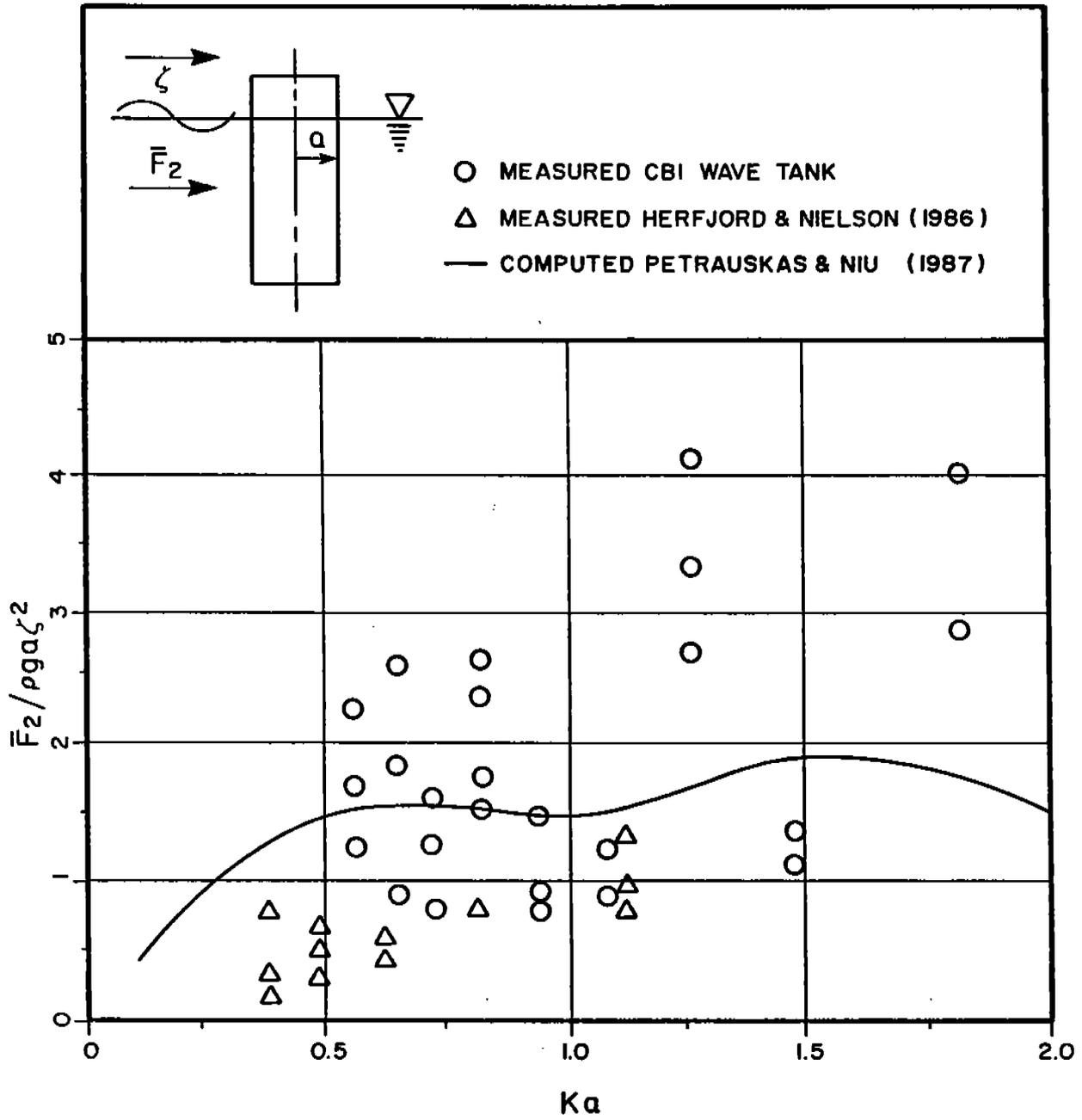
FIGURE 2.22   HIGH FREQUENCY FORCES ON A FIXED VERTICAL CYLINDER [PETRAUSKAS AND LIU (1987)]
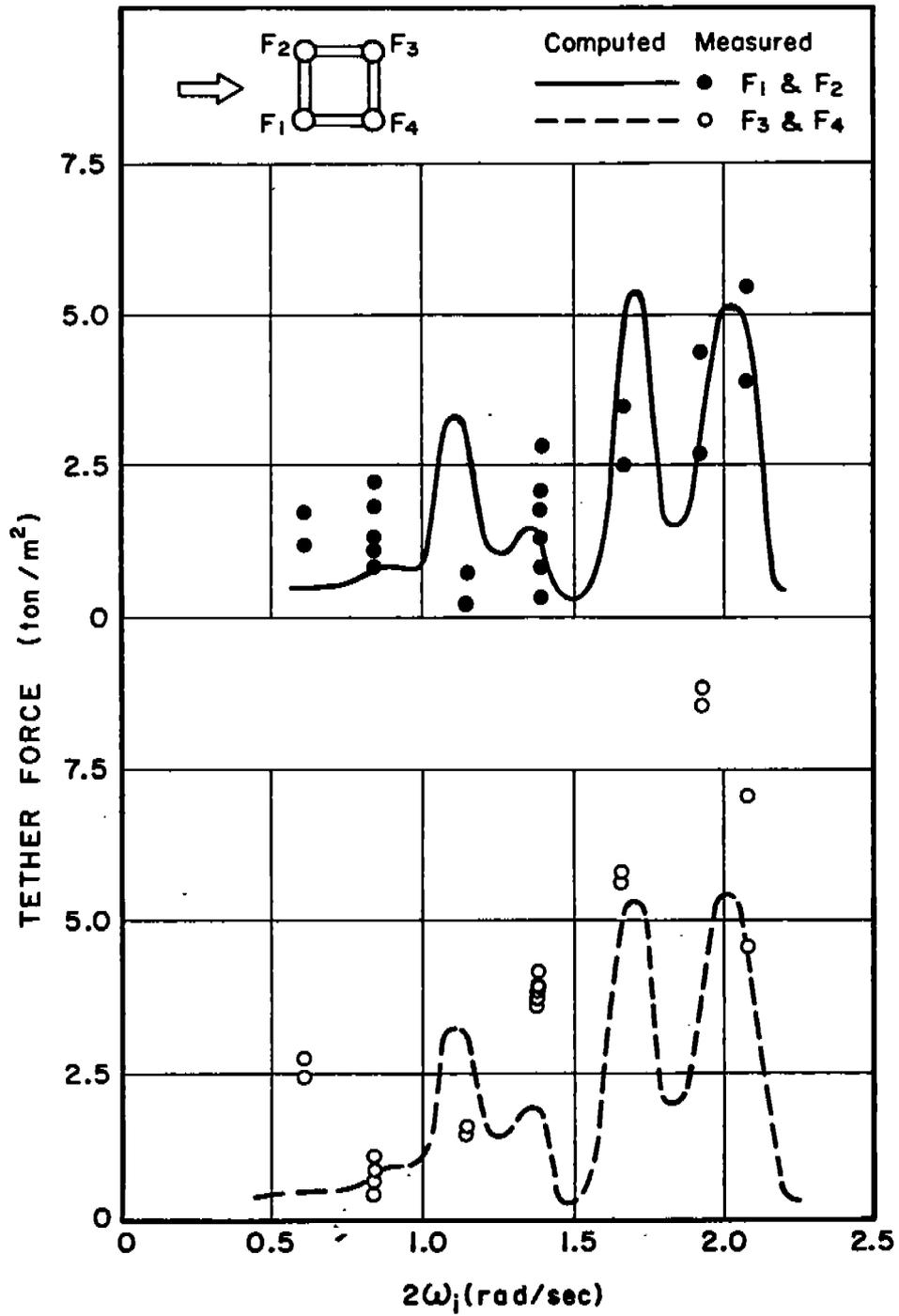
FIGURE 2.23 COMPUTED AND MEASURED SPRINGING TETHER FORCES IN REGULAR HEAD WAVES [DEBOOM, ET AL. (1984)]
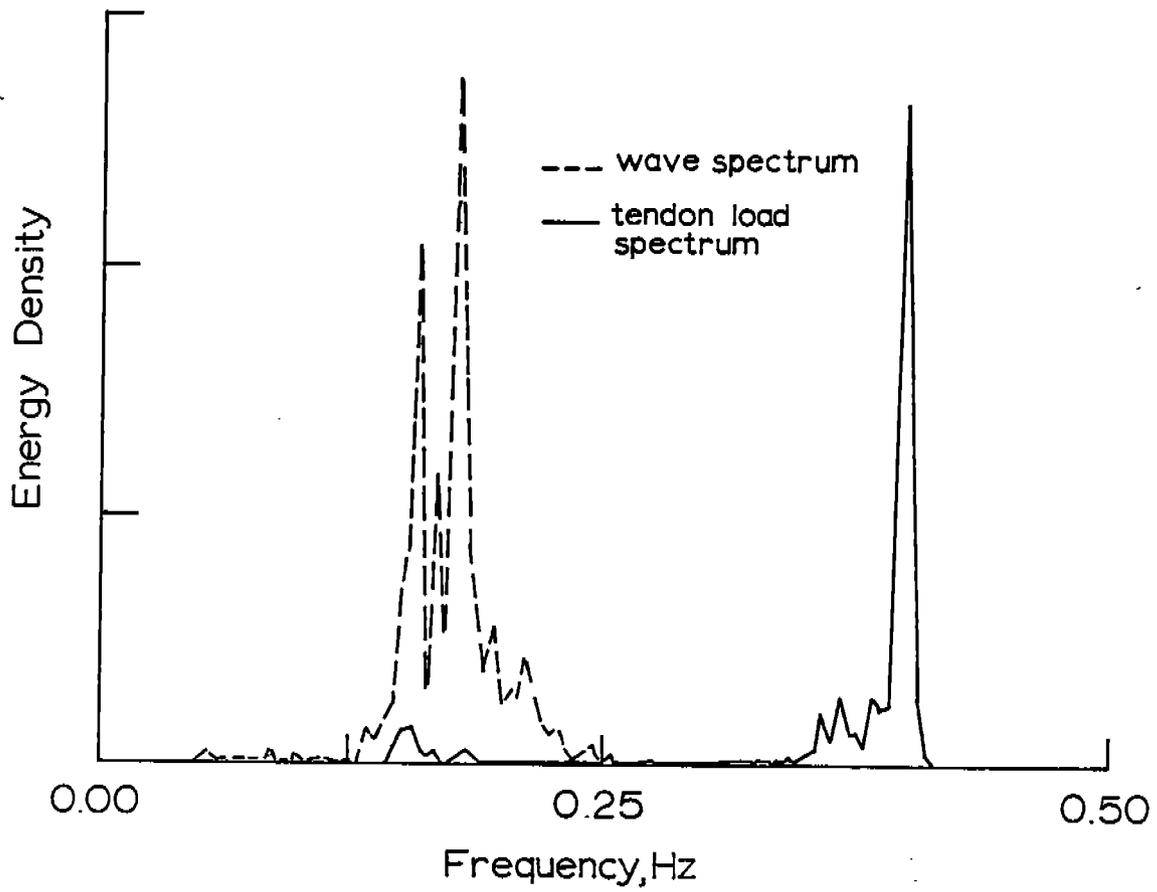
FIGURE 2.24   RANDOM   WAVES   ON   A   TLP   AND   CORRESPONDING   TENDON   LOADS
[PETRAUSKAS AND LIU (1987)]

(Eq. 2.99) so that the corresponding motion was also nonlinear. While the fore and aft tether forces are the same theoretically, the measurement showed different values. The force being second-order is difficult to measure accurately and hence the discrepancy and somewhat poor correlation.

The springing forces on a large scale (1:16) TLP model were measured in a test in the CBI tank [Petrauskas and Liu (1987)] with a four-legged TLP hull connected to the sea floor with four vertical tendons. The springing forces arised from the resonant pitch periods of about 3 seconds. Regular waves at twice the pitch period amplified the resonant springing force in the tendon. The amplification of the force at the tendon due to a random wave is clearly shown in Fig. 2.24. The tendon load at the wave frequencies is almost negligible compared to the resonant load at twice the wave frequencies. The corresponding correlation of the regular wave (averaged) springing load in the tendons is shown in Fig. 2.25. The computed results for different damping values show the importance of the knowledge of damping in determining the springing force.

2.8.1 Damping at Low and High Frequency Responses

The resonant response of a mooring structure, e.g., a TLP, is limited by the amount of damping present in the system. The TLP system experiences damping from two natural sources, e.g., material and hydrodynamic. Sometimes, mechanical dampers [Katayama (1984)] or other active damper systems are introduced externally. The material damping appears from the tendons and their attachments to the TLP as well as to the bottom. The subsea template also provides some damping. The hydrodynamic damping appears in the form of the radiation damping as well as nonlinear viscous damping. Additionally, a slow drift of the structure in the presence of waves produces an added damping force which may be called wave drift damping (or wave damping). For the surge motion of a slender body, the contribution of the quadratic viscous damping was found to be small by Nakamura, et al. (1986). However, for the yaw motion, it was important.

The contributions from the material and radiation damping are nearly equal. In an example problem, Nordgren (1986) considered the material damping factor to be 0.1 while the radiation damping for the dominant pitch response was 0.13. The heave response at a natural period of 2.5 seconds was small
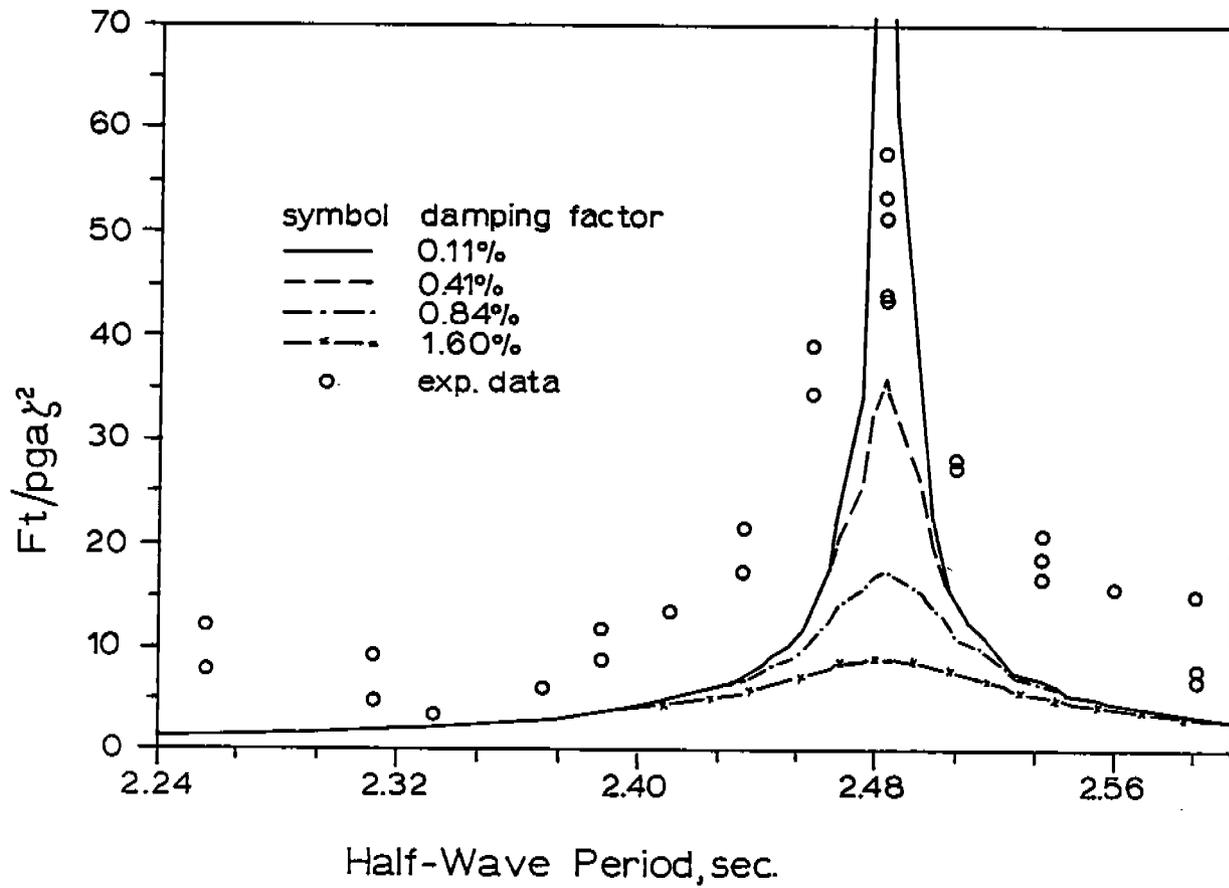
FIGURE 2.25   CORRELATION OF HIGH-FREQUENCY TENDON LOADS ON A TLP MODEL
[PETRAUSKAS AND LIU (1987)]
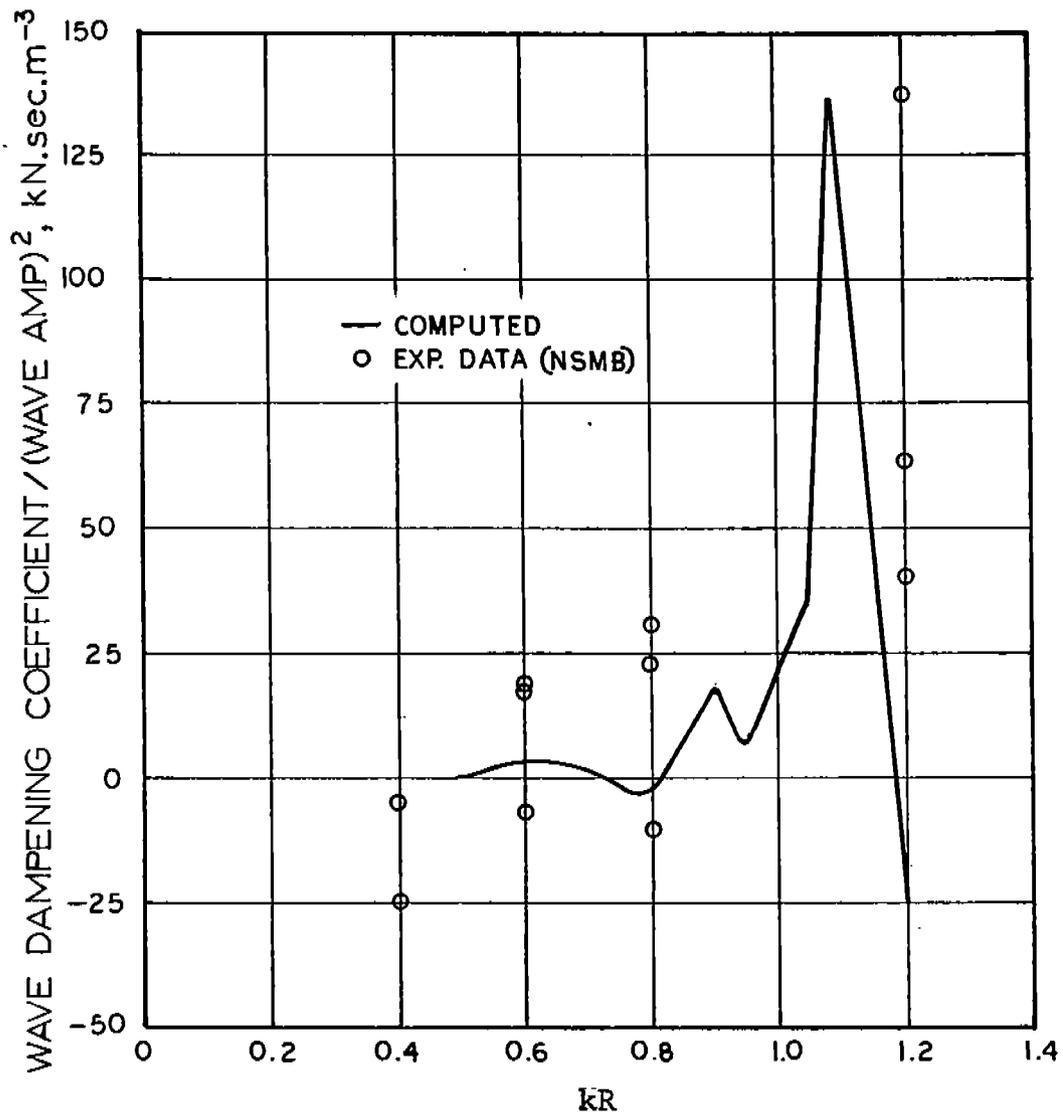
FIGURE 2.26 WAVE DRIFT DAMPING COEFFICIENTS FOR A SEDCO 700 SEMISUBMERSIBLE
MODEL [HEARN, ET AL. (1987)]

compared to the pitch response at a natural period of 3.0 seconds. However, the drag-induced damping in the high frequency resonance modes in heave, roll and pitch motions of a TLP is rather negligible because the amplitude of platform motion is extremely small.

Chakrabarti (1984) presented the low-frequency hydrodynamic coefficients in surge and sway for several floating vessels including a semisubmersible and a vertical cylinder. The results from the vertical cylinder showed that the radiation damping in surge is negligible (less than 0.02 percent) and most of the still water damping is linear viscous damping (about 1 percent). The wave damping factor in regular waves was proportional to the square of the wave amplitude and was equally important.

The heave damping factor obtained from the pluck test of a TLP model discussed earlier [Petrauskas and Liu (1987)] was found to range from 0.11 percent to 1.6 percent. The corresponding prototype values should be even smaller if they are assumed to be dependent on the Reynolds number.

The wave damping at the low frequency in surge of a TLP may be treated analytically in the following way [see Hearn, et al. (1987) for details]. Since the period of slow drift oscillation is an order of magnitude higher than the wave period, the problem may be assumed to be equivalent to computing the added resistance of the TLP advancing at a slow forward speed during half the drift cycle in regular waves. This approach was taken by Hearn et al. (1987) in computing wave damping coefficient in slow drift of a semisubmersible. Once the added resistances for different forward speeds and wave frequencies are known, the wave drift damping coefficients' quadratic transfer function may be computed from the velocity derivative of the added resistance as the forward speed approaches zero.

$$b_{21} = \frac{\partial R_W(U)}{\partial U} \Big|_{U = 0} \tag{2.102}$$

where b_{21} = wave drift damping coefficient, U = forward speed from slow drift and R_W = added resistance in waves. A comparison of the computed wave damping coefficients with the model test results on a SEDCO 700 semisubmersible has been made by Hearn, et al. (1987). This is reproduced in Fig. 2.26. Note that near a wave frequency of $\omega = 1.1$ rad/sec., the damping is large whereas at lower frequencies, it is quite small. This observation is, however, only

valid for the particular geometry but is made to illustrate that the wave drift damping could be quite significant in surge drift oscillation computation.

As mentioned earlier, the surge natural period for a typical TLP is long, being of the order of 100 seconds. Qi, et al. (1986) tested a four-legged TLP model at a scale of 1:64 for low frequency hydrodynamic coefficients in surge. The measured surge period of the model was about 12.5 seconds (100 second prototype). The natural period in waves was slightly higher due to additional added mass. The damping was computed in still water and in regular and random waves. The pontoon geometry was changed from circular section to rectangular section of the same cross-sectional area.

The still water linear damping was obtained from a pluck test using the transient equation of motion. The damping factor in surge was found to be a function of the initial displacement, possibly due to the presence of viscous damping. As expected, rectangular pontoons provided higher damping values. From the information presented by Qi, et al., the damping factor was approximately estimated as follows:

	Damping Factor
Circular pontoon	0.03 - 0.06
Rectangular pontoon	0.03 - 0.09

In regular waves, the damping increased for the rectangular pontoon whereas the damping showed a slight decrease in value for circular section. The radiation damping component was dependent on the wave frequency.

2.9 MATERIAL PROPERTIES

Often the nonlinearities are encountered in the properties of the material involved in the offshore structure system. This is particularly true for the flexible members of an offshore structure. Examples of these components that exhibit nonlinear behavior are risers, mooring lines, etc.

2.9.1 Catenary System

The type of nonlinearities encountered in a catenary type mooring system is illustrated here. Consider a mooring system that is composed of two

different line materials with a clump weight attached to their intersection. The clump weight may be considered acting positive upwards in which case it is replaced by a buoy. The two elements of the line may have different weight and elastic properties. In a mooring system it is often customary to use a cable element at the upper part and a chain element at the lower part of the catenary. A clump weight is also often used at the junction. Thus, the upper part of the catenary reacts to the smaller waves and behaves as a soft system while the lower part is provided to make the system stiff in response to occasional big waves.

Given these conditions, Fig. 2.27 demonstrates the four possible conditions where both parts of the line assume a catenary shape. The quantities in the figure and in the subsequent analysis are defined as follows: Q = length of lower element lying on seafloor; B = weight of clump or buoyancy of buoy at the intersection of two elements; $\{a_1, b_1\}$ = coordinates of element intersection; $\{a_2, b_2\}$ = coordinates of upper element at surface vessel; ψ_1 = angle lower element makes with horizontal at anchor; ψ_4 = angle upper element makes with horizontal at surface vessel. The four possibilities of Fig. 2.27 can be broken down into two cases. Either the line touches the seafloor or it does not. If these two situations can be analyzed, then the only problem remaining is to choose the proper location for the intersection $\{a_1, b_1\}$ such that the summation of forces at the intersection is zero. See Fig. 2.28.

Turning first to the situation described by Fig. 2.29a, the following assumptions are made: the lines are uniform and supported at two points and the line can only carry loads along its axis. Then, the summation of forces on a small element, Δs (Fig. 2.29a) in the horizontal and vertical directions must equate to zero. This gives rise to the following differential equation for the catenary:

$$\frac{d^2y}{dx^2} = \frac{w}{F_x} \left[1 + \left(\frac{dy}{dx} \right)^2 \right]^{1/2} \qquad (2.103)$$

where w = weight per unit length, which may be reduced to a first order differential equation by substituting

$$k = \frac{w}{F_x} \qquad (2.104)$$
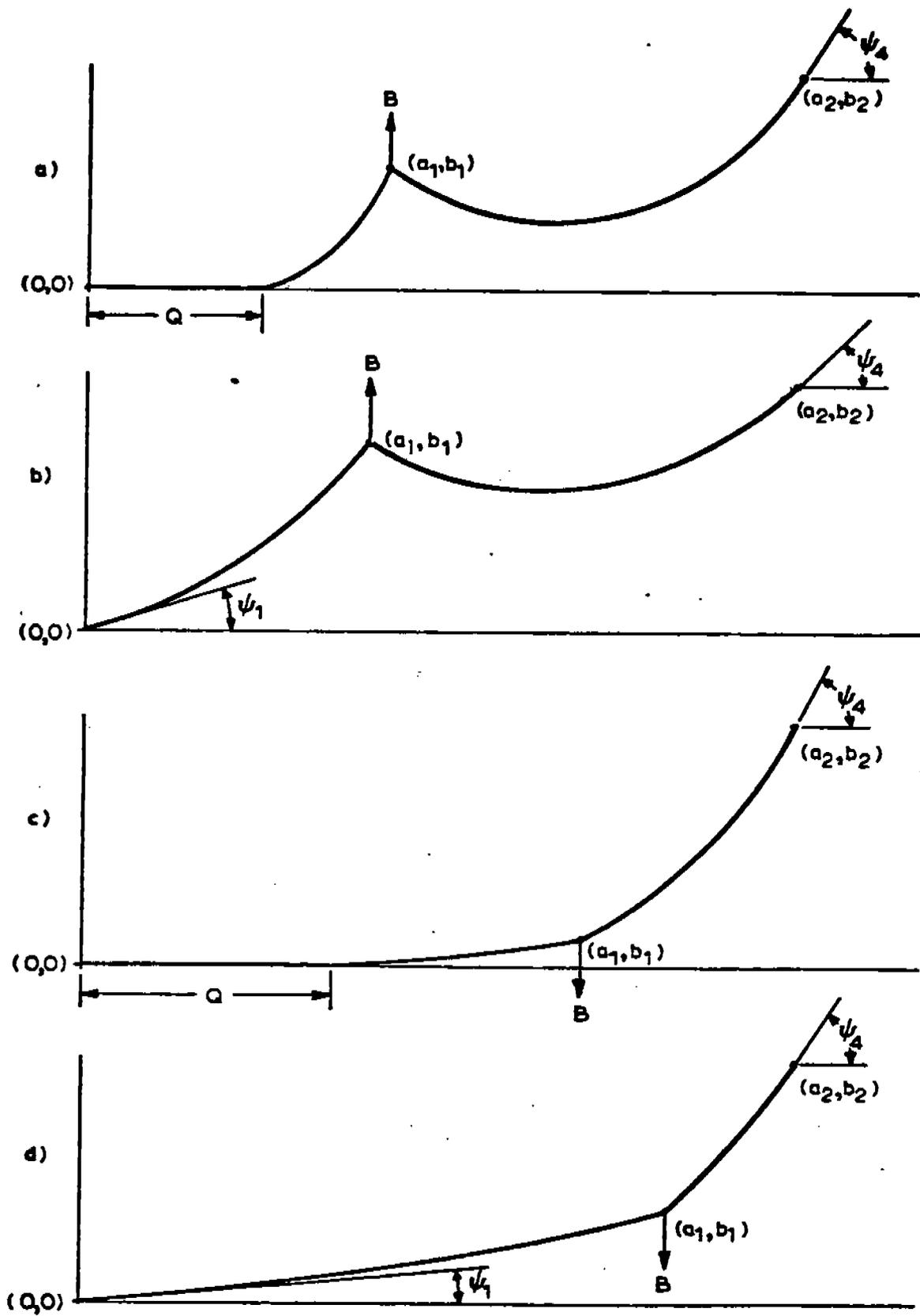
FIGURE 2.27   POSSIBLE CONFIGURATIONS OF TWO ELEMENT CATENARY SYSTEM

B

TO SURFACE

(a_1, b_1)

TO ANCHOR

$$\Sigma F_x = 0$$
$$\Sigma F_y = 0$$
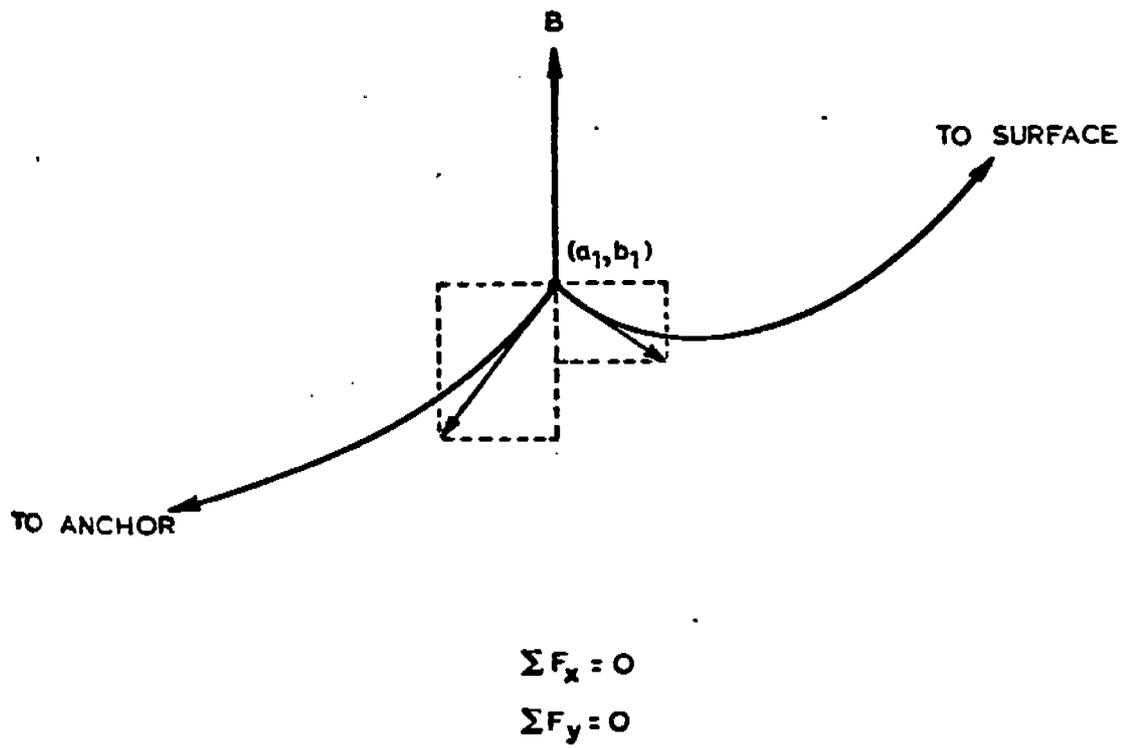
FIGURE 2.28   EQUILIBRIUM CONDITIONS FOR POINT OF INTERSECTION OF TWO LINES
IN CATENARY
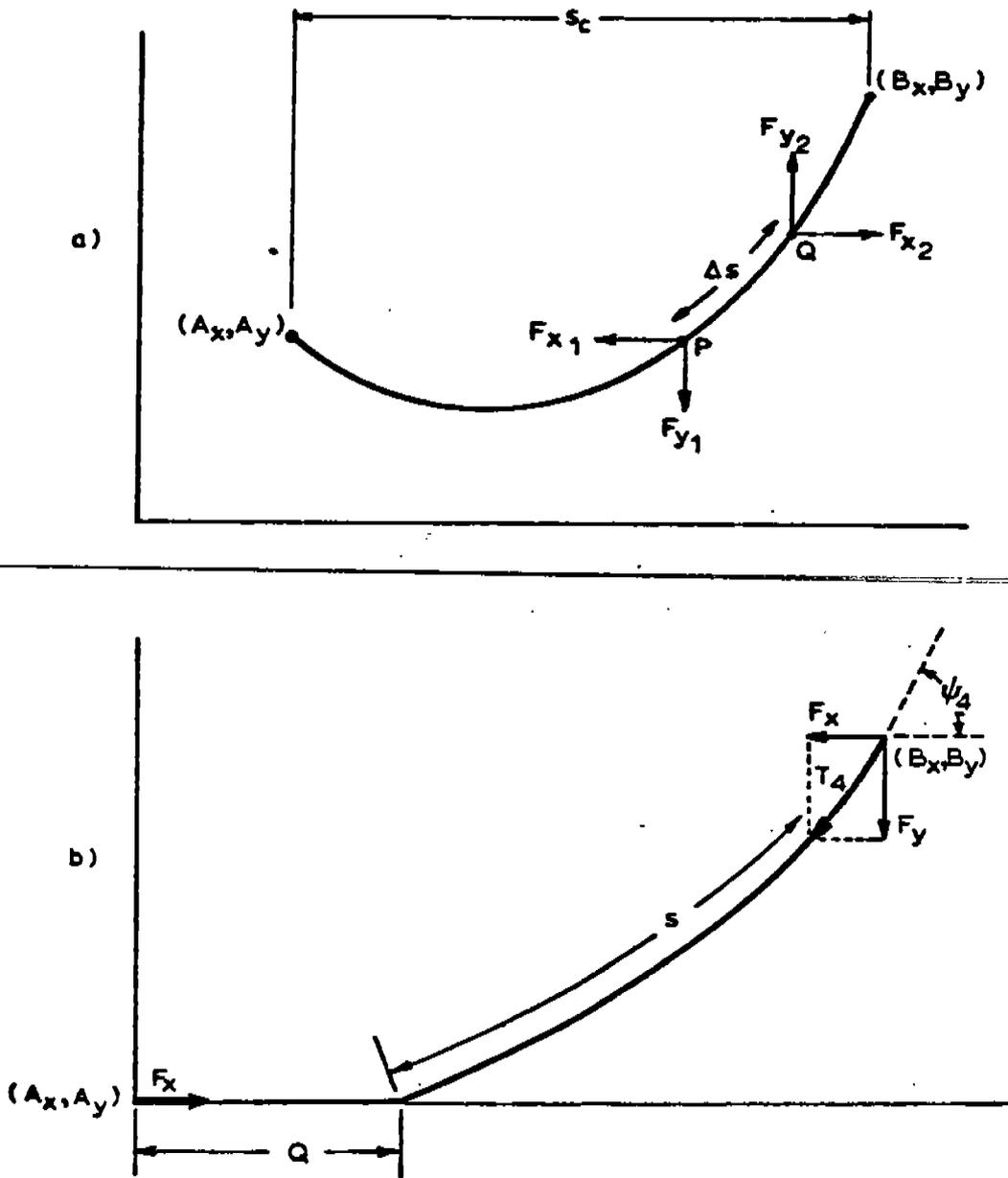
FIGURE 2.29 TWO POSSIBLE CONFIGURATIONS OF A CATENARY

$$p = \frac{dy}{dx} \qquad\qquad (2.105)$$

Thus

$$\frac{dp}{dx} = k \, (1 + p^2)^{1/2} \qquad\qquad (2.106)$$

The form of the solution of Eq. 2.103 is

$$y = \frac{1}{k} \cosh (kx + C_1) + C_2 \qquad\qquad (2.107)$$

Equation 2.107 must be solved in terms of boundary conditions. Since there are three unknowns, k, C_1, and C_2, there must be three boundary conditions. In this development these are line length, ℓ; scope, $s_c = B_x - A_x$; and elevation, $e = B_y - A_y$. Using these boundary conditions the following equation can be derived:

$$\frac{[\ell^2 - e^2]}{s_c^2} = (\frac{\sinh u}{u})^2 \qquad\qquad (2.108)$$

where $u = \frac{ks}{2}$.

Equation 2.108 is solved by a computer program using standard numerical technique such as the Newton Rhapson method. When u is known, C_1 and C_2 can be derived from Eq. 2.107.

The above analysis gives the classical catenary solution. It will depart, however, from the classical theory if stretch is added to the analysis. Throughout the line, the horizontal component of tension is constant. The vertical component is constantly changing as the slope of the line changes. Thus, the tension in the line is a function of position which will change with the stretch in the line. It is assumed that the stretch can be added to the initial line length and the weight per unit length can be modified uniformly which is considered a valid assumption.

Employing Hooke's law for elastic deformation

$$d\delta = \frac{F_x ds}{AE} \qquad\qquad (2.109)$$

43

where $d\delta$ = incremental deformation; F_x = load; ds = incremental length, A = cross-sectional area of cable; and E = Young's modulus.

On substitution of various quantities on the right hand side, the form of δ becomes

$$\delta = \frac{F_x}{AE} \int_{A_x}^{B_x} \frac{1}{2} [1 + \cosh 2(kx + C_1)] \, dx \qquad (2.110)$$

After δ is determined from Eq. 2.110 it is added to the initial line length and a new line length, ℓ, is used in Eq. 2.108. This procedure is repeated until the tension in the line balances the stretch in the line.

Turning to the situation described in Fig. 2.29b, part of the mooring line now lies on the seafloor. For simplicity, assume that $\{A_x, A_y\}$ = $\{Q, 0\}$. At this point, the slope of the line is zero; therefore, Eq. 2.107 can be rewritten in the form

$$y = 1/k \cosh k(x - Q) - 1/k \qquad (2.111)$$

The length s is determined such that

$$s = 1/k \sinh k(B_x - Q) \qquad (2.112)$$

and

$$\ell = Q + s \qquad (2.113)$$

Upon substitution of the coordinates of the surface vessel $\{B_x, B_y\}$ into Eq. 2.111, two simultaneous equations with two unknowns are derived.

$$B_y = 1/k \cosh k(B_x - Q) - 1/k \qquad (2.114)$$

$$\ell = Q + 1/k \sinh k(B_x - Q) \qquad (2.115)$$

Upon solution of this set of simultaneous equations for k and Q, C_1 and C_2 can be easily derived and the catenary equation defined. Stretch may then be added to the line in a fashion similar to the prior situation with the slight change that no integration is required for the line lying on the

44

bottom. In this part of the line, the tension is constant and equal to $F_x = w/k$. Therefore,

$$\delta_1 = \frac{F_x Q}{AE} \tag{2.116}$$

$$\delta_2 = \frac{F_x}{AE} \int_Q^{B_x} \frac{1}{2} [1 + \cosh 2(kx + C_1)] dx \tag{2.117}$$

and the total stretch, δ, equals

$$\delta = \delta_1 + \delta_2 \tag{2.118}$$

This total stretch is added to the initial line length and a new line length, ℓ, is substituted into the pair of simultaneous equations. This process is repeated until convergence is achieved.

It is clear from the above analysis that this type of system will produce a nonlinear spring constant in the mooring line, making the motion analysis of a floating moored system nonlinear. Such a system is quite prevalent in offshore operations. Examples of application of such systems are moored storage tankers, pipelay barges, single point mooring systems, floating production systems, and guyed towers.

A typically moored tanker system with catenary chains is shown in Fig. 2.30 where four chains have been used on a turntable. Figure 2.31 gives an example of the load-elongation characteristic of the catenary chain model used in a wave tank model test. The solid line is the theoretical curve obtained from the above equations while the symbols represent actual data obtained from the simulation of the catenary in the test setup.

2.9.2 Flexible Structures

The material stiffness of the components of a flexible structure contributes to the dynamic characteristics of the structure. The application of such an element in the marine field may be seen in the marine risers, OTEC cold-water pipes, and members or conductors in a production platform. Various end conditions for a flexible member are possible, e.g., fixed-fixed, fixed-free, pinned-free, etc. The basic horizontal equation of motion of such a

45
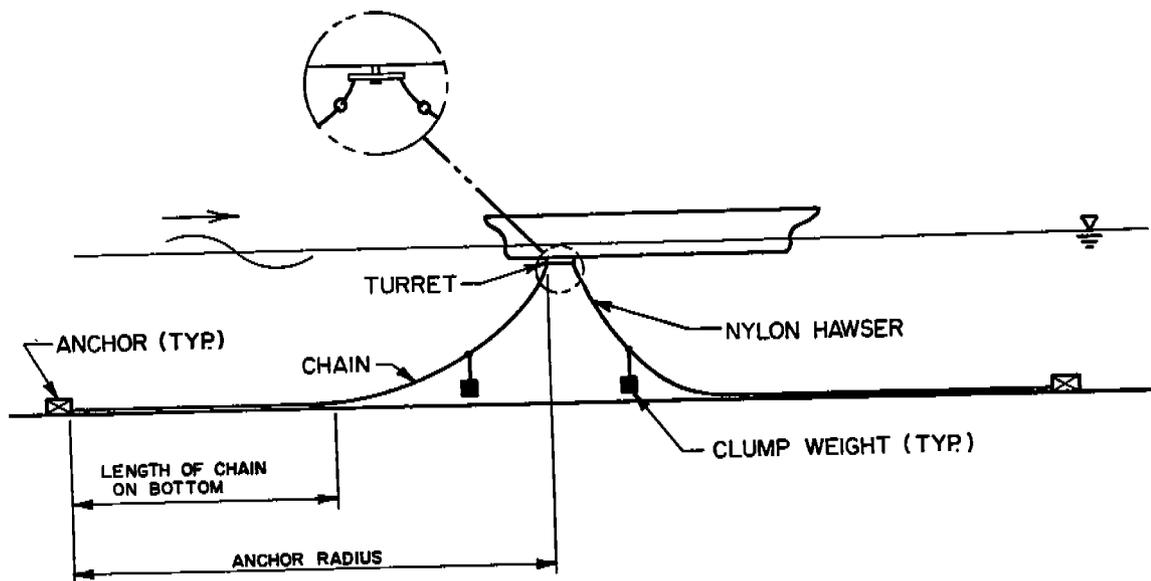
FIGURE 2.30 TYPICAL SETUP OF A SHALLOW WATER TURRET MOORING SYSTEM
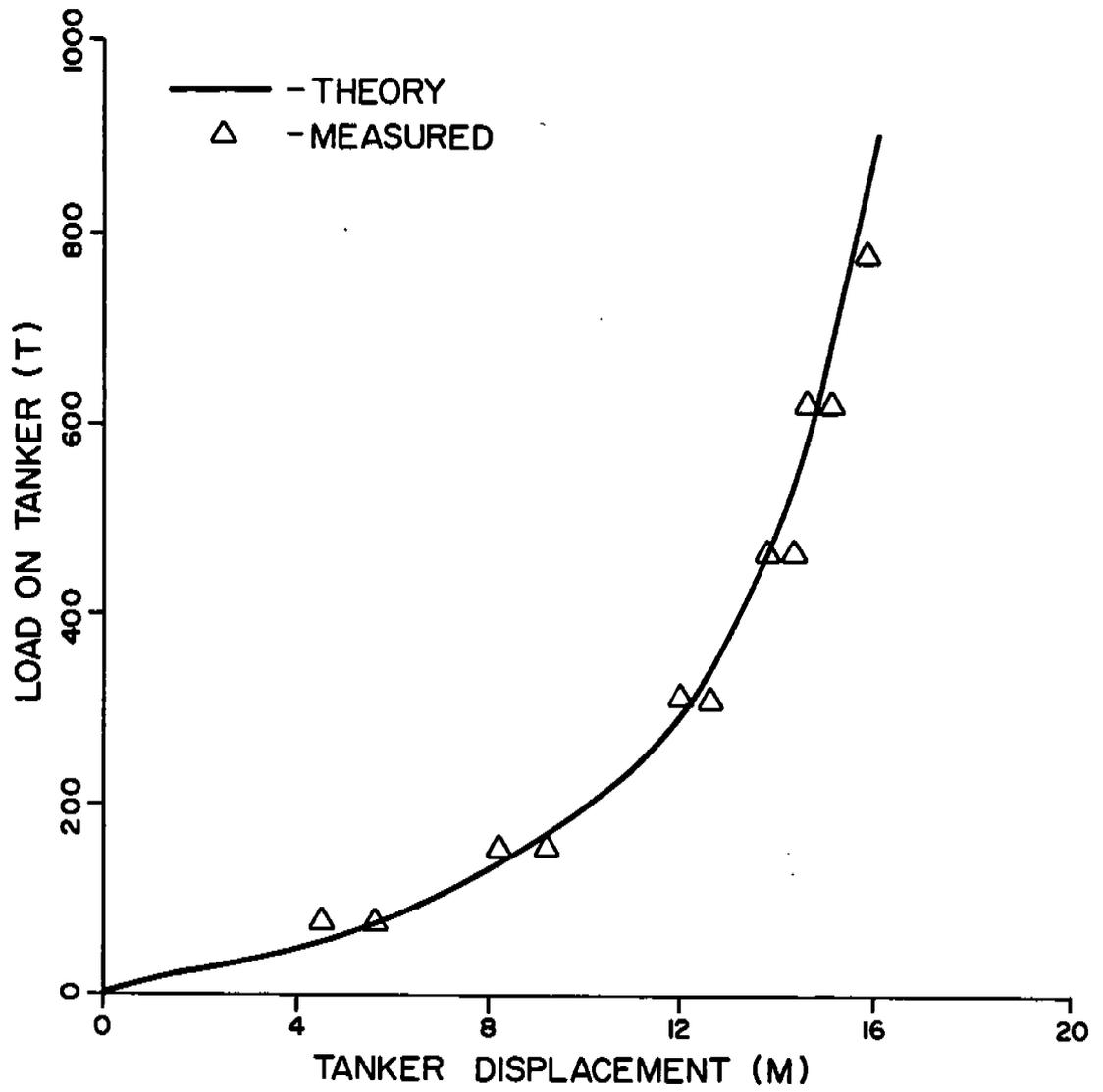
FIGURE 2.31 LOAD-ELONGATION CURVE OF A CATENARY SYSTEM ATTACHED TO A TANKER

flexible cylindrical member including its internal forces, surface and body forces may be written in the x-y coordinate system as

$$\frac{\partial^2}{\partial y^2} \left[EI(y) \frac{\partial^2 x}{\partial y^2} \right] - T_e(y) \frac{\partial^2 x}{\partial y^2} - w(y) \frac{\partial x}{\partial y} + m_x(y) \frac{\partial^2 x}{\partial t^2} = f(y,t) \qquad (2.119)$$

The first term on the left hand side in Eq. 2.119 is the horizontal reaction from the flexural rigidity, the second and third terms arise from the effective tension, T_e, and buoyant weight, w, respectively. The final term is the inertia of the riser accelerating in the horizontal direction. The right hand term represents the external forcing function.

For static riser problems, the value of the last term is zero and the right hand side of Eq. 2.119 is replaced by the time independent drag term due to a constant current profile as

$$f(y) = \frac{1}{2} \rho C_D(y) D(y) U^2(y) \qquad (2.120)$$

where ρ = mass density of water, C_D = drag coefficient and $U(y)$ = horizontal current velocity as a function of the vertical coordinate, y.

For a dynamic riser analysis, the right-hand side of Eq. 2.119 may include the wave inertia and drag forces. In this case, the right hand side is given as a forcing function, $f(y,t)$ which may be expressed by the modified Morison equation (including relative velocity, e.g., Eq. 2.35). An added mass effect from Eq. 2.35 is included in the last term of the left hand side of Eq. 2.119.

The solution of Eq. 2.119 for the static or dynamic case requires additional constraints or boundary conditions, e.g., deflection and rotation at the two ends or the top horizontal offset for a marine riser. The solutions are achieved in one of several available numerical techniques, e.g., direct or indirect finite difference or finite element methods. A frequency domain analysis is possible only after the linearization of all the nonlinear terms, and may not be suitable in many riser applications.

3.0 PROBABILISTIC METHODS FOR EXTREME VALUES

The design and performance of an offshore structure depends largely upon the response of the structure to the environmental loading such as waves. The response analyses outlined in Chapter 2 are generally applicable to regular waves. However, the extreme responses of a structure in random ocean waves should be known for the adequate design of the offshore structure. The extreme response chosen for the design of a structure should meet, as a minimum, the following criteria:

- **LIFETIME RESPONSE**
  The expected maximum response during its lifetime should be known to ensure the integrity of the structure.

- **OPERATIONAL RESPONSE**
  The responses of the structure under its normal operating conditions must be known to ensure the intended operability of the structure.

- **FATIGUE DAMAGE**
  The accumulated responses of the structure during its entire lifetime must be known to assess the cumulative damage of the structure over this period.

The design criterion of a structure is governed by the failure of its structural members due to the environment it is exposed to during its lifetime. This failure may be caused by the maximum instantaneous stress experienced by the member due to a given environment. Alternatively, it may fail due to fatigue damage resulting from an accumulated number of cycles at varying stress levels. Thus, the design value should be an upper bound to these quantities.

The primary concern of this report is to discuss available computational methods of the extreme event due to the environmental loading. The design of an offshore structure is based on either a deterministic or a probabilistic approach. In a deterministic method, the response analyses described in Chapter 2 for a given wave and wave theory may be applied. The probabilistic method of design may include a short-term prediction or a long-term

prediction. The short-term response statistics are obtained on the basis of one particular seastate. This seastate is specified by an energy spectral model having a given significant wave height and a characteristic period. On the other hand, the long-term prediction method includes all seastates which the structure is expected to encounter during its design lifetime.

For fixed structures, for example, steel piled and concrete gravity structures, a deterministic method of extreme value prediction is normally used. However, in fatigue assessment, a long term probabilistic method is often used for these cases. For an extreme value analysis of floating structures, a probabilistic method is common, but only for the short-term seas. The operational mode of floating structures is generally analyzed on the basis of long-term prediction.

A short-coming of the deterministic and probabilistic extreme value predictions based on short-term statistics is in the choice of the environment. It is not always obvious which set of environmental conditions will produce the largest responses. On the other hand, the long-term environmental data over the entire service life of a structure, e.g., in the form of a wave scatter diagram is scarce. Therefore, the reliability of the choice of long term data on which the responses are based may be questionable. The extrapolation of a few (typically, 2-5) years' direct measurements of data to the structure's lifetime and beyond introduces uncertainties in the subjective evaluation. Sometimes, hindcast methods are used to obtain similar information.

For Gaussian response processes, the probability of system failure may be related to the excitation process statistics. This relationship is well established and straight-forward to perform. Unfortunately, however, small nonlinearities are invariably present in the response of a real system. This nonlinearity, however small, may cause significant departures of the response characteristics from the Gaussian form in the extreme "tails" of the response distributions. Since the extreme responses are derived from the tail end of the response distribution, such derivations have a very profound effect on the probability of the system failure. It is thus of vital importance to develop methods of predicting the distribution of the response in the nonlinear case. The general nonlinear problem is largely unsolved. Some limited information on the response characteristics may be obtained from the

perturbation methods and equivalent linearization techniques. Distribution functions of some nonlinear problems may be obtained by the series method in probability theory.

Tickell (1978) presented a review of the state-of-the-art on the probabilistic approach to the problem of fluid loading on an offshore structure. Linear random wave theory is generally used to describe the water particle kinematics. While it represents a versatile model for the random sea, it has certain limitations. For example, the spectra of the particle kinematics and their derivatives become increasingly large at the high frequencies (tail end of the spectra) where wave energy is generally small. This is particularly enhanced in the free surface zone. The higher moments of the spectra, m_n, which depend on the nth power of frequency, likewise "blow up" due to this divergence of spectra at the high frequencies. These moments are often needed for the computation of the distribution functions. Moreover, the linear process of describing a surface cannot account for the vertical or horizontal asymmetry seen in steep storm waves.

For a particular seastate characterized by the random wave parameters, H_s, T_z and θ_0, where H_s = significant wave height, T_z = zero-crossing period and θ_0 = angle of mean wave direction, the short term response of the structure may be obtained by the spectral and probabilistic techniques. For a linear system, this procedure is straight forward. In this case, since the waves are assumed to be a stationary Gaussian random process, so will be the responses for which all the statistical properties are known. Thus, the spectral analysis technique may be used to determine the statistics of the linear system. For structures whose responses are linear with respect to the excitation force, once the force distribution function is known, the probability distributions of response normalized with respect to standard deviation will have the same form.

The prediction of the effect of nonlinearities either due to the environmental loading or due to nonlinear structural behavior for an offshore structure in random seas is not straightforward and a general procedure is not known. For a linear system subject to Gaussian excitation, the response is also Gaussian. However, if the system contains nonlinear elements, the response will no longer be Gaussian. In this case, the solutions for the probabilistic responses may be obtained only in special types of

nonlinearities. Often approximations are necessary before a probabilistic theory may be applied to the nonlinear responses. One of the methods of prediction is the nonlinear transformation of random variables.

3.1 SOME COMMON TYPES OF PROBABILITY DISTRIBUTION FUNCTIONS

The probability density function (pdf) henceforth denoted by p, is defined as the fraction of a designated period of time that a particular event is expected to occur. The probability distribution or the cumulative distribution function (CDF), denoted by P, is the fraction of the time period that this event is not exceeded. The probability of exceedance, denoted by Q, is the fraction of time the event is exceeded. Thus, P is related to Q by the relation, $Q = 1 - P$.

3.1.1 Normal or Gaussian Distribution

The probability density of a normal or Guassian distribution of a random variable, x, is given by

$$p(x) = \frac{1}{\sqrt{2\pi}\ \sigma_x} \exp \left[- \frac{(x - \mu_x)^2}{2\sigma_x^2} \right] \tag{3.1}$$

where μ_x is the mean value of x, and σ_x is its standard deviation. This formula applies to the entire range of x from $-\infty$ to $+\infty$. From Eq. 3.1, it is clear that $p(x)$ is symmetric about the mean value of x and has a maximum at μ_x. It drops off fast in the shape of a bell. The value of σ_x determines the width of the bell. If Eq. 3.1 is integrated between $\pm\sigma_x$ about μ_x, it will give a value of about 0.68. Thus a range of $\pm\sigma_x$ about the center of the bell-shaped curve contains 68 percent of the area of population, a $\pm2\sigma_x$ covers 95 percent while a $\pm3\sigma_x$ gives 99.7 percent of a normal population.

The expression for the cumulative probability, P, is not known in closed form, and the values of P are obtained from Eq. 3.1 by integration

$$P(x) = \int_{-\infty}^{x} p(x)\ dx \tag{3.2}$$

The plots of the probability density, p, and the probability distribution function, P, for a zero mean ($\mu_x = 0$) and unit variance (σ_x) are shown in Fig. 3.1. The shaded area in the density curve is represented by the value of the cumulative probability, P, on the distribution curve.

If the variable x is transformed to a quantity z by

$$z = \frac{x - \mu_x}{\sigma_x} \qquad (3.3)$$

then this transformation is called normalization and z is called the "standard" normal distribution, because it has a zero mean ($\mu_z = 0$) and standard deviation of unity ($\sigma_z = 1$). The symbols that are commonly used to represent the probability density and cumulative probability of the standard normal are $\phi(z)$ and $\Phi(z)$ respectively, which are given by

$$\phi(z) = \frac{1}{\sqrt{2\pi}} e^{-z^2/2} \qquad (3.4)$$

and

$$\Phi(z) = \int_{-\infty}^{z} \phi(z) \, dz \qquad (3.5)$$

The values of $\Phi(z)$ are tabulated in many textbooks on mathematical statistics [e.g., Tobias and Trindade (1986)].

3.1.2 Rayleigh Distribution

Unlike the Gaussian distribution, the Rayleigh distribution applies to a random variable, x, which is always positive $(0 < x < \infty)$. The probability density function for the Rayleigh distribution is given in terms of the mean value of x, μ_x, as

$$p(x) = \frac{\pi x}{2\mu_x^2} \exp \left[-\frac{\pi}{4} \left(\frac{x}{\mu_x} \right)^2 \right] \qquad (3.6)$$

This function may be integrated in a closed form using Eq. 3.2 to obtain the expression for P(x).

51
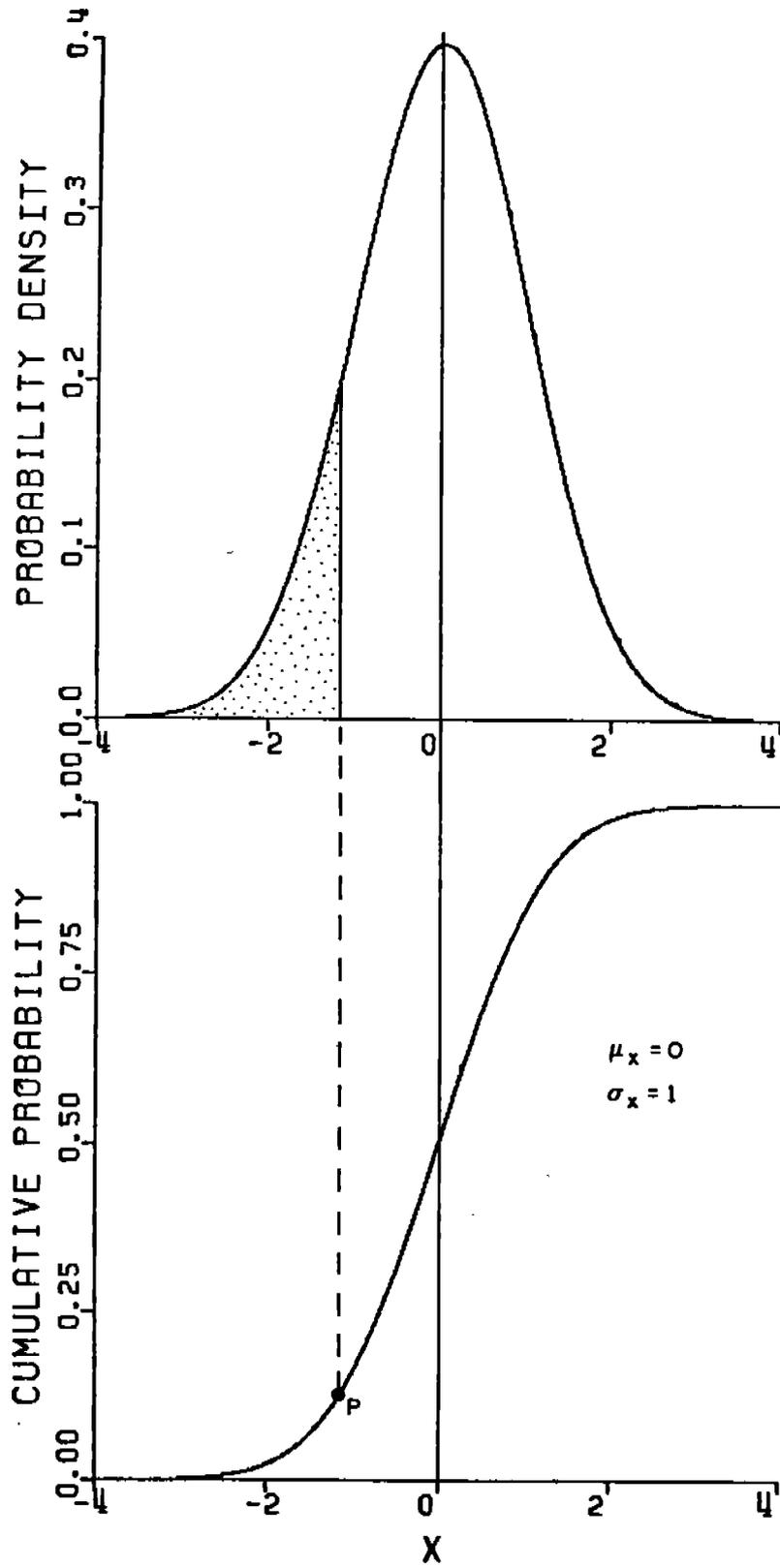
FIGURE 3.1 GAUSSIAN PROBABILITY DENSITY AND DISTRIBUTION FUNCTION
(MEAN = 0.0; VARIANCE = 1.0)

$$P(x) = 1 - \exp\left[-\frac{\pi}{4} \left(\frac{x}{\mu_x} \right)^2 \right] \tag{3.7}$$

The probability density and the cumulative probability of Rayleigh distribution are shown in Fig 3.2. The mean value of x in these plots is taken as one (μ_x = 1). In other words, the plots represent the independent variable as normalized with respect to μ_x.

3.1.3 Gumbel Distribution

The Gumbel distribution is given by the formula

$$P(x) = \exp\left[-\exp\{ -\alpha(x - \beta) \} \right] \tag{3.8}$$

This first asymptotic (Type I) distribution is not bounded and grows without limit, albeit in a logarithmic scale. A reduced variate is introduced as

$$y = \alpha(x - \beta) \tag{3.9}$$

The quantities α and β are the slope and the mode defined as

$$\alpha = E(\sigma_N)/\sigma_N \tag{3.10}$$

and

$$\beta = \overline{x}_N - E(y_N)/\alpha \tag{3.11}$$

where $E(\sigma_N)$ and $E(y_N)$ are the expected value of the dispersion of N values and the expected value of the reduced variate, respectively, σ_N is the standard deviation, and $\overline{x}_N$ is the mean of the variables, x_i (i = 1, 2, . . . N). The Gumbel distribution for a slope, α = 1, and mode, β = 3, is plotted in Fig. 3.3.

The reduced variate is related to the probability value as

$$y = -\ln\left[-\ln P \right] \tag{3.12}$$

obtained from the formula given in Eq. 3.24.
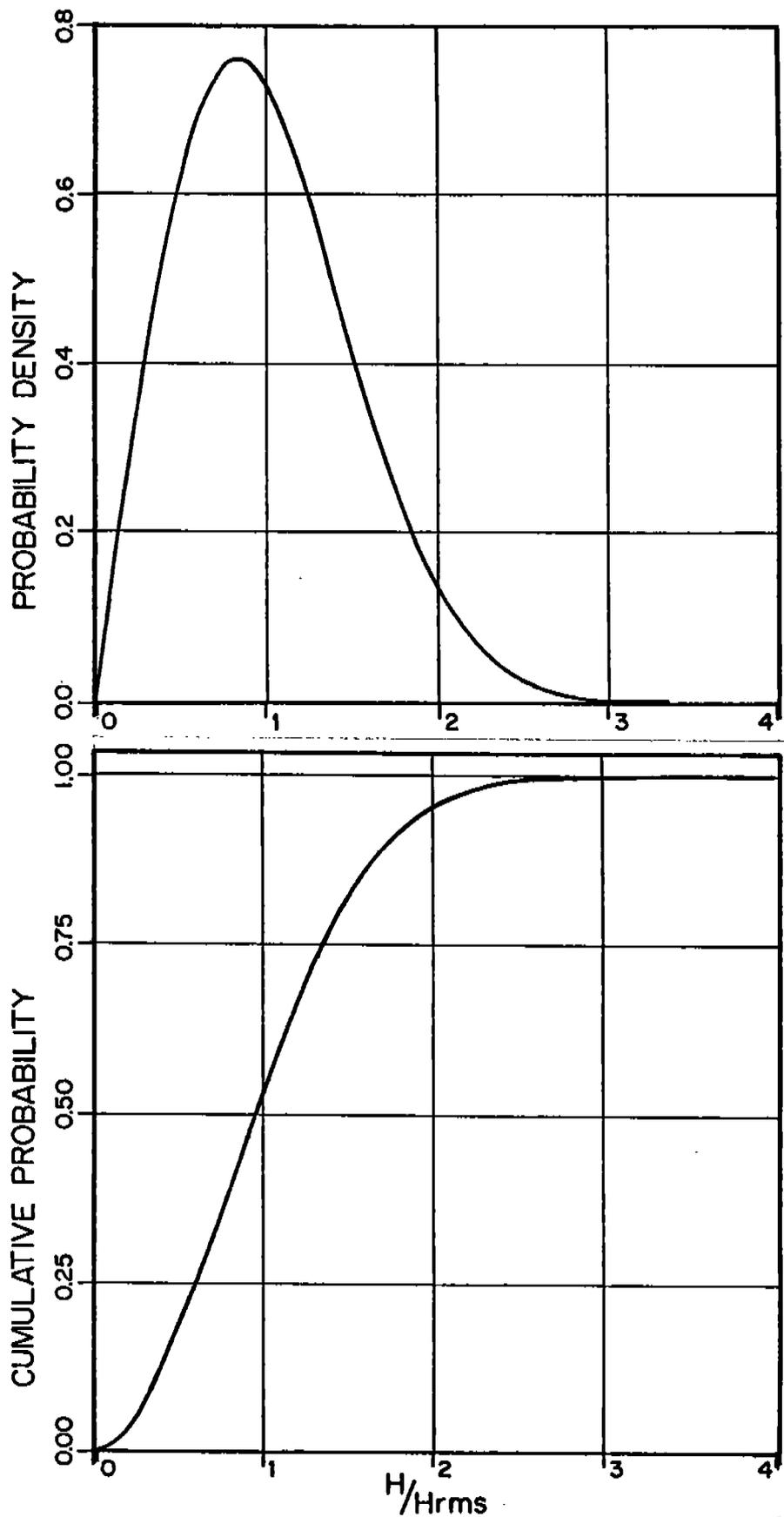
FIGURE 3.2 RAYLEIGH PROBABILITY DENSITY AND DISTRIBUTION FUNCTION (MEAN = 1.0)
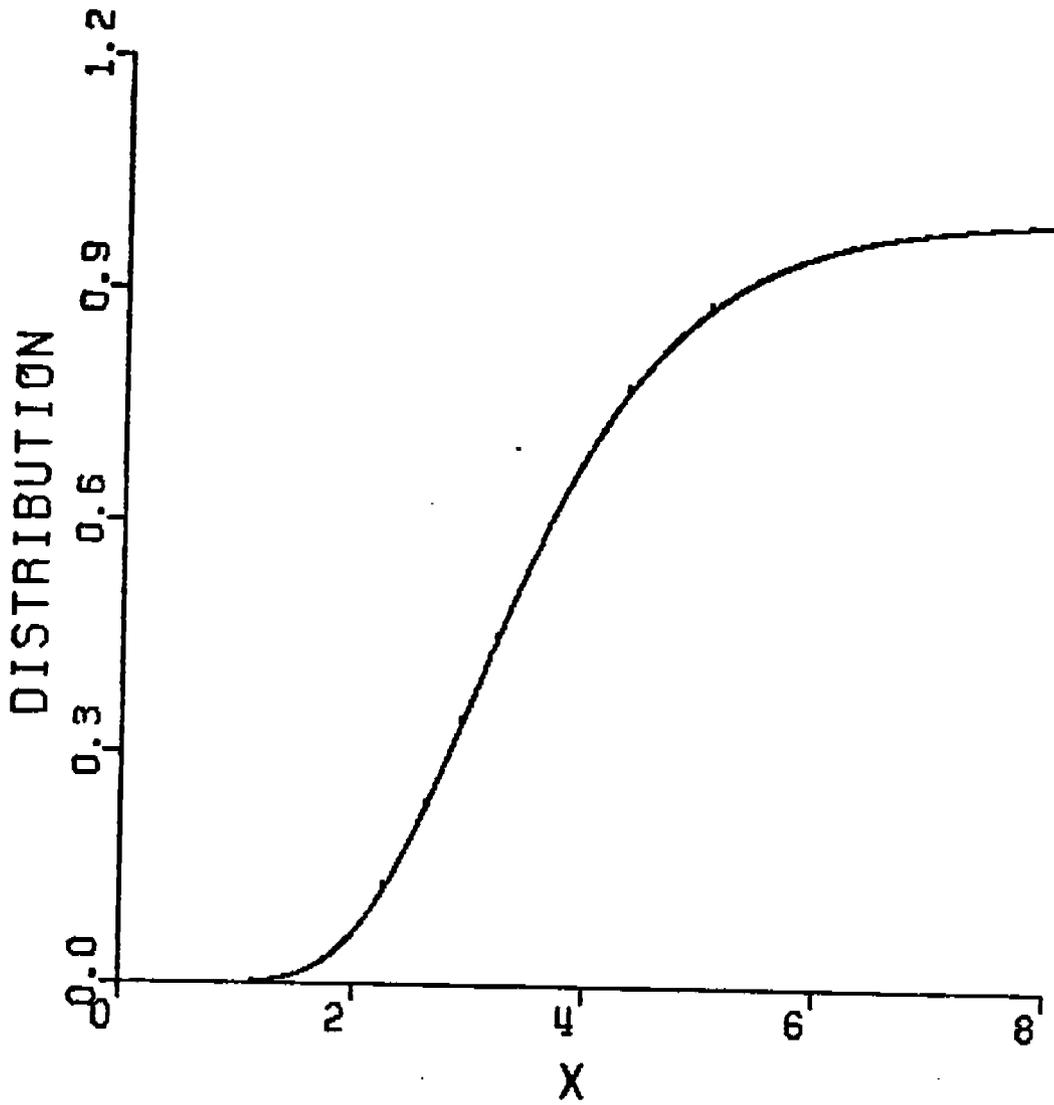
FIGURE 3.3   GUMBEL DISTRIBUTION FOR SLOPE, α = 1, AND MODE, β = 3

The expected values $E(\sigma)$ and $E(y)$ are functions of the total number of observations. Their asymptotic values for an infinite number of observations are

$$E(\sigma) = \pi/\sqrt{6} \qquad (3.13)$$

and

$$E(y) = 0.5772 \qquad (3.14)$$

which may be used for large but finite number of observations. The curve for the extreme values is then given by

$$\begin{aligned} x &= \beta + y/\alpha \\ &= \bar{x}_N + \sigma_N \sqrt{6/\pi} \,(y - 0.5772) \end{aligned} \qquad (3.15)$$

3.1.4 Weibull Distribution

The Weibull distribution function is given as

$$P(x) = 1 - \exp\left[-\left(\frac{x-B}{A}\right)^k\right] \qquad (3.16)$$

The quantity k is called the shape parameter and is generally assigned a value between 0.75 and 2.0. The parameters A and B are determined from observed data by the least-square method.

An alternate form of the Weibull distribution is given by

$$P(x) = 1 - \exp\left[-B\,x^m\right] \qquad (3.17)$$

The probability density is obtained by differentiating the above equation with respect to the variable, x

$$p(x) = m\,B\,x^{m-1} \exp\left[-B\,x^m\right] \qquad (3.18)$$

If Eq. 3.17 is rearranged, it may be written as a linear equation

$$\ln\left[\ln\frac{1}{1-P}\right] = \ln B + m \ln x \qquad (3.19)$$

where ln B is the intercept and m is the slope. The values of B and m may be determined by fitting data.

The Weibull cumulative probability distribution for wave height may be written as

$$p(H) = 1 - e^{-A\left(\frac{H}{H_{rms}}\right)^m} \tag{3.20}$$

where A and m are constants. The probability density function is written as

$$p(H) = Am\left(\frac{H}{H_{rms}}\right)^m H^{-1} e^{-A\left(\frac{H}{H_{rms}}\right)^m} \tag{3.21}$$

Taking the logarithm twice and rearranging terms

$$\ln \ln \frac{1}{1 - P(H)} = \ln A + m \ln \frac{H}{H_{rms}} \tag{3.22}$$

which is the equation of a straight line of intercept ln A and slope m. The parameters A and m are determined by the empirical fitting of data. For A = 1 and m = 2, the expressions reduce to the Rayleigh distribution.

3.1.5 Frechet Distribution

A distribution function of the Frechet type was proposed by Thom (1973) for annual maxima of extreme wave heights

$$P(x) = \exp\left[-\left(\frac{x}{A}\right)^{-k}\right] \tag{3.23}$$

This equation may be written as a linear equation

$$\ln[-\ln P] = -k \ln x + k \ln A \tag{3.24}$$

in which -k is the slope and klnA is the intercept of the line. An example of the Frechet distribution for a slope of 2 and an intercept of 1 is shown in Fig. 3.4. The probability density is obtained as

54
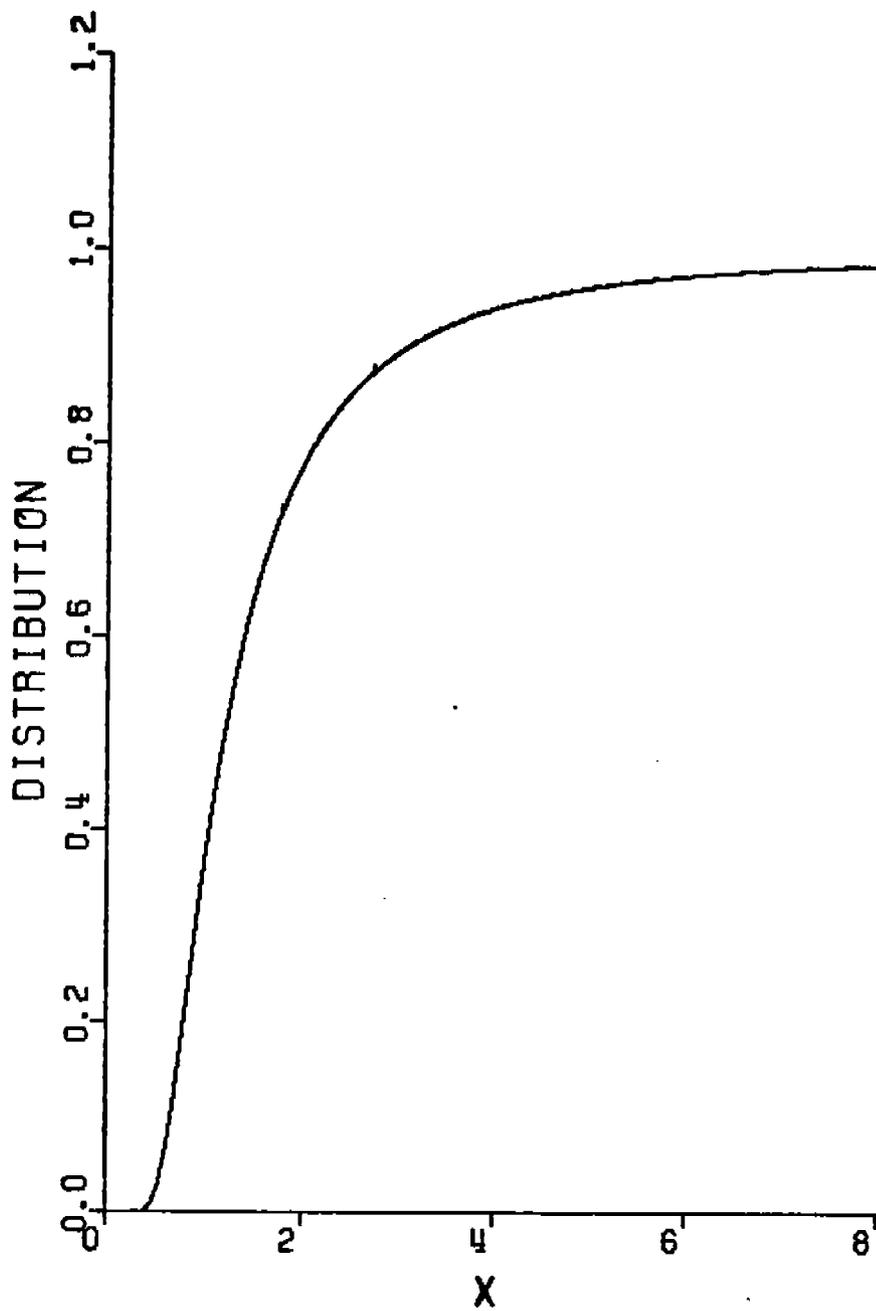
FIGURE 3.4   FRECHET DISTRIBUTION FOR A SLOPE OF 2 AND AN INTERCEPT OF 1
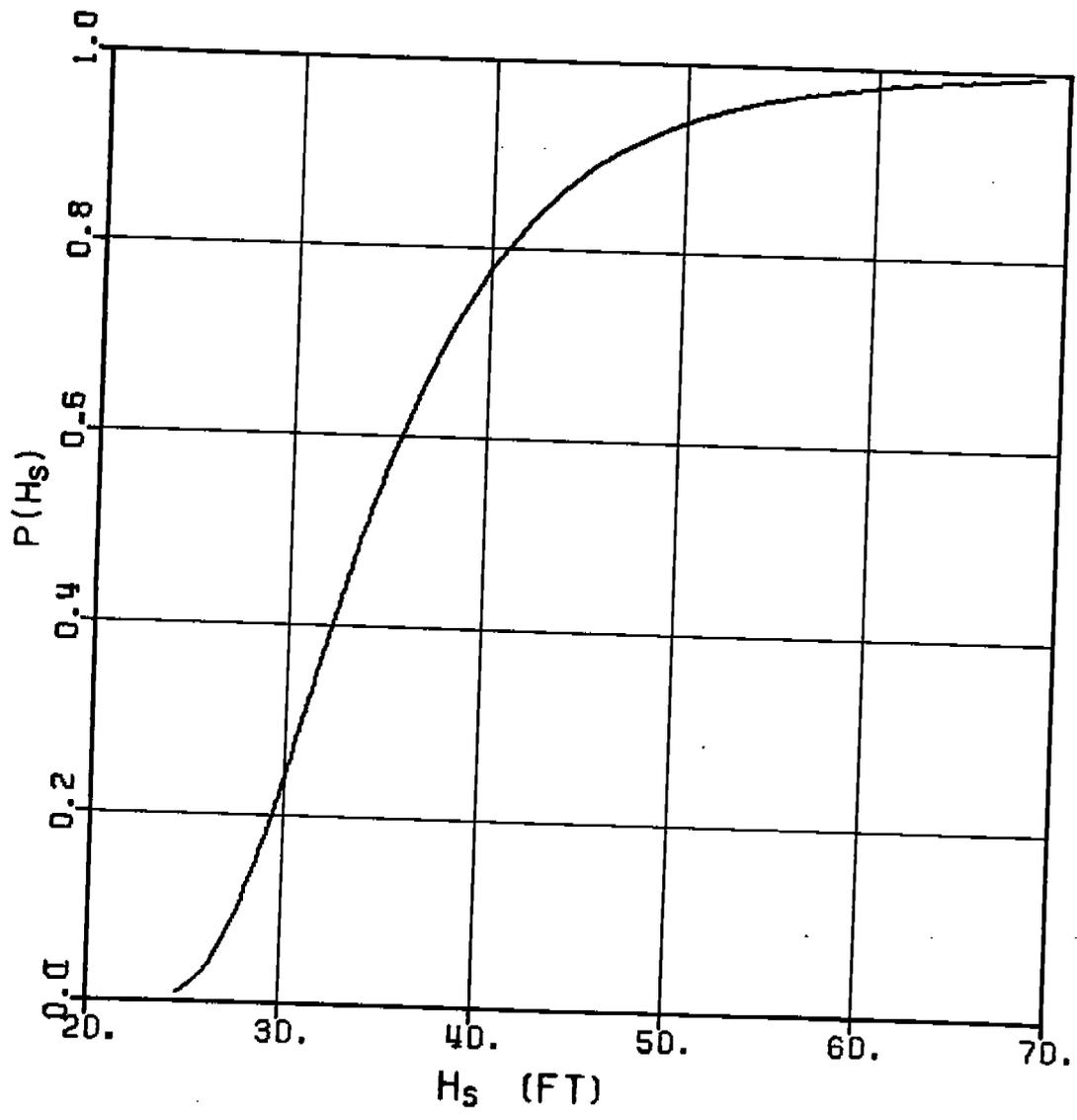
FIGURE 3.5   PROBABILITY DISTRIBUTION OF SIGNIFICANT WAVE HEIGHT, H_s, FOR
               EXAMPLE PROBLEM

$$p(x) = \frac{k}{A} \left(\frac{x}{A} \right)^{-k-1} \exp \left[- \left(\frac{x}{A} \right)^{-k} \right] \tag{3.25}$$

This type of Frechet distribution is known as Fisher-Tippett Type II distribution. The Type II distribution is related to the Type I (Gumbel) distribution by an exponential transformation. Thus, ln P will provide a Type I distribution. The parameters for the Type I distribution are simpler and more efficient to compute, from which the Type II parameters may be obtained by a transformation.

Analyzing the significant wave height data from Ocean Station Vessel (OSV), Thom (1973) obtained the significant wave height distribution function as

$$P(H_s) = \exp \left[- \left(\frac{H_s}{b_s} \right)^{-6.0} \right] \tag{3.26}$$

in which the scale parameter of the wave distribution is related to the scale parameter of the wind distribution by

$$b_s = 0.455 \ b_v \tag{3.27}$$

where b_s is in feet of wave height and b_v is in mph of wind velocity. The scale of wind is obtained from OSV data as

$$b_v = [373.8 \ \overline{U}_{max} + 542.4]^{1/2} - 23.3 \tag{3.28}$$

in which $\overline{U}_{max}$ = maximum of the monthly mean wind speed in a year in mph. These values of the wind speed have been charted for all oceans by Thom (1973). The quantile for the significant wave is then obtained as

$$H_s(P) = \exp \left[\ln b_s - \frac{1}{6} \ln \ln \left(\frac{1}{P} \right) \right] \tag{3.29}$$

The extreme waves may be derived from H_s on the assumption of Rayleigh distribution for the short-term waves.

EXAMPLE: For a North Sea location 55N-5E find the maximum wave height for a probability level of 0.98.

The maximum monthly mean wind speed, $\bar{\bar{U}}_{max}$, for the above North Sea location is 19 knots or 21.8 mph (9.8 m/s). This value is obtained from the figures provided by Thom (1973). Then

$$b_v = [373.8 \times 21.8 + 542.4]^{1/2} - 23.3$$
$$= 70 \text{ mph } (31.3 \text{ m/s})$$

Using Eq. 3.27

$$b_s = 0.455 \times 70 = 31.9 \text{ ft. } (9.75 \text{ m})$$

The probability distribution of H_s based on this value of b_s is shown in Fig. 3.5. The significant wave height, H_s, for a probability level of 0.98 is computed from Eq. 3.29

$$H_s(0.98) = \exp \left[\ln 31.9 - \frac{1}{6} \ln \ln \left(\frac{1}{0.98} \right) \right]$$
$$= 61 \text{ ft. } (18.6m)$$
$$H_{max} = 1.8 \times 61 = 110 \text{ ft. } (33.6m)$$

where a factor of 1.8 has been used considering 900-1000 waves in the record to achieve the maximum wave height.

3.1.6 Cumulants and Gram-Charlier Series

The nth cumulant of a random process x is defined as

$$k_n = \frac{1}{i^n} \frac{d^n}{d\theta^n} [\ln M(\theta)] \bigg|_{\theta = 0} \tag{3.30}$$

where $M(\theta)$ is the characteristic function. Note that the probability density function $p(x)$ and $M(\theta)$ are a Fourier transform pair

$$M(\theta) = \frac{1}{2\pi} \int_{-\infty}^{\infty} p(x) e^{i\theta x} dx \tag{3.31}$$

The quantity, k_1, can be shown to be the mean value of x, μ say , while k_2 is the variance, σ^2 say. The importance of the cumulants lies in the fact that the probability density function of a general non-Gaussian random process can be written in the form of a series, the coefficients of which are functions of

the cumulants. One of the common forms of these series is called the Gram-Charlier series given by

$$p(x) = \frac{1}{\sqrt{2\pi}\,\sigma}\, e^{-1/2\, z^2}\, \{\, 1 + \frac{1}{3!}\, (\frac{k_3}{\sigma^3})\, (z^3 - 3z)$$

$$+ \frac{1}{4!}\, (\frac{k_4}{\sigma^4})\, (z^4 - 6z^2 + 3) + \dots\} \qquad (3.32)$$

where

$$z = \frac{x - \mu}{\sigma} \qquad (3.33)$$

Besides k_1 and k_2 defined above, two other quantities of importance are the skewness, defined as $k_3\, /\, _\sigma 3$ and the kurtosis, given as $k_4\, /\, _\sigma 4$. For a Guassian random process

$$k_n = 0 \quad \text{for} \quad n > 2 \qquad (3.34)$$

Thus, for a random process if higher cumulants are evaluated, e.g., k_3 and k_4, they provide a measure of the deviation of the process from the Gaussian process.

3.2 DISTRIBUTION OF SHORT-TERM WAVE PARAMETERS

3.2.1 Wave Elevation Distribution

The sea surface elevation is assumed to follow a Gaussian distribution with a zero mean. Therefore, for the sea surface elevation, η (where μ_η is assumed to be zero)

$$p(\eta) = \frac{1}{\sqrt{2\pi}\,\sigma_\eta}\, e^{-\frac{\eta^2}{2\sigma_\eta^2}} \qquad (3.35)$$

where $\sigma_\eta = \sqrt{m_0}$ and m_0 is the area under the wave energy spectral density curve.

3.2.2 Wave Height Distribution

For a narrow-band Gaussian ocean wave whose components are in random phase uniformly distribution over $\pm\pi$, the wave height follows Rayleigh distribution given by its probability density function,

$$p(H) = \frac{2H}{H^2_{rms}} \exp \left(- \frac{H^2}{H^2_{rms}} \right) \tag{3.36}$$

where H = individual wave heights in a wave record and H_{rms} = root-mean-square wave height.

Based on this distribution the most probable maxima in a given number of waves can be determined. According to Cartwright and Longuet-Higgins (1956) the largest expected value is related to the rms value in terms of the number of zero upcrossings, N, by the formula

$$H_{max} = \sqrt{\ell n\ N} \left(1 + \frac{G}{2\ell n\ N} \right) H_{rms} \tag{3.37}$$

where the Gamma function, G = 0.5772. For example, in 1000 waves the most probable maximum is related to the significant wave height, H_s by

$$H_{max} = 1.86\ H_s$$
where
$$H_s = 1.416\ H_{rms}$$

This constitutes the short-term extreme value prediction for wave heights. If the input waves are assumed to be Rayleigh distributed, then the linear responses may be shown to be Rayleigh distributed as well. In this case the extreme value of the response is computed from this distribution as above. This analysis is called the short-term extreme value analysis for a linear system.

3.2.3 Wide Band Spectrum

The extreme values of a short-term stationary random process having an arbitrary bandwidth spectrum have been predicted by Ochi (1973). The most probable extreme value as well as the extreme value at a prescribed

probability level have been derived, the latter of which was recommended for the design of offshore structures. Selected points on a scalar random process are illustrated in Fig. 3.6. In evaluating the extreme value, it is clear that only the maxima of the random process with positive values (or minima with negative values) need be considered. It should be noted that the presence of several maxima between consecutive zero crossings indicate a broad band spectrum for the random process.

The probability density function of the maxima, x, is given by

$$p(x) = \frac{\left(\frac{2}{\sqrt{m_0}} \right)}{1 + \sqrt{1 - \epsilon^2}} \left[\frac{\epsilon}{\sqrt{2\pi}} \exp \left\{ -\frac{1}{2\epsilon^2} \left(\frac{x}{\sqrt{m_0}} \right)^2 \right\} \right.$$

$$+ \sqrt{1 - \epsilon^2} \left(\frac{x}{\sqrt{m_0}} \right) \exp \left\{ -\frac{1}{2} \left(\frac{x}{\sqrt{m_0}} \right)^2 \right\}$$

$$\left. + \left\{ 1 - \Phi \left(-\frac{\sqrt{1 - \epsilon^2}}{\epsilon} \frac{x}{\sqrt{m_0}} \right) \right\} \right] \qquad 0 < x < \infty \qquad (3.38)$$

in which the spectral moments are given by

$$m_n = \int_0^\infty \omega^n S(\omega) \, d\omega \qquad (3.39)$$

ϵ = spectral width parameter defined as

$$\epsilon^2 = 1 - \frac{m_2^2}{m_0 m_4} \qquad (3.40)$$

and Φ is referred to as the standard normal distribution given by

$$\Phi(u) = \frac{1}{\sqrt{2\pi}} \int_{-\infty}^u e^{-\frac{u^2}{2}} \, du \qquad (3.41)$$

If the variable x is nondimensionalized by dividing by $\sqrt{m_0}$, then the probability density function of

$$\bar{x} = \frac{x}{\sqrt{m_0}} \qquad (3.42)$$
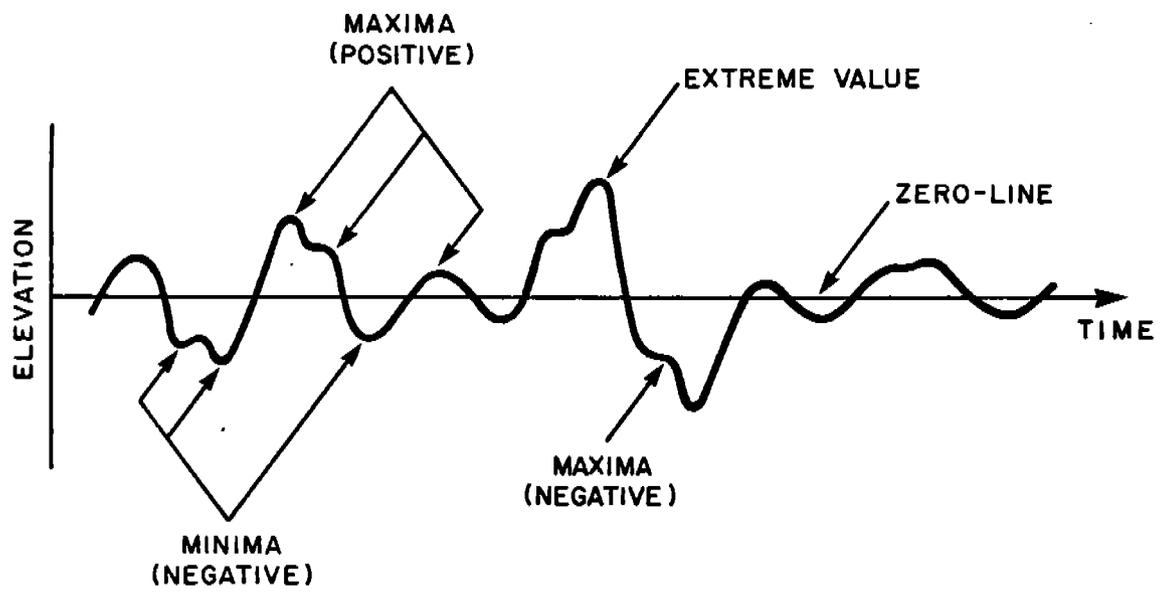
FIGURE 3.6   DEFINITION SKETCH OF A RANDOM PROCESS X(t) [OCHI (1973)]
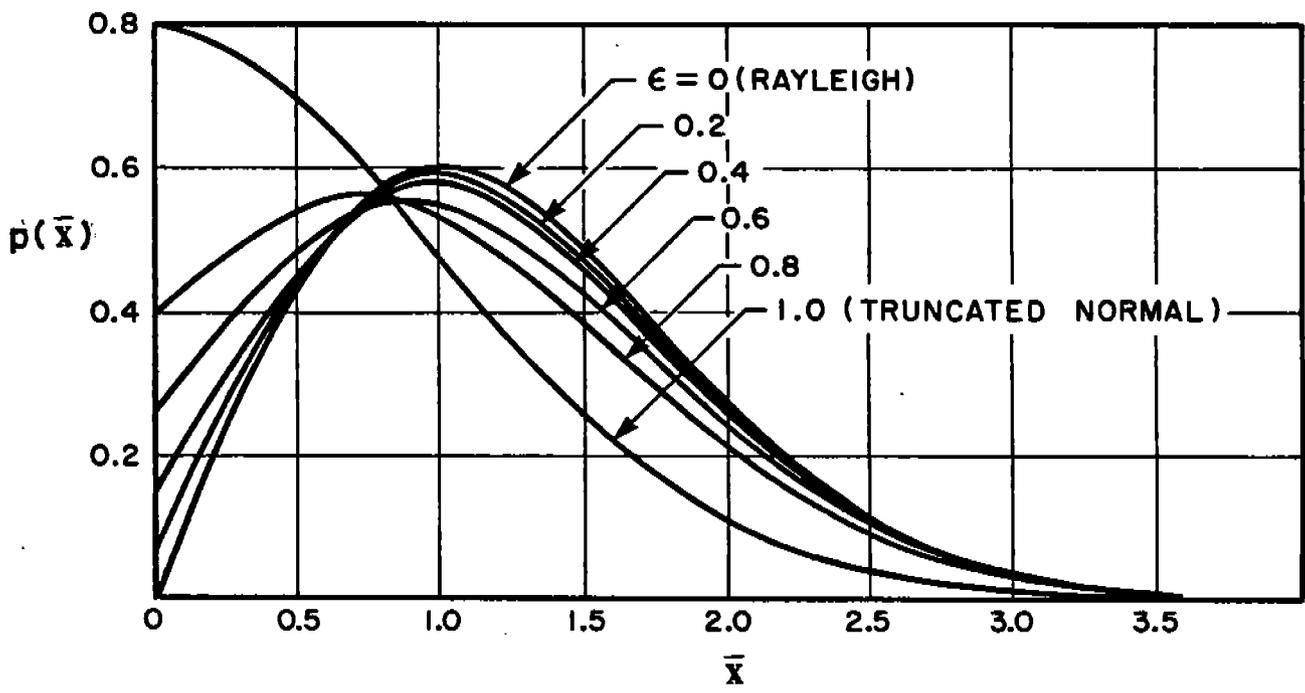
FIGURE 3.7   PROBABILITY   DENSITY   FUNCTION   OF   RANDOM   VARIABLE, $\overline{x}$
$\left(= x/ \sqrt{m_0} \right)$ AS A FUNCTION OF BANDWIDTH PARAMETER [OCHI (1973)]

becomes

$$p(\bar{x}) = \frac{2}{1 + \sqrt{1 - \varepsilon^2}} \left[\frac{\varepsilon}{\sqrt{2\pi}} \exp\left\{ -\frac{\bar{x}^2}{2\varepsilon^2} \right\} + \right.$$

$$\left. \sqrt{1 - \varepsilon^2}\ \bar{x}\ e^{-\frac{\bar{x}^2}{2}} \left\{ 1 - \Phi\left(-\frac{\sqrt{1 - \varepsilon^2}}{\varepsilon} \bar{x} \right) \right\} \right] \qquad 0 < \bar{x} < \infty$$

(3.43)

If the random process is assumed to have a narrow-band spectrum ($\varepsilon = 0$) then Eq. 3.43 reduces to

$$p(\bar{x}) = \bar{x}\ e^{-\frac{\bar{x}^2}{2}} \qquad\qquad 0 < \bar{x} < \infty \qquad (3.44)$$

which is the form of the Rayleigh distribution. Similarly, for a wide-band spectrum ($\varepsilon = 1$),

$$p(\bar{x}) = \sqrt{\frac{2}{\pi}}\ e^{-\frac{\bar{x}^2}{2}} \qquad\qquad\qquad (3.45)$$

which is the truncated (at $\bar{x} = 0$) normal (Gaussian) distribution. Figure 3.7 shows the probability density function for various values of ε.

The cumulative distribution functions of x and $\bar{x}$ are derived by integration as follows:

$$P(x) = \frac{2}{1 + \sqrt{1 - \varepsilon^2}} \left[-\frac{1}{2} \left(1 - \sqrt{1 - \varepsilon^2} \right) + \Phi\left(\frac{x}{\varepsilon \sqrt{m_0}} \right) \right.$$

$$\left. - \sqrt{1 - \varepsilon^2} \exp\left\{ -\frac{1}{2} \left(\frac{x}{\sqrt{m_0}} \right)^2 \right\} \left\{ 1 - \Phi\left(-\frac{\sqrt{1 - \varepsilon^2}}{\varepsilon} \frac{x}{\sqrt{m_0}} \right) \right\} \right]$$

(3.46)

and

$$P(\bar{x}) = \frac{2}{1 + \sqrt{1 - \varepsilon^2}} \left[-\frac{1}{2} \left(1 - \sqrt{1 - \varepsilon^2} \right) + \Phi\left(\frac{\bar{x}}{\varepsilon} \right) \right.$$

$$\left. - \sqrt{1 - \varepsilon^2} \exp\left\{ -\frac{\bar{x}^2}{2} \right\} \left\{ 1 - \Phi\left(-\frac{\sqrt{1 - \varepsilon^2}}{\varepsilon} \bar{x} \right) \right\} \right] \qquad (3.47)$$

60

In order to derive extreme values, let us consider that there are N observations of the type of Fig. 3.6. Let $\overline{x}_i$ be the observed maxima of these N records in nondimensional form. We first arrange $\overline{x}_i$ in ascending order of values ζ_i. Let α be a small probability level that ζ_N be exceeded. Then for $\varepsilon < 0.9$, a simple formula for the extreme value may be obtained as

$$\hat{\zeta}_N = \left[\; 2 \ln \left(\frac{\sqrt{1 - \varepsilon^2}}{1 + \sqrt{1 - \varepsilon^2}} \; \frac{2N}{\alpha} \right) \right]^{1/2} \qquad \text{for } \varepsilon < 0.9 \qquad (3.48)$$

This formula is valid when α is small, on the order of 0.10 or less. For $\varepsilon = 0$ (narrow band process)

$$\hat{\zeta}_N = \sqrt{2 \ln \frac{N}{\alpha}} \qquad\qquad (3.49)$$

Figure 3.8 shows the relationship in Eq. 3.48 for various values of ε when $\alpha = 0.01$. Note that the dimensional values, x_N, may be obtained by multiplying by $\sqrt{m_0}$. It is interesting to compare the extreme value for the narrow-band spectrum with the corresponding most probable extreme value, $\overline{\zeta}_N$.

$$\overline{\zeta}_N = \sqrt{2 \ln N} \qquad \text{for } \varepsilon = 0 \qquad\qquad (3.50)$$

Thus for small α, $\hat{\zeta}_N$ is considerably larger. This should be expected because for a large value of N, the probability of exceeding $\overline{\zeta}_N$ may be shown to be quite high

$$\lim_{N \to \infty} P \left[\; \hat{\zeta}_N > \overline{\zeta}_N \; \right] = 1 - e^{-1} = 0.632 \qquad\qquad (3.51)$$

The most probable extreme value for $0 < \varepsilon < 0.9$ is

$$\overline{\zeta}_N = \left[\; 2 \ln \left\{ \frac{2 \sqrt{1 - \varepsilon^2}}{1 + \sqrt{1 - \varepsilon^2}} \; N \right\} \right]^{1/2} \qquad\qquad (3.52)$$

which reduces to Eq. 3.50 for $\varepsilon = 0$.

61
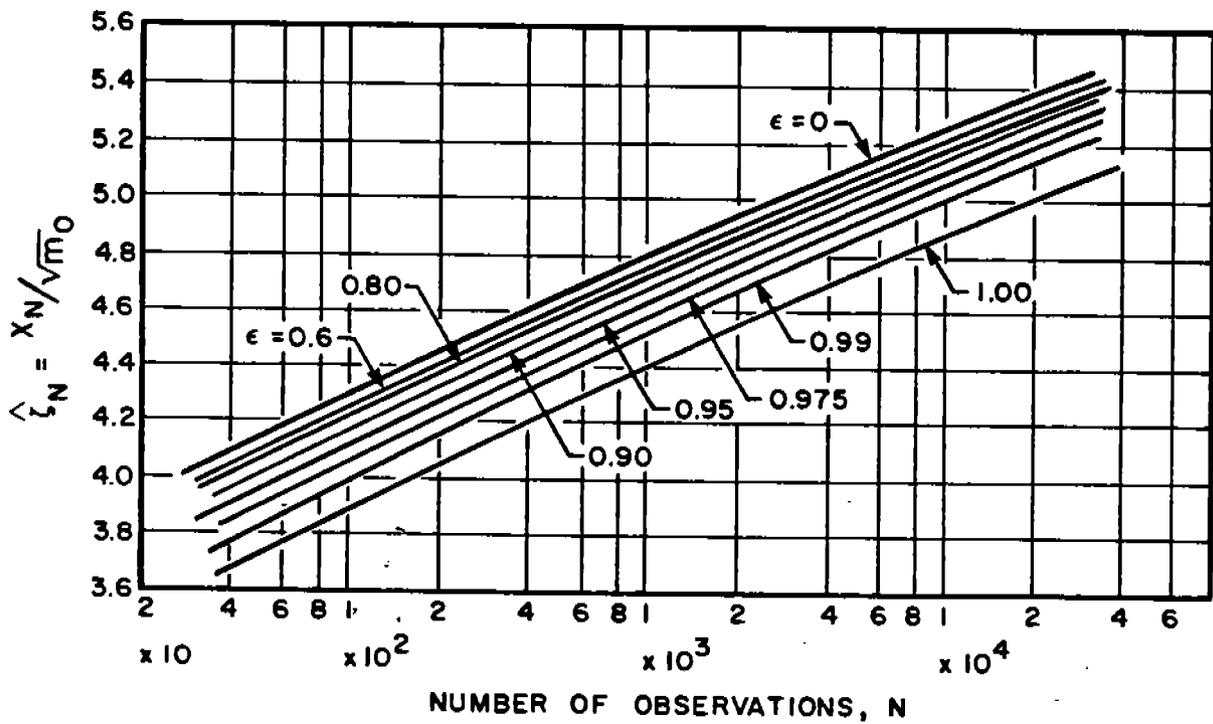
FIGURE 3.8   EXTREME VALUES OF $\hat{\zeta}_N$ (NONDIMENSIONAL AMPLITUDES) AS FUNCTION OF NUMBER OF OBSERVATIONS FOR VARIOUS BANDWIDTH PARAMETERS, ε AND FOR $\alpha = 0.01$ [OCHI (1973)]
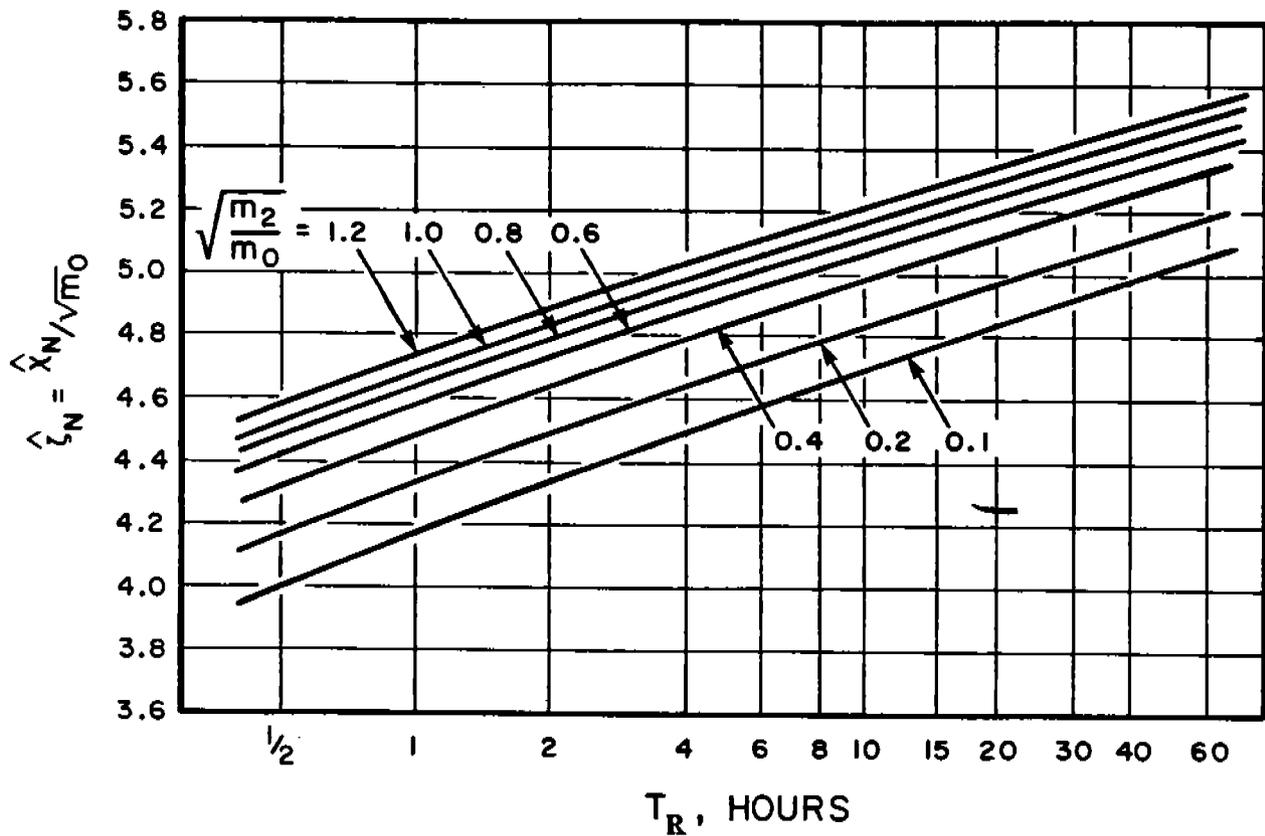
FIGURE 3.9   EXTREME VALUES OF $\hat{\zeta}_N$ (NONDIMENSIONAL AMPLITUDES) AS FUNCTION OF
TIME FOR VARIOUS VALUES OF PARAMETER $\sqrt{m_2/m_0}$ WHERE α = 0.01
[OCHI (1973)]

Expressing N as a function of time, T_R, in seconds the extreme value for a narrow-band process is obtained as

$$\hat{\zeta}_N = 2 \ln \left[\left\{ \frac{T_R}{(2\pi)\alpha} \sqrt{\frac{m_2}{m_0}} \right\} \right]^{1/2} \qquad \text{for small } \alpha \qquad (3.53)$$

This value is plotted in Fig. 3.9 for $\alpha = 0.01$ and for different values of zero crossing frequency, $(\sqrt{m_2/m_0})$ as a function of time. The corresponding most probable value is

$$\bar{\zeta}_N = \left[2 \ln \left\{ \frac{T_R}{2\pi} \sqrt{\frac{m_2}{m_0}} \right\} \right]^{1/2} \qquad (3.54)$$

3.2.4 Nonlinear Gaussian Waves

The statistical prediction of wave heights assume the waves to be Gaussian. In this case, Rayleigh distribution is applicable (for narrow-banded waves). For nonlinear waves, the distribution is not Gaussian. Longuet-Higgins (1980) suggests that the Rayleigh distribution may still be valid as long as the rms value of the linear Gaussian waves are adjusted by a factor of 0.925 in the distribution.

Forristall presented a two-parameter Weibull distribution to fit wave data from the Gulf of Mexico given by

$$P(\xi) = \exp\left(\frac{-\xi^\alpha}{\beta} \right) \qquad (3.55)$$

where ξ is nondimensional wave amplitude (half the trough-to-crest height) and α and β are empirical parameters. The values of α and β were found to be $\alpha = 2.126$ and $\beta = 1.052$ by fitting the wave data.

Longuet-Higgins (1952) derived Rayleigh distribution for narrow-banded surface seas of sinusoidal components as the distribution function for the wave amplitudes

$$P(a) = \exp \left(\frac{-a^2}{\bar{a}^2} \right) \qquad (3.56)$$

where $\bar{a}$ denotes the rms wave amplitude. For linear waves when the individual wave crests are approximately sinusoidal, the zeroth moment is related to $\bar{a}$ by

62

$$m_0 = \frac{1}{2} \bar{a}^2 \qquad (3.57)$$

In this case, the distribution function may also be written as

$$P(a) = \exp\left(\frac{-a^2}{2m_0} \right) \qquad (3.58)$$

However, for nonlinear waves where crests are narrower and higher than troughs as well as for finite bandwidth, the relationship in Eq. 3.58 is not valid. In the latter case, for example,

$$\frac{\bar{a}^2}{2m_0} = 1 - 0.734\nu^2 \qquad (3.59)$$

where

$$\nu^2 = \frac{\mu_2}{\bar{\omega}^2 m_0} \qquad (3.60)$$

where μ_2 is the second moment of the spectrum about the mean frequency, $\bar{\omega}$. For a P-M spectrum, the correction factor becomes 0.931. Using

$$\bar{a} = 0.925 \ (2m_0)^{1/2} \qquad (3.61)$$

Longuet-Higgins showed that the same Gulf of Mexico data was fitted by the Rayleigh distribution as good as the Weibull distribution.

3.2.5 Nonlinear Non-Gaussian Waves

It has already been noted that the response (output) of a nonlinear system is a non-Gaussian random process even though the waves (input) are Gaussian. Therefore, even though linearization technique works quite well for many nonlinear systems, marine systems with strong nonlinear characteristics, e.g., tension leg platform, may require the probabilistic prediction of non-Gaussian random processes. In recent years, several prediction methods have been made available in the literature that deal with this subject applicable to ocean structure.

The deep-water waves have been shown to follow Gaussian distribution from measurement at sea as well as in the laboratory. A correlation of the

probability density of time history of random laboratory waves in deep water is shown in Fig. 3.10. Note that the wave follows a Bretschneider spectral model. On the other hand, the wave profile becomes highly nonlinear in shallow water due to the bottom effect, showing excessively high crests and shallow troughs. This is illustrated in Fig. 3.11. Thus, the histogram in this case will not be symmetric with respect to the mean value but rather skewed to the positive side which will increase with the increase in the severity of the sea.

Bitner (1980) obtained an expression for the probability density function of the crest-to-trough wave height for non-normal waves. She assumed that the wave profile is a quasinormal random process and narrow-banded about a central frequency. The time-varying sine, $x_s(t)$, and cosine, $x_c(t)$, components of the central frequency, however, are considered nearly normal. Written in terms of a combined parameter, k_4, of the sine and cosine components, the probability density for height H becomes

$$p(H) = \frac{H}{4\sigma^2} \exp\left(-\frac{H^2}{8\sigma^2} \right) \left[1 + \frac{H^4}{1024\sigma^2} - \frac{H^2}{32\sigma^2} + \frac{1}{8} \right] k_4 \qquad (3.62)$$

where

$$k_4 = (\eta_1^4 - 3) + (\eta_2^4 - 3) + (\eta_1^2 \eta_2^2 - 1)$$

$$= \eta_1^4 + \eta_2^4 + \eta_1^2 \eta_2^2 - 7 \qquad (3.63)$$

and

$$\eta_1 = (x_c - \bar{x}_c) / \sigma \qquad (3.64)$$

$$\eta_2 = (x_s - \bar{x}_s) / \sigma \qquad (3.65)$$

The quantity, k_4, is determined numerically from η_1 and η_2. The mean wave height, $\bar{H}$, has a form

$$\bar{H} = \sqrt{2\pi}\sigma \left[1 - \frac{k_4}{64} \right] \qquad (3.66)$$

64
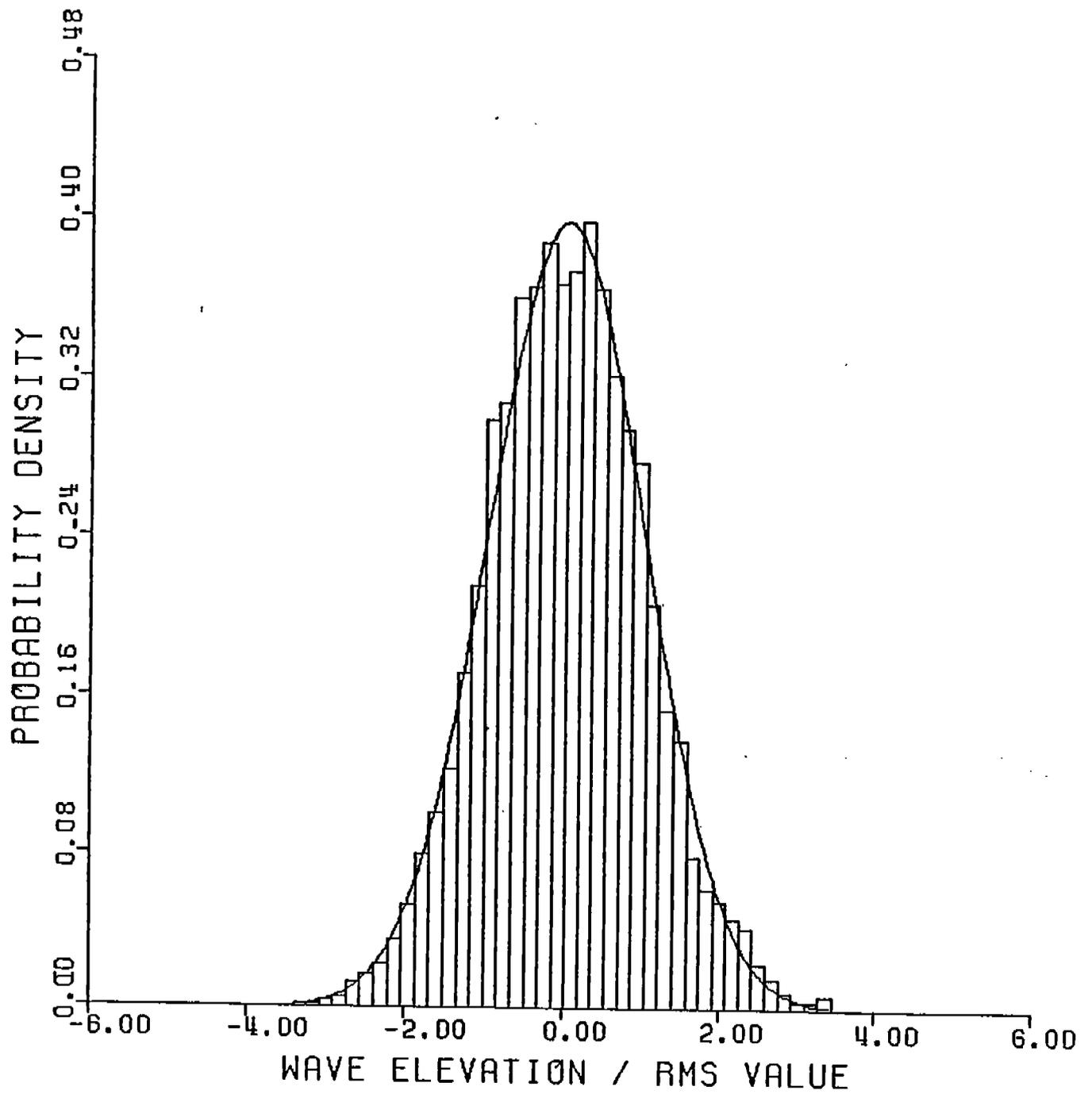
FIGURE 3.10   LABORATORY MEASURED WAVE ELEVATION PROBABILITY
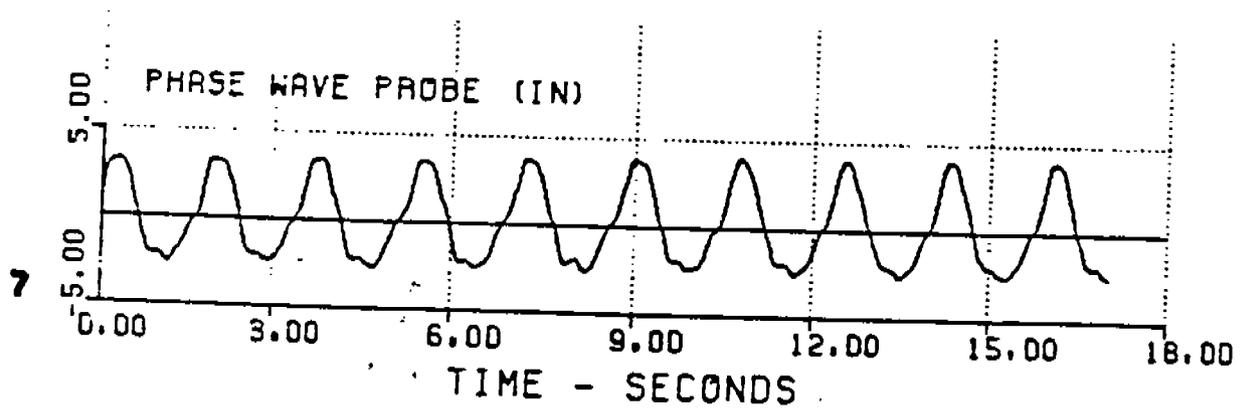
FIGURE 3.11   SHALLOW WATER WAVE IN WAVE BASIN

This density function is compared with the Rayleigh density function in Fig. 3.12.

In the derivation of non-Gaussian wave probability distribution, assumptions are made that the waves are narrow-banded and the nonlinearity is weak. For strong nonlinearity, the problem is extremely complicated.

In obtaining the Rayleigh distribution for the wave heights, the magnitudes of the statistical properties of wave height are assumed to be simply twice those of the wave amplitudes. However, more appropriately as shown above, the magnitude of the crest-to-trough heights should be determined disregarding this assumption which is often invalid. In this case, the height is taken as the sum of an upper-envelope value and a lower-envelope value for the profile that are separated by half the average period. Tayfun (1981) used this concept to determine the probability density function of the average of the two envelope values [namely, $a = (a_1 + a_2) / 2$] separated by $T/2$ where T = wave period. It is given as an integral of the joint probability distribution $p(2\bar{a} - \bar{a}_2, \bar{a}_2 ; T/2)$ and $p(T)$, where $p(T)$ is the period probability density function. The joint density function between a_1, and a_2 is written as

$$p(\bar{a}_1, \bar{a}_2 ; \tau) = \frac{\bar{a}_1\bar{a}_2}{(1 - r^2)} I_0\left(\frac{\bar{a}_1\bar{a}_2 r}{1 - r^2}\right) \exp\left[-\frac{(\bar{a}_1^2 + \bar{a}_2^2)}{2(1 - r^2)}\right] \qquad (3.67)$$

where $\bar{a}_1, \bar{a}_2$ (>0) = dimensionless amplitudes = $\dfrac{a_i}{\sqrt{m_0}}$, (i = 1, 2),

$$a_1 = A(t) \quad ; \quad a_2 = A(t + \tau) \qquad (3.68)$$

$$r(\tau) = \sqrt{\rho^2 + \lambda^2} \qquad (3.69)$$

$$\rho(\tau) = \frac{1}{m_0} \int_0^\infty S(\omega) \cos(\omega - \omega_0)\tau \, d\omega \qquad (3.70)$$

$$\lambda(\tau) = \frac{1}{m_0} \int_0^\infty S(\omega) \sin(\omega - \omega_0)\tau \, d\omega \qquad (3.71)$$

The computation of this expression is very complex, and Tayfun suggested the following simplification on the assumption of narrow-bandedness around the mean frequency, $\bar{\omega}$. Then

65
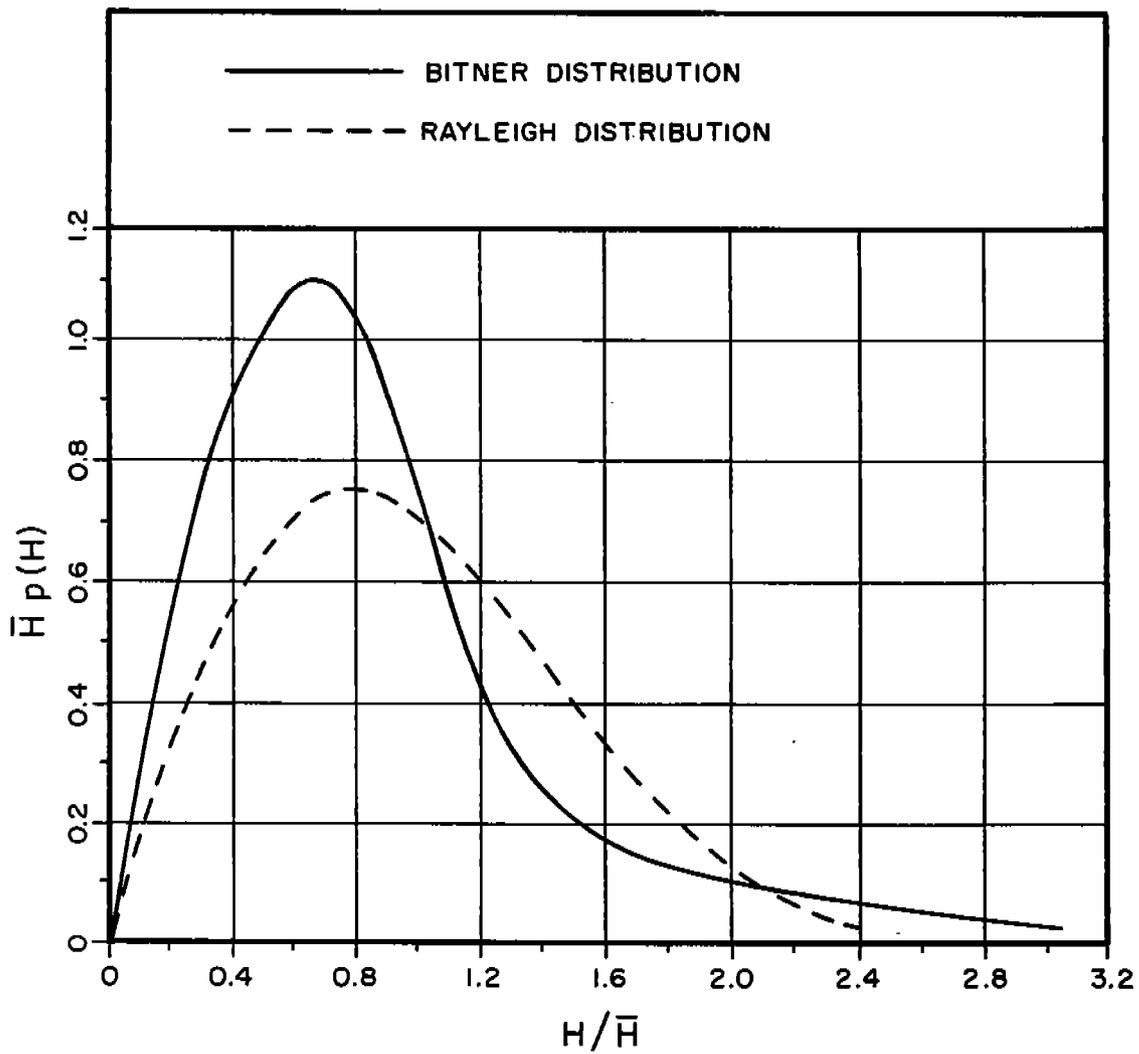
FIGURE 3.12 COMPARISON OF NON-NORMAL CREST-TO-TROUGH DISTRIBUTION WITH RAYLEIGH PROBABILITY DENSITY [BITNER (1980)]
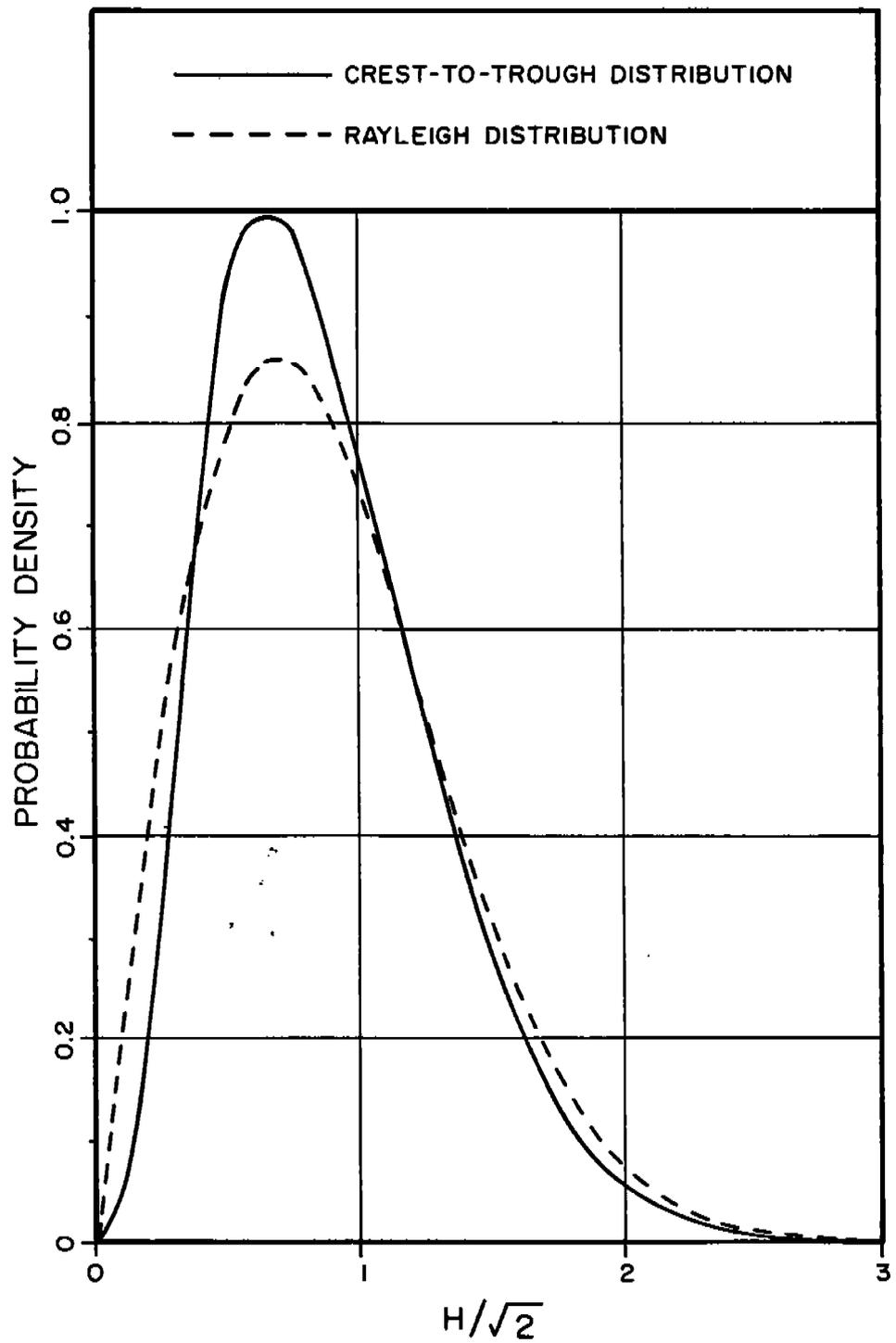
FIGURE 3.13   COMPARISON OF CREST-TO-TROUGH DISTRIBUTION FOR WAVE HEIGHT WITH
RAYLEIGH [TAYFUN (1981)]

$$\lambda(\tau) = 0, \text{ and} \tag{3.72}$$

$$\rho(\tau) = r(\tau) = 1 - \frac{1}{2}(\overline{\omega}\nu\tau) \tag{3.73}$$

The probability density function of a, then becomes

$$p(a) = 2 \int_0^{2a} p(\ 2a - a_2 \ , \ a_2 \ ; \ \frac{\pi}{\omega}\ )\ da_2 \tag{3.74}$$

This density function is plotted in Fig. 3.13 along with the Rayleigh density function and observed data. It is noted that this density function has a higher maximum value than Rayleigh.

There are several distribution functions available to represent the non-Gaussian random phenomena, e.g., observed in the wave profiles in finite water depth. These generally have series representation and are obtained either from the probability theory or nonlinear wave theory. Examples of non-Gaussian probability theory distributions are Gram-Charlier series, Edgeworth series and Longuet-Higgins series. The nonlinear wave theory uses, for example, Stokes' wave series. These have been derived by Ochi (1986). Here, only the essential results will be given.

The Gram-Charlier theory starts with the normal probability density function and writes a series in terms of the derivatives of the standardized (by subtracting mean and dividing by standard deviation) normal density function. This gives rise to the Hermite polynomials. The non-Gaussian density function then has the form for a random variable with zero mean and a variance of σ^2 as follows:

$$p(x) = \frac{1}{\sqrt{2\pi}\sigma} \ e^{\frac{-x^2}{2\sigma^2}} \ \sum_{n=0}^{\infty} C_n H_n \ (\frac{x}{\sigma}) \tag{3.75}$$

and the coefficients, C_n have the following values:

$$C_0 = 1, \ C_1 = C_2 = 0, \ C_3 = \frac{\lambda_3}{3!} \ , \qquad C_4 = \frac{\lambda_4}{4!} \ , \ C_5 = \frac{\lambda_5}{5!} \ ,$$

$$C_6 = \frac{\lambda_6}{6!} + \frac{\lambda_3^2}{2!(3!)^2} \ , \ C_7 = \frac{\lambda_7}{7!} + \frac{\lambda_3\lambda_4}{3!4!} \tag{3.76}$$

and so on, where H_n is the Hermite polynomial of order n, x is the value of a standardized normal variable

$$\lambda_j = \frac{k_j}{(k_2)^{\frac{j}{2}}} = \frac{k_j}{\sigma^j} \tag{3.77}$$

and k_j are the cumulants having the following properties

$$E[(x - \mu)^2] = k_2 = \sigma^2 \tag{3.78}$$

$$E[(x - \mu)^3] = k_3 \tag{3.79}$$

$$E[(x - \mu)^4] = k_4 + 3k_2^2 \tag{3.80}$$

$$E[(x - \mu)^5] = k_5 + 10k_3k_2 \tag{3.81}$$

$$E[(x - \mu)^6] = k_6 + 15k_4k_2 + 10k_3^2 + 15k_2^3 \tag{3.82}$$

and so on. Note that the quantity, λ_3 in Eq. 3.77 is called the skewness, and λ_4 is equal to the kurtosis minus 3.

It has been shown by Ochi (1986) that the Edgeworth and the Longuet-Higgins series reduce to the same form. In fact, the normalized Longuet-Higgins series in terms of non-zero standardized values of $Z[= (x - \mu) / \sigma]$ may be obtained by replacing x/σ by Z on both sides of Eq. 3.75.

It is interesting to note that the first term of the series reduces to the Gaussian density function (since $H_0 = 1$). In order to examine the effects of various terms in the series on the density function as well as their correlation with a measured severe wave ($H_s = 2.05$m) record in shallow water (d = 1.4m), an example from Ochi and Wang (1984) is reproduced in Fig. 3.14. It is found that the higher order terms introduce negative density values (albeit small) at large negative value of the variable, x. Ochi and Wang concluded from this and many other such correlation that the second term is the most dominant in the non-Gaussian distribution and the first three terms best describe the non-Gaussian waves.

67
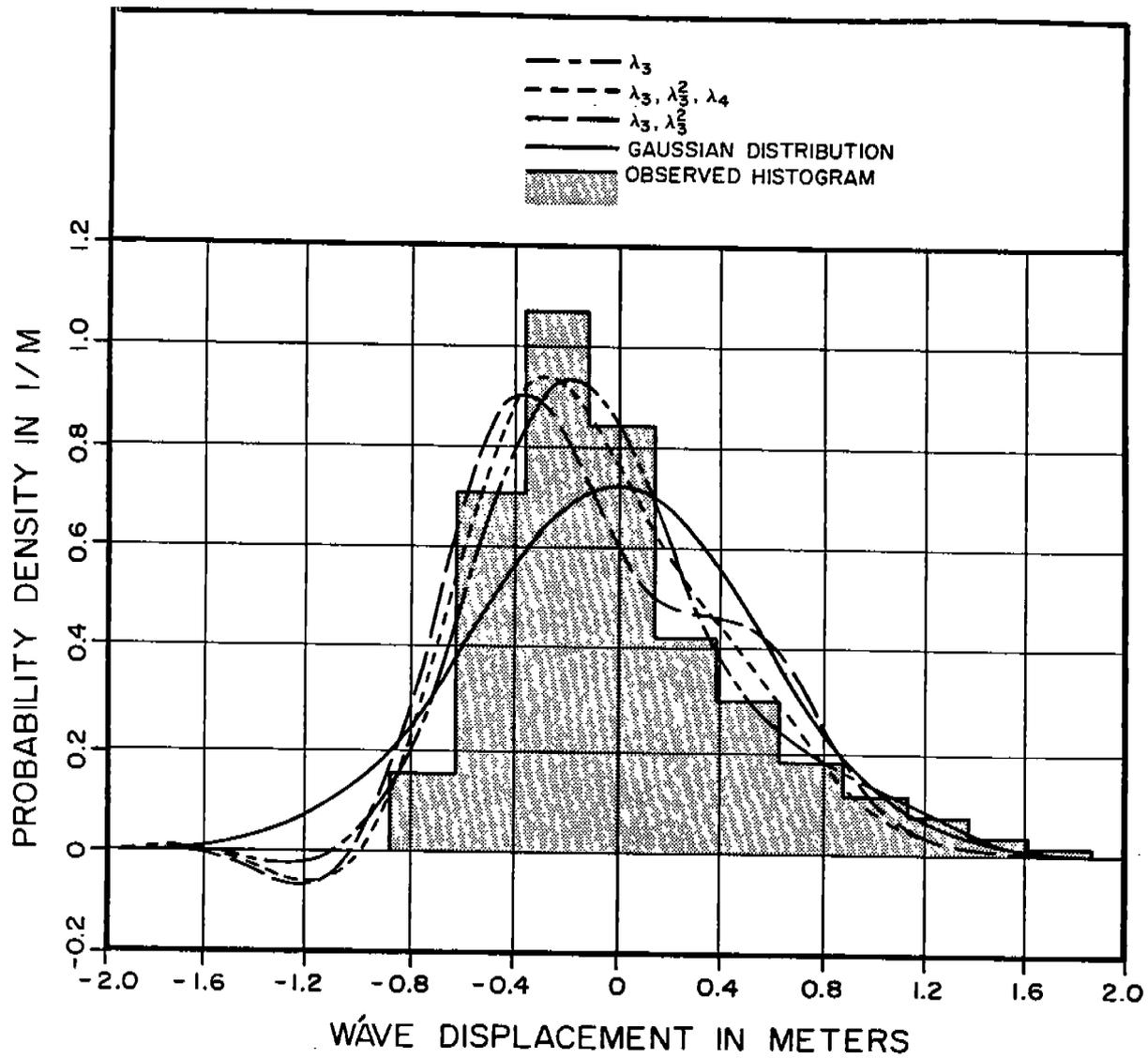
FIGURE 3.14   COMPARISON OF GAUSSIAN AND NON-GAUSSIAN DISTRIBUTIONS WITH
MEASURED DATA IN SHALLOW WATER [OCHI AND WANG (1984)]

Knowing the initial distributions of the wave profile, the distribution of the peaks and troughs (including their extreme values) and the wave heights may be determined. In this respect, it should be emphasized that for nonlinear waves, e.g., shown in Fig. 3.13, the probability functions for peaks and troughs are different and should be derived separately. The variance of peaks is obtained from the variance of x as

$$
\sigma_{x^+}^2 = \left(\frac{6\sqrt{\pi} + 2\sqrt{2} \; \lambda_3}{6\sqrt{\pi} - 2\sqrt{2} \; \lambda_3} \right) \sigma_x^2
\tag{3.83}
$$

For the variance of troughs, the term inside the parenthesis is inversed. The probability density function of peaks, ξ_+, is obtained from the expression

$$
p(\xi_+) = \frac{-\dfrac{d}{d\xi_+} \displaystyle\int_{-\infty}^{\infty} |x'| \; p(\xi_+, x') \; dx'}{\displaystyle\int_{-\infty}^{\infty} |x'| \; p(0, x') \; dx'}
\tag{3.84}
$$

where $p(x, x')$ is the joint probability density function of displacement and velocity. The non-Gaussian density function of displacement is known from Eq. 3.75 having a variance given by Eq. 3.83. The velocity, x', is assumed to be Gaussian with zero-mean and variance obtained from a given wave spectrum. The displacement and velocity are assumed to be statistically independent. The probability density function of wave heights (peak-to-trough) can be derived from the convolution integral of the individual density functions of peaks and troughs.

The linearization technique or the perturbation technique are appropriate only when the nonlinearity in the system is weak. This allows the response of the system to be expressed as a Gaussian system. The above examples of nonlinear waves show that the response of a nonlinear system will not be Gaussian. For a stronger nonlinear system, the Fokker-Planck equation may be applied. In this case, no restriction is applied to the degree of nonlinearity in the system. For a white-noise spectrum, the probability density function is obtained for a non-Gaussian response. Among others, such

an analysis was carried out by Ochi and Malakar (1984). They applied this technique to a single degree of freedom system having the following nonlinear equation

$$\ddot{x} + g(\dot{x}) + h(x) = f(t) \tag{3.85}$$

where $f(t)$ is the excitation force function for unit (total) mass of the system. The damping per unit mass is expressed as

$$g(\dot{x}) = a\dot{x} + \beta|\dot{x}|\dot{x} \tag{3.86}$$

the first term of which is linear while the second term is the viscous drag term. The restoring force per unit mass is written as

$$h(x) = \omega_N^2 x + rx^3 \tag{3.87}$$

including a linear spring and cubic spring term; ω_N is the natural frequency = $\sqrt{k/m}$.

The Fokker-Planck equation for this nonlinear system may be derived as

$$-\dot{x} \frac{\partial}{\partial x} p(x, \dot{x}) + \frac{\partial}{\partial \dot{x}} \left[\{g(\dot{x}) + h(x)\} p(x, \dot{x}) \right] + \frac{\pi S}{2} \frac{\partial^2}{\partial \dot{x}^2} p(x, \dot{x}) = 0 \tag{3.88}$$

where $p(x, \dot{x})$ = joint probability density function of x and $\dot{x}$, x = displacement from the mean, $\dot{x}$ = vertical velocity deviation from the mean, and S = white-noise spectrum of force, f. This equation is solved numerically.

Once the joint density function, $p(x, \dot{x})$, is known, the probability density function, $p(x)$, may be derived following the previously described method (Eq. 3.84) by applying least square fitting technique. The other quantities, e.g. density function of peaks, trough, etc., may then be obtained as before.

Note that the method is limited by the use of a white-noise spectrum. Therefore, it is desirable to find a white-noise spectrum which is equivalent to the excitation spectrum. Ochi (1986) suggests equating the variances of an equivalent linear system obtained by superposition and Fokker-Planck equation

69

methods and obtaining the equivalent white-noise spectrum. An example of the probability density function of the peak-to-trough surge motion of a TLP having nonlinear damping and restoring characteristics in a sea of H_s = 9.15m is shown in Fig. 3.15. The corresponding Rayleigh distribution on a linear system assumption is shown as dotted line.

According to the probability theory [Cramer (1970)], the characteristic function, $\phi(x)$ can be defined as the expected value of $e^{ix\zeta}$. Thus, $\phi(x)$ can be written as the Fourier transform of the probability distribution function of the random variable ζ, i.e., $P(\zeta)$ as follows

$$\phi(x) = \int_{-\infty}^{\infty} e^{ix\zeta} P(\zeta)\, d\zeta \qquad (3.89)$$

It can be shown that the right hand side may be expanded in a power series of $e^{ix\zeta}$ to give

$$\phi(x) = 1 + \mu_1' \frac{(ix)}{1!} + \mu_2' \frac{(ix)^2}{2!} + \ldots + \mu_r' \frac{(ix)^r}{r!} + \ldots$$

$$= \exp\left\{\lambda_1 \frac{(ix)}{1!} + \lambda_2 \frac{(ix)^2}{2!} + \ldots + \lambda_r \frac{(ix)^r}{r!} + \ldots\right\} \qquad (3.90)$$

where μ_r' and λ_r are the rth order moment and cumulant respectively. If μ_r represents rth order moment about the mean, then the first eight cumulants are related explicitly to these moments as follows

$$\lambda_1 = 0$$
$$\lambda_2 = \mu_2$$
$$\lambda_3 = \mu_3$$
$$\lambda_4 = \mu_4 - 3\mu_2^2$$
$$\lambda_5 = \mu_5 - 10\mu_3\mu_2 \qquad (3.91)$$
$$\lambda_6 = \mu_6 - 15\mu_4\mu_2 - 10\mu_3^2 + 30\,\mu_2^3$$
$$\lambda_7 = \mu_7 - 21\mu_5\mu_2 - 35\mu_4\mu_3 + 210\mu_3\mu_2^2$$
$$\lambda_8 = \mu_8 - 28\mu_5\mu_2 - 56\mu_5\mu_3 - 35\mu_4^2 + 420\mu_4\mu_2^2 + 560\mu_3^2\mu_2 - 630\mu_2^4$$

For a Gaussian distribution

$$\mu_{2r} = \frac{(2r)!}{2^r r!} \mu_2^r \qquad (3.92)$$
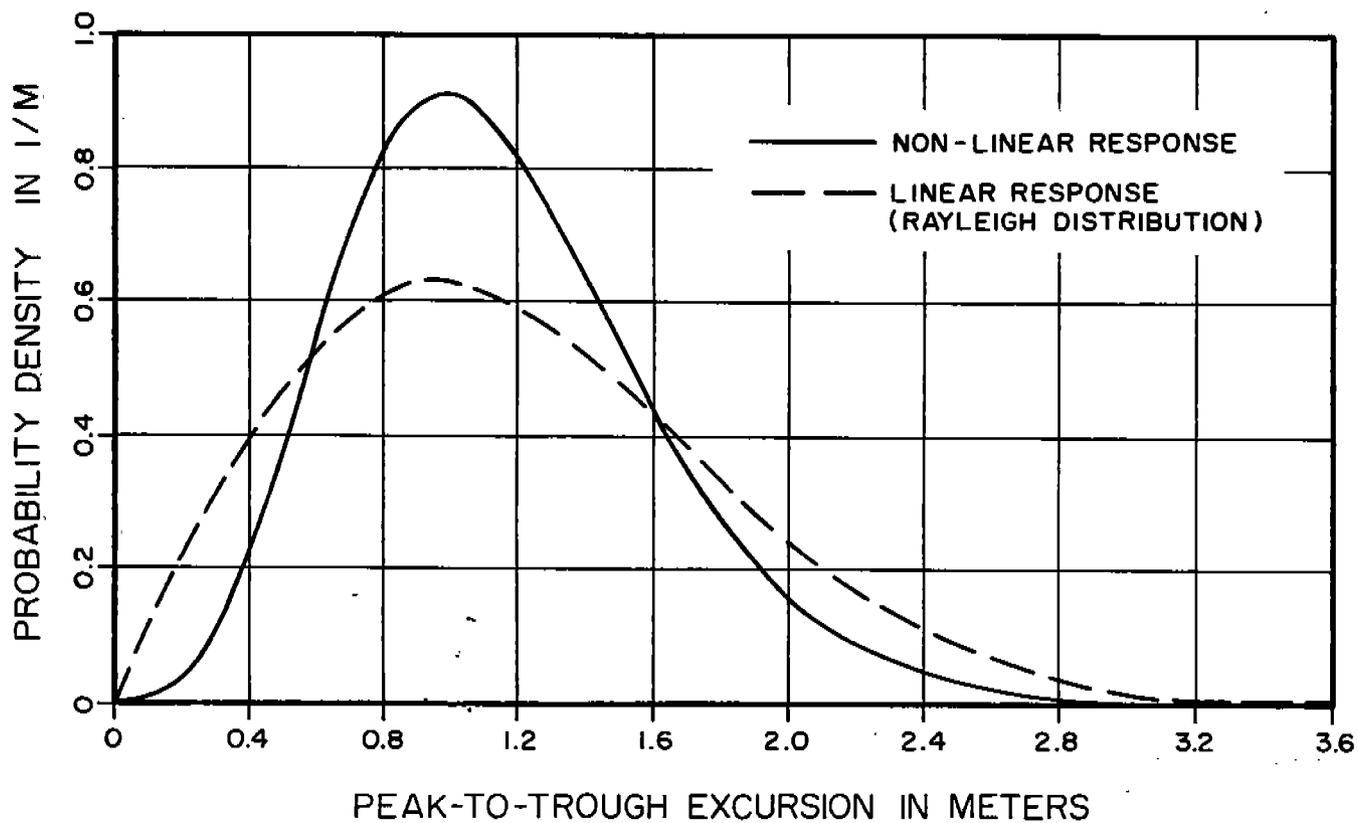
FIGURE 3.15   COMPARISON OF PEAK-TO-TROUGH PROBABILITY DENSITY OF LINEAR AND
NONLINEAR SURGING MOTION OF A TENSION LEG PLATFORM [OCHI
(1986)]

$$\mu_{2r+1} = 0 , \qquad r > 1 \qquad\qquad (3.93)$$

and

$$\lambda_2 = \mu_2$$
$$\lambda_r = 0 , \quad r > 2 \qquad\qquad (3.94)$$

for all r.

The values of moments and cumulants offer a quantitative measure to determine if a process is Gaussian or not. For a non-Gaussian process, higher-order approximations are necessary requiring higher moments and cumulants. Longuet-Higgins showed that Edgeworth's form of the type A Gram-Charlier series [Kendall and Stuart (1963)] is a good approximation for nonlinear waves. In terms of the Hermite polynomial of degree r defined as

$$H_r = t^r - \frac{r(r-1)}{1!} \frac{t^{r-2}}{2} + \frac{r(r-1)(r-2)(r-3)}{2!} \frac{t^{r-4}}{2^2} - \dots \qquad (3.95)$$

where t is the normalized wave elevation, $t = \zeta / \sqrt{\mu_2}$, the distribution function of ζ is given by Longuet-Higgins (1963) as

$$P(\zeta) = (2\pi k_2)^{-\frac{1}{2}} e^{-\frac{1}{2} t^2} [1 + \frac{1}{6} k_3 H_3 + (\frac{1}{24} k_4 H_4 + \frac{1}{72} k_3^2 H_6) + \dots] \qquad (3.96)$$

where $k_r = \lambda_r / \lambda_2^{r/2}$. The full Edgeworth's form up to eight terms has been given by Huang and Long (1980) as

$$P(\zeta) = (2\pi k_2)^{-\frac{1}{2}} e^{-\frac{1}{2} t^2} [1 + \frac{1}{6} k_3 H_3 + \frac{1}{24} k_4 H_4 + \frac{1}{120} k_5 H_5$$
$$+ \frac{k_6 + 10k_3^2}{720} H_6 + \frac{k_7 + 35k_4 k_3}{5040} H_7$$
$$+ \frac{k_8 + 56k_5 H_3 + 35k_4^2}{40320} H_8 + \dots] \qquad (3.97)$$

The series up to the sixth term reduces to Longuet-Higgins' series (Eq. 3.96) for $k_r = 0$, $r > 5$. Huang and Long (1980) showed with the laboratory experimental data that additional terms make the approximation worse. Moreover, even for highly non-Gaussian waves for which the skewness, k_3, approaches one, the four-term approximation in Eq. 3.97 does a good job in

71

predicting the wave elevation distribution. This is illustrated in Fig. 3.16. Another interesting feature evidenced in this figure is that a gentle hump appears near the mean amplitude of waves given by $1.4\sqrt{\overline{\zeta^2}}$. This indicates that the amplitudes of waves have a preferred range of height rather than appearing completely random. Note that the Gram-Charlier expansion introduces a slightly negative density value at large negative surface elevation as discussed earlier.

If the wave field is described by denumerably many independent pure sinusoidal components, by the central limit theorem, the probability density function of the surface profile becomes Gaussian. The sinusoidal components, however, satisfy only the first-order wave theory and are applicable for wave slopes, ka, approaching zero (k = wave number, a = wave amplitude).

For many real wave fields, the value of ka is finite and higher-order nonlinear theories for individual wave components are applicable. One of the most obvious effects of nonlinearity in waves appears as sharper peaks and shallower troughs. In this case, the waves are no longer symmetric with respect to the mean water line and, consequently, the surface elevation will no longer be Gaussian.

We have already discussed the non-Gaussian distribution using Edgeworth's form of the type A Gram-Charlier series. It was shown that for steep waves, the probability density function becomes negative for large trough values. The other disadvantage of this distribution is that it requires the values of skewness (k_3) and flatness (k_4) which are extremely difficult to compute.

For nonlinear waves, Tayfun (1980) obtained the probability density function of deep water second-order waves. He used the standard technique of transformation of a pair of random variables and the computation of marginal probability density function from the joint density function (mapping approach).

Huang, et al. (1983) presented the probability density function for waves to third order. They used a perturbation scheme on the assumption of small wave steepness. The third-order approximation for the probability density function for the surface profile is given by
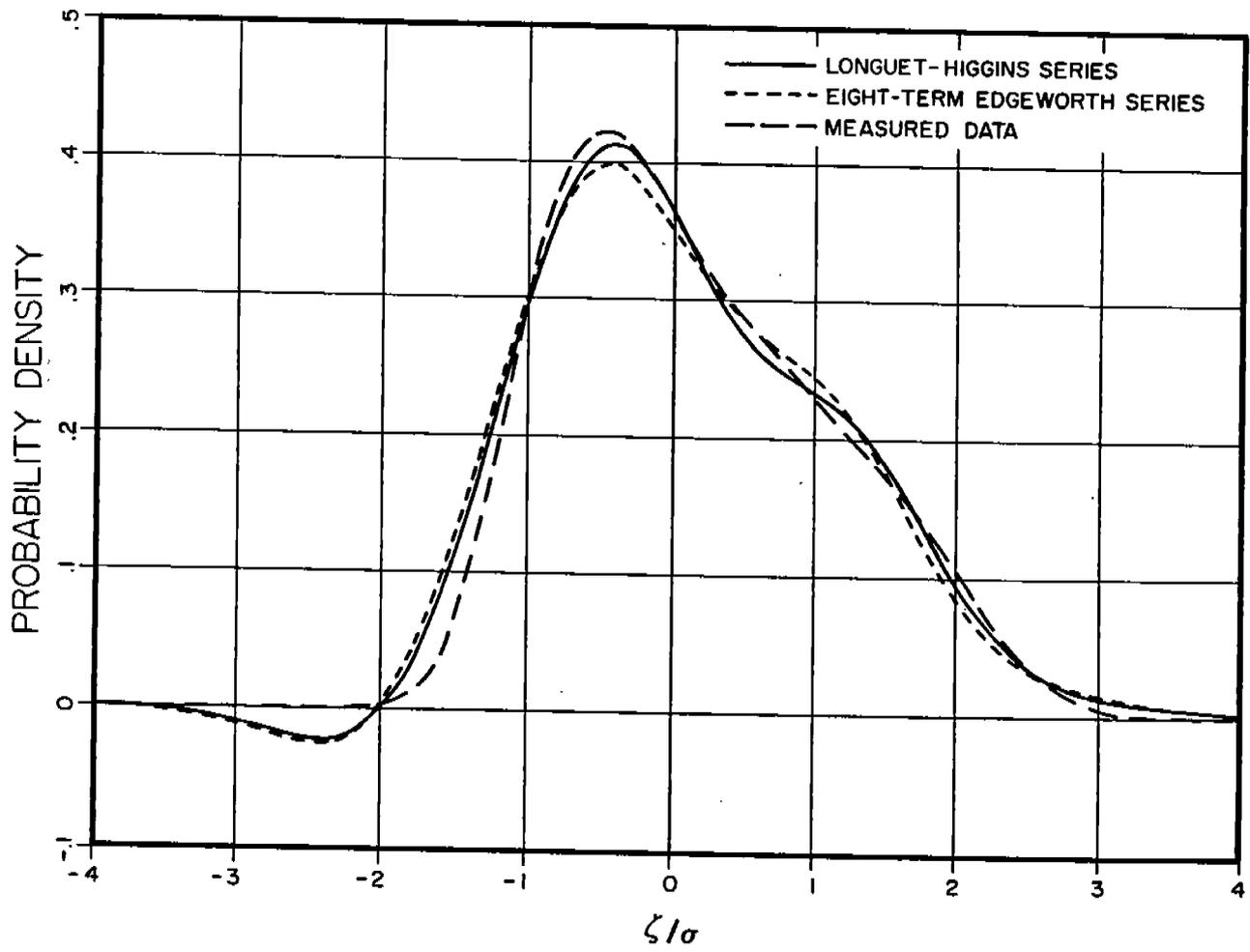
FIGURE 3.16   CORRELATION OF PROBABILITY DENSITY OF LONGUET-HIGGINS AND
   EDGEWORTH SERIES WITH MEASURED DATA [HUANG AND LONG (1980)]
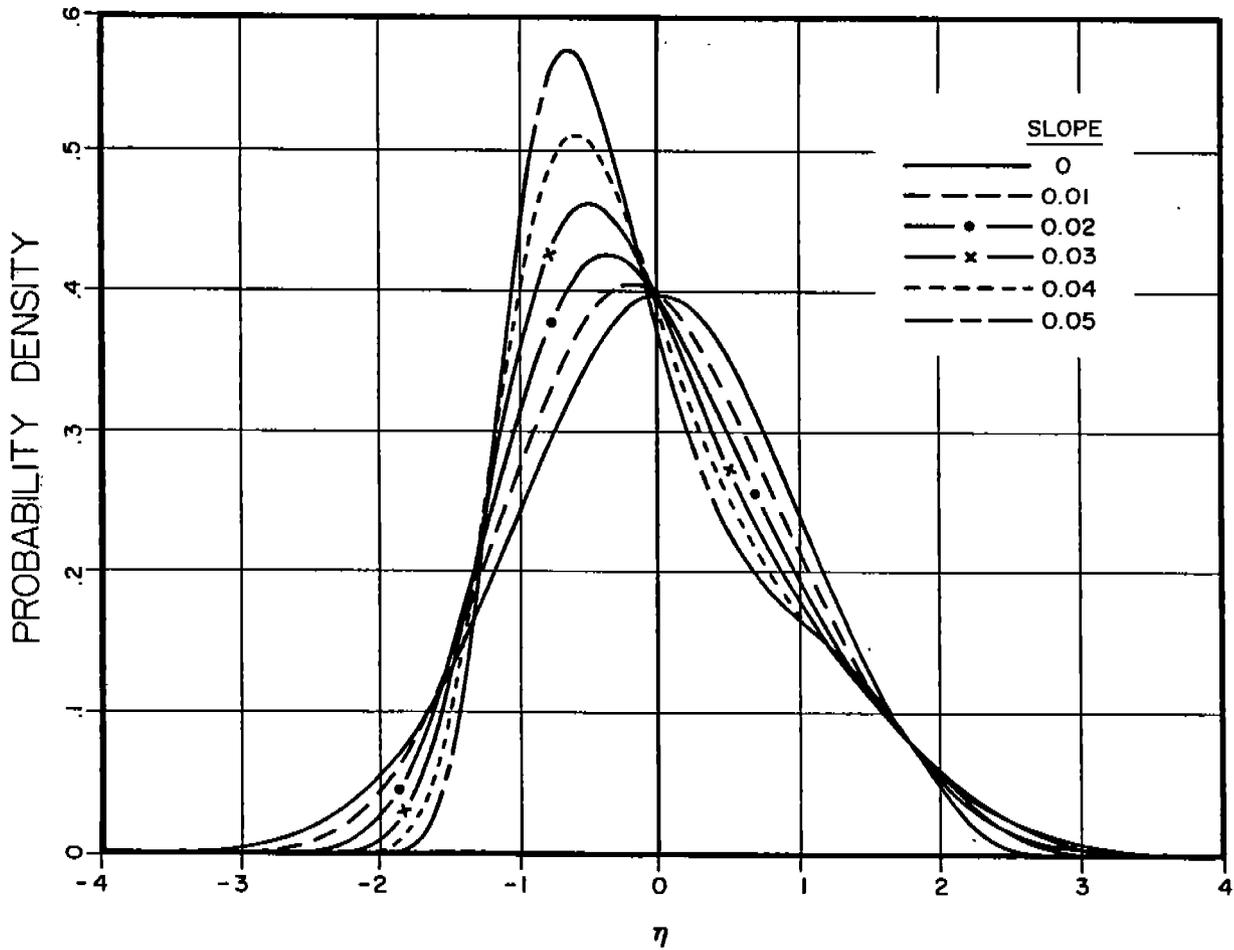
FIGURE 3.17   PROBABILITY DENSITY OF SURFACE ELEVATION OF THIRD-ORDER STOKES
WAVE [HUANG, ET AL. (1983)]

$$p(\eta) = \frac{e^{-\frac{H_\eta^2}{2}}}{\sqrt{2\pi}} \left[\frac{J_\eta}{\sqrt{R}} + \frac{9}{8} \frac{\sigma^2 k^2}{N} \frac{1}{\sqrt{R^3}} \right] \qquad (3.98)$$

where

$$R = 1 + \frac{9}{4} \sigma^2 k^2 \eta^2 \qquad (3.99)$$

$$J_\eta = N \left[1 - 2\sigma k \eta + \sigma^2 k^2 \left(\frac{39}{8} \eta^2 - 2 \right) \right] \qquad (3.100)$$

$$N = 1 + \sigma^2 k^2 \qquad (3.101)$$

$$H_\eta = N \left[\eta - \sigma k (\eta^2 - 1) + \sigma^2 k^2 \left(\frac{13}{8} \eta^3 - 2\eta \right) \right] \qquad (3.102)$$

and η is the normalized surface elevation given by

$$\eta = \frac{\zeta - \tilde{\zeta}}{\sigma} \qquad (3.103)$$

where $\tilde{\zeta} = \sigma^2 k$ to third order. The probability density function depends on σ as well as σk (slope parameter).

Note that σk is proportional to the significant slope, $s = \sigma/\lambda$ where σ is the rms value and λ is wave length corresponding to the peak frequency. The probability density of surface profile for $s = 0$, 0.01, 0.02, 0.03, 0.04 and 0.05 is plotted in Fig. 3.17. The density values are always non-negative unlike the Gram-Charlier approximation.

Moreover, a hump is evident for high s values (larger skewness) for η between 1 and 2. This hump appears because of the constant term in the third-order Stokes' wave profile and has been found earlier in experimental data in Fig. 3.16.

A third-order approximation for the density function can be derived in finite water depth following similar a procedure. In this case, the expression for $p(\eta)$ is similar but more involved.

$$p(\eta) = \frac{e^{-\frac{H_s^2}{2}}}{\sqrt{2\pi}} \left\{ \tilde{J}_\eta \left[\frac{1}{\sqrt{R_s}} - \frac{3\sigma^2 k^2}{2N_s^2} \frac{h_s^2}{\sqrt{R_s^5}} \right] - \frac{\tilde{J}_\omega \sigma^2 k^2}{N_s} \frac{1}{\sqrt{R_s^3}} \right\} \qquad (3.104)$$

73

where the subscript s stands for shallow water and

$$N_s = (1 + \sigma^2 k^2 S_0^2 S_3)^{1/2} \tag{3.105}$$

$$S_0 = \coth kd \tag{3.106}$$

$$S_1 = \frac{3}{4} \frac{\coth kd}{\sinh^2 kd} \tag{3.107}$$

$$S_2 = 1 + \frac{3}{\sinh^2 kd} + \frac{3}{\sinh^4 kd} + \frac{9}{8 \sinh^6 kd} \tag{3.108}$$

$$S_3 = 1 + \left(1 + \frac{3}{2 \sinh^2 kd} \right)^2 \tag{3.109}$$

$$H_s = N_s \{ \eta - \sigma k [(S_0 + S_1)\eta^2 - S_0] $$
$$+ \sigma^2 k^2 [2(S_0 + S_1)^2 \eta^3 - \frac{3}{8} S_2 \eta^3 - 2S_0 (S_0 - S_1)\eta] \} \tag{3.110}$$

$$h_s = S_1 - \sigma k (2S_0 S_1 + 2S_1 - \frac{9}{8} S_2)\eta \tag{3.111}$$

$$\mathfrak{J}_\eta = \{ 1 - 2\sigma k (S_0 + S_1)\eta + \sigma^2 k^2 [6(S_0 + S_1)^2 - \frac{9}{8} S_2]\eta^2 $$
$$- 2\sigma^2 k^2 S_0 (S_0 + S_1) \} N_s \tag{3.112}$$

$$\mathfrak{J}_\omega = 2S_1 (S_0 + S_1) - \frac{9}{8} S_2 \tag{3.113}$$

$$R_s = 1 + \sigma k H_s h_s \tag{3.114}$$

In this case, additional dependence on the depth parameter, kd is clear. One should note, however, that the Stokes' higher order waves have limited applications in shallow water.

The non-Gaussian response characteristics of an offshore structure may be linked to the nonlinearity in the wave kinematics, as discussed earlier, as well as the free-surface fluctuations of the water at the structure free-board and the nonlinearity in the force due to the presence of the drag effect. The first of these make the waves non-Gaussian. The effect of the free-surface fluctuations is that the loading on the structure is intermittent near the mean sea level and is therefore no longer Gaussian. Thus conventional

74

spectral analysis is no longer sufficient to fully define the response. The spectral analysis indicates only the variance. Higher order moments of the response must be known for a complete probabilistic description of the response in terms of its mean, variance, skewness and kurtosis coefficients. The nonlinear forces make the response non-Gaussian.

Kanegaonkar and Haldar (1987) analyzed the dynamic response of an offshore platform of the jacket type. The equation of motion was written in a matrix form for a lumped mass system. The nonlinearity was introduced in the relative-velocity drag term which was linearized in terms of a relative velocity rms value. The analysis considers the free-surface fluctuations and their effects on the spectral and probabilistic analysis.

Near the mean water level where the structure is intermittently loaded, the horizontal water particle velocity is given as

$$\hat{u} = uH(\eta - y) \tag{3.116}$$

where $\hat{u}$ is the effective velocity, u = velocity by the Stokes' wave theory and H = Heaviside unit-step function. Assuming that the effective velocity is stationary, Tung (1975) showed that the approximate spectral density function of velocity is

$$S_{\hat{u}}(\omega) = \left(\frac{\sigma_u}{\sigma_\eta}\right)^2 \left[\beta z(\beta) + Z(\beta) \right]^2 S(\omega) \tag{3.117}$$

where

$$\beta = \frac{y}{\sigma_\eta} \tag{3.118}$$

$$z(\beta) = \frac{1}{\sqrt{2\pi}} \exp\left(-\frac{\beta^2}{2}\right) \tag{3.119}$$

and

$$Z(\beta) = \int_\beta^\infty z(\beta)d\beta \tag{3.120}$$

Also, the acceleration spectra

75

$$S_{\ddot{u}}(\omega) = \omega^2 \, S_{\hat{u}}(\omega) \tag{3.121}$$

Based on this effective velocity, $\hat{u}$, the equation of motion is modified and the spectral density of the displacement is obtained in terms of $S_{\hat{u}}(\omega)$ and $S_{\ddot{u}}(\omega)$, the frequency transfer function and modified and linearized Morison equation. These then were used to express the first four moments (mean, variance, skewness and kurtosis) of the load which are necessary for the probabilistic analysis. The derivation is shown by Kanegaonkar and Haldar (1987).

The unknown non-Gaussian distribution for the displacement response can be assumed to be a mixture of a set of distributions, P_i, each one having a weighing factor, w_i, associated with each so that

$$\sum_{i=1}^{I} w_i = 1 \quad \text{and} \quad w_i > 0 \tag{3.122}$$

The distribution, P_i, is chosen such that it has the same mean and variance as the net distribution, P_x. The response distribution, P_x, is assumed to be of the form

$$P_x = w_1 P_1 + w_2 P_2 \tag{3.123}$$

where P_1 = standard normal and P_2 = shifted exponential distribution given by its density function

$$p_2(x) = \frac{1}{\beta} \exp \left(\frac{x - \alpha}{\beta} \right) \tag{3.124}$$

For this distribution, mean = $\alpha + \beta$, variance = β^2 , skewness = 2.0 and kurtosis = 6.0. Through numerical examples, it was shown that if the surface fluctuations are included in the analysis, the high seastates yielded $w_1 \simeq$ 0.3. On the other hand, at low seastates as well as without fluctuations, the displacement of the jacket structure at its deck was Gaussian $(w_1 = 1, w_2 = 0)$. The non-Gaussian distributions showed significant deviations from the Gaussian at the upper tails with much higher probability of exceedance values for the same displacements. The rms values were slightly reduced. The skewness and kurtosis were near zero at lower significant wave heights and increased in value as the height increased.

3.2.6 Wave Period Distribution

The probability functions for evaluating the statistical properites of the ocean wave periods have been derived by Longuet-Higgins (1975), Cavanie et al. (1976) and Arhan, et al. (1976). They derived the joint probability density function of wave height and period. Once the joint density function and the individual density function of one of the variables, namely the wave height, is known, the density function for the other single variable, namely the wave period, is simply the marginal probability density function of the joint distribution. Longuet-Higgins derived the density function of the zero crossing period while Cavanie, Arhan, et al. (1976) obtained the density function of the crest period (between the maxima).

Defining a nondimensional period having a mean of zero-crossing period, $\bar{T}$, as

$$\eta = \frac{T - \bar{T}}{\upsilon \bar{T}} \tag{3.125}$$

where υ is a measure of spectrum width defined as

$$\upsilon = \frac{m_0 m_2 - m_1^2}{m_1^2} \tag{3.126}$$

Then the Longuet-Higgins probability density of nondimensional period is given by

$$p(\eta) = \frac{1}{2(1 + \eta^2)^{3/2}} \tag{3.127}$$

The probability density is symmetric about the mean period having a bell-shaped curve similar to a normal distribution.

It is noted from the definition of η, that the period T becomes negative for $\eta < -(1/\upsilon)$. Therefore, in order to limit the probability density to the positive periods, η should be truncated at $\eta = -(1/\upsilon)$. In this case, the probability density function of η becomes [Ochi (1982)]

$$p(\eta) = \frac{\sqrt{1 + \upsilon^2}}{(1 + \sqrt{1 + \upsilon^2})} \quad \frac{1}{(1 + \eta^2)^{3/2}} \qquad -\frac{1}{\upsilon} < \eta < \infty \qquad (3.128)$$

In dimensional form, the density function of T is

$$p(T) = \frac{\sqrt{1 + \upsilon^2}}{(1 + \sqrt{1 + \upsilon^2})} \quad \frac{(\upsilon\bar{T})^2}{[(\upsilon\bar{T})^2 + (T - \bar{T})^2]^{3/2}} \qquad 0 < T < \infty \qquad (3.129)$$

The Longuet-Higgins formulation is based on a narrow-band spectrum. On the other hand, Arhan, et al. obtained an expression for a wide band spectrum in terms of the parameter, ε. The probability density function for the time interval between two maxima is given in terms of dimensionless period is

$$p(\tau) = \frac{\alpha^3 \beta^2 \tau}{[(\tau^2 - \alpha^2)^2 + \alpha^4 \beta^2]^{3/2}} \qquad -\infty < \tau < \infty \qquad (3.130)$$

where $\tau = T / \bar{T}_m$, $\bar{T}_m$ is the expected time between two successive positive maxima given by

$$\bar{T}_m = 4\pi \left(\frac{\sqrt{1 - \varepsilon^2}}{1 + \sqrt{1 - \varepsilon^2}} \right) \left(\frac{m_0}{m_2}\right)^{1/2} \qquad (3.131)$$

$$\alpha = \frac{1}{2} (1 + \sqrt{1 - \varepsilon^2}) \qquad (3.132)$$

$$\beta = \frac{\varepsilon}{\sqrt{1 - \varepsilon^2}} \qquad (3.133)$$

Note that for $\varepsilon = 0$, $\alpha = 1$ and $\beta = 0$, and the probability density function does not exist. A comparison of this relationship with that derived by Longuet-Higgins was made by Goda (1978) assuming $\tau = \eta$. The correlation showed that at least for small correlation coefficient values (ε between 0.5 and 0.7) between H and T, there is little difference between the two forms.

3.2.7 Wave Height-Period Distribution

While it is important in a statistical analysis to know the wave height distribution and maximum wave heights, in a response analysis the joint distribution of the wave heights and periods is often needed. The statistical description of the sea surface is usually divided into short-term and long-term statistics. The short-term seastates are usually assumed to be stationary even though the seas are often expected to vary over a few hour period. For a varying seastate at a given location, the probability distribution of the height and period of the highest wave has been derived by Krogstad (1985). Consider a wave record over a time period, T_R, during a constant seastate, s, where the individual wave height and period are denoted by $\{(H_i, T_i), i = 1, \ldots N\}$, and H_{max} is the maximum of all the heights. The CDF of H_i with the seastate, s is given by

$$P(H_i < H) = F(H,s) \tag{3.134}$$

If the wave heights are independent

$$P(H_{max} < H) = F(H,s)^N \tag{3.135}$$

Assuming

$$T_z = \frac{1}{2\pi} \sqrt{\frac{m_2}{m_0}} \tag{3.136}$$

the maximum wave height in a time interval $[0,T_R]$ is

$$P(H_{max} < H) = F(H,s)^{T_R/T_z} \tag{3.137}$$

If s varies over $[0,T_R]$, then the interval is partitioned into subintervals over which the seastate is constant and in the limit

$$P(H_{max} < H \mid [0,T_R]) = \exp \left\{ \int_0^{T_R} \log F [H, s(\tau)] \frac{d\tau}{T_z(\tau)} \right\} \tag{3.138}$$

The conditional probability distribution for the period of the maximum wave is identical to the conditional probability distribution of the wave period for that particular seastate and wave height, $p(T|H,s)$. The

conditional probability distribution of T_{max} for given H_{max} for the whole time interval which is partitioned into subintervals is given by

$$p(T|H = H_{max}) = \sum_{i=1}^{N} p(T|H = H_{max}, s_i) \times p(H_{max} \text{ occurred in } I_i) \qquad (3.139)$$

which reduces to the following form for max $(\Delta I_i) \to 0$

$$p(T|H = H_{max}) = \frac{\int_0^{T_R} \frac{d}{dH} \log F [H,s(\tau)] \; p(T|H,s(\tau)) \; d\tau/T_z(\tau)}{\int_0^{T_R} \frac{d}{dH} \log F[H,s(\tau)] \; d\tau/T_z(\tau)} \qquad (3.140)$$

If the distribution of the seastate is known and is equal to $P(s)$ where $\int P(s)$ ds $= 1$ for an observation time, T_R, then

$$P(H_{max} < H) = \exp \left\{ T_R \int P(s) \frac{1}{T_z} \log [F(H,s)] \; ds \right\} \qquad (3.141)$$

and

$$p(T|H_{max} = H) = \frac{\int P(s) \frac{d}{dH} \log F(H,s) \; p(T|H,s) \; ds/T_z(s)}{\int P(s) \frac{d}{dH} \log F(H,s) \; ds/T_z(s)} \qquad (3.142)$$

Now we require the short-term distribution functions $F(H,s)$ and $p(T|H,s)$. Assuming F as a function of H_s only, Forristall (1978) gives

$$F(H,s) = 1 - \exp \{-(4H/H_s)^\alpha/\beta\} \qquad (3.143)$$

This is a two parameter Weibull distribution. It corresponds to the Rayleigh distribution for $\alpha = 2$ and $\beta = 8$. However, for extreme value analysis, it is the upper tail ($H > H_s$) distribution of wave height that is important, not the overall distribution. Thus, we are interested in the values of α and β that fit the upper tail.

Considering the normalized variable

$$x = \frac{4H_{max}}{\hat{H}_s} \qquad (3.144)$$

where $\hat{H}_s$ is an estimate of H_s, x is modified by

80

$$x = (4H_{max}/\hat{H}_s) \ (\log N_0/\log N)^{1/2} \qquad (3.145)$$

where N_0 is fixed and $N = T_R/T_z$. Then x has a CDF of

$$F(x) = \left[1 - \exp \ (-x^{\alpha}/\beta) \ \right]^{N_0} \qquad (3.146)$$

The parameters α and β are computed from a plot of $\log \ [-\log \ (1 - F^{1/N_0})]$ vs. $\log(x)$. Based on the Norwegian Sea wave rider data, these values are obtained as shown in Table 3.1. Note that these values are quite different from the Rayleigh distribution parameters, $\alpha = 2$, and $\beta = 8$.

The joint height-period distribution in a record was obtained by Wooding (1955), Longuet-Higgins (1975), Ezraty, et al. (1978) and Chen, et al. (1979). Both Longuet-Higgins and Ezraty, et al. assumed a narrow-band, Gaussian model. Longuet-Higgins' formula is easy to apply and shows symmetric distribution in the wave period. On the other hand, Ezraty, et al. showed a complex distribution form which is difficult to apply. They found an asymmetric distribution with respect to period, but the distribution is a function of the spectral width parameter, ε, depending on occasionally unstable fourth-spectral moment, m_4. The conditional probability distribution of the wave period following Chen, et al. (1979) is assumed to be normal, $N(\mu,\sigma^2)$ where

$$\mu = C_{\mu}T_z \qquad (3.147)$$

and

$$\sigma = C_{\sigma}T_z \frac{H_s}{H_{max}} \qquad (3.148)$$

The values of C_{μ} and C_{σ} were found to be functions of T_z only as shown in Table 3.2. These values are shown as functions of T_p in Table 3.3.

The numerically computed expectation of H_{max} coincides with the asymptotic relation derived by Forristall (1978)

$$E(H_{max}/H_s) = 0.25 \ (\beta \log N)^{1/\alpha} \ [1 + 0.5722/(\alpha \log N)] \qquad (3.149)$$

81

TABLE 3.1

BEST FIT VALUE OF α AND β
FROM OFFSHORE NORWAY WAVE DATA

SITE LOCATION	H_s m	NO. OF RECORDS	α	β
Utsira	>5	230	2.37	12.5
Halten	>5	405	2.50	15.6
Tromsoflaket	>5	384	2.38	12.9

TABLE 3.2

VALUES OF C_μ AND C_σ VERSUS T_z
IN THE EMPIRICAL DISTRIBUTION OF WAVE PERIOD
CORRESPONDING TO MAXIMUM HEIGHT

T_z(s)	C_μ	C_σ
4	1.50	0.50
6	1.41	0.39
8	1.32	0.30
10	1.30	0.25
12	1.20	0.23

TABLE 3.3

VALUES OF C_μ AND C_σ VERSUS T_P
IN THE EMPIRICAL DISTRIBUTION WAVE PERIOD
CORRESPONDING TO MAXIMUM HEIGHT

$T_P(s)$	C_μ	C_σ
6	1.05	0.26
8	0.94	0.21
10	0.89	0.19
12	0.85	0.20
14	0.82	0.22
16	0.76	0.26
18	0.70	0.30

Note that this expression reduces to Eq. 3.37 for $\alpha = 2$ and $\beta = 8$. An example of the joint distribution of H_{max} and T_{Hmax} is shown in Fig. 3.18 for given H_s and T_z.

The distribution in Fig. 3.18 shows that it is symmetric around the mean period, T_z. However, field data have shown that the joint distribution is generally asymmetric [cf. Chakrabarti and Cooley (1977)]. Longuet-Higgins (1983) revised his earlier derivation by introducing an asymmetric joint distribution of wave amplitudes and periods. This revised distribution also depends on the first three moments of wave spectrum (m_0, m_1 and m_2) which are simpler to use.

Defining nondimensional wave amplitude and period as

$$\xi = \frac{a}{(2m_0)^{1/2}} \quad , \quad \eta = \frac{T}{\bar{T}} \tag{3.150}$$

where $\bar{T} = 2\pi m_0/m_1$, we can write the joint probability density function

$$p(\xi, \eta) = \frac{2}{\sqrt{\pi}} \frac{\xi^2}{\nu \eta^2} e^{-\eta^2 \left[1 + \left(1 - \frac{1}{\eta}\right)^2 / \nu^2\right]} L(\nu) \tag{3.151}$$

and $L(\nu)$ is defined as a normalization factor to account for positive η

$$L(\nu) = \frac{2}{(1 + \sqrt{1 + \nu^2})} \tag{3.152}$$

Note that for small ν, $L \approx 1 + \frac{1}{4} \nu^2$ and at $\nu = 0$, the distribution is symmetric about the mean period, independent of the normalized wave amplitude. Joint density plots for low and high ν values are shown in Fig. 3.19. Note that at $\nu = 0.1$, it is almost symmetric about $\eta = 1$, while at $\nu = 0.6$, it is not.

The density function of the wave amplitude may be obtained by integration with respect to the period η over its positive range

$$p(\xi) = 2\xi e^{-\xi^2} L(\nu) \, \phi(\frac{\xi}{\nu}) \tag{3.153}$$
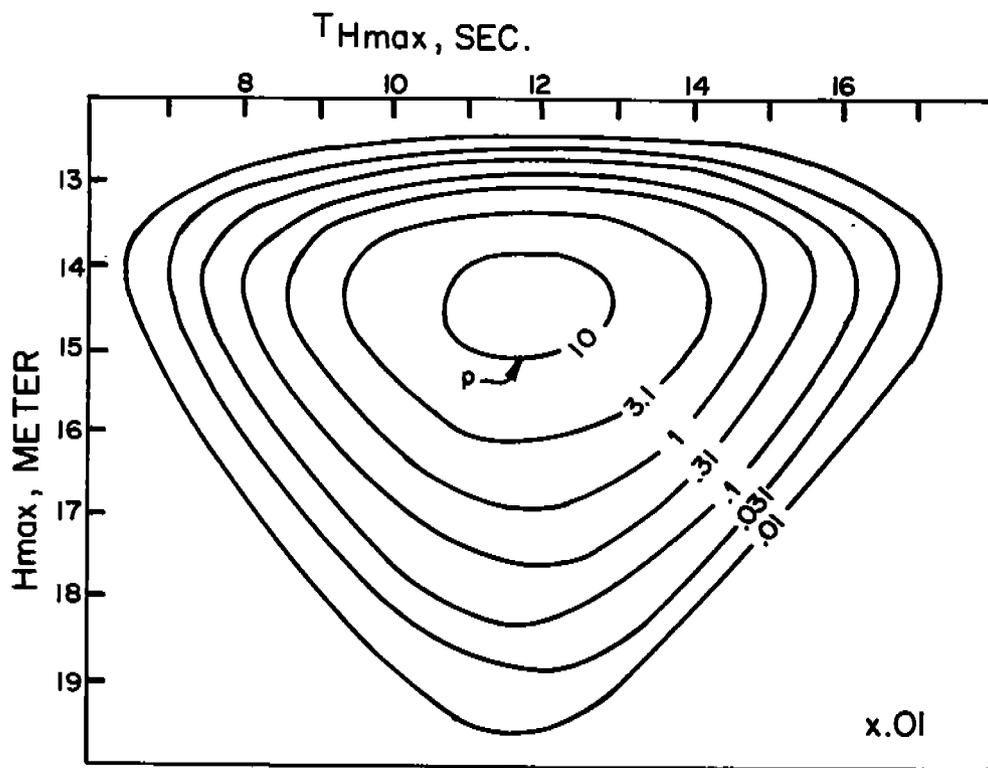
FIGURE 3.18   JOINT DISTRIBUTION FUNCTION OF H_{max} AND T_{Hmax} FOR H_s = 8m, T_z = 9s, AND A TIME INTERVAL OF 12 HOURS
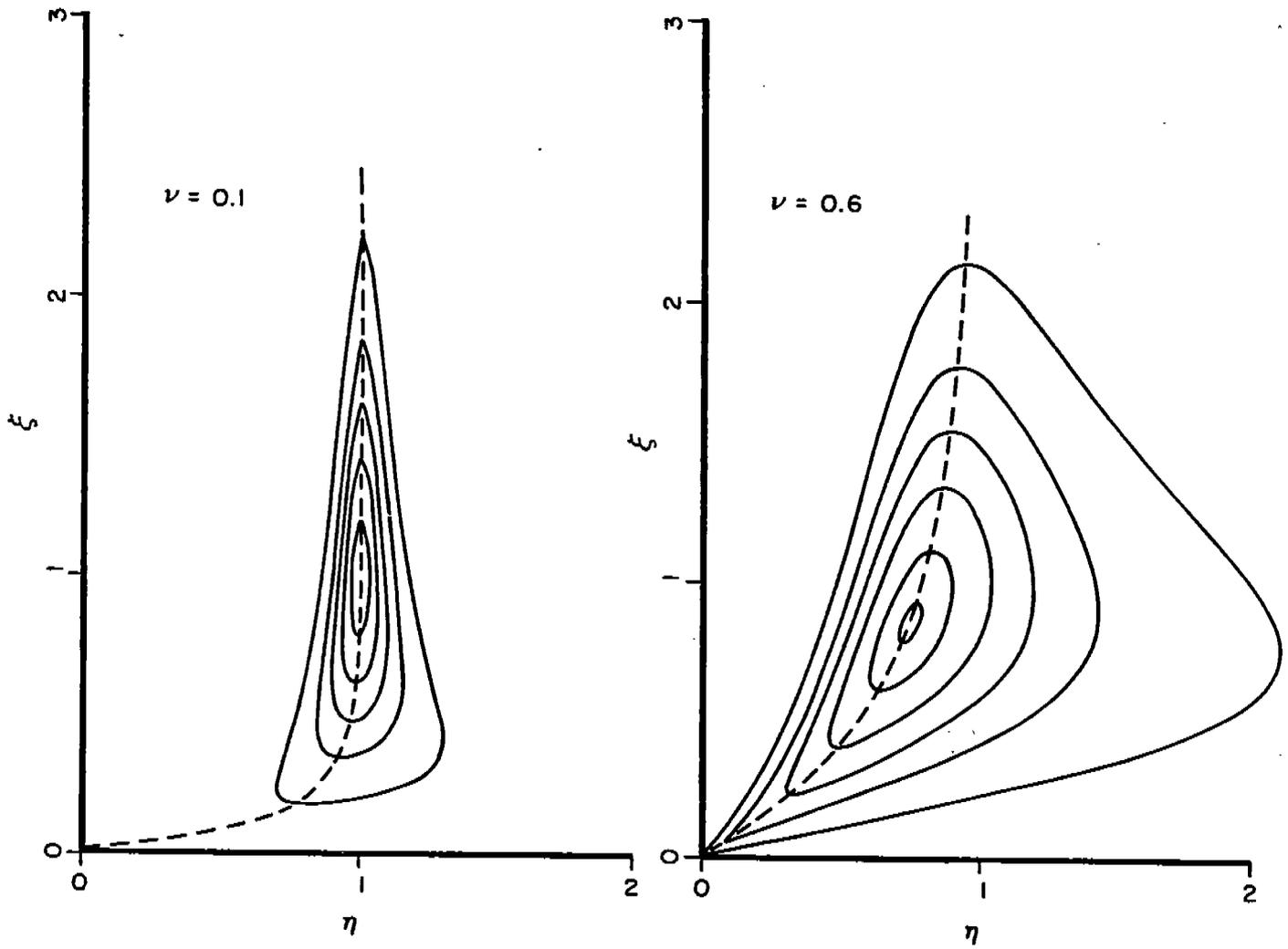
FIGURE 3.19   WAVE HEIGHT-PERIOD JOINT DENSITY PLOT FOR NARROW AND WIDE-BAND
SPECTRAL WIDTH PARAMETERS [LONGUET-HIGGINS (1983)]

where ϕ is the well known error function. Thus, the density is almost Rayleigh differing by the factor $L\phi(\frac{\xi}{v})$ which is small for small v. The density of the period η may be similarly obtained by integration with respect to ξ over its positive range,

$$p(\eta) = \frac{L}{2v\eta^2} \left[1 - (1 - \frac{1}{\eta})^2 / v^2 \right]^{-3/2} \qquad (3.154)$$

The conditional distribution of η for a fixed value of ξ may be found as

$$p(\eta|\xi) = \frac{p(\xi, \eta)}{p(\xi)} \qquad (3.155)$$

Lindgren and Rychlik (1982) derived approximate expressions for the joint distribution functions of crest-to-trough heights and periods of a stationary random process irrespective of its covariance or spectral structure. The process, however, was assumed Gaussian with mean zero. They compared their solutions with the approximate theory of Cavanie', et al. (1976), who considered only the positive maxima, thus excluding the shorter waves. It works for relatively narrow-band spectra ($\varepsilon < 0.7$) and agrees with an approximation of an exact model process shown by Lindgren and Rychlik. The latter method requires time-consuming numerical integration, but can handle many practical cases including low-frequency noise and bimodal spectra. Another approximation based on a simplified model has also been developed by Lindgren and Rychlik and is simpler to use and is similar to the Cavanie' approximation in accuracy, but includes shorter waves.

Nolte (1979) derived the joint probability density function including an additional order of approximation for the wave period which provided better agreement with the measured data [Nolte and Hsu (1979)].

Truncating the joint probability density function at $\eta = -\frac{1}{v}$ in order to avoid negative period, Ochi (1982) showed

$$p(\xi, \eta) = \frac{1}{1 - \phi(-\xi/v)} \frac{1}{\sqrt{2\pi}} \xi^2 \exp \left[-\frac{\xi^2(1 + \eta^2)}{2} \right] \qquad (3.156)$$

3.2.8 Extreme Wave Height - Steepness Distribution

The extremely high waves in deep water are responsible for capsizing smaller vessels as well as for damaging marine structures with their slamming

loads. Thus, the estimates of the encounter probabilities of occurrence of
these waves are very important from the design point of view. These waves are
invariably asymmetric. In describing these individual waves, one would
require additional parameters besides wave height and wave period. Myrhaug
and Kjeldsen (1984, 1987) presented the following three additional parameters
to describe their steepness and asymmetry:

(1) Crest front steepness, ε

$$\varepsilon = \frac{\eta_c}{(\frac{g}{2\pi})T \, T'} \qquad (3.157)$$

where η_c = crest elevation measured from MWL, and T' = time between crest and
zero-upcrossing.

(2) Vertical asymmetry factor, λ

$$\lambda = \frac{T''}{T'} \qquad (3.158)$$

where T'' = time between crest and zero-downcrossing so that $T_c = T' + T''$.

(3) Horizontal asymmetry factor, μ

$$\mu = \frac{\eta_c}{H} \qquad (3.159)$$

Thus, the estimation of the probability of occurrence of steep waves
should include these parameters. Myrhaug and Kjeldsen (1987) derived the
joint distribution of crest-front steepness and wave height. The joint
probability density distribution for this purpose may be written as the
product of the marginal density distribution of wave height and the
conditional distribution of wave steepness:

$$p(\hat{\varepsilon}, \hat{h}) = p(\hat{\varepsilon}|\hat{h}) \, p(\hat{h}) \qquad (3.160)$$

where $\hat{h} = H/H_{rms}$ and $\hat{\varepsilon} = \varepsilon/\varepsilon_{rms}$ normalized height and crest steepness respectively, $p(\hat{h})$ is marginal probability density of $\hat{h}$ and $p(\hat{\varepsilon}|\hat{h})$ is the conditional density distribution of $\hat{\varepsilon}$ and $\hat{h}$.

Based on the measured wave data on the Norwegian continental shelf, the Wiebull distribution was found to be suitable for $p(\hat{h})$. For the conditional distribution, both Weibull and log-normal distribution were found to work equally well.

The Weibull probability density function for a parameter, x, is given by

$$p(x) = \frac{\beta_x x^{\beta_x - 1}}{\rho_x^{\beta_x}} \left[- \left(\frac{x}{\rho_x}\right)^{\beta_x} \right] \tag{3.161}$$

where β_x and ρ_x are the Weibull parameters. For $\beta_x = 2$, one obtains Rayleigh distribution.

The log-normal probability density distribution is given by

$$p(x) = \frac{1}{\sqrt{2\pi} \, v_x x} \exp\left[\frac{(\ln x - \theta x)^2}{2v_x^2} \right] \, , \, x > 0 \tag{3.162}$$

where θ_x and v_x^2 denote the mean value and variance of $\ln \chi$, respectively.

The rms values, ε_{rms} and H_{rms} used in the normalization were obtained by fitting data as   , .

$$H_{rms} = 2.8582 \sqrt{m_0} \tag{3.163}$$

and

$$\varepsilon_{rms} = 0.0202 + 32.4\kappa \; ; \; \kappa = \frac{m_2}{g \sqrt{m_0}} \tag{3.164}$$

Thus, κ is related to a steepness parameter, $\kappa = H_s/ 4g\bar{T}_z^2$.

Use of Weibull distribution as the marginal distribution of $\hat{h}$ from data gave

$$\rho_{\hat{h}} = 1.05 \text{ and } \beta_{\hat{h}} = 2.39 \tag{3.165}$$

The Weibull distribution fitted to the conditional distribution of $\hat{\varepsilon}$ given $\hat{h}$ for the Norwegian shelf data, yielded the following functional relationships

$$\rho_{\hat{\varepsilon}}(\hat{h}) = \begin{cases} 1.37 - 1.10\hat{h} + 0.57\hat{h}^2 & \text{for } \hat{h} < 1.9 \\ 0.36 \tan^{-1}[2.80(\hat{h} - 1.9)] + 1.34 & \text{for } \hat{h} > 1.9 \end{cases} \qquad (3.166)$$

$$\beta_{\hat{\varepsilon}}(\hat{h}) = 0.56 \tan^{-1}[3.57(\hat{h} - 1.7)] + 2.28 \qquad (3.167)$$

On the other hand, the log-normal distribution fitted to the conditional distribution of the same data gave the following relationships for the parameters θ and γ^2 .

$$\theta_{\hat{\varepsilon}}(\hat{h}) = \begin{cases} 0.024 - 1.065\hat{h} + 0.585\,\hat{h}^2 & \text{for } \hat{h} < 1.7 \\ 0.32 \tan^{-1}[3.14(\hat{h} - 1.7)] - 0.096 & \text{for } \hat{h} > 1.7 \end{cases} \qquad (3.168)$$

$$\gamma_{\hat{\varepsilon}}^2 = -0.21 \tan^{-1}[2.0(\hat{h} - 1.4)] + 0.325 \qquad (3.169)$$

Both these models fit the data reasonably well. However, the log-normal distribution seemed to do better at the higher values of $\hat{\varepsilon}$ and $\hat{h}$. The estimates of the probability of occurrence of extremely steep waves were significantly higher for the log-normal conditional distribution.

3.3 SHORT-TERM RESPONSE PREDICTION

The short term is defined as the period of time in which the ocean waves may be considered stationary and ergodic. Thus, a given wave record and a corresponding energy density spectrum is needed to describe the short-term probabilistic properties of the sea of a particular severity level. The severity level may be described by the mean wind speed or the characteristic wave height (H_s) and wave period (T_z). The duration of a short-term sea is typically a few hours whereas the wave record is typically on the order of 30 mins. long.

The short-term response analysis is then based on the short-term waves. If a frequency domain analysis is possible, then only the wave energy density spectrum is required. In the case of a numerical time domain analysis, a time history of the short-term waves is needed. It has already been shown how the time history may be generated from a wave spectrum. If a time domain analysis is performed where a frequency domain solution is not possible, then the amplitudes of the response time history may be fitted to a distribution function to generate the short-term distribution of the response. This method may be used in the short-term prediction of a nonlinear system. It is, however, time consuming.

For a linear system in which the response is linearly related to the waves, a spectral analysis provides all the necessary information regarding the responses, as will be shown shortly. For a nonlinear system, approximations are often made in both frequency and time domain analysis. The approximation chosen depends on the extent and complexity of the nonlinearity in the system. The majority of the work on nonlinear problems deals with the short-term responses and the statistics related to the short-term responses.

Section 3.2 is the longest section of Chapter 3 as most of the available techniques on handling nonlinear problems in offshore mechanics are reviewed in this section. In some cases, brief derivations of the equations for the statistical probabilities are shown. While a few distribution (or density) functions for the response time history are shown, the important aspect addressed here is the probability distribution of the amplitude of response. Of course, once the distribution is known, the distribution of the maximum response amplitude at a chosen probability level may be easily determined. Methods of projecting this short-term response to a long-term response, corresponding to the design life of the structure under consideration, are briefly outlined in the following section.

3.3.1 Linear Systems

The inertia force on an object including the forces obtained by the linear wave diffraction theory is a linear force. The inertia part of Morison's equation can be written for a vertical cylinder per unit length as

$$f_I(t) = k_M \dot{u}(t) \qquad (3.170)$$

where $\dot{u}$ (t) is the water particle acceleration. Under linear wave theory

$$\dot{u}(t) = -\frac{gHk}{2} \frac{\cosh ks}{\cosh kd} \sin (kx - \omega t) \qquad (3.171)$$

or

$$\dot{u}(t) = gk \frac{\cosh ks}{\cosh kd} \eta(t + T/4) \qquad (3.172)$$

where T is the wave period and T/4 in this case represents a phase lead of 90°, i.e. the acceleration is zero at the wave crest. Therefore,

$$f_I(t) = k_M gk \frac{\cosh ks}{\cosh kd} \eta_{90^\circ} (t) \qquad (3.173)$$

Then writing the covariance of f_I in terms of the covariance of η and taking the Fourier transform of both sides

$$S_{f_I}(\omega) = H^2_{f_I}(\omega) S(\omega) \qquad (3.174)$$

where

$$H_{f_I} = k_M gk \frac{\cosh ks}{\cosh kd} \qquad (3.175)$$

The significant amplitude of the force is obtained from the area under the response spectrum curve.

$$f_s = 2 \sqrt{\int S_{f_I}(\omega) d\omega} \qquad (3.176)$$

Assuming a mean period of 9 seconds and a short-term period (T_R) of 2.5 hours, the probable maximum value of the force amplitude (for 1000 waves) is

$$f_{max} = 1.86 f_s \qquad (3.177)$$

In usual extreme value analysis, the maxima (or minima) are assumed to be uncorrelated and statistically independent. This may be a crude approxi-

mation. If the random process under investigation is Gaussian and narrow banded, then one may work with the derived process, namely, the envelope of the narrow-band process. The neighboring maxima of an envelope process are generally not as well correlated as those of the underlying process. Moreover, the extreme values of the envelope process may be taken as an upper estimate of the extreme values of the base process. Naess (1982) developed analytical formulas for the envelope process of a narrow band Gaussian system. Assuming that the random variable under investigation is given by $x(t)$ for a time interval, T_R, the expected maximum value of $x(t)$ is given by

$$E[\max x(t)] \leqslant m_0 \left(\eta + \frac{G}{\eta}\right) \tag{3.178}$$

where G denotes the Euler's constant, $G = 0.5772$, and η is obtained from the solution of

$$\eta = 2 \ln(\kappa\eta N) \tag{3.179}$$

where N = number of maxima in $x(t)$, and

$$\kappa = 2 \sqrt{2\pi(1 - \rho^2)} \sqrt{1 - \varepsilon^2} \left(1 + \sqrt{1 - \varepsilon^2}\right)^{-1} \tag{3.180}$$

ε = spectral width parameter, ρ = correlation coefficient defined as

$$\rho = \frac{m_1^2}{m_0 m_2} \tag{3.181}$$

and the spectral moments, m_n, are defined by

$$m_n = \int_0^\infty \omega^n S(\omega) \, d\omega \qquad n = 0, 1, 2, \ldots \tag{3.182}$$

It was shown through numerical examples that the introduction of statistical dependence between neighboring maxima (through ρ) into the extreme value prediction generally leads to a decrease of the resulting extreme value estimates.

3.3.2 Nonlinear Systems

When the response function has a nonlinear relationship with the wave amplitude, the system is called nonlinear. Thus, when drag is present in a system, it constitutes a nonlinear system. The same is true for nonlinear damping for a moving body. In these cases, approximate methods are employed in predicting extreme response values. One of these approximations is a series representation of the nonlinear term so that only a few terms in the series require consideration, depending on the extent of nonlinearity. If only the first term of the series is retained, then the system is called linearized.

3.3.2.1 Wave Drag

In the case where drag is important and cannot be ignored, the conversion of the wave spectrum to the response spectrum is not straight forward. In this case, a linearization technique is often used for the drag force.

Since the drag force is proportional to the square of the velocity, the linear approximation of the normalized drag force is written as

$$|x(t)|x(t) \approx C_1 x(t) \tag{3.183}$$

where $x(t) = u(t)/\sigma_u$ and σ_u is the rms value of the velocity profile. Assuming that $u(t)$ is normally distributed with zero mean and standard deviation, σ_u, the most accurate linear estimate of $|u|u$ gives

$$C_1 = \sqrt{\frac{8}{\pi}} \tag{3.184}$$

Similarly, the cubic approximation

$$|x|x \approx C_1 x + C_3 x^3 \tag{3.185}$$

will yield

$$C_1 = \sqrt{\frac{2}{\pi}}, \quad C_3 = \sqrt{\frac{2}{9\pi}} \tag{3.186}$$

90

The quintic approximation

$$|x|x \approx C_1 x + C_3 x^3 + C_5 x^5 \qquad (3.187)$$

will give

$$C_1 = \frac{3}{4}\sqrt{\frac{2}{\pi}}, \quad C_3 = \frac{1}{2}\sqrt{\frac{2}{\pi}}, \quad C_5 = -\frac{1}{60}\sqrt{\frac{2}{\pi}} \qquad (3.188)$$

In terms of the dimensionless quantity, $x = u/\sigma_u$, the linear approximation does a fair job for $|x| < 2$; that is, if the velocity is within $\pm 2\sigma_u$. Since according to normal theory this happens 95% of the time, the linear approximation will do a good job of estimating the spectral density most of the time.

The cubic approximation is quite an improvement over the linear expression, yielding results accurate to more than $3\sigma_u$. The quintic approximation is only slightly better than cubic producing results accurate to nearly $4\sigma_u$.

3.3.2.2 Wave-Plus-Current Drag

When current is present and drag is not negligible compared to inertia, then the relationship between the wave force and wave profile is further complicated by the presence of current, U. If the current is considered uniform and flows in the same direction as the wave (or opposing it, in which case U is negative) then the drag force per unit length of a vertical cylinder is written in terms of the relative velocity between current and water particle velocity.

$$f_D(t) = k_D |u(t) - U|[u(t) - U] \qquad (3.189)$$

In Eq. 3.189 the current is in the opposite direction of the wave. In the presence of current, the mean value of the relative velocity is not zero as before. In this case, the linearization is more complicated. If we approximate $v|v|$ as

$$v|v| \approx C_0 + C_1 v \qquad (3.190)$$

91

where $v = u(t) - U$, μ_v is the mean value of v, and σ_v^2 is its variance about the mean, then

$$C_0 = (\sigma_v^2 - \mu_v^2) [2 \, \Phi \, (\gamma) - 1] - 2 \, \mu_v \, \sigma_v \, \phi \, (\gamma) \qquad (3.191)$$

and

$$C_1 = 2 \, \mu_v \, [2 \, \Phi \, (\gamma) - 1] - 4 \, \sigma_v \, \phi \, (\gamma) \qquad (3.192)$$

where the mean value $\mu_v = -U$ and $\gamma = -U/\sigma_u$ is the strength of the current. The quantity, $\phi(x)$, is written as

$$\phi(x) = \frac{e^{-x^2/2}}{\sqrt{2\pi}} \qquad (3.193)$$

whereas $\Phi(x)$ is given by its integral and known as the error function

$$\Phi(x) = \int_{-\infty}^{x} \frac{e^{-t^2/2}}{\sqrt{2\pi}} \, dt = \int_{-\infty}^{x} \phi(t) \, dt \qquad (3.194)$$

3.3.2.3 Structural Dynamics Response

When a structure responds to waves, the motion of the structure results in a relative velocity between the wave velocity and the structure velocity. The modified form of the Morison equation is used in analyzing structural dynamic response in random waves.

In many cases, the structural motions are small compared to the water particle motion. Assuming that the response velocity is small compared to the water particle velocity, the nonlinear drag term is expressed in a Taylor series, and higher order terms in structural velocity are neglected.

$$|u - \dot{x}| \, (u - \dot{x}) = |u|u - 2|u|\dot{x} \qquad (3.195)$$

Further the term involving absolute values of u are replaced by their polynomial approximations

$$|u|u = \sqrt{2/\pi} \, \sigma_u \, u + \frac{1}{3} \sqrt{2/\pi} \, \frac{u^3}{\sigma_u} \qquad (3.196)$$

92

$$|u| = \sqrt{8/\pi}\; \sigma_u + \alpha\; \sqrt{2/\pi}\; \frac{u^2 - \sigma_u{}^2}{\sigma_u} \qquad\qquad (3.197)$$

The parameter, α, is introduced in Eq. 3.197 which indicates a small fluctuation in damping about its time average. On using these approximations, the solution may be obtained by a perturbation method.

A second method, known as an equivalent damping method, transforms the equation of motion to its fundamental resonance mode and uses the approximations of the wave drag force outlined above, including a time varying damping in a series form. An equivalent constant damping is obtained as a first approximation by replacing the time varying terms with equivalent constant term. The equivalence is obtained in terms of work done over a cycle. To a first approximation, the resonant response as well as the nonresonant response are considered to be Gaussian.

The linear and cubic estimates of the spectral density of the wave drag force on a cylinder of unit diameter and unit length are shown in Fig. 3.20. For this example, the random wave is chosen as having H_s = 24m and T_z = 14 sec. The spectrum is computed at the surface and 40m below the surface. It is seen that the cubic representation of the drag force provides more energy at about 3 times the predominant frequency. This gives rise to the super-harmonic response of the structure at higher frequencies in waves.

Eatock Taylor and Rajagopalan (1981) compared the method of equivalent linearization for the nonlinear term with the complete nonlinear time history simulation. They found that the response spectra produced by the linearization technique may be underestimated, particularly in high waves. Inclusion of the cubic term significantly improves the estimation.

Dao and Penzien (1982) investigated the effect of linearizing the drag force through an example where a single degree of freedom system was subjected to a harmonic excitation. They considered the forcing function for the second order linear differential equation to be nonlinear and composed of the modified relative velocity model of the Morison equation. Three different cases were considered; (1) the coupled relative velocity form of the nonlinear drag term, (2) the uncoupled nonlinear drag term and, (3) the linearized form of the drag term.
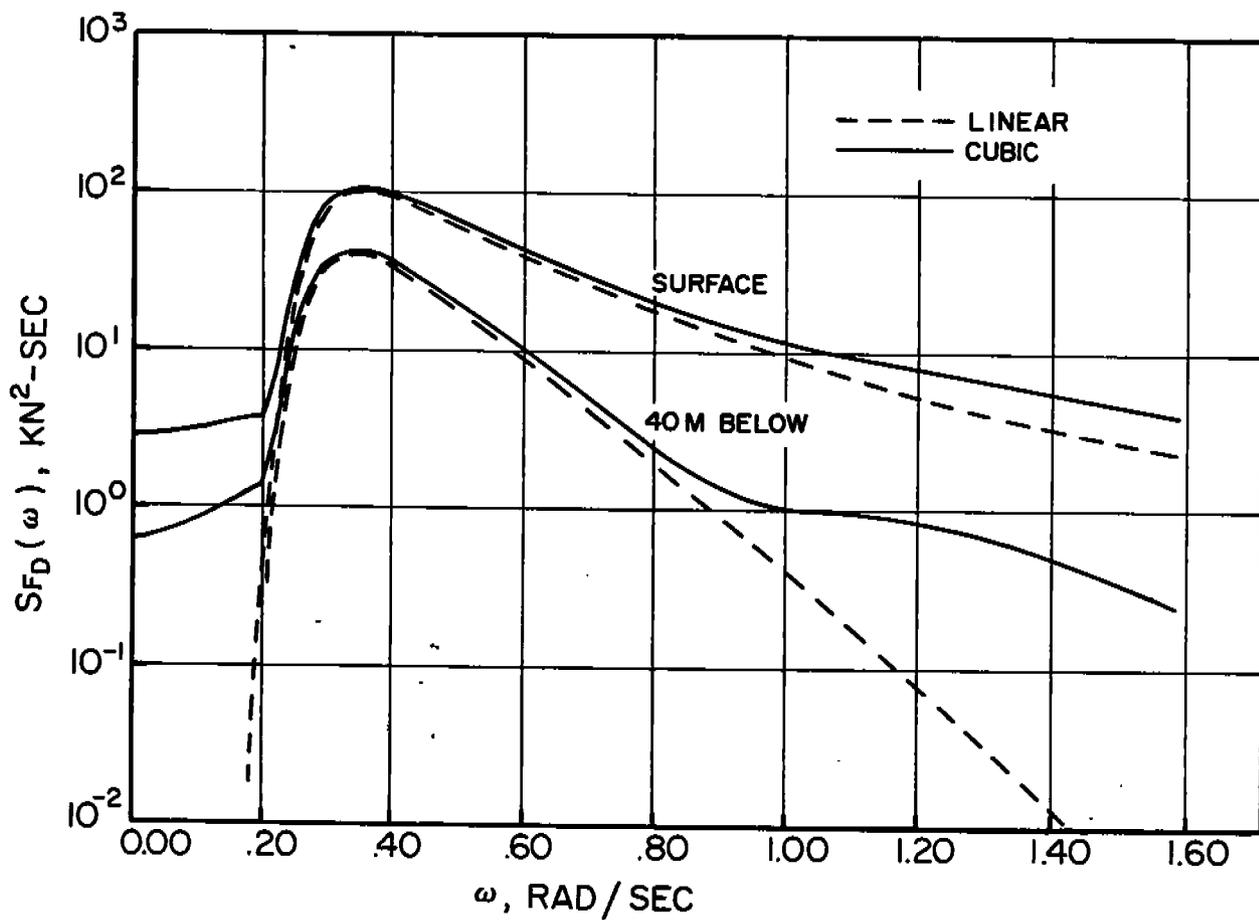
FIGURE 3.20   DRAG FORCE SPECTRUM FOR A UNIT-DIAMETER CIRCULAR CYLINDER AT
THE WATER SURFACE AND 40M BELOW SURFACE IN P-M WAVES [EATOCK
TAYLOR ET AL. (1981)]
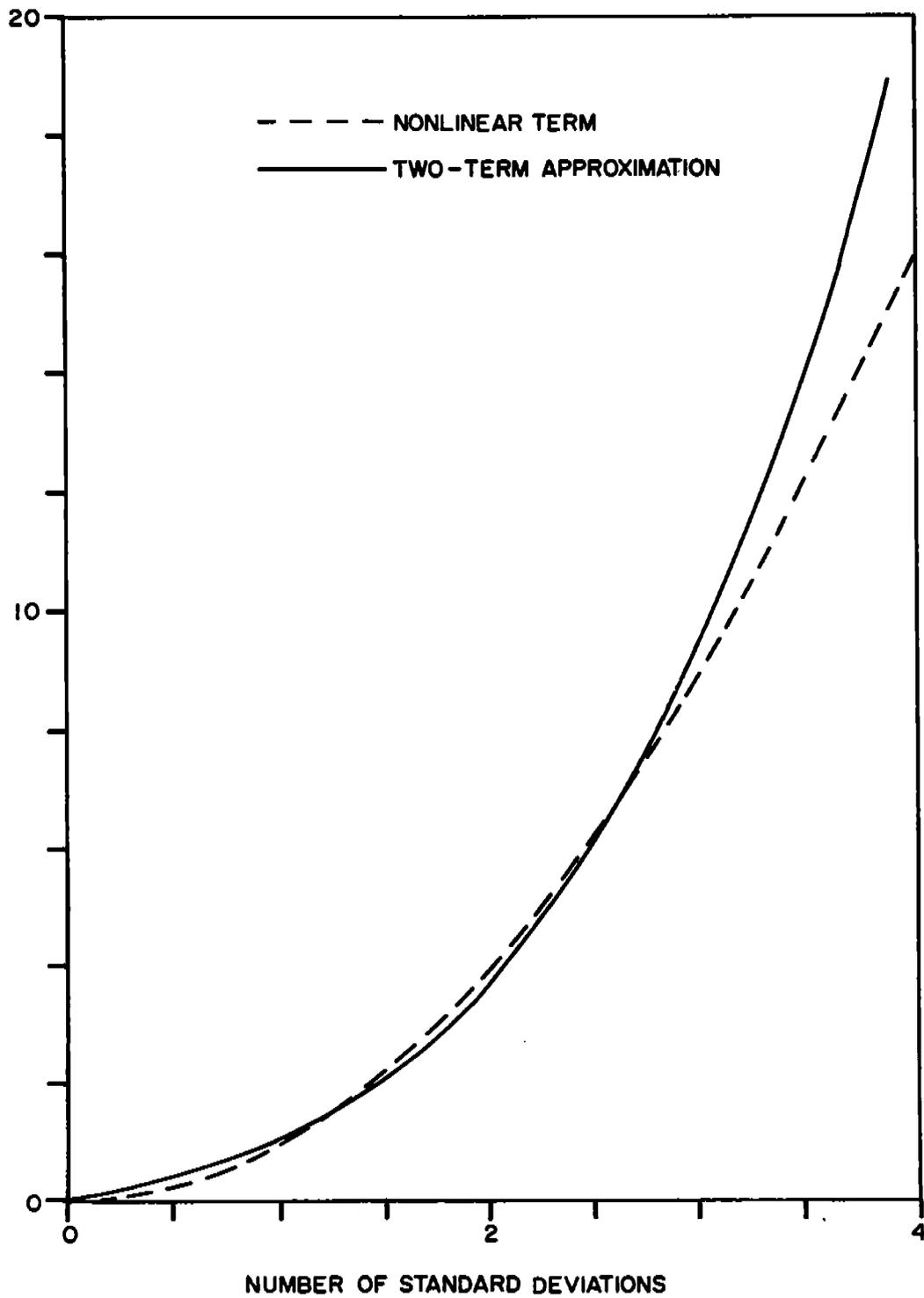
FIGURE 3.21   COMPARISON OF TWO-TERM POLYNOMIAL APPROXIMATION WITH THE
NONLINEAR DRAG TERM IN RELATIVE VELOCITY MODEL [DUNWOODY AND
VANDIVER (1981)]

In the second case, the drag term was uncoupled, assuming that the water particle velocity is much larger than the structure velocity, e.g., for a jacket structure. Then the approximation takes the form given by Eq. 3.195. The quantity $|u|u$ is replaced by a Fourier series by writing $u = u_0 \cos \omega t$ and using

$$|\cos \omega t| \cos \omega t = \sum_m a_m \cos m\omega t, \qquad m = 1, 3, 5, \ldots \qquad (3.198)$$

where

$$a_m = \begin{cases} -8/[m\pi(m^2 - 4)] & \text{for } m = 1, 5, 9, \ldots \\ \\ 8/[m\pi(m^2 - 4)] & \text{for } m = 3, 7, 11, \ldots \end{cases} \qquad (3.199)$$

Also, $|u|$ is replaced by its temporal average,

$$|u| = u_0 \overline{|\cos \omega t|} = \sqrt{\frac{2}{\pi}} u_0 \qquad (3.200)$$

Thus, the nonlinear terms are linearized and the equation of motion can be solved for $x(t)$ in a series form as functions of $m\omega t$.

In the third case, linearization is achieved by writing

$$|u - \dot{x}| (u - \dot{x}) = C_1 (u - \dot{x}) \qquad (3.201)$$

where C_1 minimizes the error in a least square sense. The value of C_1 is given by

$$C_1 = \frac{[v_R |v_R|]}{[v_R^2]} \qquad (3.202)$$

If v_R ($= u - \dot{x}$) is assumed harmonic, then

$$C_1 = 1.20 \, \sigma_{v_R} \qquad (3.203)$$

where σ_{v_R} is the rms value of v_R. Once this linearization is introduced in the equation of motion, the expression for $x(t)$ may be obtained in terms of σ_{v_R} which may be solved by an iterative technique.

94

The numerical results for a single degree of freedom system in regular waves showed that the first two solutions are quite close while the linearized solution produces large error. The analysis was then extended to random waves. For random waves, the extreme values of the response were found to closely follow the Gumbel Type I distribution given by Eq. 3.8. This was true irrespective of the method of representation of the drag force. In random waves, the mean square values produced by the three methods are similar, while the mean extreme value determined by the linearized method can be as low as 65% of the maxima for large values of H_s/D (> 20).

Dunwoody and Vandiver (1981) predicted the dynamic response of offshore structures to the random wave excitation. The response included the effect of the separated flow drag force in terms of the relative velocity formulation. The equation of motion had the form similar to Eq. 2.67 with the nonlinear damping replaced by the relative velocity terms. The drag term of the Morison formula was approximated by a cubic polynomial in the relative velocity between the fluid and the structure. Thus, following an approach similar to that developed by Borgman (1969) the relative velocity drag is written as

$$|v_R|v_R = C_1 v_R + C_3 v_R^3 \tag{3.204}$$

where $v_R = u - \dot{x}$.

The coefficients C_1 and C_3 have the values

$$C_1 = \sqrt{\frac{2}{\pi}} \sigma_{v_R} \tag{3.205}$$

and

$$C_3 = \sqrt{\frac{2}{\pi}} \frac{1}{3\sigma_{v_R}} \tag{3.206}$$

which are equivalent to Borgman's expressions with σ_{v_R} as the rms value of v_R. The correlation between the nonlinear term and the approximation in Eq. 3.204 is quite good over a large range of σ_{v_R} (up to about 3) as shown in Fig. 3.21. The cubic term is handled through the convolution integral (see next section) similar to Borgman except for the relative velocity form. The solution is obtained by iteration due to this coupling. The linear and

95

nonlinear components of the hydrodynamic force spectra for a single degree of freedom of cylinder motion in a random fluid field are shown in Fig. 3.22. Note that at the low frequency, the drag contribution is large. The quantity α is the ratio of the fluid added mass to the sum of the cylinder mass and the added mass, while $\sigma_{\dot{x}}$ is the rms value of the cylinder velocity. The linear term is proportional to the fluid velocity spectrum only.

Sigbjörnsson and Mörch (1982) analyzed the effect of the second term of the series (cubic approximation) representing a nonlinear drag term that includes the three-term convolution of the autospectral density of waves. The main peak of the wave force spectral density appears at the modal frequency. From the series expression, Eq. 3.204, it is evident that superharmonics may appear in the load spectral density in frequency bands near 3, 5, 7, . . ., respectively times the modal frequency of a single peaked wave spectral density. Inclusion of the lowest superharmonics made the load spectral density bimodal. This method was applied to the example of a jacket-type fixed tower which was permitted to deflect.

A JONSWAP type wave spectrum was chosen for this purpose, as shown in Fig. 3.23, having a significant height of H_s = 15m, a modal frequency of ω_0 = 0.35 rad/sec. and a peakedness parameter of γ = 3.78. The autospectral density of drag forces acting on a 0.5m diameter vertical pile at different elevations is given in Fig. 3.24. The computation includes two terms of the series approximation for the drag force. No secondary peak is visible close to the free surface. This is because the linear contribution of the drag force is large and overshadows the convolution contribution. In deeper waters the secondary peaks become clearly visible because of the slower depth attenuation of the cubic contribution compared to the linear one. The auto spectral density of the total load on the pile (including inertia) shown in Fig. 3.25 has the same general trend as the drag force spectral density. This is a result of drag force dominance in this case. However, a certain amount of reduction is seen in the relative size of the secondary peak because of the presence of the inertia forces.

Table 3.4 shows the mean square (ms) force contributions due to the inertia forces and the linearized and nonlinear (second-order) drag forces, respectively, for different water elevations (depths). The nonlinear drag is obtained from the three-fold convolution contribution of the energy density

96
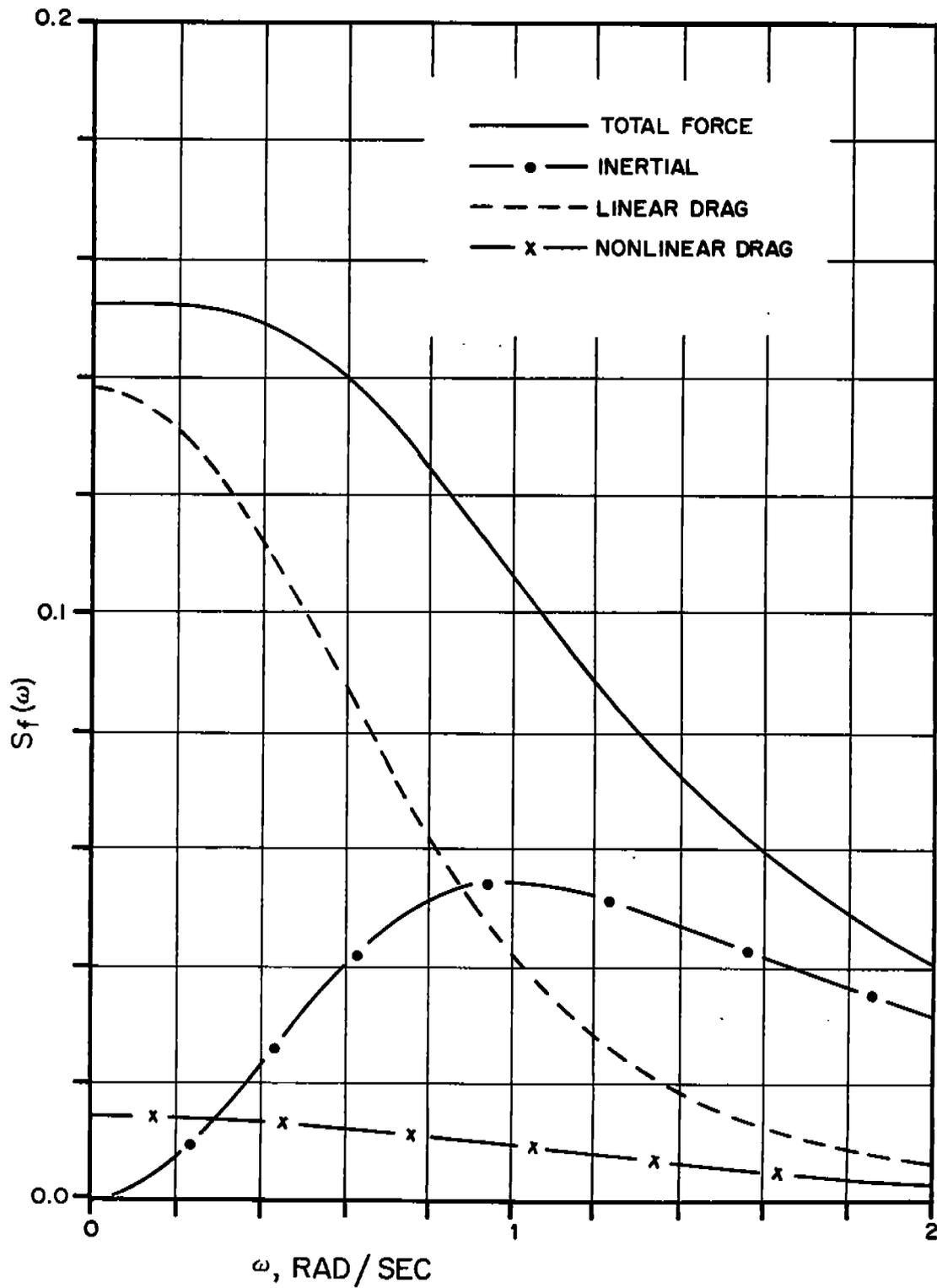
FIGURE 3.22   COMPONENTS OF HYDRODYNAMIC FORCE SPECTRA ON A MOVING CYLINDER
IN A RANDOM FLUID FIELD (α = 0.079, $\sigma_{\dot{x}}$ = 2.5) [DUNWOODY AND
VANDIVER (1981)]
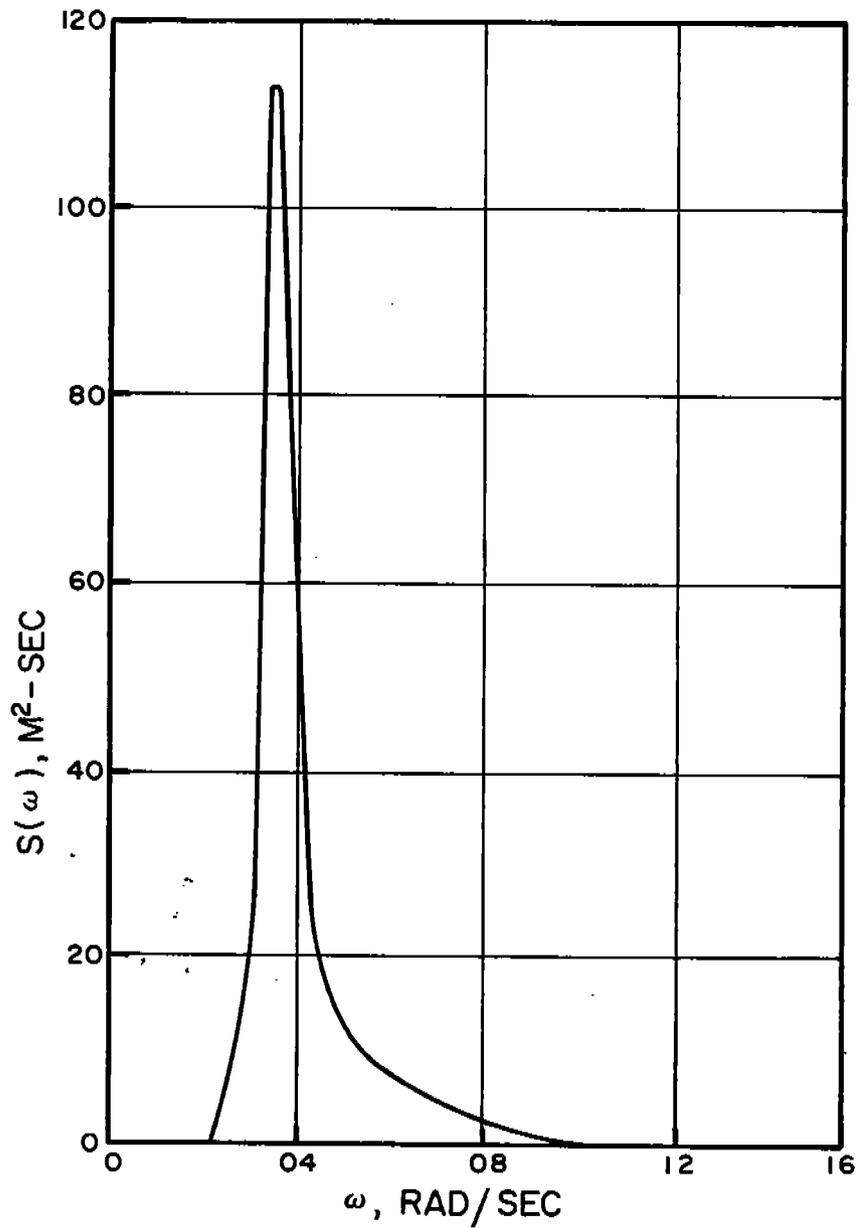
FIGURE 3.23   AUTOSPECTRAL DENSITY OF EXAMPLE SEASTATE GIVEN BY A JONSWAP
SPECTRUM; SIGNIFICANT WAVE HEIGHT = 15m; MODEL FREQUENCY = 0.36
rad/s; AND PEAKEDNESS PARAMETER = 3.78 [SIGBJORNSSON ET AL.
(1982)]
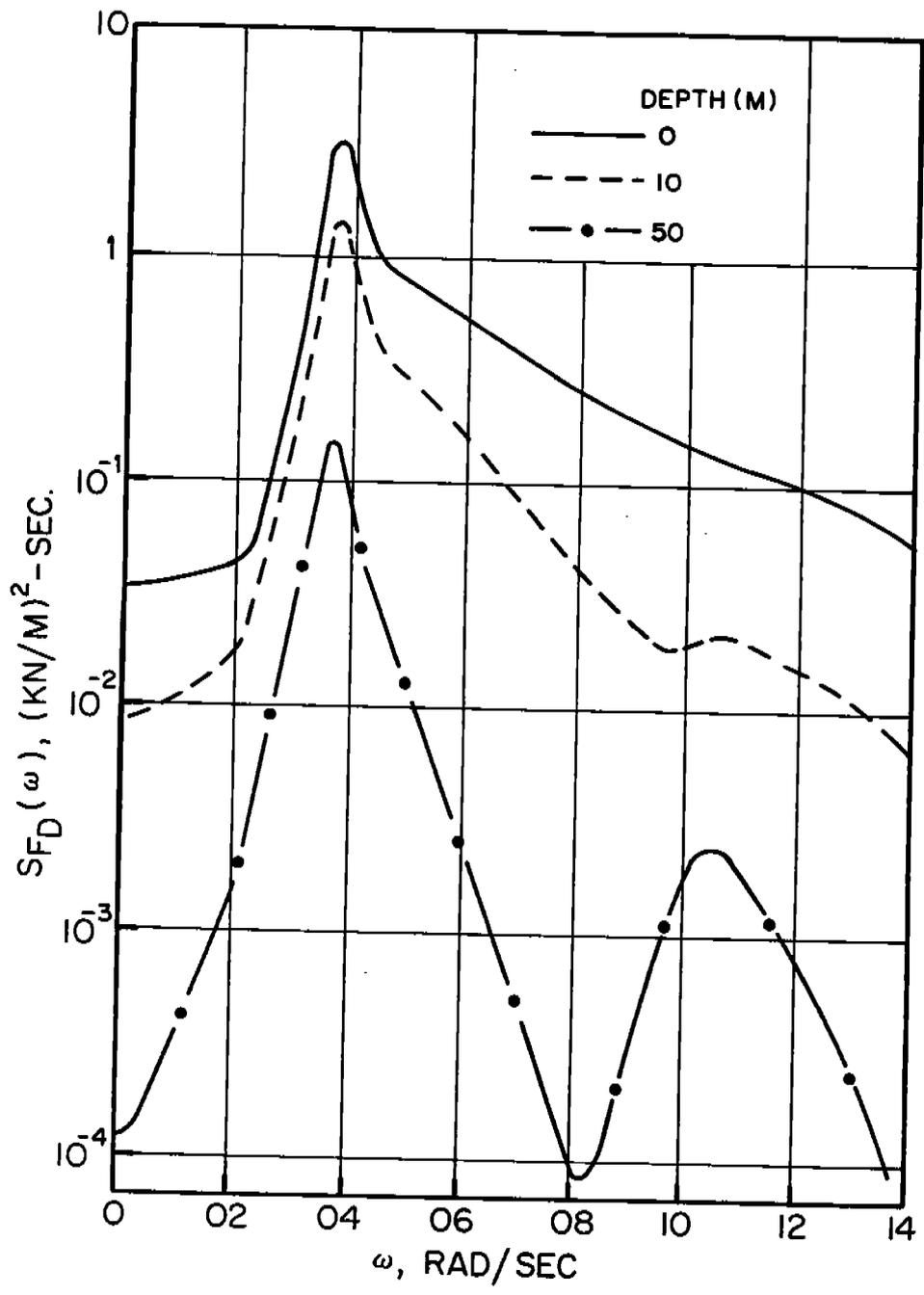
FIGURE 3.24   AUTOSPECTRAL DENSITY OF DRAG FORCES ACTING ON RIGID CIRCULAR
VERTICAL CYLINDER OF DIAMETER = 0.5m [SIGBJORNSSON ET AL.
(1982)]
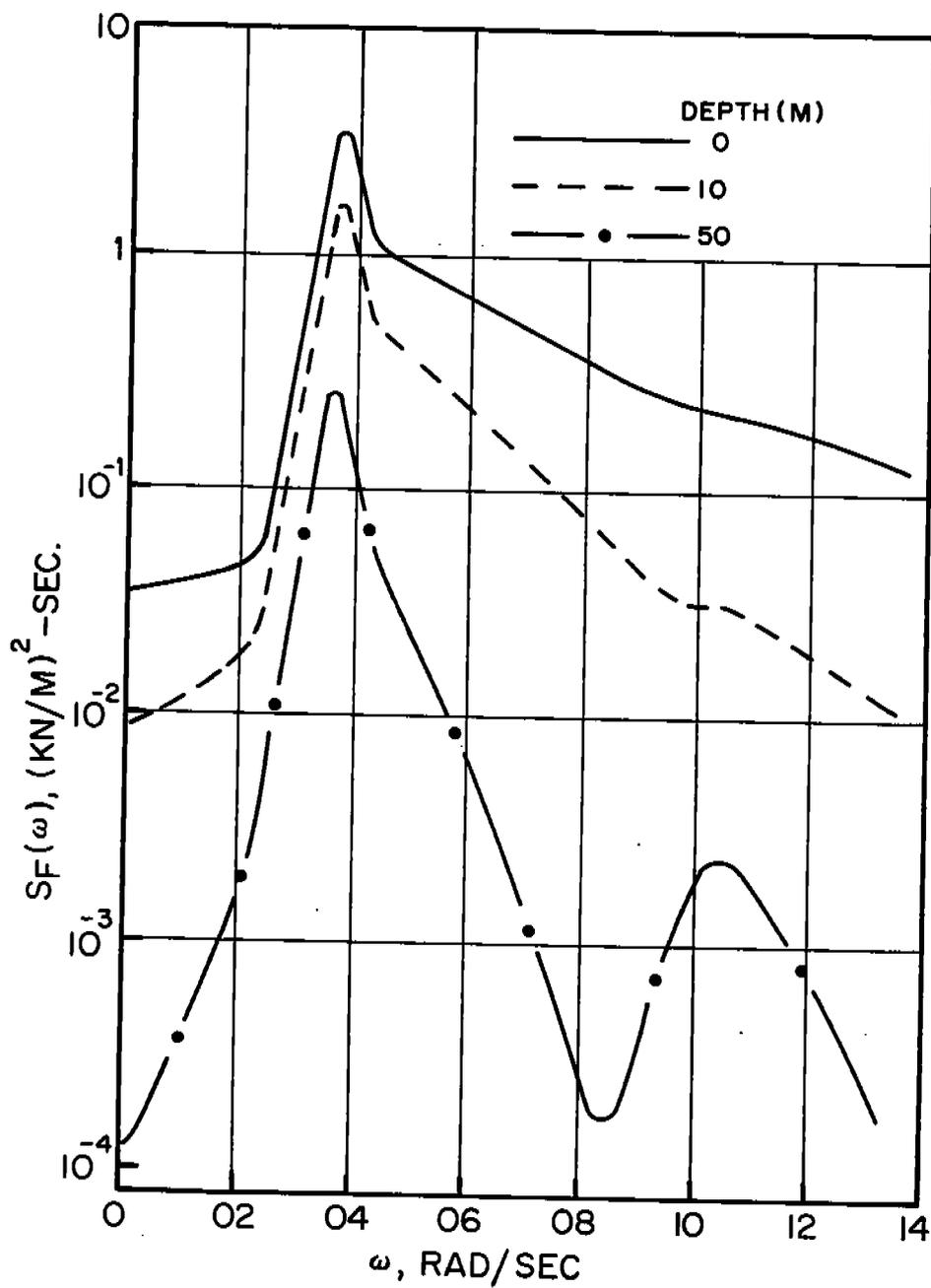
FIGURE 3.25   AUTOSPECTRAL DENSITY OF TOTAL WAVE FORCES ACTING ON RIGID
CIRCULAR VERTICAL CYLINDER OF DIAMETER = 0.5m [SIGBJORNSSON
ET AL. (1982)]

TABLE 3.4

MEAN SQUARE WAVE FORCE COMPONENTS
FOR VERTICAL PILES FOR A JONSWAP SEASTATE
SIGNIFICANT WAVE HEIGHT = 15m; MODAL FREQUENCY = 0.35 rad/s
[SIGBJORNSSON, ET AL. (1982)]

| DEPTH (m)	DIAMETER (m)	INERTIA FORCE	LINEAR DRAG FORCE	NONLINEAR DRAG FORCE
0	0.5	29.6	60.4	10.0
	5.0	96.3	3.2	0.5
10	0.5	20.1	68.5	11.4
	5.0	96.2	3.3	0.5
50	0.5	37.0	54.0	9.0
	5.0	98.3	1.4	0.2
100	0.5	58.8	35.3	5.9
	5.0	99.3	0.6	0.1
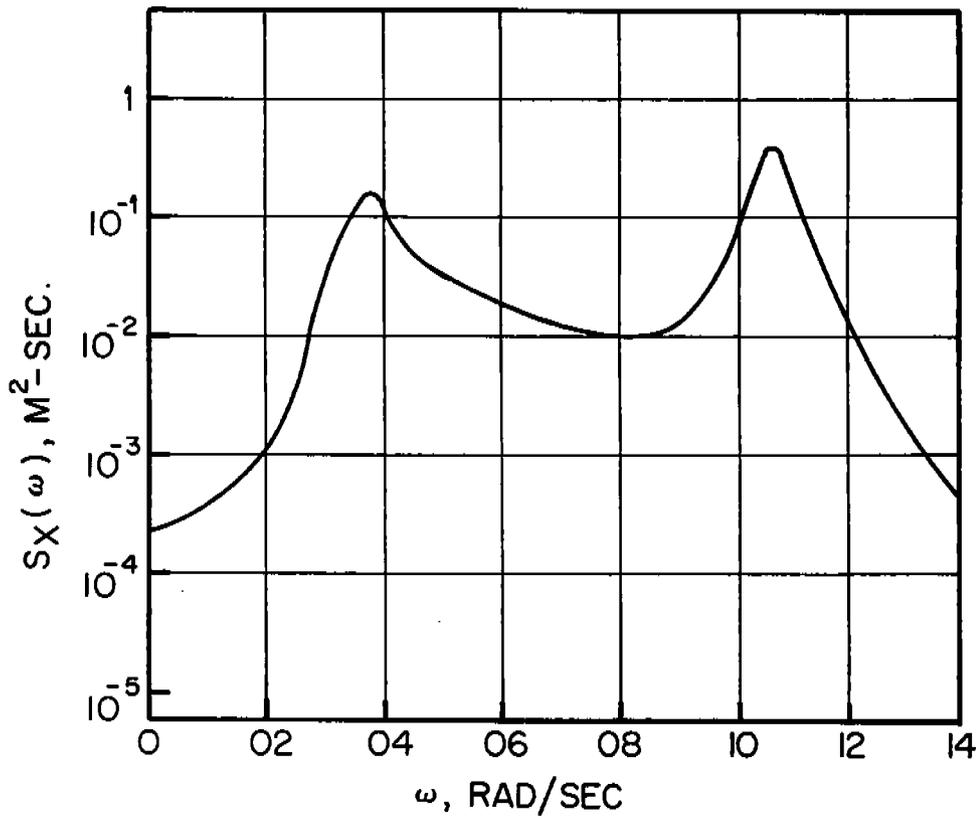
FIGURE 3.26   AUTOSPECTRAL DENSITY OF DECK DISPLACEMENTS OF EXAMPLE PLATFORM
SUBJECTED TO JONSWAP SEASTATE; SIGNIFICANT WAVE HEIGHT = 15m;
MODEL FREQUENCY = 0.35 rad/s [SIGBJORNSSON ET AL. (1982)]

spectrum (second term of the series approximations of the nonlinear drag force). The results are given for two different pile diameters. The contribution due to the nonlinear term is not significant for the inertia dominated pile, D = 5m, as can be expected. In fact, even the linear drag term is of secondary importance compared to inertia. For the drag dominated pile, D = 0.5m, the nonlinear term is only about 15% of the linear drag term.

These examples indicate that the stochastic linearization method represents the mean squared wave forces quite reasonably for engineering purposes. However, the "super harmonics" present in the drag forces may produce secondary spectral peaks which may be extremely important in the evaluation of dynamic structural responses.

Let us illustrate this by the following example of a structural response. Assume a jacket structure in 300m water depth having a fundamental natural frequency, ω_0 = 1.05 rad/sec., and a corresponding modal damping factor, ζ = 0.027. The displacement of the deck of the structure due to the JONSWAP wave of Fig. 3.22 was investigated by Sigbjörnsson and Mörch (1982) in terms of a single degree of freedom linear equation of motion, but with nonlinear excitation derived earlier. Assuming that for a fixed offshore platform in severe seas, the water particle velocity is much larger than the structure velocity, or in other words, $E[|\dot{u}|] > E[|\dot{x}|]$, the matrix equation of motion of the platform is

$$m\ddot{x} + C|\dot{u}|\dot{x} + Kx = F(t) \qquad (3.207)$$

The displacement spectrum is obtained from

$$S_x(\omega) = H(\omega) \, S(\omega) \, H^{T*}(\omega) \qquad (3.208)$$

where

$$H(\omega) = [\, K - \omega^2 M + i\omega C \, \sqrt{\tfrac{2}{\pi}} \, \sigma_{\dot{u}} \,]^{-1} \qquad (3.209)$$

where the superscript, T, refers to transform and a star refers to the complex conjugate. The autospectral density of the deck displacement is shown in Fig. 3.26. The secondary peak in the loading spectra, being in resonance with

97

the fundamental natural frequency of the platform, produces a sharp secondary peak in the displacement spectra. Thus, in designing fixed platforms, the fundamental natural frequency of the platform should be matched against the superharmonic frequencies of the drag force contribution to investigate the possibility of amplification. If such possibilities exist, then these terms may have to be included in the analysis of the response. Of course, the higher order terms may make the analysis extremely complicated and time consuming. A time domain simulation would, of course, include these effects explicitly.

For fixed platforms that respond statically, the extreme value analysis is carried out in the usual way by computing the short-term force distributions on the platform and quasi-static structural and foundation analysis. However, deepwater platforms may be excited at the lower wave frequencies of about 3 to 4 secs. and the super-harmonic loads discussed above. In this case, the dynamic response of the structure should be accounted for in terms of the dynamic inertia forces. The degree of dynamic response will depend on the frequency content of the exciting force from random waves and the structural and hydrodynamic damping. Thus, to account for the dynamic inertial loads, the regular wave static solutions are corrected by the dynamic amplification factors (DAF) computed by random wave analysis. Larrabee (1982) provided a method of selection of the dynamic amplification factor. The method is based on selecting a given probability level (of exceedance) over a given duration of seastate for both the dynamic response and static response and then defining DAF as the ratio between the two.

3.3.2.4 General Linearization Technique

The technique of equivalent linearization for the specific cases outlined in the earlier section is often used as an approximation method of solution of nonlinear problems. A general method may be described to approximate the nonlinear term as a linear one such that the mean square error between the two terms is a minimum. Thus, for a nonlinear damping term of the form $|\dot{x}|^{\alpha-1}\dot{x}$, we write

$$|\dot{x}|^{\alpha-1}\dot{x} = c_1\dot{x} \qquad (3.210)$$

98

Then the form of C_1 becomes

$$C_1 = \sqrt{2/\pi} \ 2^{\alpha/2} \ \Gamma \left(\frac{\alpha+2}{2} \right) \ \sigma_{\dot{x}}^{\alpha-1} \qquad (3.211)$$

where $\sigma_{\dot{x}}$ is the root mean square velocity. In the above expression, C_1 is not dimensionless but has a dimension dependent upon the value of α. Note that α = 2 gives

$$C_1 = \sqrt{\frac{8}{\pi}} \ \sigma_{\dot{x}} \qquad (3.212)$$

For the linear approximation, the drag force becomes

$$f_D(t) \approx k_D \ \sqrt{\frac{8}{\pi}} \ \sigma_u u(t) \qquad (3.213)$$

In this case, the drag term may be treated as a linear system in constructing a transfer function and calculating the response spectrum using the appropriate equation, e.g. Eq. 3.174.

Roberts (1977, 1978) obtained an approximation to the stationary joint density function of the displacement and velocity response for oscillators with nonlinear damping and excitation by white noise. An approximate one-dimensional (Markov envelope) equation to the resulting Fokker-Planck equation was obtained. The results were compared with digital simulation, as well as perturbation and equivalent linearization methods. The stiffness was considered linear and the damping nonlinear, taking the form

$$f(\dot{x}) = \dot{x}(1 + \varepsilon|\dot{x}|^n) \qquad (3.214)$$

An example of this correlation is shown in Fig. 3.27 in which the quantity σ^2/σ_0^2 is plotted versus ε^* for n = 2. The quantity ε^* is a non-dimensional nonlinearity parameter

$$\varepsilon^* = \varepsilon \ \omega_0^n \sigma_0^n \qquad (3.215)$$

in which ε = nonlinearity parameter, ω_0 = natural frequency, σ = standard deviation of the nonlinear response and σ_0 = standard deviation of the linear
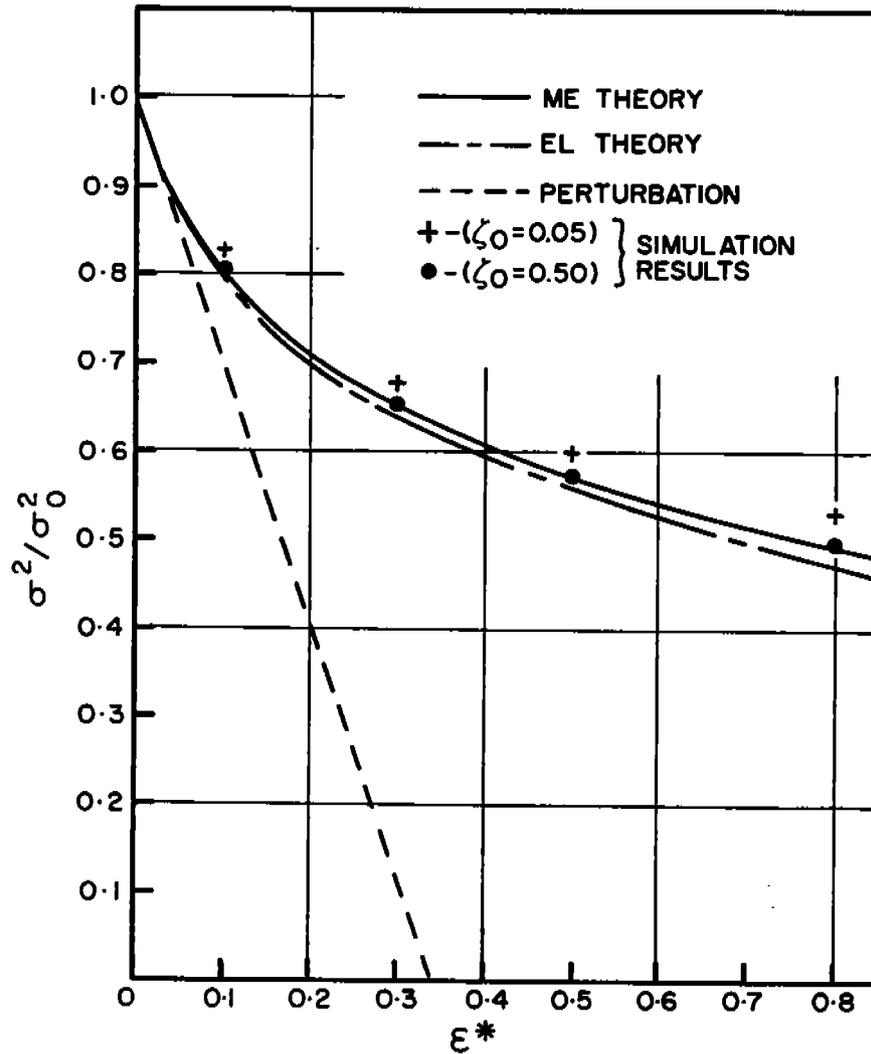
FIGURE 3.27   VARIATION OF THE NORMALIZED MEAN SQUARE OF THE RESPONSE WITH ε^*
FOR $n = 2$; SIMULATION RESULTS ARE SHOWN AS ● FOR $\zeta_0 = 0.05$; AND
AS + FOR $\zeta_0 = 0.50$ [ROBERT (1977-78)]

response (i.e., for ε = 0). The figure shows that the equivalent linearization (EL theory) result is very close to the Markov envelope (ME theory) result over the entire range of ε^* shown. The digital simulation for the damping ratio values of ζ_0 = 0.05 and 0.50 are also shown. For a low damping factor, the simulation results are in excellent agreement with the ME theory. At the higher damping factor, the correlation is less satisfactory, but still close. The perturbation solution matches others only when ε^* is small (< 0.05), i.e., for small nonlinear damping compared to the linear term.

3.3.2.5 Nonlinear Response Spectra

The drag force per unit length of a vertical cylinder is given by the second term of Eq. 2.18. In order to compute the response spectra due to the drag force, the covariance of both sides of this expression is taken. In this case, the covariance function of the drag force has a highly nonlinear relationship with the covariance function of the water particle velocity.

$$R_{f_D}(\tau) = k_D^2 \sigma_u^4 \; \psi[R_u(\tau)/\sigma_u^2] \qquad (3.216)$$

where τ = time, σ_u^2 the variance of the velocity spectrum given by

$$\sigma_u^2 = \int_0^\infty S_u(\omega) \; d\omega \qquad (3.217)$$

and $R_u(\tau)$ is the covariance of the velocity, u. Substituting $r = R_u(\tau)/\sigma_u^2$, $\psi(r)$ is a function defined by the formula

$$\psi(r) = [(4r^2 + 2) \sin^{-1}r + 6r (1 - r^2)^{1/2}]/\pi \qquad (3.218)$$

$\psi(r)$ can be expanded in a power series in r as follows:

$$\psi(r) = \frac{1}{\pi} (8r + \frac{4r^3}{3} + \frac{r^5}{15} + \frac{r^7}{70} + \ldots) \qquad (3.219)$$

The spectral density for f_D is the Fourier transform of the covariance function. Hence

$$S_{f_D}(\omega) = \int_{-\infty}^\infty R_{f_D}(\tau) \; e^{-i\omega\tau} \; d\tau \qquad (3.220)$$

100

or,

$$S_{f_D}(\omega) = k_D^2 \sigma_u^4 \int_{-\infty}^{\infty} \psi \left[R_u(\tau)/\sigma_u^2 \right] e^{-i\omega\tau} \, d\tau \tag{3.221}$$

In terms of the series expansion of $\psi(r)$,

$$S_{f_D}(\omega) = k_D^2 \sigma_u^4 \int_{-\infty}^{\infty} \frac{1}{\pi} \left[8 \frac{R_u(\tau)}{\sigma_u^2} + \frac{4R_u^3(\tau)}{3\sigma_u^6} + \frac{R_u^5(\tau)}{15\sigma_u^{10}} + \ldots \right] e^{-i\omega\tau} \, d\tau \tag{3.222}$$

This yields the following expression for the drag force spectral density in terms of the velocity spectral density.

$$S_{f_D}(\omega) = \frac{k_D^2 \sigma_u^4}{\pi} \left[\frac{8S_u(\omega)}{\sigma_u^2} + \frac{4}{3\sigma_u^6} S_u(\omega) * S_u(\omega) * S_u(\omega) + \ldots \right] \tag{3.223}$$

in which the asterisk means convolution. Note that a product in the time domain appears as a convolution integral in the frequency domain. Thus

$$S_u(\omega)*S_u(\omega)*S_u(\omega) = \frac{1}{4\pi^2} \int_{-\infty}^{\infty} \int_{-\infty}^{\infty} S_u(\omega'')S_u(\omega'-\omega'') \, d\omega'' S_u(\omega - \omega') d\omega' \tag{3.224}$$

or the triple convolution of $S_u(\omega)$ with itself. The other higher order terms in the series, Eq. 3.223 may be similarly written.

The discussion in the previous paragraph suggests a reasonable approximation for S_{f_D}, namely, the linearization of $\psi(r)$ by

$$\psi(r) \approx \frac{8r}{\pi} \tag{3.225}$$

Then

$$S_{f_D}(\omega) = \frac{8k_D \sigma_u^2}{\pi} S_u(\omega) \tag{3.226}$$

101

It is found [Borgman (1969)] that the maximum error introduced by the linear approximation of $\psi(r)$ is of the order of 15%. If the first two nonlinear terms are introduced, then the error is reduced to about 1%.

When current is present along with the waves, the drag force is represented in terms of the relative velocity. The presence of current alters the energy density of waves which, in deep water, has been represented by Eq. 2.15. Under the deep water assumption, an expression for the drag force spectrum due to relative velocity is shown by Tung and Huang (1972, 1973). To the first order of approximation, the spectrum of the Morison force may be shown to have the form

$$S_f^*(\omega) = 16 \; k_D^2 \; \sigma_u^2 \; [\phi(\gamma) + |\gamma| \; \Phi(\gamma)]^2 \; S_u^*(\omega) + k_M^2 \; S_{\dot{u}}^* \; (\omega) \tag{3.227}$$

where recall that γ is defined as the strength of the current $(\gamma = U/\sigma_u)$ and σ_u^2 is the variance of the fluid particle velocity spectrum. The asterisk indicates that the spectrum has been modified by current. The rms force magnitude may be written as

$$\sigma_f = \{E[f^2] - E^2[f]\}^{1/2} \tag{3.228}$$

where

$$E[f] = 2 \; k_D \; \sigma_u^2 \; [\gamma \; \phi(\gamma) + (1 + \gamma^2) \; \Phi(\gamma)] \tag{3.229}$$

and

$$E[f^2] = \frac{1}{4} \; k_M^2 \; \sigma_{\dot{u}}^2 \; [4 + K^2(\gamma^4 + 6\gamma^2 + 3)] \tag{3.230}$$

in which the quantity K is defined as

$$K = \frac{2k_D \sigma_u^2}{k_M \; \sigma_{\dot{u}}} \tag{3.231}$$

In the absence of current $(\gamma = U/\sigma_u = 0)$, the expression for $E[f^2]$ reduces to that given by Borgman (1965),

$$E[f^2] = k_M^2 \; \sigma_{\dot{u}}^2 + 3 \; k_D^2 \; \sigma_u^4 \tag{3.232}$$

102

Note that the linear combination of the Gaussian inertia force and non-Gaussian drag force is non-Gaussian.

The parameter, K, is a measure of the relative importance of the drag to inertia components of the fluid force. It, therefore, serves as an indicator of the degree of closeness of the force by Morison equation, f(t), to a Gaussian process. Thus, the larger the value of K, the more important is the drag force compared to the inertia force, and the more the force deviates from Gaussian. In the presence of current, a similar conclusion may be drawn with the σ_u replaced by σ_v. The effect of current on the non-Gaussian property of f(t) is more pronounced when current is negative. The expression for the probability density function of f'(t) = f(t)/ρ was derived by Tung (1974) and is given by

$$
p(f') = \sqrt{2/K} \; \frac{1}{2\pi \, k_M^{'} \sigma_{\dot{u}}} \left\{ \int_0^\infty \exp \left[-\frac{1}{2} \left(\frac{f'}{k_M^{'} \, \sigma_{\dot{u}}} + s^2 \right)^2 \right. \right.
$$

$$
\left. -\frac{1}{K} \left(s + \frac{\gamma K}{2} \right)^2 \right] ds + \int_0^\infty \exp \left[-\frac{1}{2} \left(\frac{f'}{k_M^{'} \, \sigma_{\dot{u}}} - s^2 \right)^2 \right.
$$

$$
\left. \left. - \gamma \left(s - \frac{\gamma K}{2} \right)^2 \right] ds \right\} \tag{3.233}
$$

in which $k_M^{'} = k_M/\rho$, γ is the current strength parameter already defined, and s is a dummy variable. The probability density function for the force time history in the absence of current may be obtained from the above expression by setting $\gamma = 0$ in Eq. 3.233. The integrals for the density function cannot be solved in a closed form and are computed numerically, as is the distribution function. This distribution, Eq. 3.233, can be obtained in terms of four parameters given as the coefficient of variation, C_u, force parameter, K, correlation

coefficient, ρ $\left(= - \dfrac{\sigma_{\dot{u}}^2}{\sigma_u \sigma_{\ddot{u}}} \right)$ and acceleration frequency, ω $\left(= \dfrac{\sigma_{\dddot{u}}}{\sigma_{\dot{u}}} \right)$. The

numerical values can only be obtained by solving the equation on a computer. Note that the expression in Eq. 3.233 can be written in a nondimensional form in terms of $\hat{f} = f/k_M \, \sigma_{\dot{u}}$. The probability density function for the (initial) distribution of f(t) normalized by $k_M \dot{u}$ has been provided by Borgman (1972) assuming that f(t) is Gaussian. A similar expression has been given by Vinje

(1980) for f(t) which includes a non-zero mean velocity, e.g., from current [similar to Eq. 3.233]. An asymptotic form of the distribution applicable to large values of the maxima was derived by Vinje (1980) and was found to match the numerical results of the distribution.

The probability density and distribution function for the force resulting from a current of $U = \pm 3$ fps (0.915 m/s) as well as for $U = 0$ are plotted in Figs. 3.28-3.31. It is clear from the figures that the distribution is non-Gaussian for non-zero current. The effect of the interaction in modifying the velocity and acceleration spectra is shown to be quite important. For the no-current case, the Gaussian approximation holds, the difference being only due to numerical error.

The density function in Eq. 3.233 is an indicator of the non-Gaussian property of the total force including inertia and drag. However, it does not provide the information on the extreme force maxima which is the quantity required for the design of an offshore structure.

3.3.2.6 Statistics of Narrow-Band Morison Force

For the wave force derived from the Morison equation the distribution of the peak values of the force may be obtained by the method of nonlinear transformation of random variables in the following ways:

1. If the sea surface is assumed to be Gaussian, the force model becomes non-Gaussian and wide banded. In this case, the distribution can only be obtained numerically on a computer [Tickell (1977)].

2. If, on the other hand, the force model is assumed to be an approximate narrow-band model for the Gaussian variables, a distribution function for peak forces may be derived analytically [Borgman (1972)].

3. If either drag or inertia is disregarded then an analytical expression may be obtained even for a wide-band model [Tickell (1977)].

104
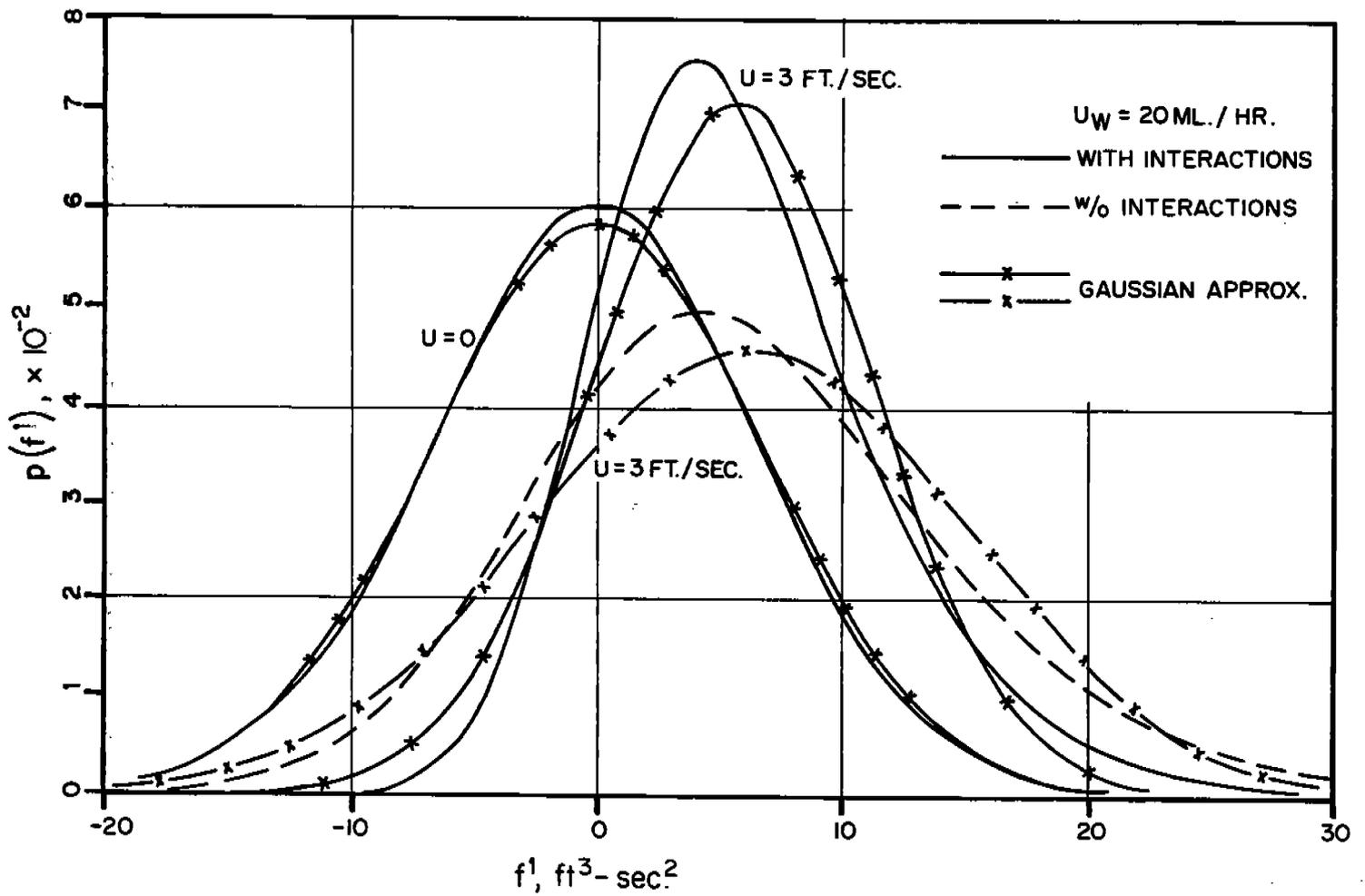
FIGURE 3.28   PROBABILITY DENSITY FUNCTION OF FORCE TIME HISTORY f'(t)
[= f(t)/ρ] FOR CURRENT VALUES OF U = 0 AND U = 3 FT/SEC [TUNG
AND HUANG (1972)]
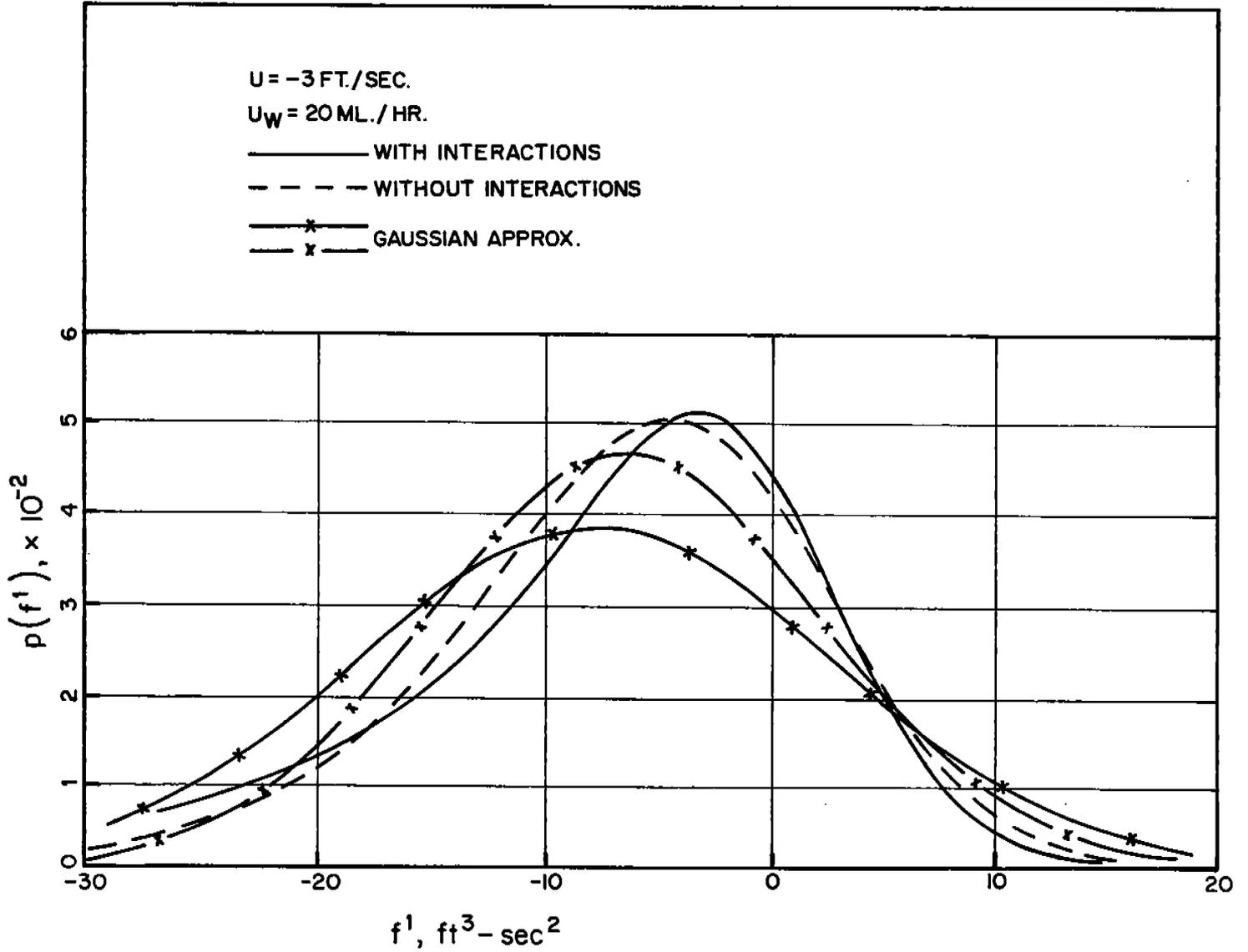
FIGURE 3.29   PROBABILITY DENSITY FUNCTION OF FORCE TIME HISTORY f'(t)
              [= f(t)/ρ] FOR A CURRENT VALUE OF U = -3 FT/SEC. [TUNG AND
              HUANG (1972)]
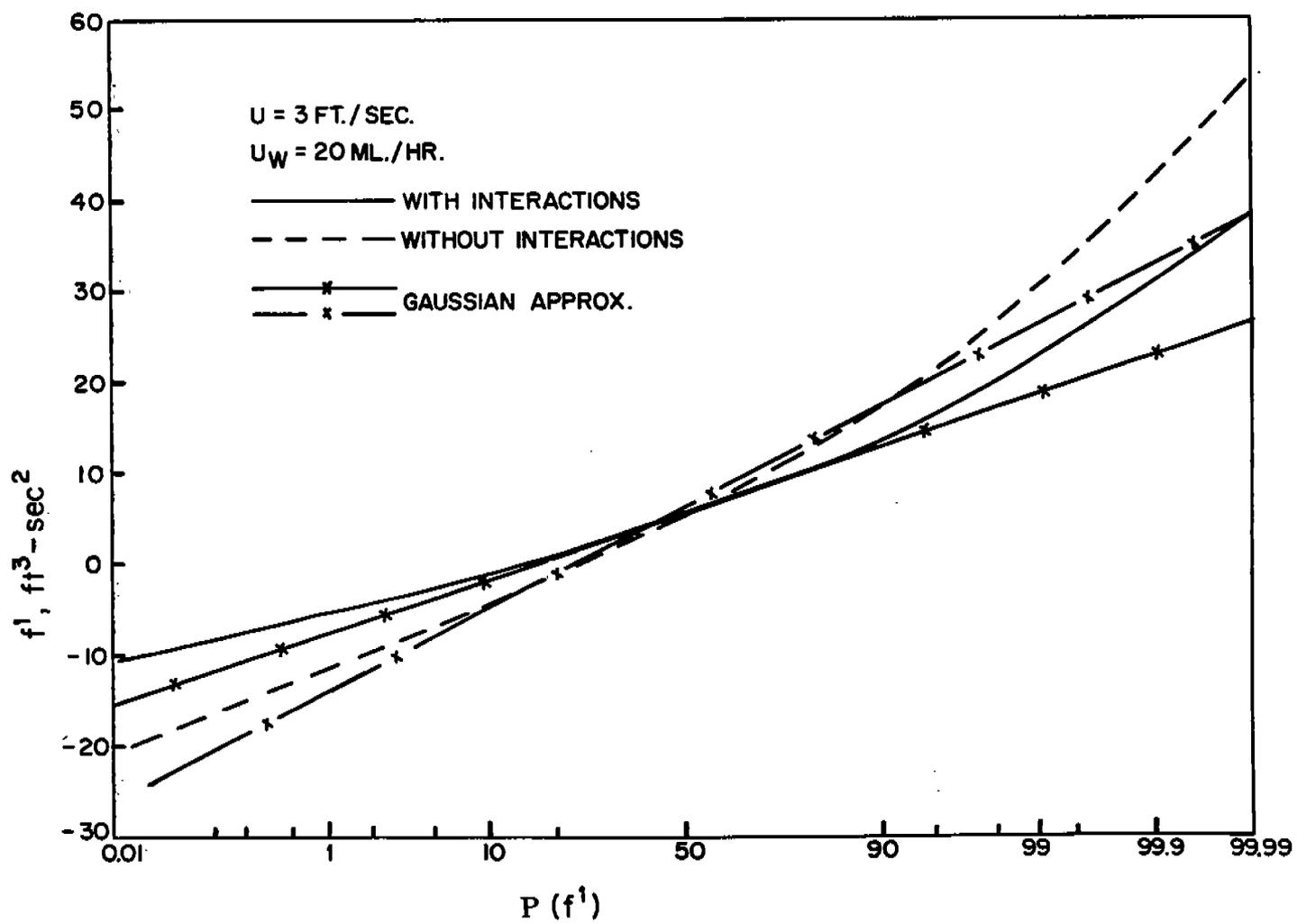
FIGURE 3.30   PROBABILITY DISTRIBUTION FUNCTION OF FORCE TIME HISTORY, f'(t)
[= f(t)/ρ] FOR A CURRENT VALUE OF U = 3 FT/SEC. [TUNG AND HUANG
(1972)]
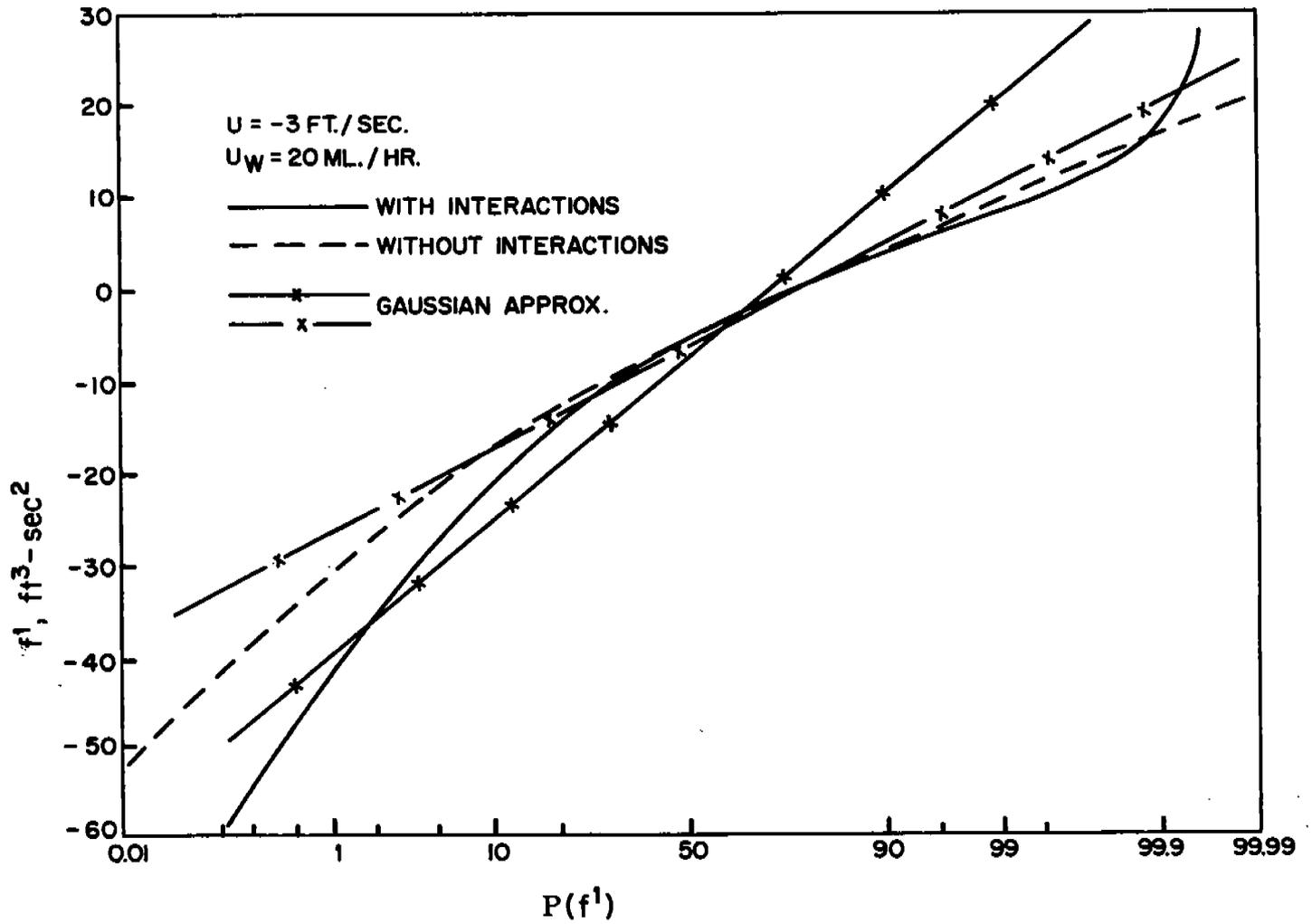
FIGURE 3.31   PROBABILITY DISTRIBUTION FUNCTION OF FORCE TIME HISTORY f'(t)
[= f(t)/ρ] FOR A CURRENT VALUE OF U = -3 FT/SEC. [TUNG AND
HUANG (1972)]

Gaussian models for ocean waves involve superposition of numerous linear waves. For a Gaussian sea, all of the probability properties of the sea surface may be predicted. In the Gaussian model, the energy density spectrum completely determines the probabilities of all wave properties especially if the spectrum is assumed to be narrow banded. A statistical model for the wave forces faces mathematical complexities if the waves are of appreciable amplitude causing nonlinearities to be introduced. Because of this difficulty, statistical treatments are frequently based on linear theory. If the Morison force with its nonlinearities is assumed to be narrow banded, then the probabilities of the extreme values for the force may be derived in a straight-forward manner.

A simple deterministic model of the short-crested directional sea condition is

$$\eta(x,y,t) = \sum_{n=1}^{\infty} a_n \cos(k_n x \cos \theta_n + k_n y \sin \theta_n - \omega_n t + \psi_n) \qquad (3.234)$$

where the subscript n represents the nth linear wave, a_n is the amplitude of the nth wave, k_n, ω_n and ψ_n are its wave number, frequency and phase, respectively. Assuming that waves are coming from directions covering an area given by the angle $-\pi < \theta < \pi$, an integral representation is

$$\eta(x,y,t) = \int_0^{\infty} \int_{-\pi}^{\pi} a(\omega,\theta) \cos [kx \cos\theta + ky \sin\theta - \omega t + \psi(\omega,\theta)] d\theta \, d\omega$$
$$(3.235)$$

On the assumption that both the amplitude and phase of the component waves are random with arbitrary probability laws, Borgman (1972) presented a stationary, second-order stochastic process for predicting the sea surface. The Gaussian model is a useful, though somewhat restricted model which assumes that the amplitude is related to the energy content, and phase is independent and random but uniformly distributed over the interval $(-\pi, \pi)$. Thus, dividing the two dimensional plane (ω, θ), into small cells of width $\Delta\omega$ and $\Delta\theta$,

$$\eta(x,y,t) = \sum_{\substack{\text{all cells} \\ (\Delta\omega, \Delta\theta)}} [2 \, S(f,\theta) \, \Delta\omega \, \Delta\theta]^{1/2} \cos (kx \cos\theta - ky \sin\theta - \omega t + \psi)$$
$$(3.236)$$

where ω and θ assume values at the midpoints of the cells. This expression may be used to derive wave profile from a directional sea given by the energy density $S(f,\theta)$ and is thus a generalization of Eqs. 2.11-2.13. Alternatively

$$\eta(x,y,t) = \int_0^\infty \int_{-\pi}^\pi [2S(f,\theta) \ d\omega \ d\theta]^{1/2} \cos(kx \cos\theta + ky \sin\theta - \omega t + \psi)$$

(3.237)

The Gaussian model implicitly assumes symmetry about the still water level. It fails to encompass the crest-trough inequality. For the latter case, a general second-order stochastic model with multivariate probability law similar to those described in Sections 3.2.2 and 3.2.4 is needed for the sea surface. In the general second-order model, the spectrum is not adequate to describe the probabilistic properties. It is just one of many characterizing functions of the wave; bispectrum is another.

A more detailed probabilistic structure can be obtained if the Gaussian model is restricted to unidirectional waves ($\theta = 0$) and a narrow spectral density. Then

$$\eta(x,t) = \int_0^\infty [2S(\omega) \ d\omega]^{1/2} \cos(kx - \omega t + \psi)$$

(3.238)

Recall that for a narrow-band model, the Rayleigh probability law applies for the wave amplitudes, a .

$$P(a) = \begin{cases} 1 - \exp(-a^2/2\sigma_0^2) & \text{if } a > 0 \\ 0 & \text{if } a < 0 \end{cases}$$

(3.239)

where σ_0 is the rms value of the wave profile. The corresponding density function is

$$p(a) = \begin{cases} a/\sigma_0^2 \exp(-a^2/2\sigma_0^2) & \text{for } a > 0 \\ 0 & \text{for } a < 0 \end{cases}$$

(3.240)

The mean-square amplitude, a_{rms}^2 is given by

$$a_{rms}^2 = 2\sigma_0^2 \tag{3.241}$$

If linear wave theory is applied to the Morison equation, then the inertia and drag force amplitudes are written as

$$f_I = C_1 H \tag{3.242}$$

and

$$f_D = C_2 H^2 \tag{3.243}$$

where C_1 and C_2 are known functions of C_M, C_D, d, D and T. Assuming these parameters to be constant, one obtains

$$p(f_I) \, df_I = p(f_D) \, df_D = p(H) \, dH \tag{3.244}$$

The probability density function for the inertia and drag force amplitudes are then obtained assuming that the wave heights follow Rayleigh distribution

$$p(f_I) = \frac{2f_I}{f_{I_r}^2} e^{-\left(\frac{f_I}{f_{I_r}}\right)^2} \tag{3.245}$$

and

$$p(f_D) = \frac{1}{f_{D_r}} e^{-\left(\frac{f_I}{f_{D_r}}\right)} \tag{3.246}$$

where

$$f_{I_r} = C_1^2 H_{rms}^2 \tag{3.247}$$

$$f_{D_r} = C_2 H_{rms}^2 \tag{3.248}$$

The cumulative distributions are written as

107

$$P(f_I) = 1 - e^{-\left(\frac{f_I}{f_{I_r}}\right)^2} \qquad (3.249)$$

$$P(f_D) = 1 - e^{-\left(\frac{f_D}{f_{D_r}}\right)} \qquad (3.250)$$

Thus, the inertia force peaks follow Rayleigh distribution while the drag force amplitudes follow exponential distribution.

Similar expressions may be obtained for the inertia and drag force peaks if the wave heights are assumed to follow two-parameter Wiebull distribution.

The wave force on a one-foot section of a vertical cylinder as a function of time is written as

$$f = k_M \dot{u} + k_D |u|u \qquad (3.251)$$

where $k_M = C_M \rho \pi D^2/4$ and $k_D = C_D \rho D/2$. A number of simplifications in the statistical theory for forces are possible if as before the wave spectrum is assumed to be quite narrow and concentrated around a single frequency. Using the linear theory to describe water particle kinematics, the force from Eq. 3.130 may be written equivalently as

$$f = \begin{cases} k_D u_0^2 \cos^2\theta + k_M \omega u_0 \sin\theta & \text{if } |\theta| \leqslant \pi/2 \\ \\ - k_D u_0^2 \cos^2\theta + k_M \omega u_0 \sin\theta & \text{if } \pi/2 < |\theta| < \pi \end{cases} \qquad (3.252)$$

where $\theta = kx - \omega t$ and $u_0 = \dfrac{\pi H \cosh ky}{T \sinh kd}$.

Since the important quantities of interest for extreme value prediction are the peak forces in the profile, the maximum force is given by

$$f_0 = \begin{cases} k_D u_0^2 + \dfrac{(k_M \omega)^2}{4k_D} & \text{if } \dfrac{k_M \omega}{2k_D u_0} < 1 \\ \\ k_M \omega u_0 & \text{if } \dfrac{k_M \omega}{2k_D u_0} \geqslant 1 \end{cases} \qquad (3.253)$$

We note here that for a narrow-band spectrum the wave height, H, is Rayleigh distributed. Hence, u_0 and $\dot{u}_0$ given by linear theory are also Rayleigh

distributed. Thus, f_0 in Eq. 3.253 is a linear combination of a first power and square of a Rayleigh random variable. The probability law of f_0 from that of H may be obtained by converting the probability of non-exceedance of f_0 to that of H.

The cumulative probability of maximum force amplitudes, $\hat{f}$, for the inertia dominated and drag-inertia regions is given by

$$P(\hat{f}) = \begin{cases} 1 - \exp\left(- \dfrac{\hat{f}^2}{(\hat{f})^2_{rms}} \right) & \text{if } \dfrac{2k_D\hat{f}}{k_M^2\omega^2} < 1 \\[3em] 1 - \exp\left\{ - \dfrac{4\,\hat{f}\,\overline{f}_D - \overline{f}_I^2}{4\,\overline{f}_D\,H^2_{rms}} \right\} & \text{if } \dfrac{2k_D\hat{f}}{k_M^2\omega^2} > 1 \end{cases} \tag{3.254}$$

The probability density

$$p(\hat{f}) = \begin{cases} \dfrac{2\hat{f}}{(\hat{f})^2_{rms}} \exp\left(- \dfrac{\hat{f}^2}{(\hat{f})^2_{rms}} \right) & \text{if } 0 < \dfrac{2k_D\hat{f}}{k_M^2\omega^2} < 1 \\[3em] \dfrac{1}{\overline{f}_D\,H^2_{rms}} \exp\left(- \dfrac{4\,\hat{f}\,\overline{f}_D - \overline{f}_I^2}{4\,\overline{f}_D\,H^2_{rms}}\right) & \text{if } \dfrac{2k_D\hat{f}}{k_M^2\omega^2} > 1 \end{cases} \tag{3.255}$$

where $\overline{f}_D = \hat{f}_D/H^2$, $\overline{f}_I = \hat{f}_I/H$, and $\hat{f}_I$ and $\hat{f}_D$ are the inertia and drag force amplitudes. Note that for the inertia dominated case (the upper expression), a Rayleigh distribution is obtained. For the drag-dominated case, the distribution is exponential.

Any normal stochastic process can be completely described by its mean and convariance functions, but an appropriate description of a non-normal stochastic process requires more information. These will yield the mean and the variance of the offshore structural response. A major shortcoming of this approach is that it essentially ignores the fact that the structural response is usually not a normal (Gaussian) process. For example, the knowledge of response kurtosis allows a substantial improvement over the usual prediction

for a normal process (with a given variance and power spectral density). Since kurtosis is a fourth moment property, it is a natural next step beyond variance.

Hu and Lutes (1987) obtained expressions for computing fourth order cumulant function for the force which provides the value of the kurtosis of the response through numerical evaluation. In the frequency domain, the non-normality may be described by a three-dimensional spectral density function.

3.3.2.7 Statistics of Wide-Band Morison Force

Tickell (1977) derived a general multivariate distribution of wave loads including the nonlinear drag force from the linear Gaussian long-crested random seas. Probability distributions of the peak loads were developed. These distributions showed the general behavior of a wide-band process in contrast to simpler distributions which resulted from the narrow-band assumptions. The probability density function of force time history, F(t), is written in an integral form as follows:

$$p(F) = \frac{1}{2\pi \, \sigma_{\psi_1} \sigma_{\psi_2}} \int_{-\infty}^{\infty} \exp \left[-\frac{1}{2} \left(\frac{\psi_1^2}{\sigma_{\psi_1}^2} + \frac{\psi_2^2}{\sigma_{\psi_2}^2} \right) \right] d\psi_1 \qquad (3.256)$$

and computed numerically. The quantities ψ_1 and ψ_2 are defined as

$$\psi_1 = \sqrt{k_D} \; u \qquad (3.257)$$

$$\psi_2 = k_M \, \dot{u} \qquad (3.258)$$

and their standard deviations are computed from the second and fourth moments of F as

$$E[F^2] = \sigma_{\psi_2}^2 + 3 \, \sigma_{\psi_1}^4 \qquad (3.259)$$

$$E[F^4] = 3\sigma_{\psi_2}^4 + 18 \, \sigma_{\psi_2}^2 \, \sigma_{\psi_1}^4 + 105 \, \sigma_{\psi_1}^8 \qquad (3.260)$$

110

This basic force distribution theory has been compared with data obtained from an offshore platform in the Southern North Sea. The cumulative distribution function of the vertical bending stress in a bracing member of the platform is shown in Fig. 3.32 along with the Gaussian CDF. A measured kurtosis (= $E[F^4]/E^2[F^2]$) of 6.9 indicates a strong deviation from the Gaussian distribution as demonstrated in the figure. For a mean zero Gaussian distribution the corresponding kurtosis is 3.0.

While this formulation indicates the importance of the non-Gaussian formulation for the nonlinear loads, it is not useful in the practical design where the distribution of the peak forces is needed. The cumulative peak distribution may be estimated from the expected number of peaks above a certain force level. However, it involves higher moments of the spectrum (e.g. sixth moment of the velocity spectrum) which are inaccurate because representation of the tail of the wave spectrum (e.g. P-M spectrum) is often inaccurate. If the time history of the force is assumed to be a narrow-band process, the distribution requires the fourth moment of the velocity spectrum. If, in addition, the force and its first time derivative are assumed to be independent, then the distribution may be obtained from the second and fourth derivatives of force only. This results in a narrow-band non-Gaussian force amplitude distribution. The theoretical and observed distribution of the stress range of the prototype data discussed earlier and the tip displacement range from a laboratory test on a vertical cantilever under random wave input are shown in Figs. 3.33 and 3.34. The ranges are defined as the highest peak to the lowest trough between successive zero crossings in a record. The Rayleigh distribution is also shown in the figures. In each case, an improved estimate of the range is achieved by use of the non-Gaussian distribution.

For a narrow-band model, the probability distribution of the peak force, $\hat{f}$, which is normalized by the standard deviation of force is given by

$$
p(\hat{f}) = \begin{cases}
(\frac{3}{4} K^2 + 1) \, \hat{f} \, \exp\left[-\frac{1}{2} (\frac{3}{4} K^2 + 1) \, \hat{f}^2 \right] \\
\qquad\qquad\qquad\qquad \text{for } \hat{f} < K^{-1}(\frac{3}{4} K^2 + 1)^{-1/2} \\[2ex]
(\frac{3}{4} K^2 + 1)^{1/2} K^{-1} \exp\left[- (\frac{3}{4} K^2 + 1)^{1/2} K^{-1} \, \hat{f} + (\frac{1}{4} K^2)^{-1}\right] \\
\qquad\qquad\qquad\qquad \text{for } \hat{f} > K^{-1} (\frac{3}{4} K^2 + 1)^{-1/2}
\end{cases} \qquad (3.261)
$$
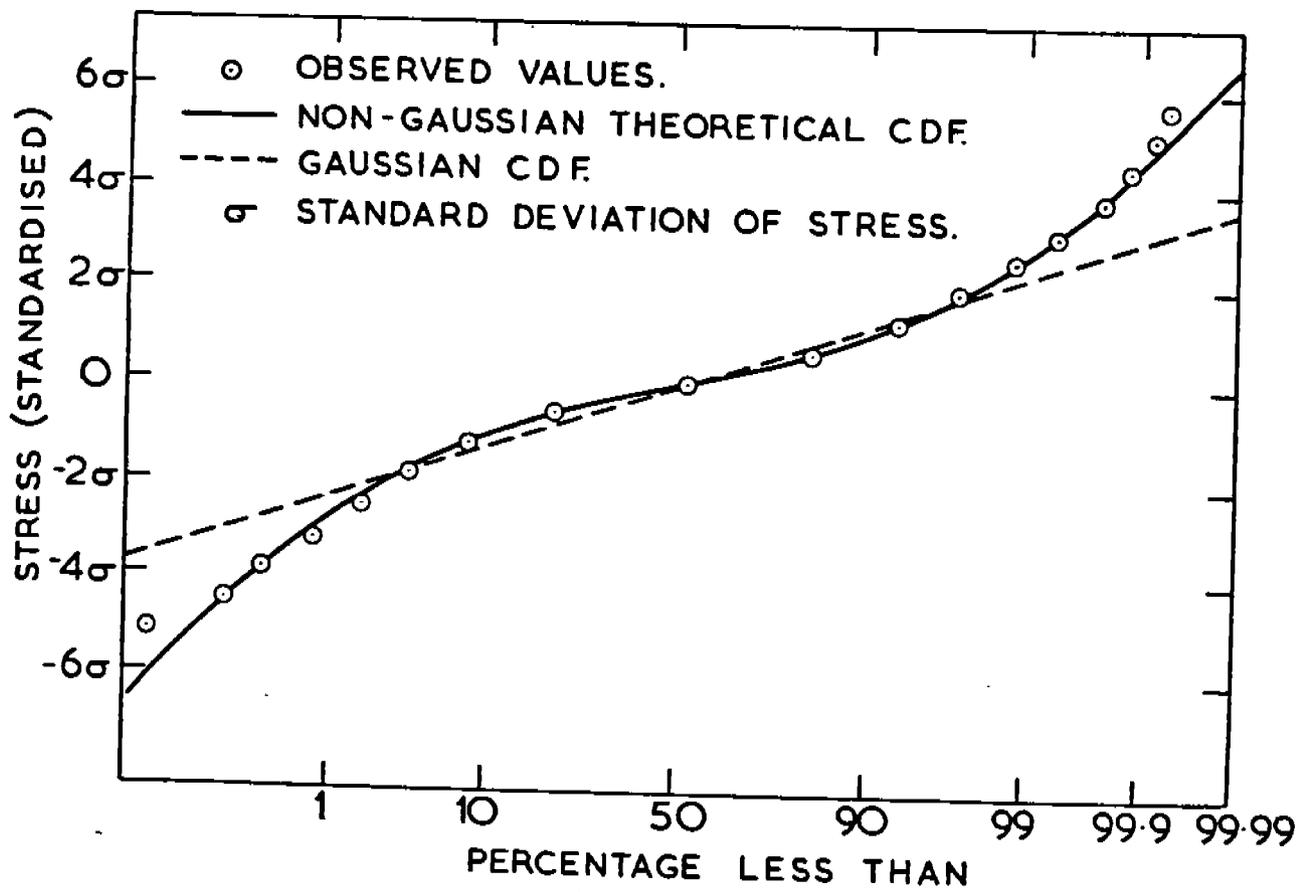
FIGURE 3.32   WIDE-BAND AND NARROW-BAND CUMULATIVE DISTRIBUTIONS OF STRESS ON
A RAYLEIGH SCALE [TICKELL (1977)]
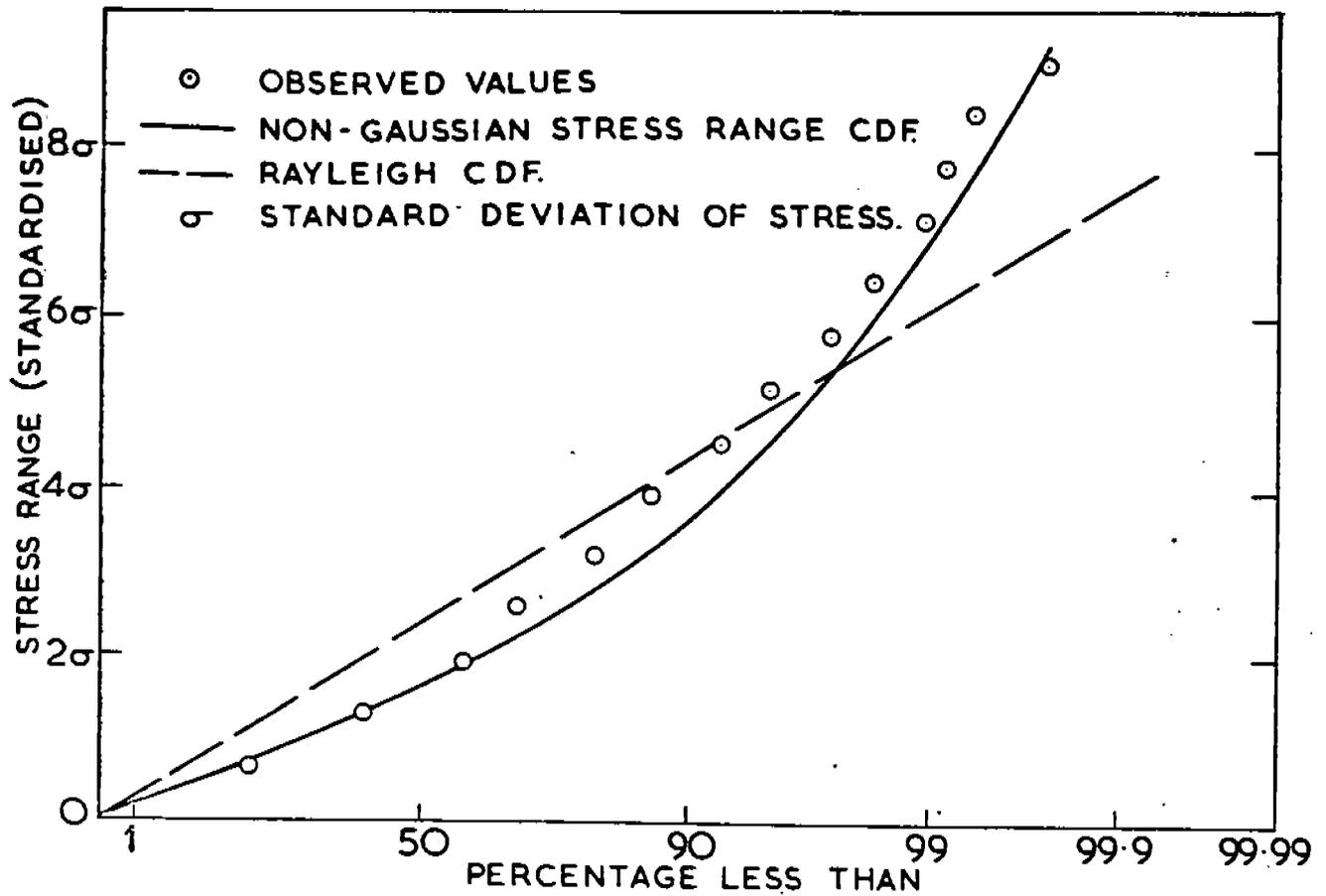
FIGURE 3.33   THE OBSERVED AND THEORETICAL CDF OF STRESS RANGE IN AN OFFSHORE
PLATFORM BRACING MEMBER [TICKELL (1977)]
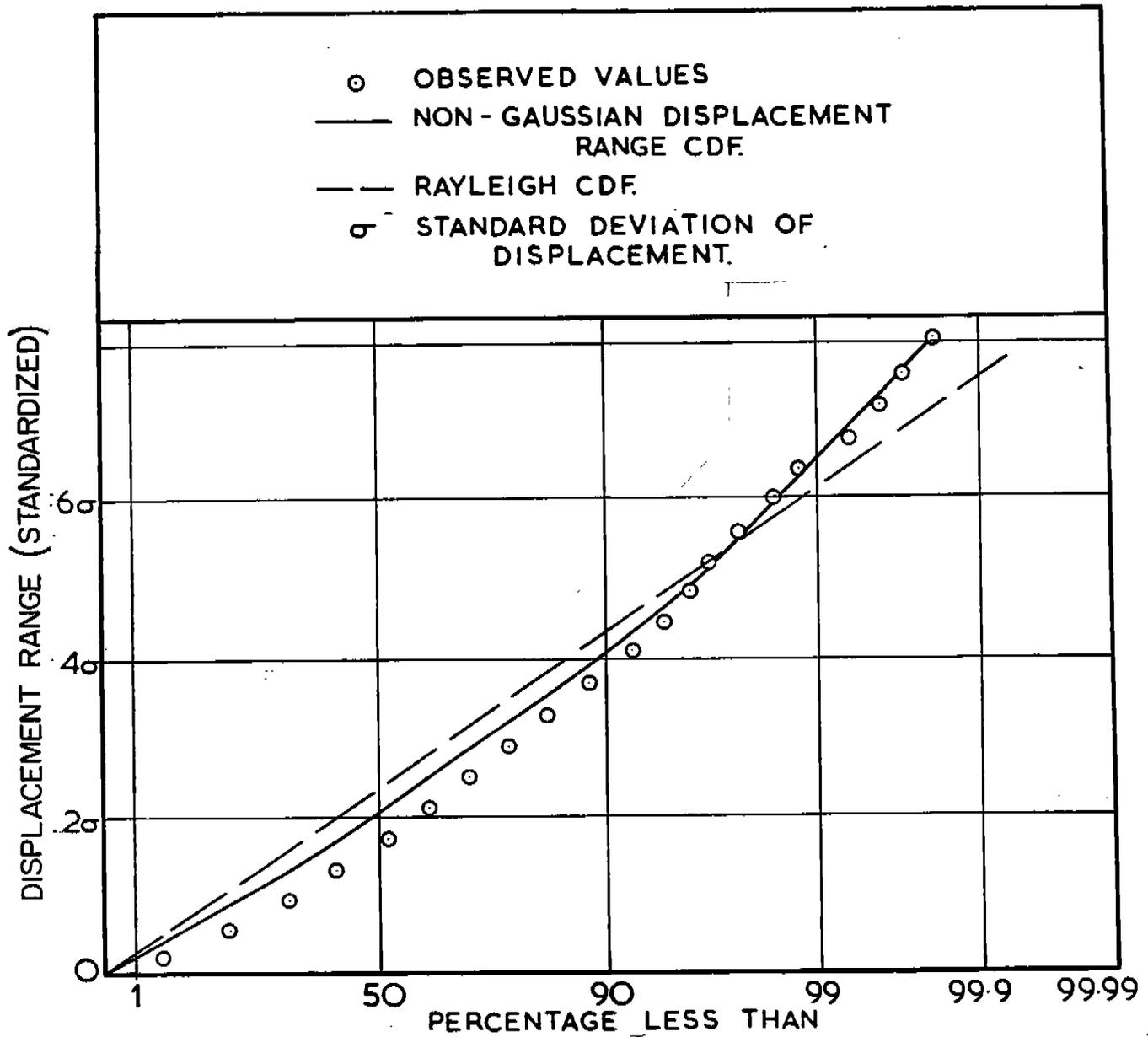
FIGURE 3.34   THE OBSERVED AND THEORETICAL CDF OF DISPLACEMENT RANGE OF A
LABORATORY CANTILEVER MODEL [TICKELL (1977)]
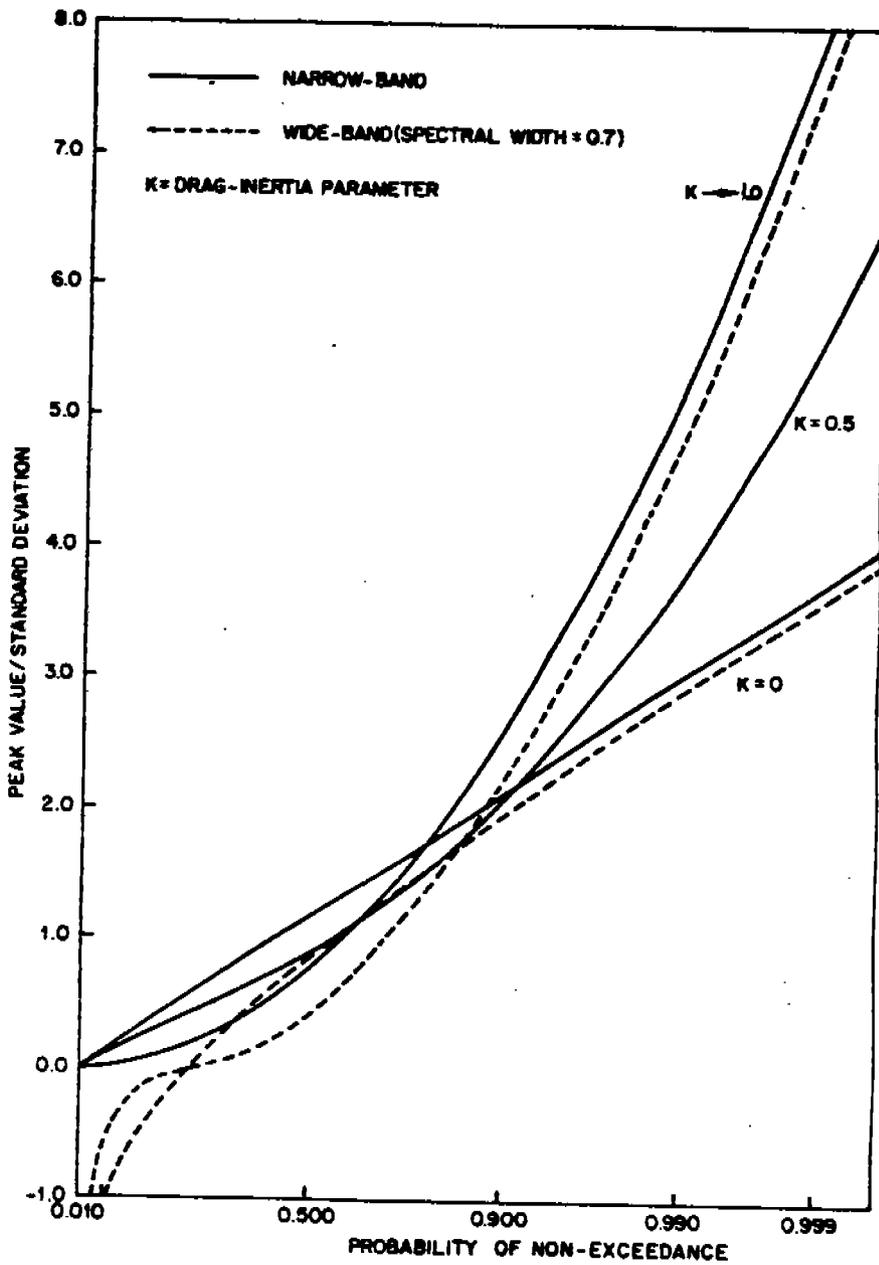
FIGURE 3.35 WIDE-BAND AND NARROW-BAND CUMULATIVE PEAK DISTRIBUTIONS OF
FORCE ON A RAYLEIGH SCALE [TICKELL (1979)]

where $\hat{f} = \dfrac{f_0}{\sigma_f}$, f_0 = peak force, σ_f = standard deviation of force, and K is defined as the drag-inertia parameter. The drag-inertia parameter is the ratio of the drag force amplitude to the inertia force amplitude given by

$$K = \frac{4}{\pi} \frac{C_D}{C_M} \frac{\sigma_u}{D \, \omega_z} = \frac{2k_D \sigma_u^2}{k_M \sigma_{\dot{u}}} \qquad (3.262)$$

where $\sigma_{\dot{u}} = \omega_z \sigma_u$, ω_z = zero upcrossing frequency of the water particle velocity, and σ_u = corresponding standard deviation.

If the inertia force predominates, then $K \rightarrow 0$ and from Eq. 3.261

$$p(\hat{f}) = \hat{f} \, \exp \left(-\frac{1}{2} \hat{f}^2 \right) \qquad (3.263)$$

which is the Rayleigh distribution describing the probability distribution of a narrow band process. On the other hand when drag forces dominate, $K \rightarrow \infty$ and Eq. 3.261 reduces to

$$p(\hat{f}) = \frac{\sqrt{3}}{2} \exp \left(-\frac{\sqrt{3}}{2} \hat{f} \right) \qquad (3.264)$$

which is the equation of an exponential distribution. The cumulative probability distribution of peak forces is obtained by integration of $p(\hat{f})$. The probability of non-exceedance of the normalized peak forces for different values of K, namely K = 0, $K \rightarrow \infty$ and K = 0.5 has been plotted in Fig. 3.35.

For a wide-band model, the peak distribution of force, f, is expressed in terms of the joint probability density of force and its first and second derivatives (obtained by differentiating Morison equation)

$$P(f) = 1 - \frac{\displaystyle\int_{-\infty}^{\infty} \int_{-\infty}^{0} \ddot{f} \, p \, (f, \dot{f}{=}0, \ddot{f}) \, d\ddot{f} \, d\hat{f}}{\displaystyle\int_{\infty}^{0} \ddot{f} \, p \, (f, \dot{f}{=}0, \ddot{f}) \, d\ddot{f}} \qquad (3.265)$$

First, a multivariate Gaussian distribution for the velocity and its derivatives is constructed. Then, it is transformed into the force variable and its derivative to form $p(f, \dot{f}, \ddot{f})$ using the Morison equation [Tickell (1977)]. A simple closed form expression for the general force case does not

112

seem possible. The individual probability densities for drag-dominated and inertia-dominated limits are obtained respectively as

$$p(\hat{f}_D) = (1 - \epsilon^2)^{1/2} \frac{\sqrt{3}}{4} \frac{\hat{f}}{|\hat{f}|} \exp \left[-\frac{\sqrt{3}}{2} |\hat{f}| \right]$$

$$\text{erf} \left[-\frac{4\sqrt{3}}{\sqrt{2}} \left(\frac{1 - \epsilon^2}{\epsilon^2} \right)^{1/2} \frac{\hat{f}}{|\hat{f}|^{1/2}} \right]$$

$$+ \left(\frac{2}{\pi} \right)^{1/2} \frac{4\sqrt{3}}{4} \frac{\epsilon}{|\hat{f}|^{1/2}} \exp \left[-\frac{\sqrt{3}}{2\epsilon^2} |\hat{f}| \right] \tag{3.266}$$

where ϵ = spectral width parameter for the water particle velocity, and erf = error function,

$$p(\hat{f}_I) = \frac{1}{2} (1 - \epsilon^2)^{1/2} \hat{f} \exp \left[-\frac{\hat{f}^2}{2} \right]$$

$$\text{erf} \left[-\left(\frac{1 - \epsilon^2}{2\epsilon^2} \right)^{1/2} \hat{f} \right] + \frac{\epsilon}{(2\pi)^{1/2}} \exp \left[-\frac{\hat{f}^2}{2\epsilon^2} \right] \tag{3.267}$$

where ϵ = spectral width parameter for the water particle acceleration. The last relationship is the Rice's distribution.

In the above expression, if $\epsilon \rightarrow 0$, then the expressions for the wide band peak distributions for both drag- and inertia-dominated areas reduce to the corresponding narrow-band solutions (Eqs. 3.263-3.264). The results from the wide-band model (for a value of $\epsilon = 0.7$) for $K = 0$ (inertia dominated, Eq. 3.267) and $K \rightarrow \infty$ (drag-dominated region, Eq. 3.266) are plotted in Fig. 3.35.

It may be observed that the effect of nonlinear drag forces is most pronounced in the upper tails of the distribution function. Thus, the probability of exceedance of large peaks increases with increasing value of the drag-inertia parameter, K. Moreover, at least for $K = 0$ and $K \rightarrow \infty$, the narrow band model yields results that are close to and higher than the wide-band model. These results suggest that these models may be conservatively used in predicting extreme responses.

If the spectral width parameter is nonzero ($\epsilon > 0$), the prediction of the extreme value is expected to be different from the case of $\epsilon = 0$. It can be

113

shown that for the inertia dominated region, the limiting relative magnitude is given by $(4 \ln N)^{-1} \ln(1 - \epsilon^2)$ whereas the drag-dominated limit can be written as $(2 \ln N)^{-1} \ln(1 - \epsilon^2)$. Therefore, if the number of force peaks, N, is large, the deviation is small. For example, if we choose N = 1000 and ϵ = 0.7, the reduction in the expected extreme values is 2.4% for the inertia-dominated case and 4.9% for the drag-dominated regions.

A slightly different approach in the extreme value analysis was adopted by Moe (1979). Instead of expressing the probability density of force maxima, Moe derived expressions for the expected rate of occurrence of force maxima at any intensity on a cylindrical member of a structure. The expected number of peaks per unit time exceeding a prescribed value of the force maxima can be found from these expressions by integration. On the assumption that the sea surface is not necessarily a Gaussian process but a non-narrow-band stochastic process, the expressions are obtained for the inertia and drag force as well as for the Morison formula. The expected number of extremes per unit time per unit increment of the loading level, f, is given in terms of the extreme rate density, $\mu(f)$.

Knowing $\mu(f)$, other statistical quantities may be readily computed. The probability density function for extremes is given as

$$p(\hat{f}) = \frac{\mu(\hat{f})}{\int_0^\infty \mu(f)\, df} \qquad (3.260)$$

The probability of $\hat{f} > f_0$ (a defined value) is

$$P[\hat{f} > f_0] = \frac{\int_{f_0}^\infty \mu(f)\, df}{\int_0^\infty \mu(f)\, df} \qquad (3.269)$$

The expected extreme value is

$$E(\hat{f}) = \frac{\int_0^\infty f\, \mu(f)\, df}{\int_0^\infty \mu(f)\, df} \qquad (3.270)$$

For the purpose of these derivations, several definitions for the frequencies are required. These are the expected frequencies of the wave profile, its derivative, the particle velocity, the particle acceleration and its derivative. They are defined as follows:

114

$$\omega_1 = \sigma_u/\sigma_{r\eta}; \qquad \omega_2 = \sigma_a/\sigma_u; \qquad \omega_3 = \sigma_{\ddot{a}}/\sigma_a$$

$$\omega_1' = \sigma_{\dot{\eta}}/\sigma_\eta; \qquad \omega_2' = \sigma_{\ddot{\eta}}/\sigma_{\dot{\eta}} \qquad\qquad (3.271)$$

in which r is the decay factor depending on the water depth and $r\eta(t)$ refers to the decayed vertical amplitude of the water particle orbit. In deepwater ($\omega^2 = kg$), we have $\omega_1' = \omega_1$ and $\omega_2' = \omega_2$.

Note that by Airy theory,

$$r = \frac{\cosh ky}{\sinh kd} \qquad\qquad (3.272)$$

$$S_u(\omega) = r^2 \omega^2 S_\eta(\omega) \qquad\qquad (3.273)$$

$$S_a(\omega) = r^2 \omega^4 S_\eta(\omega) \qquad\qquad (3.274)$$

The peak rate density of the wave height for a sea surface of any bandwidth, $\varepsilon (0 < \varepsilon < 1)$ is given by

$$\mu(\hat{H}) = \frac{\omega_2'}{4\pi \sqrt{m_0}} \left[\frac{\varepsilon}{\sqrt{2\pi}} \exp\left(-\frac{\hat{H}^2}{8 \varepsilon^2 m_0} \right) \right.$$

$$+ (1 - \varepsilon^2)^{1/2} \frac{H}{2\sqrt{m_0}} \exp\left(-\frac{H^2}{8 m_0} \right)$$

$$\left. \left\{ 1 - \Phi \left[-\frac{H}{\varepsilon} \left(\frac{1 - \varepsilon^2}{4 m_0} \right)^{1/2} \right] \right\} \right] \qquad\qquad (3.275)$$

where $\varepsilon^2 = 1 - m_2^2/(m_0 m_4) = 1 - (\omega_1'/\omega_2')^2$ and $\Phi(x)$ is the cumulative distribution function for a Gaussian variable.

The short-term rate density for the inertia force maxima is given by

$$\mu(\hat{f}) = \frac{\omega_3}{2\pi} \frac{\hat{f}}{k_M^2 \sigma_a^2} \exp\left(-\frac{\hat{f}^2}{2 k_M^2 \sigma_a^2} \right) \qquad\qquad (3.276)$$

Note that for a narrow-band process $\omega_3 \approx \omega_1 \approx \omega_1'$ and the above expression corresponds to a Rayleigh distribution. The short-term rate density for the integrated total inertia force on a cylinder has the same form as Eq. 3.276 if

$k_M^2 \, \sigma_a^2$ is replaced by the corresponding integral representation for the total force.

The rate density for the short-term drag force was derived by Moe (1979) for the deepwater case assuming relatively narrow-banded waves. In this case the total drag force on the pile may be approximated by

$$F_D(t) \approx 0.5 \, k_D \, g \, |\eta(t)| \, \eta(t) \tag{3.277}$$

and the rate density of the drag force maxima has the form

$$\mu(\hat{F}_D) = \frac{\omega_1}{2\pi} \frac{1}{g \, k_D \sigma_\eta^2} \exp\left(-\frac{\hat{F}_D}{g \, k_D \, \sigma_\eta^2}\right) \tag{3.278}$$

When the wave amplitude is such that both inertia and drag components are important in the Morison formula then both terms are needed. This criterion is established from the parameter

$$\eta_0 = \frac{k_M}{2rk_D} = \frac{\pi}{2} \frac{C_M}{r \, C_D} D \tag{3.279}$$

Note that η_0 has a unit of length as opposed to K in Eq. 3.262 which is a dimensionless parameter. Thus, η_0 may be thought of as a measure of wave amplitude which determines the importance of the drag force compared to the inertia force. For small values of $\eta < \eta_0$, inertia is predominant while drag becomes significant for large values of $\eta > \eta_0$. Once the expected rate density of force maxima for a given amplitude is known, the expected number of peaks for this limiting value of force may be determined by integration of the density function. For a point at the surface, we have $r = 1$ and $\eta_0 = 1.5D$ to $3.0D$, depending on the cylinder roughness. For $\hat{\eta} > \eta_0$ (which means both terms are important in the Morison formula)

$$\mu(\hat{f}) = \frac{\omega_2}{2\pi} \frac{1}{2 \, k_D \sigma_u^2} \exp\left(-\frac{\hat{f} - f_0/2}{2 \, k_D \, \sigma_u^2}\right), \qquad f > f_0 \tag{3.280}$$

and

$$f_0 = \frac{\omega_2^2 \, k_M^2}{2k_D} \tag{3.281}$$

116

EXAMPLE

Consider an ITTC wave spectrum model

$$S(\omega) = \frac{\alpha g^2}{\omega^5} \exp\left(-\frac{B}{\omega^4} \right) \tag{3.282}$$

in which $\alpha = 0.0081$ and $B = 3.11/H_s^2$. Since higher order moments of the spectra are required in considering a distribution of peak forces, and since the higher order moments of this type of spectra are divergent, an upper cut-off frequency must be specified in these cases. A cut-off frequency of $\omega_{cut} = 1.257$ (period = 5 sec.) was chosen to limit σ_a. Then

$$\sigma_\eta = 3.75m, \quad \sigma_u = 1.69 \text{ m/sec. and } \sigma_a = 0.943 \text{ m/sec}^2$$

Assuming the pile diameter $D = 1m$, $\rho g = 1026$ kg/m^3, $C_D = 1$, and $C_M = 1.5$, we have $k_D = 513$ and $k_M = 1209$, $\omega_1 = 0.4507$ rad/sec and $\omega_2 = 0.5580$ rad/sec. The force, f_0, is obtained as $f_0 = 444$ N/m. Then from Eq. 3.280 the force at the surface per unit length has the rate density

$$\mu(\hat{f}) = \frac{0.0888}{2930} \exp\left(-\frac{\hat{f} - 222}{2930} \right) \tag{3.283}$$

and the drag force has the rate density (Eq. 3.278)

$$\mu(\hat{F}_D) = \frac{0.0717}{70770} \exp\left(-\frac{\hat{F}_D}{70770} \right) \tag{3.284}$$

Thus the number of peaks in the surface process is 0.0717/sec and in the velocity process 0.0848/sec. The expected number of peaks per unit time exceeding a given limiting value of $\hat{f}$ and $\hat{F}_D$ is found by integration.

$$M(f') = 0.0786 \, e^{-f'/2930} \tag{3.285}$$

$$M(F_D') = 0.0717 \, e^{-F_D'/70770} \tag{3.286}$$

For example, about 37% (e^{-1}) of the peaks will exceed 2930 N/m (at the surface) and 70770N (total drag force), respectively. These functions are shown graphically in Fig. 3.36.
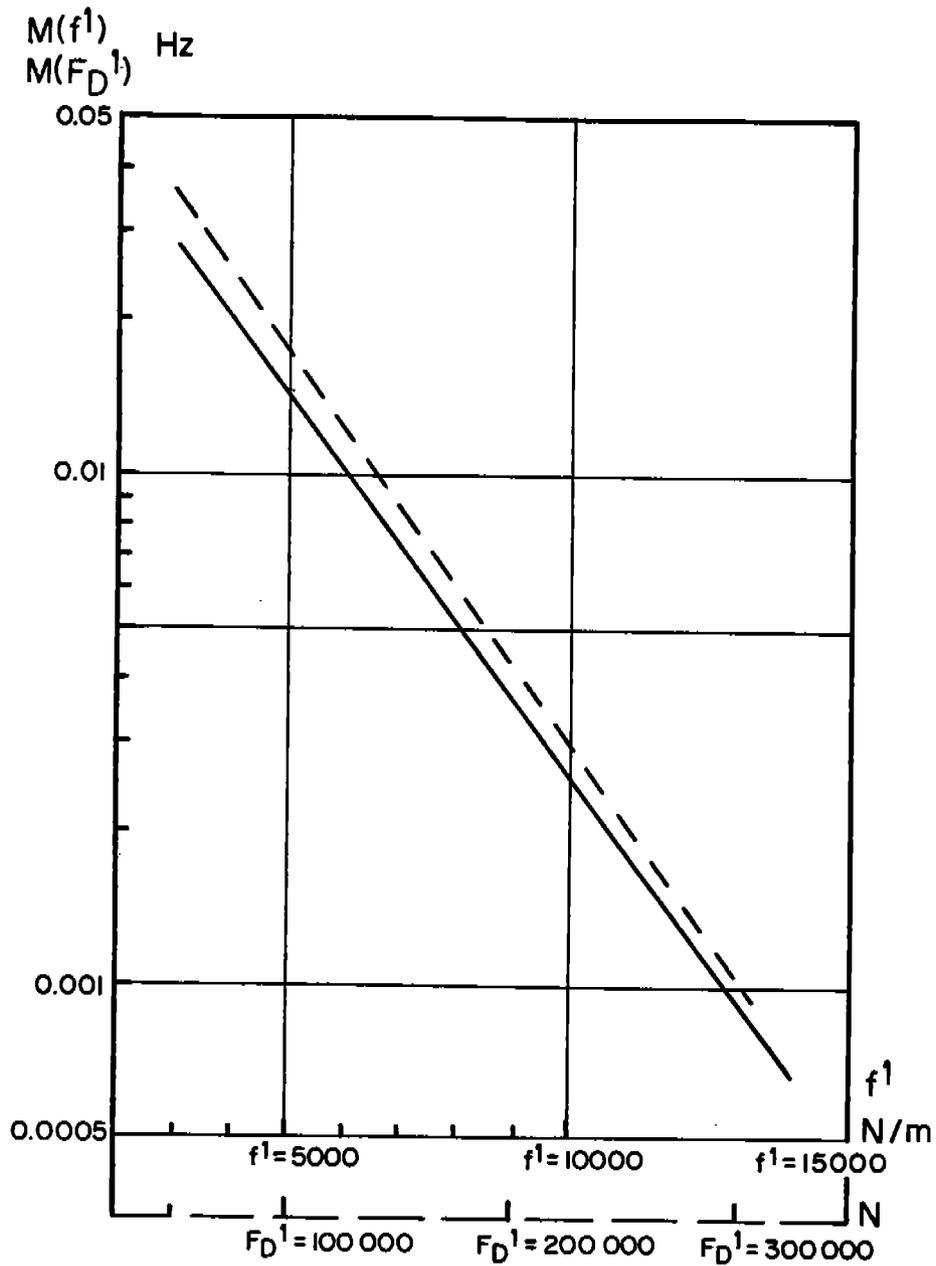
FIGURE 3.36   THE NUMBER OF PEAKS PER UNIT TIME (SEC) THAT EXCEEDS A FORCE
PER UNIT LENGTH EQUAL TO f' AT THE SURFACE (FULL LINE) AND A
TOTAL FORCE OF F_D (HATCHED LINE) [MOE (1979)]

3.3.2.8 Statistics of Wave-Current Force

When current is added to the waves, the velocity is given by the relative velocity between the two and the force has a non-zero mean. The extreme value analysis for this case may be obtained by the above analysis if further simplifying assumptions are made. Moe and Crandall (1978) derived the extreme statistics of the wave-current force based on the extreme rate density, $\mu(f)$.

3.3.2.8.1 Narrow-Band Gaussian Wave and Small Current

The assumption of narrow bandedness implies that ω_1, ω_2, etc. (Eq. 3.271) are nearly equal. The amplitude or envelope $\hat{n}(t)$ of a narrow-band Gaussian process is distributed according to the Rayleigh distribution

$$p(\hat{n}) = \frac{\hat{n}}{\sigma_n^2} \exp \left\{ - \hat{n}^2/2\sigma_n^2 \right\} \tag{3.287}$$

In the presence of a small steady current, U

$$u = U + \hat{n} \, r \, \omega_1 \cos [kx - \omega_1 t + \psi(t)] \tag{3.288}$$

$$a = \hat{n} \, r \, \omega_1'^2 \sin [kx - \omega_1 t + \psi(t)] \tag{3.289}$$

where $\hat{n}(t)$ and $\psi(t)$ are slowly varying. Then

$$p(\hat{f}) \, d\hat{f} = p(\hat{n}) \, d\hat{n} \tag{3.290}$$

and

$$p(\hat{f}) = \begin{cases} \dfrac{\hat{f}}{k_M^2 \, \omega_1^2 \, \sigma_u^2} \exp \left\{ - \dfrac{\hat{f}^2}{2k_M^2 \, \omega_1^2 \, \sigma_u^2} \right\} , & 0 < \hat{f} < f_0 \\[4mm] \dfrac{\exp \left\{ - [\hat{f} - f_0/2 - 2(k_D \, U^2 \, [\hat{f} - f_0])^{1/2}]/(2 \, k_D \, \sigma_u^2) \right\}}{2 \, k_D \, \sigma_u^2 \, [1 + (k_D \, U^2/[\hat{f} - f_0])^{1/2}]} , & \hat{f} > f_0 \end{cases} \tag{3.291}$$

where

$$f_0 = \frac{\omega_1^2 \, k_M^2}{2 \, k_D} \tag{3.292}$$

118

correct to the first order in U/σ_u. For $U = 0$

$$p(\hat{f}) = \frac{\exp\{-(\hat{f}-f_0/2]/(2\ k_D\ \sigma_u^2)\}}{2\ k_D\ \sigma_u^2} \qquad \hat{f} > f_0 \qquad (3.293)$$

which is the same as that given by Borgman (1972). Also, note the similarity between Eqs. 3.293 and 3.280.

Now consider surface elevation, $\eta(t)$ not necessarily a narrow-band process. Asymptotic estimates of extreme force statistics may be obtained in this case. If the joint probability density function for the force $f(t)$ per unit length on a cylinder and its time derivative, $\dot{f}$ is $p(f, \dot{f})$, the peak rate density is given by

$$\mu(f) = - [\ \frac{d}{df} \int_0^\infty \dot{f}\ p(f,\dot{f})\ d\dot{f}\ ]_{f=\hat{f}} \qquad (3.294)$$

The asymptotic approximation of $p(f, \dot{f})$ is

$$p(f,\dot{f}) \simeq \frac{1}{8\pi\sigma\ \sigma\ k_D\dot{f}} \exp\{-\frac{1}{2k_D\sigma_u^2}[f-f_0/2 - 2U\ (k_Df)^{1/2} + \dot{f}^2/(4\omega_2^2 f)]\} \qquad (3.295)$$

where $f_0 = \frac{\omega_2^2\ f_I^2}{2f_D}$. The peak rate density $\mu(\hat{f})$ is

$$\mu(\hat{f}) = \frac{\omega_2}{2\pi} \frac{\exp\{-[\hat{f}-f_0/2 - 2U(k_D\hat{f})^{1/2}]\ /(2k_D^2\sigma_u)\}}{2k_D\ \sigma_u^2[1+(k_DU^2/\hat{f})^{1/2}]} \qquad (3.296)$$

Comparing the two expressions in Eqs. 3.291 and 3.296, the former is valid for any $\hat{f} > 0$ but is restricted to narrow-band waves. The latter has no band width restriction but is only valid for large $\hat{f}$ asymptotically. Both results are restricted to small currents, i.e. $U/\sigma_u < 1$. When $U = 0$, the only difference is ω_2 vs. ω_1. This suggests that the frequency of larger extremes is determined by the frequency ω_2 of the velocity, $u(t)$, process rather than by the frequency, ω_1 of the surface elevation, $\eta(t)$, process.

119

<u>EXAMPLE</u>

Let us investigate the large-force behavior of $\mu(\hat{f})$ for a cylindrical pile 1.3m (4.3 ft.) in diameter for a P-M spectrum seastate for wind speed of 30 m/s (67.1 mph) in the absence of current. The spectrum is truncated at a frequency of 0.98 rad/s. The result is calculated at a section where $\sigma_u = 1.8$ m/s (5.9 ft/s), $\sigma_a = 0.90$ m/s^2 (3.0 ft/s^2), $f_0 = 68$ kgf/m (4.6 lb/ft), and $2f_D\sigma_u^2 = 450$ kgf/m (310 lb/ft). The extreme rate density is shown in Fig. 3.37 from Eq. 3.296 by setting U = 0. The peak rate density, $\mu(f)$, has an exponential decay here.

Grigoriu (1984) considered the extremes of the modified Morison force in the presence of current by two different methods. In the first case the extremes were predicted based on the assumption of Gaussian force through linearization. The corresponding Gaussian approximation for the drag force will have the form

$$p(\overline{f}_D) = [\frac{1}{\sqrt{2\pi}} + N\,\overline{f}_0\,\Phi\,(\overline{f}_D)]\,\exp\,\{-\frac{\overline{f}_D^2}{2} - N\,e^{-\overline{f}_D^2/2}\} \qquad (3.297)$$

in which N is the number of peaks defined as $N = 2\pi T_R/\omega_2$ where ω_2 is defined in Eq. 3.271 and T_R is the duration of the storm under consideration. In the second case the actual distribution of force was considered. Expressions for extreme value density functions were obtained for the drag force alone and for the drag-inertia force combination from the Morison formula. The probability density function of the peak drag force (in the presence of current) is given in terms of the nondimensional force

$$\overline{f}_D = \frac{f_D - \mu_{f_D}}{\sigma_{f_D}} \qquad (3.298)$$

where f_D = peak drag force amplitudes, μ_{f_D} = mean value of the peak drag force and σ_{f_D} = corresponding standard deviation. The dependence of current is introduced in the expression of the density function in terms of α which is the inverse of γ. Thus, α can be defined as:

$$\alpha = \frac{\sigma_u}{U} \qquad (3.299)$$

120
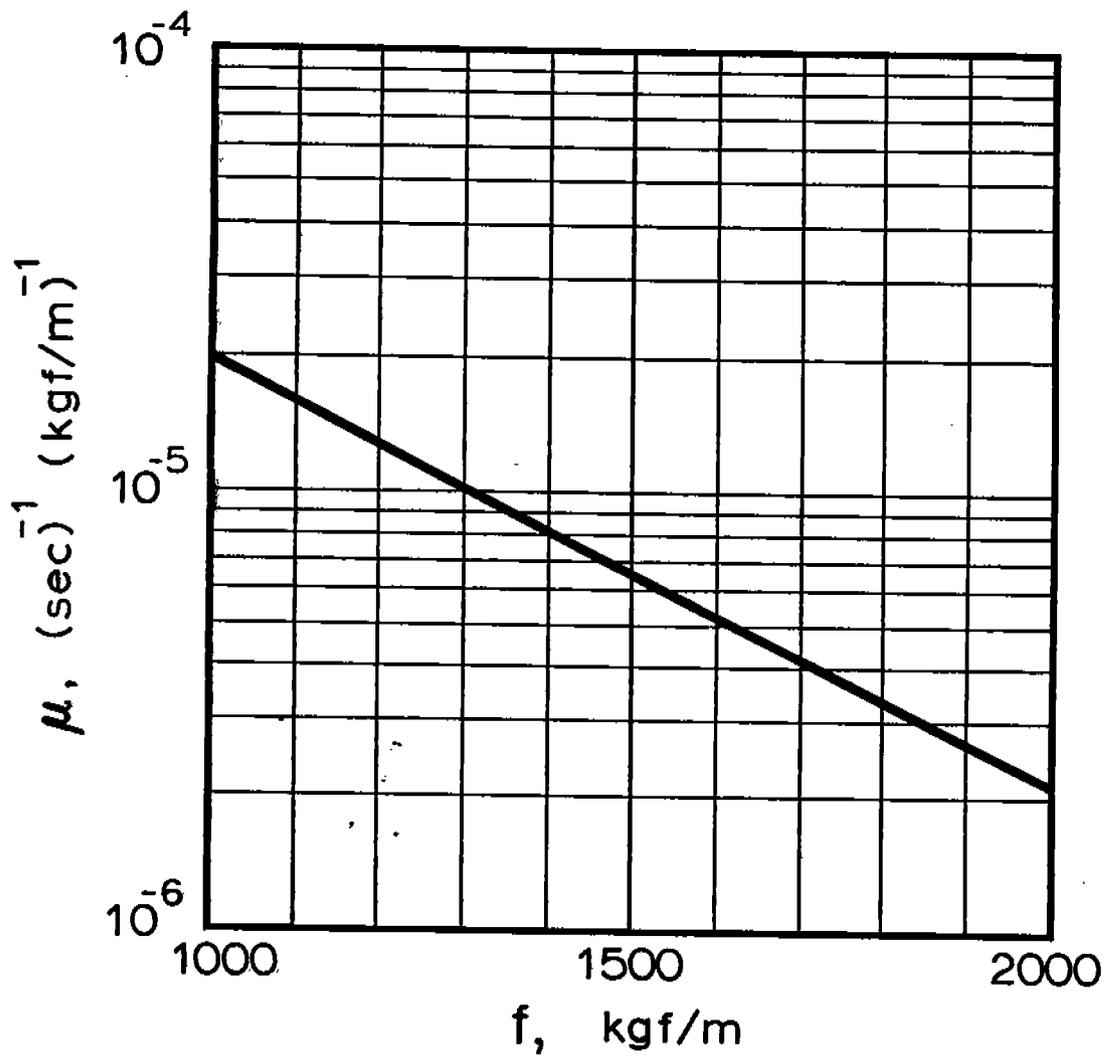
FIGURE 3.37   EXTREME RATE DENSITY FOR FORCE PER UNIT LENGTH OF A CYLINDER
   [MOE AND CRANDALL (1978)]
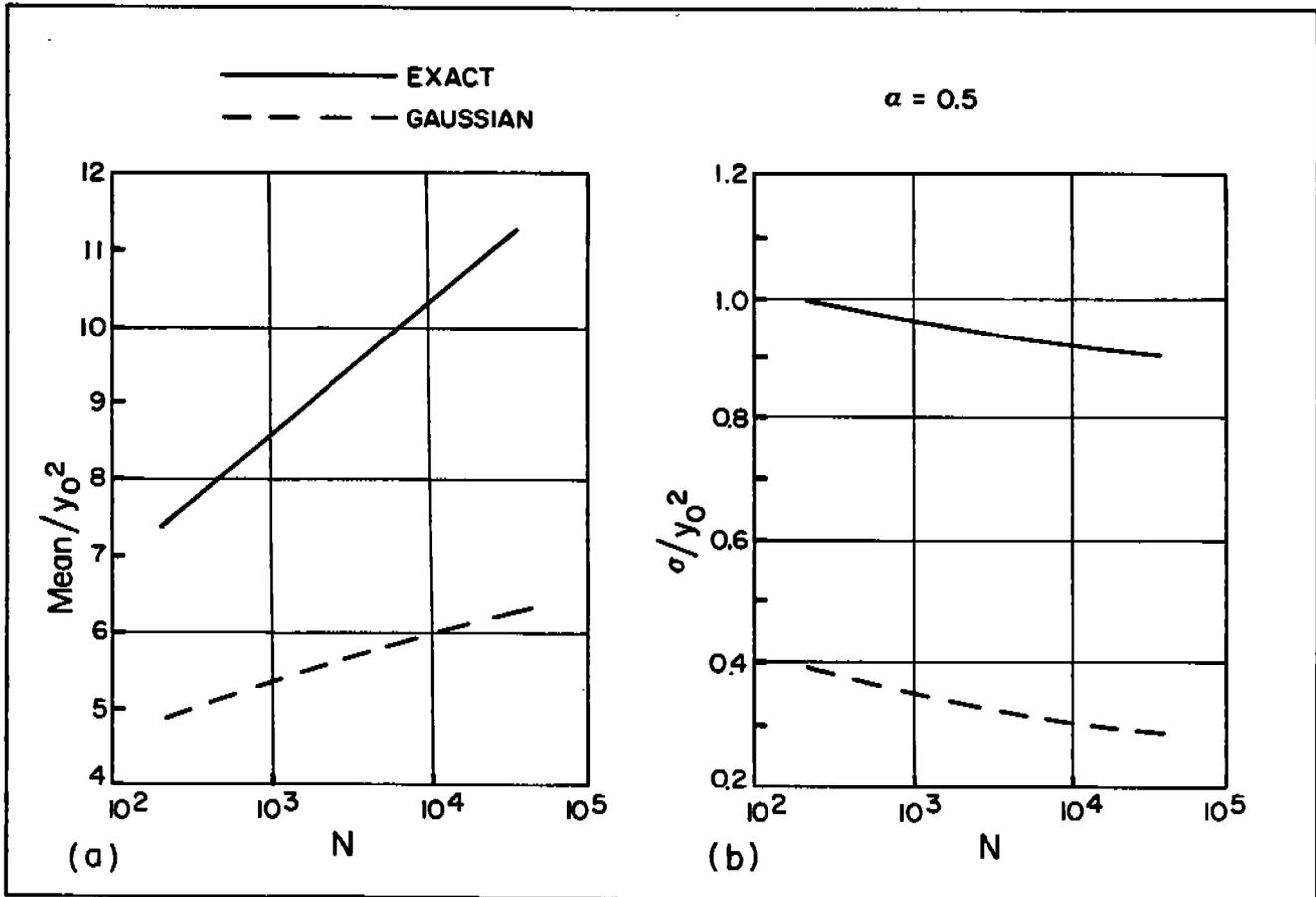
FIGURE 3.38   (A) NORMALIZED MEAN AND (B) STANDARD DEVIATION OF PEAK MORISON
FORCES IN THE PRESENCE OF CURRENT [GRIGORIU (1984)]

where U = current velocity. Thus, $\alpha \to 0$ when U is dominant ($\gamma \to \infty$) and $\alpha \to \infty$ as current approaches zero. ($\gamma \to 0$). The probability densities for the exact and approximate expressions were used to determine the mean and standard deviations of the peak drag force by numerical integrations. The mean and standard deviation of the peak drag forces from the exact and approximate methods are normalized by U^2 and shown in Fig. 3.38 versus N for $\alpha = 0.5$. The figure shows that the Gaussian hypothesis yields approximations which significantly underestimate the mean and standard deviations of the peak drag force. For example, these values from the exact formula are 10.4 U^2 and 0.86 U^2, respectively, while the corresponding values from the approximate formula are 6.0 U^2 and 0.26 U^2 for N = 10,000 and $\alpha = 0.5$.

3.3.2.8.2 Finite Current

Naess (1983) developed a general method of investigating extreme values of a compound stochastic process. The method relies upon the mean upcrossing frequency, $f_\xi^+(f)$ at a level ξ of a process, e.g., force, f(t). In the extreme situations these upcrossings are rare events. Such upcrossings are assumed to be statistically independent which is at least conservative. The zero crossing frequency is derived in the following way.

By the Poisson probability law, the probability that f(t) stays below a level ξ during a time interval of length, T_R, is given by

$$P[f(t) < \xi] = \exp \{- f_\xi^+(f)T_R\} \tag{3.300}$$

Thus, if f_ξ^+ is known for all large values of ξ the probability distribution function of max {f(t)} is known.

The general procedure of obtaining the zero upcrossing frequency, $f_\xi^+(f)$ is applied to the forcing function computed by the Morison formula. The problem is to obtain the upcrossing frequency of the forcing function, f(t). The fluid velocity, u(t), is assumed to be a stationary Gaussian process and is differentiable. The quantities u(t) and $\dot{u}(t)$ are independent random variables. In the presence of a current U, the mean value of u(t), is given by E[u(t)] = U. Normalizing the velocity and acceleration terms as

$$\bar{\dot{u}}(t) = \frac{\dot{u}(t)}{\sigma_{\dot{u}}} \text{ and } \bar{u}(t) = \frac{u(t)}{\sigma_u} \tag{3.301}$$

121

and the forcing function f(t) by

$$\overline{f}(t) = \frac{f(t)}{k_M \sigma_{\ddot{u}}} \qquad (3.302)$$

Eq. 3.251 is written in a nondimensional form as

$$\overline{f}(t) = h[\overline{\dot{u}}(t), \overline{u}(t)]$$

$$= \overline{\dot{u}}(t) + \frac{1}{2} K|\overline{u}(t)|\overline{u}(t) \qquad (3.303)$$

The variables, $\overline{\dot{u}}(t)$ and $\overline{u}(t)$ are two stationary Gaussian processes of unit variance

$$E[\overline{\dot{u}}_1(t)] = 0 \qquad (3.304)$$

and

$$E[\overline{u}(t)] = \frac{U}{\sigma_u} \equiv \gamma, \qquad \gamma > 0 \qquad (3.305)$$

The mean upcrossing frequency $f_\xi^+ = f_\xi^+(f)$ of f(t) is determined by the well-known formula of Rice.

Using the law of marginal distribution and transformation of variables, the probability density of mean upcrossing frequency may be written as an integral of the product of conditional probability density function between $\overline{\dot{u}}$ and $\overline{u}$ and the probability density function, p_f. The expression for f_ξ^+ is

$$f_\xi^+ = \int_{-\infty}^{\infty} \int_{-\infty}^{\infty} \frac{\dot{\phi}d\dot{\phi}}{(2\pi)^{3/2}\,\overline{\sigma}} \exp\left\{-\frac{1}{2}\left(\frac{\dot{\phi} - \overline{\mu}}{\overline{\sigma}}\right)^2\right\} \exp\left\{-\frac{1}{2}[\hat{\dot{u}} + (\hat{u} - \gamma)^2]\right\} d\hat{u} \qquad (3.306)$$

where

$$\overline{\mu} = E[\overline{\dot{F}}|\overline{\dot{u}} = \hat{\dot{u}}, \overline{u} = \hat{u}] = -\omega_2(\hat{u} - \gamma) + K\omega_2|\hat{u}|\hat{\dot{u}} \qquad (3.307)$$

and

$$\overline{\sigma} = \text{Var}[\overline{\dot{F}}|\overline{\dot{u}} = \hat{\dot{u}}, \overline{u} = \hat{u}] = \frac{\omega_2^2}{\rho^2}(1 - \rho^2) \qquad (3.308)$$

122

where $\omega_2 = \sigma_{\dot{u}}/\sigma_u$, and the correlation coefficent, $\rho = \dfrac{\sigma_{\dot{u}}^2}{\sigma_u \sigma_{\ddot{u}}}$. Alternately,

$$f_\xi^+ = \frac{1}{2\pi} \int_{-\infty}^{\infty} \left[\frac{\overline{\sigma}}{\sqrt{2\pi}} e^{-\frac{1}{2}(\overline{\mu}/\sigma)^2} + \overline{\mu} \, \Phi \left(\frac{\overline{\mu}}{\sigma} \right) \right] \exp \left\{ -\frac{1}{2} [\hat{\dot{u}} + (\hat{u} - \gamma)^2] \right\} d\hat{u} \tag{3.309}$$

where

$$\hat{\dot{u}} = \xi - \frac{1}{2} K |\hat{u}| \hat{u} \tag{3.310}$$

This equation for the zero upcrossing frequency can be solved numerically. An asymptotic relation for f_ξ^+ valid for all current speeds is obtained by Vinje (1980)

$$\hat{f}_\xi^+ = \frac{\omega_2}{2\pi} \exp \left\{ -\frac{\xi}{K} + 2U \left(\frac{\xi}{K} - \frac{1}{K^2} \right) - \frac{U^2}{2} + \frac{1}{2K^2} \right\} \tag{3.311}$$

Note that Borgman considered the case of $U = 0$ while Moe and Crandall (1977) investigated the case of $\gamma \ll 1$.

For a long time interval (i.e., large ξ), the probability distribution function of the largest value of $f(t)$ is obtained assuming a time interval length, T_R and defining

$$\overline{f} = \overline{\mu}^1 \; \max \{f(t)\} \tag{3.312}$$

as

$$P_{\overline{f}}(\eta) = \text{Prob} \, \{\overline{f} \leqslant \eta\}$$

$$= \text{Prob} \, \{\max[f(t) \leqslant \mu\eta\}$$

$$\approx \exp \, \{ -f_{\mu\eta}^+ T_R \} \tag{3.313}$$

The expected value of the maximum force is obtained from

$$E[\max \{f(t)\}] = KE[\overline{f}] = 2K \left[\theta_0(T_R)^2 + U \, \theta_1(T_R) + \frac{G\theta_1(T_R)}{U + \theta_1(T_R)} \right]$$

$$+ 0 \left[(\ln \Omega \, T_R)^{-3/2} \right] \tag{3.314}$$

where G = Euler's constant (= 0.5772),

$$\Omega = \frac{\omega_2}{2\pi} \exp \left\{ -\frac{U^2}{2} + \frac{1}{2K^2} \right\} \qquad (3.315)$$

and

$$\theta_n(T_R) = \left[(n + 1)\, \ell n\, \Omega\, T_R + U^2 - \frac{2n}{K^2} \right]^{1/2}, \qquad n = 0,1 \qquad (3.316)$$

Note that as $T_R \rightarrow \infty$ the variance of the maximum values of $f(t)$ approach $\pi^2 K^2/6$.

It may be similarly derived that the component of the drag force has the expected extreme values given by

$$E[\max \{f_D(t)\}] = \mu\left[(2\ell n\, \frac{\omega_2 T_R}{2\pi})^{1/2} + U \right]^2 + 2KG\left[1 + U(2\ell n\, \frac{\omega_2 T_R}{2\pi})^{-1/2} \right]$$

$$+ 0\left[(\ell n\, \frac{\omega_2 T_R}{2\pi})^{-3/2} \right] \qquad (3.317)$$

which has the same asymptotic variance as the total force.

EXAMPLE: Consider a pile of diameter D = 1m and a seastate given by the significant height, H_S = 6m and zero upcrossing period T_z = 8 sec. Assume C_M/C_D = 1 and U = 1.

For this case, σ_u = 1.21 m/sec and $\sigma_{\dot{u}}$ = 1.70m/sec^2. Then

$$\omega_2 = \frac{\sigma_{\dot{u}}}{\sigma_u} \approx 1.4\ \text{sec}^{-1}$$

and

$$K = \frac{2k_D \sigma_u^2}{k_M \sigma_{\dot{u}}} = 1.1$$

The mean upcrossing frequencies f_ξ^+ are plotted versus the load level, ξ in Fig. 3.39 along with the upcrossing frequencies $f_\xi^+(f_D)$ of the drag force component. The expected largest values of the total force, $f(t)$ and drag force, $f_D(t)$ are shown as functions of time interval, T_R, in Fig. 3.40. The expected values of the inertia force, $f_I(t)$ is a Gaussian process. Since

124
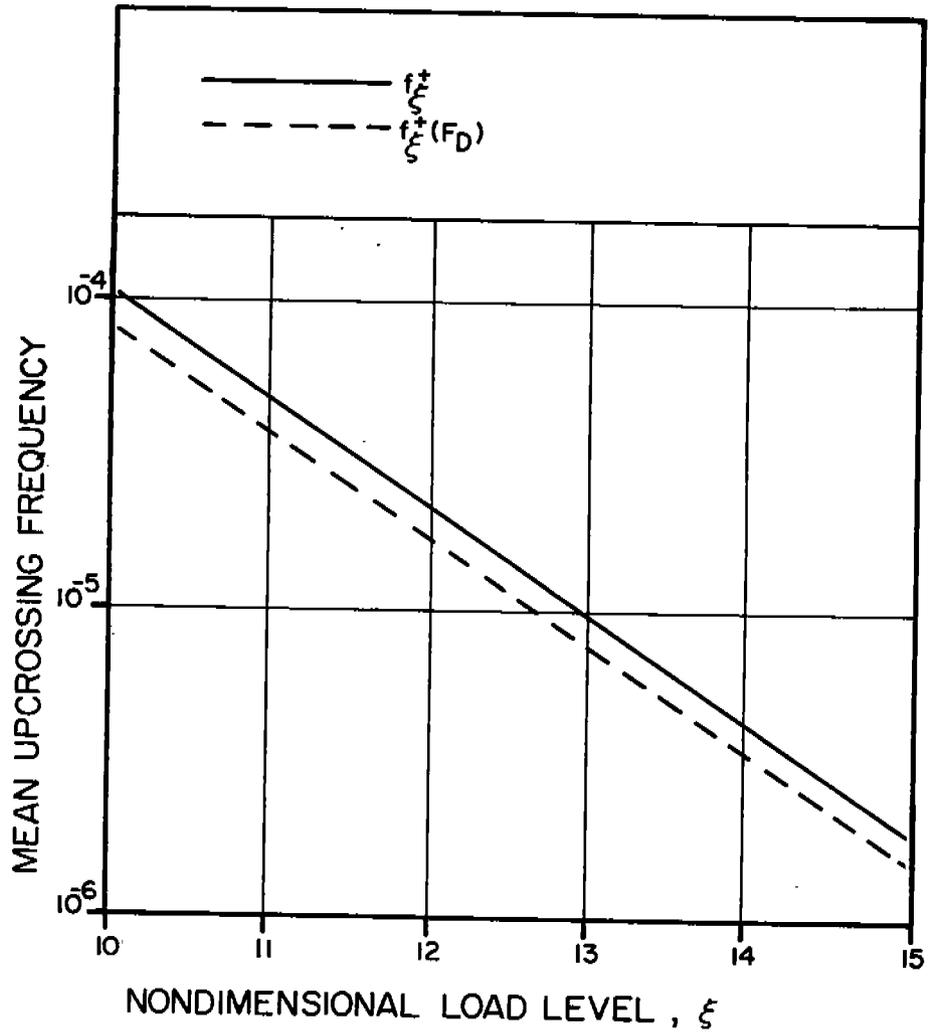
FIGURE 3.39   MEAN UPCROSSING FREQUENCY, f_ξ^+ OF THE TOTAL MORISON FORCE (SOLID
LINE) AND DRAG FORCE (DOTTED LINE) [NAESS (1983)]
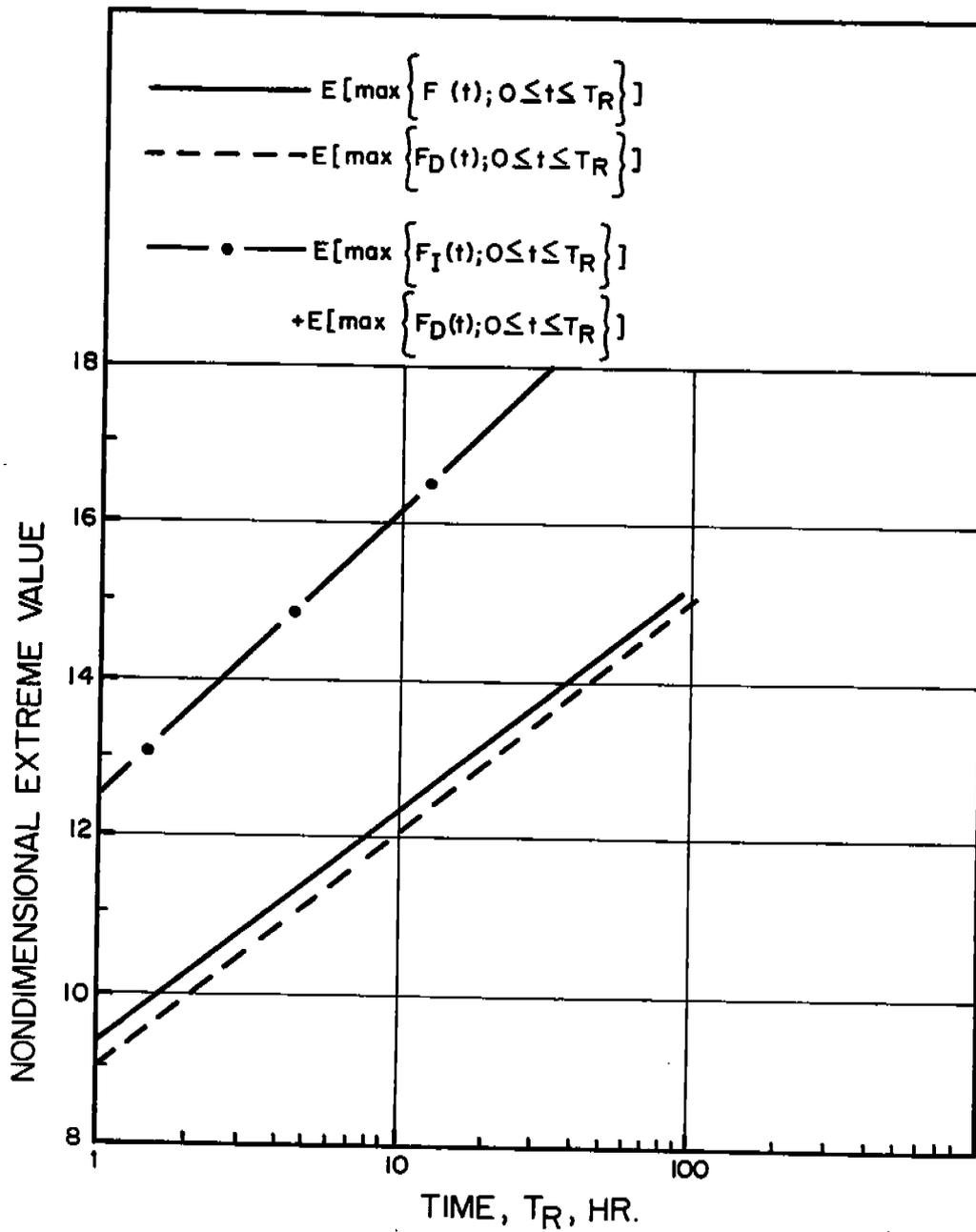
FIGURE 3.40   EXPECTED LARGEST VALUES OF TOTAL MORISON FORCE (SOLID LINE),
DRAG FORCE (DOTTED LINE) AND EXPECTED INERTIA PLUS EXPECTED
DRAG FORCE (CENTER LINE) FOR TIME INTERVAL, T_R [NAESS (1983)]

loading is high and mainly in the drag regime, the extreme value analysis can be performed on the drag force component alone with reasonable results. On the other hand, a term by term extreme value analysis of the Morison equation (centerline, Fig. 3.40) substantially overpredicts the expected value.

3.3.2.9 Statistics of Nonlinearly Damped Systems

If the excitation for a single or multi-degree of freedom system is assumed Gaussian and the damping in the system is linear, the prediction of extreme values of the response of the system is straightforward by computing the response spectra first. This has already been demonstrated. However, if the damping is nonlinear, then the prediction formula is difficult to obtain in general. The problem of the response of a nonlinearly damped system subject to a Gaussian excitation has been addressed by Brouwers (1982) and approximate expressions for the probability distributions for small damping have been derived.

The derivation is based on the fact that if damping is small in a system, the response near resonance is finite (unlike an undamped system) but still extremely large compared to the response away from the resonance. This is, of course, true if the natural frequency falls near the center of the excitation spectrum. For a natural frequency far in the tails of the excitation spectrum where there is very little energy the response will be small even if the damping is small. The overall solution in the former case is dominated by the response near resonance.

Therefore, for small damping the response is narrow banded (but non-Gaussian for nonlinear damping) over a small band of frequencies. The excitation spectrum over this band may be considered constant. An example of this scenario is shown in Fig. 3.41. The frequency, ω_0 corresponds to the natural frequency of the system and the relative magnitudes of the width and height of the response spectrum is indicated in the figure. In this case, the input spectrum may be treated as a white noise for which solutions have been obtained by Roberts (1977). Because of the narrow bandedness of the solution, it may be represented by a sinusoidal wave of slowly and randomly varying amplitude and phase. An exact solution for the joint probability density of

125
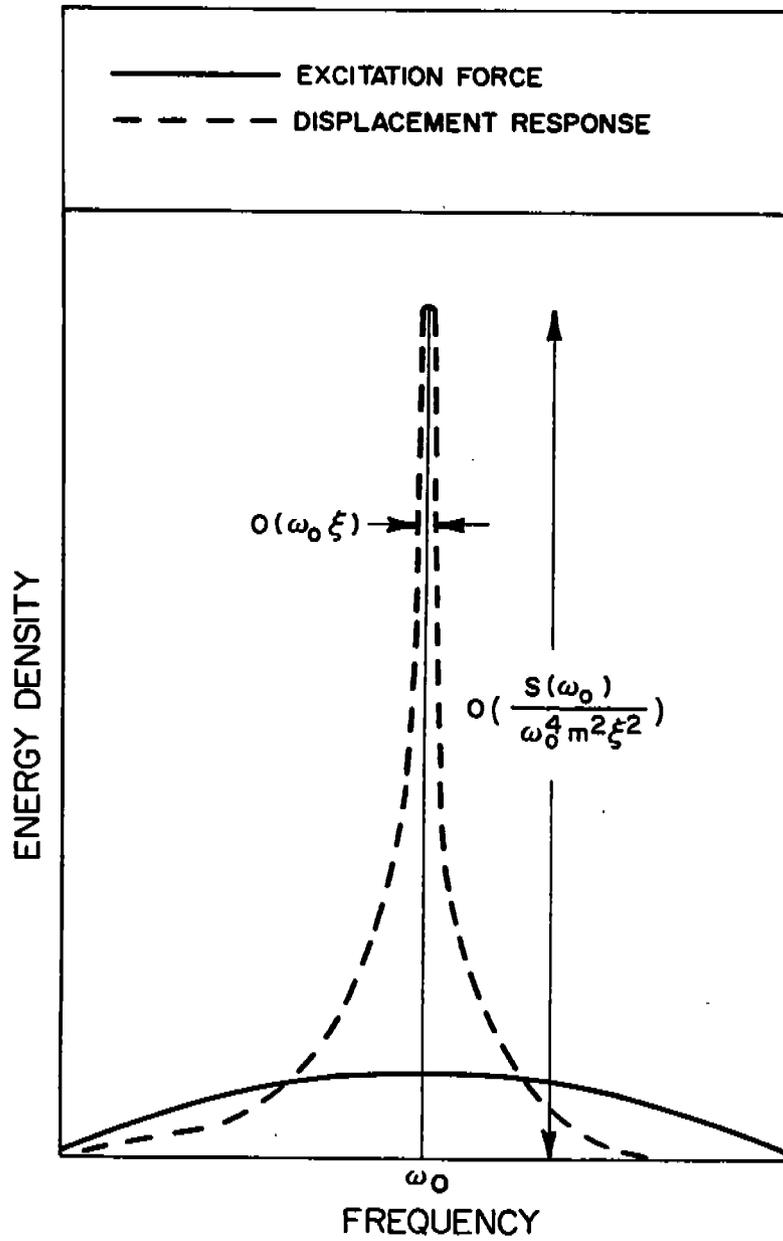
FIGURE 3.41   SCHEMATICS OF THE ENERGY DENSITY SPECTRA OF EXCITATION AND
RESPONSE [BROUWERS (1982)]

the amplitude and phase has been obtained by Roberts (1977). Brouwers (1982) provided an alternate method of solution for these density functions for amplitude and phase in integral form.

The equation of motion of a single degree of freedom system involving nonlinear damping is written as

$$m\ddot{x} + g(\dot{x}) + m\omega_0^2 x = f(t) \tag{3.318}$$

where m = mass of the system, ω_0 = undamped natural frequency, x = displacement response, $g(\dot{x})$ = damping force as an odd function of $\dot{x}$, and f(t) = stationary Gaussian excitation with zero-mean. If the damping term is assumed to have the form

$$g(\dot{x}) = N|\dot{x}|^{\alpha-1} \dot{x} \tag{3.319}$$

then a simplified expression for the integral representation of the probability density function may be obtained. Note that for $\alpha = 0$, Coulomb friction is represented. If $\alpha = 1$, the damping is linear viscous while if $\alpha = 2$, it is the usual fluid dynamic drag. The probability density for the response maxima (amplitude a) is

$$p(a) = \frac{(\alpha + 1) \ \Gamma \left(\frac{4}{\alpha + 1} \right) a}{2 \ \sigma_a^2 \ \Gamma^2 \left(\frac{2}{\alpha + 1} \right)} \ \exp \left[- \left\{ \frac{\Gamma \left(\frac{4}{\alpha + 1} \right) a^2}{2\sigma_a^2 \ \Gamma \left(\frac{2}{\alpha + 1} \right)} \right\}^{\frac{\alpha + 1}{2}} \right] \tag{3.320}$$

where Γ is the gamma function tabulated in mathematical handbooks. For $\alpha = 2$, the expression for p reduces to that for a Rayleigh distribution. The variance of the response may be computed from

$$\sigma_a^2 = \frac{\Gamma \left(\frac{4}{\alpha + 1} \right)}{2 \ \omega_0^2 \ \Gamma \left(\frac{2}{\alpha + 1} \right)} \left\{ \frac{\pi^{3/2} \ (\alpha + 1) \ S(\omega_0) \ \Gamma \left(\frac{\alpha + 3}{2} \right)}{4 \ mN \ \Gamma \left(\frac{\alpha + 2}{2} \right)} \right\}^{\frac{2}{\alpha + 1}} \tag{3.321}$$

The probability density function is plotted in Fig. 3.42 for $\alpha = 0, 1$ and 2.

The expected extreme response may be obtained from the probability density of the largest amplitude

$$p(a_{max}) = \{ \frac{dP^n(a)}{da} \}_{a = a_{max}} \qquad (3.322)$$

by an asymptotic approximation.

$$E[a_{max}] = \sigma_a \{ \frac{2\Gamma (\frac{2}{\alpha + 1})}{\Gamma (\frac{4}{\alpha + 1})} \}^{1/2} \kappa^{- \frac{1}{\alpha + 1}} \{ 1 + \frac{\alpha - 1}{\alpha + 1} \kappa \ln \kappa \}^{- \frac{\alpha}{\alpha + 1}}$$

$$[1 + \frac{\alpha - 1}{\alpha + 1} \kappa \ln \kappa + (\frac{G - \ln \Gamma (\frac{2}{\alpha + 1})}{\alpha + 1}) \kappa$$

$$- \frac{(\alpha - 1)^2}{(\alpha + 1)^3} \kappa^2 \ln \kappa + 0 (\kappa^2)] \qquad (3.323)$$

where G is Euler's constant (= 0.57722) and

$$\kappa = \frac{1}{\ln N} \qquad (3.324)$$

The expected extreme values of the response for different values of α and large N (= 1000 and 2000) are tabulated in Table 3.5. The extreme value is seen to decrease as α increases.

If an equivalent linearization technique as shown in Section 3.3.2.4 is employed then the mean square displacement has the form

$$\sigma_{eq}^2 = \frac{1}{2\omega_0^2} \{ \frac{\pi^{3/2} \, S (\omega_0)}{2 \, \Gamma (\frac{\alpha + 2}{2}) \, mN} \}^{\frac{2}{\alpha + 1}} \qquad (3.325)$$

The ratio of the mean square displacement between the general solution and linear approximation has the form

127
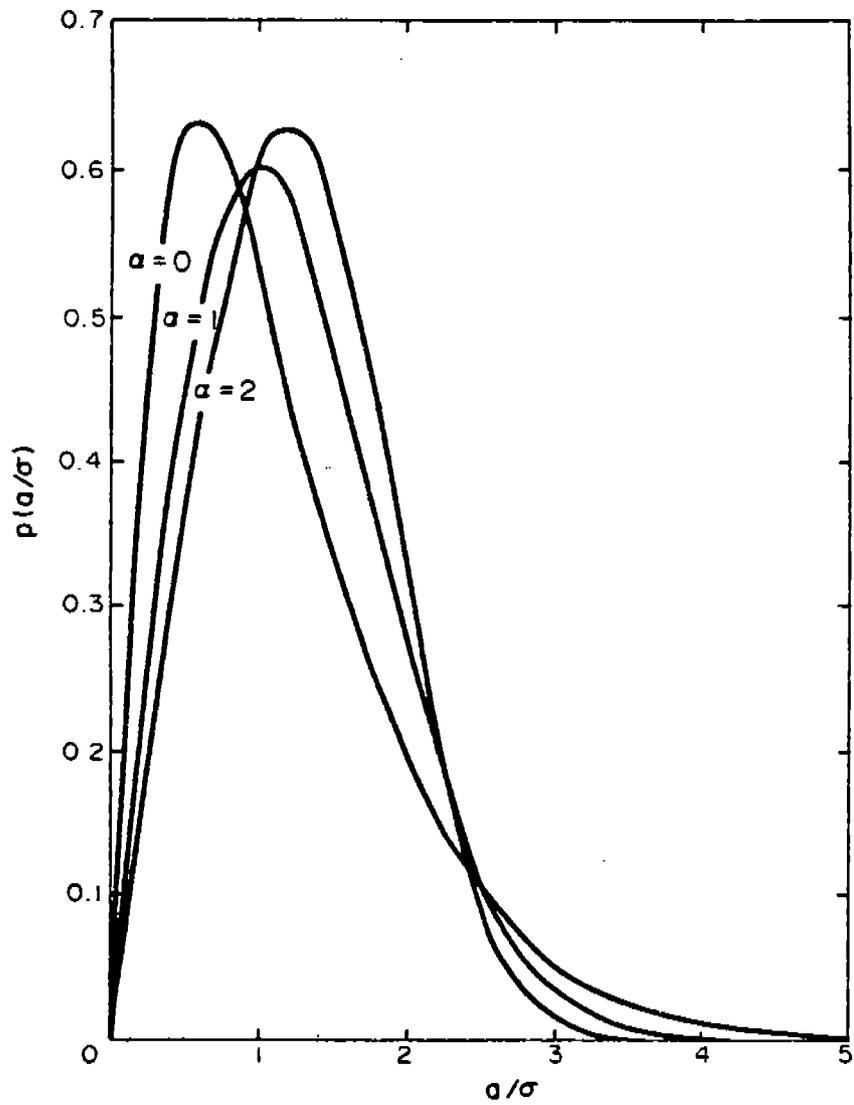
FIGURE 3.42   PROBABILITY DENSITY OF MAXIMA FOR A DAMPING FORCE WHICH IS
PROPORTIONAL TO A POWER α OF THE VELOCITY [BROUWERS (1982)]

TABLE 3.5

RATIO OF THE EXPECTED EXTREME RESPONSE OF NONLINEAR
AND LINEARIZED SYSTEM TO THE ROOT MEAN SQUARE RESPONSE
VS. THE NONLINEARITY PARAMETER α
[BROUWERS (1982)]

	N	$\alpha =$ 0	1	2	3	4	5
	1000	5.60	3.87	3.26	2.95	2.76	2.63
$E[\bar{\alpha}]/\sigma$							
	2000	6.05	4.05	3.37	3.02	3.83	2.68
σ_{eq}^2/σ^2		0.85	1.0	0.96	0.89	0.82	0.75
	1000	0.64	1.0	1.16	1.24	1.27	1.28
$E[\bar{a}]_{eq}/E[\bar{a}]$							
	2000	0.62	1.0	1.18	1.27	1.30	1.31

$$\frac{\sigma_{eq}^2}{\sigma^2} = \frac{\Gamma\left(\frac{2}{\alpha+1}\right)}{\Gamma\left(\frac{4}{\alpha+1}\right)} \left\{\frac{2}{(\alpha+1)\,\Gamma\left(\frac{\alpha+3}{2}\right)}\right\}^{\frac{2}{\alpha+1}} \tag{3.326}$$

These values for $\alpha = 0, 1, \ldots 5$ are shown in Table 3.5. In all cases (except $\alpha = 1$, linear case), the equivalent linearization method underpredicts the mean square value which increases with increasing nonlinearity, i.e., increasing α.

For an equivalent linear representation of the damping force which is considered small, the probability density of maxima reduces to a Rayleigh distribution whose extreme value formula is known as

$$E[a_{max}]_{eq} = \sqrt{2}\ \sigma_{eq}\ \ell n^{-1/2} N\ \{1 + \frac{1}{2} \gamma\ \ell n\ N + 0\ (\ell n^2 N)\ \} \tag{3.327}$$

A comparison for the expected extreme values between this solution and the general solution is shown in Table 3.5. The linearized solution overpredicts the extreme response in all cases (except for $\alpha < 1$). Thus, this simplified method may be applied as a conservative method in this case.

An example problem was provided by Brouwers (1982). For certain types of offshore structures the response is governed by resonance. (If the response at resonance is not important, on the other hand, the nonlinear damping term is of no consequence in the analysis.) The riser of a Single Anchor Leg Storage (SALS) system for oil production (Fig. 3.43) may fall in this category. Consider a 4m diameter riser in 140m water depth. The riser responds predominantly in the first mode at a natural frequency of 1.4 rad/sec. which is well in the center of typical wave spectra. The second natural frequency of 5.5 rad/sec is outside the range of energy spectra. Assuming a small damping, Brouwers (1982) obtained the distribution for extreme amplitudes by the present approximate method as well as by numerical time domain solution. The results for $\alpha = 0$, (Coulomb friction) and 2 (quadratic damping) are shown in Fig. 3.44. Note that the approximate solutions in both cases are quite satisfactory.

Roberts (1987) considered a class of nonlinear motion response problems which have a linear-plus-quadratic damping and linear-plus-cubic stiffness, with a softening spring characteristic. Thus, the problem involved a second-

128

Universal joint

12 m

Mean sea level

Yoke

Vessel

Buoyancy chamber

132 m   Riser

Longitudinal section
of riser

2 m
31 mm

4 m
31 mm

Buoyancy chamber

Flow lines

8 m   Gravity
base
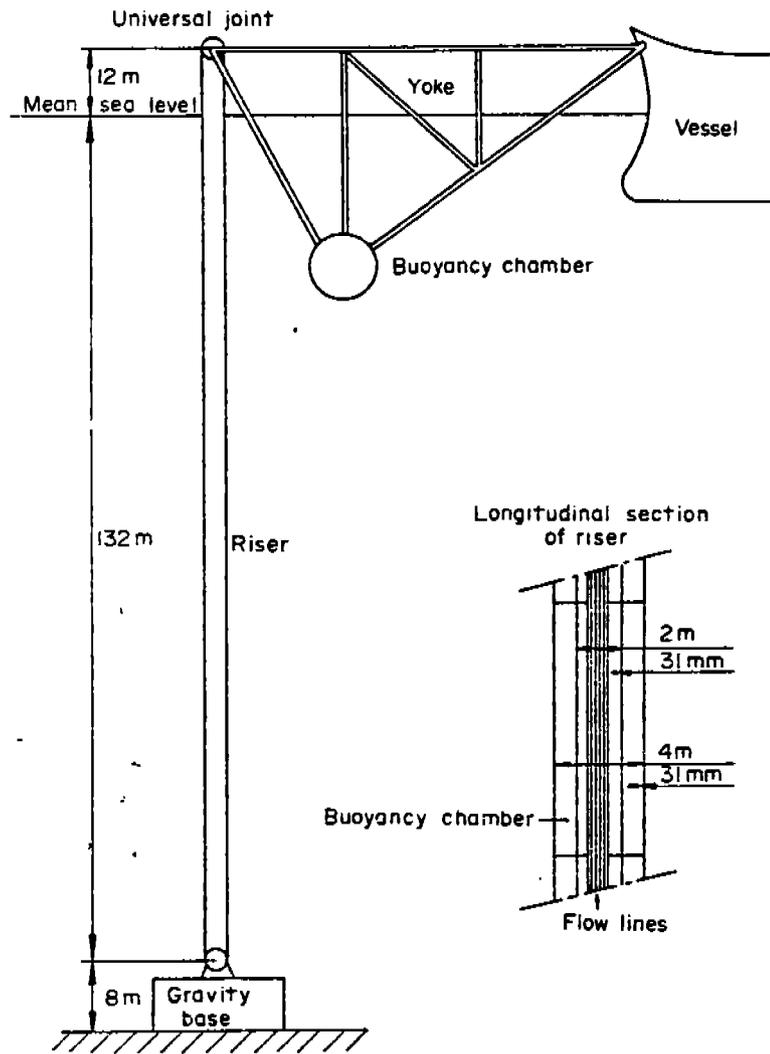
FIGURE 3.43   SCHEMATIC OF SINGLE ANCHOR LEG STORAGE (SALS) SYSTEM FOR
EXAMPLE PROBLEM [BROUWERS (1982)]

Figure axes and labels:
- Y-axis: Response maximum / standard deviation (0 to 4)
- X-axis: Probability less than (0.01, 0.5, 0.9, 0.99, 0.999)
- Legend: ● ● ● Numerical results for SALS riser; ——— Analytical solutions
- Curve labels: Rayleigh, Coulomb friction, Quadratic damping
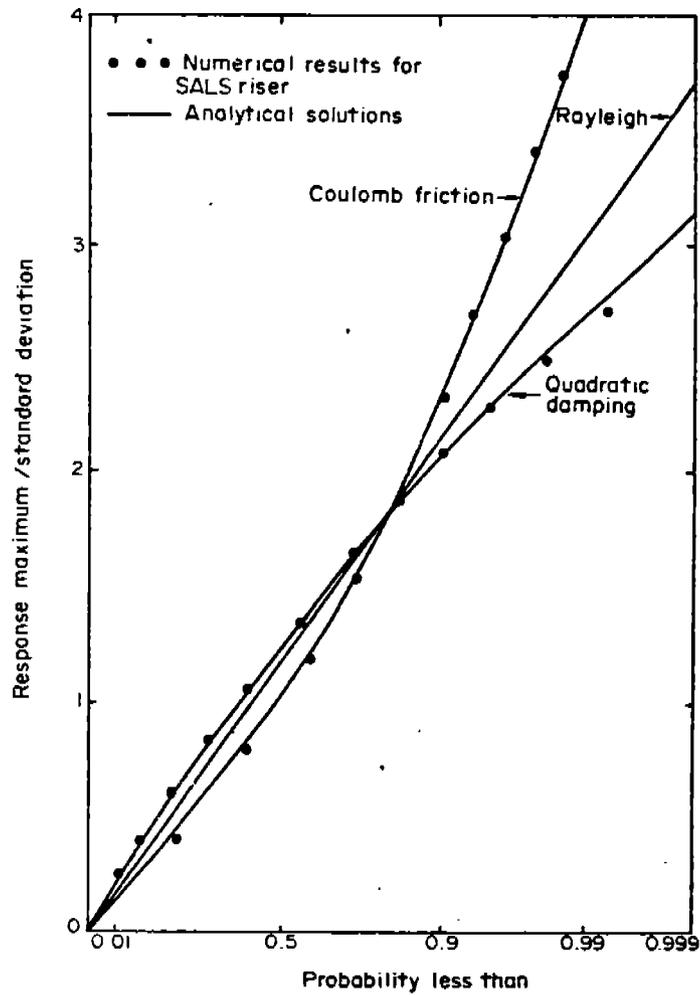
FIGURE 3.44   NUMERICALLY CALCULATED DISTRIBUTION OF RESPONSE AMPLITUDES FOR THE SALS RISER AND THE ANALYTICAL DISTRIBUTIONS FOR COULOMB FRICTION AND QUADRATIC DAMPING [BROUWERS (1982)]

order equation of motion of a moored floating system having drag-type damping and hawser lines. A generalized method of stochastic averaging was applied to deduce expressions for various response statistics. A modification of the Markov process allowed use of a non-white spectrum shape. The excitation was assumed to be a stationary process with zero mean.

The cumulative distribution based on this modified theory is compared in Fig. 3.45 with the experimental data on roll peak amplitudes of a ship model in a random beam sea. The results from the previous theory [Roberts (1982)] are also shown on the figure. The modified theory seems to match the experimental data well.

3.3.2.10 Statistics of Drift Force Response

In order to predict the maximum values of the slow drift responses of a moored vessel, the statistical distribution of the slow drift response must be known. In this case, the exciting forces are non-Gaussian. In addition, the mooring system generally has nonlinear restoring properties, but that nonlinearity has not been discussed in this section.

For an infinitely narrow-banded wave spectrum, the slow drift response follows an exponential distribution [Stansberg (1983)]. However, for a wave force spectrum of finite bandwidth, the statistical distribution of the second-order wave force differs from an exponential distribution [Langley (1984)].

The second-order force may be expressed in regular waves in terms of a reflection coefficient

$$F = C(\omega) \left(\frac{H}{2} \right)^2 = C(\omega) \, a^2 \tag{3.328}$$

Thus, the force is proportional to the square of the wave amplitude, and the reflection coefficient, $C(\omega)$, is a function of the wave frequency, ω. A random sea is written as a superposition of linear wave components

$$\eta(t) = \sum_{n=1}^{N} (a_n \cos\omega_n t + b_n \sin\omega_n t) \tag{3.329}$$

This process may be equivalently written in terms of a single wave component with time varying amplitude and frequency
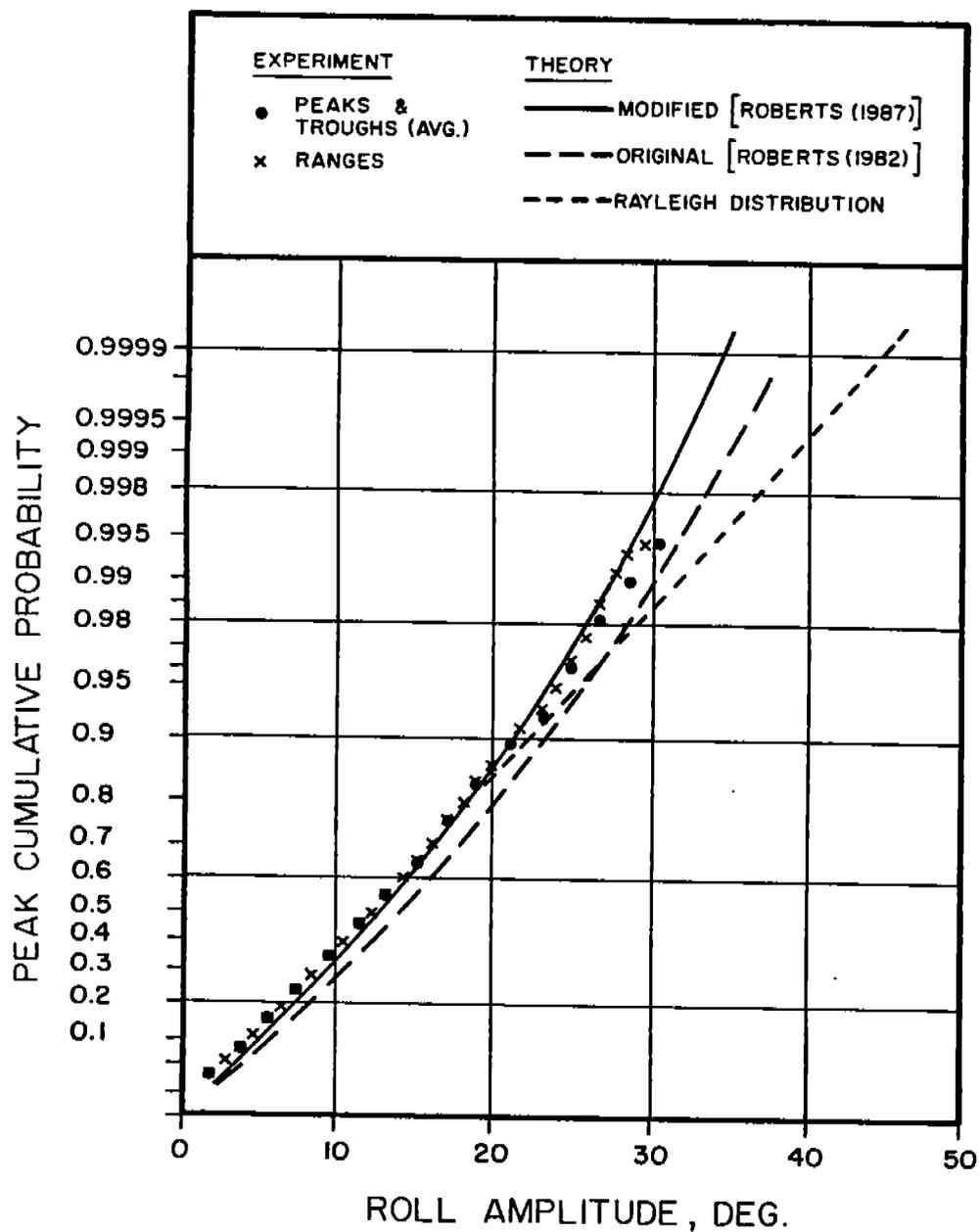
FIGURE 3.45   CUMULATIVE PROBABILITY DISTRIBUTION OF ROLL PEAK AMPLITUDES
[ROBERTS (1987)]

$$\eta(t) = a(t) \cos [\bar{\omega}t + \theta(t)] \tag{3.330}$$

where

$$a(t) = (A^2 + B^2)^{1/2} \tag{3.331}$$

$$\theta(t) = \tan^{-1} (B/A) \tag{3.332}$$

$$A = \sum_{n=1}^{N} \{a_n \cos (\omega_n - \bar{\omega})t + b_n \sin(\omega_n - \bar{\omega})t\} \tag{3.333}$$

$$B = \sum_{n=1}^{N} \{a_n \sin(\omega_n - \bar{\omega})t + b_n \cos(\omega_n - \bar{\omega})t\} \tag{3.334}$$

and $\bar{\omega}$ is a central frequency, e.g., the mean frequency of the spectrum. The time varying amplitude, $a(t)$ is known as the envelope of $\eta(t)$. The time varying frequency is given as $\bar{\omega} + \dot{\theta}$ where dot represents derivation and $\dot{\theta}$ is variation about the mean frequency. With this definition, then, the second order force due to a random sea may be approximately written as

$$F_2(t) = C(\bar{\omega} + \dot{\theta}) [a(t)]^2 \tag{3.335}$$

The joint probability density function, $p(a, \dot{\theta})$ may be written as

$$p(a,\dot{\theta}) = \frac{a^2}{\sqrt{2\pi} \, \sigma_\eta^2 \, \sigma_u} \exp \left\{ -\frac{1}{2} \left[a^2 \left(\frac{1}{\sigma_\eta^2} + \frac{\dot{\theta}^2}{\sigma_u^2} \right) \right] \right\} \tag{3.336}$$

where σ_η is the rms surface elevation and $\sigma_u = q \, \sigma_{\dot{\eta}}$; $\sigma_{\dot{\eta}}$ is the rms surface velocity and q is a measure of the spectral width given in terms of the moments of the spectrum

$$q^2 = 1 - \frac{m_1^2}{m_0 m_2} \tag{3.337}$$

Thus, $q \to 0$ represents a narrow banded spectrum.

The joint density function, $p(F_2, \dot{\theta})$ may be obtained by transforming from $(a, \dot{\theta})$ to $(F_2, \dot{\theta})$

$$p(F_2, \dot{\theta}) = \frac{\sqrt{F_2}}{\sqrt{8\pi} \, \sigma_\eta^2 \, \sigma_u \, [C(\bar{\omega} + \dot{\theta})]^{3/2}} \exp \left\{ -\frac{1}{2} \left[\frac{F_2}{C(\bar{\omega} + \dot{\theta})} \left(\frac{1}{\sigma_\eta^2} + \frac{\dot{\theta}^2}{\sigma_u^2} \right) \right] \right\} \tag{3.338}$$

The density function of the second-order force F_2 can be found by integrating $p(F_2, \dot{\theta})$ over $\dot{\theta}$. Nondimensionalizing F_2 and $\dot{\theta}$ as

$$\bar{F}_2 = \frac{F_2}{\sigma_n^2}, \qquad \bar{\dot{\theta}} = \frac{\dot{\theta}}{q\bar{\omega}} \qquad (3.339)$$

where $\bar{\omega}$ is chosen such that $\bar{\omega} = \omega_1' = \frac{\sigma_{\dot{n}}}{\sigma_n}$

$$p(\bar{F}_2) = \sqrt{\frac{\bar{F}_2}{8\pi}} \int_{-\infty}^{\infty} [C_1(\bar{\dot{\theta}})]^{-3/2} \exp \left\{ -\frac{1}{2} \left[\frac{\bar{F}_2}{C_1(\bar{\dot{\theta}})} (1 + \bar{\dot{\theta}}^2) \right] \right\} d\bar{\dot{\theta}} \qquad (3.340)$$

where

$$C_1(\bar{\dot{\theta}}) = C(\omega_1' + q\omega_1'\bar{\dot{\theta}}) \qquad (3.341)$$

In the limiting case of $q = 0$, the expression may be integrated analytically

$$p(\bar{F}_2) = \frac{1}{2C(\omega_1')} \exp \left\{ -\frac{1}{2} \left[\frac{\bar{F}_2}{C(\omega_1')} \right] \right\} \qquad (3.342)$$

which is the exponential distribution.

The probability density function of $\dot{\theta}$ is given by integration over the envelope, and

$$p(\dot{\theta}) = \frac{1}{2\sigma_n^2 \sigma_u} \left(\frac{1}{\sigma_n^2} + \frac{\dot{\theta}^2}{\sigma_u^2} \right)^{-3/2} \qquad (3.343)$$

Letting $r = \frac{\dot{\theta}}{\omega_1'}$, the probability density function of the modulus of r is obtained as

$$P(|r|) = 2 \int_0^{|r|} p(r)dr = |r| [r^2 + q^2]^{-1/2} \qquad (3.344)$$

For $q = 0.3$ (a typical North Sea wave spectrum bandwidth), $\dot{\theta}$ will exceed $0.4\omega_1'$ 20% of the time for which the exponential form for narrow band spectrum will be inaccurate.

131

The probability density function of $\overline{F}_2$ is shown for $\omega_1' = 0.38$ and $q = 0$ to 0.5 in Fig. 3.46. This illustration shows that even for a slightly wide band spectrum, the second order slow drift force may not follow exponential distribution. Note that the distribution described here refers to the marginal probability density function of the process (force time history) which does not say anything about the distribution of the force maxima.

3.3.2.11 Statistics of Low Frequency Motion

Pinkster and Wichers (1987) examined the statistical properties of the slow-drift motions of floating moored structures through time-domain simulation as well as from model tests. They derived the expression of optimum duration of simulation so that the convergence in the statistical properties is achieved. They assumed a band width limited white noise spectrum for the drift force with an exponential distribution. Then the surge drift motions become normally distributed about its mean value.

It was shown using experimental data that as long as linear mooring systems are used, the assumption of normal distribution of the surge motion is quite valid. The troughs and peaks likewise follow Rayleigh distribution. On the other hand, for a nonlinearly moored system, the deviation of the surge motion distribution from the normal distribution is significant (Fig. 3.47). Likewise, the amplitudes of motion do not follow Rayleigh.

It was also found that the duration has a significant effect on the statistical properties of the slow drift motion. Longer duration reduced statistical variance. Typical length of 18-20 cycles of surge period oscillation may not be enough to achieve stability. About 5 times this duration (i.e., 90-100 cycles) are needed for a small variance in the statistical results.

It is clear from Eqs. 2.89 and 2.84 for forces and motions, that they may be written in a general matrix form as

$$x(t) = u^T H u^*$$ (3.345)

where H is the matrix given by the tensor notations $\overline{H}_{mn}$ or G_{mn}^j , u is the vector given by $\hat{u}_m$ e$^{T\omega_m t}$ and u* is its conjugate. The matrix, H, is complex Hermitian,
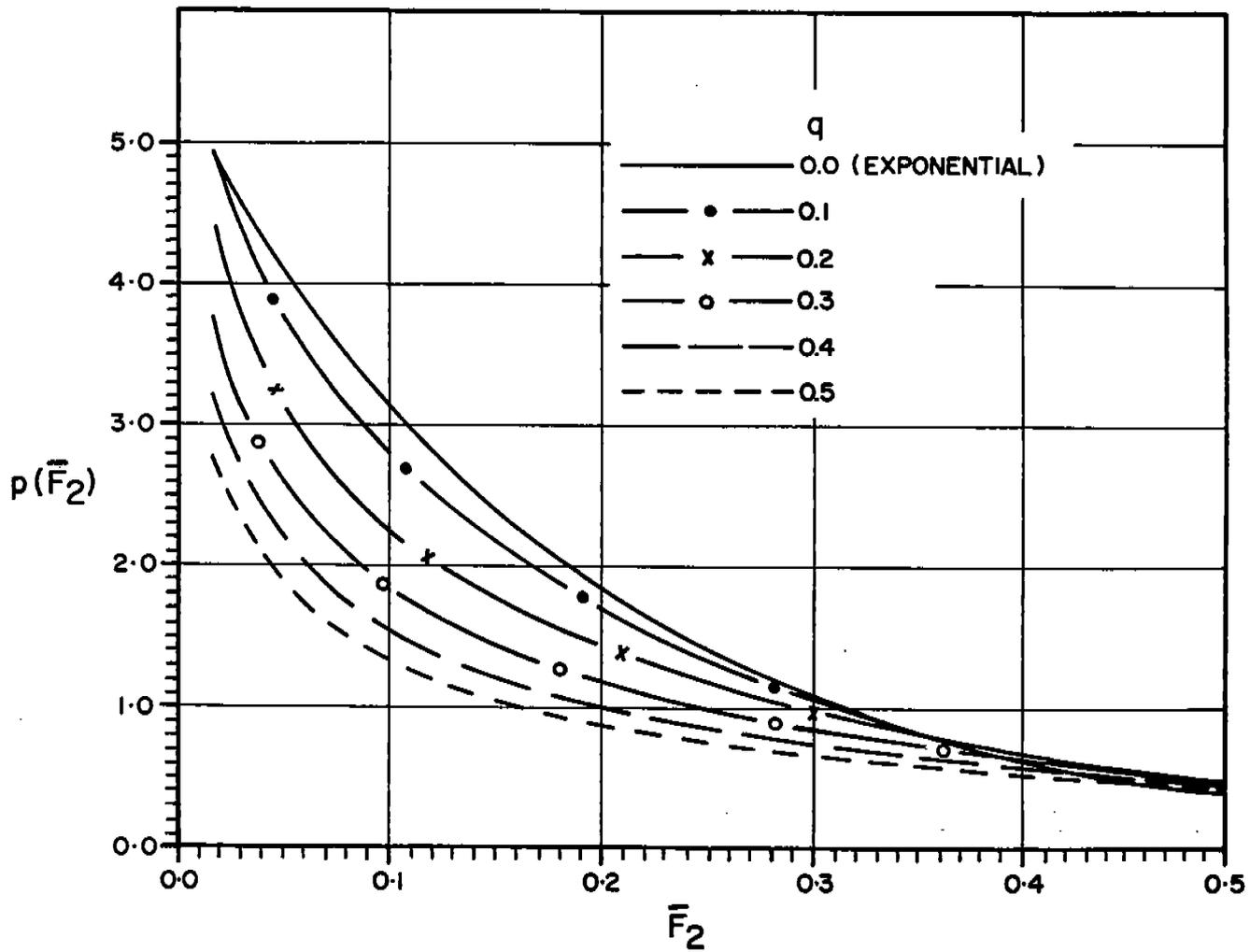
FIGURE 3.46 PROBABILITY DENSITY FUNCTION OF THE NON-DIMENSIONAL SECOND ORDER FORCE $(\overline{F}_2$) FOR $\omega_1' = 0.38$ [LANGLEY (1984)]
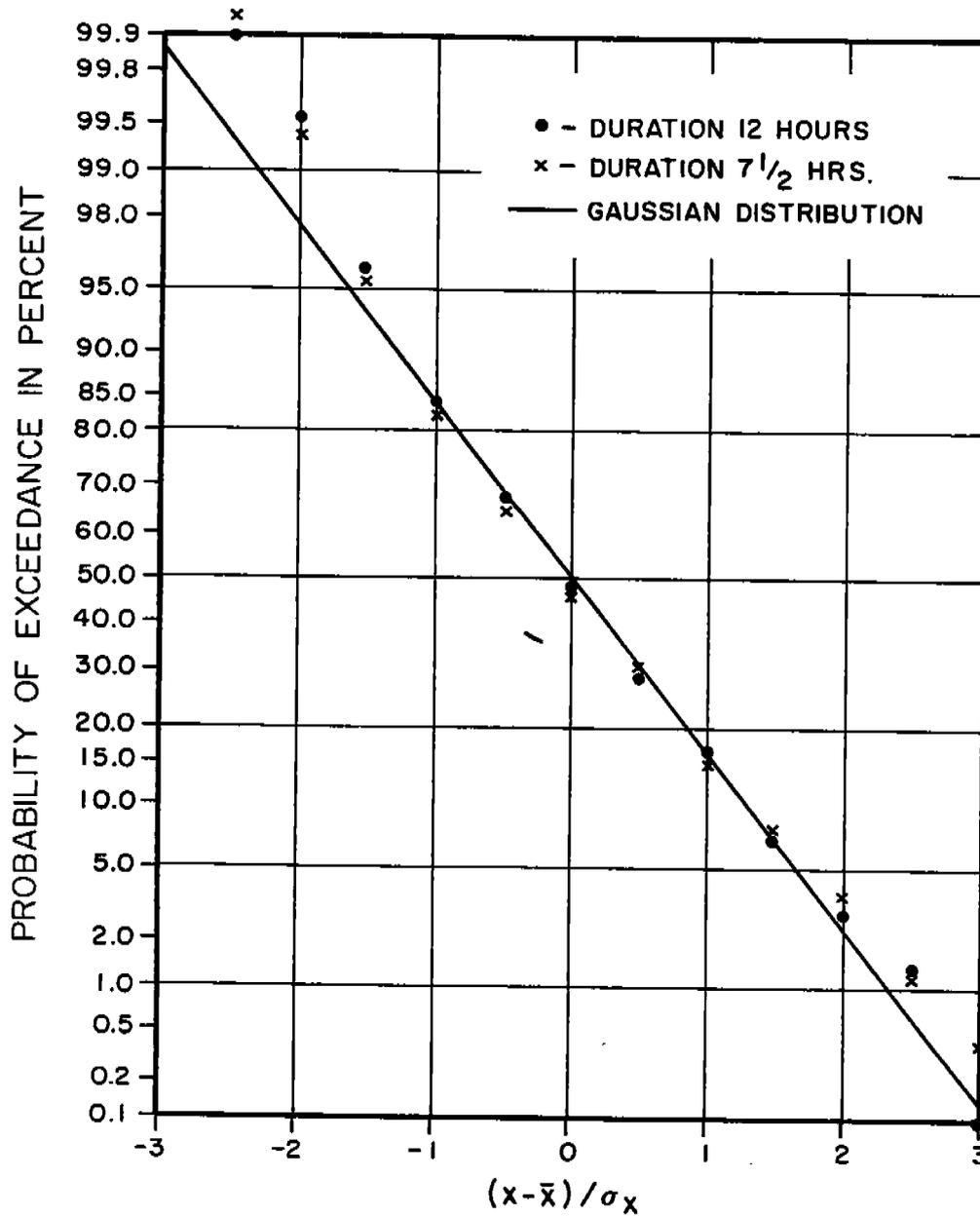
FIGURE 3.47 PROBABILITY DISTRIBUTION OF LOW-FREQUENCY SURGE MOTION [PINKSTER AND WICHERS (1987)]

$$H^* = H^T \qquad (3.346)$$

so that a diagonal matrix Λ may be obtained where

$$H = R^T \Lambda R^* \qquad (3.347)$$

The properites of R and Λ are as follows:
(1) Λ contains the eigenvalues of H which are real.
(2) The rows of R* contain the eigen vectors of H.
(3) $R^T R^* = I$
(4) The eigenvalues λ_j, and eigen vectors, v_j, satisfy the relationship

$$v_j^T H = \lambda_j v_j^T \qquad (3.348)$$

Substituting these relationships in Eq. 3.345, the second-order quantity, x(t), becomes

$$x(t) = \sum_{j=1}^{N} \lambda_j \mid X_j \mid^2 \qquad (3.349)$$

where the vector X has the form

$$X = Ru \qquad (3.350)$$

Since u is a complex Gaussian random variable and X is a linear combination of the components of u, X is also a complex Gaussian random variable at a given time and from Eq. 2.76.

$$E[\mid X_j \mid^2] = 1; \quad E[X_i \, X_j] = 0; \quad E[X_i \, X_j^*] = 0, \quad i \neq j \qquad (3.351)$$

Then, writing

$$z_j = \lambda_j \mid X_j \mid^2 \qquad (3.352)$$

the second-order quantity x(t) is a sum of independent random variables, z_j.

The following is according to Naess (1986) and Langley (1987). The real and imaginary parts of X_j are independent Gaussian random variables each having a mean squared value of 1/2 (Eq. 3.35). Under these conditions, it can be shown that $|X_j|$ has a Rayleigh distribution [see Stansberg (1983)]. Similarly, $|X_j|^2$ has an exponential distribution with a mean value of unity. Then the probability density function is given by

$$p(z_j) = \frac{1}{|\lambda_j|} e^{-z_j/\lambda_j} \qquad (3.353)$$

This equation is valid for positive z_j if $\lambda_j > 0$ and negative z_j if $\lambda_j < 0$. The characteristic function, $M_j(\theta)$ of z_j is defined as the expected value of $e^{i\theta z_j}$

$$M_j(\theta) = E\,[e^{i\theta z_j}] = \int_{-\infty}^{\infty} e^{i\theta z_j}\,p(z_j)\,dz_j = (1 - i\lambda_j\theta)^{-1} \qquad (3.354)$$

From this and the relationship in Eq. 3.352, the characteristic function of x is given by

$$M(\theta) = E\,[e^{i\theta x}] = \prod_j (1 - i\lambda_j\theta)^{-1} \qquad (3.355)$$

The probability density function of x, p(x) is a Fourier transform of $M(\theta)$,

$$p(x) = \frac{1}{2\pi} \int_{-\infty}^{\infty} e^{-i\theta x} M(\theta)\,d\theta \qquad (3.356)$$

Substituting the value of $M(\theta)$, the integral is evaluated by contour integration [Naess (1986)]

$$p(x) = \begin{cases} \displaystyle\sum_{j=1}^{M} \frac{\mu_j}{\lambda_j}\, e^{-x/\lambda_j} & x \geqslant 0 \\[2em] \displaystyle\sum_{j=M+1}^{N} \frac{\mu_j}{|\lambda_j|}\, e^{-x/\lambda_j} & x < 0 \end{cases} \qquad (3.357)$$

where the eigenvalues have been ordered such that λ_j, j = 1,2,.....M are positive and λ_j, j = M + 1, ...,N are negative. The quantities μ_j are given by

$$\mu_j = \prod_{\substack{k = 1 \\ k \neq j}}^{N} \left(1 - \frac{\lambda_k}{\lambda_j}\right)^{-1}$$

(3.358)

Langley (1987) has shown through numerical computation that the value of N, the number of frequency components, should be in the neighborhood of 200. Vinje (1983) and Naess (1986) used N = 8 in their computation with a slightly different approach through matrix inversion which is too small for convergence of results.

In Langley's (1987) method of pdf for second-order forces and motions, the cumulants may be evaluated from the eigenvalues, λ_j, as

$$k_n = (n - 1)! \sum_j \lambda_j^n$$

(3.359)

Langley considered an example of a half-submerged circular horizontal cylinder of 10m radius in long-crested beam seas. Only the sway motion of the cylinder was considered. The incident wave field was given by an ISSC spectrum. Fig. 3.48 shows the probability density function of the force. The force is highly non-Gaussian having a skewness of 1.96 and a kurtosis value of 5.87. The pdf of the sway motion for a damping factor of 0.005 is shown in Fig. 3.49. It compares quite well with the corresponding Gaussian distribution having the same mean and variance. However, it should be cautioned that at the tail of the pdf, the agreement is poor so that the extreme value prediction is expected to be quite different with an assumed Gaussian distribution.

The total second-order response includes a linear and a second-order term. Naess (1986) derived expressions for pdf of the pure quadratic response term. On the other hand, Vinje (1976) derived the pdf of a weakly nonlinear response from Taylor expansions of cumulants. Kato et al. (1987) obtained a total second-order response probability based on the approximate theory of continuous distribution. The total second-order response process of a moored floating structure was obtained in a closed form by the difference of two random variables which yield the Gamma distribution. In this case, the pdf of the second-order response, x, was obtained as
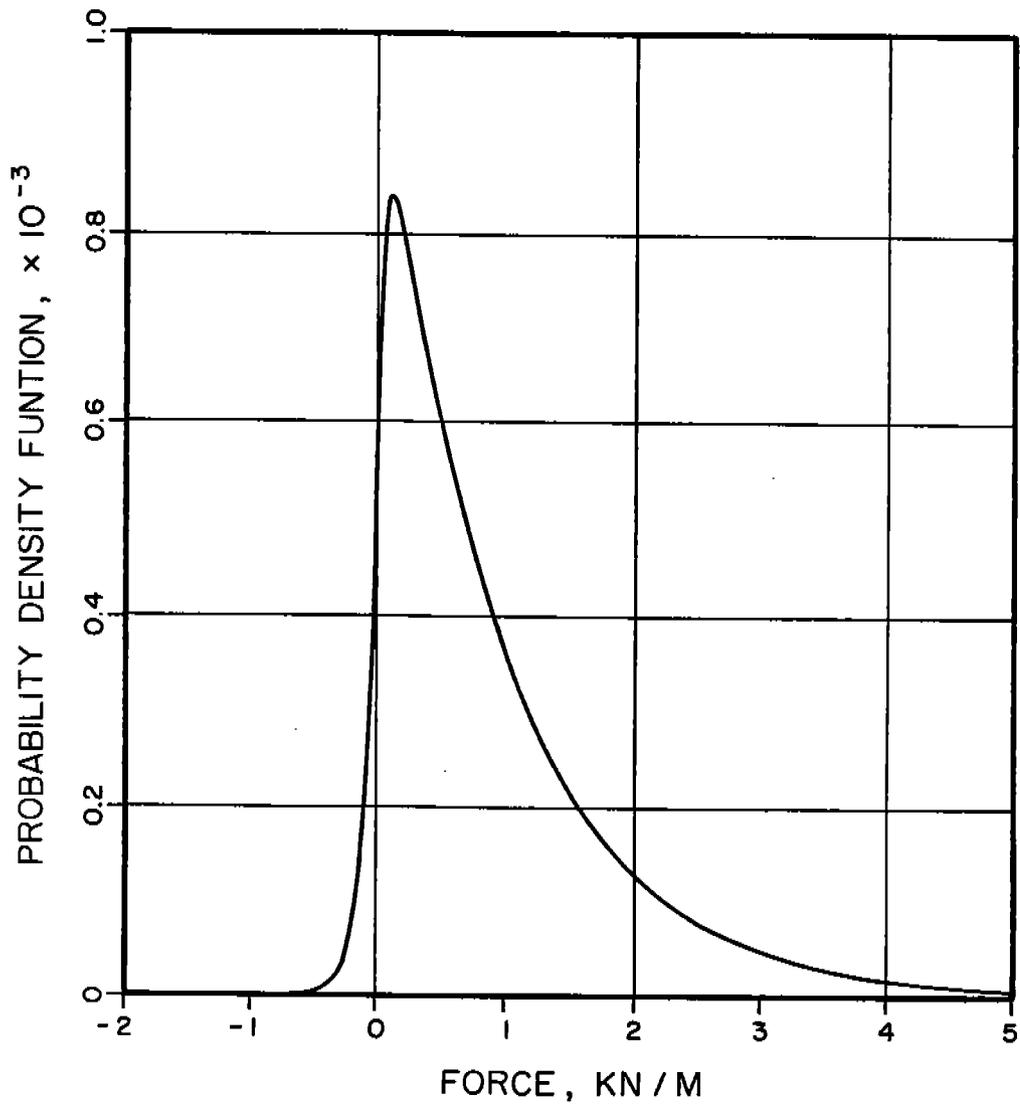
FIGURE 3.48   PROBABILITY DENSITY FUNCTION OF SECOND-ORDER FORCE [LANGLEY (1987)]
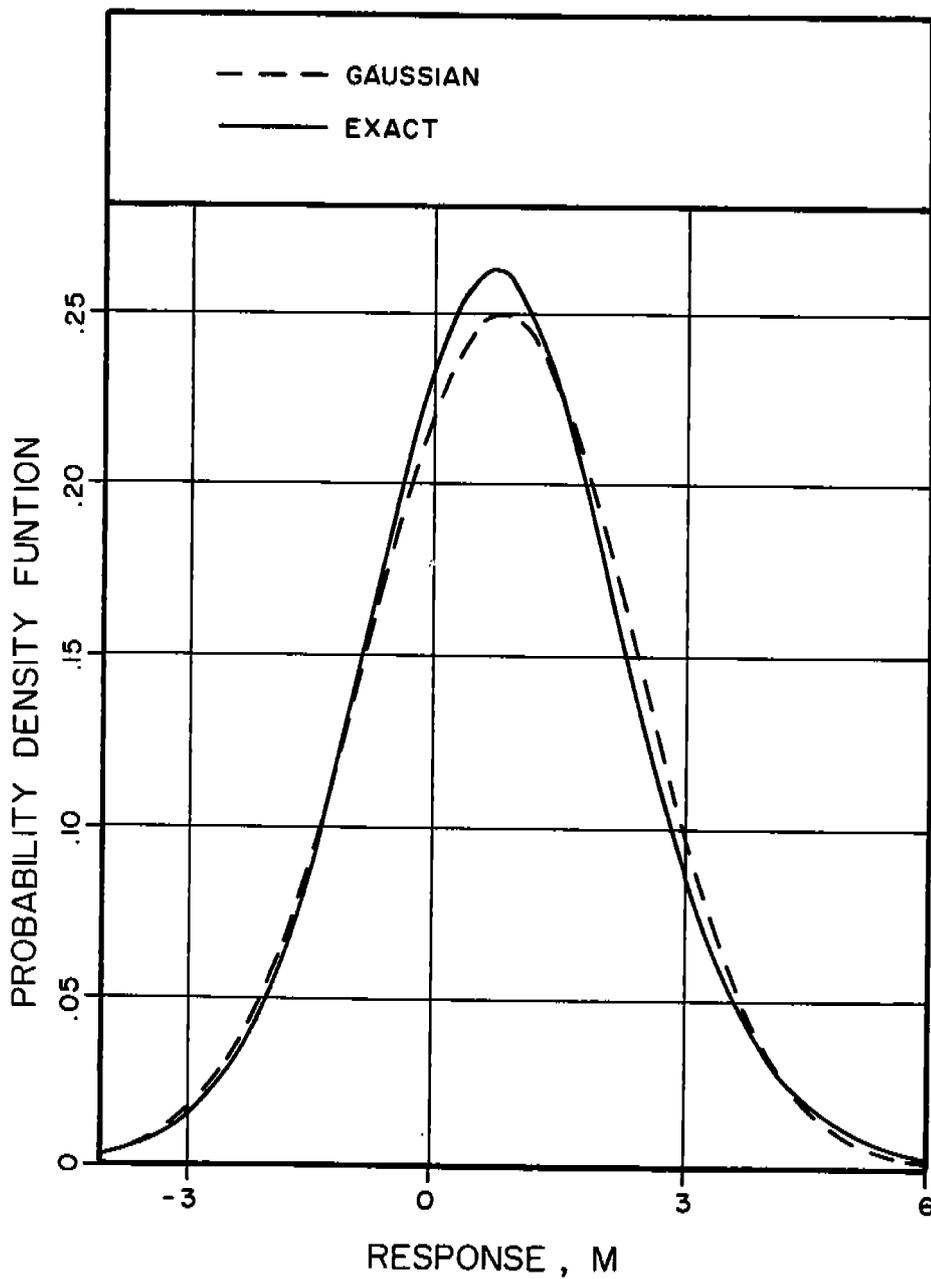
FIGURE 3.49   PROBABILITY DENSITY FUNCTION OF SECOND-ORDER RESPONSE FOR β = 0.05 [LANGLEY (1987)]

$$p(x) = C \sum_{r=0}^{m_1-1} \frac{\Gamma(m_1) \, \Gamma(m_1 + r)}{\Gamma(m_1 - r) \, \Gamma(r + 1)} \, x^{m_1-r-1} \left(\frac{1}{a}\right)^{m_2 + r} e^{-x/2\tilde{\theta}_1}$$

$$\text{for } x > 0 \qquad (3.360)$$

and

$$p(x) = C \sum_{r=0}^{m_2-1} \frac{\Gamma(m_2) \, \Gamma(m_2 + r)}{\Gamma(m_2 - r) \, \Gamma(r + 1)} \, (-x)^{m_2-r-1} \left(\frac{1}{a}\right)^{m_1 + r} e^{x/2\tilde{\theta}_2}$$

$$\text{for } x < 0 \qquad (3.361)$$

where

$$a = \frac{\tilde{\theta}_1 + \tilde{\theta}_2}{2\tilde{\theta}_1 \tilde{\theta}_2} \quad , \quad m_i = \frac{\tilde{\nu}_i}{2} \; (i = 1,2) \; , \qquad (3.362)$$

and

$$C = \frac{1}{(2\tilde{\theta}_1)^{m_1} (2\tilde{\theta}_2)^{m_2} \, \Gamma(m_1) \, \Gamma(m_2)} \qquad (3.363)$$

The parameters, $\tilde{\theta}_i$, and degrees of freedom, $\tilde{\nu}_i$, are given by

$$\tilde{\theta}_i = \left(\sum \lambda_{ij}^2 + \sum c_j^2 / 4 \right) \sum | \lambda_{ij} | \qquad (3.364)$$

$$\tilde{\nu}_i = \frac{(\sum \lambda_{ij})^2}{(\sum \lambda_{ij}^2 + c_j^2 / 4)} \; , \; i = 1,2; \; j = 1,2,\ldots. \qquad (3.365)$$

and Γ is a Gamma function, λ_j ($j = 1,2,\ldots,n$) are the eigenvalues while λ_{1j} ($j = 1,2,\ldots n_1$) and λ_{2j} ($j = 1,2,\ldots,n_2$) are the positive and negative eigenvalues ($n = n_1 + n_2$), c_j are the coefficients of linear Gaussian random variables. The summation in Eqs. 3.364 and 3.365 is on j.

From the statistical properties of the Gamma distribution, the first- and second-order cumulants are given by

$$K_1 \equiv \sum_j \lambda_j = 2m_1 \tilde{\theta}_1 - 2m_2 \tilde{\theta}_2 \qquad (3.366)$$

$$K_2 = 2 \Sigma \lambda_j^2 + \Sigma c_j^2 = 4m_1 \tilde{\theta}_1^2 + 4m_2 \tilde{\theta}_2^2 \qquad (3.367)$$

where K_1 is the mean value $E(x)$ and K_2, the variance $V(x)$ of the second-order response.

The pdf of the slowly varying sway motion of a moored floating rectangular cylinder obtained from the above formulation is given in Fig. 3.50. The Gaussian distribution as well as the pdf from Naess formulation is also shown. The latter matches well with Kato, et al. (1987).

Fig. 3.51 compares the probability distribution of a pure second-order response with that of the total response including the first-order term. The asymmetry of the total second-order response is higher.

3.4 SHORT-TERM RESPONSE MEASUREMENTS

Many offshore structural models have been tested in the CBI wave tank. These tests involved both fixed and floating structures and included random waves generated in the tank.

Waves are generated in the test tank using a pneumatic type wave maker. The wave maker consists of a low pressure blower connected to a large open bottom plenum chamber that is partially submerged in the tank. A flapper valve between the plenum and the blower controls the pressure in the plenum chamber. By changing the position of the flapper, the inlet or the outlet of the blower can be connected alternately to the plenum, causing the water level in the chamber to alternately rise and fall. The cyclic motion of the water in the plenum chamber generates the waves in the tank.

The position of the flapper valve is controlled by a hydraulic servo system. The system accepts both a flapper position feedback signal from a transducer at the flapper and a reference signal, and operates a hydraulic cylinder to cause the flapper position to match the reference. The amplitude and frequency of the generated waves are directly related to the amplitude and frequency of the reference signal.

The method of random wave generation is similar to that described in section 2.2. Random waves are created through the summation of a large number, e.g. 200, of sinewave components of various amplitudes and random

137
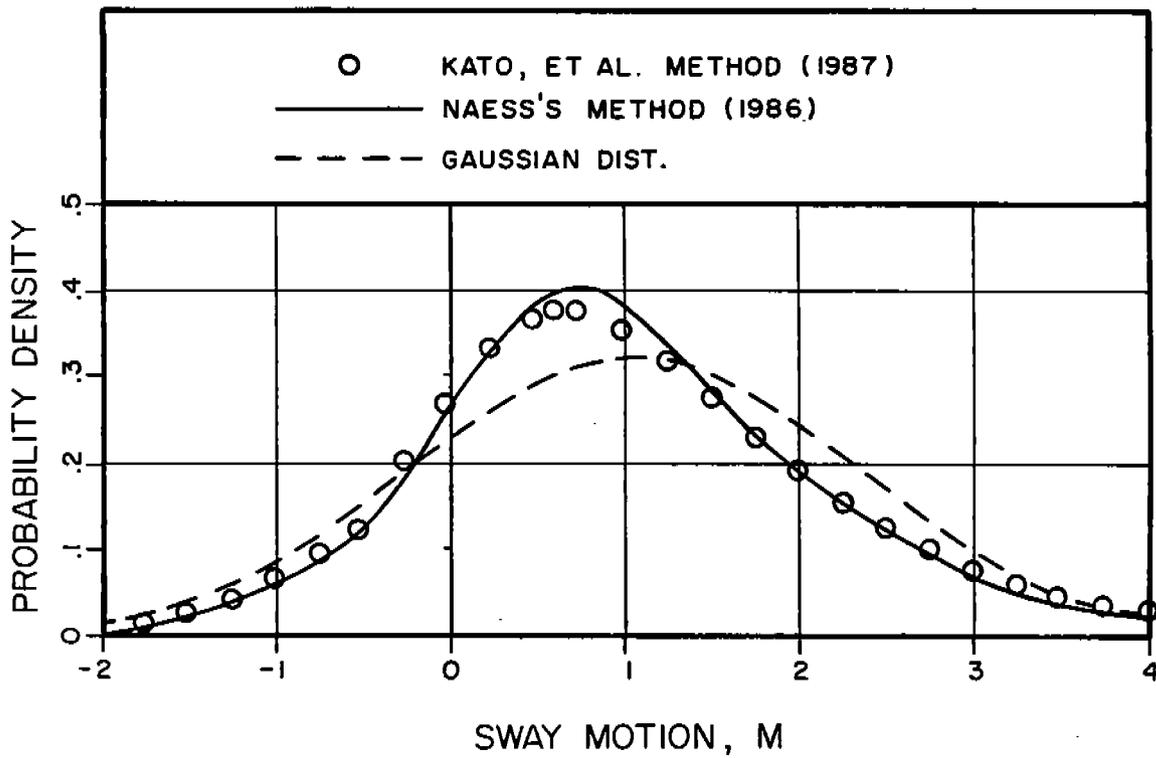
FIGURE 3.50   COMPARISONS OF THE PROBABILITY DENSITY OF SLOWLY VARYING SWAY
MOTION OF A MOORED RECTANGULAR CYLINDER [KATO, ET AL. (1987)]
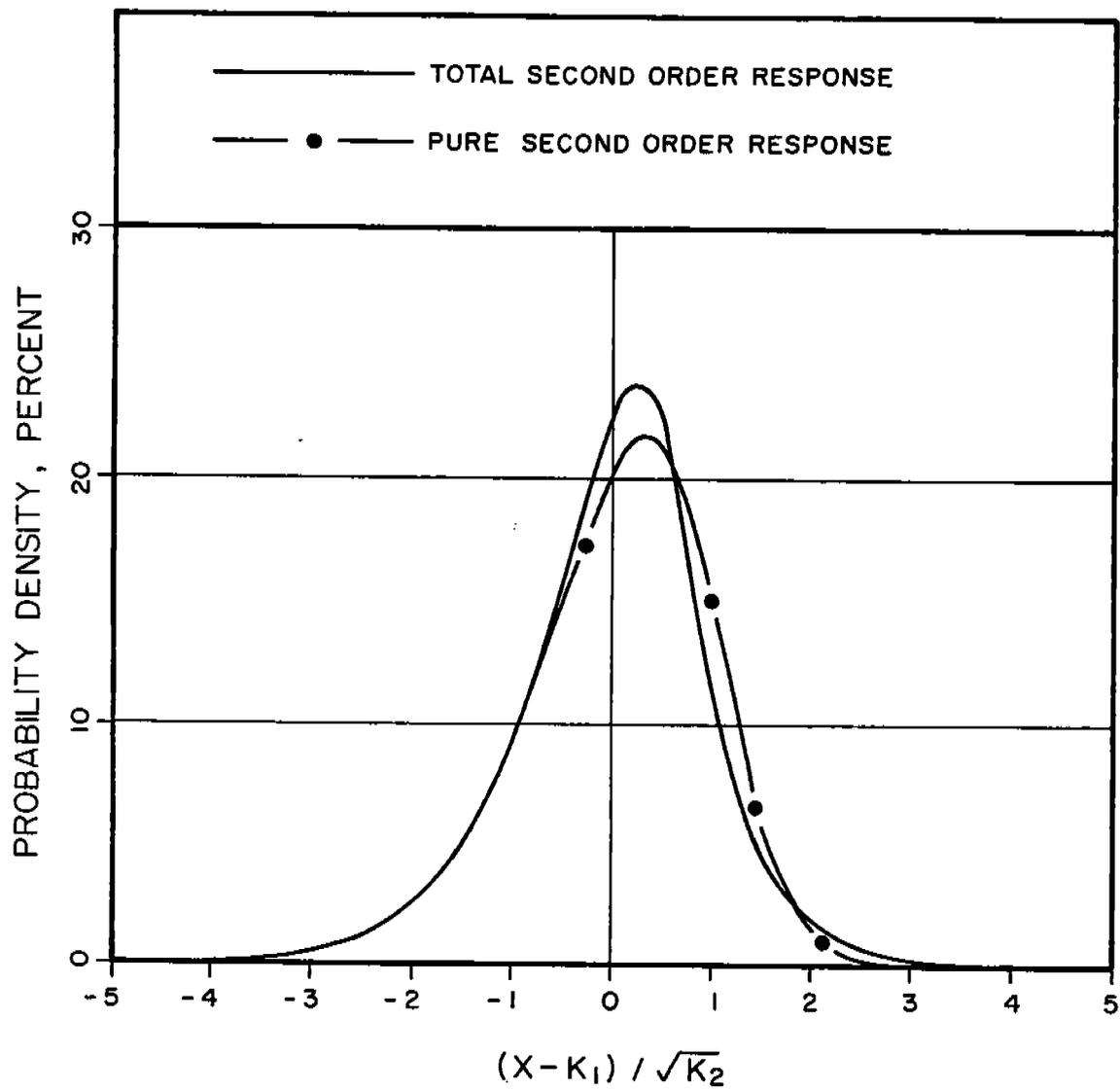
FIGURE 3.51   COMPARISON OF THE PROBABILITY DENSITY OF A PURE SECOND-ORDER
RESPONSE WITH A COMBINED FIRST- AND SECOND-ORDER RESPONSE
[KATO, ET AL. (1987)]

phases. By tailoring the amplitudes of the frequency components, a desired ocean wave spectrum can be modeled. The wave reference signal is initially calculated and stored as a digital time series. To generate the analog reference required by the servocontroller, the stored time trace is output one point at a time through a digital to analog converter under the control of a dedicated microcomputer. By generating waves from a stored time series, identical waves can be repeated for any number of tests.

The results on the responses of structures tested in the tank in random waves are presented in this section. The structures that are considered for this presentation are fixed vertical and inclined cylinders, articulated towers, barges, tankers and semisubmersibles. For the fixed structures, the wave loads were measured whereas for the moving structures, the loads and motions were recorded. The short-term distribution of these quantities are presented and compared with theoretical distribution function. Where appropriate, discussions have been presented in correlating the measured distribution with the theoretical techniques presented in the earlier sections.

3.4.1 Random Wave Load Tests

A series of tests were conducted with circular cylinders of various diameters fixed in waves. A small section of the cylinders was instrumented to measure two component local forces. The cylinder was orientated to measure the inline and transverse or lift forces on them. The instrumented sections were placed under water so that they were never exposed in air during the passing of waves. The orientations of the cylinders were changed from the vertical to inclined in a few test setups. In some cases, currents were generated along with the random waves. This section provides results of the waves generated, kinematics measured at the instrumented sections and forces on these sections.

3.4.1.1 Vertical Cylinder

In a test series in the CBI tank with a 3 inch diameter fixed vertical cylinder, forces due to random waves on two 1 ft. smooth sections of the cylinder were measured. Two random waves were chosen having broad band spectra with a bandwidth parameter, ε of about 0.70 but different frequency distribution. A plot of one of the wave spectrum is shown in Fig. 3.52. A

138

WAVE

$\omega_0 = 2.1$

$H_s = 9.8$ in.

ENERGY DENSITY IN² – SECOND

FREQUENCY-HZ
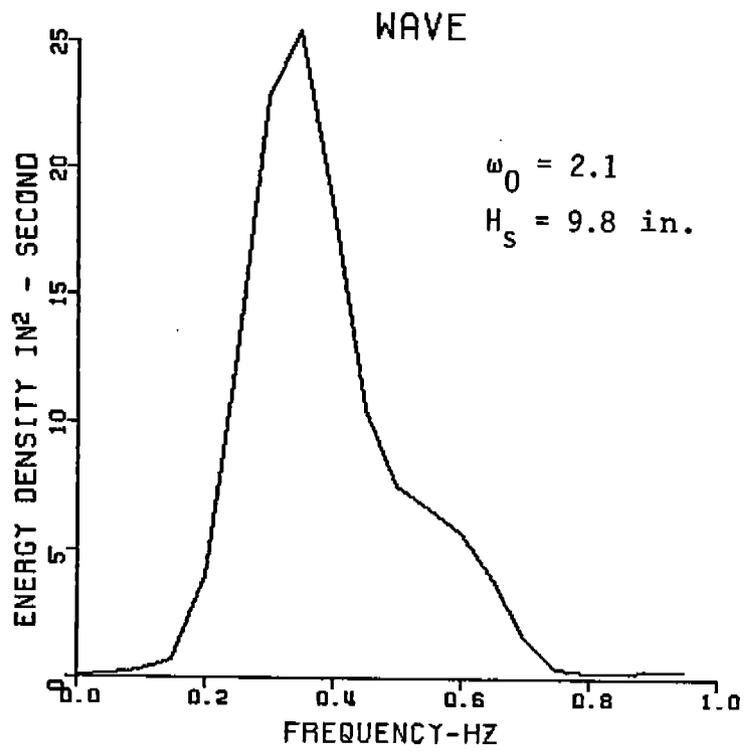
FIGURE 3.52   SAMPLE WAVE ENERGY DENSITY SPECTRUM
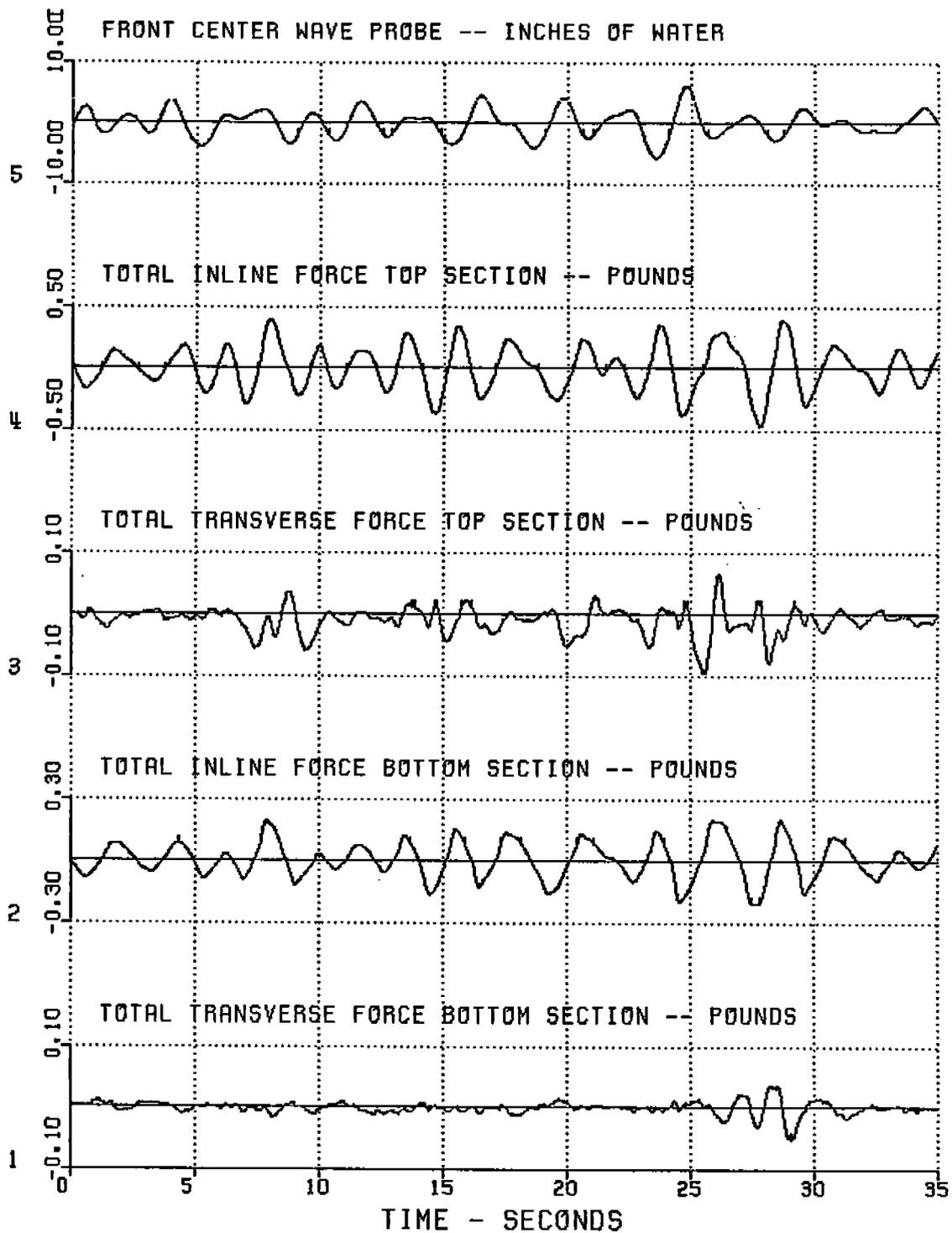
FIGURE 3.53 SAMPLE RANDOM WAVE AND FORCE PROFILES RECORDED ON TWO INSTRUMENTED VERTICAL CYLINDRICAL SECTIONS

small portion of the measured wave profile and in-line and transverse forces on the two instrumental sections is shown in Fig. 3.53.

Correlations are made of the measured in-line force spectra with the theoretically computed spectra. The hydrodynamic coefficients are considered constant over the frequency range of the wave spectrum and are chosen based on an equivalent KC number. In this regard it should be noted that it does not seem appropriate to assign values of C_M and C_D based on individual waves in the spectrum depending on a small frequency band. In fact, an attempt to derive the KC number on this basis by dividing the spectrum into several small frequency bands of equal width showed that the method is rather impractical and produced values that are not realistic. An equivalent KC number may be defined in several different ways. An equivalent KC number may be obtained, for example, based on the rms value of the water particle velocity and a mean zero-crossing period obtained from the moments of the wave spectrum. Calculation for one of the measured wave spectra showed that $\sigma_u = 0.388$ ft/sec. and $\overline{T}_z = 2.2$ sec. so that the equivalent KC number is computed as

$$KC_{eq} = \frac{\sigma_u \overline{T}_z}{D} = 3.4 \qquad (3.368)$$

From Fig. 2.6, this value of KC gives a mean $C_M = 2.2$ (± 0.35) and a mean $C_D = 0.8$ (± 0.5).

Correlation of force spectra is based on Borgman's (1972) method with the drag force spectra approximated by its linearized term. The values of C_M and C_D chosen for all measured force spectrum correlations are

$$C_M = 1.90$$
$$C_D = 0.10$$

These values correspond to a KC value near the equivalent KC number of 3.4, but are chosen strictly to give a good fit of the computed force spectra to the measured. While the chosen C_M and C_D values are within the range shown in Fig. 2.6 for $KC_{eq} = 3.4$, these values are low and fall near the lower limit of the variation at this KC value. The correlations of the force spectra are shown in Fig. 3.54 Note that the correlation is good in general. Thus, it has been possible to obtain good correlation with constant C_M and C_D values
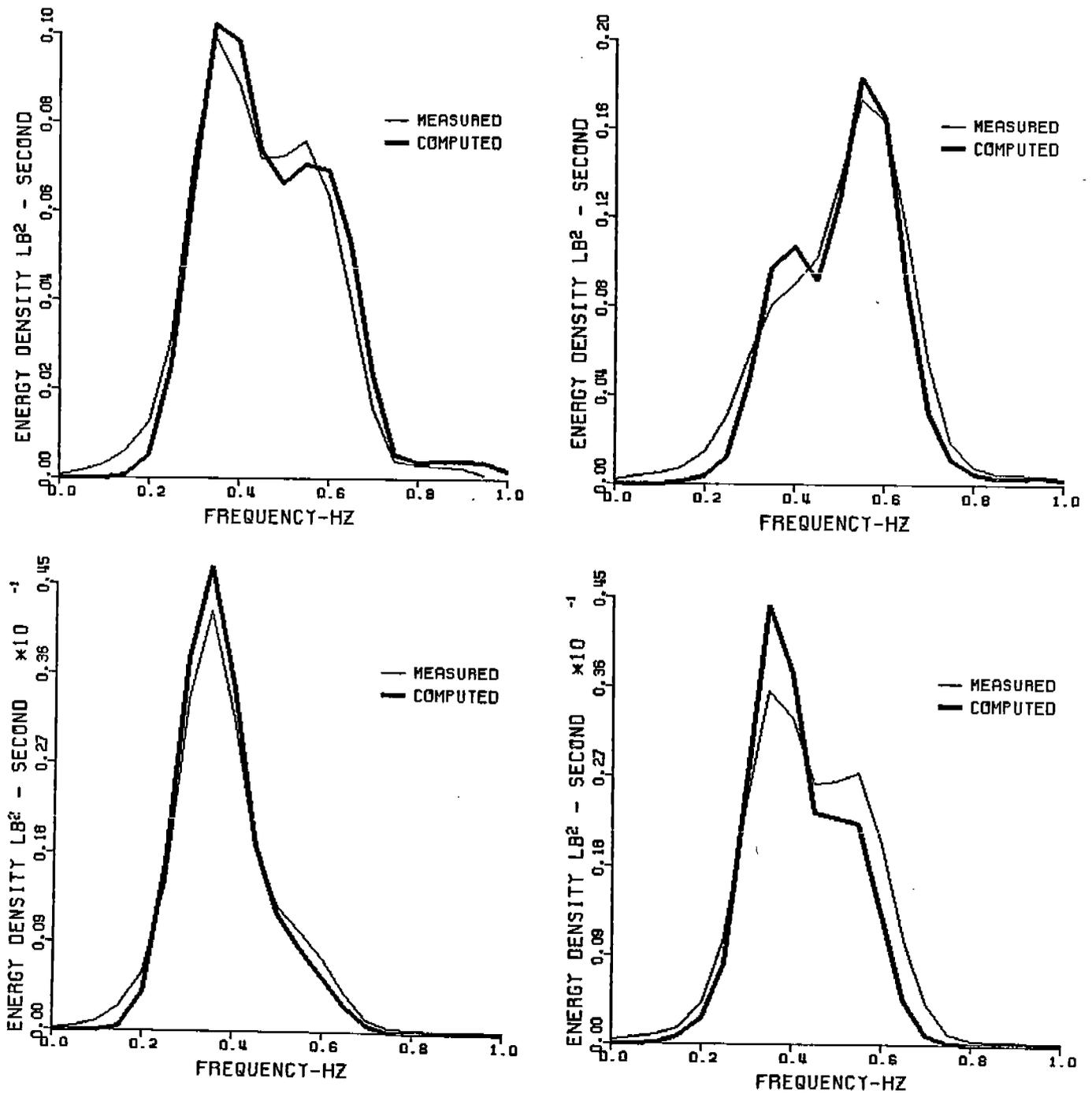
FIGURE 3.54   CORRELATION OF MEASURED IN-LINE FORCE SPECTRA WITH COMPUTED
FORCE SPECTRA USING C_M = 1.90 AND C_D = 0.10
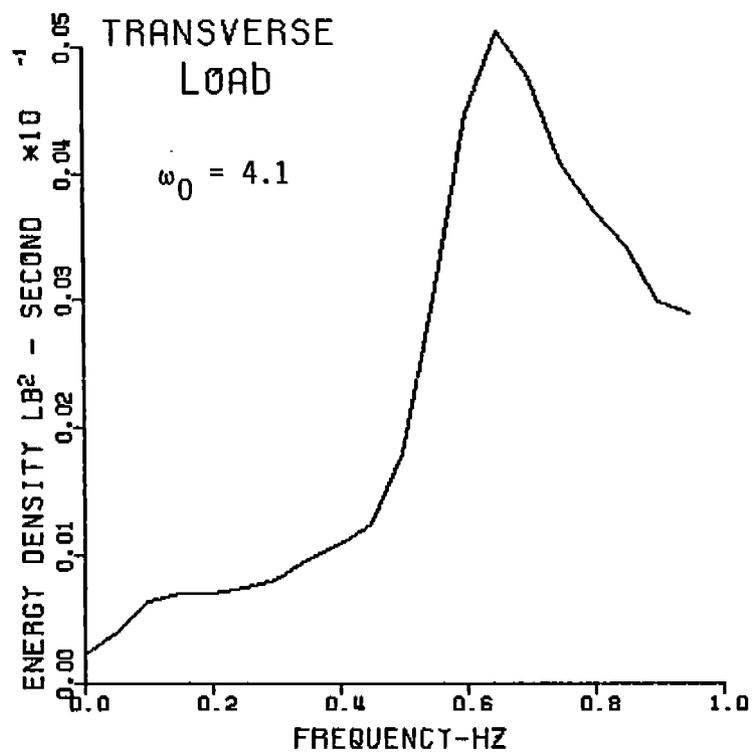
FIGURE 3.55   TRANSVERSE FORCE SPECTRUM ON AN INSTRUMENTED SECTION DUE TO THE
WAVE OF FIGURE 3.52

over the frequency range of the wave spectrum. Moreover, these values correspond to an equivalent KC number based on the rms velocity and mean period of the wave spectrum, albeit at their low end of the range, in these cases.

The transverse force on the cylinder due to these random waves has been generally small. A measured transverse force spectrum is given in Fig. 3.55. Note that the peak frequency of the spectrum (ω_0) is at about twice the frequency of the peak of the wave (or in-line force) spectrum. Thus, the transverse force, while irregular in nature, has frequencies that are generally twice the component frequencies of the random waves.

3.4.1.2 Inclined Cylinder

Similar tests were conducted with a 6 inch diameter inclined cylinder near an inclined plane boundary. The slope of the boundary was changed from 0^0 to 40^0 and 70^0 with respect to the horizontal. Similarly, the uniform gap between the cylinder and the boundary was varied from 0.25 inches to 2.5 inches and 4.5 inches. Several random waves were generated past the cylinder for each boundary gap and each slope. The random waves were modeled after the Bretschneider spectrum and were three minutes in duration.

A sample spectrum from the wave generated in the tank is shown in Fig. 3.56. A small portion of the corresponding measured wave profile, water particle velocity and in-line and normal forces on the instrumented section is shown in Fig. 3.57. The data are presented from the smallest cylinder-boundary gap of 0.25 ins. The velocity and load in the in-line (X) direction follow the wave profile reasonably well with one-to-one peaks. However, the normal load (in the Y direction) has twice as many peaks as the wave. The additional peaks are due to the second harmonic component in the force. Moreover, the downward force is much larger than the upward force. At the larger gaps, the normal force frequencies follow the wave frequencies and the asymmetry in the profile disappears. A sample calculation was made of the linearized drag force spectra. For the wave spectrum chosen, we obtain the rms velocity, $\sigma_u = 0.2$ ft/sec. and the mean zero-crossing period, $T_z = 2.0$ sec. Then, an equivalent KC number is computed as
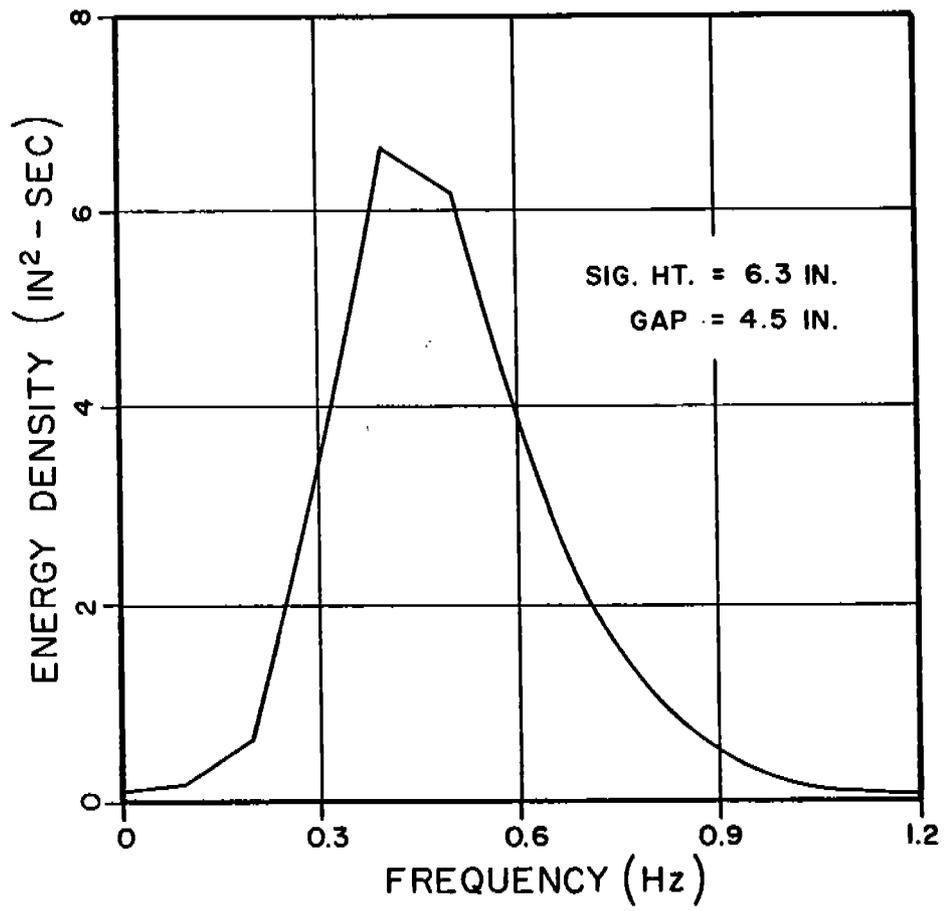
FIGURE 3.56   SAMPLE MEASURED WAVE SPECTRUM
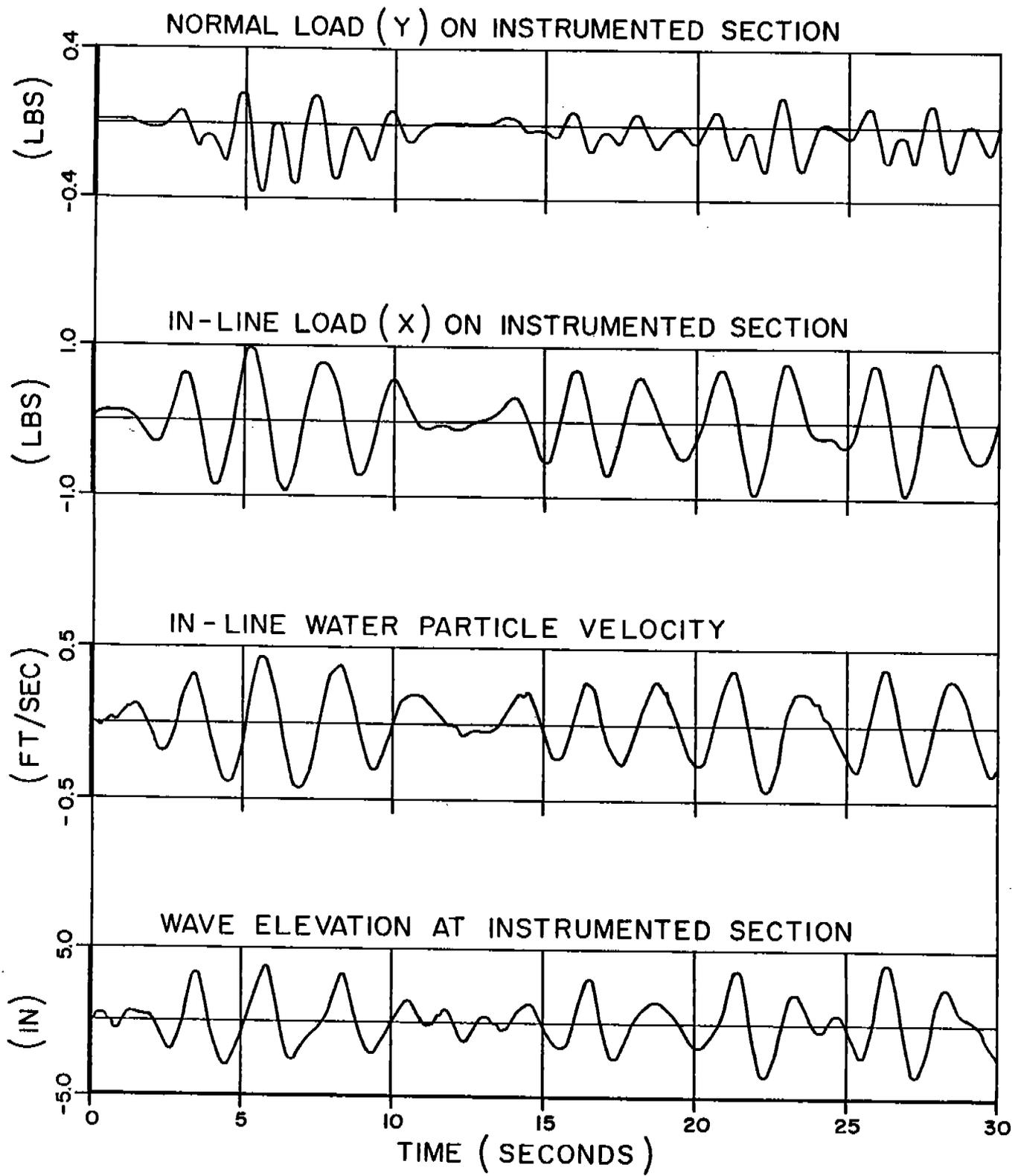
FIGURE 3.57   SAMPLE MEASURED DATA FROM RANDOM WAVES

$$KC_{eq} = \frac{\sigma_u \overline{T}_z}{D} = 0.8 \qquad (3.369)$$

For this KC value, the drag coefficient from Sarpkaya's (1981) data is $C_D \approx 1.0$. The drag force spectra computed with these values was on the order of 1% of the inertia force spectra. Since the drag force contribution is insignificant, for the subsequent calculations C_D is taken as zero. Therefore, the computation of the force spectrum is rather straightforward. The correlations for the in-line force spectra for all gaps and the three slopes of 0°, 40° and 70° are shown in Figs. 3.58 - 3.60, respectively. Note that the correlation is good in all cases.

The normal force on the cylinder due to random waves was generally small in all cases except for the smallest gap of 0.25 ins. This is evident from the measured normal force spectra given in Fig. 3.61 for gaps of 4.5 and 0.25 in. Note that there are two distinct peaks in the spectrum for the 0.25 in. gap; one at the peak frequency of the wave and in-line force and one at twice this frequency. There is a third peak at a low frequency corresponding to the set-down shown in Fig. 3.57. The correlation of the linear part is made using the above procedure. The spectra due to second harmonic is computed from the transfer function measured in regular waves [Chakrabarti and Libby (1987)] and the following relationship

$$S_F(2f) = 8S^2(f) \, [RAO(f)]^2 (\Delta f) \qquad (3.370)$$

where RAO = transfer function and Δf = frequency increment in the estimate of S(f). This formula is similar in form to that used in the drift force spectrum computation [Rye, et al. (1975)]. The shape of the two spectra in Fig. 3.61 is similar. However, the correlation may only be termed fair.

3.4.1.3 Force Distributions

It has been shown by several investigators earlier [Goda (1985)] that even for a relatively broad band wave spectrum ($\varepsilon < 0.7$) Rayleigh distribution provides a good approximation to the individual wave heights defined by the zero-upcrossing method. If the wave heights follow Rayleigh distribution and responses due to waves are linear with the wave heights then it is straight-forward to show that the response amplitudes also follow the Rayleigh
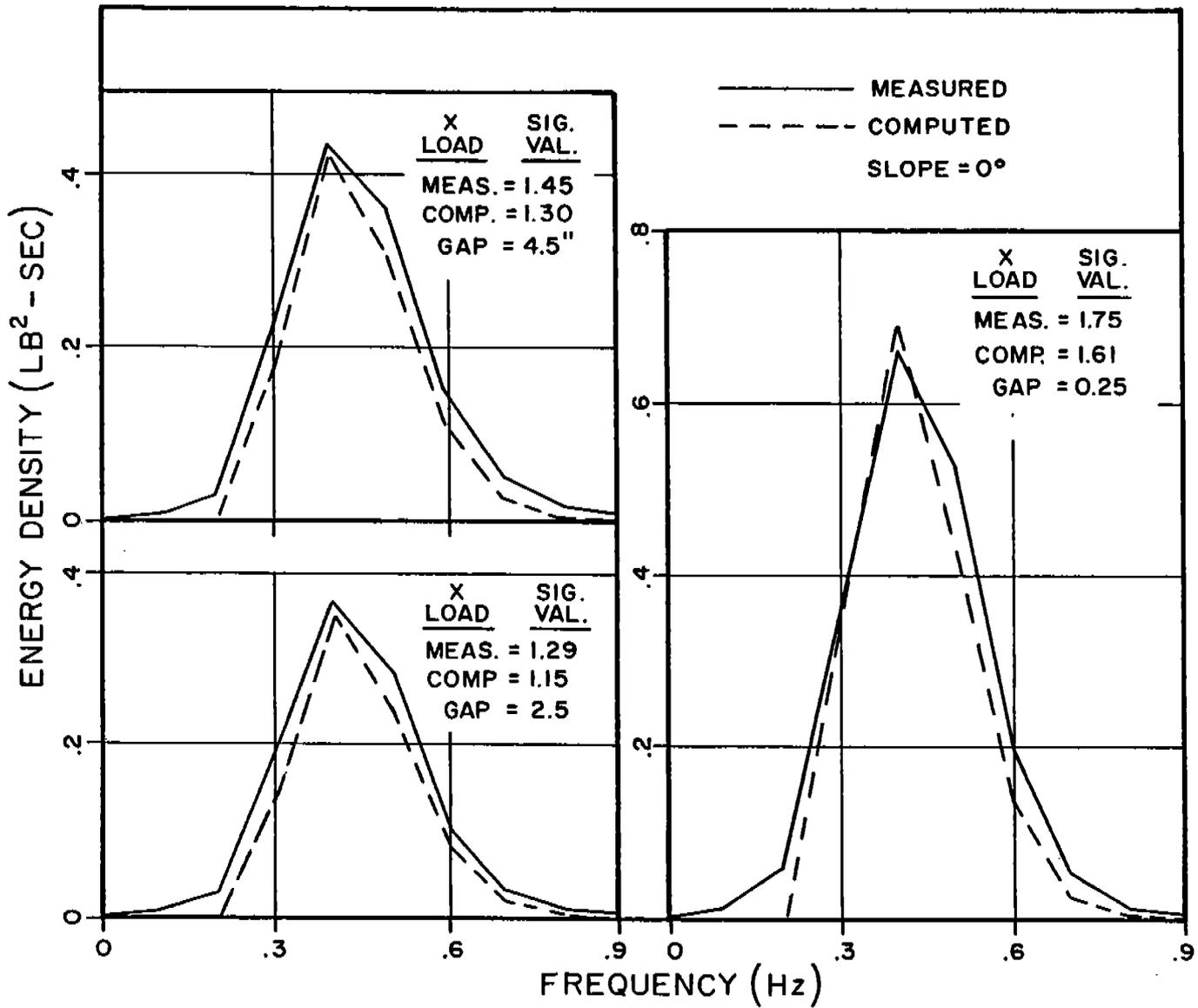
FIGURE 3.58   CORRELATION OF IN-LINE FORCE SPECTRA FOR 0° SLOPE
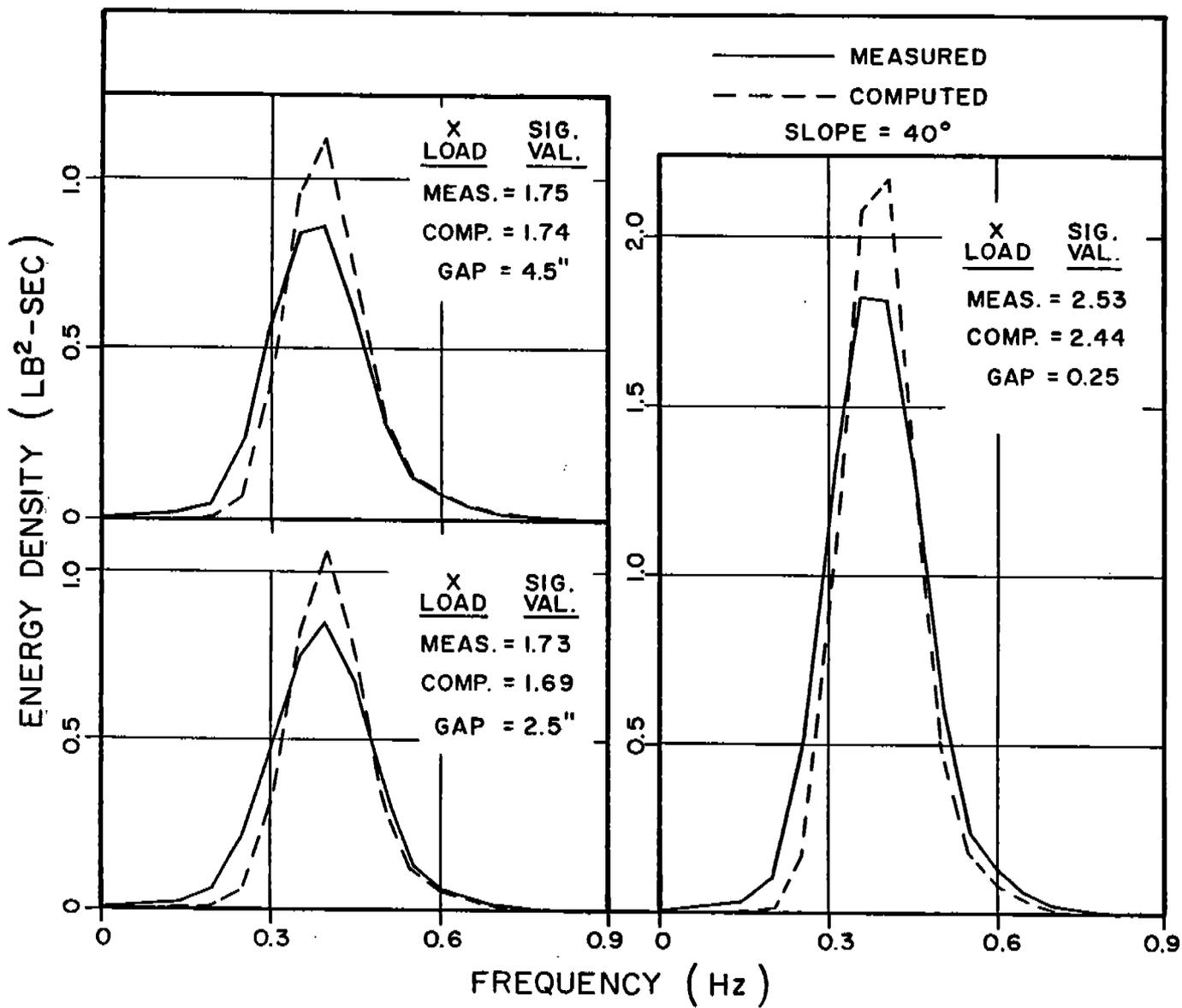
FIGURE 3.59   CORRELATION OF IN-LINE FORCE SPECTRA FOR 40° SLOPE
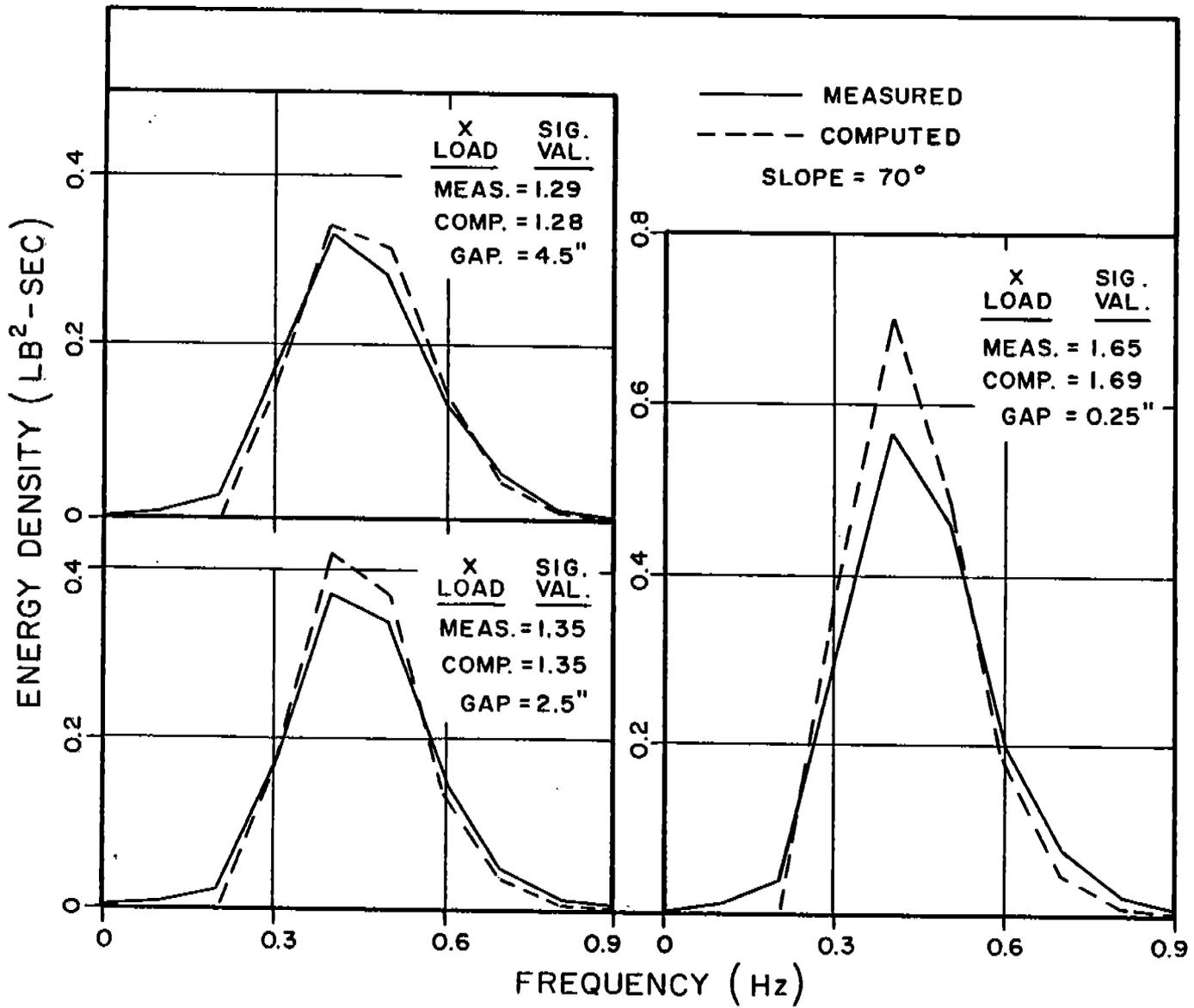
FIGURE 3.60   CORRELATION OF IN-LINE FORCE SPECTRA FOR 70° SLOPE
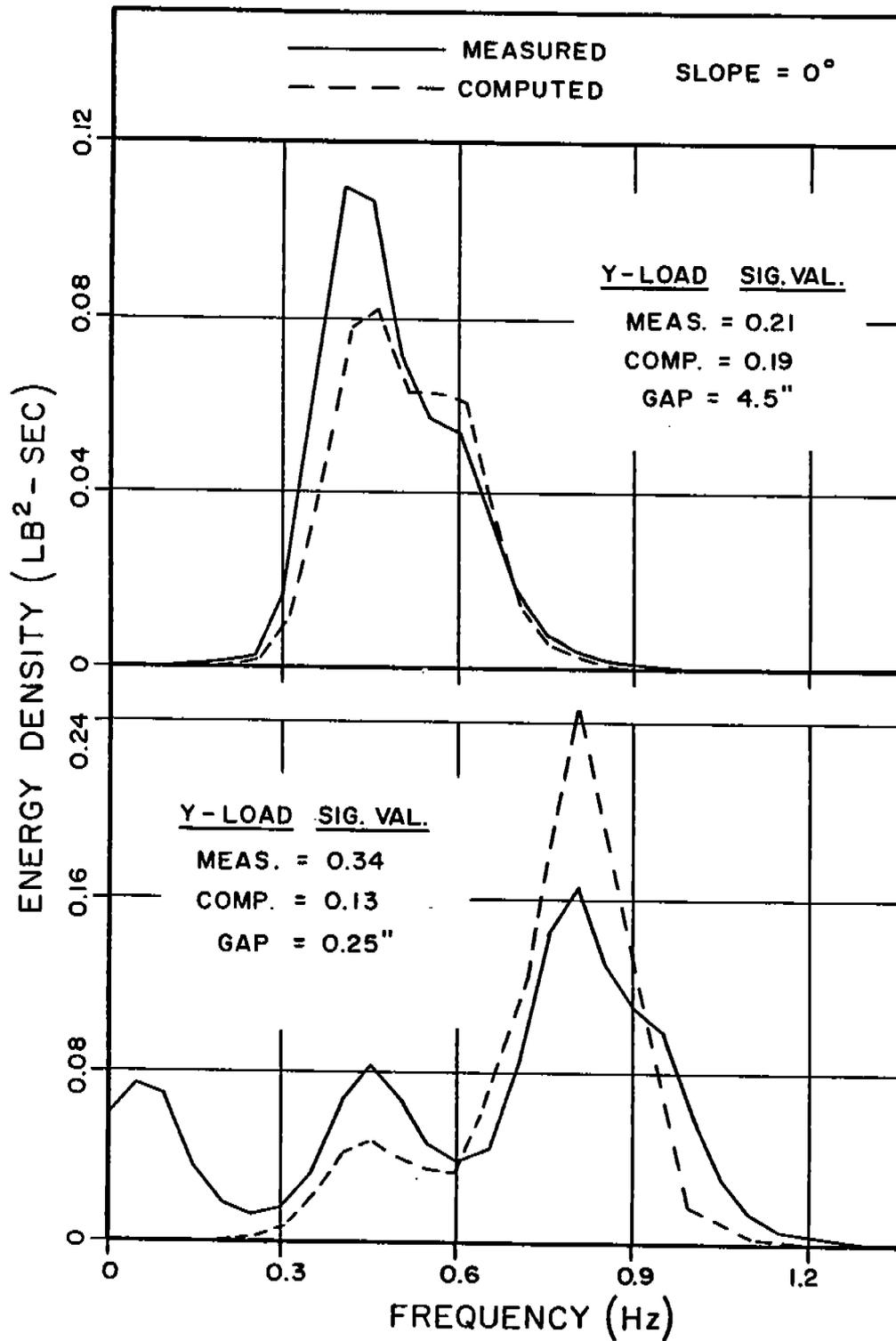
FIGURE 3.61   CORRELATION OF NORMAL FORCE SPECTRA FOR 0° SLOPE

distribution. Thus, if the forces measured on the cylinder are strictly inertial then these random force amplitudes may be described by the Rayleigh distribution function.

From the earlier force correlation it is found that the drag force contribution in the total force is quite small. For the vertical cylinder tests, the cummulative distribution of the wave heights and in-line force double amplitudes (heights) are shown in Figs. 3.62 and 3.63, respectively. It is found that the forces follow the Rayleigh distribution function as good as or better than the wave heights. The wave heights show some departure at the high end of the distribution function. The in-line response has a somewhat similar trend. While the overall correlation seems satisfactory in both cases, this deviation at the upper tail may be important from the point of view of the extreme value analysis.

The transverse force, on the other hand, while small in magnitude, shows a significant departure from the Rayleigh distribution. Note that the lift force has a form

$$f_L(t) = \frac{1}{2} C_L \rho D [u(t)]^2 = C[u(t)]^2 \qquad (3.371)$$

i.e., the lift force is proportional to the velocity squared. In the above expression, the value of C_L is assumed to be constant with time. This assumption is not strictly correct because the lift force is irregular. However, if the most predominant lift force frequency is twice the wave frequency, this assumption is reasonable. This form is similar to the wave drift force profile. Langley (1984) showed that for a wave drift force, the asymptotic initial distribution of the drift force profile for a narrow band spectrum follows an exponential distribution. For a wider band spectrum, the distribution is sharper depending on the value of q. Borgman (1972) has shown that on a narrow band assumption, the drag force amplitudes follow an exponential distribution. The lift force due to regular waves may be approximated by the formula

$$f_L = k_L u_m^2 \cos 2\omega t \qquad (3.372)$$

142
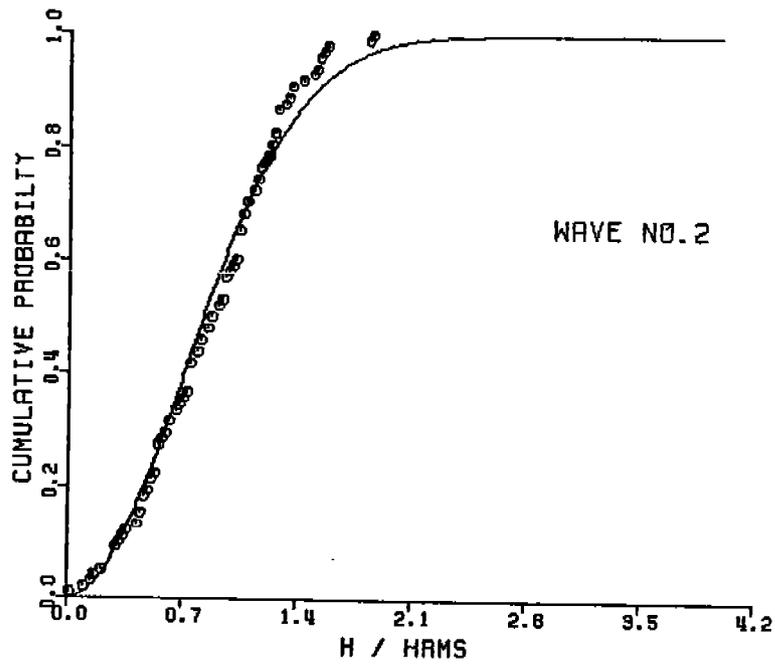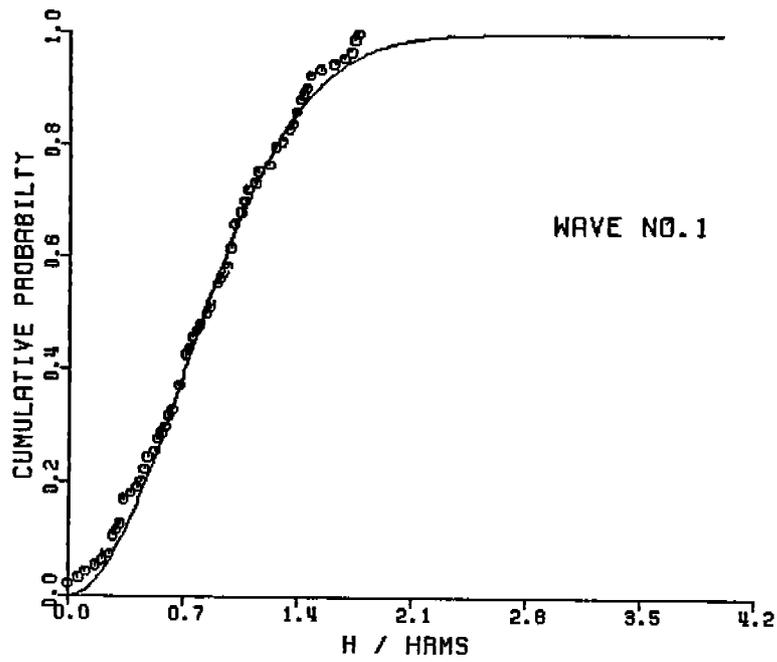
FIGURE   3.62   CORRELATION   OF   WAVE   HEIGHT   DISTRIBUTION   WITH   RAYLEIGH
DISTRIBUTION FUNCTION
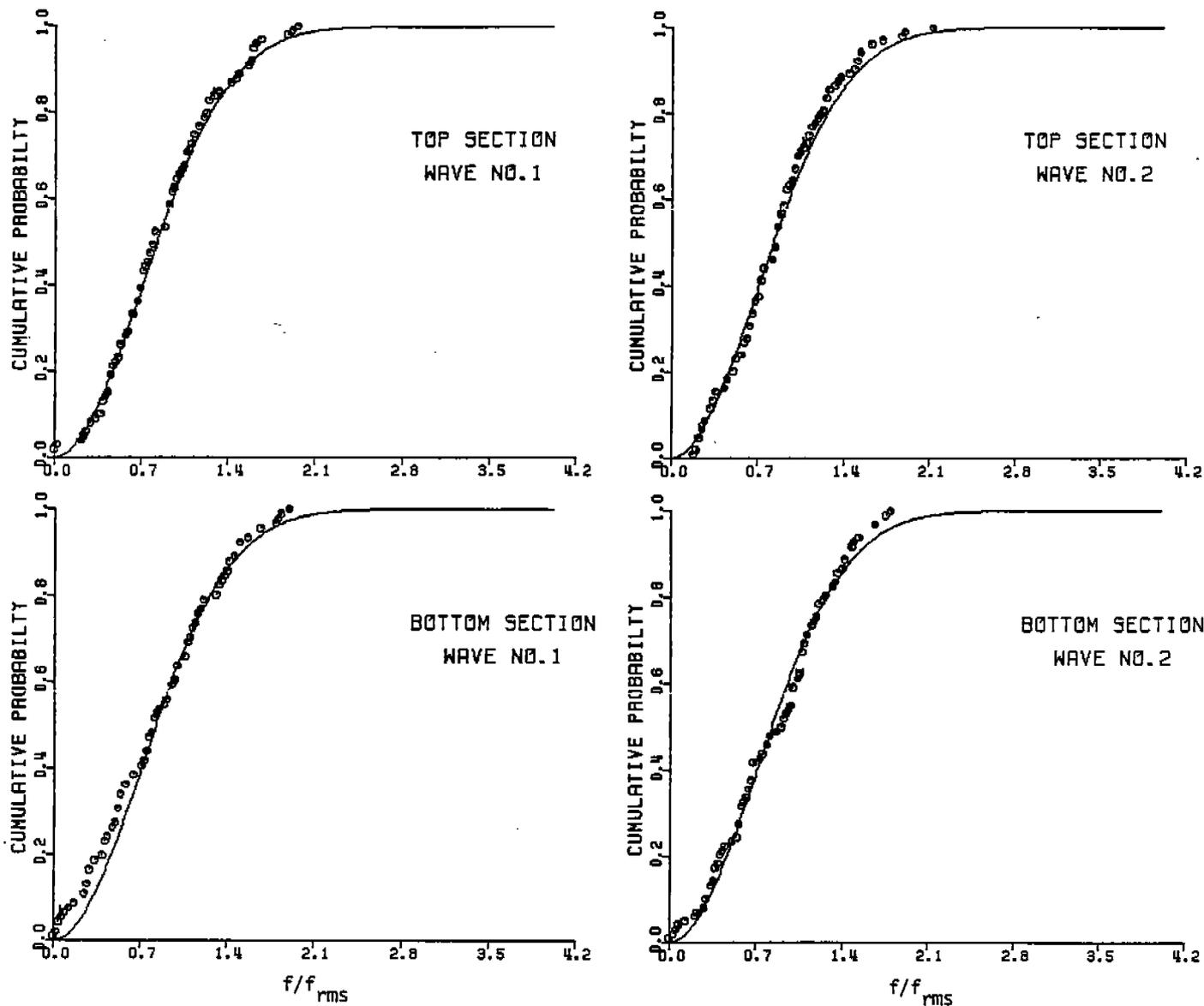
FIGURE 3.63 CORRELATION OF IN-LINE FORCE DISTRIBUTION WITH RAYLEIGH
DISTRIBUTION FUNCTION

where $k_L = 1/2 \, C_L \, \rho \, D$. In this form, the other frequencies in the irregular lift force profile are ignored as small. Then, the maximum lift force in regular waves is given by

$$f_{L_m} = k_L \, u_m^2 \qquad (3.373)$$

Following a method similar to Borgman's (1972) for the drag force amplitudes, the lift force amplitudes may be expected to follow the exponential distribution at least on a narrow band spectrum assumption. This distribution may then be given by

$$P(\hat{f}_L) = 1 - \exp\left[-\frac{\hat{f}_L}{k_L \, u_{rms}^2}\right] = 1 - \exp\left[-\frac{\hat{f}_L}{(f_L)_{rms}}\right] \qquad (3.374)$$

where $\hat{f}_L$ = amplitudes of f_L and u_{rms} = rms value of the water particle velocity and $(f_L)_{rms} = k_L \, u_{rms}^2$. The correlation between the measured lift force amplitudes and the exponential distribution is shown in Fig. 3.64. From this correlation it is seen that at least at the low end of KC number (< 10) the lift forces do not follow the exponential distribution well, especially at the intermediate range of the independent variable. On examining the lift force profile, it is found that the frequency contents of the lift force correspond to the wave and the inline force frequencies as well as twice these frequencies. Thus, the distribution of the lift force amplitudes is between the Rayleigh distribution and the exponential distribution function and may have to be obtained as a distribution of a polynomial series in the powers of velocity.

The forces measured on the instrumented section of the inclined cylinder in the in-line (X) and normal (Y) directions with respect to the cylinder axis are mostly inertial. Therefore the random force amplitudes are described by the Rayleigh distribution function. At the smallest gap, however, the normal force had larger force components at twice the frequencies of the wave frequencies and may not be expected to follow the Rayleigh distribution function well. The normal force is expected to be a mixed distribution. When the second harmonic is small, e.g., for larger gaps, the distribution will be closer to the Rayleigh distribution.

The cummulative distribution of the wave heights, in-line and normal force amplitudes for random wave runs with a 0° slope and gaps of 2.5 in. and 0.25 in. are presented in Figs. 3.65 and 3.66, respectively. The wave heights and in-line forces are found to follow the Rayleigh distribution reasonably well even though the departure from the theoretical curve is not insignificant. Part of this deviation may be due to a large bandwidth. The normal force for the larger cylinder/boundary gap of 4.5 ins. has a similar correlation. However, the normal force at the 0.25 in. gap compares poorly with the Rayleigh distribution. The distribution of the measured force amplitudes rises more sharply than the Rayleigh curve and corresponds more nearly to the exponential distribution. It is possible that the correction required for a larger band width may improve this correlation as shown by Langley (1984) for the initial drift force distribution.

Additional test runs were recently made with a 2.5 inch diameter vertical cylinder with a 1 ft. instrumental section submerged 1 ft. below the still water level (SWL). Besides the wave profile, the velocity components at the center of the instrumented section (18 inches below SWL) were measured. Two random waves having similar significant wave heights (H_s = 8.4 - 8.5 inches) but slightly different peak frequency (Fig. 3.67) were chosen. The probability density of the wave elevation and horizontal velocity for these runs is compared with the Gaussian distribution on the top of Figs. 3.68 and 3.69. The probability density of the inline load and the cumulative distribution of its amplitudes are shown in the middle along with Gaussian and Rayleigh probability respectively. The transverse (or lift) force is correlated with the exponential distribution at the bottom of the figures. The wave and the velocity profiles follow Gaussian distribution even though there is some random departure in the case of the velocity. The inline force seems to be asymmetric and skewed to the right in both cases. This trend is definitely comparable to the distributions derived for linear-plus-quadratic terms by Kato, et al. (1987) in Fig. 3.51.

The transverse force probability density function is generally symmetric and sharply peaked compared to the Gaussian density function. This is, however, expected as there are numerous small peaks due to higher harmonics
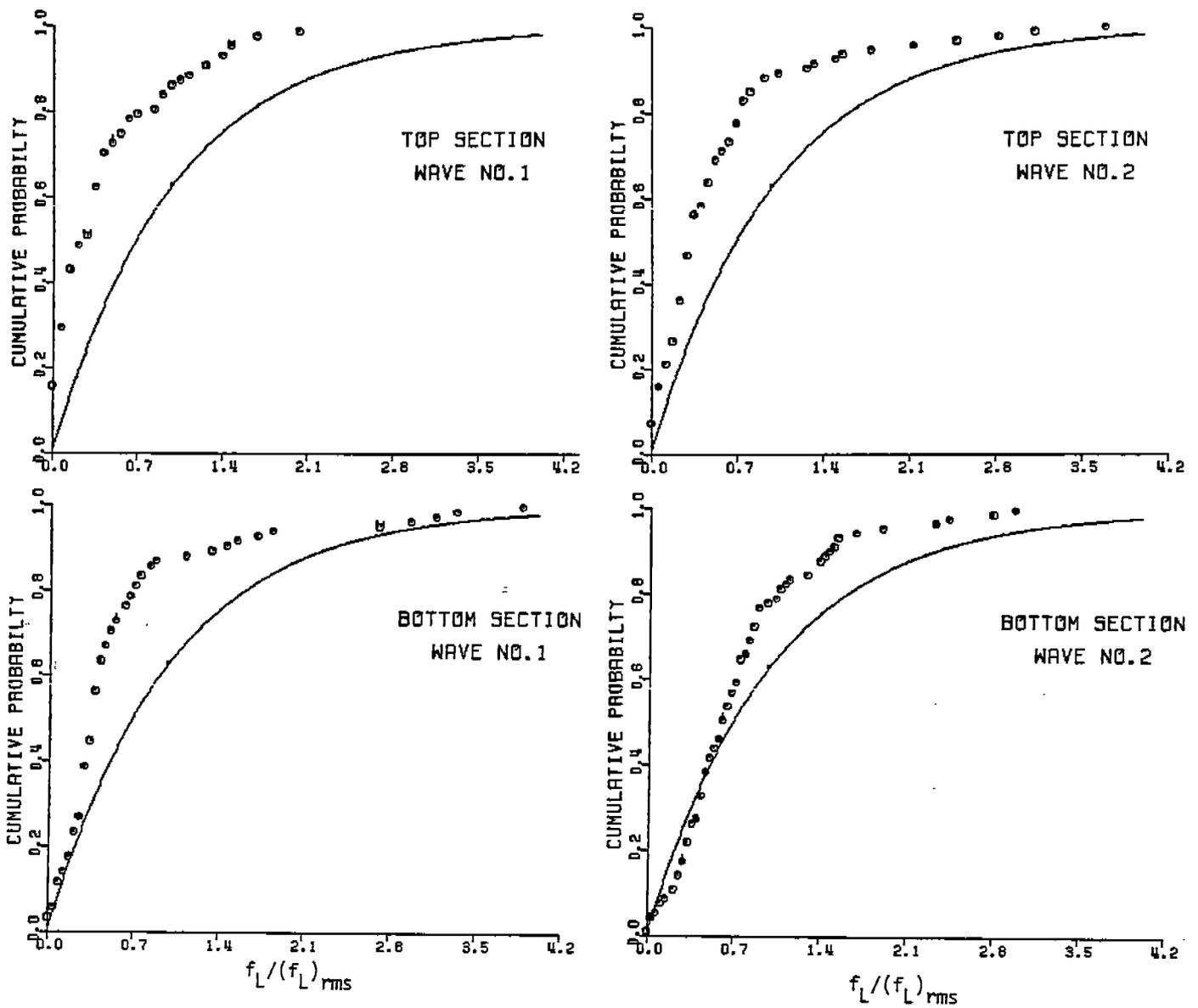
FIGURE 3.64   CORRELATION OF TRANSVERSE FORCE DISTRIBUTION WITH EXPONENTIAL
DISTRIBUTION FUNCTION
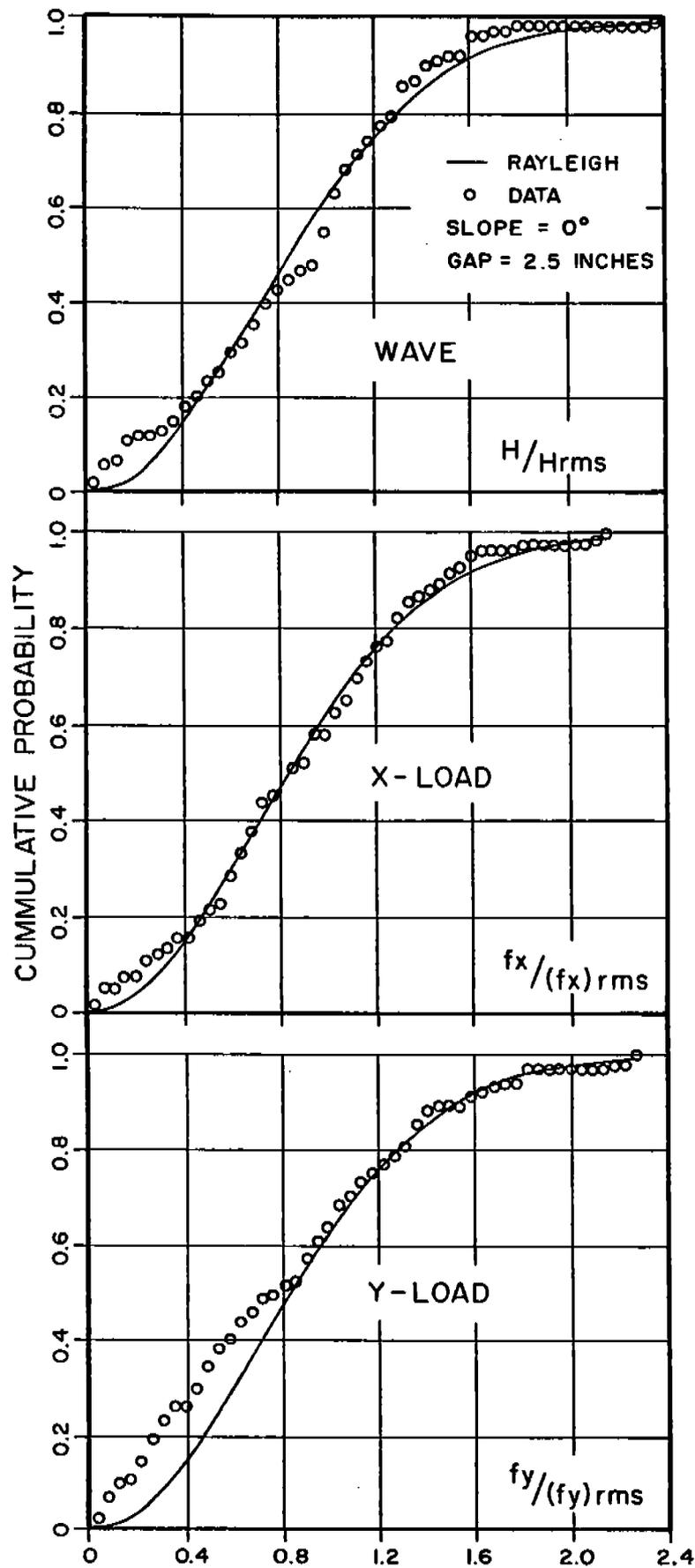
FIGURE 3.65   WAVE, IN-LINE AND NORMAL FORCE DISTRIBUTIONS FOR A 2.5 IN. GAP
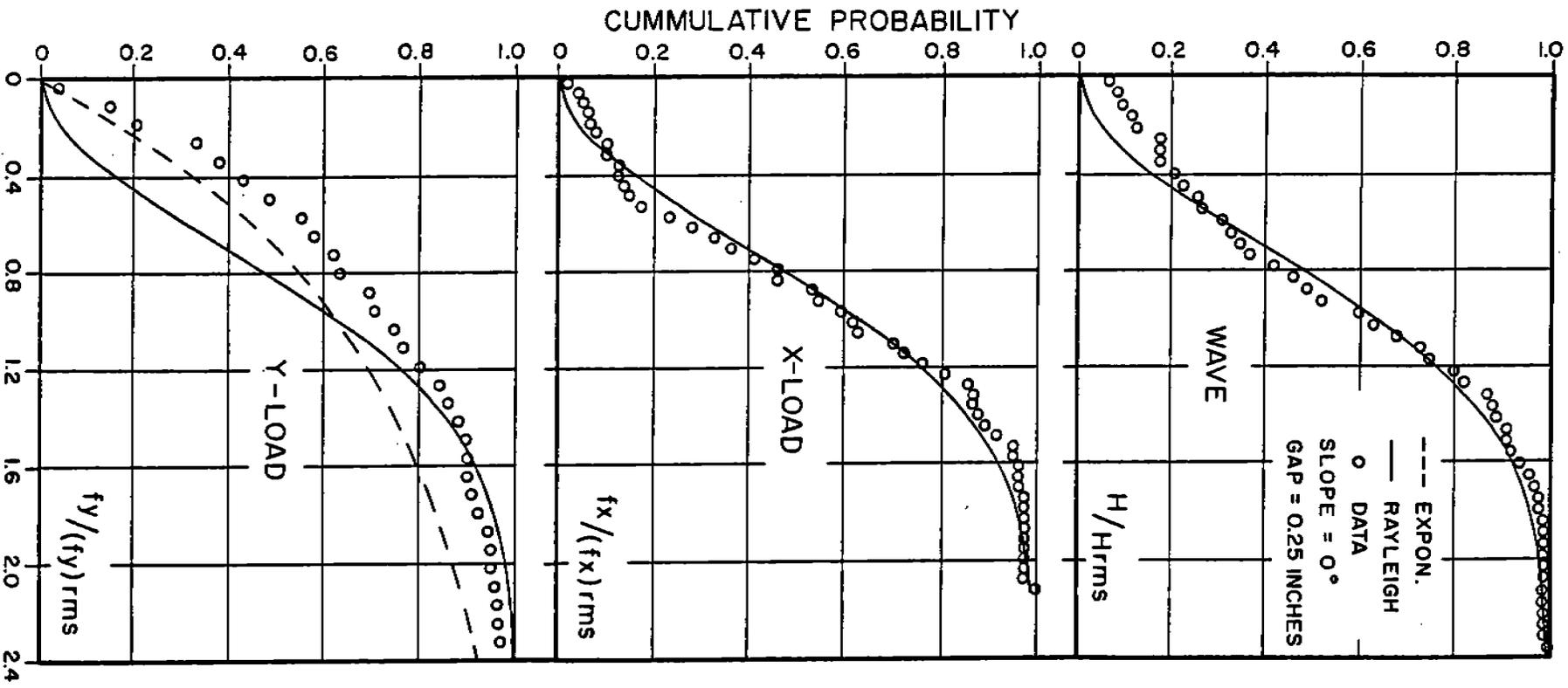
FIGURE 3.66   WAVE, IN-LINE AND NORMAL FORCE DISTRIBUTIONS FOR A 0.25 IN. GAP
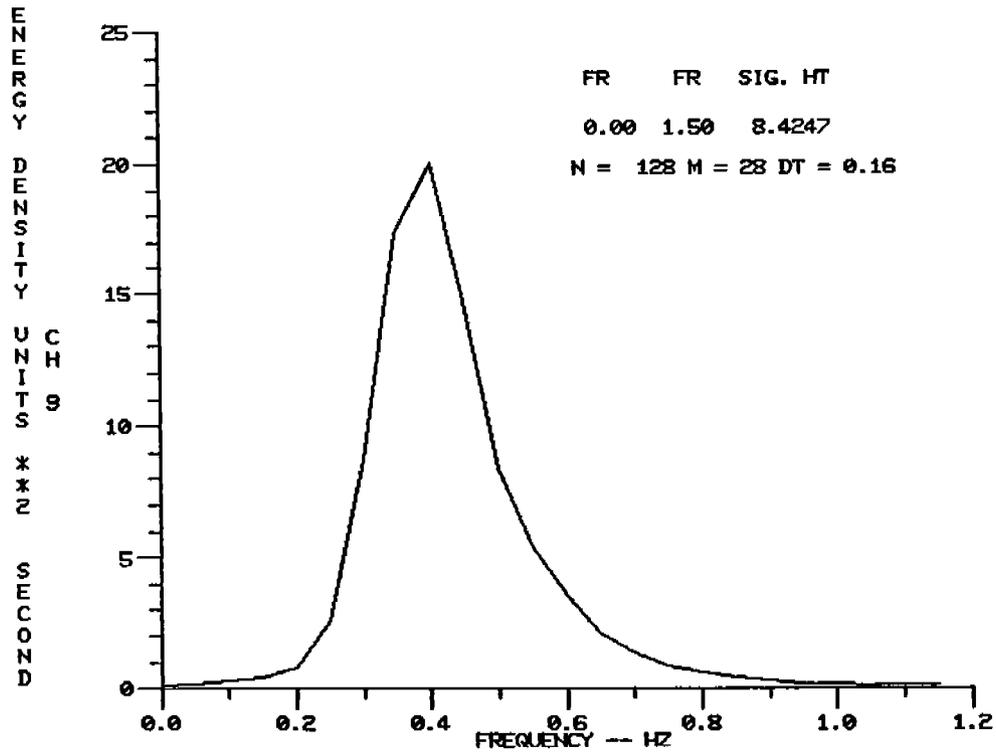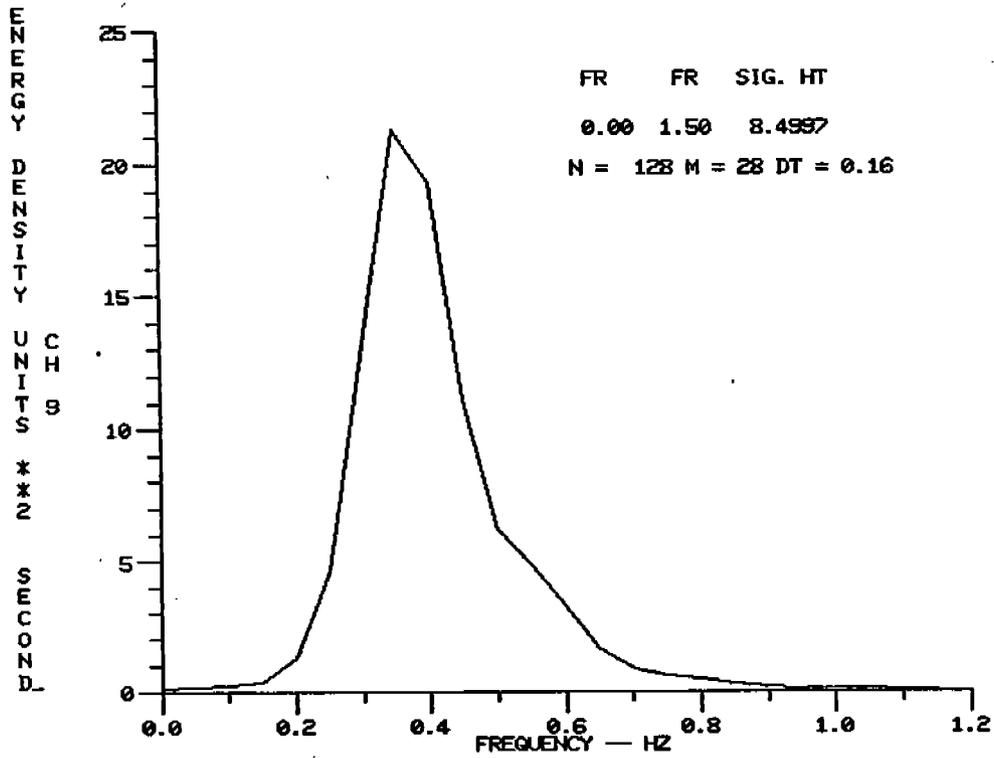
FIGURE 3.67   WAVE ENERGY DENSITY SPECTRA OF RANDOM WAVES EXPERIENCED BY
2.5 IN. DIAMETER VERTICAL CYLINDER
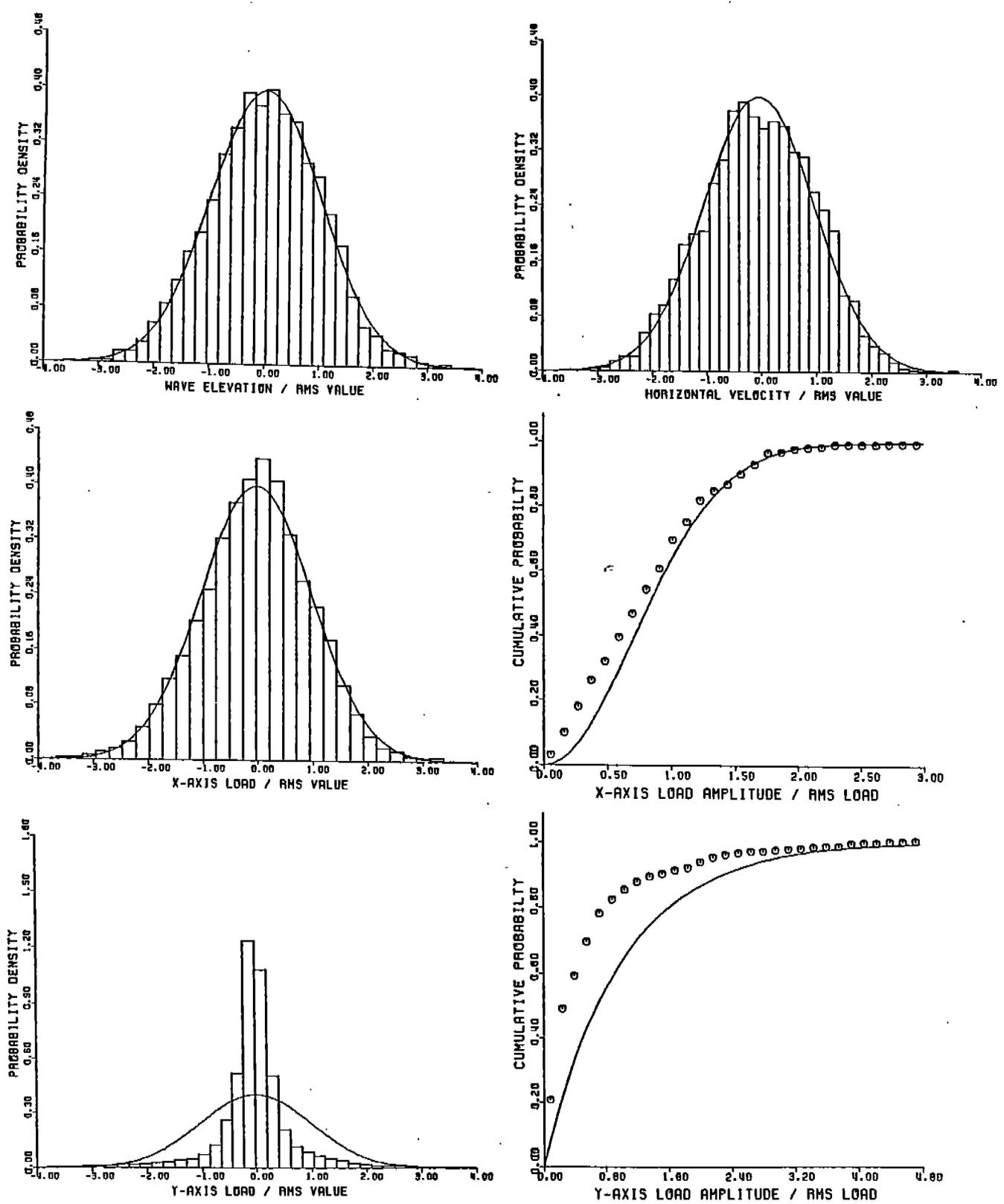
FIGURE 3.68   CORRELATION OF WAVE ELEVATION, HORIZONTAL PARTICLE VELOCITY,
IN-LINE AND TRANSVERSE LOADS WITH GAUSSIAN DISTRIBUTION AS WELL
AS IN-LINE LOAD AMPLITUDES WITH RAYLEIGH AND TRANSVERSE LOAD
AMPLITUDES WITH EXPONENTIAL DISTRIBUTION
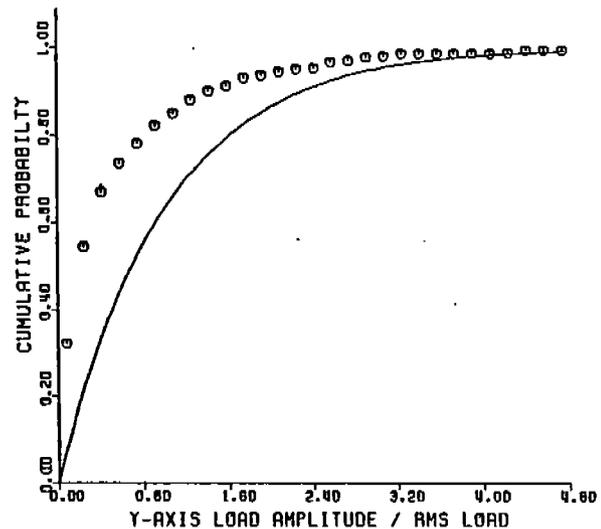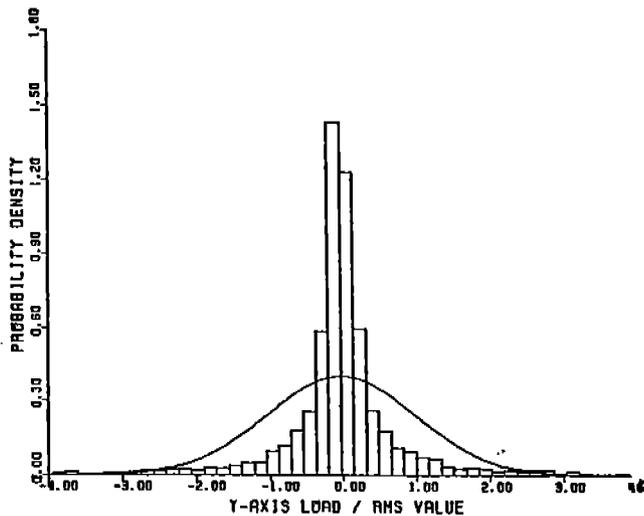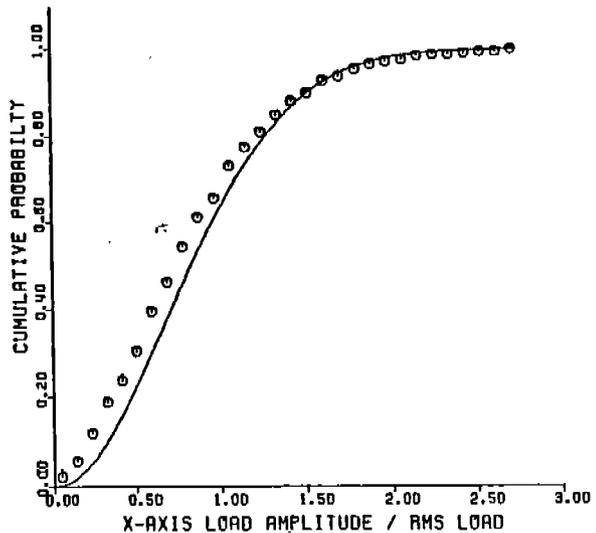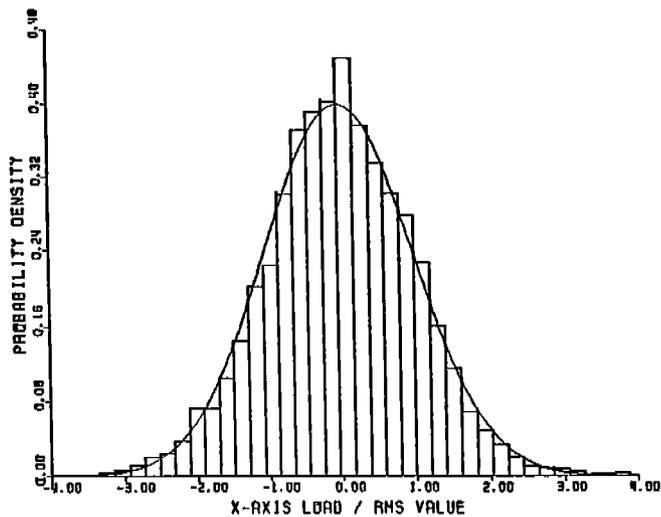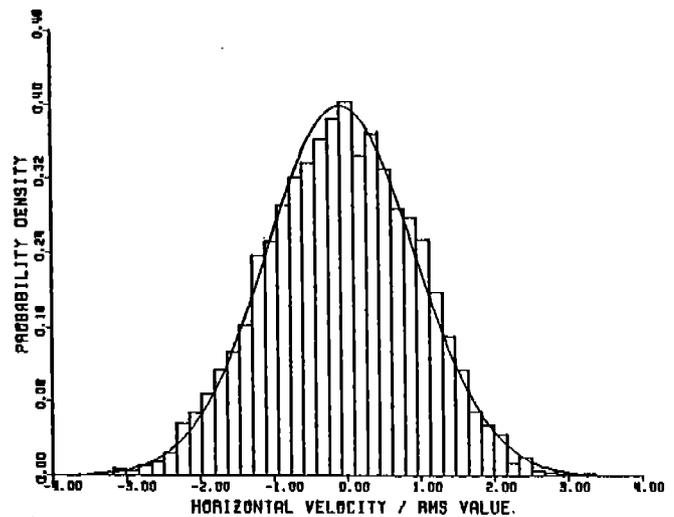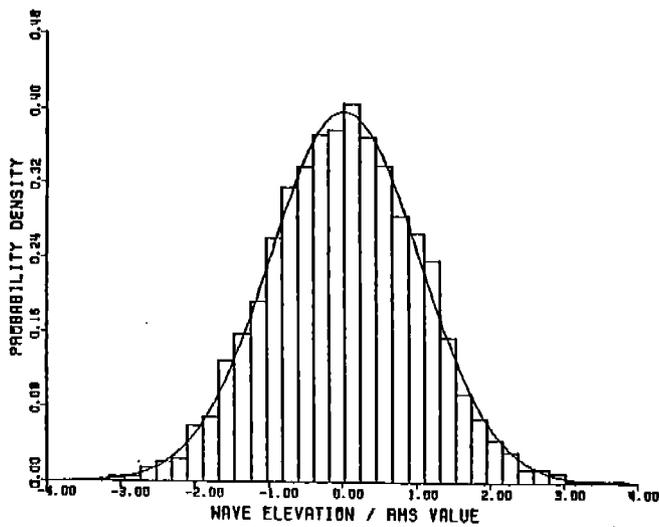
FIGURE 3.69   CORRELATION OF WAVE ELEVATION, HORIZONTAL PARTICLE VELOCITY,
               IN-LINE AND TRANSVERSE LOADS WITH GAUSSIAN DISTRIBUTION AS WELL
               AS IN-LINE LOAD AMPLITUDES WITH RAYLEIGH AND TRANSVERSE LOAD
               AMPLITUDES WITH EXPONENTIAL DISTRIBUTION.

present in the lift force which provides a bias towards its mean value. Because of the presence of multiple harmonics, correlation with the exponential distribution is not satisfactory.

Additional test runs were made in the presence of uniform current. In these cases, the horizontal particle velocity was measured as well at the center of the instrumented section. The random wave run was repeated with an inline and an opposing current having a strength of $\gamma = 1.0$. The horizontal velocity and the inline load histograms are correlated with the Gaussian distribution in Fig. 3.70. The top plots represent waves without current while the bottom ones correspond to the inline and opposing current respectively with the waves. The horizontal velocity and inline loads follow the Gaussian distribution in the absence of current. While current is present, the distribution represents a non-zero mean, positive or negative depending on the direction of current. Moreover, there is a small tendency of the histograms to be skewed towards the zero value with respect to the mean. This skewness is more pronounced for the inline load in the opposing current.

The distributions of the transverse forces are shown in Fig. 3.71. The left-hand sides show the correlation of the force histograms with the Gaussian distribution while the right-hand side plots represent the cumulative probability distribution of the force amplitudes with the theoretical Rayleigh distribution function. The departure from the Rayleigh distribution is quite evident and is more pronounced in the adverse current case. Similarly, the force profiles are more peaked compared to the Gaussian distribution, particularly for the opposing current case. The transvere force, however, has a zero mean in all cases.

3.4.2 Response of an Articulated Tower

An articulated tower was tested in random waves in which the inline oscillation angle of the tower at the bottom as well as the horizontal load at the universal joint were measured (Fig. 3.72). The random wave represented a modified P-M spectrum. The tower was subjected to a steady load from the simulated wind. The histograms of the wave elevation, horizontal U-joint load and tower oscillation are compared with the Gaussian distribution in Fig. 3.73. Note the non-zero mean values in the latter two cases due to the applied steady load. The amplitudes of these measurements are compared with

145
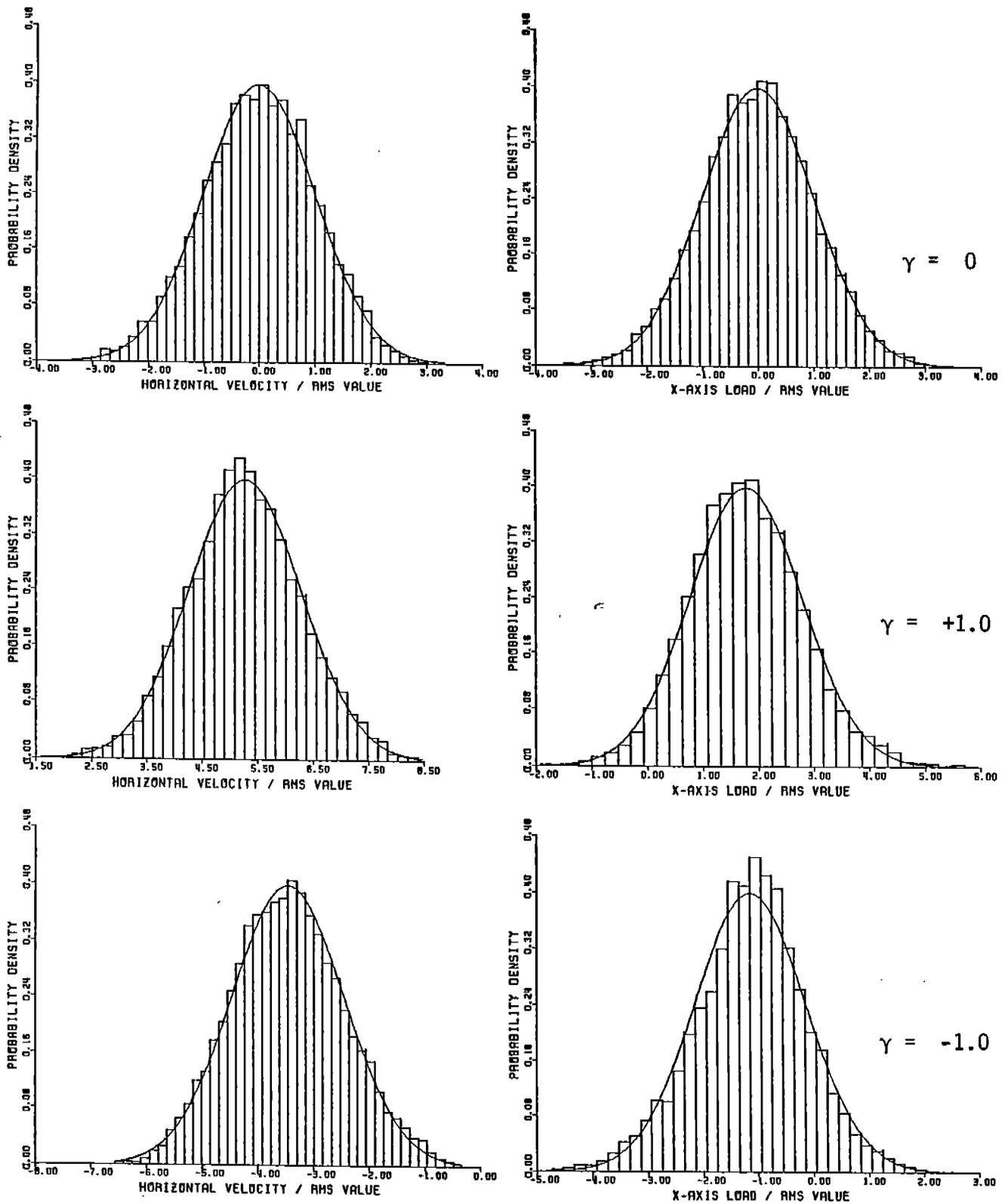
FIGURE 3.70 CORRELATION OF HORIZONTAL WATER PARTICLE VELOCITY AND IN-LINE LOADS ON A VERTICAL CYLINDER IN THE ABSENCE OF, AS WELL AS PRESENCE OF, IN-LINE AND OPPOSING CURRENT WITH GAUSSIAN DISTRIBUTION
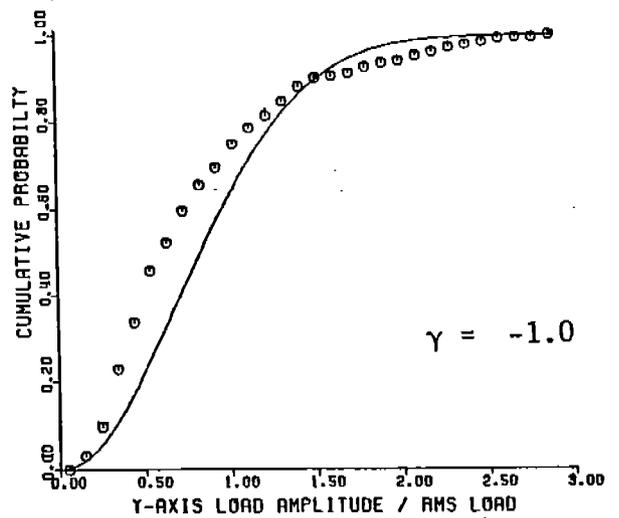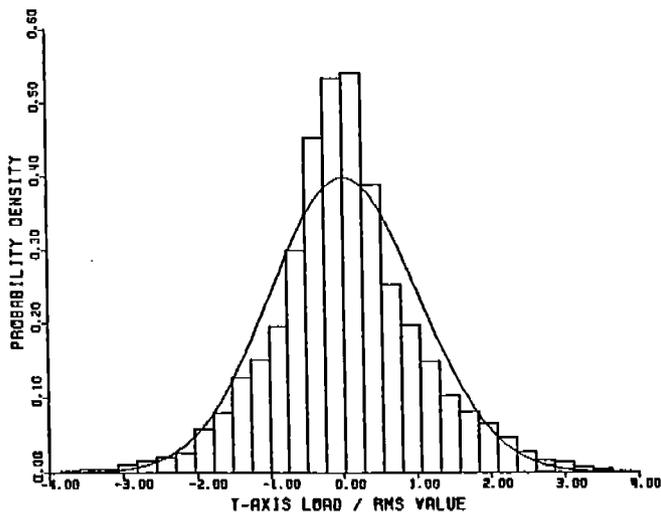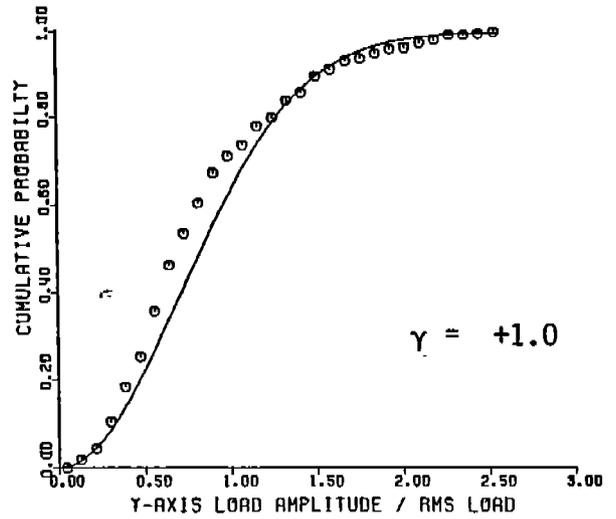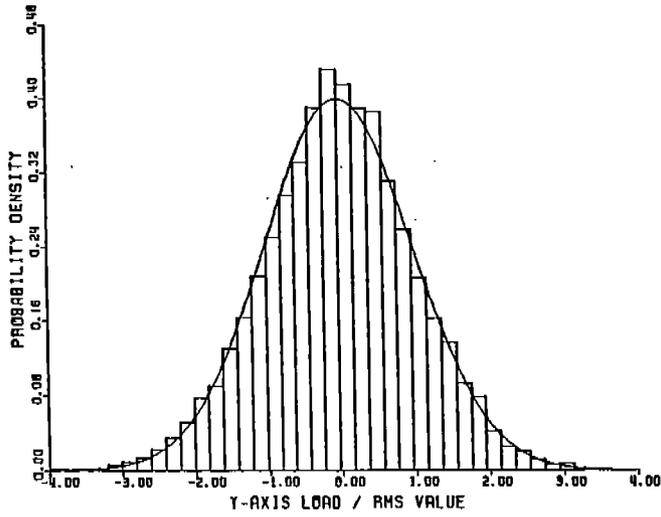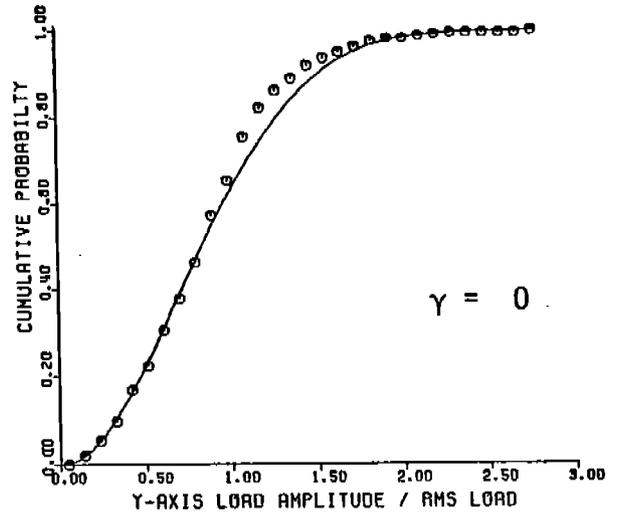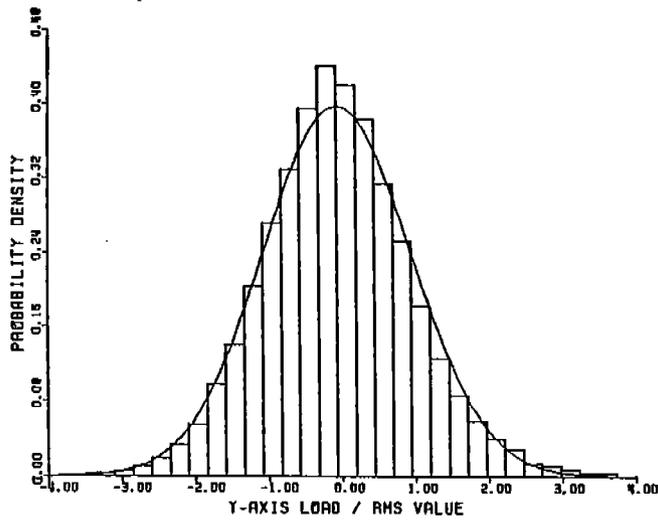
FIGURE 3.71 CORRELATION OF TRANSVERSE LOADS WITH GAUSSIAN AND RAYLEIGH
DISTRIBUTIONS FOR THE SAME CASE AS FIGURE 3.70
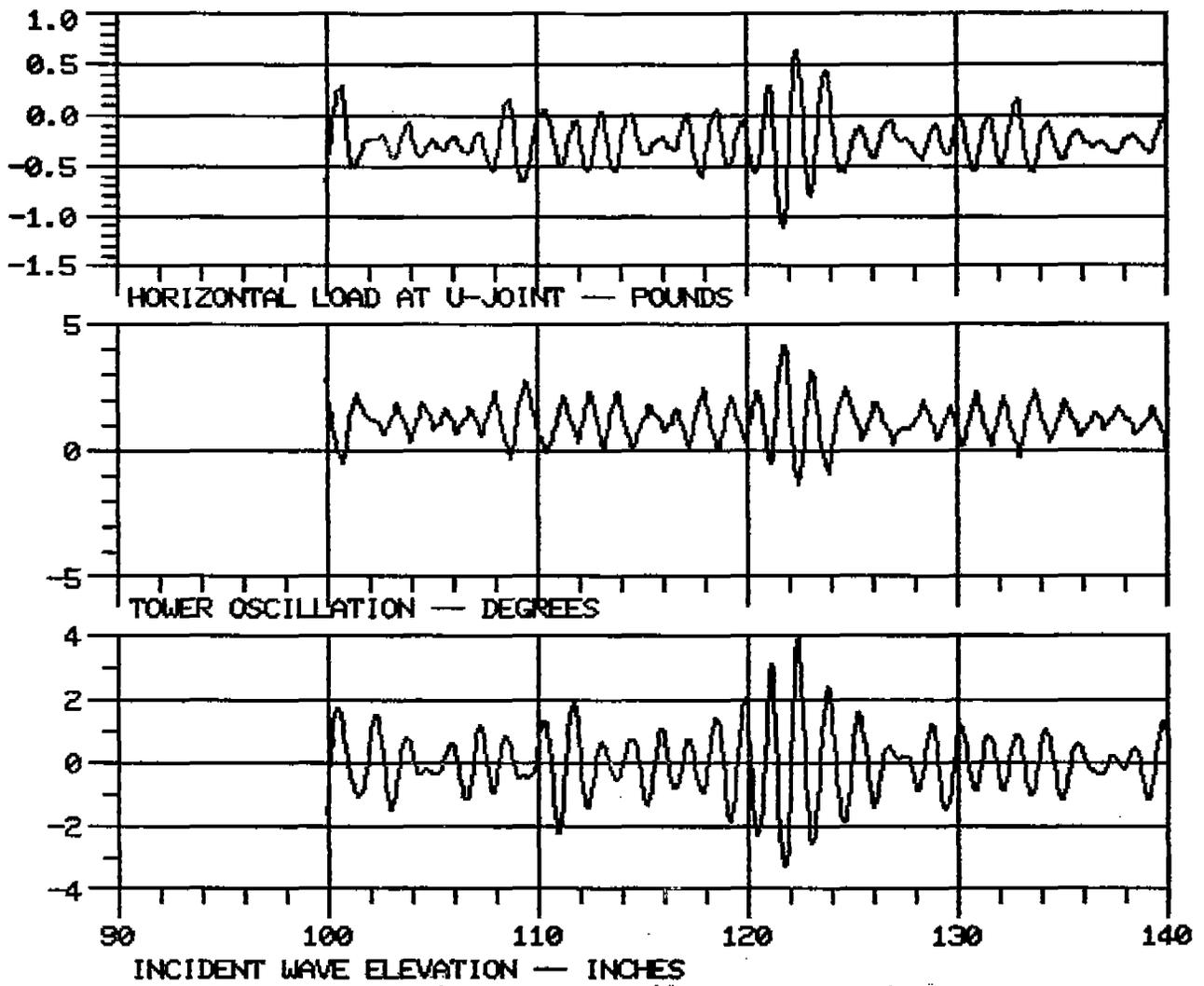
FIGURE 3.72   SAMPLE DATA RECORDED IN A WAVE TANK TEST OF AN ARTICULATED
                TOWER
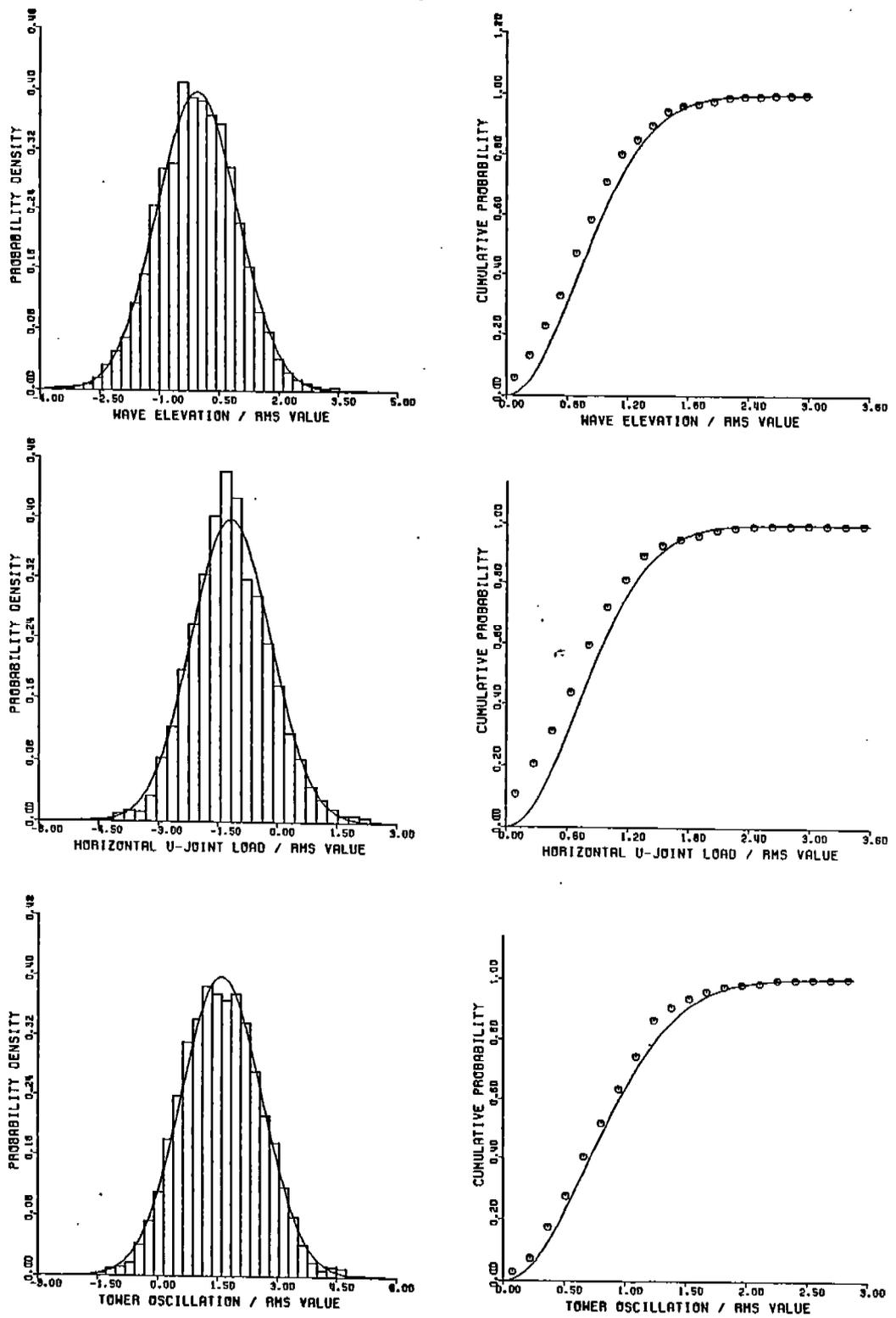
FIGURE 3.73   CORRELATION OF WAVE ELEVATION, HORIZONTAL U-JOINT LOAD AND IN-
LINE OSCILLATION OF AN ARTICULATED TOWER WITH GAUSSIAN AND
RAYLEIGH DISTRIBUTIONS

the Rayleigh distribution in the same figure. The correlation of the tower oscillation with the Gaussian and Rayleigh distributions is reasonably good. The horizontal load, however, show some deviation. The dimensions of the buoyant tower relative to the wave were such that some drag dependence of the load may be expected.

3.4.3 Response of a Moored Tanker

A tanker model moored by catenary anchored lines was tested in the wave tank. The tanker model represented a 100,000 dwt displacement tanker class, and the mooring arrangement was similar to the one shown in Fig. 2.30. The load-elongation characteristics of the catenary system are shown in Fig. 2.31. During the test in random waves, the surge of the tanker as well as the line tension in the forward mooring line were measured. The tanker was ballasted at 50 percent and was subjected to a steady wind load. One run also included a steady current load.

The results for the line tension and tanker surge are presented here. These data are digitally filtered to remove the high frequency oscillations corresponding to the wave frequencies so that the responses correspond to the low-frequency oscillation only. The histograms and cumulative distribution of amplitudes of the line tension and tanker surge are correlated with the Gaussian and Rayleigh distribution respectively in Figs. 3.74 and 3.75. These runs correspond to two different random waves and wind; the second one having steady current as well. The distributions are somewhat asymmetric about the non-zero mean value, but otherwise, close to the Gaussian distribution function.

3.4.4 Response of a Barge

A conventional barge model was tested in the CBI wave tank. The barge was 12.5 ft. long, 3.25 ft. wide and had a draft of 0.42 ft. It was moored in head seas by a linear spring fore and aft such that it had a natural period in surge of approximately 30 seconds. The details of the barge characteristics have been reported by Chakrabarti (1982). The mooring line load and surge motion of the barge were measured in random waves.

The data was filtered as before to remove the high frequency oscillations using a high pass filter with a cut-off frequency of 0.2 Hz. The results are

146
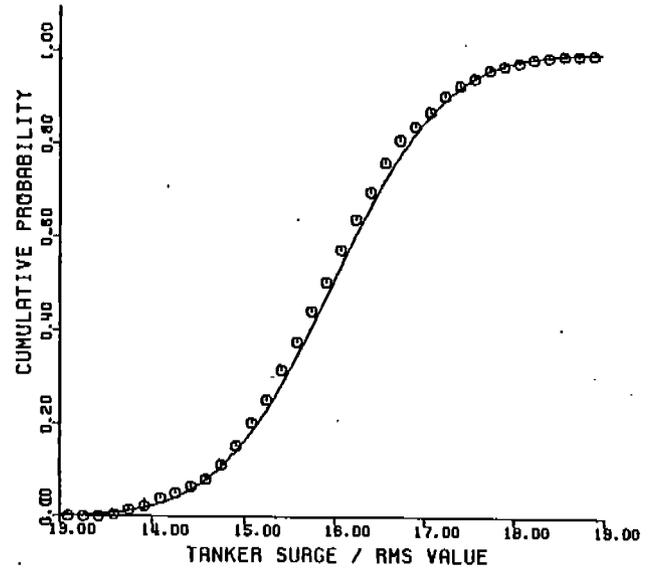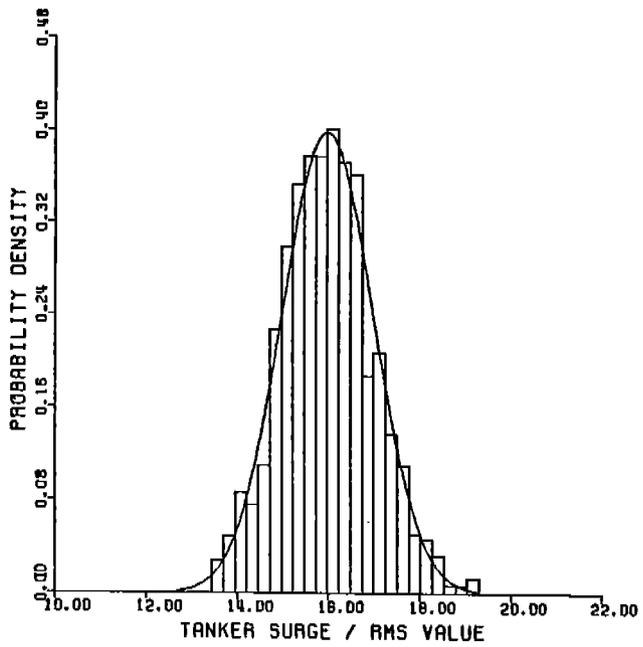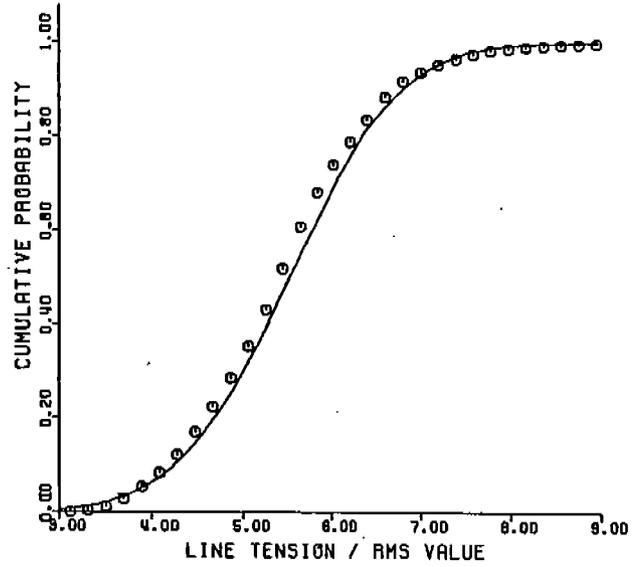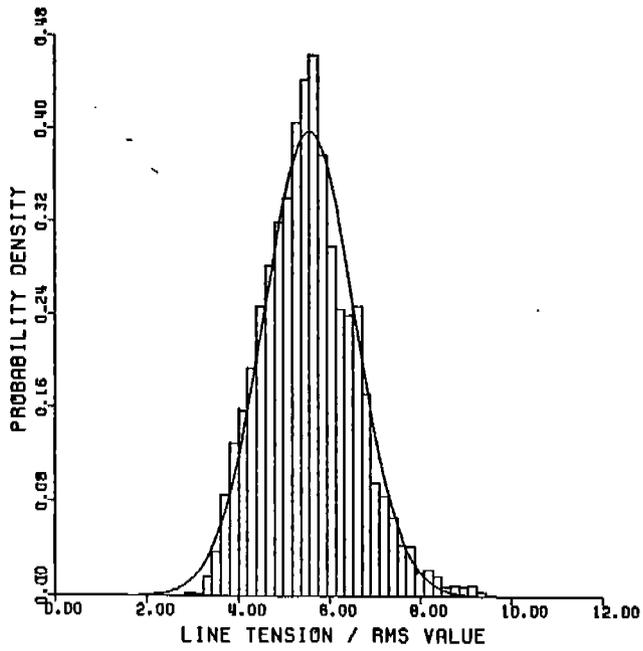
FIGURE 3.74 CORRELATION OF LOW-FREQUENCY SURGE MOTION AND CORRESPONDING
LINE TENSION OF A SPREAD-MOORED TANKER IN WAVES AND WIND WITH
GAUSSION AND RAYLEIGH DISTRIBUTION
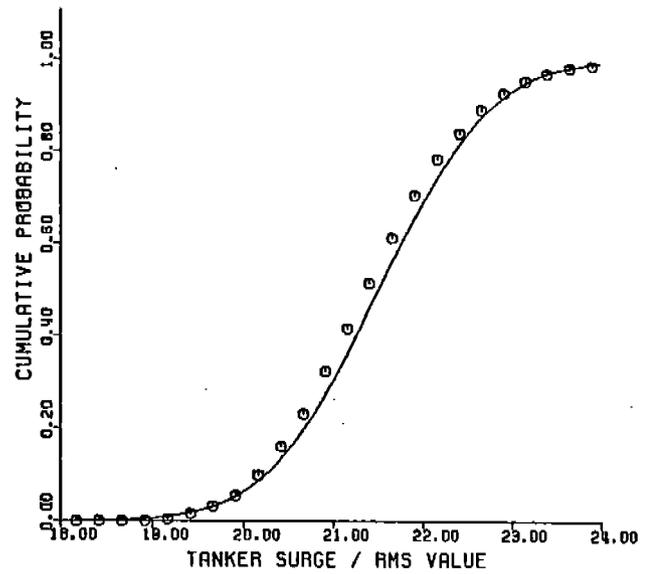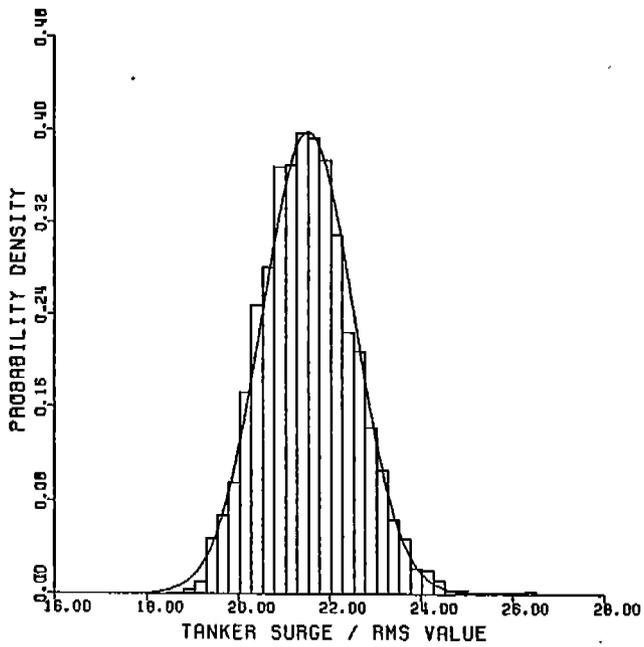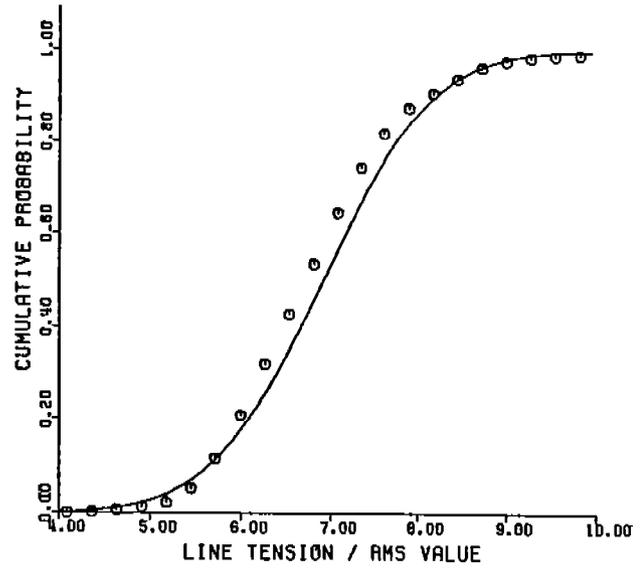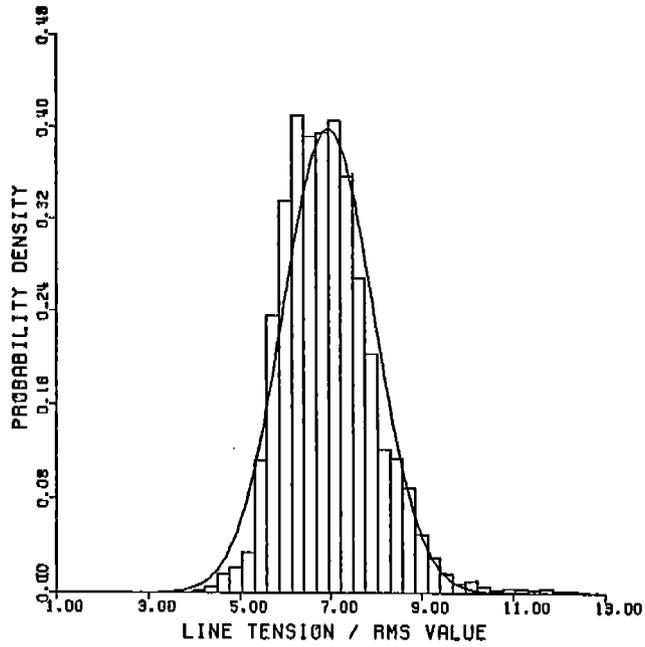
FIGURE 3.75 CORRELATION OF LOW-FREQUENCY SURGE MOTION AND CORRESPONDING LINE TENSION OF A SPREAD-MOORED TANKER IN WAVES, WIND AND CURRENT WITH GAUSSIAN AND RAYLEIGH DISTRIBUTION

presented in Figs. 3.76 and 3.77. There are two limitations that can be stated regarding this set of data. First of all, the length of data runs was limited (five minutes of model time). It has been shown by Pinkster, et al. (1987) that the statistical parameters should be unstable for short duration of runs. Moreover, the number of components used to generate waves were also small. These limitations are evidenced in Figs. 3.76 and 3.77. While the individual measurements correspond to each other, any trend in the histogram data is lacking.

3.4.5 Response of a Semisubmersible

A model of a semisubmersible pipelay barge design was tested in the CBI wave tank. The major dimensions of the semisubmersible were 8.1 ft. long and 2.8 ft. wide. The barge was composed of twin hulls and six legs supporting a box superstructure. It was ballasted at the legs to a draft of 0.78 ft. The model was moored to two fixed points by linear springs. The springs on the fore and aft sides of the model were identical with a spring constant of 0.49 lbs/ft. each. The spring constants were chosen so that the translational natural period of the moored system was about 30 sec. The mooring lines were instrumented with load cells. In addition to the wave elevations, the dynamic pressure in the free-stream flow, one foot below the still water level, was also recorded.

The results for these measurements are shown in Fig. 3.78 for a P-M wave spectrum and in Fig. 3.79 for a JONSWAP wave spectrum. The data for the line load was likewise filtered as before to retain only the low-frequency loads. Thus, the correlations with the Gaussian distribution in Figs. 3.78 and 3.79 correspond to the high-frequency wave as well as corresponding dynamic pressure and low-frequency line load. Note that the line loads are biased towards positive values and show poor correlation with Gaussian.

3.5 LONG-TERM RESPONSE PREDICTION

The long-term refers to the desired lifetime of a marine system or an ocean structure. During this period of time, the structure experiences a large number of seas from very small to very large. Each of these individual seastates is a short-term phenomenon and may be treated as a linear or nonlinear excitation depending on its size. Similarly, the responses may be

147
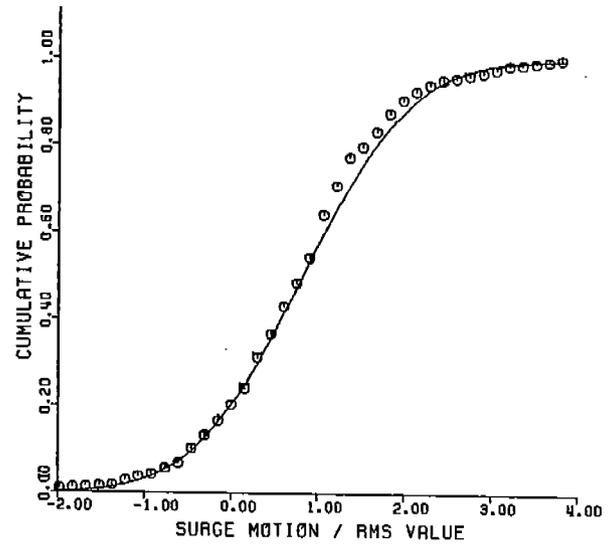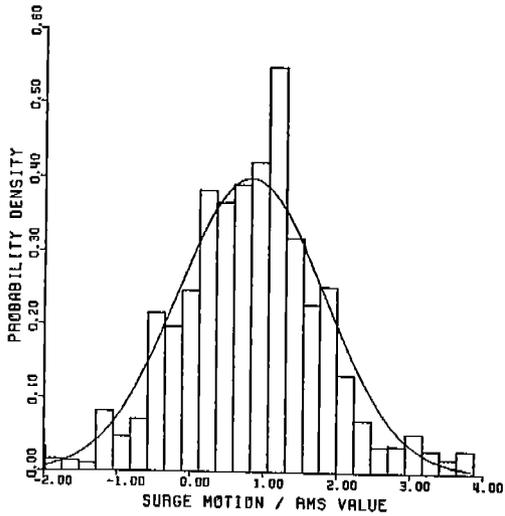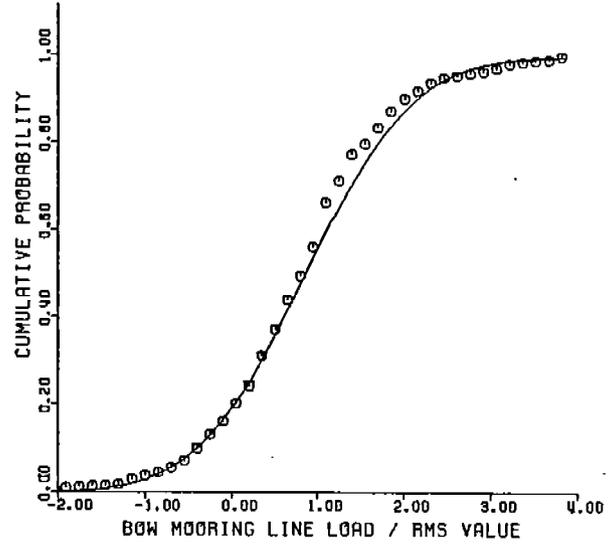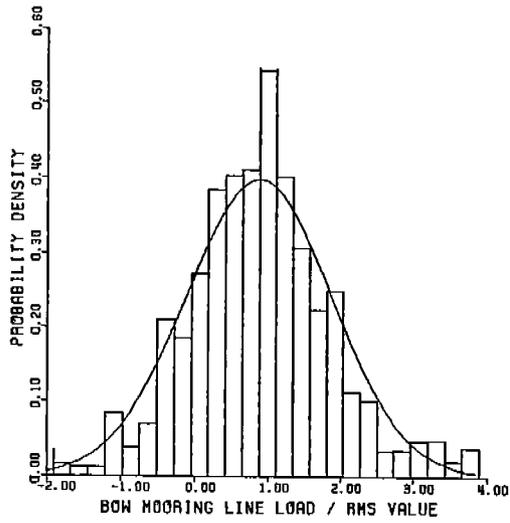
FIGURE 3.76   CORRELATION OF MOORING LINE LOAD AND SURGE MOTION OF A BARGE
WITH GAUSSIAN DISTRIBUTION
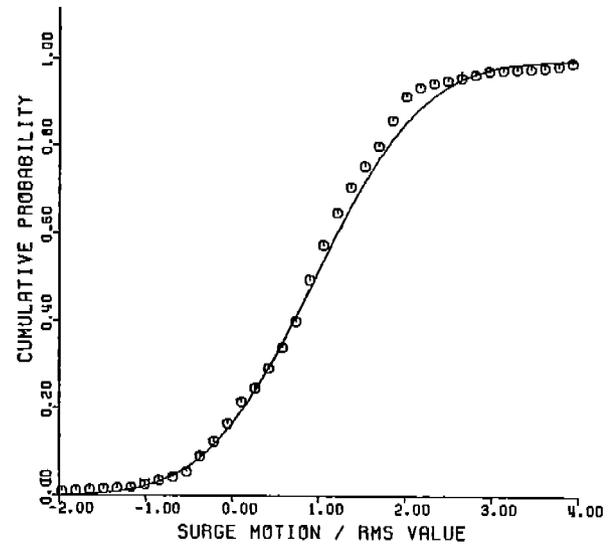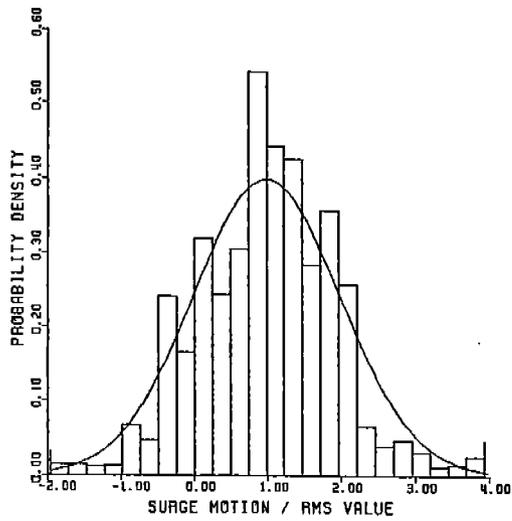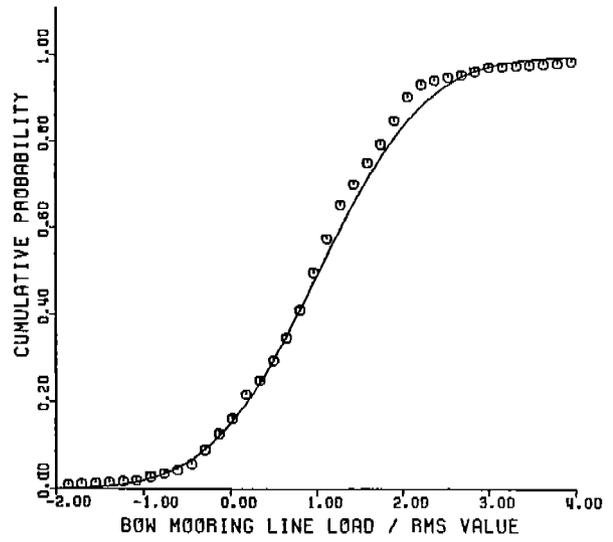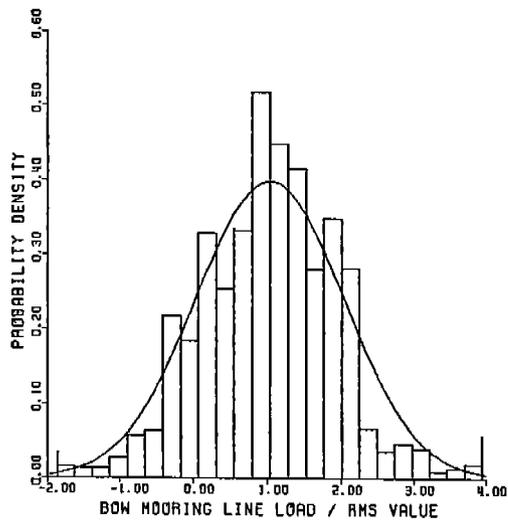
FIGURE 3.77   CORRELATION OF MOORING LINE LOAD AND SURGE MOTION OF A BARGE
WITH GAUSSIAN DISTRIBUTION
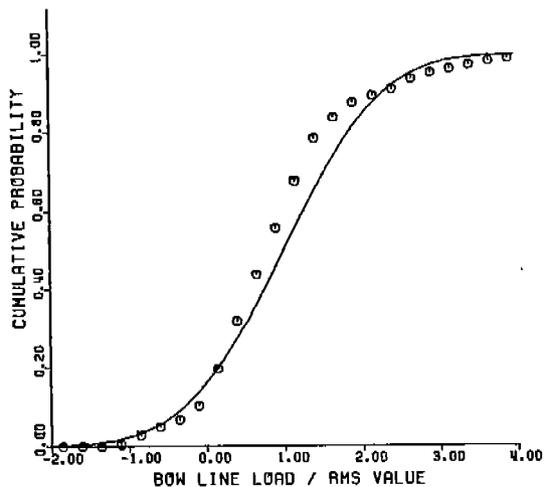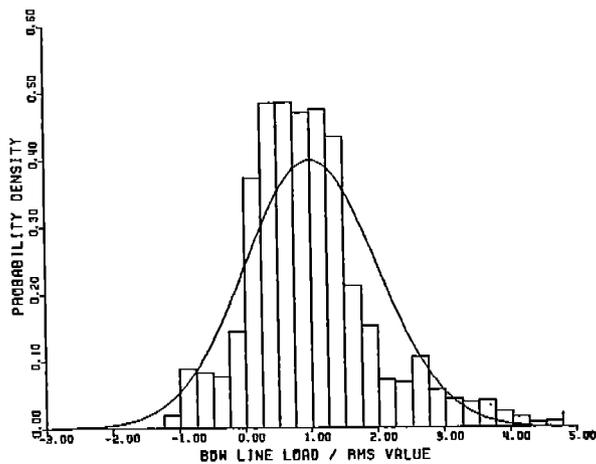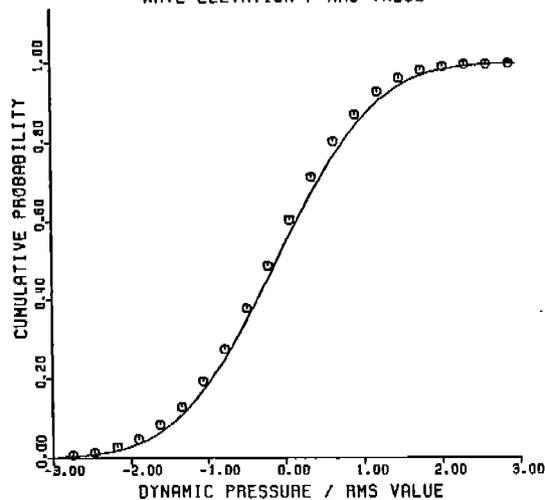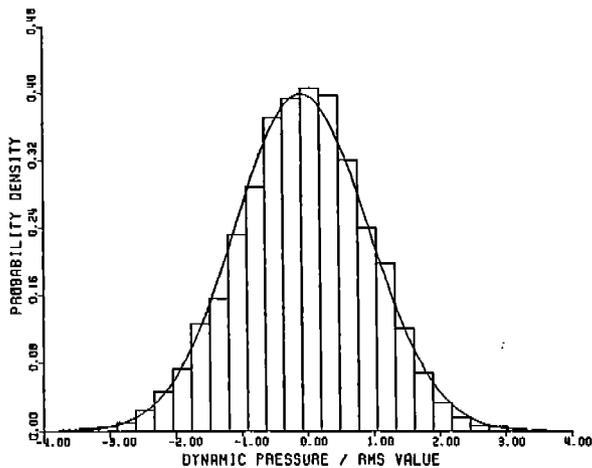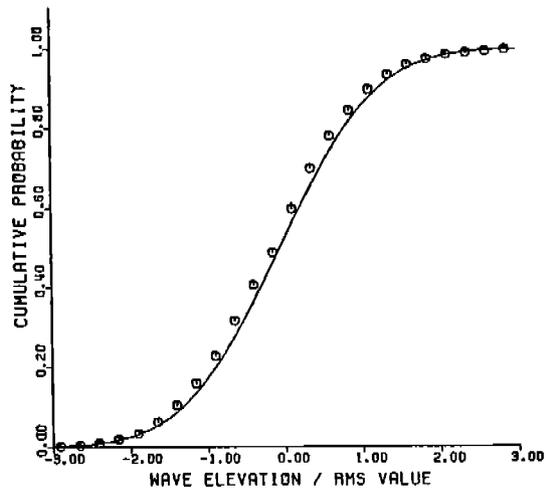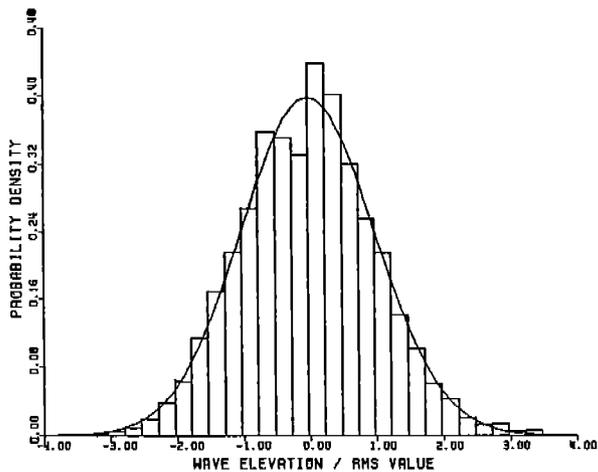
FIGURE 3.78 CORRELATION OF MEASURED WAVE, PRESSURE AND LINE LOAD DISTRIBUTIONS WITH GAUSSIAN FOR P-M WAVE ON A SEMISUBERMSIBLE
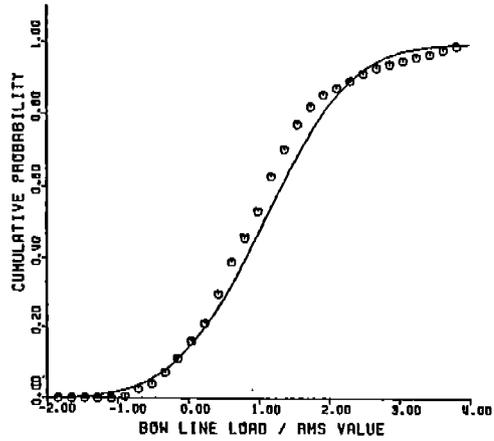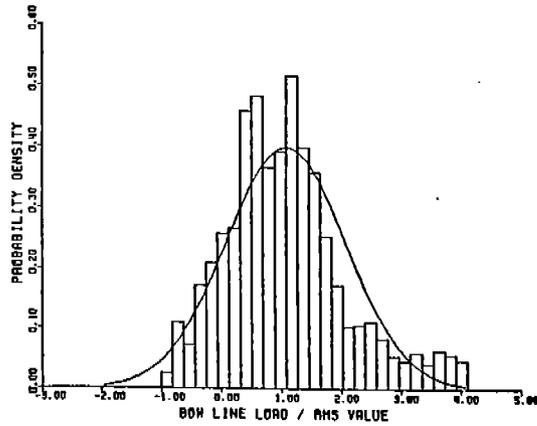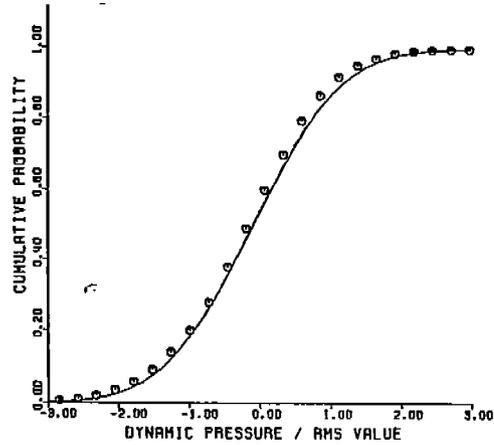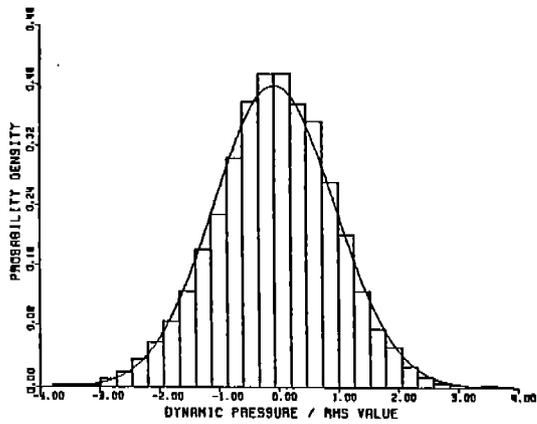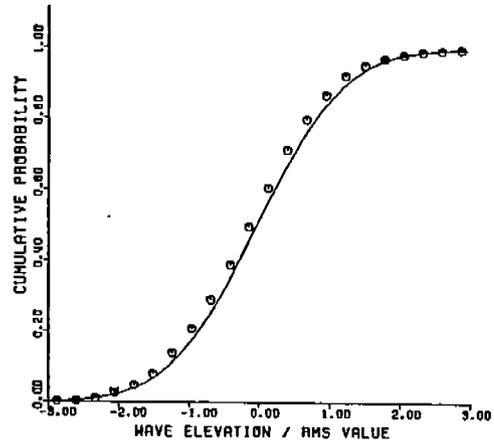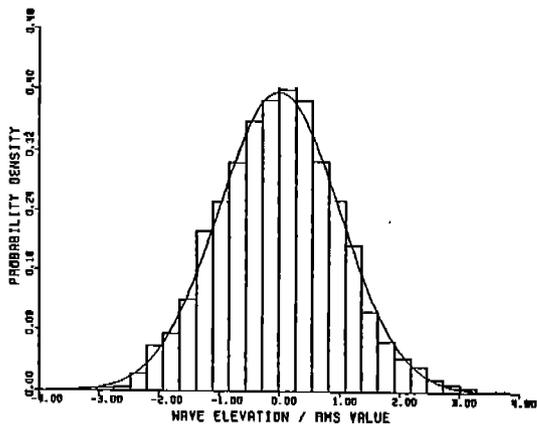
FIGURE 3.79 CORRELATION OF MEASURED WAVE, PRESSURE AND LINE LOAD
DISTRIBUTIONS WITH GAUSSIAN FOR JONSWAP WAVE ON A
SEMISUBMERSIBLE

linear or nonlinear depending on the type and size of them. Thus, it is understood that long-term response statistics would include both linear and nonlinear response parameters. In long-term statistics, a few statistical parameters representing individual short-term seas, whether linear or nonlinear, are required. Thus, the long-term statistics involve parameters obtained from both linear and nonlinear analysis, even though many of the severe seas will produce parameters involving a nonlinear system.

There are two types of information useful in the study of the long-term statistics of waves. One is the sea severity. The severity of sea is generally expressed in terms of the significant wave height or significant wave height coupled with the associated zero-crossing or modal wave periods. In this case, the probability distribution of H_s or the joint distribution of H_s and $\bar{T}_z$ (or T_0) is needed. The other type of information is the long-term probability of individual wave heights.

Unlike individual waves in the short-term record, no theoretical method is available to derive the probability distribution of the significant wave heights or the joint distribution of H_s and T_z. These distributions are obtained from actual measurements in the oceans at frequent intervals over a reasonable period of time (e.g., several years). The distributions of these significant wave heights have been compared with known distribution functions in order to examine their suitability. Of the available distribution functions, e.g., described in Section 3.1, the common ones considered most often are the Weibull and log-normal distribution. Correlations have shown [Ochi (1982)] that the Wiebull distribution is poor at small H_s values while log-normal underestimates H_s, at the large values of H_s. The log-normal distribution seems to be slightly better, in general, and has certain advantages, as well.

The zero-crossing wave periods have also been found to follow log-normal distribution quite well. Since both height and period individually follow log-normal distribution, it may be shown [Ochi (1978)] that their combined statistical properties follow bivariate log-normal probability law.

A long-term probability defines events and extreme value statistics for a period on the order of 20-100 years, as opposed to a few hours for the short-term probability. The concept of extreme waves is associated with that of design waves for an offshore structure. In order to obtain a long-term

148

probability of wave heights, the wave height data at a particular site are collected over the period of a few years. The wave heights are plotted on a suitable probability distribution paper so that the distribution of the data appears as a straight line. Then the straight line is extended to the desired return period to obtain the extreme wave height.

If information is available for numerous short-term statistics of the wave heights then the long-term probability of wave heights may be obtained by the following simple method of order statistics. The short-term wave heights are ranked in the order of higher wave heights. If there are N short-term wave heights over a long-term period such that T_L is the long-term period and T_S is the short-term period, then

$$N = \frac{T_L}{T_S} \qquad (3.375)$$

T_L is also termed the return period or recurrence interval of the maximum wave. The probability distribution of the wave height is given by

$$P(H_m) = \frac{m}{N + 1} \qquad (3.376)$$

and the probability of exceeding a given height is

$$Q(H_m) = 1 - \frac{m}{N + 1} \qquad (3.377)$$

In order to obtain the total probability, this figure should be multiplied by the short-term probability. The long-term probability could seldom be obtained by the above method because of lack of long-term wave data. Therefore, one has to rely on a theoretical probability distribution function. There are several such formulas available as discussed in Section 3.1. Suitability of these formulas to a particular instance may be established with limited field data that may be available. Since little or no data are usually available at the upper tail of the probability distribution, fitting different distributions and choosing the most suitable one is always a difficult task.

3.5.1 Bivariate Short- and Long-Term Distribution

3.5.1.1 Short Term

Because of the variability of wave spectral shape, Ochi (1978) advocated use of a family of wave spectra for given significant wave height and peak frequency. Using the two-parameter spectral model of modified P-M, he showed that in the short term ($P(\bullet) < 0.99$), the significant wave height and peak frequency follow log-normal distribution. The statistical properties of combined wave height and wave period then follow a bivariate log-normal probability distribution. The conditional distribution of the peak frequency, ω_0, for a given significant wave height, H_s, is written as

$$p(T_0|H_s) = \frac{1}{\sqrt{1-\rho^2}\,\sigma_{T_0}\,\sqrt{2\pi}\,T_0} \exp\left[-\frac{1}{2} \frac{\ln T_0 - \mu_{T_0|H_s}}{\sqrt{1-\rho^2}\,T_0} \right] \quad (3.378)$$

where the probability of T_0 refers to a given H_s, $\omega_0 = 2\pi / T_0$ $\rho =$ correlation coefficient between wave height and period, μ and σ refer to mean and standard deviation and

$$\mu_{T_0|H_s} = \mu_{T_0} \rho \frac{\sigma_{T_0}}{\sigma_{H_s}} (\ln H_s - \mu_{H_s}) \quad (3.379)$$

Analyzing the recorded North Atlantic wave data, Ochi (1978) obtained the expressions for the most probable as well as the upper and lower values of the peak period. The most probable peak period is given by

$$T_0(m) = \exp\left[\mu_{T_0} + \rho \frac{\sigma_{T_0}}{\sigma_{H_s}} (\ln H_s - \mu_{H_s}) - \sqrt{1-\rho^2}\,\sigma_{T_0} \right] \quad (3.380)$$

while the upper and lower values of the peak period for a given confidence, γ, is written as

150

$$T_0(\gamma) = \exp \left[\mu_{T_0} + \rho \frac{\sigma_{T_0}}{\sigma_{H_s}} (\ln H_s - \mu_{H_s}) \pm x \sqrt{1 - \rho^2} \, \sigma_{T_0} \right] \qquad (3.381)$$

where the confidence level, γ (= Φ) is a standard normal for the argument x,

$$\Phi(x) = \frac{1}{\sqrt{2\pi}} \int_{-\infty}^{x} e^{-t^2/2} \, dt \qquad (3.382)$$

In particular, the values of x are

x	Φ
1.96	0.95
1.44	0.85
1.15	0.75
0.67	0.50

If x is set equal to 1 in Eq. 3.381, then the most probable value of T_0 (Eq. 3.380) is obtained. From the mean North Atlantic data the peak period for various confidence coefficients are shown as functions of the significant wave heights. The equations for the peak frequency for the various confidence values are given in Table 3.6.

An example of how this family of spectra may be used to predict the extreme responses, the formulas for the most probable extreme value and the design extreme value are considered as follows. The design extreme value of a response amplitude, $\hat{y}_n$, is given in

$$\hat{y}_n(R) = 2 \ln \left\{ \frac{T_s}{2\pi(R/N)} \sqrt{\frac{m_0}{m_2}} \right\} \sqrt{m_0} \qquad (2.383)$$

in which R = risk factor, T_s = largest duration of sea in secs., and N = number of encounters with a specified sea in the structure's lifetime. For the most probable value, $\overline{y}_n$, in the above equation, R = 1, and N = 1.

Ochi (1978) presented results of a numerical analysis on a semi-submersible in which the transverse forces in a beam sea are computed. The extreme values of the transverse forces for various seastates are shown in

151

Fig. 3.80. The most probable as well as upper and lower extreme values for the modified P-M spectra are given in the figure. In the computation, the beam seas are assumed to be exposed a quarter of the assumed 20 year life.

3.5.1.2 Long Term

In contrast to the short-term prediction, the long-term prediction experiences all waves encountered by the structure, large and small. This is important from the standpoint of the fatigue life of the structure. The long-term predictions also deal with the extreme of the response in the lifetime of the structure. In order to evaluate the long-term extreme response, the long-term wave statistics must be known. This may be accomplished in the form of the frequency of occurrences of all possible seastates or the long-term joint probability distribution of wave height and wave period.

The frequency of occurrence for the seastates in the North Atlantic was obtained by Ochi (1978) and is shown in Table 3.7. The product of this and the short-term probability of a family of seastates may be obtained as the long-term probability. The short-term probability will depend on whether the system is linear or nonlinear. The probability function for the nonlinear system depends on the type of nonlinearity, some of which have already been covered in Chapter 3.

The short-term distribution of a narrow-banded Gaussian response variable, x, follows the Rayleigh distribution function

$$P_s(x) = 1 - \exp(-x/\sqrt{E})^2 \qquad (3.384)$$

where $\sqrt{E}$ varies linearly with wave amplitude, and is estimated from wave spectra and transfer functions by means of the linear superposition principle. Thus, the statistical short-term distribution of a response variable is completely defined by one single parameter, E, for given structure size, heading angle, forward speed and seastate $(\bar{T}, H_s)$. For nonlinear systems, E will not vary linearly with H, but a single response value may be obtained for a given seastate. In this case, Rayleigh distribution function is not appropriate, and additional parameters may be needed to describe the probability.

152

TABLE 3.6

MODAL FREQUENCIES FOR THE (MEAN) NORTH ATLANTIC WAVE SPECTRA

AS FUNCTIONS OF SIGNIFICANT WAVE HEIGHT [OCHI (1978)]

	γ	VALUE OF ω_0
Lower ω_0	0.95	$0.048 \ (8.75 - \ell n \ H_s)$
	0.85	$0.054 \ (8.44 - \ell n \ H_s)$
	0.75	$0.061 \ (8.07 - \ell n \ H_s)$
	0.50	$0.069 \ (7.77 - \ell n \ H_s)$
Most Probable		$0.079 \ (7.63 - \ell n \ H_s)$
Upper ω_0	0.50	$0.099 \ (6.87 - \ell n \ H_s)$
	0.75	$0.111 \ (6.67 - \ell n \ H_s)$
	0.85	$0.119 \ (6.65 - \ell n \ H_s)$
	0.95	$0.134 \ (6.41 - \ell n \ H_s)$

NOTE: ω_0 in rps

H_s in meters
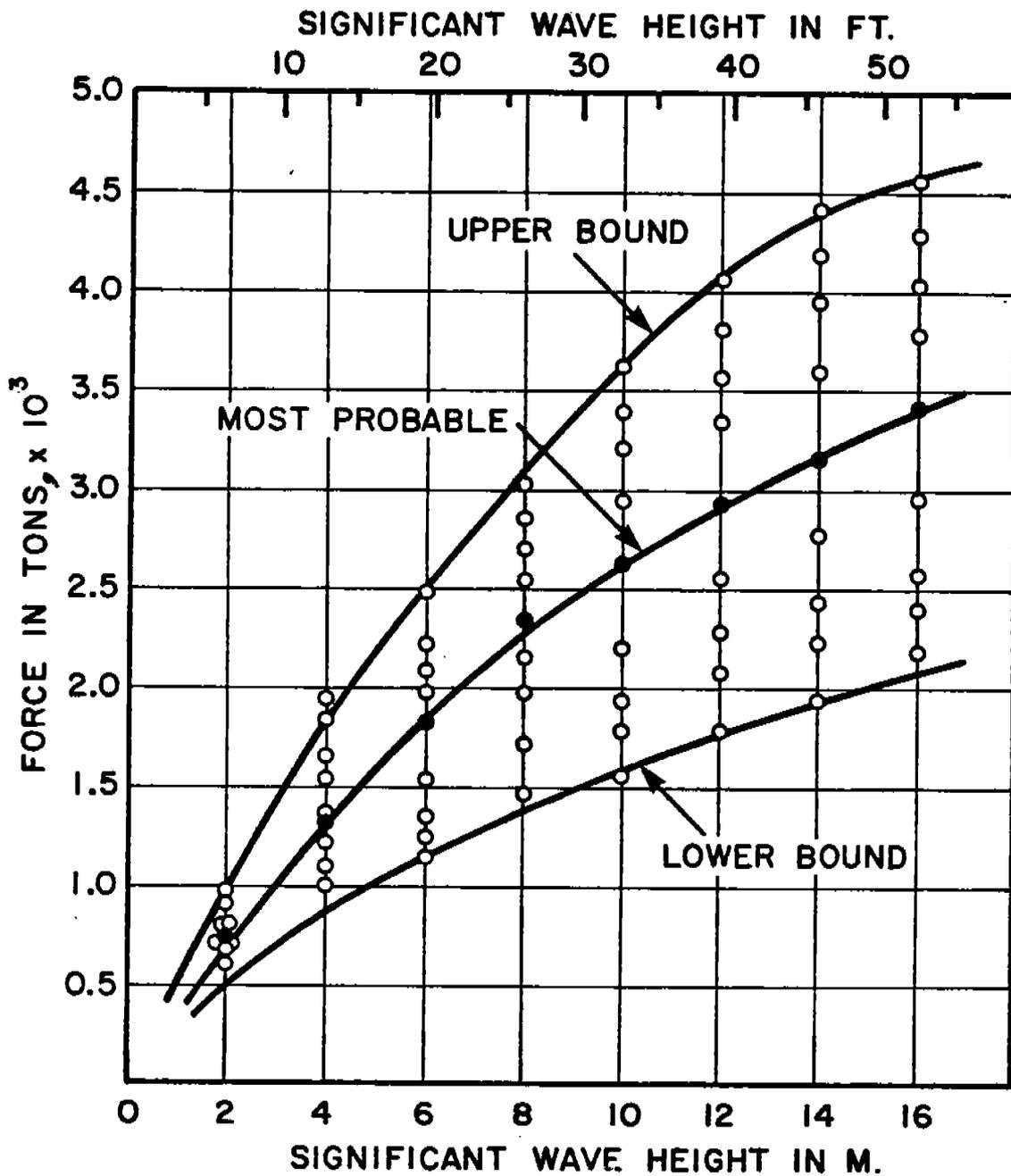
FIGURE 3.80 PROBABLE EXTREME VALUES OF TRANSVERSE FORCE IN VARIOUS SEASTATES COMPUTED BY USING TWO-PARAMETER FAMILY OF WAVE SPECTRA [OCHI (1978)]

TABLE 3.7

FREQUENCY OF OCCURRENCE OF VARIOUS SEASTATES

IN THE (MEAN) NORTH ATLANTIC [OCHI (1978)]

SIGNIFICANT WAVE HEIGHT (m)	FREQUENCY OF OCCURRENCE	SIGNIFICANT WAVE HEIGHT (m)	FREQUENCY OF OCCURRENCE
<1	0.0503	9 - 10	0.0079
1 - 2	0.2665	10 - 11	0.0054
2 - 3	0.2603	11 - 12	0.0029
3 - 4	0.1757	12 - 13	0.0016
4 - 5	0.1014	13 - 14	0.00074
5 - 6	0.0589	15 - 16	0.00045
6 - 7	0.0346	16 - 17	0.00012
7 - 8	0.0120	> 17	0.00009
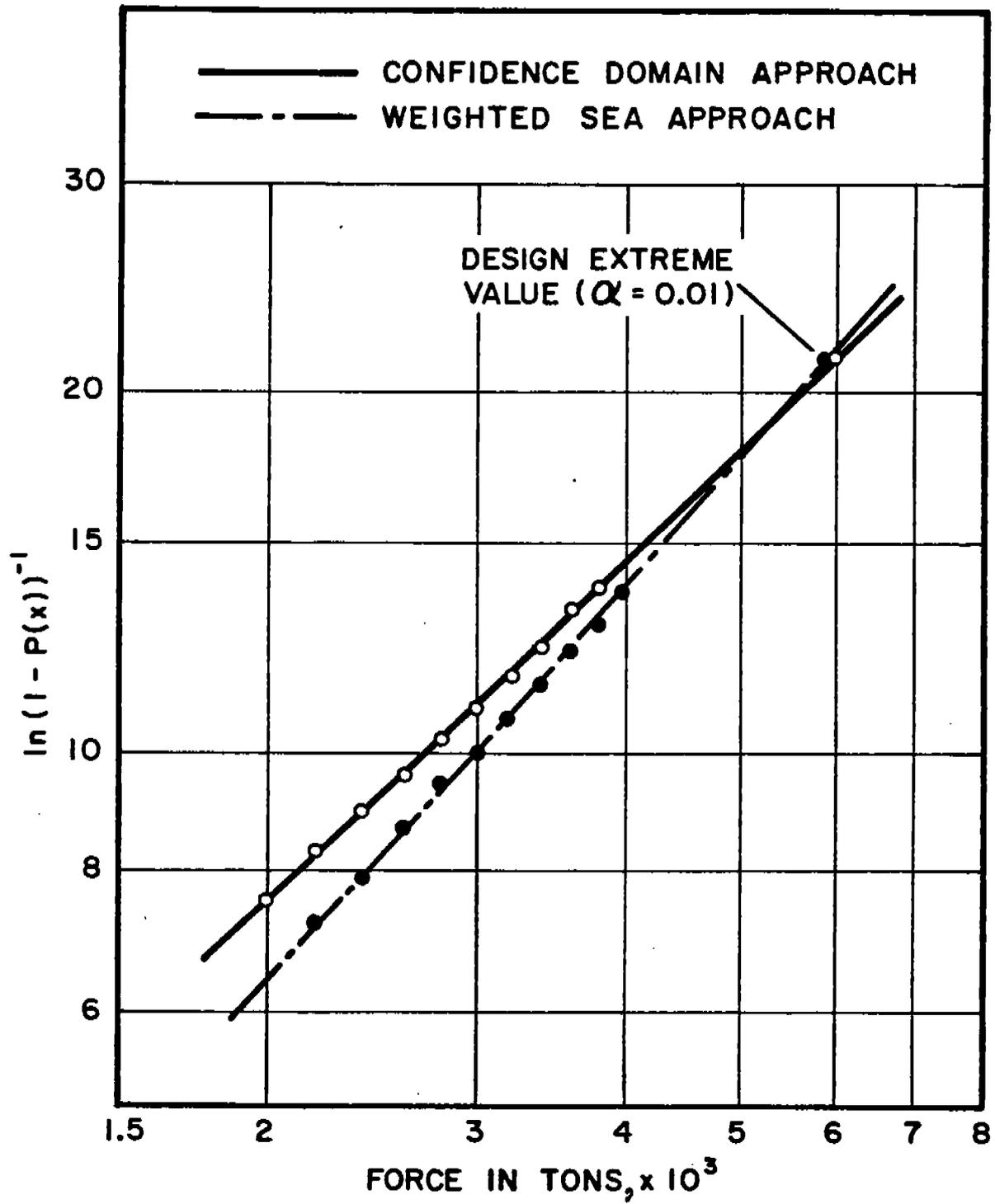
FIGURE 3.81   DESIGN EXTREME VALUE OF TRANSVERSE FORCE EVALUATED BY USING
TWO-PARAMETER FAMILY OF WAVE SPECTRA [OCHI (1978)]

The long-term non-stationary response process is written as a sum of a large number of short-term stationary processes. Therefore,

$$P_L(x) = \int_0^\infty P(x)p(\sqrt{E}) \, d\sqrt{E} \qquad (3.385)$$

where P_L is the long-term probability.

The long-term distribution of $\sqrt{E}$ is sometimes assumed log-normal. Likewise, the long-term distribution of response amplitudes is assumed log-normal [Jasper, et al. (1956)].

Nordenstrom, et al. (1973) obtained a long-term distribution from data from seven different ships by formal integration of the above equation. They grouped the measured $\sqrt{E}$ values (of longitudinal bending moments) into five Beaufort groups and found that the long-term distribution of $\sqrt{E}$ within each group was approximately a normal distribution. The integration was carried out separately for each Beaufort group and the final long-term distribution of amplitudes was obtained as a weighted sum of long-term distributions for Beaufort groups.

Lewis (1973) made a similar analysis for ship bending stress. The actual stress (trough to peak) in any record were Rayleigh distributed. The total weather system was divided into n weather groups. In each weather group, the mean square values of stress, $\sqrt{E}$ from many records were normally distributed.

Nordenstrom (1973) investigated a distribution function which was in-between the normal and log-normal, but closer to the normal one and was capable of describing the entire range of $\sqrt{E}$. This function was found as the Weibull distribution function

$$P(\sqrt{E}) = 1 - \exp\left[-\left(\sqrt{E}/a \right)^m \right] \qquad (3.386)$$

where a and m are parameters. Note that $m = 1$ gives exponential distribution while $m = 2$ yields the Rayleigh distribution. The Weibull distribution was based on 1577 full scale recordings of longitudinal stress amidships on seven ships, as well as other published data. The resulting long-term distribution of amplitudes was found to be another Weibull distribution

153

$$P(x) = 1 - \exp \left[\frac{1}{b} \left(\frac{x}{a} \right)^2 \right]^k \tag{3.387}$$

where the parameters b and k are functions of m. A method of obtaining this Weibull distribution and the values of the parameters involved has been described by Nordenstrom.

The long-term response depends at least on the following quantities each having an assigned weighting factor: (a) sea severities, (b) spectral shape, and (c) number of cycles in the response due to a seastate. Considering these factors, the long-term probability density function is given by

$$p_L(x) = \frac{\sum\limits_i \sum\limits_j N_s \, p_i \, p_j \, p(x)}{\sum\limits_i \sum\limits_j N_s \, p_i \, p_j} \tag{3.388}$$

where $p(x)$ = short-term response probability density function

N_s = number of short-term responses = $\frac{1}{2\pi} \sqrt{m_2/m_0}$

p_i = weighting factor for sea condition (state)

p_j = weight factor for wave spectrum shape

The total number of response expected for the lifetime of the structure is given by

$$N = \sum\limits_i \sum\limits_j N_s \, p_i \, p_j T_L \tag{3.389}$$

where T_L is lifetime in seconds.

Ochi (1978) utilized the above approach in computing the long-term response of the semisubmersible loads in beam sea. Two different methods produced two probability functions from which the extreme values are shown in Fig. 3.81. Note that the extreme values estimated by the two methods of long-term prediction agree quite well.

3.5.2 Time and Frequency Domain Long-Term Predictions

When the long-term probability density function for a response is not known, whereas the long-term distribution of waves is given in a tabular form

154

in terms of probability level for the pair of wave parameters, H_s and T_z, then the short-term response due to long or short-crested waves are computed first. It is then extended to a long-term distribution based on the available wave data. This method is applicable in the frequency domain for a linear system [e.g., Fukuda (1968)].

Assuming that the response, e.g., the bending moment of a ship addressed by Fukuda is a linear function of the regular wave amplitude, the short-term distribution of the bending moment in a short-term sea follows the Rayleigh distribution. The standard deviation, σ_m of the bending moment in a short-crested wave of constant heading is given by

$$\sigma_m^2 = \int_{-\pi}^{\pi} \int_0^{\infty} [H(\omega, \theta - \theta_0)]^2 \, S(\omega, \theta) \, d\omega \, d\theta \qquad (3.390)$$

where θ = angle between wave component and mean wave direction, θ_0 = ship heading angle with respect to the mean wave direction, and the transfer function, H, corresponds to the heading angle, θ_0. The directional sea may be assumed to be given by the cosine square law

$$S(\omega, \theta) = \begin{cases} \dfrac{2}{\pi} S(\omega) \cos^2\theta, & -\dfrac{\pi}{2} \leqslant \theta \leqslant \dfrac{\pi}{2} \\[2mm] 0, & \text{elsewhere} \end{cases} \qquad (3.391)$$

Then, the variance due to a short-crested sea is given by

$$\sigma_m^2 = \frac{2}{\pi} \int_{-\pi/2}^{\pi/2} \int_0^{\infty} [H(\omega, \theta - \theta_0)]^2 \, S(\omega) \cos^2\theta \, d\omega \, d\theta \qquad (3.392)$$

where $S(\omega)$ is a theoretical or measured spectral energy density. It should be noted here that for the long-term response prediction the shape of the response spectrum is not important; only the variance of the short-term response is needed.

Once the short-term response parameter, σ, for a linear system is known, the probability of exceedance of the variable M (e.g., the amplitude of the bending moment) beyond a given M_1, is given by

$$q(M > M_1) = \exp\left[-\frac{M_1^2}{2 \sigma_m^2} \right] \qquad (3.393)$$

155

Assuming that the probability density function of σ is given by $p_L(\sigma)$, the long-term probability of exceedance is obtained from the integral

$$Q_L(M > M_1) = \int_0^\infty \exp\left[-\frac{M_1^2}{2\sigma^2}\right] p(\sigma)d\sigma \qquad (3.394)$$

which is evaluated by replacing the integral by a summation.

Let p_{ij} denote the long-term frequency of occurrence of a short term wave given by the significant wave height, H_i, and the average period, T_j. Also, let σ_{ijk} denote the short term response parameter for this wave and for a wave angle of θ_k where k is the kth equal interval between $-\pi/2$ and $\pi/2$. Then the probability for all waves at this heading angle, θ_k is given by

$$Q_k(M > M_1) = \sum_i \sum_j \exp\left(-\frac{M_1^2}{2\sigma_{ijk}^2}\right) p_{ij} \qquad (3.395)$$

If it is assumed that the long-term probability is uniformly distributed for heading angles between 0 and 2π, then the total probability is obtained from

$$Q(M > M_1) = \frac{1}{N_\theta} \sum_k Q_k (M > M_1) \qquad (3.396)$$

where N_θ is the total number of intervals of heading angle between $-\pi/2$ to $\pi/2$. Usually a 10-15° increment of heading angle is sufficient for response calculation for the short-crested waves.

The above method is applicable only to linear systems, i.e., systems in which the response function is related to the excitation, e.g., waves, in a linear fashion such that if the wave amplitude is doubled the response amplitude also increases by a factor of two. When this relationship between the wave and the response does not exist, a more elaborate time domain analysis, sometimes termed total system analysis, may be used. It should be noted that this method is extremely time consuming and is prohibitive to use routinely in the design of a structure. It may be used as a benchmark for other more efficient albeit approximate methods.

The time domain analysis is applied to the short-term response prediction. For a given wave energy density spectrum, e.g., given by the

parameters, H_i and T_j, a time history of the wave is generated by one of the methods such as outlined in Chapters 2 and 3.

From the relationship between the response and the regular wave (e.g., wave force given by the Morison equation in terms of the water particle velocity and acceleration), the time history of the response due to the short-term wave (H_i, T_j) may be computed. The method of computation may include a finite-difference or a finite-element scheme and may involve one of the analysis methods outlined in Chapter 2. Considering the variability of the spectral shape for a given (H_i, T_j), it has been proposed by Ochi (1978) and Hoffman and Walden (1977) that a family of wave energy density spectra be used in place of a single spectral model. In this case, several time histories of the response are generated, one for each spectral shape. Similarly, if the wave direction is an important consideration for the response, then a response time history for each increment of wave direction is needed.

From these short-term time histories, a histogram of the extreme values may be constructed. This then will provide the probability density function of the response from which the expected value and variance of the response may be computed. It is sometimes possible to consistently fit a known theoretical distribution through these histograms. In this case, the subsequent analysis is much simpler as illustrated by the Rayleigh distribution for a linear system earlier. Once all the short-term parameters for all possible wave conditions are known by this method, the long term prediction of the response may be carried out by the ordinary statistical method outlined earlier.

3.5.3 Extrapolation of Wave Scatter Diagram to Longer Duration

In order to cover all wave conditions over the entire service life of a structure and obtain statistically reliable response predictions, particularly the extremes, one should choose a period much longer than the period of wave measurements, generally encountered in literature. Thus, extrapolation of the measured wave scatter diagram is needed. Inglis, et al. (1985) showed that it is desirable for the aforementioned reasons to consider a scatter diagram of the sea states that is at least ten times the service life of the structure. This will provide a much better value for the average occurrence of various sea states.

157

A simple method is outlined below to extrapolate a wave scatter diagram to a period that is long compared to the structure's service life. It can be achieved in the following steps [Inglis, et al. (1985)].

1. Plot the cumulative probability distribution of the significant wave height, $P(H_s)$ for the available observations on Weibull scales.

2. Determine the parameters A, B and C of the three parameter Weibull distribution

$$P(H_s) = 1 - \exp\left(-\frac{H_s - A}{B}\right)^C \qquad (3.397)$$

which fits the data.

3. Calculate $P(H_s)$ for a range of values of H_s in excess of the largest H_s in the observations using the above Weibull distribution.

4. Assuming one observation every 3 hours, the total number of observations in 1000 years is 2921940. The number of occurrences in 1000 years, smaller than or equal to H_s^* is

$$N(H_s < H_s^*) = 2921940 \ P(H_s < H_s^*) \qquad (3.398)$$

The number of occurrences of each H_s^* value chosen is

$$N(H_s^*) = N_1(H_s < (H_s^* + \delta)) - N_2(H_s < (H_s^* - \delta)) \qquad (3.399)$$

where δ is half the difference between two adjacent H_s^* values. Sum all numbers of occurrences $N(H_s^*)$ for H_s^* values exceeding the highest H_s in the actual observations; this sum is N_T.

5. The number of occurrences $N(H_s^*)$ are associated with an estimated mean wave period, T_z, such as, assuming a constant wave steepness.

6. The number of actual observations for each (H_s, T_z) pair is finally scaled up by the factor

158

$$\frac{2921940 - N_T}{N_a}$$

<div align="right">(3.400)</div>

where N_a is the actual number of observations. This gives the total number of observations in 1000 years to the required total of 2921940.

3.6 Extreme Value Statistics

The extreme value is defined as the largest value expected to occur in a certain specified period of time. Since the specified time may be equivalently expressed in terms of number of observations of the variable under investigation, extreme value may refer to a specified number of observations. This specified time may be a short-term interval, e.g., within a wave record of 30 min. duration, which is considered statistically invariant. Alternately, it could be long term in terms of the lifetime of the structure. The distribution function, $P(\bullet)$ of the short-term wave heights, as a random variable, is called the initial cumulative distribution for extreme-value statistics. Similarly, the corresponding density function is the initial probability density function. On the other hand, the extreme wave height as a random variable in N observations has a different probability law.

If the initial probability distribution is known, e.g., Rayleigh distribution of wave heights in a short-term sea, then the extreme value is straightforward to compute by the order statistics. On the other hand, the extreme values may be estimated without the precise knowledge of initial distribution if the measured data or maxima are available. In the latter case, an asymptotic extreme-value distribution is obtained.

As mentioned earlier, the probability distribution of extremes is different from the initial distribution. Thus, the probability density function of extreme wave heights, y_n is

$$q(y_n) = n \left[p(x) \left[P(x) \right]^{n-1} \right]_{x = y_n}$$

<div align="right">(3.401)</div>

and the cumulative distribution is

$$Q(y_n) = \left[\left[P(x) \right]^n \right]_{x = y_n}$$

<div align="right">(3.402)</div>

From the above two equations, the probable extreme wave height, $\bar{y}_n$, is derived as

$$\frac{d}{dy_n} q(y_n) = 0 \qquad (3.403)$$

which gives

$$p'(y_n) \, P(y_n) + (n - 1) \, [p(y_n)]^2 = 0 \qquad (3.404)$$

Assuming P to follow Rayleigh distribution, Longuet-Higgins (1952) showed that

$$2 \frac{y_n^2}{x_{rms}^2} \left[n \exp\left(-\frac{y_n^2}{x_{rms}^2} \right) \right] - \left[\exp\left(-\frac{y_n^2}{x_{rms}^2} \right) - 1 \right] = 0 \qquad (3.405)$$

Neglecting second term as small for large N, y_n is solved as

$$\bar{y}_n = \sqrt{2 \ln n} \; x_{rms} \qquad (3.406)$$

which is equivalent to Eq. 3.70.

In the previous discussions, the maxima were assumed to be statistically independent which render the derivation simple. On the other hand, for a narrow-band spectrum, the maxima changes slowly through envelope process and are, therefore, highly correlated. The statistical dependence of maxima may be included through the concept of Markov chain condition. In this method, the magnitude of a maximum point depends on the immediately previous one, but not any other prior ones. In this case, the joint probability distribution of two successive maxima is needed. This is illustrated and derived by Ochi (1982).

In the approximate method, measured or observed maxima over a certain period (e.g., a number of years) are ranked and fitted with known probability distribution curve. If the fit is good, the distribution function is used to obtain extremes. In case the match is poor, the ranked data are plotted on a probability paper as

$$1 - P(x) = \frac{1}{n} \qquad\qquad (3.407)$$

and extended for extremes over a certain return period. However, this method may not be satisfactory as it relies on highest waves whose measurement may not be very reliable. An alternative scheme of representation by fitting the entire data by a least squares method has been discussed by Ochi and Whalen (1980).

TABLE 4.1
POLYNOMIAL APPROXIMATION OF NONLINEAR RESPONSES

TYPE OF NONLINEARITY	NONLINEAR TERM	POLYNOMIAL APPROXIMATION	REMARKS	SOURCE
Wave Drag	$\|u\|u$	$2\sqrt{\frac{2}{\pi}}\,\sigma_u u$	Linear Term	Borgman (1969)
Wave Drag	$\|u\|u$	$\sqrt{\frac{2}{\pi}}\,\sigma_u u + \frac{1}{3}\sqrt{\frac{2}{\pi}}\frac{u^3}{\sigma_u}$	Linear & Cubic	Borgman (1969)
Wave Drag	$\|u\|u$	$\frac{3}{4}\sqrt{\frac{2}{\pi}}\,\sigma_u u + \frac{1}{2}\sqrt{\frac{2}{\pi}}\frac{u^3}{\sigma_u} - \frac{1}{60}\sqrt{\frac{2}{\pi}}\frac{u^5}{\sigma_u^3}$	Linear & Cubic & Quintic	Borgman (1969)
Hydrodynamic Damping	$\|\dot{x}\|\dot{x}$	$2\sqrt{\frac{2}{\pi}}\,\sigma_{\dot{x}}\dot{x}$	Linear Damping	
General Damping Term	$\|\dot{x}\|^{\alpha-1}\dot{x}$	$2^{\alpha/2}\sqrt{\frac{2}{\pi}}\,\Gamma\left(\frac{\alpha+2}{2}\right)\sigma_{\dot{x}}^{\alpha-1}\dot{x}$	$\alpha = 0$ Coulomb, $\alpha = 1$ linear, $\alpha = 2$ drag	Brouwers (1982)
Wave Plus Current Drag	$\|u - U\|(u - U)$	$C_0 + C_1(u - U)$ $C_0 = (\sigma_u^2 - U^2)[2\beta(\gamma)-1]+2U\sigma_u\phi(\gamma)$ $C_1 = -2U[2\Phi(\gamma)-1]-4\sigma_u\phi(\gamma)$ $\gamma = \frac{U}{\sigma_u};\ \phi(x) = \frac{e^{-x^2/2}}{\sqrt{2\pi}};\ \Phi(x) = \int_{-\infty}^{x}\phi(t)dt$	Steady & Linear Terms	Borgman (1972)
Relative Velocity Drag	$\|u - \dot{x}\|(u - \dot{x})$	$\|u\|u - 2\|u\|\dot{x}$	$\dot{x} \ll u$	Eatock Taylor et al. (1982)
Relative Velocity Drag	$\|u - \dot{x}\|(u - \dot{x})$	$2\sqrt{\frac{2}{\pi}}\,\sigma_u(u - \dot{x})$	Linear Terms Only	Eatock Taylor, et al. (1982)

TABLE 4.1 CONT'D

TYPE OF NONLINEARITY	NONLINEAR TERM	POLYNOMIAL APPROXIMATION	REMARKS	SOURCE
Relative Velocity Drag	$\lvert u - \dot{x}\rvert(u - \dot{x})$	$\sqrt{\dfrac{2}{\pi}}\,\sigma_u\, u + \dfrac{1}{3}\sqrt{\dfrac{2}{\pi}}\,\dfrac{u^3}{\sigma_u} - [\,\sqrt{\dfrac{2}{\pi}}\,\sigma_u$ $-\,\varepsilon\,\sqrt{\dfrac{1}{2\pi}}\,\dfrac{u^2 - \sigma_{u2}}{\sigma_u}\,]\dot{x}$	Linear and Cubic Terms for Small $\dot{x}$	Eatock Taylor, et al. (1982)
Relative Velocity Drag	$\lvert u - \dot{x}\rvert(u - \dot{x})$	$c(u - \dot{x});\ c = 2\sqrt{\dfrac{2}{\pi}}\,\sigma_{V_R};\ V_R = u - \dot{x}$	V_R is Harmonic	Dao & Penzien (1982)
Relative Velocity Drag	$\lvert u - \dot{x}\rvert(u - \dot{x})$	$u_0^2\,\Sigma\,a_m\,\cos m\,\omega t + 2\sqrt{\dfrac{2}{\pi}}\,u_0\,\dot{x}$ a_m = Fourier Coefficients	u is Harmonic	Dao & Penzien (1982)

NOTE: $u = u(t)$ and $\dot{x} = \dot{x}(t)$ are random functions of time, t, and the current U is steady.

4.0 EVALUATION OF PROBABILISTIC APPROACHES

Several different methods have been described in the previous chapter (Chapter 3) in handling nonlinear problems in the prediction of extreme response values. These methods are evaluated here regarding their assumptions and limitations. Limiting values of their application are prescribed wherever possible.

4.1 DISCUSSION OF LINEARIZATION TECHNIQUE

One of the common methods of handling the stochastic description of nonlinear responses is to linearize the nonlinear terms. Sometimes it is convenient to retain the first few terms of the polynomial approximation thus maintaining some of the nonlinearities in the system. In the linear case the probabilistic description of the responses is simple and straightforward specially if the sea surface is assumed to be a Gaussian random variable. When higher order terms of the polynomial series are retained the problem is somewhat more complex but is still solvable in a number of cases.

Different methods of linearization have already been presented in Section 3. Let us discuss the limits of applicability of these various linearized terms. The often used polynomial approximations of several common nonlinear terms are summerized in Table 4.1. The nonlinear terms in the table relate to the drag term of the Morison formula or its modified form including damping and relative velocity terms. As such, they have wide applications in the analysis of marine and offshore structures for both the evaluation of exciting forces and corresponding responses.

On small members of a jacket structure, or on structures with flat surfaces and sharp corners where flow experiences separation the wave drag or wave-current drag is important. On moving structures, e.g. most of the floating structures that experience resonance the hydrodynamic damping term may be significant. On moving members, e.g., risers, tendons, catenary lines, the relative velocity drag term should be included.

On large floating structures moored with soft springs, e.g., single-point mooring system, catenary anchored ships and semisubmersibles, slow-drift oscillation occurs in certain degrees of freedom, e.g., surge. In this case, nonlinearity appears from the nonlinear exciting forces (drift force) as well

as nonlinear mooring line characteristics. Floating structures that are tethered with taut vertical lines, e.g., TLP, experiences springing force in their tendons that are nonlinear. In this case, the damping is small and any contribution from the nonlinear damping term may be important.

The most common form of nonlinearity that is often linearized for convenience in the analysis is the nonlinear drag term found in the Morison equation. The nonlinear wave drag term and the corresponding linear, cubic and quintic approximations are shown in Fig. 4.1. The independent variable in these plots is taken as the nondimensional quantity, u/σ_u. The nonlinear term is quadratic. According to this figure, the linear approximation seems to be reasonable for velocities of up to about two standard deviations. The cubic term is good for $u \approx 3\sigma_u$ while the quintic term is close for the velocity up to about 4 standard deviations. In the spectral estimate of the load, the cubic term has been shown to give rise to a triple convolution of the velocity spectrum. Similarly, the quintic term will yield a fifth convolution integral and, thus, will require more time-consuming computations.

The linear approximation of the hydrodynamic damping will provide a similar plot as for the linear term in Fig. 4.1. In fact a similar higher order polynomial approximation may be written for the hydrodynamic damping term. The nonlinear damping term of this form may be handled in an equation of motion by several approximate methods of solution, e.g., the Rayleigh-Ritz averaging technique.

A general damping term may be written in terms of the power of the absolute velocity where $\alpha = 0$ refers to the Coulomb friction. $\alpha = 1$ corresponds to linear damping term while $\alpha = 2$ is the velocity-squared term. Plots are presented in Figs. 4.2-4.3 showing the correlations between the nonlinear and linearized damping terms for $\alpha = 2$ and 3. For $\alpha = 0$, the nonlinear term takes on positive or negative constant values. $\alpha = 1$ corresponds to the linear term and is, thus, exact. The region of correlations for $\alpha = 2$ and 3 is similar.

When current is present in waves the drag force is written in terms of the relative velocity between the waves and current. In this case, the linearization involves a constant term plus a linear term and depends on the strength of the current given by γ (= U/σ_u) in addition to the two coefficients in the two terms. The correlation of the nonlinear drag term and
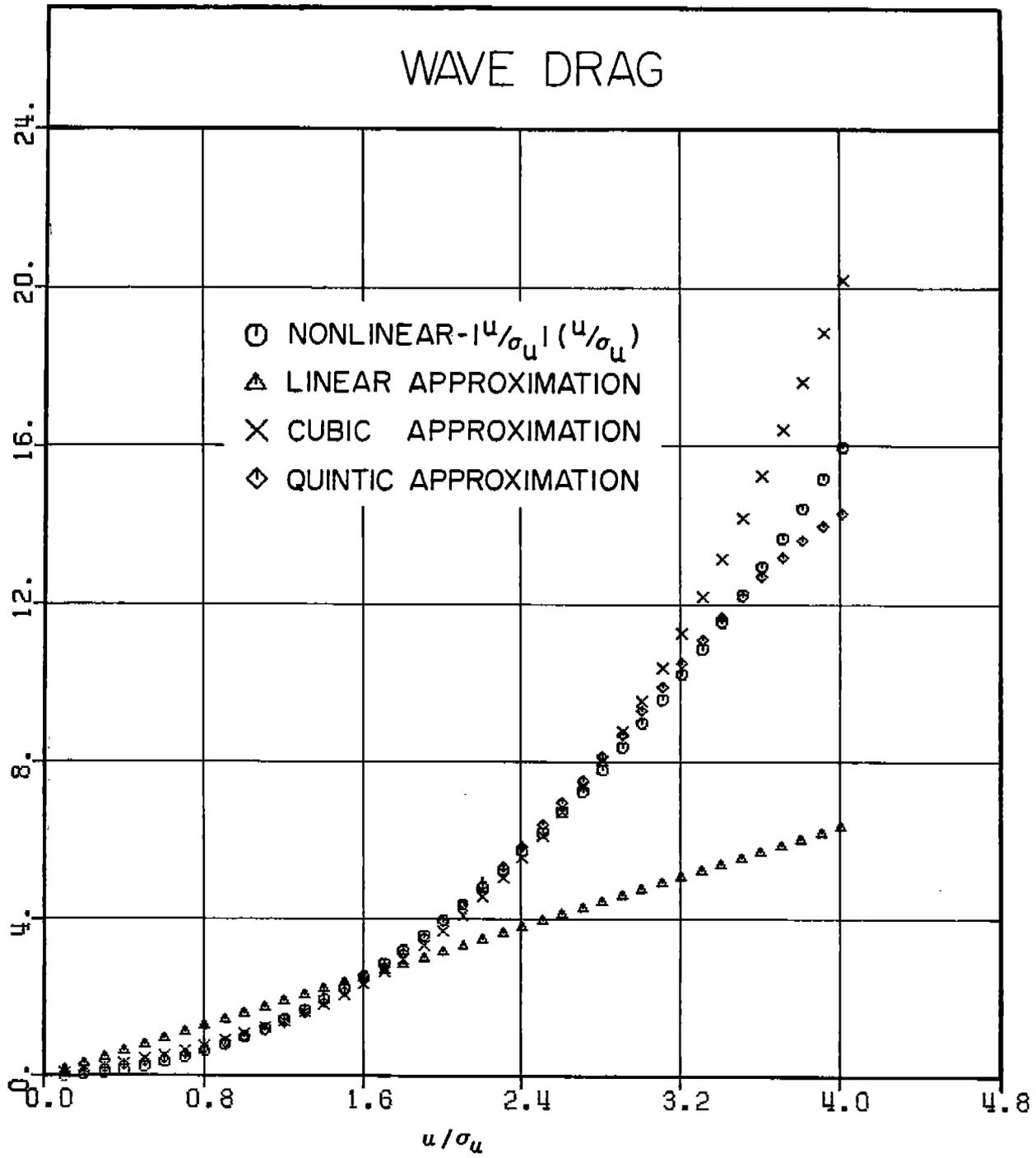
FIGURE 4.1   POLYNOMIAL APPROXIMATIONS OF NONLINEAR WAVE DRAG FORCE
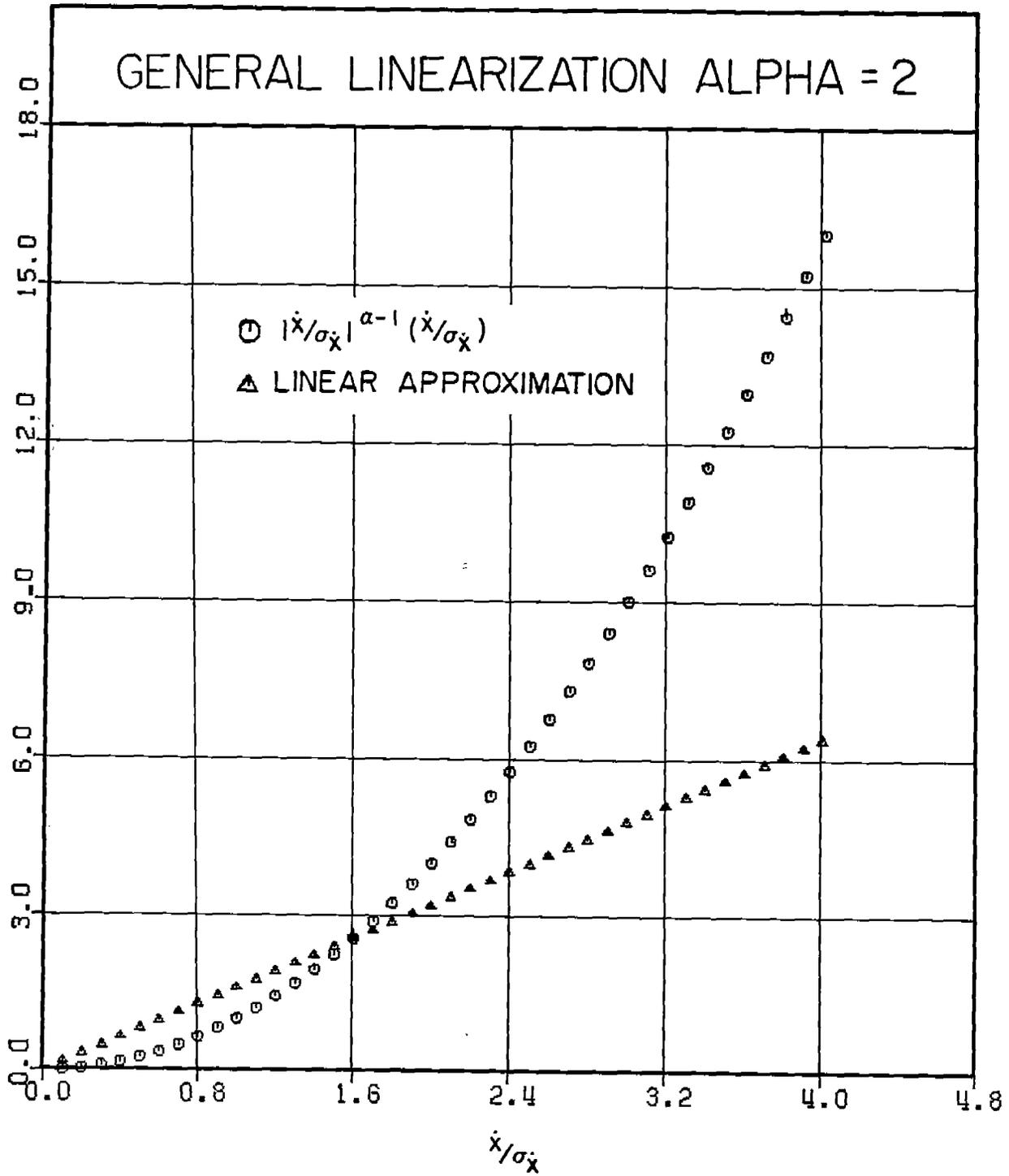
FIGURE 4.2   LINEARIZATION OF NONLINEAR DRAG DAMPING TERM (α = 2)
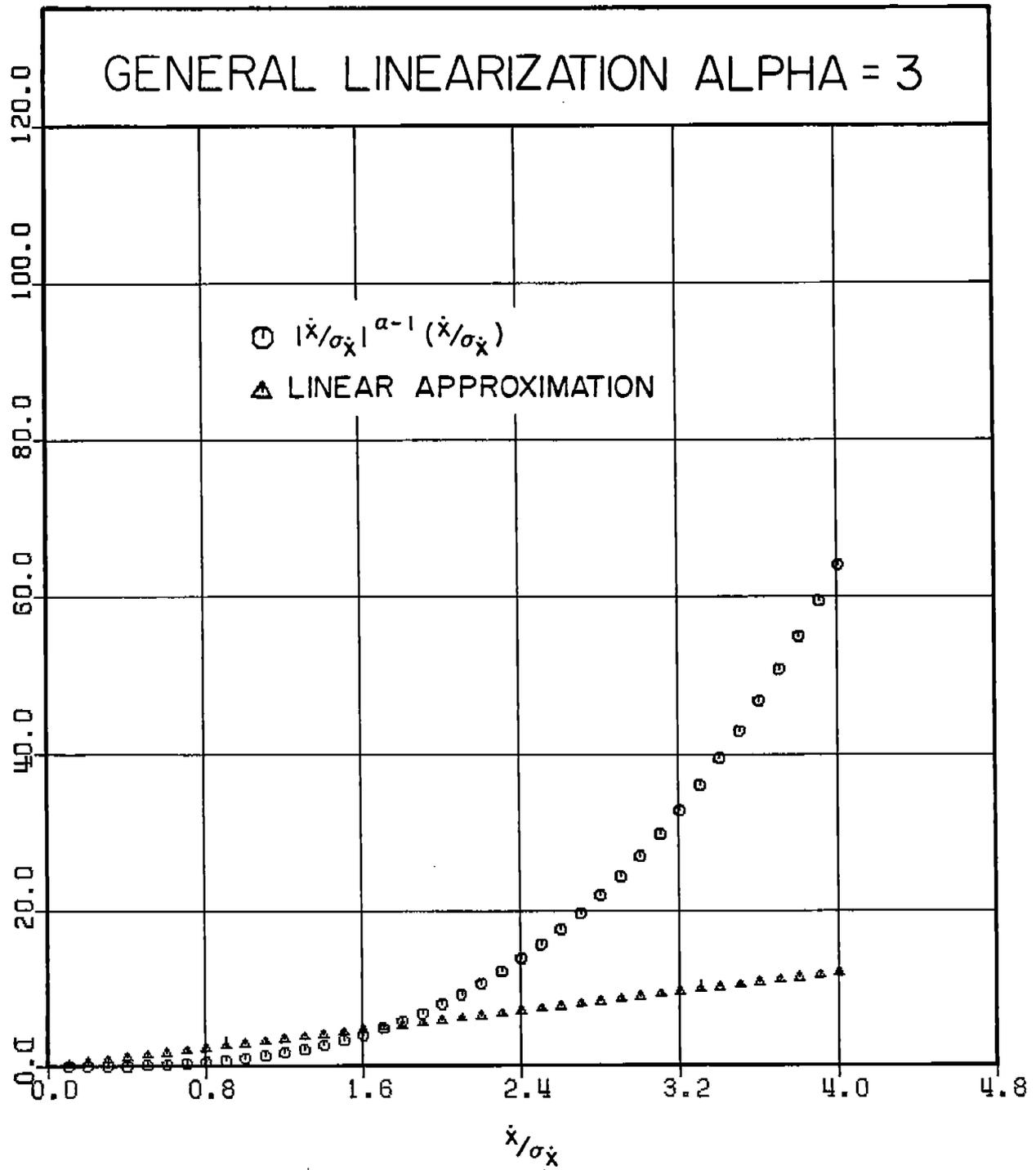
FIGURE 4.3 LINEARIZATION OF HIGHER ORDER NONLINEAR DAMPING TERM
(α = 3)

its linearization is shown in Figs. 4.4-4.6 for different values of γ (= 0.1, 0.5 and 1.0, respectively). Note that the correlation of the linear term becomes poorer as the strength of the current increases.

If the structure is allowed to move, the drag force on the structure is given in terms of the relative velocity between the structure motion and the water particle. In this case, the linearization is achieved [Eatock Tayor, et al. (1982)] in terms of the relative velocity, $u - \dot{x}$, as shown in Table 4.1. The correlation between the nonlinear relative velocity drag term and the linearization for different structural motion amplitudes $\dot{x}/\sigma_u$ = 0.1, 0.2 and 0.3 are shown in Figs. 4.7, 4.8 and 4.9, respectively. In all cases the correlation seems to be good for u/σ_u values of about 2.

4.2 DISCUSSION OF NONLINEAR EXCITATION STATISTICS

The linearization of nonlinear systems is only possible when the non-linearity in the system is relatively small. In Chapter 5, the limits of arguments of nonlinear systems for which linearization technique is applicable without serious errors will be discussed. For predominantly nonlinear systems, this simplified technique is not useful. In these cases, one of the methods outlined for non-Gaussian systems is applicable.

The non-Gaussian random waves found, for example, in shallow waters have several available representations of distribution functions. These take the form of a series either in the probability theory or in the nonlinear wave theory. When waves are nonlinear with sharper peaks than throughs, the series expression in Eq. 3.62 provides one representation for the probability density for the wave heights. This expression is easy to apply, but assumes narrow-banded waves of weak nonlinearity. Another representation of the wave amplitudes (half the crest-to-trough height) is given by the integral representation of Eq. 3.74. In this case, computation of the probability density is more involved in terms of the joint probability of crests and troughs. Both these distributions show that the density value is higher than Rayleigh and occurs slightly ahead of the Rayleigh distribution.

The non-Gaussian probability theory for waves provided the distribution functions represented by the Gram-Charlier series, Edgeworth series and Longuet-Higgins series. These series representations can be extended to any number of terms with added complexity for each additional term. However, the

164
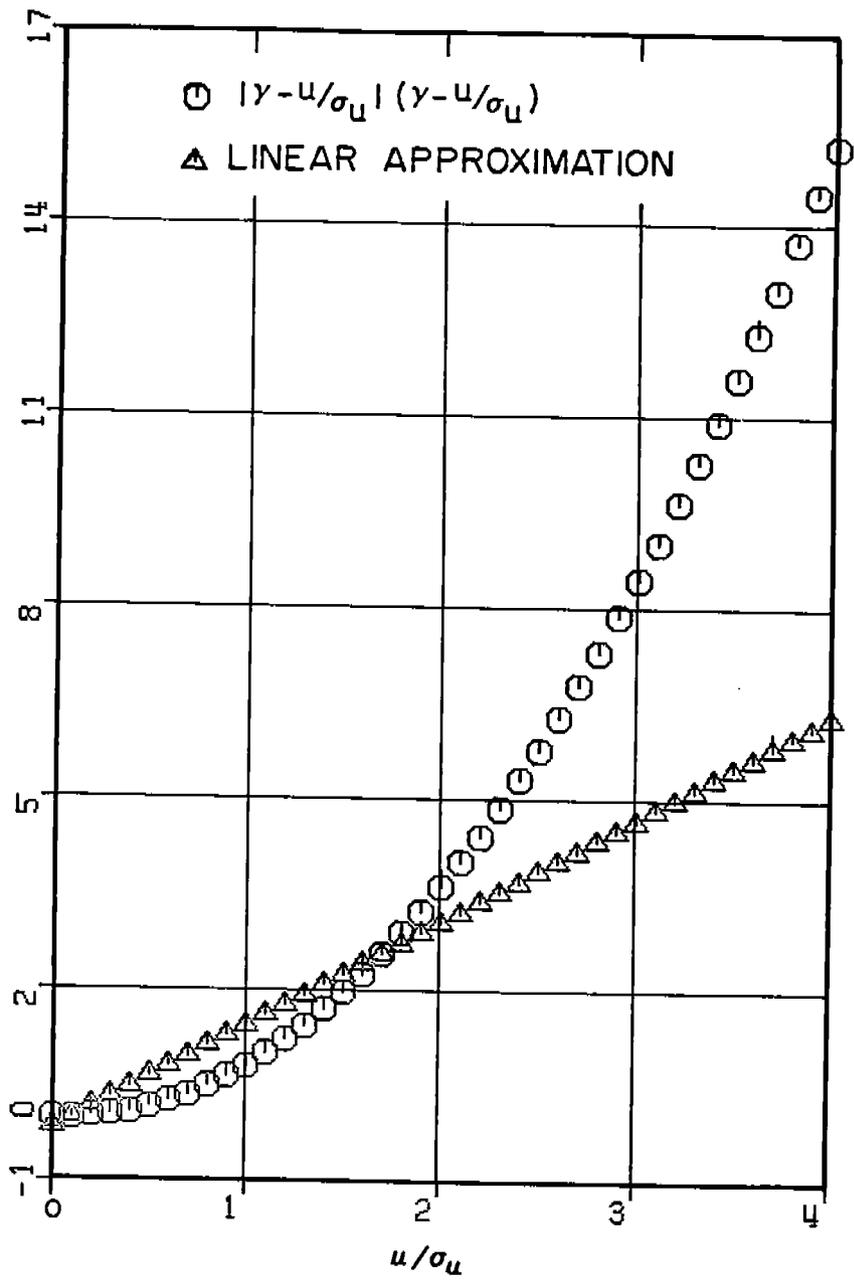
FIGURE 4.4   LINEARIZATION OF WAVE-CURRENT DRAG FOR A CURRENT STRENGTH
OF γ = 0.1
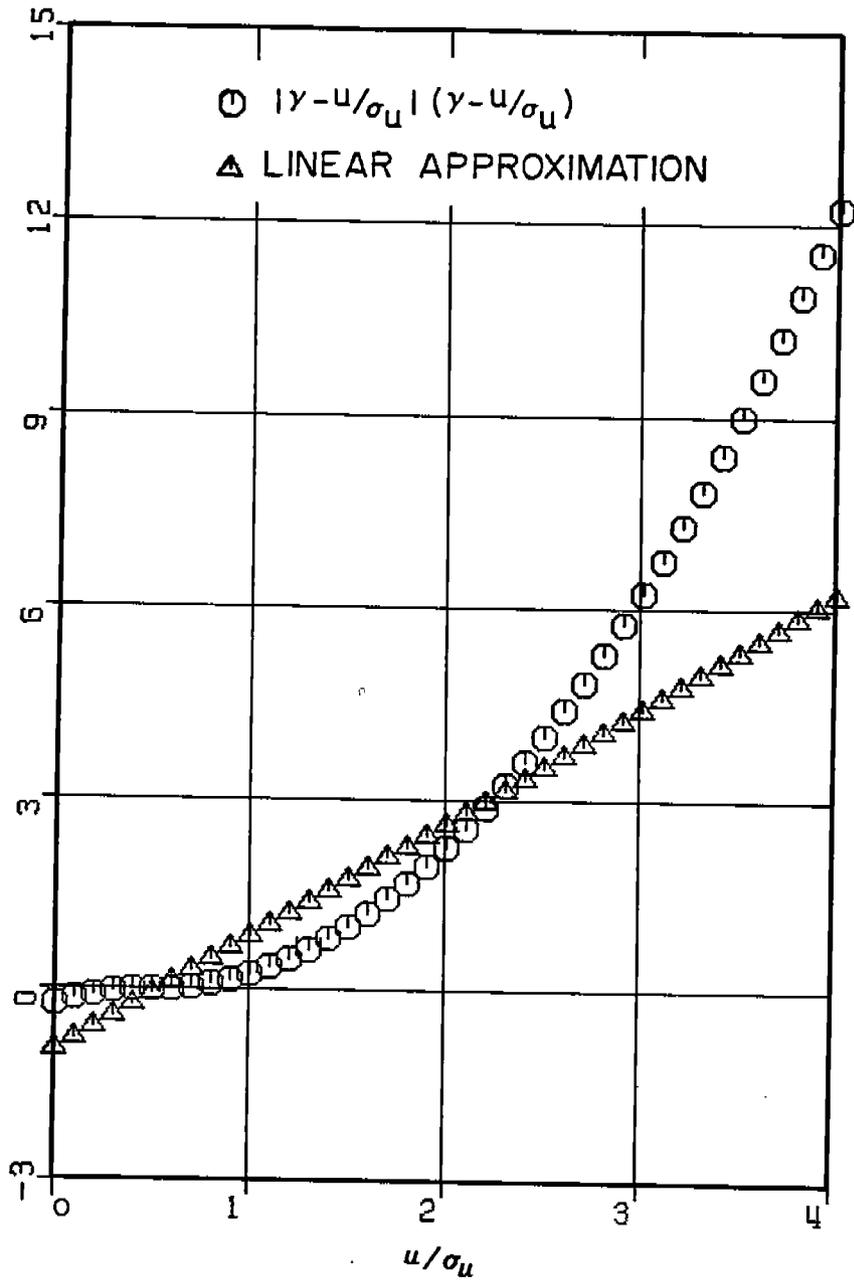
FIGURE 4.5   LINEARIZATION OF WAVE-CURRENT DRAG FOR A CURRENT STRENGTH
OF γ = 0.5
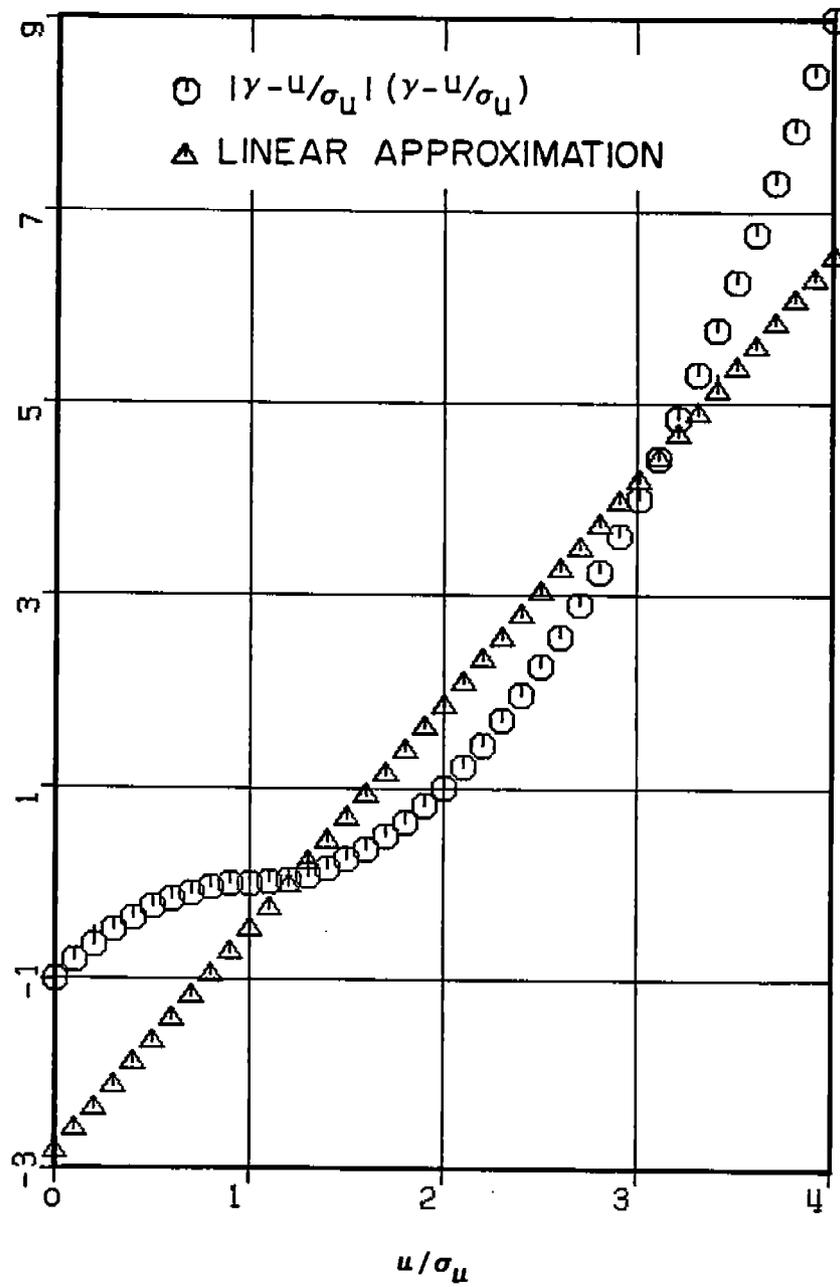
FIGURE 4.6   LINEARIZATION OF WAVE-CURRENT DRAG FOR A CURRENT STRENGTH
OF γ = 1.0
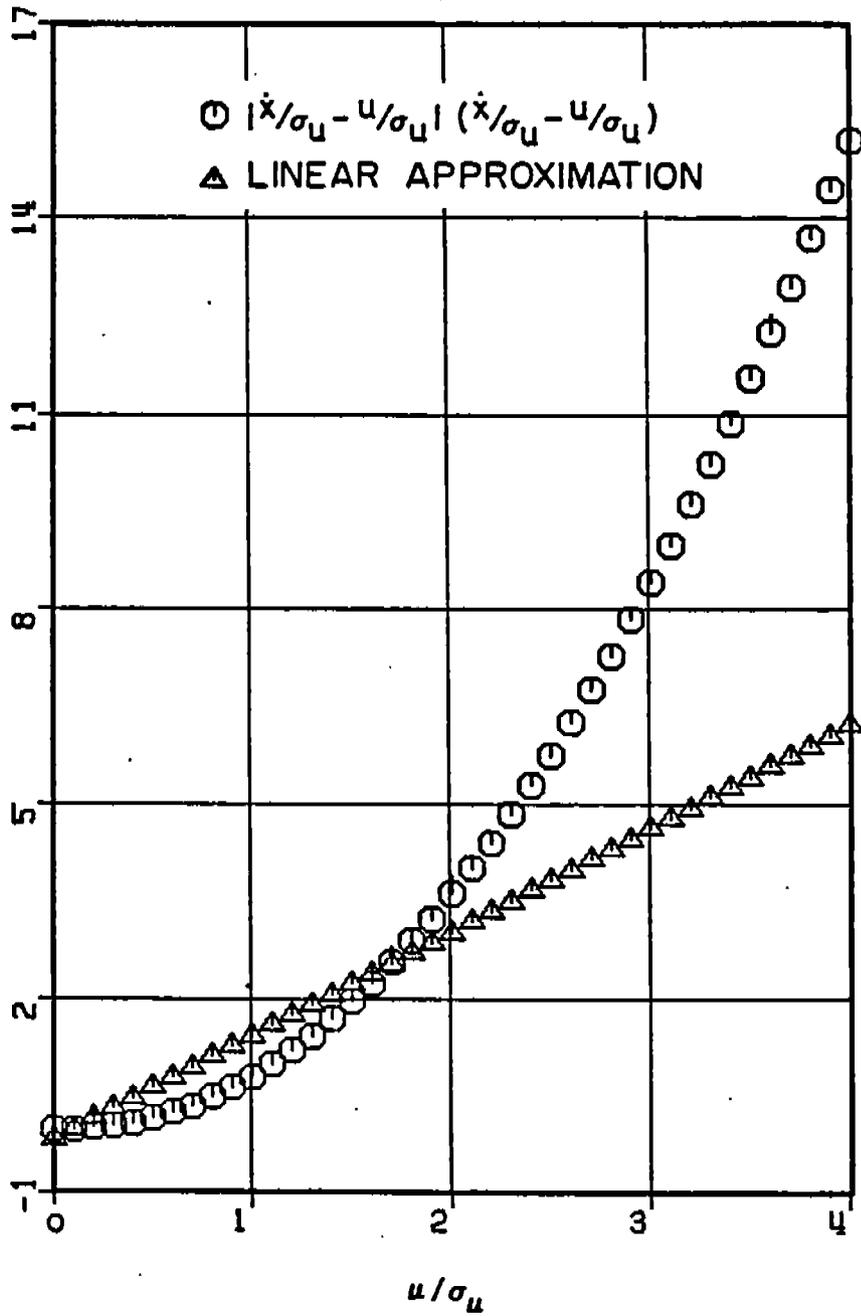
FIGURE 4.7   LINEARIZATION OF RELATIVE VELOCITY DRAG FOR $\sigma_v/\sigma_u = 0.1$
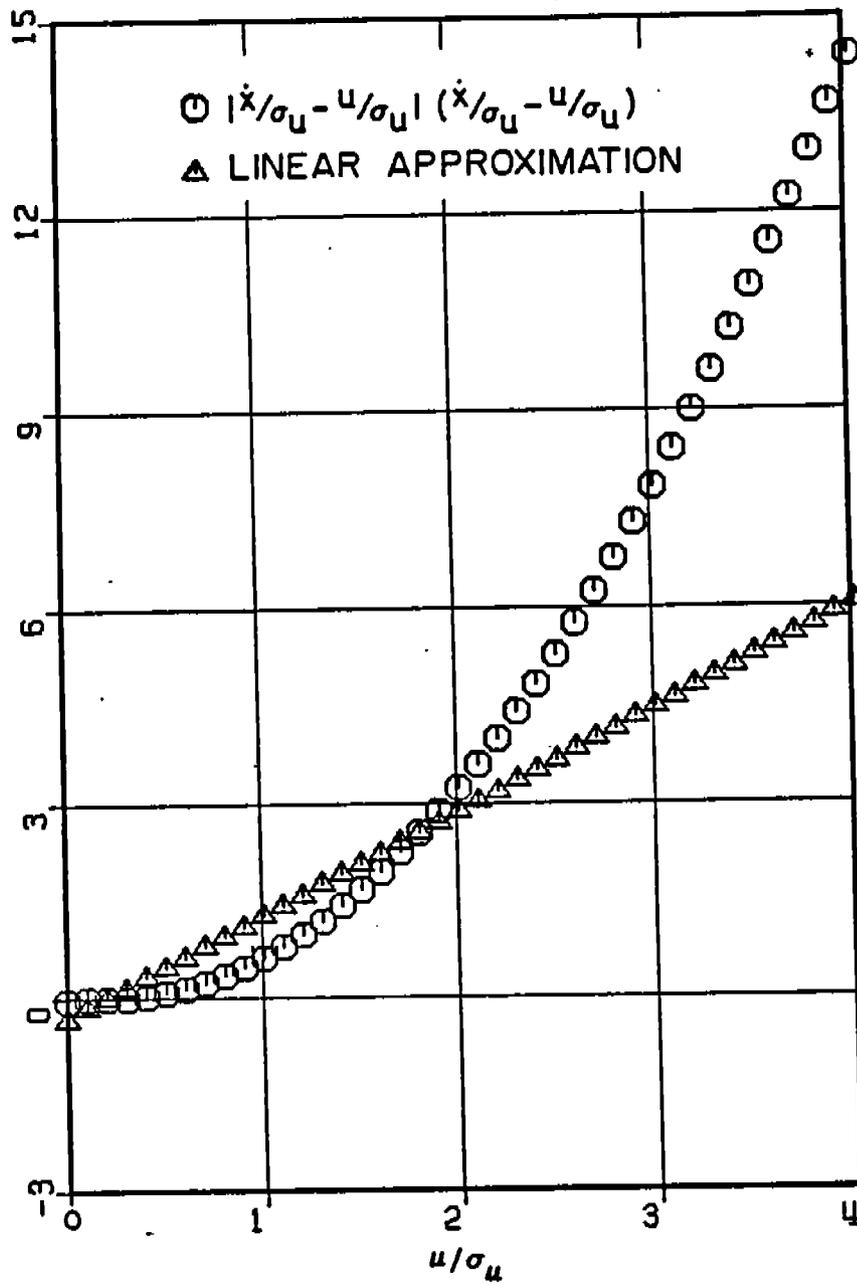
FIGURE 4.8   LINEARIZATION OF RELATIVE VELOCITY DRAG FOR $\sigma_v/\sigma_u = 0.2$
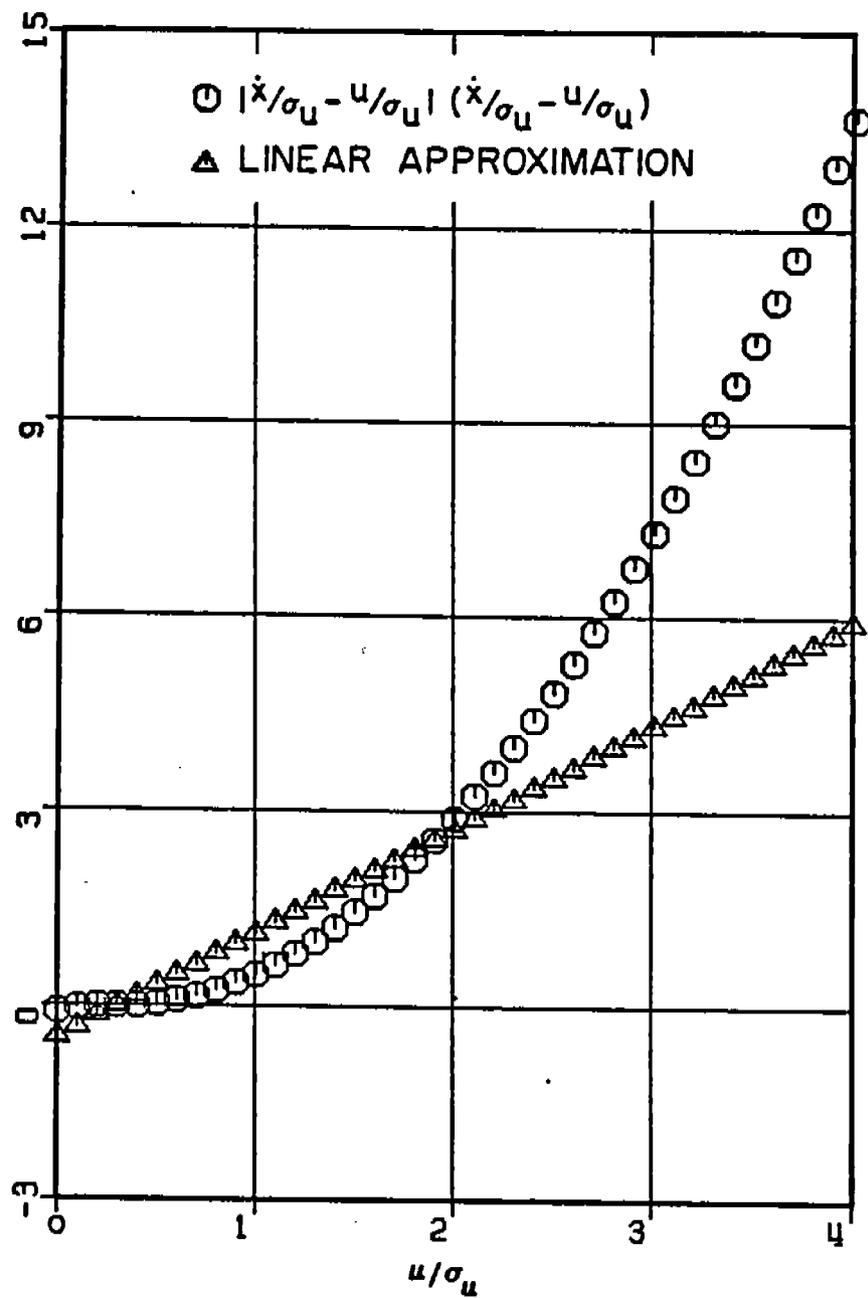
FIGURE 4.9   LINEARIZATION OF RELATIVE VELOCITY DRAG FOR σ_v / σ_u = 0.3

representation does not necessarily improve with added terms, but in fact may deteriorate. For example, the first three terms of the Gram-Charlier series best describes the non-Gaussian waves. Another limitation of this function is that it produces negative density values at large negative wave troughs. The Edgeworth and Longuet-Higgins series suffer from the same drawback. Moreover, the skewness and flatness required by the Edgeworth series are difficult to compute. For the Edgeworth series, approximations up to four terms are sufficient. Another interesting feature of the series is the presence of a second hump indicating a preferred range in the density function near the mean wave amplitude.

For a strong nonlinear system, The Fokker-Planck equation may be applied in which case the degree of nonlinearity may be left as arbitrary. For a single degree of freedom motion system, the equation may be written in terms of a joint probability density function of displacement and velocity (Eq. 3.88). Once the numerical solution is known, the probability density of displacement is obtained. For a practical multi degree of freedom system, however, this procedure is quite involved and time consuming. Moreover, it uses a white noise spectrum as the input for the excitation force.

The probability density functions for nonlinear third-order Stokes waves in deep water as well as in finite water depth are known. For these waves, the probability density values are always positive. The expressions are obtained (Eqs. 3.98 and 3.104) in a closed form in terms of nondimensional surface elevation. This function shows that the non-Gaussian nature of the distribution increases with the increasing value of a slope parameter. For higher slope parameters, the maximum density values increase, and the distribution becomes more and more skewed. For zero slope, it reduces to the Gaussian distribution.

4.3 DISCUSSION OF NONLINEAR RESPONSE STATISTICS

There are basically three types of nonlinearities that are encountered in the analysis and design of an offshore structure. These nonlinearities are grouped according to the stages at which they appear: (1) nonlinear waves, (2) nonlinear external forces and (3) nonlinear responses.

The incident waves based on nonlinear wave theories are non-Gaussian. Theories are available to describe the non-Gaussian characteristics of these waves, some of which are included in Chapter 3 and discussed in Section 4.2. However, they have found limited use thus far in the extreme value analysis. While some attempts have been made in developing nonlinear wave spectra, these have not found applications in the extreme value analysis.

The nonlinear external forces may appear in the form of drag forces exerted on the structural member or may be due to the time varying wetted height of structure. The general form for the nonlinear drag forces is included in the Morison formula (including inertia and drag force) and its several modifications. Some of these modifications discussed in Section 2 are wave-plus-current effect, relative velocity model, etc. The nonlinear drift force appears from the wetted-free surface and convective-inertia terms. The exciting force for TLP springing has the same origin.

The nonlinear responses may arise from the responses at frequencies other than the imposed wave frequencies (e.g., second-order frequencies, low frequency drift, etc.) or nonlinear damping or restoring force in a dynamic offshore structure system. The latter case arises from the material properties or geometric nonlinearities of the components present in the offshore structure system. Two of these, namely the catenary system and flexible structures, are included in Section 2.

Some attempts have been made in examining the extreme value analysis in all these areas of nonlinearities. Because of the complex nature of the nonlinear problem, it may be solved numerically using time domain simulation on a computer which is time-consuming and difficult to use in a design case. The other approach in obtaining the probability distribution of the extreme values has been to make simplified assumptions so that the solution may be obtained in a closed-form or a semi-closed form expression. These approaches are discussed in Chapter 3 and summarized by nonlinear categories in Table 4.2. As can be seen from the table, the sea surface has been invariably chosen as Gaussian.

For the nonlinear drag force, a polynomial approximation developed by Borgman is popular. The second term of the force spectral estimate gives rise to a triple convolution integral of the velocity spectra. Similarly, the third term may be shown to yield a quintic convolution integral and so on.

TABLE 4.2
SUMMARY OF METHODS OF NONLINEAR RESPONSE PREDICTION

NONLINEAR TERM	SEA	APPROXIMATION	METHOD OF SOLUTION	REMARKS	SOURCE
1. Nonlinear Drag	Zero-Mean Gaussian	Polynomial; Linear Wave Theory	Triple Convolution of Velocity Spectra	May be extended with mathematical complexity	Borgman (1972)
2. Nonlinear Drag	Zero-Mean Gaussian	Polynomial; Kinematics are unidirectional & Gaussian & water particle velocity substantially larger than structure velocity	Triple Convolution Velocity Spectra	Effect of superharmonics in load spectrum shown on displacement response of a fixed platform	Sigbjörnsson & Mörch (1982)
3. Morison Formula	Zero-Mean Gaussian	Narrow Band Spectrum	Transformation from the distribution of wave height, H, to force amplitude, f_0	Two expressions for the inertia (Rayleigh) & drag predominance (exponential) are obtained	Borgman (1972)
4. Morison Formula	Zero-Mean Gaussian	Wide Band Spectrum	Moments of the velocity spectrum upto 6th order are needed for computation	From joint distribution function of force and its second derivative	Tickell (1977)
5. Morison Formula	Zero-Mean Gaussian	Force is narrow banded; but non-Gaussian	2nd & 4th derivatives of force only required for computation	Force & its 1st time derivative are statistically independent	Tickell (1977)
6. Morison Formula	Zero-Mean Gaussian	Any band width, but $$\text{force} > \frac{\omega_z^2 k_M^2}{2k_D}$$	Extreme value is based on peak rate density whose expressions are derived	Separate expressions for inertia, drag & Morison force	Moe (1979)

TABLE 4.2 CONT'D

NONLINEAR TERM	SEA	APPROXIMATION	METHOD OF SOLUTION	REMARKS	SOURCE
7. Morison Formula	Zero-Mean Gaussian	Statistically independent mean up-crossing frequency	Numerical solution	Expressions for total force as well as drag force	Naess (1983)
8. Wave-Plus Current Drag	Zero-Mean Gaussian	Polynomial; deep water	First approximation to the relative velocity	Effect of current on wave in deep water accounted for	Tung & Huang (1972-1973)
9. Wave-Plus Current Drag	Zero-Mean Gaussian	Narrow Band Small current; $\gamma = U/\sigma_u < 1$	Based on extreme rate density related to pdf	Expressions for the probability density given	Moe & Crandall (1978)
10. Wave-Plus Current Drag	Zero-Mean Gaussian	Wide band but large extreme force	Based on extreme rate density related to pdf	Expressions for the peak rate density given	Moe & Crandall (1978)
11. Wave-Plus Current Drag	Zero-Mean Gaussian	Gaussian force	Linearized method	Mean & standard deviation of peak drag force	Grigoriu (1984)
12. Wave-Plus Current Drag	Zero-Mean Gaussian	Exact form	Numerical solution	Presented actual distribution of force	Grigoriu (1984)
13. Relative Velocity Drag	Zero-Mean Gaussian	Cubic Polynomial; relative velocity term is assumed to be Gaussian with zero mean	Triple convolution of relative velocity spectra; simplified by Gaussian closure approach; iterative method of solution due to relative velocity	Finite wave height effect ignored as is almost always done	Dunwoody & Vandiver (1981)

TABLE 4.2 CONT'D

NONLINEAR TERM	SEA	APPROXIMATION	METHOD OF SOLUTION	REMARKS	SOURCE
14. Nonlinear Damping	Zero-Mean Gaussian	One dimensional equation	Markov envelope method	Excited by white noise; correlated with digital simulation	Roberts (1977)
15. Nonlinear Damping	Gaussian	Small damping and very narrow band spectrum	Asymptotic approximation for expected extreme	General form of damping is used	Brouwers (1982)
16. Slow Drift	Zero-Mean Gaussian	Wide band	From joint pdf of force and derivative of phase function. For narrow band, reduces to exponential function	Initial distribution describes the 2nd order force time history	Langley (1984)
17. Linear & Quadratic Damping & Linear & Cubic Stiffness	Zero-Mean Gaussian	Stochastic averaging	Generalized Markov process	Non-white spectrum shape; Experimental correlation	Roberts (1987)
18. Low Frequency Force and Motion	Zero-Mean Gaussian	Ordered Eigenvalue Series	Characteristic function and contour integration	Square of response vector assumed to have exponential distribution	Langley (1987)
19. Total Second-Order Response	Zero-Mean Gaussian	Continuous distribution; Series representation	Gamma distribution	Positive and Negative Eigenvalues are used in the Series	Kato (1987)

Therefore, in principle, as many terms of the polynomial expression as desired may be added. The complexity and computer time consumption for the evalution of the integrals are enormous. In general, the inclusion of the second term of the approximation provides a reasonable estimate unless the drag contribution is extremely high. An example in Fig. 3.25 shows that for a near surface KC number of 94 based on the significant wave height and modal frequency and the relative drag contribution parameter, K, of about 117, the second term contributes about 16% of the first term and about 10% of the maximum total force.

There is another effect of these higher order terms on offshore structures (e.g., jackets) whose modal frequencies of vibration are at frequencies higher than the wave frequency. Since these higher components appear at higher harmonics of the load spectrum and since damping is small at the natural frequency of the jacket structures, the responses (e.g., stress, displacement, etc.) are amplified at these frequencies. An example of this phenomenon is shown in Fig. 3.26. The responses at the second harmonic are of the same order of magnitudes as those at the first harmonic.

Besides the Gaussian assumption if the wave heights are assumed to follow Rayleigh distribution (narrow band assumption) then the distribution of the maximum forces for the Morison formula may be readily obtained from that of the wave height [Borgman (1972)]. Another approach was taken by Tickell (1977) in which force spectrum, instead, was assumed to be narrow banded. For a wide-band spectrum, expressions are obtained for the limiting cases of all drag or all inertia situation. These solutions are compared in Fig. 3.26 with the corresponding numerical solution and are found to be acceptable in these areas. A general numerical procedure was developed by Naess (1983) for the prediction of extreme forces by the Morison formula. The expressions for the expected extreme values are given for the compound inertia and drag terms and are obtained in terms of the level up-crossing frequency.

For the wave-plus-current drag or the relative velocity drag, a similar polynomial approximation as for the wave drag is possible. In these cases, a force spectrum may be obtained including inertia and drag term of the modified Morison equation. This was shown by Tung and Huang (1972-1973) and Grigoriu (1984) for the wave-current drag and by Dunwoody and Vandiver (1981) for the relative velocity drag. In the first case of waves, the current influences

167

the incident wave as well through the kinematic interaction. Only linear terms of the polynomial were used in these analyses. The extreme rate density method was used by Moe and Crandall (1978) to obtain expression of extreme forces in the presence of small current for both narrow-band and wide-band Gaussian sea. In the latter case, the expressions for the extreme forces were approximated by an asymptotic formulation. An exact form was solved numerically by Grigoriu (1984) for the wave-plus-current drag.

The case of nonlinear damping in the differential equation of motion for an offshore structure has been considered in an approximate way by Brouwers (1982) on the assumption that the damping is small and the motion response is extremely narrow-banded in the area of the natural frequency of the structure. In this case, any motion of consequence is from the resonance at the natural frequency of the structure. If the excitation is considered to be a white noise having nearly equal amount of energy at all frequencies over the narrow band of interest, then a method of solution was developed by Roberts (1977) based on the Markov envelope method. For a spectrum model used for ocean waves this procedure is adaptable. Most ocean structures are inherently designed to have natural periods away from the wave periods. In these cases, the responses are generally some combination of resonance plus mass (or stiffness) controlled response. When both of these separate responses are significant, this method is not applicable. However, in cases where the resonance response is much higher than the wave excited response, e.g., the oscillating surge drift motion of a ship or the high frequency springing load on a TLP tendon, the method of Brouwers and Roberts is suitable. In a recent work by Roberts (1987), the limitation of white noise spectrum was waived by modifying the Markov process and using a generalized stochastic averaging. The revised theory produced higher values of cumulative probability compared to Rayleigh distribution as well as the earlier results. The new theory seemed to match the experimental data on ship roll well.

The slow drift force is nonlinear being proportional to the square of the wave height. For a narrow-band spectrum the initial distribution of the force reduces to an exponential distribution function. However, Langley (1984) obtained an expression for a wide-band spectrum which is markedly different from the exponential distribution.

168

In a recent important study by Pinkster and Wichers (1987) through numerical and experimental simulation of slow drift oscillation, e.g., surge motion, it was found that as long as the mooring system is linear, the low frequency surge motion follows Gaussian distribution quite well. However, for a nonlinear mooring characteristic, the deviation from the normal distribution is large. The expressions for the probability density function for the second-order forces and motions have been given by Langley (1987). It is obtained by contour integral and expressed in terms of eigenvalues of the matrix equation of motion as a series expression. The number of terms which is equal to the number of wave components in the irregular wave should be large (about 200) according to Langley. The non-Gaussian characteristics of the nonlinear force is given by high values of skewness (~2) and kurtosis (>5). However, the motion probability density of an example problem showed that it is close to Gaussian.

The total second-order response including the first and second-order terms has been investigated by Kato, et al. (1987), and an expression for the pdf of this response is given. It is expressed as a series of Gamma functions and eigenvalues. Numerical examples showed that the addition of linear term makes the pdf of the response more skewed.

5.0 CONSISTENT METHODOLOGY

The response of an offshore structure to random wave excitation is usually computed in two distinct stages. First, the excitation force on the structure due to the wave kinematics around the structure is computed. Then the responses of the structure such as displacements, stresses, etc. due to the application of this excitation force are obtained. If the responses are linear with respect to the wave amplitudes, then the relationship between the force and the wave and that between the response and the force must be linear. The nonlinearities in this analysis may enter in either one of these two steps. The excitation may be nonlinear from higher order effects in the wave loading, e.g., the drag force, the drift force, etc. On the other hand, the responses may be nonlinear even if forces are linear due to nonlinear damping or restoring force etc.

It is clear from the discussion in the previous sections that one consistent methodology for all types of nonlinearities that appear in predicting the responses of an offshore structure cannot be prescribed. In fact most of the probabilistic methods available today that are used in predicting extreme values of a nonlinear system are based on simplified assumptions that are dependent upon the type and characteristic of nonlinearity.

Let us discuss the type of nonlinear problems in offshore applications that have been dealt with using the extreme value analysis. The most common nonlinearity that appears in the marine structure design is in the calculation of the exciting forces. This takes the form of the nonlinear drag force, e.g., in the Morison formula. There are several variations of the Morison formula in terms of the presence of current or structure motion. Some of these areas are also investigated in predicting extreme response values. Other areas include nonlinear damping and slow drift oscillation.

In all these formulations, the sea has been invariably assumed to be zero mean Gaussian. If the sea surface is high which usually produces the extreme responses then the crests are higher than the troughs and sea surface in all likelihood will not have a zero mean nor will it follow a Gaussian distribution. In these cases, the non-Gaussian properties of the waves should be known. The non-Gaussian distribution is usually represented in a series

form based on a nonlinear wave theory, e.g., Stokes' higher order theory or probability theory, e.g., Gram-Charlier series. These theories show that the waves generally have a non-zero negative mean and higher skewed density than Gaussian. The distribution of wave heights similarly have higher density than Rayleigh. However, the effect of non-Gaussian sea on a nonlinear response is generally not known. On the other hand, probability distribution of several specific nonlinear non-Gaussian responses of marine structures has been presented.

Because of the above limitations and various simplified approximations involved in nonlinear extreme value analysis a cookbook method for an engineer to follow is not possible at this stage of the development. The state-of-the-art is such that various simplified methods may be recommended. None of these techniques may be applicable to a particular problem in which case several methods should be tried to find the differences in the results. Then an engineering judgment should be used in choosing the appropriate extreme values.

5.1 EXTREME VALUE PREDICTION FOR NONLINEAR SYSTEMS

A simple flow chart for the evaluation of the extreme responses of a marine structure is shown in Table 5.1. Depending on the type of the extreme value that is sought for in the design, the computation may be stopped at the short-term level or continued to obtain long-term statistics or extreme and a fatigue analysis. The process is similar whether the response is a linear or a nonlinear function of the environmental input variable, which is the waves in our case.

For a linear system, the rms value of the response defines the short-term statistics of the response. This may then be extended directly to the long-term statistics if the long-term probability of the short-term waves is known. For a nonlinear system, the rms value of the response is generally only one of the parameters that determines the response statistics. Other statistical parameters are needed to complete the description of the short-term extremes of the response. Therefore, in the long-term response analysis the appropriate statistical dependence of the short-term response must be included along with the long term wave statistics.

171

TABLE 5.1

FLOW CHART FOR EXTREME RESPONSE VALUE ANALYSIS

```
┌──────────────┐                    ┌──────────────┐
│  STRUCTURE   │                    │  SHORT-TERM  │
│  RESPONSE    │                    │    WAVE      │
│  FORMULA     │                    │  PARAMETERS  │
└──────┬───────┘                    └──────┬───────┘
       │                                   │
┌──────▼───────┐                    ┌──────▼───────┐
│  NONLINEAR   │                    │WAVE SPECTRUM │
│  RESPONSE    │                    │  MODEL AND   │
└──────┬───────┘                    │ STATISTICAL  │
       │                            │ PARAMETERS   │
       │                            └──────┬───────┘
       │         ┌──────────────┐          │            ┌──────────────┐
       └────────►│  RESPONSE    │◄─────────┘            │ WAVE SCATTER │
                 │  SPECTRUM    │                       │   DIAGRAM    │
                 │AND SHORT TERM│                       └──────┬───────┘
                 │ STATISTICS   │                              │
                 └──────┬───────┘                              │
        ┌───────────────┼───────────────┐                     │
┌───────▼──────┐ ┌──────▼───────┐ ┌──────▼───────┐            │
│  LONG-TERM   │ │STATISTICS OF │ │   FATIGUE    │◄───────────┘
│ RMS RESPONSE │ │  LONG-TERM   │ │  ANALYSIS    │
│              │ │  RESPONSE    │ │              │
└──────────────┘ └──────────────┘ └──────────────┘
```
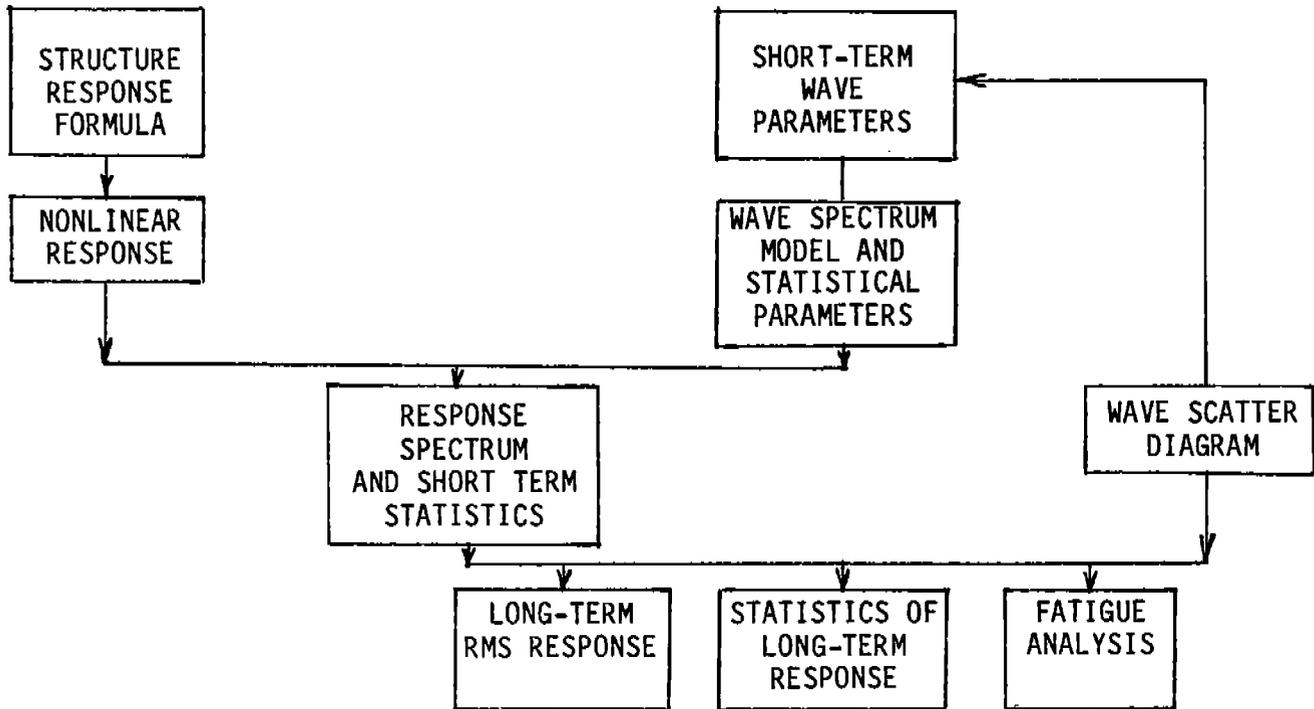
TABLE 5.2

RANGE OF APPLICABILITY OF

LINEAR APPROXIMATION OF COMMON NONLINEAR TERMS

NONLINEAR TERM	PARAMETER	VELOCITY
Wave Drag		$u < 2\sigma_u$
Wave Current Drag	$\gamma = 0.1$	$v < 2\sigma_v$
	$\gamma = 0.5$	$v < 2.5\sigma_v$
	$\gamma = 1.0$	$10 < v < 3\sigma_v$
Relative Velocity Drag	$\sigma_v/\sigma_u = 0.1$	$v < 2\sigma_v$
	$= 0.2$	$v < 2\sigma_v$
	$= 0.3$	$v < 2\sigma_v$

Different approximation methods that are available and are described in Chapters 3 and 4 are summarized here in a logical order. In the extreme value analysis for the design of a marine structure, the random waves are customarily assumed to have a Gaussian distribution. A suitable spectrum model, e.g., P-M, JONSWAP, etc., is chosen as the wave model to represent the seastates for a long-term prediction depending on the sea severity. Sometimes, more than one spectrum model is suitable. For example, the lower waves may follow a P-M model while the JONSWAP model may be suitable for the higher seastates. Once the wave environmental model is chosen, the next step in the prediction is computation of the environmental forces on the offshore structure.

If the forces are linear, then the forces may be obtained in the form of a force spectrum. For a linearized approximation of a nonlinear system a similar approach may be taken. One of the most common forms of nonlinear forces is given by the Morison equation representing a drag and an inertia force. The values of the velocity for which the linear approximation may be used with reasonable accuracy have been given in Table 5.2. If current is present with waves, the validity of a linear approximation is measured in terms of the strength of the current as well. These limiting values are also given in the table.

Higher order terms in the force spectrum may be estimated based on the series expansion of the nonlinear terms. These higher terms in the estimate are time-consuming to compute but may become significant if the nonlinearity of the force term is large. The extreme values are difficult to obtain from these spectrum extimates without knowing the distribution of the force maxima which is not generally Rayleigh.

However, the additional terms in the spectrum produce peaks in the spectrum in the higher frequency range which may coincide with the natural frequency of vibration of the structure under investigation. In this case, if the structural damping is small, the response may be peaked at this frequency leading to a narrow band spectrum. This response spectrum may then be treated as Rayleigh distributed so that the response extremes may be easily determined.

If the force spectrum is narrow banded, then the distribution of the force extremes may be given in terms of inertia or drag dominance. For the inertia-dominated region, the force maxima are distributed according to the Rayleigh distribution. For the drag-dominated area, the distribution is exponential.

For a wide-band wave force model, similar separate expressions for the drag-dominated and inertia-dominated areas are known but now in terms of an additional parameter, ε. These expressions are, however, only valid for the limiting values of the drag-inertia parameter, K, namely, K = 0 and K $\rightarrow$ ∞. The comparison between the two cases shows that the narrow-band assumption overpredicts for the same probability level at both the limiting values of K.

The extreme value analysis for a wide-band spectrum was also provided in terms of the expected rate of occurrence of force maxima. These expressions use the appropriate frequencies corresponding to kinematics involved in the process. The expected number of peaks per time unit are obtained from these expressions by integration.

Similar analysis have been made for wave-current force. The latter was derived on the assumption of large force. Separate expressions for narrow-band and wide-band process have been given. In this case the modified form of the Morison equation is used. However, current is assumed small in the sense that only the terms in the first order in U/σ_u are retained. Thus, the expressions are valid for current of the order of 10-20% of the rms water particle velocity.

The expression for the expected extreme value for the component of the drag force in the presence of a finite current is shown in Eq. 3.317. The extreme value depends on a time interval, T_R.

If a dynamic system is nonlinearly damped, the simplest solution for the extreme responses is to derive the solution of an equivalent linearly damped system. The damping is particularly important near the natural frequency. Moreover, if the damping is small then the response may be treated as an extremely narrow-band process. Then, the input spectrum over this area of response may be treated as a white noise process for which the solution is known. The Markov process is a powerful tool for these derivations and a generalized method has been derived to waive the requirement of white noise.

173

5.2 A CONSISTENT LINEARIZATION METHOD

A common technique of handling these problems is a linearization technique in which the nonlinear problem is linearized by one of many means, e.g., the Fourier averaging, least square error technique, Taylor series expansion, etc.

Table 4.2 includes the polynomial approximations of various forms of nonlinear terms that appear in the structure response calculations. These may be generalized in the following way. Let

$$f = f(x) \qquad (5.1)$$

be a nonlinear function of x. Let x be a variable that follows a zero mean normal (Gaussian) probability law. Thus, x could be such quantities as the wave profile, velocity profile, relative velocity profile, etc. The problem is to compute a polynomial approximation of f(x) given by

$$f(x) = \sum_n C_n x^n \qquad (5.2)$$

such that the quantity

$$Q = \int_{-\infty}^{\infty} [f(x) - \sum_n C_n x^n]^2 \frac{1}{\sqrt{2\pi}\,\sigma_x} \exp[-x^2/2\sigma_x^2]\, dx \qquad (5.3)$$

is minimized. The last part of the integrand is the Gaussian formulation. The values of C_n (n = 1, 2, . . .) may be obtained by differentiating Q with respect to C_n and setting the result equal to zero. Thus, depending on the number of terms desired in the polynomial, an equal number of equations in the unknowns C_n may be obtained. The values of C_n are then obtained by setting up a matrix equation and its inversion. For example if

$$f(x) = |x|x \qquad (5.4)$$

and only one term in the polynomial (linearized) is desired then

$$C_1 = \sqrt{\frac{8}{\pi}}\,\sigma_x \qquad (5.5)$$

174

This is then a generalized method that can be used for any nonlinear function f(x) as long as the function f(x) is explicitly known as a function of x where x is an independent variable. Many of the nonlinear response terms for a marine structure have already been worked out and the results are tabulated in Table 4.1.

Once the problem is linearized then the usual procedure of a short-term Gaussian process is applicable. For example, in the case of wave drag

$$f(u) = k_D |u| u \tag{5.6}$$

Once the right hand side is linearized through the formulation in Eq. 5.3, we have

$$f(u) = k_D \sqrt{\frac{8}{\pi}} \sigma_u u \tag{5.7}$$

Since u(t) is assumed to follow Gaussian distribution with a zero mean so would the force f(u). Thus, the amplitudes of force, f, will follow Rayleigh distribution for which extreme values may be predicted. This linearization will apply only for small nonlinearity.

The adequacy of assuming Gaussian response statistics of a linearized nonlinear problem depends on the type of nonlinearity and the sea severity. The ranges of the values of u for which this linearization is reasonably valid along with all the other nonlinear terms included in Table 4.1 are summarized for convenience in Table 5.1.

5.3 RESPONSE SPECTRUM COMPUTATION

In some cases of nonlinearity, more exact solution is possible by spectral or stochastic averaging technique. This may provide nonlinear relationship between the wave spectrum and force spectrum depending on the area of nonlinearity. In a few cases, a probabilistic description of the response is also possible. However, because of simplification of the structure, etc. in these analyses, the practical application is quite limited.

For a linear system the response may be related to the waves by a relationship of the type

175

$$x(t) = H(\omega)\eta(t) \qquad (5.8)$$

where x = response function, η = wave profile, t = time, and H = a function of the frequency, ω. This relationship can be directly converted from the time to the frequency domain through the autocovariance method. Thus, taking the lagged product of both sides and integrating

$$\int_0^\infty x(t)\, x(t + \tau)\, dt = H^2(\omega) \int_0^\infty \eta(t)\eta(t + \tau)\, dt \qquad (5.9)$$

or

$$R_x(\tau) = H^2(\omega)\, R_\eta(\tau) \qquad (5.10)$$

Then the Fourier transform of both sides provides the wellknown relationship between the wave spectrum and the response spectrum for a linear system

$$\int_0^\infty R_x(\tau)\, e^{i\omega\tau}d\tau = H^2(\omega) \int_0^\infty R_\eta(\tau)\, e^{i\omega\tau}\, d\tau \qquad (5.11)$$

or

$$S_x(\omega) = H^2(\omega)\, S_\eta(\omega) \qquad (5.12)$$

Here, $H(\omega)$ is called the transfer function between the wave profile and the response. Since the wave profile is assumed to follow the Gaussian distribution and wave height, the Rayleigh distribution and since the transformation is linear, the response amplitudes also follow the Rayleigh distribution from which the extreme values are easy to determine.

This approach may be extended to nonlinear systems as well, if the nonlinear functional relationship is expressed in a polynomial form as shown in the previous section. Let us take the example of drag force related to the water particle velocity

$$f = k_D|u|u \qquad (5.13)$$

176

In this case, after the autocorrelation function for the force is written, the right hand side is expanded in a series form the first three terms of which take the form

$$R_f(\tau) = H_1(f) \, R_u(\tau) + H_2(f) \, R_u^3(\tau) + H_3(f) \, R_u^5(\tau) + \ldots \quad (5.14)$$

where $H_1(f) = 8/\pi k_D^2 \sigma_u^2$, $H_2(f) = 4 \, k_D^2/(3 \, \pi \sigma_u^2)$ and $H_3(f) = k_D^2/(15\pi\sigma_u^4)$.

By taking the Fourier transform of both sides, the drag force spectrum may be related to the velocity spectrum. Note that the powers of the autocorrelation function appear in the frequency domain as the convolution integral. Thus,

$$\int_0^\infty R_u^3(\tau) \, e^{i\omega\tau} d\tau = \int_0^\infty \int_0^\infty S(\omega) \, S(\omega' - \omega'') \, S(\omega - \omega') \, d\omega' \, d\omega'' \quad (5.15)$$

This integral is easy to evaluate numerically even though it is time consuming. Thus, in principle as many terms in the series in Eq. 5.14 may be included in the evaluation of $S_f(\omega)$ even though in the practical sense anything beyond the second term may be prohibitive in terms of execution time requirements of a computer.

Moreover, even though the response spectrum is known and its significant value may be calculated, the computation of the extreme value is not straightforward. Since the relationship is nonlinear the force amplitudes do not necessarily follow Rayleigh distribution even though the velocity amplitudes do. Therefore, it is difficult to predict the extreme values for the force.

The importance of this analysis, however, may be stated in the following way. Let us examine Eq. 5.14. If the first term on the right hand side produces the first harmonic frequency of the force, the second term will have a peak at the third harmonic, the third term at the fifth harmonic and so on. These higher order terms will generally be reduced in magnitude in succession. However, many fixed structures have natural frequencies of vibrational modes at frequencies much higher than the wave frequency range. One of these vibrational modes may coincide with this higher frequency in the force spectrum in which case an amplification of the response, e.g., stresses, etc. may be generated. Moreover, if the structural and hydrodynamic damping

are small in this region the response, e.g., stress or displacement, will appear as a narrow-band spectrum in this frequency range. The response then may follow Rayleigh distribution even if the force does not. The extreme values may be derived for the responses due to this nonlinear excitation.

5.4 RESPONSE PROBABILITY DENSITY FUNCTION

Consider two random processes, $x(t)$ and $y(t)$, where $x(t)$ is an excitation and $y(t)$ is the corresponding response. If $x(t)$ is Gaussian while $y(t)$ is not there is strong indication that the physical system is nonlinear. Unlike linear systems, no general methodology exists for nonlinear system analysis.

For a class of nonlinear systems, however, a consistent method exists for deriving the initial distribution of the response if the excitation is assumed Gaussian. While the initial distribution of the response does not provide information regarding the extreme values, it may give some insight into the nonlinear nature of the response and a degree of departure from the linear system. Thus, it may help provide and evaluate the validity of an approximate method of the extreme value analysis of the nonlinear system. The following analysis is according to Bendat (1985).

Let us consider that the excitation function, $x(t)$, is a stationary ergodic random process with zero mean value such that at any time, t, the random variable $x = x(t)$ has the first-order Gaussian probability density function

$$p(x) = \frac{1}{\sigma_x \sqrt{2\pi}} \exp\left(-\frac{x^2}{2\sigma_x^2} \right) \qquad (5.16)$$

where the mean value, μ_x, and the variance, σ_x of x are given by

$$\mu_x = E[x] = 0 \qquad (5.17)$$

$$\sigma_x^2 = E[x^2] \qquad (5.18)$$

For the pair of random variables $x_1 = x(t)$ and $x_2 = x(t + \tau)$, the joint probability density function is given by the second-order Gaussian form

$$p(x_1,x_2) = \frac{1}{2\pi \, \sigma_x^2 \, \sqrt{1 - \rho^2}} \left\{ \exp \frac{-1}{2\sigma_x^2 \, (1 - \rho^2)} \left[x_1^2 - 2\rho \, x_1 \, x_2 + x_2^2 \right] \right\}$$

(5.19)

where ρ is the correlation coefficient between x_1 and x_2

$$\rho = \rho_{xx} = \frac{E[x_1,x_2]}{\sqrt{E[x_1^2] \, E[x_2^2]}} = \frac{E[x_1 \, x_2]}{\sigma_x^2}$$

(5.20)

The auto correlation function

$$R_{xx}(\tau) = E[x(t) \, x(t + \tau)] = E[x_1 \, x_2]$$

(5.21)

$$R_{xx}(0) = E[x(t) \, x(t)] = E(x_1^2] = E[x_2^2] = \sigma_x^2$$

(5.22)

Hence

$$\rho(\tau) = \rho_{xx}(\tau) = \frac{R_{xx}(\tau)}{R_{xx}(0)} = \frac{R_{xx}(\tau)}{\sigma_x^2}$$

(5.23)

The expected value of the response and its moments can be obtained from $g(x)$ and $p(x)$ as follows:

$$E(y) = E[g(x)] = \int_{-\infty}^{\infty} g(x) \, p(x) \, dx$$

(5.24)

$$E(y^n) = E[g^n(x)] = \int_{-\infty}^{\infty} g^n(x) \, p(x) \, dx$$

(5.25)

$$\sigma_y^2 = E[y^2] - (E[y])^2$$

(5.26)

If the response $y = g(x)$ is a zero memory nonlinear system that is single-valued and one-to-one, the response probability density function $p_2(y)$ for the response $y(t)$ is given by

$$p_2(y) = \frac{p(x)}{|dy/dx|}$$

(5.27)

expressed in terms of y. If each value of $y = g(x)$ corresponds to n values of x which are equally likely, then

$$p_2(y) = \frac{n \, p(x)}{|dy/dx|}$$

(5.28)

179

Whenever $p(x)$ is Gaussian and $g(x)$ is nonlinear, the resulting $p_2(y)$ will be non-Gaussian.

Example: Two Slope Systems

A nonlinear mooring line may be approximated, sometimes, by two straight lines of two different slopes (often within the range of its application in an offshore system). Let us consider the example of the nonlinear two slope system given by

$$y = g(x) = x \qquad\qquad \text{for } x < A$$
$$= A + b(x - A) \qquad\qquad x > A$$

where $g(x)$ is an odd function, $g(x) = g(-x)$. Then

$$\frac{dy}{dx} = 1 \qquad\qquad \text{for } |x| \geqslant A$$

$$= b \qquad\qquad |x| > A$$

Note that (dy/dx) is discontinuous at $|x| = A$.

The response probability density function is obtained from

$$p_2(y) = p(x) = p(y) \qquad\qquad \text{for } y < A \qquad\qquad (5.29)$$

$$= \frac{1}{b} \{ p (A + [(y - A)/b]) \} \qquad y > A \qquad\qquad (5.30)$$

$$= \frac{1}{b} \{ p[-A + [y + A]/b] \} \qquad y < -A \qquad\qquad (5.31)$$

If it is assumed that the excitation follows the normal (Gaussian) distribution with unit variance ($\sigma_x = 1$)

$$p(x) = \frac{1}{\sqrt{2\pi}} \exp (-x^2/2) \qquad\qquad (5.32)$$

then the response probability density function is given by

180

$$p_2(y) = \frac{1}{\sqrt{2\pi}} \exp(-y^2/2) \qquad\qquad |y| < A \quad (5.33)$$

$$= \frac{1}{b\sqrt{2\pi}} \exp\left\{ \frac{-(A + [(y - A)/b])^2}{2} \right\} \qquad y > A \quad (5.34)$$

$$= \frac{1}{b\sqrt{2\pi}} \exp\left\{ \frac{-(A - [(y + A)/b]^2}{2} \right\} \qquad y < -A \quad (5.35)$$

It is clear from the above expressions (Eqs. 5.33-5.35) that there is a discontinuity of the response density function at $y = A$. Depending on the case of clipping for $0 < b < 1$ or hardening for $b > 1$, the quantity $p_2(A+)$ is either greater than or less than $p_2(A-)$.

Example: Square-Law System

The second-order wave force, e.g., the wave drift force follows a square law with respect to the waves. Let us consider a response

$$y = g(x) = x^2$$

Then

$$\frac{dy}{dx} = g'(x) = 2x \quad \text{and} \quad x = \pm\sqrt{y} \qquad\qquad (5.36)$$

The response probability density function

$$p_2(y) = \frac{2\ p(x)}{|2x|} = \frac{p(\sqrt{y})}{\sqrt{y}} \qquad\qquad \text{for } y > 0 \qquad (5.37)$$

with $p_2(y) = 0$ for $y > 0$ and $p_2(0) = \infty$. If $p(x)$ has a Gaussian distribution, then

$$p(\sqrt{y}) = \frac{1}{\sigma_x\sqrt{2\pi}} \exp(-y/2\sigma_x^2) \qquad\qquad \text{for } y > 0 \qquad (5.38)$$

Hence

$$p_2(y) = \frac{1}{\sigma_x\sqrt{2\pi}\ y} \exp(-y/2\sigma_x^2) \qquad\qquad \text{for } y > 0 \qquad (5.39)$$

This is the form of an exponential distribution. Note that

$$E[y^n] = E[x^{2n}] = 1, 3, 5, \ldots (2n - 1) \, \sigma_x^{2n} \tag{5.40}$$

$$\mu_y = E[y] = \sigma_x^2 \tag{5.41}$$

$$R_{yy}(0) = E[y^2] = 3 \, \sigma_x^4 \tag{5.42}$$

$$\sigma_y^2 = 2\sigma_x^4 \tag{5.43}$$

Example: Cubic System

The load-elongation characteristics of a mooring system may often be expressed by the cubic law. A nonlinear cubic system is given by

$$y = g(x) = x^3$$

Hence

$$\frac{dy}{dx} = 3x^2 \quad \text{and} \quad x = y^{1/3} \tag{5.44}$$

Then the response probability density function is given by

$$p_2(y) = \frac{p(x)}{|3x^2|} = \frac{p(y^{1/3})}{3 \, y^{2/3}} \tag{5.45}$$

Assuming a Gaussian distribution for $p(x)$

$$p_2(y) = \frac{1}{3 \, \sigma_x \, y^{2/3} \, \sqrt{2\pi}} \exp \, (-y^{2/3}/2\sigma_x^2) \tag{5.46}$$

In this case, $p_2(-y) = p_2(y)$ and $p_2(0)$ approaches infinity. Note that

$$\mu_y = E[y] = E[x^3] = 0 \tag{5.47}$$

$$R_{yy}(0) = E[y^2] = E[x^6] = 15 \, \sigma_x^6 \tag{5.48}$$

182

Example: Square-Law System with Sign

The wave drag force is expressed as the square law with sign in terms of the water particle velocity. A nonlinear square-law system with sign is defined as

$$y = g(x) = |x|x$$

i.e.

$$y = x^2 \qquad\qquad\qquad \text{for } x < 0$$

$$= -x^2 \qquad\qquad\qquad \text{for } x < 0$$

Then

$$x = + \sqrt{y} \qquad\qquad\qquad \text{for } y > 0$$

$$= - \sqrt{-y} \qquad\qquad\qquad \text{for } y < 0$$

Also

$$\frac{dy}{dx} = g'(x) = 2x \qquad\qquad\qquad \text{for } x > 0$$

$$= -2x \qquad\qquad\qquad x < 0$$

Hence, the response probability density function

$$p_2(y) = \frac{p(x)}{|2x|} = \frac{p(\sqrt{y})}{2\sqrt{y}} \qquad\qquad \text{for } y > 0$$

$$= \frac{p(\sqrt{-y})}{2\sqrt{-y}} \qquad\qquad \text{for } y < 0$$

Then $p_2(y) = p_2(-y)$ and $p_2(0)$ tends to infinity. Also

$$\mu_y = E[y] = E[|x|x] = 0 \qquad\qquad\qquad (5.49)$$

183

$$R_{yy}(0) = E[y^2] = E[x^4] = 3\sigma_x^4 \qquad (5.50)$$

The above theory provides a simple method in obtaining the initial distribution of a nonlinear system subjected to Gaussian excitation. As mentioned before, an initial distribution (distribution of the profile values) does not indicate the extreme values for the system. But it may aid in examining the nonlinear system against any approximation used in deriving the extreme value of the nonlinear system.

5.5 RESPONSE EXTREMES BY ORDER STATISTICS

The extreme value of the maxima of a Gaussian (linear) response may be derived by applying order statistics. The extreme value defined in this respect is the largest value of the maxima that will occur in N observations in a short interval of time (of the order of a few hours).

If the value of the bandwidth parameter, ϵ, for a random variable is known, then the probability density function of the variable may be estimated. For example, if the spectrum of the response, e.g., the force spectrum derived in a previous section, is known, the bandwidth parameter, ϵ, may be estimated from its moments. The distribution function for the broad band spectrum (varying between truncated normal, $\epsilon = 1$, and Rayleigh, $\epsilon = 0$) is then known from Eq. 3.67.

For a random sample, x_1, x_2, . . ., x_N of size N which are the observed maxima of a random process, the samples may be ordered in ascending values, ζ_1, ζ_2, . . ., ζ_N where ζ_N is the largest. Each one of ζ_i will have its own probability density function different from that of x_i (Eq. 3.63). For example, for a given probability level, α, such that

$$P[\zeta_N > \hat{\zeta}_N] = \alpha \qquad (5.52)$$

we can obtain the relationship

$$[P(\hat{\zeta}_N)]^N = 1 - \alpha \qquad (5.53)$$

where $P(\hat{\zeta}_N)$ is given by Eq. 3.67 for $\bar{x}_1 = \hat{\zeta}_N$. The problem then is to compute $\hat{\zeta}_N$ for a given value of α. This is a difficult task from an equation of the type of Eq. 5.53.

However, considerable simplification may be made if the following two assumptions are made:

- α is small being of the order of 0.1 or less
- N is large
- $\varepsilon < 0.9$

All these assumptions are reasonable from practical standpoint since most response spectra will lie in the range of $0 < \varepsilon < 0.9$ and the extreme values will generally be sought from large number of observations with the cumulative probability of 99% or more.

Under the above assumptions the error functions in Eq. 3.67 reduce to either zero or one and the extreme value, $\hat{\zeta}_N$, is derived as

$$\hat{\zeta}_N = \left[2 \ln \left(\frac{\sqrt{1 - \varepsilon^2}}{1 + \sqrt{1 - \varepsilon^2}} \frac{2N}{\alpha} \right) \right]^{1/2} \tag{5.54}$$

Note that Eq. 5.54 is a "peak factor" applicable to a Gaussian process. Note also that $\hat{\zeta}_N$ is normalized so that the extreme value of the amplitude of the response (as a random process) is obtained by multiplying this value by $\sqrt{m_0}$.

The number of observations, N, is difficult to work with, but it can be related directly to the time length, T_R. For practical purposes, it is more meaningful to express the extreme value as a function of T_R.

$$\hat{\zeta}_N = \left[2\ln \left\{ \frac{T_R}{(2\pi)\alpha} \sqrt{\frac{m_2}{m_0}} \right\} \right]^{1/2} \tag{5.55}$$

where T_R is given in seconds.

Ochi (1973) worked out examples for extreme values from data from a wave basin. The examples include various random waves generated in the tank and the recorded pitching motion of a ship model in random seas. The results are summarized in Table 5.3. The predicted values are based on the moments of the spectrum computed from the recorded data. The most probable extreme value, $\bar{x}_N$, corresponds to the value at which the probability density is

185

TABLE 5.3
COMPARISON OF PREDICTED AND OBSERVED EXTREME VALUES
FROM MODEL TESTS
[OCHI (1973)]

RESPONSE	SEA STATE	SPEED (knots)	TEST TIME (min)	BAND WIDTH PARAMETER (ϵ)	NO. OF MAXIMA OBSERVED	EST.	EXTREME VALUE OBSERVED	$\bar{x}_N$	PREDICTED $\hat{x}_N$ $\alpha=0.10$	$\hat{x}_N$ $\alpha=0.05$	$\hat{x}_N$ $\alpha=0.01$	UNIT
Waves	5		27.5	0.513	177	186	22.3	20.6	24.8	26.0	28.4	ft
Waves	6		24.8	0.616	282	308	32.0	33.3	39.6	41.3	45.0	ft
Waves	7		32.9	0.598	213	220	48.7	45.1	54.2	56.6	61.9	ft
Pitching Angle	7	10	23.5	0.378	160	172	18.9	16.3	19.7	20.6	22.5	deg
Pitching Angle	6	15	24.8	0.350	233	211	11.2	12.1	14.4	15.1	16.5	deg
Bow Acceleration	7	10	37.4	0.231	360	326	1.78	1.75	2.07	2.16	2.35	deg

TABLE 5.4

SHORT AND LONG TERM MOTION RESPONSE EXTREMES

	WAVE FREQUENCY SWAY ONLY	COMBINED WAVE AND LOW FREQUENCY SWAY
Short term most probable maximum in 10 year seastate	9.1m	11.5m
Long term maximum with a 10% probability of being exceeded at least once in 1 year	9.8m	12.9m

maximum. The extreme values are obtained for three different probability of exceedance values of $\alpha = 0.1$, 0.05 and 0.01.

The agreement between the predicted most probable extreme values and the observed extreme values is satisfactory. But the probability of exceeding this value is quite high (about 0.63 for $\epsilon \approx 0$). Therefore, for design purposes the extreme values corresponding to $\alpha = 0.01$ or so are more appropriate. These values are about 25-40% higher than the most probable values.

5.6 LONG-TERM RESPONSE PREDICTIONS FOR NONLINEAR SYSTEMS

There is no universally applicable theory for describing the response behavior of general nonlinear systems either spectrally in the frequency domain or probabilistically in the amplitude domain. Under certain conditions, however, solutions may be obtained in a few cases. Two such cases discussed earlier are second-order drift force along with associated low frequency motion and Morison type force. The short- and long-term predictions of two such examples are provided here [Inglis, et al. (1985)].

EXAMPLE 1 - LOW FREQUENCY MOTION RESPONSE

It has been shown [Pinkster (1980)] that the time-domain description of the second-order force on a floating structure due to a wave group having frequency components, ω_i ($i = 1, 2, \ldots N$) is given by

$$F_2(t) = \sum_{i=1}^{N} \sum_{j=1}^{N} \zeta_i \zeta_j P_{ij} \cos \{(\omega_i - \omega_j)t + (\epsilon_i - \epsilon_j) +$$

$$\sum_{i=1}^{N} \sum_{j=1}^{N} \zeta_i \zeta_j Q_{ij} \sin \{(\omega_i - \omega_j)t + (\epsilon_i - \epsilon_j)\} +$$

$$\text{high frequency terms} \tag{5.55}$$

where P_{ij} and Q_{ij} are the in-phase and out-of-phase components of the time independent transfer functions. The mean second-order force is found by setting $\omega_i = \omega_j$

$$\bar{F}_2(t) = \sum_{i=1}^{N} \zeta_i^2 P_{ii} = \sum_{i=1}^{N} \zeta_i^2 P(\omega_i, \omega_i) \tag{5.56}$$

which may be generated as

$$\overline{F}_2(t) = 2 \int_0^\infty S(\omega) \, P(\omega,\omega) \, d\omega \tag{5.57}$$

where $S(\omega) \, d\omega = \frac{1}{2} \zeta^2$ and ζ is the wave amplitude.

The spectral density of the low frequency components of the force is computed from the square of the transfer function as

$$S_F(\omega) = 8 \int_0^\infty S(\omega + \omega') \, S(\omega') \, T^2 \, (\omega + \omega', \, \omega') \, d\omega' \tag{5.58}$$

where

$$T^2(\omega + \omega', \omega') = P^2(\omega + \omega', \omega') + Q^2(\omega + \omega', \omega') \tag{5.59}$$

and T = amplitude of the quadratic transfer function.

The motion response spectrum may be obtained from the force spectrum if the system is considered to be a single degree of freedom system having linear damping. For a catenary moored system, this approximation usually provides a good estimate of the motion. Assuming that the system is lightly damped, as the case is for a low frequency oscillation, the motion response spectrum becomes quite narrow-banded acting as an effective filter. Thus, even though the force spectrum follows a non-Gaussian process, force being proportional to the square of the wave amplitude, the probability distribution of the resonant response is almost independent of the probability distribution of the excitation. Thus, for a linear transfer function between force and motion, the motion response can be well represented by a Gaussian process. The motion response spectrum describes the short term probability of the low frequency motion response. If the high frequency and the low frequency responses are assumed to be statistically independent, the two response spectra can be added together. Once the short-term response is known it can be combined with the wave scatter diagram to generate the long-term response.

The short-term estimates are made in terms of a storm with a 10 year return period having a significant wave height, H_s = 14.2m and a mean zero crossing period, T_z = 13.6 sec. The long-term response may be estimated for a

return period of 10 years. On the other hand, the maximum response may be determined which is experienced (at least) once during a given period (say, 1 year) with a given probability level.

The cumulative probability of a response exceeding a particular value, M, is Q(M). Then the probability of not exceeding this value is 1 - Q(M). Assuming a period of L years (e.g., the lifetime of the structure) and the number of peaks, N, in a year, the probability of not exceeding the prescribed value M in L years is $(1 - Q(M))^{N*L}$. If it is assumed that this value M will be exceeded once in L years, the probability $Q_1(M)$ is given by

$$Q_1(M) = 1 - (1 - Q(M))^{N*L} \tag{5.60}$$

An acceptable probability of exceeding the design value of M is chosen as 10%. The short-term most probable value for a 10 year storm and the long term response for a 10% probability of being exceeded once a year are shown in Table 5.4.

In the above example, the difference between the short- and long-term response extremes is quite small. However, the long-term extreme is obtained on the basis of exceedance in one year as opposed to the 10 year storm for the short-term response.

EXAMPLE 2 - EXTREME FORCE BY MORISON FORMULA

The Morison formula describing force on a vertical cylindrical member of an offshore structure is given by

$$f = k_M \dot{u} + k_D |u|u \tag{5.61}$$

where $k_M = C_M \rho \pi D^2/4$, $k_D = 1/2\ C_D\ \rho\ D$, u = horizontal water particle velocity and $\dot{u}$ = horizontal acceleration. In order to derive a force spectrum, Eq. 5.61 is statistically linearized as

$$f = k_M \dot{u} + \sqrt{8/\pi}\ k_D\ \sigma_u\ u \tag{5.62}$$

188

where σ_u = standard deviation of the water particle velocity. Thus, once the seastate is known, σ_u is known and force is strictly linear with the wave height. A transfer function for force may be determined which, however, will depend on the seastate under consideration.

For a short-term response prediction, the transfer function can be used directly without any difficulty similar to any linear system. However, for a long-term prediction method, the transfer function has to be modified with each seastate. An example of the difference in the transfer function is shown in Fig. 5.1. In order to overcome this problem, a further approximation is made by choosing one seastate to obtain the transfer function which is then used to derive σ_f for all seastates.

Using the narrow band solution, the probability density function of the normalized force amplitude, $\bar{f}$, is given by

$$p(\bar{f}) = (\tfrac{3}{4} K^2 + 1) \, \bar{f} \, \exp \left(- \frac{\tfrac{3}{4} K^2 + 1}{2} \bar{f}^2 \right) \qquad \text{for } \bar{f} < h \tag{5.63}$$

$$p(\bar{f}) = \frac{(\tfrac{3}{4} K^2 + 1)^{1/2}}{K} \, \exp \left(- \frac{(\tfrac{3}{4} K^2 + 1)^{1/2}}{K} \left(\bar{f} - \frac{\bar{f}_0}{2} \right) \right) \text{ for } \bar{f} > h \tag{5.64}$$

where

$$h = \frac{1}{K(\tfrac{3}{4} K^2 + 1)^{1/2}} \tag{5.65}$$

and

$$\bar{f} = \frac{f_0}{\sigma_f} \tag{5.66}$$

Thus, the peak force amplitude distribution depends on σ_f and K.

The standard deviation for the force using the Morison equation is

$$\sigma_f^2 = 3 \, k_D^2 \, \sigma_u^4 + k_M^2 \, \sigma_u^2 \tag{5.67}$$

whereas the linear approximation gives
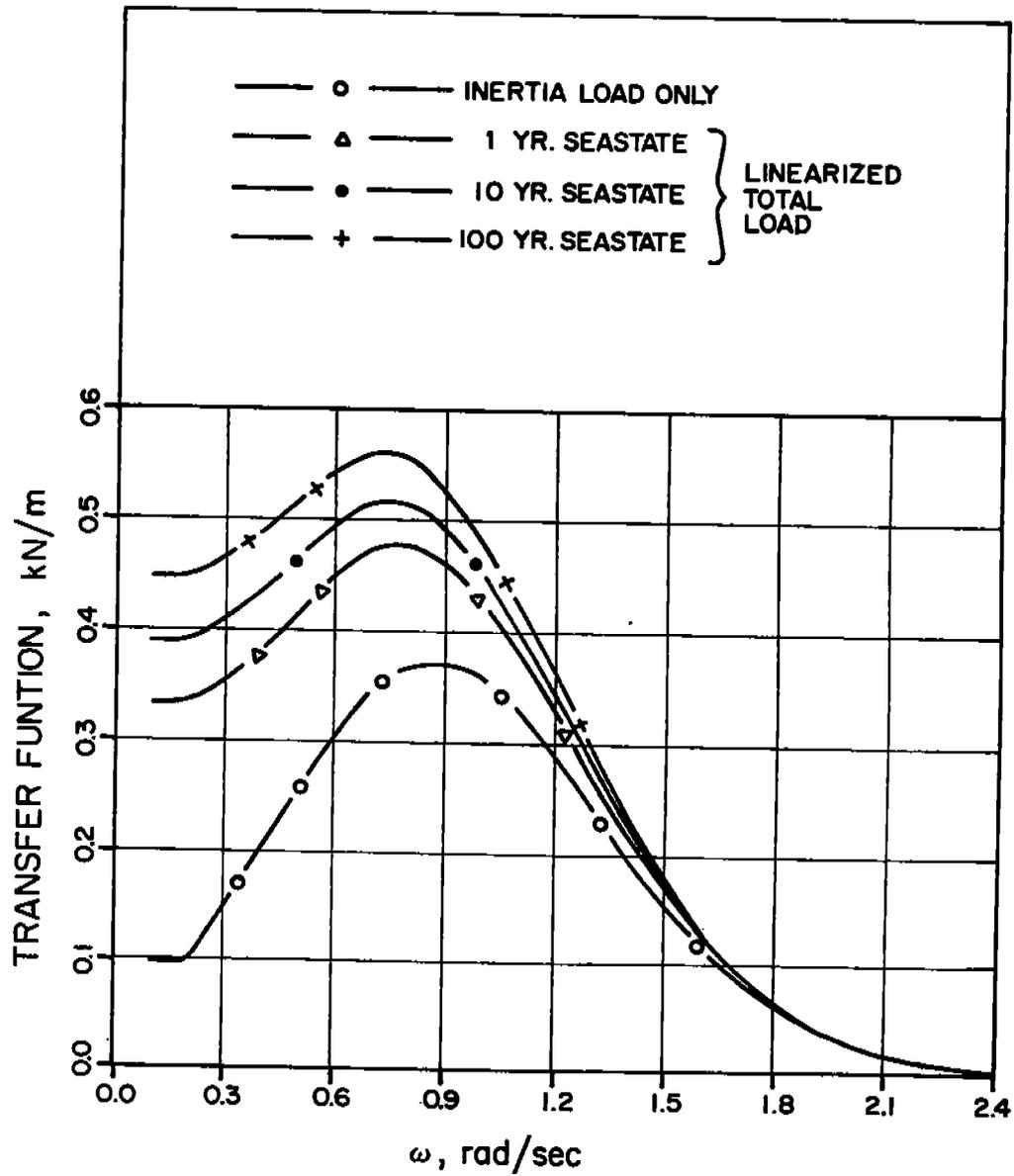
FIGURE 5.1   TRANSFER FUNCTIONS FOR THE MORISON FORCE FOR DIFFERENT
SEASTATES [INGLIS, ET AL. (1985)]

TABLE 5.5

EXTREME VALUE FORCES ACTING ON 1 m

ELEMENT OF PILE AT 13 m BELOW SEA LEVEL

BY MORISON FORMULA

FORCE CALCULATIONS	PEAK PROBABILITY DISTRIBUTION	MOST PROBABLE EXTREME FORCE	(kN)
Short Term 10 Year	Gaussian Response	3.7 x RMS =	5.7
Sea-State H_s = 14.2 m, T_z = 13.6 sec.	Non-Gaussian Response $K = 1.11$	7.7 x RMS =	11.9
Long Term	Linearization in each sea state	Non-Gaussian $K = 0.00579 * H_s * T_z$	14.3
	Single transfer function linearization in 1-year sea state	Non-Gaussian $K = 0.00579 * H_s * T_z$	12.8
	Single transfer function linearized in 10 year sea state	Non-Gaussian $K = 0.00579 * H_s * T_z$	14.4
	Single transfer function linearized in 100 year sea state	Non-Gaussian $K = 0.00578 * H_s * T_z$	16.0
	Linearization in each sea state	Gaussian (Rice distribution)	7.0

$$\sigma_f^2 = \frac{8}{\pi} k_D^2 \sigma_u^4 + k_M^2 \sigma_{\dot{u}}^2 \tag{5.68}$$

Then the error in the estimate of K given by the ratio of drag to inertia force components is of the order of 8%. Note that K is a function of H_s. In the present example the dependence of K to T_z is found to be linear in T_z given by

$$K = K_0 T_z H_s \tag{5.69}$$

where $K_0 = 0.00579$. These formulations were used to predict long-term extreme force. The results are given in Table 5.5. In the example, both the nonlinear peak distribution for a narrow-band non-Gaussian process and the linear exponential (Rice) distribution for a general wide-band Gaussian process have been used. The short-term prediction is based on a 10 year storm while the long-term prediction assumed a 10% probability of exceeding once in a year. The factors for the extremes for the short-term prediction are used as 7.7 times the standard deviation for the non-Gaussian process and 3.7 times the standard deviation for the Gaussian process [Brouwers and Verbeek (1983)]. From the table it is seen the non-Gaussian response more than doubles the extreme value prediction. The long-term predictions in this case are higher than the short-term ones by about 20%.

6.0 CONCLUDING REMARKS

The nonlinear analysis for various responses of an offshore structure and the extreme value prediction of those responses are reviewed in this report. Different classes of offshore structures are introduced and the applicability of the nonlinear systems to these structures is discussed wherever appropriate. Because of the complexity of determining the probabilistic properties of a general class of nonlinear responses, only approximate solutions in the extreme value analysis is possible. Various methods of approximating nonlinear systems and the limitations in their application in an offshore structure design are discussed. Nonlinear problems leading to the non-Gaussian distribution and the extent of their departure from a Gaussian distribution are investigated. Based on these solutions, techniques of predicting extreme values of both linear and nonlinear responses for marine structures that are consistent within the particular methods are given.

The discussions included in this report warrant the following conclusions:

1. For a nonlinear system, the response parameter is nonlinearly related to the wave elevation through nonlinear elements in the wave force excitation or in the structure's system characteristics. In either case, the response becomes non-Gaussian. No consistent method exists for such a system. In a few special cases, the solutions may be found by approximations or modification of the analysis procedure. Sometimes the response characteristics of the system act as a linear filter, e.g., for a lightly damped system even when force excitation is nonlinear in wave elevation. Examples of such possible systems is the finely-tuned springing of a TLP tendon. Thus, even if force probability distribution is non-Gaussian the response is nearly Gaussian.

2. The structural response time history for a single degree of freedom system is similar between uncoupled, coupled and linearized drag forces. In the latter case, the error is about 20% for large $H/D > 20$. For random waves, the mean square values are similar, but the linearized method produces considerably lower (60% at $H_s/D > 20$)

191

extreme values of response. The nonlinear drag also alters the spectral distribution of wave forces providing an increased energy at higher frequencies. This may increase the resonant response compared to a linearized analysis.

3. The expected extreme responses of members of offshore structures by the nonlinear drag forces exceed significantly those predicted by equivalent linear methods, particularly when drag forces are predominant. Nonlinear effects can be expected to be important in fatigue damage computed when for a significant portion of the life of the structure the drag forces constitute a significant part of the total force. Typical example of such members are the small diameter members of jacket structures in water near the free surface, conductors and risers in areas of severe wave action. For extreme value analysis, the effect of drag nonlinearity may be important even for larger members.

4. If a linearized method is applied in a complex numerical analysis, the effect of the nonlinear probability distribution not taken into account in the analysis should be corrected. While this is not an easy task, in a limited number of cases, a reasonable correction factor may be achieved by the comparison of results presented in the report. For example, Fig. 3.47 shows the amount of deviation in the probability of exceedance of a low-frequency surge motion from Gaussian. Care should be exercised in using these data, however, as they are limited.

5. The surge periods of a large compliant structure (for example, catenary anchored) is very long, of the order of one minute. The second-order wave forces based on difference frequencies of component waves excite the structure at its natural frequency giving rise to large anchor loads. On the other hand, a compliant structure held by taut cables, such as a tension leg platform has a high frequency natural period in the vertical direction. Second-order wave forces at the sum frequencies of component waves can resonate the structure in the vertical direction introducing large

192

tendon loads which is important consideration for fatigue damage evaluation. This phenomenon, known as springing load, is proportional to the square of wave amplitude and, thus, has similar characteristics as the wave drift load. The response probability is expected to be similar in this case.

6. The deterministic design wave and the probabilistic short-term procedures fail to adequately predict consistent maximum responses in a structure's lifetime for which a long-term statistical distribution method is far more appropriate. Wave data for this method, however, are rather lacking in many sites particularly on a long term basis. In this case, a so-called '1000 year wave scatter diagram' may be extrapolated by the method presented herein. This provides a rational and consistent criterion of acceptability in the form of a uniform chance that a given response level is exceeded in the lifetime of the structure as opposed to the non-uniformity present in the first two methods.

7. For short-term as well as long term prediction, a family of wave spectra for a specified seastate has been advocated. Since the shape of the energy density spectrum varies considerably based on the environmental input, even for a given energy level (or, equivalently, given significant wave height), this method is more reliable in predicting extreme responses. For a two-parameter family, the wave height and the wave period were found to follow log-normal probability law (for $P < 0.99$). Since the responses are computed for a series of spectra, the upper and lower bounds as well as standard deviation of short-term responses may be obtained.

8. For estimating short-term extreme values of the responses for design consideration, various factors such as operation (or exposure) time, frequency of encounter with seas, speed (in the case of a ship), and risk parameter should be considered. In the long-term response prediction, factors such as seas of various severities, a variety of wave spectral shapes, various speeds (in case of a moving vehicle), various headings to waves, and the expected number of cycles of the response should be included in the prediction routine.

193

9. For non-Gaussian waves, a popular method of obtaining the distribution function for the time history of waves is to use a series representation in the probability theory. A common series available is the Gram-Charlier series. Several probability density functions for nonlinear waves are known. The non-Gaussian nature of nonlinear responses generally based on linear waves is characterized by the eigenvalue-eigenvector approach. This is particularly true for quadratic and linear plus quadratic response. Examples of such responses are slow drift oscillations, drift force, springing force, etc. Several probability density functions are derived in series forms by this method. Once the initial distribution is known, extreme values may be predicted from it.

7.0 RECOMMENDATION FOR FUTURE WORKS

It is clear that no systematic procedure exists to handle nonlinear problems in predicting extreme value responses by probabilistic means either long term or short term. Only a few special cases may be treated at this time and those too only after certain linearization or other approximations. Based on the present review the following recommendations are made to further the state-of-the-art of the nonlinear extreme value analysis.

1. Various energy spectral models to describe random ocean waves are known. They do an adequate job of describing the ocean waves at a particular site for a given set of wave statistical parameters, i.e., a suitable form of the spectral model may be chosen based on the statistical parameters that match the energy distribution reasonably well. However, the knowledge of the upper tail of the spectrum at the high frequency end is less confident and often poor. Since the extreme values (including higher moments of spectra for such derivation) are highly dependent on this upper tail, care must be taken to describe them accurately. Therefore, more research work is needed to study this area in terms of reliable field data in the area and the corresponding mathematical description.

2. Most of the probability methods start with the assumption of Gaussian waves. However, waves are not necessarily Gaussian. In fact, high waves which produce the extreme values are seldom Gaussian. The distribution of nonlinear and non-Gaussian waves has received some attention in the past several years. Several methods have been presented here that deal with non-Gaussain waves and excitation. The treatment of corresponding non-Gaussain responses is relatively few. More theoretical and general statistical description of non-Gaussian response behavior of more practical marine structures should be developed. Such developments should include cases of non-Gaussian random excitation of a linear system, and Gaussian random excitation of a nonlinear system as well as a combination of the two.

195

3. The interaction of waves and currents and the resulting influence on the responses should be thoroughly investigated. The influence of currents on the random wave loading both for Morison type loading and of second-order drift forces is not known adequately.

4. The probability of simultaneous occurrence of waves (with parameter H_s, T_z and θ_0) and current (with parameter U, θ_0 and profile with depth) should be known.

5. The formulation of the long-term probability distribution for the characteristic wave height and wave period is limited. More knowledge of the actual distribution function for these parameters is needed so that accurate long-term prediction of responses is possible.

6. The probabilistic description of the water particle kinematics in the free surface zone is limited. Further work is needed, particularly through experiments with high waves, to collect data in this area so that a better understanding of the free surface effect on marine structures may be achieved in a probabilistic sense.

7. Most of the statistical treatments of nonlinear problems have been centered around the wave exciting forces in the form of Morison equation. While a few studies have been made regarding nonlinear structural responses, more work is needed to determine the effect of nonlinear forces on the structural responses (both linear and nonlinear) and how they can be used to derive the extreme response values.

The above is a list of some of the general areas of nonlinear extreme value analysis that are required in the future years to come so that the state-of-the-art may be extended to the point where it may be incorporated in the design of marine structures in a routine manner. These investigations are complicated and will require considerable time to develop. Because of the limited knowledge in this area this technique is not used routinely by offshore design engineers for nonlinear systems. It is hoped that the

196

strengths and limitations of various methods described here will enable the design engineer to attempt to use these methods more often where appropriate.

However, additional work may be performed to make this report more valuable to the designer. This will require performing several case studies based on various approximate methods described here. Since many of the simplified methods outlined do not need complicated numerical computation and simple expressions have been included in many cases, such an analysis will be relatively straight-forward compared to the work under Recommendations 1-7 above. Hypothetical but practical structures along with their design parameters may be chosen for the design calculation purposes. The structures will be kept simple so that the calculation process is not too involved and comparison of various methods is not difficult. The design computations will be made in a systematic manner and extreme values of the responses will be predicted for each method chosen. Where the methods are not applicable because of inherent assumptions it will be so stated. This then, may be used as a cookbook by a designer in his own design. He may also be able to use his engineering judgment regarding the choice of a suitable method and its effect on the extreme value prediction. Any necessary correction to this value because of his model may then be easier to make.

8.0 REFERENCES

REVIEWS ON STATISTICS

1. Cramer, H., "Mathematical Methods of Statistics", Princeton University Press, Princeton, New Jersey, 1946.

2. Ochi, M.K., "Stochastic Analysis and Probabilisitc Prediction of Random Seas", Advances in Hydroscience, Vol. 13, 1984, pp. 217-375.

3. Tobias, P.A. and Trindade, D., Applied Reliability, Van Nostrand Reinhold Company, New York, 1986.

NONLINEAR ANALYSIS

1. Burns, G.E., "Calculating Viscous Drift of a TLP," Proceedings of Second International Offshore Mechanics and Arctic Engineering Symposium, ASME, New York, 1983.

2. Chakrabarti, S.K., "Inline Forces on Fixed Vertical Cylinder in Waves," Journal of the Waterway, Port, Coastal and Ocean Division, ASCE, Vol. 106, May 1980.

3. Chakrabarti, S.K., "Impact of Analytical, Model and Field Studies on the Design of Offshore Structures," International Symposium on Ocean Engineering Ship Handling, SSPA, Gothenburg, Sweden, September 1980.

4. Chakrabarti, S.K. and Frampton, R.E., "Review of Riser Analysis Techniques," Applied Ocean Research, Vol. 4, No. 2, April 1982.

5. Chakrabarti, S.K. and Cotter, D.C., "First and Second Order Interaction of Waves with Large Offshore Structures", Second International Symposium on Offshore Mechanics and Arctic Engineering, ASME, Houston, Texas, February 1983.

6. Chakrabarti, S.K., "Nonlinear Wave Effects on Large Offshore Structures," Second International Symposium on Ocean Engineering and Ship Handling, Gothenburg, Sweden, March 1983.

7. Chakrabarti, S.K. and Cotter, D.C., "Hydrodynamic Coefficients of Mooring Tower," Proceedings of Fifteenth Annual Offshore Technology Conference, Houston, Texas, May 1983.

8. Chakrabarti, S.K., Cotter, D.C. and Libby, A.R., "Hydrodynamic Coefficients of a Harmonically Oscillated Tower," Applied Ocean Research, Vol. 5, No. 4, 1983.

9. Chakrabarti, S.K. and Cotter, D.C., "Nonlinear Wave Interaction with a Moored Floating Cylinder," Proceedings of the Sixteenth Annual Offshore Technology Conference, Houston, Texas, May 1984.

10. Chakrabarti, S.K., "Steady Drift Force on Vertical Cylinder - Viscous vs. Potential", Applied Ocean Research. Vol. 6, No. 2, 1984, pgs. 73-82.

11. Chakrabarti, S.K., "Moored Floating Stuctures and Hydrodynamic Coefficients," Presented at the Ocean Structural Dynamic Symposium, Corvallis, Oregon, September 1984.

12. Chakrabarti, S.K., "Hydrodynamic Coefficients and Depth Parameter," Journal of Waterway, Port, Coastal and Ocean Engineering, Vol. 111, No. 1, January 1985, pp. 123-127.

13. Cotter, D.C. and Chakrabarti, S.K., "Wave Force Tests on Vertical and Inclined Cylinders," Journal of Waterways, Ports, Coastal and Ocean Division, ASCE, Vol. 110, February 1984, pp. 1-14.

14. Dahong, Q., and Quihau, Z., "The Dynamic Response of an Underwater Column Hinged at the Sea Bottom Under the Wave Action," Proceedings on Behavior of Offshore Structures, MIT, Boston, Vol. 2, 1982, pp. 523-531.

15. Dalrymple, R.A., "Waves and Wave Forces in the Presence of Currents," Proceedings on Conference on Civil Engineering in Oceans III, Delaware, Vol. 2, 1975, pp. 999-1017.

16. Dao, V., V., and Penzien, J., "Comparison of Treatments of Nonlinear Drag Forces Acting on Fixed Offshore Platforms," Applied Ocean Research, Vol. 4, No. 2, 1982.

17. Dean, R.G., "Stream Function Representation of Nonlinear Ocean Waves," Journal of Geophysical Research, Vol. 70, 1965, pp. 4561-4572.

18. Dean, R.G., "Relative Validities of Water Wave Theories," Journal of Waterways, Harbors and Coastal Engineering Division, ASCE, Vol. 96, No. WW1, 1970, pp. 105-119.

19. DeBoom, W.C., Pinkster, J.A., and Tan, P.S.G., "Motion and Tether Force Prediction for a TLP," Journal of Waterway, Port, Coastal and Ocean Division, ASCE, Vol. 110, No. 4, November 1984, pp. 472-486. (Also, 15th OTC, Houston, Texas, May 1983.)

20. Elgar, S., Guza, R.T., and Seymour, R.J., "Wave Group Statistics from Numerical Simulations of a Random Sea," Applied Ocean Research, Vol. 7, No. 2, 1985, pp. 93-96.

21. Faltinsen, O.M., and Loken, A.E., "Drift Forces and Slowly Varying Forces on Ships and Offshore Structures in Waves," Norwegian Maritime Research, No. 1, 1978.

22. Hallam, M.G., Heaf, N.J., and Wootton, L.R., "Dynamics of Marine Structures: Methods of Calculating the Dynamic Response of Fixed Structures Subject to Wave and Current Action," CIRIA Underwater Engineering Group, London, Report UR8, 1977.

23. Hearn, G.E., Tong, K.C. and Ramzan, F.A., "Wave Drift Damping Coefficient Predictions and Their Influence in the Motions of Moored Semisubmersibles", Proceedings of the Nineteenth Annual Offshore Technology Conference, Houston, Texas, OTC 5455, 1987, pp. 297-331.

24. Hudspeth, R., "Wave Force Predictions from Nonlinear Random Sea Simulations," Proceedings on Seventh Offshore Technology Conference, Houston, Texas, OTC 2193, 1975, pp. 471-485.

25. Hsu, F.H., and Blenkarn, K.A., "Analysis of Peak Mooring Forces Caused by Slow Vessel Drift Oscillations in Random Seas," Offshore Technology Conference, OTC, 1159, Houston, Texas, May 1970.

26. Isaacson, M. de St. Q., "Nonlinear Wave Effects on Fixed and Floating Bodies," Journal of Fluid Mechanics, Vol. 120, 1982, pp. 267-281.

27. Iwagaki, Y., Asano, T., and Nagai, F., "Hydrodyanmic Forces on a Circular Cylinder Placed in Wave-Current Coexisting Fields," Memoirs of the Faculty of Engineering, Kyoto University, Japan, Vol. XLV, Part 1, January 1983, pp. 11-23.

28. Garrison, C.J., "Comments on the Cross-Flow Principle and Morison's Equation," Journal of Waterway, Port, Coastal and Ocean Engineering Division, ASCE, Vol. 111, No. 1, 1985.

29. Jain, R.K., and Kirk, C.L., "Dynamic Response of a Double Articulated Offshore Loading Structure to Non-Collinear Waves and Currents," Proceeding of the Energy Technology Conference, ASME, Preprint No. 80-PET-56, New Orleans, Louisiana, February 1980.

30. Kinsman, B., Wind Waves, Prentice-Hall, Englewood Cliffs, New Jersey, 1965.

31. Kobsyashi, M., Shimada, K., and Fujchira, T., "Study on Dynamic Response of a TLP in Waves," Proceedings of the Fourth International Offshore Mechanics and Arctic Engineering Symposium, ASME, Vol. 1, February 1985, pp. 29-35.

32. Larsen, C.M., et al., "Nonlinear Static and Dynamic Behavior of Tension Leg Platform Tethers", Proceedings of the Third International Offshore Mechanics and Arctic Engineering Symposium, New Orleans, Louisiana, ASME, 1984, pp. 41-50.

33. LeMéhauté, B., An Introduction to Hydrodynamics and Water Waves, Springer-Verlag, Dusseldorf, 1976.

34. Lighthill, M.J., "Waves and Wave Loading," Proceedings on Second Conference on Behavior of Offshore Structures, BOSS '79, London, Vol. 1, 1979, pp. 1-40.

35. Longuet-Higgins, M.S., and Stewart, R.W., "The Changes in Amplitude of Short Gravity Waves on Steady Non-Uniform Currents," Journal of Fluid Mechanics, 1981.

36. Lyons, G.J. and Patel, M.H., "Comparisons of Theory with Model Test Data for Tensioned Buoyant Platforms", Journal of Energy Resources Technology, Transactions ASME, Vol. 106, 1984, 426-436.

37. Moe, G., and Verley, R.L.P., "Hydrodynamic Damping of Offshore Structures in Waves and Currents," Proceedings of the Twelvth Offshore Technology Conference, Houston, Texas, OTC 3798, May 1980, pp. 37-44.

38. Morison, J.R., O'Brien, M.P., Johnson, J.W., and Shaaf, S.A., "The Forces Exerted by Surface Waves on Piles," Transactions AIME, Vol. 189, 1950, pp. 149-154.

49. Nakamura, S., Saito, K., and Takagi, M., "On the Increased Damping of a Moored Body During Low-Frequency Motions in Waves", Proceedings of the Fifth International Offshore Mechanics and Arctic Engineering Symposium, Vol. I, ASME, Tokyo, Japan, 1986, pp. 281-288.

50. Nichols, J.D., and Hirt, C.W., "Nonlinear Hydrodynamic Forces on Floating Bodies," Proceedings on Second Conference on Numerical Ship Hydrodynamics, Berkeley, 1977, pp. 382-394.

41. Nordgren, R.P., "Analysis of High-Frequency Vibration of Tension Leg Platform", Proceedings of the Fifth International Offshore Mechanics and Arctic Engineering Symposium, Vol. III, ASME, Tokyo, Japan, 1986, pp. 149-156.

42. Patel, M.H. and Lynch, E.J., "The Coupled Dynamics of Tensioned Buoyant Platforms and Mooring Tethers", Journal of Engineering Structures, Vol. 5, 1983, pp. 299-308.

43. Petrauskas, C. and Liu, S.V., "Springing Force Response of a Tension Leg Platform", Proceedings of the Nineteenth Annual Offshore Technology Conference, Houston, Texas, OTC 5458, 1987, pp. 333-341.

44. Pinkster, J.A., "Low Frequency Second Order Wave Exciting Forces on Floating Structures," Publication No. 650, Netherlands Ship Model Basin, Wageningen, 204 pages.

45. Pinkster, J.A., and Oortmerssen, G., "Computation of the First and Second Order Wave Forces on Bodies Oscillating in Regular Waves," Second International Conference on Numerical Ship Hydrodynamics, University of California, Berkeley, 1977.

46. Pinkster, J.A., "Mean and Low Frequency Wave Drifting Forces on Floating Structures," Ocean Engineering, October 1974.

47. Qi, X.Y., Fang, Y., and Zhang, J.L., "Low-Frequency Surge Motion of TLP in Survival Sea State", Proceedings of the Fifth International Offshore Mechanics and Arctic Engineering Symposium, Vol. III, ASME, Tokyo, Japan, 1986, pp. 120-125.

48. Roberts, J.B., "Nonlinear Analyis of Slow Drift Oscillations of Moored Vessels in Random Seas," Journal of Ship Research, 1980.

49. Rye, H., Rynning, S. and Moshagen, H., "On the Slow Drift Oscillation of Moored Structures", Proceedings of the Seventh Annual Offshore Technology Conference, OTC 2366, 1975, pp. 299-310.

50. Salvesen, N., Meinhold, M.J., and Yue, D.K., "Nonlinear Motions and Forces on Tension Leg Platform," U.S. Coast Guard, Washington, DC., USCG-M-84-4, May 1984.

51. Salvesen, N., von Kerczek, C.H., Yue, D.K., and Stern, F., "Computations of Nonlinear Surge Motions of Tension Leg Platforms," Proceeding of Fourteenth Offshore Technology Conference, Houston, Texas, OTC 4394, May 1982, pp. 199-215.

52. Sarpkaya, T., and Isaacson, M. de St. Q., Mechanics of Wave Forces on Offshore Structures, von Nostrand Reinhold, New York, 1981.

53. Sarpkaya, T., Bakmis, C., and Storm, M.A., "Hydrodynamic Forces from Combined Wave and Current Flow on Smooth and Rough Circular Cylinders at High Reynolds Number," Proceedings of the Sixteenth Offshore Technology Conference, Houston, Texas, OTC 4830, 1984, pp. 455-462.

54. Sarpkaya, T., Collins, N.J. and Evans, S.R., "Wave Forces on Rough-Walled Cylinders at High Reynolds Numbers," Proceedings on the Ninth Offshore Technology Conference, Houston, OTC 2701, May 1977.

55. Skjelbreia, L., and Hendrickson, J.A., "Fifth Order Gravity Wave Theory," Proceedings on the Seventh International Coastal Engineering Conference, The Hague, 1960, pp. 184-196.

56. Tucker, M.J., Challenor, P.J., and Carter, D.J.T., "Numerical Simulation of a Random Sea: A Common Error and Its Effect Upon Wave Group Statistics," Applied Ocean Research, Vol. 6, No. 2, 1984, pp. 118-122.

57. Vandiver, J.K., "Prediction of the Damping-Controlled Response of Offshore Structures to Random Wave Excitation", Society of Petroleum Engineering Journal, 1980, pp. 5-14.

58. Vugts, J.H., and Bouquet, A.G., "A Nonlinear, Frequency Domain Description of Wave Forces on an Element of a Vertical Pile in Random Seas," Proceedings on the Behavior of Offshore Structures, Amsterdam, Elsevier Science, July 1985, pp. 239-253.

59. Wichers, J.E.W., "On the Low-Frequency Surge Motions of Vessel Moored in High Seas", Proceedings on the Fourteenth Annual Offshore Technology Conference, OTC 4437, 1982, Houston, Texas.

60. Wichers, J.E.W. and Huijsmans, R.M.H., "On the Low Frequency Hydrodynamic Damping Forces Acting on Offshore Moored Vessels", Proceedings of the Sixteenth Annual Offshore Technology Conference, OTC 4813, 1984, Houston, Texas.

61. Wiegel, R.L., "A Presentation of Cnoidal Wave Theory for Practical Application," Journal of Fluid Mechanics, Vol. 7, 1960, pp. 273-286.

SHORT TERM WAVE HEIGHT STATISTICS

1. Ahren, M.K. and Plaisted, R.O., "Nonlinear Deformation of Sea-Wave Profiles in Intermediate and Shallow Water", Oceanological Acta, Vol. 4, No. 2, 1981, pp. 107-115.

2. Battjes, J.A., "Probabilistic Aspects of Ocean Waves", Report No. 77-2, Delft University of Technology, Netherlands, 1977.

3. Bitner, E.M., "Nonlinear Effects of the Statistical Model of Shallow-Water Wind Waves", Applied Ocean Research, Vol. 2, No. 2, 1980, pp. 63-74.

4. Bowden, K.F., "Some Observations of Waves and Other Fluctuations in a Tidal Current", Proc. Royal Society of London, Vol. A192, 1948, pp. 403-425.

5. Cartwright, D.E., and Longuet-Higgins, M.S., "The Statistical Distribution of the Maxima of the Random Function," Proceedings of Royal Society, London, Series A, Vol. 237, 1956, pp. 212-232.

6. Chakrabarti, S.K., and Snider, R.H., "Wave Statistics for March 1968 North Atlantic Storm," Journal of Geophysical Research, Vol. 79, No. 24, August 1974.

7. Chakrabarti, S.K. and Cooley, R.P., "Ocean Wave Statistics for 1961 North Atlantic Storm," Journal of Waterways, Port, Coastal and Ocean Division, ASCE, Vol. 103, November 1977.

8. Chakrabarti, S.K. and Cooley, R.P., "The Stability of Some Currently Used Wave Parameters - A Discussion," Coastal Engineering, Vol 1, 1977, pp. 359-365.

9. Edgeworth, F.Y., "The Law of Error", Trans. Camb. Phil. Soc., Vol. 20, No. 1, 1904, pp. 36-65.

10. Forristall, G.Z., "On the Statistical Distribution of Wave Heights in a Storm," Journal of Geophysical Research, Vol. 83, 1978, pp. 2353-2358.

11. Goda, Y., "Numerical Experiments on Wave Statistics with Spectral Simulation," Report of Port and Harbour Research Institute, Japan, Vol. 9, No. 3, 1970, pp. 320-337.

12. Goda, Y., "Estimation of Wave Statistics From Spectra Information," Proceedings International Symposium on Ocean Wave Measurement and Analysis, ASCE, New Orleans, 1974, pp. 320-337.

13. Goodknight, R.C., and Russell, T.L., "Investigation of the Statistics of Wave Heights," Journal of the Waterways and Harbors Division, ASCE, Vol. 89, No. WW2, 1963.

14. Huang, N.E. and Long, S.R., "An Experimental Study of the Surface Elevation Probability Distribution and Statistics of Wind-Generated Waves", J. of Fluid Mechanics, Vol. 101, No. 1, 1980, pp. 179-200.

15. Huang, N.E., et al., "A Non-Gaussian Statistical Model for Surface Elevation of Nonlinear Random Wave Fields", J. of Geophysical Research, Vol. 88, No. C12, 1983, pp. 7597-7606.

16. Jasper, N.H., "Statistical Distribution Patterns of Ocean Waves and Wave-Induced Ship Stresses and Motions with Engineering Applications," Society of Naval Architects and Marine Engineers, Transactions, Volume 64, 1956.

17. Longuet-Higgins, M.S., "On the Statistical Distribution of the Heights of Sea Waves," Journal of Marine Research, Vol. 11, 1952, pp. 245-266.

18. Longuet-Higgins, M.S., "The Effect of Non-Linearities on Statistical Distributions in the Theory of Sea Waves, J. Fluid Mechanics, 1963, 17(3), pp. 459-480.

19. Longuet-Higgins, M.S., "On the Distribution of the Heights of Sea Waves: Some Effects of Nonlinearity and Finite Band Width", J. of Geophysics Research, Vol. 80, No. 18, 1975, pp. 2688-2694.

20. Ochi, M.K. and Whalen, J.E., "Estimation of Extreme Waves Critical for the Safety of Offshore Structures", Proc. Offshore Technology Conference, OTC 3596, 1979, 2085-2090.

21. Ochi, M.K. and Whalen, J.E., "Prediction of the Severest Significant Wave Height", Proc. on Seventeenth International Conference of Coastal Engineering, Vol. 1, 1980, pp. 587-599.

22. Ochi, M.K. and Wang, W.C., "Non-Gaussian Characteristics of Coastal Waves", Proceedings of Nineteenth International Conference on Coastal Engineering, 1984.

23. Putz, R.R., "Statistical Distribution for Ocean Waves," Transactions of American Geophysical Union, Vol. 33, No. 5, 1952, pp. 685-692.

24. Tayfun, M.A., "Narrow-Band Nonlinear Sea Waves", J. of Geophysical Research, Vol. 85, No. C3, 1980, pp. 1548-1552.

25. Tayfun, M.A., "Distributuion of Crest-to-Trough Wave Heights", Proc. of Waterways, Harbors & Coastal Engrg., ASCE, Vol. 107, No. WW3, 1981, pp. 149-158.

26. Walden, A.T., and Prescott, P., "The Asymptotic Distribution of the Maximum of N Wave Crest Heights for Any Value of the Spectral Width Parameter," Journal of Geophysical Research, Vo. 85, No. C4, April 1980, pp. 1905-1909.

SHORT-TERM PERIOD DISTRIBUTION

1. Buckley, W.H., "Climatic Wave Spectra for Use in Design of Ships and Offshore Platforms", DTCG23-85-F-20014, David W. Taylor NSRDC, Bethesda, Maryland, August, 1986, 119 pages.

2. Epstein, B., "The Distribution of Extreme Values in Sample Whose Members are Subject to Markov Chain Condition", Ann. Math. Stat. 20, 1949, pp. 590-594.

3. Ezraty, R., et al., "Comparison with Observation at Sea of Period or Height Dependent Sea State Parameters from a Theoretical Model", Proceedings of Offshore Technology Conference, OTC 2744, 1977, pp. 149-154.

4. Longuet-Higgins, M.S., "The Distribution of Intervals Between Zeros of a Stationary Random Function," Philosophical Transactions of Royal Society, Series A, Vol. 254, 1962, pp. 557-599.

SHORT-TERM HEIGHT-PERIOD DISTRIBUTION

1. Arhan, M.F., Cavanie, A.G., and Ezraty, R.S., "Determination of the Period Range Associated to the Design Wave," Offshore Technology Conference, OTC 3643, Houston, Texas, May 1979.

2. Chakrabarti, S.K. and Cooley, R.P., "Statistical Distribution of Periods and Heights of Ocean Waves," Journal of Geophysical Research, Vol. 82, No. 9, March 1977.

3. Ezraty, R., Laurent, M., and Arhan, M., "Comparison with Observation at Sea of Period or Height Dependent Sea State Parameters from a Theoretical Model," OTC 2744, Offshore Technology Conference, May 1977, pp. 149-154.

4. Goda, Y., "The Observed Joint Distribution of Periods and Heights of Sea Waves", Proceedings on the Sixteenth International Conference of Coastal Engineering, Vol. 1, 1978, pp. 151-170.

5. Longuet-Higgins, M.S., "On the Joint Distribution of the Periods and Amplitudes of Sea Waves," Journal of Geophysical Research, Vol. 80, 1975, pp. 2688-2694.

6. Longuet-Higgins, M.S., "On the Joint Distribution of Wave Periods and Amplitudes in a Random Wave Field", Proceedings of Royal Society of London, Series A, Vol. 389, 1983, pp. 241-258.

LONG-TERM WAVE HEIGHT STATISTICS

1. Battjes, J.A., "Long-Term Wave Height Distribution at Seven Stations Around the British Isles," National Institute of Oceanography, Godalming, England, Report No. A44, 1970.

2. Bretschnieder, C.L. (Editor), "On Wind Generated Waves," Topics in Ocean Engineering, Gulf Publishing Co., Houston, Texas, 1969.

3. Gumbel, E.J., Statistics of Extremes, Columbia University Press, New York, 1958.

4. Isaacson, M.Q. and MacKenzie, N.G., "Long-Term Distributions of Ocean Waves", Waterways Harbors and Coastal Engineering Division, ASCE, No. WW2, 1981, pp. 93-109.

5. Krogstad, H.E., "Height and Period Distributions of Extreme Waves," Applied Ocean Research, Vol. 7, No. 3, 1985, pp. 158-165.

6. Phillips, O.M., The Dynamics of the Upper Ocean, Second Edition, Cambridge University Press, 1977.

7. Price, W.G., and Bishop, R.E.D., Probabilistic Theory of Ship Dynamics, Chapman and Hall, London, 1974.

8. Thom, H.C.S., "Asymptotic Extreme Value Distributions of Wave Heights in the Open Ocean," Journal of Marine Research, Vol. 29, 1971, pp. 19-27.

9. Thom, H.C.S., "Distribution of Extreme Winds Over Oceans," Journal of Waterways, Harbors and Coastal Engineering Division, ASCE, Vol. 99, No. WW1, 1973, pp. 1-17.

10. Thom, H.C.S., "Extreme Wave Height Distribution Over Oceans," Journal of Waterways, Harbors and Coastal Engineering Division, ASCE, Vol. 99, No. WW3, 1973, pp. 355-374.

SHORT-TERM RESPONSE STATISTICS

1. Anastasiou, K., Tickell, R.G., and Chaplin, J.R., "The Nonlinear Properties of Random Wave Kinematics," Proceedings on Behavior of Offshore Structures, MIT, Boston, BOSS '82, August, 1982, pp. 493-515.

2. Bendat, J.A., and Piersol, A.G., "Spectral Analysis of Nonlinear Systems Involving Square-Law Operations," Journal of Sound and Vibration, Vol. 81, No. 2, 1982, pp. 199-213.

3. Bendat, J.A., "Statistical Errors for Nonlinear System Measurements Involving Square Operations," Journal of Sound and Vibration, Vol. 90, No. 2, 1983, pp. 275-302.

4. Bendat, J.A., "Decomponsition of Wave Forces into Linear and Nonlinear Components," Journal of Sound and Vibration, 1986.

5. Borgman, L.E., "Statistical Models for Ocean Waves and Wave forces," Chow, V.T., Editor, Advances in Hydroscience, Vol. 8, Academic Press, 1972, pp. 139-181.

6. Borgman, L.E., "Wave Forces on Piling for Narrow-Band Spectra," Journal of Waterways and Harbors Division, ASCE, Vol. 91, No. WW3, 1965, pp. 65-90.

7. Borgman, L.E., "Ocean Wave Simulation for Engineering Design," Journal of Waterways and Harbors Division, ASCE, Vol. 95, No. WW4, 1969, pp. 557-583.

8. Brouwers, J.J.H., and Verbeek, P.H.J., "Expected Fatigue Damage and Expected Extreme Response for Morison-Type Wave Loading," Applied Ocean Research, Vol. 5, No. 3, 1983, pp. 129-133.

9. Brouwers, J.J.H, "Response Near Resonance of Nonlinearly Damped Systems Subject to Random Excitation with Application to Marine Risers," Ocean Engineering, Vol. 9, 1982, p. 235-257.

10. Chakrabarti, S.K., "Statistical Properties of Wave-Current Force," (discussion), Journal of Waterways, Harbors and Coastal Engineering Division, ASCE, Vol. 100, May 1974.

11. Chakrabarti, S.K. and Libby, A.R., "Random Forces on Cylinder Near a Boundary", Proceedings on Coastal Hydrodynamics, ASCE, University of Delaware, Newark, July 1987.

12. Chakrabarti, S.K., "Forces on a Vertical Cylinder Due to Random Waves", Journal of Waterway, Harbor, Coastal and Ocean Engineering, ASCE, Vol. 114, 1988, (to be published).

13. Dunwoody, A.B., and Vandiver, J.K., "The Influence of Separated Flow Drag on the Dynamic Response of Offshore Structures to Random Waves," International Symposium on Hydrodynamics in Ocean Engineering, NIT, Trondheim, Norway, 1981.

14. Eatock Taylor, R., and Rajagopalan, A., "Superharmonic Resonance Effects in Drag Dominated Structures," Integrity of Offshore Structures, Edited by D. Faulkner, Cowling and Frieze, Applied Science Publishers, Proceedings of Symposium at Glasgow, July 1981, pp. 85-104.

15. Grigoriu, M., "Extremes of Wave Forces," Journal of Engineering Mechanics Division, ASCE, Vol. 110, No. 12, December 1984, pp. 1731-1742.

16. Herfjord, K., and Nielsen, F.G., "Nonlinear Wave Forces on a Fixed Vertical Cylinder due to the Sum Frequency of Waves in Irregular Seas," Applied Ocean Research, Vol. 8, No. 1, 1986, pp. 8-21.

17. Hu, S.J. and Lutes, L.D., "Non-Normal Descriptions of Morison-Type Wave Forces", Journal of Engineering Mechanics, ASCE, Vol. 113, No. 2, February, 1987, pp. 196-203.

18. Kato, S., Ando, S., and Kinoshita, T., "On the Statistical Theory of Total Second-Order Response of Moored Floating Structures", Proceedings on the Nineteenth Offshore Technology Conference, OTC 5579, Houston, Texas, 1987, pp. 243-257.

19. Langley, R.S., "The Statistics of Second Order Wave Forces," Applied Ocean Research, Vol. 6, No. 4, 1984, pp. 182-186.

20. Langley, R.S., "A Statistical Analysis of Low Frequency Second-Order Forces and Motions", Applied Ocean Research, Vol. 9, No. 3, 1987, pp. 163-170.

21. Larabee, R.D., "Extreme Wave Dynamics of Deepwater Platforms," Proceedings on Third International Conference on Behavior of Offshore Structures, BOSS 82, MIT, Cambridge, Massachusetts, 1982.

22. Moe, G., and Crandall, S.H., "Extremes of Morison-Type Wave Loadings on a Single Pile," Journal of Mechanical Design, ASME Transactions, Vol. 100, January 1978, pp. 100-104.

23. Moe, G., Sack, R.L., "Extremes of Morison Type Loading on Complex Structures," Safety of Structures under Dynammic Loading, pp. 752-759.
24. Moe, G., "Long Term Wave Force Statistics for a Vertical Pile," Coastal Engineering, No. 2, 1979, pp. 297-311.

25. Myrhaug, D. and Kjeldsen, S.P., "Prediction of Occurrences of Steep and High Waves in Deep Water", Journal of Waterway, Port, Coastal and Ocean Engineering, ASCE, Vol. 113, No. 2, March, 1987, pp. 122-138.

26. Naess, A., "The Effect of the Markov Chain Condition on the Prediction of Extreme Values," Journal of Sound and Vibration, Vol. 94, No. 1, 1984, pp. 87-103.

27. Naess, A., "Statistical Analysis of Second-Order Response of Marine Structures", Journal of Ship Research, Vol. 29, 1985, pp. 270-284.

28. Naess, A., "The Statistical Distribution of Second-Order Slowly-Varying Forces and Motions", Applied Ocean Research, Vol. 8, 1986, pp. 110-118.

29. Naess, A., "On the Statistical Analysis of Slow-Drift Forces and Motions of Floating Offshore Structure", Fifth OMAE Symposium, Vol. 1, 1986, pp. 317-329.

30. Neal, E., "Second Order Hydrodynamic Forces Due to Stochastic Excitation", Proceedings of Tenth ONR Symposium, 1974, pp. 517-537.

31. Ochi, M.K., "Generalization of Rayleigh Probability Distribution and Its Application," Journal of Ship Research, Vol. 22, No. 4, 1973, pp. 259-265.

32. Ochi, M.K., "Extreme Values of Waves and Ship Responses Subject to the Markov Chain Condition", J. of Ship Research, Vol. 23, No. 3, 1979, pp. 188-197.

33. Ochi, M.K. and Malakar, S.B., "Non-Linear Response of Ocean Platforms with Single Degree of Freedom in a Seaway", Rep. UFL/COEL-TR/050, University of Florida, Gainsville, 1984.

34. Ochi, M.K., "Non-Gaussian Random Processes in Ocean Engineering", Probabilistic Engineering Mechanics, Vol. 1, No. 1, 1986, pp. 28-39.

35. Pierson, W.J., Jr., and Holmes, P., "The Forces on a Pile to Irregular Waves," Journal of the Waterways and Harbors Division, ASCE, Vol. 91, No. WW4, Proceeding Paper 4528, 1965, pp. 1-10.

36. Pinkster, J.A. and Wichers. J.E.W., "The Statistical Properties of Low-Frequency Motions of Nonlinearly Moored Tankers", Proceedings of the Nineteenth Offshore Technology Conference, OTC 5457, Houston, Texas, 1987, pp. 317-331.

37. Roberts, J.B., "Stationary Response of Oscillators with Nonlinear Damping to random Excitation," Journal of Sound and Vibration, Vol. 50, No. 1, 1977, pp. 145-156.

38. Roberts, J.B., "First Passage Time for Oscillators with Nonlienar Damping," Journal of Applied Mechanics, No. 45, 1978, pp. 175-180.

39. Roberts, J.B., "Response of an Oscillator with Nonlinear Damping and a Softening Spring to Non-White Random Excitation", Probabilistic Engineering Mechanics, Vol. 1, No. 1, 1986, pp. 40-48.

40. Shinozuka, M., Yun, C., and Vaicaitis, R., "Dynamic Analysis of Fixed Offshore Structures Subject to Wind-Generated Waves", J. Structural Mechanics, Vol. 5, No. 2, 1977, pp. 135-146.

41. Sharma, J.N., and Dean, R.G., "Second Order Directional Seas and Associated Wave Forces," Proceedings on Eleventh Offshore Technology Conference, Houston, Texas, OTC 3645, May 1979, pp. 2505-2514.

42. Sigbjornsson, R. and Morch, M., "Spectral Analysis of Nonlinear Wave Load Effects on Offshore Platforms," Engineering Structures, Vol. 4, January 1982, pp. 29-37.

43. Stansberg, C.T., "Statistical Analysis of Slow-Drift Responses," Proceedings on Second International Conference on Offshore Mechanics and Arctic Engineering, ASME, Houston, Texas, 1983, pp. 188-197.

44. Tickell, R.G., "Continuous Random Wave Loading on Structural Members," The Structural Engineer, Vol. 55, No. 5, May 1977, pp. 209-222.

45. Tickell, R.G., "The Probabilistic Approach to Wave Loading on Marine Structures," Mechanics of Wave Induced Forces on Cylinders, (T.L. Shaw, Editor), Pitman, San Francisco, California, 1979, pp. 152-178.

46. Tung, C.C., and Huang, N.E., "Some Statistical Properties of Wave-Current Force on Objects," Sea Grant Publication, UNC-SG-72-14, December 1972, 24 pgs.

47. Tung, C.C., and Huang, N.E., "Statistical Properties of Wave-Current Force," Journal of Waterways, Harbors, and Coastal Engineering Division, ASCE, Vol. 99, No. WW3, August 1973, pp. 341-354.

48. Tung, C.C., "Statistical Properties of Wave Force," Journal of Engineering Mechanics Division, ASCE, Vol. 100, No. EM1, February 1974, pp. 1-11.

49. Tung, C.C., "Peak Distribution of Random Wave-Current Force," Journal of Engineering Mechanics Division, ASCE, Vol. 100, EM5, October 1974, pp. 873-884.

50. Vinje, T., "Statistical Distribution of Hydrodynamic Forces on Objects in Current and Waves," Norwegian Maritime Research, Vol. 8, No. 2, 1980.

51. Vinje, T., "On the Statistical Distribution of Second-Order Forces and Motion," International Shipbuilding Progress, Vol. 30, No. 343, March 1983, pp. 58-68.

52. Vinje, T., and Bitner-Gregersen, E., "Determination of the Statistical Distribution of Maxima of Responses to Narrow Banded Incoming Waves," Report No. 210, A.S. Veritas Research, January 1986, 15 pgs.

53. Vinje, T., "On the Statistical Distribution of Maxima of Slightly Nonlinear Stochastic Variables," Report SK/M 27, Division of Ship Structures, NIT, Trondheim, Norway, 1974, 95 pgs.

54. Vinje, T., "On the Calculation of Maxima of Nonlinear Wave Forces and Wave Induced Motions", I.S.P., Vol. 23, 1987, pp. 393-400.

55. Vinje, T., "On the Statistical Distribution of Second Order Forces," Report No. 2.6, VERITEC, January 1985, 48 pgs.

56. Vinje, T., "On the Statistical Distribution of Maxima of Slightly Nonlinear Stochastic Variables," Report SK/M 27, Division of Ship Structures, NIT, Trondheim, Norway, 1974, 95 pgs.

57. Vinje, T., "On the Statistical Distribution of Second Order Forces," Report No. 2.6, VERITEC, January 1985, 48 pgs.

LONG-TERM RESPONSE STATISTICS

1. Borgman, L.E., "Risk Criteria," Journal of Waterways and Harbors Division, ASCE, Vol. 89, No. WW3, 1963, pp. 1-35.

2. Fukuda, T., "Long Term Predictions of Wave Bending Moment," Journal of the Society of Naval Architects of Japan, Selected Papers, Vol. 5, 1968, pp. 33-55.

3. Hoffman, D., Van Hooff, R., and Lewis, W.V., "Evaluation of Methods for Extrapolation of Ship Bending Stress Data," Report SSC-234, Ship Structure Committee, Webb Institute of Naval Architecture, Glen Cove, New York, 1972.

4. Hoffman, D., and Lewis, E.V., "Analysis and Interpretation of Full-Scale Data on Midship Bending Stresses of Dry Cargo Ships," Report SSC-196, Ship Structure Committee, Webb Institute of Naval Architecture, Glen Cove, New York, 1969.

5. Hoffman, D., and Walden, D. A., "Environmental Wave Data for Determining Hull Structural Loadings," Ship Structures Committee, Report No. SSC 268, U. S. Coast Guard Headquarters, Washington, D. C., 1977.

6. Hoffman, D., and Karst, O.J., " The Theory of Rayleigh Distribution and Some of Its Applications," Journal of Ship Research, Vol. 19, No. 3, September 1975.

7. Houmb, O.G., and Overvik, T. "Parameterization of Wave Spectra and Long Term Joint Distribution of Wave Height and Period," Proceedings on Behaviour of Offshore Structures, BOSS '76, Trondheim, Vol. I, 1976, pp. 144-169.

8. Huntington, S.W., and Gilbert, G., "Extreme Forces in Short Crested Seas," Proceedings on Offshore Technology Conference, Houston, Texas, OTC 3595, May 1979.

9. Jasper, N.H., "Statistical Distribution Patterns of Ocean Waves and Wave-Induced Ship Stresses and Motions with Engineering Applications," Society of Naval Architecture and Marine Engineers, Transactions, Vol. 64, 1956.

10. Lewis, E.V., "Comparison of Long-Term Stress Distributions," Summer Seminar, Webb Institute of Naval Architecture, Glen Cove, New York, 1973.

11. Moe, G., "Long-Term Wave-Force Statistics for a Vertical Pile," Coastal Engineering, Vol. 2, 1979, pp. 297-311.

12. Naess, A., "Technical Note: On a Rational Approach to Extreme Value Analysis," Applied Ocean Research, Vol. 6, No. 3, 1984, pp. 173-174.

13. Naess, A., "Prediction of Extremes of Morison-Type Loading, An Example of a General Method," Ocean Engineering, Vol. 10, No. 5, 1983, pp. 313-324.

14. Naess, A., "Extreme Value Estimates Based on the Envelope Concept," Applied Ocean Research, Vol. 4, No. 3, 1982, pp. 181-187.

15. Nordenstrom, N., "A Method to Predict Long-Term Distributions of Waves and Wave-Induced Motions and Loads on Ships and Other Floating Structures," Det Norske Veritas, Report No. 81, 1973, pp. 9-39.

16. Ochi, M.K., "On Prediction of Extreme Values," Journal of Ship Research, March 1973, pp. 29-37.

17. Ochi, M.K., "Wave Statistics for the Design of Ships and Ocean Structures," Society of Naval Architecture and Marine Engineers, Vol. 86, 1978, pp. 47-76.

FATIGUE ANALYSIS

1. Burrow, R., "Expected Value Analysis for the Quasi-Static Response of Offshore Structures", Applied Mathematical Modeling, Vol. 7, No. 5, October, 1983, pp. 317-328.

2. Chaudhury, G.K. and Dover, W.D., "Fatigue Analysis of Offshore Platforms Subject to Sea Wave Loading", International Journal of Fatigue, Vol. 7, No. 1, January, 1985, pp. 13-19.

3. Chen, Y.N. and Wirsching, P.H., "Probability Based Fatigue Design Criteria for TLP Tendons", Proceedings on Fifth International Symposium on Offshore Mechanics and Arctic Engineering, ASME, Tokyo, Japan, 1986.

4. Grigoriu, M., "Dynamic Response of Offshore Platforms to Environmental Loads", Proceedings of Fourth Specialty Conference on Probabilistic Mechanics and Structural Reliability, ASCE, New York, NY, January, 1984, pp. 115-118.

5. Kenegaonkar, H.B. and Haldar, A., "Non-Gaussian Response of Offshore Platforms: Dynamic", Journal of Structural Engineering, ASCE, Vol. 113, No. 9, September, 1987, pp. 1899-1908.

6. Lutes, L.D., et al., "Stochastic Fatigue Damage Accumulation", Journal of Structural Engineering, ASCE, Vol. 110. No. 11, November, 1984, pp. 2585-2601.

7. Maddox, N.R. and Wildenstein, A.W., "A Spectral Fatigue Analysis for Offshore Structures", Proceedings of the Offshore Technology Conference, OTC 2261, May, 1975, pp. 185-197.

8. Miner, M.A., "Cumulative Damage in Fatigue", Transactions of the American Society of Mechanical Engineers, Vol. 12, 1945, pp. A-159-165.

9. Winterstein, S.R. and Cornell, C.A., "Fatigue and Fracture Under Stochastic Loading", Proceedings of Fourth International Conference on Structural Safety and Reliability, Kobe, Japan, Vol. 3, May, 1985, pp. 745-749.

10. Wirsching, P.H. and Light, M.C., "Probability-Based Fatigue Design Criteria for Offshore Structures", Final Report, American Petroleum Institute, Production Research Advisory Committee Project #15, November, 1979.

11. Wirsching, P.H. and Light, M.C., "Fatigue Under Wide Band Random Stresses", Journal of the Structural Division, ASCE, Vol. 106, No. ST7, July, 1980.

12. Wirsching, P.H. and Chen, Y.N., "Fatigue Design Criteria for TLP Tendons", Journal of Structural Engineering, ASCE, Vol. 113, No. 7, July, 1987, pp. 1398-1414.

13. Vugts, J.H., and Kinra, R.K., "Probabilistic Fatigue Analysis of Fixed Offshore Structures," Offshore Technology Conference, OTC 2608, Houston, Texas, May 1976.

CONSISTENT METHODOLOGY

1. Bendat, J.S., "Nonlinear System Dynamic Analysis Using Random Data," Naval Civil Engineering Laboratory, Report No. CR-85-006, Department of Navy, March 1985, 149 pages.

2. Inglis, R.B., Pijfers, J.G.L., and Vugts, J.H., "A Unified Probabilistic Approach to Predicting the Response of Offshore Structures, Including the Extreme Response," Proceedings on Behavior of Offshore Structures, 1985.

COMMITTEE ON MARINE STRUCTURES

Commission on Engineering and Technical Systems

National Academy of Sciences - National Research Council

The COMMITTEE ON MARINE STRUCTURES has technical cognizance over the interagency Ship Structure Committee's research program.

Stanley G. Stiansen (Chairman), Riverhead, NY
Mark Y. Berman, Amoco Production Company, Tulsa, OK
Peter A. Gale, Webb Institute of Naval Architecture, Glen Cove, NY
Rolf D. Glasfeld, General Dynamics Corporation, Groton, CT
William H. Hartt, Florida Atlantic University, Boca Raton, FL
Paul H. Wirsching, University of Arizona, Tucson, AZ
Alexander B. Stavovy, National Research Council, Washington, DC
Michael K. Parmelee, Ship Structure Committee, Washington, DC

LOADS WORK GROUP

Paul H. Wirsching (Chairman), University of Arizona, Tucson, AZ
Subrata K. Chakrabarti, Chicago Bridge and Iron Company, Plainfield, IL
Keith D. Hjelmstad, University of Illinois, Urbana, IL
Hsien Yun Jan, Martech Incorporated, Neshanic Station, NJ
Jack Y. K. Lou, Texas A & M University, College Station, TX
Naresh Maniar, M. Rosenblatt & Son, Incorporated, New York, NY
Solomon C. S. Yim, Oregon State University, Corvallis, OR

MATERIALS WORK GROUP

William H. Hartt (Chairman), Florida Atlantic University, Boca Raton, FL
Fereshteh Ebrahimi, University of Florida, Gainesville, FL
Santiago Ibarra, Jr., Amoco Corporation, Naperville, IL
Paul A. Lagace, Massachusetts Institute of Technology, Cambridge, MA
John Landes, University of Tennessee, Knoxville, TN
Mamdouh M. Salama, Conoco Incorporated, Ponca City, OK
James M. Sawhill, Jr., Newport News Shipbuilding, Newport News, VA

SHIP STRUCTURE COMMITTEE PUBLICATIONS

SSC-334 Influence of Weld Porosity on the Integrity of Marine Structures by William J. Walsh , Brian N. Leis, and J. Y. Yung,   1989

SSC-335 Performance of Underwater Weldments by R. J. Dexter, E. B. Norris, W. R. Schick, and P. D. Watson   1986

SSC-336 Liquid Sloshing in Cargo Tanks by N. A. Hamlin   1986

SSC-337 Part 1 - Ship Fracture Mechanisms Investigation by Karl A. Stambaugh and William A. Wood   1987

SSC-337 Part 2 - Ship Fracture Mechanisms - A Non-Expert's Guide for Inspecting and Determining the Causes of Significant Ship Fractures by Karl A. Stambaugh and William A. Wood 1987

SSC-338 Fatigue Prediction Analysis Validation from SL-7 Hatch Corner Strain Data by Jen-Wen Chiou and Yung-Kuang Chen 1985

SSC-339 Ice Loads and Ship Response to Ice - A Second Season by C. Daley, J. W. St. John, R. Brown, J. Meyer, and I. Glen 1990

SSC-340 Ice Forces and Ship Response to Ice - Consolidation Report by C. Daley, J. W. St. John, R. Brown, and I. Glen   1990

SSC-341 Global Ice Forces and Ship Response to Ice by P. Minnick, J. W. St. John, B. Cowper, and M. Edgecomb   1990

SSC-342 Global Ice Forces and Ship Response to Ice - Analysis of Ice Ramming Forces by Yung-Kuang Chen, Alfred L. Tunik, and Albert P-Y Chen   1990

SSC-343 Global Ice Forces and Ship Response to Ice - A Second Season by P. Minnick and J. W. St. John   1990

SSC-344 Development of an Onboard Strain Recorder by Eric Greene and William A. Wood   1987

SSC-345 Elastic-Plastic Fracture Mechanics by T. L. Anderson   1990

SSC-346 Fatigue Characterization of Fabricated Ship Details - Phase 2 by K. K. Park and F. V. Lawrence, Jr.   1988

None Ship Structure Committee Publications - A Special Bibliography   1983